COULOMB EXCITATION IN
ODD-A RARE-EARTH NUCLEI

by

Edwin Vandewater Bishop

B.A., Swarthmore College, 1958
M.S., Yale University, 1960

Edwin V. Bishop

A Dissertation Presented to the Faculty of the
Graduate School of Yale University in
Candidacy for the Degree of
Doctor of Philosophy

1966

ABSTRACT

The spectroscopy of the low-lying collective levels of the odd-A nuclei terbium-159, holmium-165 and lutetium-175 have been studied by detecting the deexcitation gamma radiation following Coulomb excitation with oxygen ions up to 65 MeV in energy. Information is presented both on the level structures and on the reduced electromagnetic transition probabilities between some of the states, and these are discussed within the framework of existing collective models. The most striking deviation from the usual axially-symmetric quasi-rigid rotor model occurs in Tb^{159}, in the form of a higher-order decoupling type term similar to the well-known Coriolis decoupling term in intrinsic $K=1/2$ bands. An analysis of possible mechanisms is presented and it is concluded that either band mixing involving a strongly decoupled band or centrifugal stretching of the core can explain the form of the energy perturbation. Although an experimental choice between the mechanisms was not possible, it is concluded that the stretching mechanism could account for the substantial part of the decoupling which a band-mixing calculation using an intrinsic matrix element computed from Nilsson wave functions does not account for. Magnitudes of the higher Coriolis and the usual vibration-rotation type perturbations in the ground-state bands are measured.

Gamma-vibrational states are located in the three nuclei, and reduced transition probabilities for their excitation, referred to ground-state band Q_0 values, are given.

ACKNOWLEDGEMENTS

I would like to express my appreciation to my research advisor, Dr. J. S. Greenberg, for suggesting this experiment and guiding and assisting in all phases of its development, and to Prof. E. R. Beringer for making the facilities of the Yale University Heavy Ion Accelerator available for this experiment.

I am grateful to G. G. Seaman and G. A. Burginyon for their valuable assistance in construction of equipment and recording of data. Special thanks are extended to Mr. Burginyon for the use of the cooled-germanium gamma-ray detection apparatus.

I would like to thank Cathy Barton, Al Nelson and my wife, Sheila Bishop, for their fine cooperation in the production of the figures in this dissertation, and the staff of the Heavy Ion Accelerator for their cooperation and technical assistance during the course of the experiment. Also, I wish to thank Mrs. D. Darling, Mrs. E. Milone and my wife for their aid in the preparation of the final manuscript.

I would particularly like to express my appreciation to my wife for her patience and encouragement during all phases of this work.

I am grateful to the U. S. Atomic Energy Commision for financial support of this research.

Table of Contents

Page

I. Introduction

The collective model for nuclear motion has been found to provide a quite adequate representation of empirical features in the low-lying spectra in large numbers of nuclei in the regions of the periodic table away from closed shells. In particular regions in which nuclei execute low-multipole-order surface vibrations about the spherical equilibrium shape and regions in which nuclei are permamently deformed into axially-symmetric nonspherical equilibrium shapes and undergo rotations as well as quadrupole and octupole vibrations are well-known experimentally and reasonably well-understood on theoretical grounds. But, on the basis of certain conceptually well-defined arguments, there arise possibilities for specific kinds of deviations from the purely collective modes of motion, arising from coupling to the other degrees of freedom. Because of the existence of pairing energies, the single-nucleon-plus-deformed-core model is expected to provide an accurate representation of low-energy nuclear phenomena in heavy odd-A nuclei in the so-called rotational regions among the Lanthanide and the Actinide elements. However, a certain amount of core elasticity is expected, which should lead to vibrational states and also, in conjunction with the Coriolis force and wave-function symmetrization for the axially-symmetric case, to certain other higher-order decoupling effects similar in character to the well-known $|K| = 1/2$ Coriolis decoupling.

Various perturbations on the simple $I(I+1)$-dependent level sequence of a pure rotator unsusceptible to elastic deformation or Coriolis effects can be predicted for an isolated rotational band, as can certain effects due to band mixing, which is brought about by these same effects in the presence of two or more rotational bands based on intrinsic or vibrational states. It is the purpose in the present thesis to observe ground-state bands up to high-lying members, via the process of E2 Coulomb excitation with heavy ions, in order to ascertain the presence or absence of the specific anticipated perturbations of the rotational motion among the odd-A rare-earth nuclei, and to identify and study experimentally such other features, especially the vibrational states, as may be present. This would provide valuable experimental checks on further implications than have previously been considered of some of the reasoning behind the collective-model phenomenology, especially as it is applied in the odd-A case.

Section I describes the relevant theoretical considerations regarding the collective models and explores their relation to the more fundamental viewpoint of the internucleon forces. In sections II, III and IV there are presented historical profiles of the three nuclei investigated in this study, Tb^{159}, Ho^{165} and Lu^{175}. Section V contains a brief description of the apparatus, targets and experimental conditions, and section VI gives details of the data reduction and of the cross-section calculations, based on available single and multiple Coulomb-excitation theory, used in the interpretation of the results. The results and their interpretation are presented in section VII, and a summary and concluding remarks are given in section VIII. Certain technical details appear in the appendices (section IX).

A. Experimental

With the experimental observation and subsequent utalization of the Coulomb-excitation process for populating excited states of nuclei in the 1950's, a very useful tool for experimental nuclear spectroscopy was realized. For bombarding energies below the Coulomb barrier of the target-projectile system, the only significant interaction is the long-range electromagnetic interaction. Because the exact form of this interaction is known from classical physics, expressions for the excitation cross sections, as functions of scattering angle and incident energy, can be separated into calculable "geometric factors", and so-called reduced electromagnetic transition probabilities or "B values" that contain information about nuclear matrix elements for known operators, thus providing, in principle, a theoretically unambiguous route to certain specific nuclear properties.

In Coulomb excitation the states most strongly populated are the low-lying collective states connected by large electromagnetic reduced transition moments, or large B(E2) values. These collective states are arranged in rotational or vibrational bands consisting of sequences of levels of increasing angular momenta, whose higher-lying members are not generally accessible to radioactive decay-scheme or to nuclear-reaction studies, and are at the same time required to obtain important information on the nuclear collective dynamics. The Coulomb excitation process provides a good complement to decay scheme work which preferentially populates low spin states, usually the low-lying "single-particle" states.

The connection of the B-value to the nuclear properties can be illustrated by following Adler et al.[1] in their semi-classical treatment of the excitation process, in which the Maxwell field is considered as a classical force field, and the projectile relative orbit is taken as a known (hyperbolic) trajectory. This treatment is accurate for the calculation of cross sections as functions of projectile energy, charge, and mass (but not scattering angle, for which quantal effects of the field are significant) provided

$$\eta = \frac{Z_1 Z_2 e^2}{\hbar v_i} \gg 1 \qquad \text{(I-1)}$$

where Z_1 and Z_2 are the charge numbers of the projectile and target nuclei respectively, e is the electronic charge, and v_1 is the initial projectile speed. The Rutherford cross section is

$$\frac{d\sigma_R}{d\Omega} = \frac{1}{4} a^2 \sin^{-4} \frac{\theta_{cm}}{2} \qquad \text{(I-2)}$$

where θ_c is the center-of-mass scattering angle, and a, half the distance of closest approach in a head-on collision, can be shown to be

$$a = \lambda\!\!\!^{-}\, \eta \qquad \text{(I-3)}$$

where $\lambda\!\!\!^{-}$ is the rationalized de Broglie wavelength of the "reduced-mass particle,"

$$\frac{\hbar}{\lambda\!\!\!^{-}} = \mu v_i = \frac{m_1 m_2}{m_1 + m_2} v_i \qquad \text{(I-4)}$$

The target nucleus alone is considered in a quantum context. If the nucleus in its initial (ground) state, described by the unperturbed Schrödinger equation

$$H_o \mid I_i M_i \rangle = E_i \mid I_i M_i \rangle \quad , \tag{I-5}$$

is subjected to the time-dependent interaction due to the electromagnetic field of the passing projectile, then the first-order time-dependent perturbation expression for the probability of excitation of the state $\mid I_f M_f \rangle$ is given by

$$b_{if} = \frac{1}{i\hbar} \int_{-\infty}^{\infty} \langle I_f M_f \mid H'(t) \mid I_i M_i \rangle \, e^{i\omega_{if} t} \, dt \tag{I-6}$$

where

$$\omega_{if} = \frac{E_f - E_i}{\hbar} \quad . \tag{I-7}$$

Into this are substituted multipole expansions of the perturbing potentials of the Maxwell field (minus the point Coulomb interaction responsible for the Rutherford scattering), which are functions of the quantities λ, μ, characterizing the multipolarity of the excitation process: $\vec{r}_p(t)$, $\vec{v}_p(t)$, and for magnetic excitations, $\vec{L}_p(t)$, specifying the projectile orbit parameters relative to the target nucleus mass center, and the quantities $\mathcal{M}(\lambda, \mu)$, which are the nuclear multipole moments:

$$\mathcal{M}(E\lambda, \mu) = \int r^{\lambda} Y_{\lambda}^{\mu}(\theta, \varphi) \rho(\vec{r}) \, d\vec{r} \tag{I-8}$$

$$\mathcal{M}(M\lambda, \mu) = \frac{i}{c(\lambda+1)} \int \vec{j}(\vec{r}) \cdot \vec{L} \left[r^{\lambda} Y_{\lambda}^{\mu}(\theta, \varphi) \right] d\vec{r} .$$

Here $\vec{L} = -i\vec{r} \times \nabla$, and $\rho(\vec{r})$ and $\vec{j}(\vec{r})$ are nuclear charge and current density operators. The results for the excitation cross sections of an unpolarized collection of target nuclei accompanying projectile scattering through angle θ_c into $d\Omega$,

$$\frac{d\sigma}{d\Omega} = \frac{1}{2I_1 + 1} \sum_{M_1} \sum_{M_f} \left| b_{1f} \right|^2 \frac{d\sigma_R}{d\Omega} \ , \qquad \text{(I-9)}$$

are, for electric and magnetic 2^λ-pole excitations respectively,

$$\frac{d\sigma_{E\lambda}}{d\Omega} = \frac{Z_1^2 e^2}{\hbar v_1 v_f} a^{-2\lambda+2} B(E\lambda) \frac{df_{E\lambda}(\theta,\xi)}{d\Omega} \qquad \text{(I-10)}$$

$$\frac{d\sigma_{M\lambda}}{d\Omega} = \left(\frac{Z_1 e}{\hbar c}\right)^2 a^{-2\lambda+2} B(M\lambda) \frac{df_{M\lambda}(\theta,\xi)}{d\Omega} \ .$$

Here $f_\lambda(\theta_1,\xi)$ are tabulated functions of the scattering angle and the parameter $\xi = \eta_f - \eta_1$, with η_f being the η parameter for the final projectile speed v_f after the exciting collision. These functions are the values of certain integrals taken over the classical projectile relative trajectories. In these expressions all the nuclear information is contained in the quantities (see also ref.2, p.599):

$$B(E\lambda) = \sum_{\mu} \sum_{M_f} \left| e \int \psi^*_{I_f M_f}(\vec{r}) r^\lambda Y_\lambda^{\mu *}(\theta,\varphi) \psi_{I_i M_i}(\vec{r}) d\vec{r} \right|^2 \qquad \text{(I-11)}$$

$$B(M\lambda) = \sum_{\mu} \sum_{M_f} \left| -\frac{i}{\lambda+1} \frac{e\hbar}{m_2 c} \int r^\lambda Y_\lambda^{\mu *}(\theta,\varphi) \nabla \cdot \left[\psi_{I_f M_f}(\vec{r}) \vec{L} \psi_{I_i M_i}(\vec{r}) \right] d\vec{r} \right|^2$$

which are essentially matrix elements of known operators with respect to the (unknown) nuclear wave functions, and are the same quantities (apart from trivial numerical factors) that appear in the expressions for the probability of radiative decay of the excited nuclear state.

The periodic table contains certain "rotational" regions characterized by large static quadrupole moments, large electromagnetic E2 transition moments, and the "rotational sequence" in the level energies and spins. The use of heavy ions as opposed to protons or alpha particles, which appreciably excite only one or two levels of the ground state bands, has some distinct advantages. The Coulomb barrier is much higher, so that considerably more center-of-mass energy is available for the excitation process, when operating at a fixed amount of energy below some criterion for the barrier height. A situation disadvantageous for the perfoming of accurate calculations is that the process is no longer adiabatic, so that perturbation treatments such as illustrated above fail to yield accurate cross sections, but is more in the character of an impulsive shock to the nucleus:

$$\xi = \eta_f - \eta_i \approx \eta_i \frac{\Delta E}{2E_{CM}} \sim \frac{\text{nuclear frequency}}{\text{collision time}} \ll 1 \quad \text{(I-12)}$$

However, the multiple excitation theory of Alder and Winther,[3] which then becomes a more applicable approximation, predicts that at higher projectile energies, and preferentially for backward projectile scattering angles, higher order multiple excitation processes become present at detectable percentages, providing a practical way to reach very high-lying members of a ground-state band, and several members of higher bands based on vibrational or single-particle excited states. Other methods might be the use of (α,xn) reactions to high-spin members of a band, or population of high-spin intrinsic states corresponding to two or three nucleons.

From considerations on these lines high-order excitation processes were judged to be both desirable and feasible for study on a heavy ion linear accelerator such as the HILAC at Yale.

B. Theoretical

For the theoretical understanding of nuclei, aside from the accidental discovery of an exact dynamical theory and a practical means of applying it in the analogue of the classical many-body context, one must take recourse to accurate phenomenological models of nuclei. This may be thought to constitute a basic limitation on the use of nuclear structure as a probe of nuclear forces. But, noting that generally reliable methods for solving n-body problems have not been forthcoming even for such simple known interactions as, for example, pure Coulomb forces, even with possession of knowledge of the nuclear force, nuclear properties probably could not be calculated without considerable foreknowledge of the results. Thus, even if the exact form of the nuclear force were known, observations of nuclear properties and their phenomenological description would still be prerequisite to successful formulation of a complete theory of nuclear structure. In the absence of such knowledge, the models that adequately describe the data can be studied in relation to their theoretical foundations in terms of fundamental nuclear forces, to check such information as may be available about them. These considerations motivate experimental studies in nuclear spectroscopy and the correlation of results with the predictions of nuclear models.

An indication of phenomena expected in heavy deformed nuclei is obtained by noting that, irrespective of the nuclear dynamics, if the Hamiltonian is formally identical to the rotating rigid-body Hamiltonian

$$T_R = \frac{1}{2} \sum_{\mu} \sum_{\nu} \omega_{\mu} \mathcal{I}_{\mu\nu} \omega_{\nu} \quad , \tag{I-13}$$

or

$$T_R = \frac{1}{2} \sum_{i=1}^{3} \mathcal{I}_i' \omega_i^2 \tag{I-14}$$

in terms of body-fixed principal-axis frame components, then the system will behave in a manner similar to an isolated, rigid, asymmetric top. Here ω_{μ} are components of the angular velocity associated with the net rotational motion, and $\mathcal{I}_{\mu\nu}$ are components of the usual rotational inertia tensor. The inertia moments will not necessarily have values characteristic of a rotating rigid body or, at the other extreme, the much smaller moments characteristic of irrotational flow in an incompressible fluid body with a time-dependent boundary like that of a rotating spheroid. The values of the inertia moments can be considered as adjustable parameters of the model.

Deviations from strict quasi-rigid-body behavior may be interpreted in a manner dependent upon the specific model employed. One approach consists of assuming a symmetric top formalism for the nucleus but allowing for centrifugal stretching by permitting the inertia moments to depend parametrically on the collective angular momentum. A second approach, pertinent to odd-A nuclei, is to separate out the angular momentum due to the collective motion of the body as a whole, $\vec{R}$, from a residual angular momentum, present in the

Euler Rotations

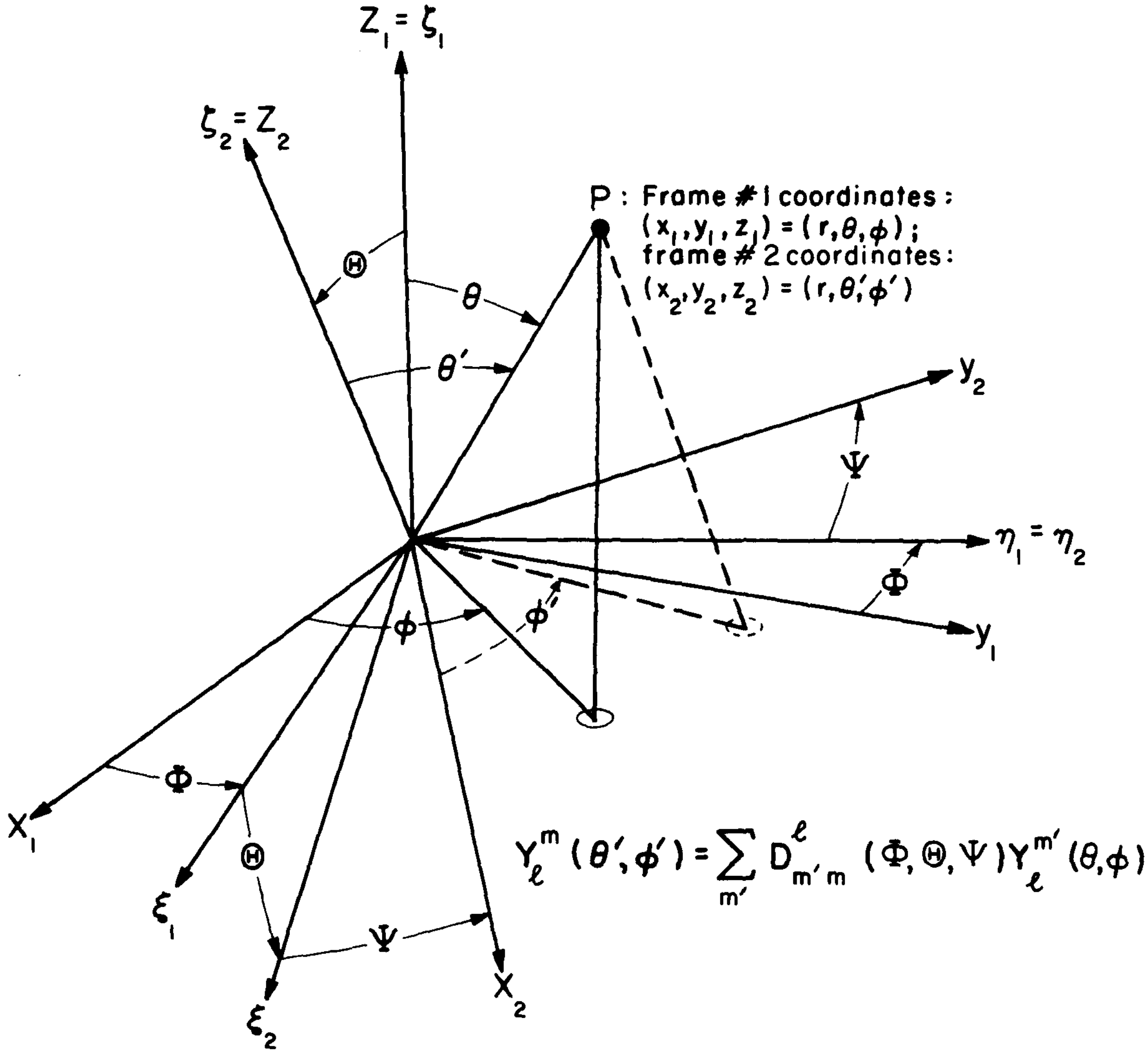

FIG I-1

absence of any collective modes, attributable specifically to individual nucleon motions, $\vec{J} = \sum_i \vec{j}_i = \sum_i (\vec{\ell}_i + \vec{s}_i)$. Even-even nuclei always couple to $\vec{J} = 0$ in the ground states. For odd-A nuclei it is generally considered that even-even cores up to the last major closed shell couple to zero intrinsic angular momentum, and $\vec{J}$ resides with the extra-core nucleons. For low-lying states $\vec{J}$ resides with the last odd nucleon. In both these approaches there occur terms in the Hamiltonian which, in conjunction with the symmetry requirements on the wave functions, result in deviations from the usual quantized rotator energy spectrum including, for odd-A systems, terms characterized by alternate elevation and depression of levels in a rotational sequence.

C. Formal Theory of an Axially-Symmetric Top

In order to understand the nature of anticipated phenomena in odd-A nuclei in the collective regions, certain theoretical developments were explored. Some of this material, which was written primarily for my own edification, has not appeared in the literature in this form.

1. Definition of $D_{m'm}^{j}(\Phi, \Theta, \Psi)$

The D-functions arise as coefficients in a transformation among the spherical-harmonic functions induced by a reorientation of coordinate axes in the following manner. Of two Cartesian frames with coincident origins but arbitrary relative orientations, frame 1 may be taken into frame 2 by the sequence of rotations: first, a rotation through the angle Φ (in the right-hand screw sense) about the z_1 axis, into the frame (ξ_1, η_1, ζ_1) (Fig. I-1); then a rotation of Θ about the η_1 axis, into the frame (ξ_2, η_2, ζ_2); and lastly, a rotation of Ψ about the ζ_2 axis, into frame 2. This results in a transformation of the coordinates of a point fixed in frame 1 which is given by:

$$\begin{pmatrix} x_2 \\ y_2 \\ z_2 \end{pmatrix} = \begin{pmatrix} \cos\Psi & \sin\Psi & 0 \\ -\sin\Psi & \cos\Psi & 0 \\ 0 & 0 & 1 \end{pmatrix} \begin{pmatrix} \cos\theta & 0 & -\sin\theta \\ 0 & 1 & 0 \\ \sin\theta & 0 & \cos\theta \end{pmatrix} \begin{pmatrix} \cos\Phi & \sin\Phi & 0 \\ -\sin\Phi & \cos\Phi & 0 \\ 0 & 0 & 1 \end{pmatrix} \begin{pmatrix} x_1 \\ y_1 \\ z_1 \end{pmatrix} \qquad \text{(I-15)}$$

If the Euler angles Φ, Θ, Ψ which specify the reorientation are restricted[4,5] to the ranges $0 \leq \Phi \leq 2\pi$, $0 \leq \Theta \leq \pi$, $0 \leq \Psi \leq 2\pi$, then there is a one-to-one correspondence between sets of angles and relative frame orientations. It can be shown[4,5] that the same net reorientation results from the rotations: first, through Ψ about the z_1 axis, then through Θ about the original y_1 axis, and finally, through Φ about the original z_1 axis.

For an isolated body whose square and z-component of angular momentum are $\hbar j(j+1)$ and $\hbar m$:

$$J^2 |jm\rangle = j(j+1)\hbar^2 |jm\rangle \qquad \text{(I-16)}$$

$$J_z |jm\rangle = m\hbar |jm\rangle \qquad \text{(I-17)}$$

frame 1 may be identified as a space-fixed inertial frame and frame 2, a body-fixed frame, the coincident origins being at the mass centroid. Then a reorientation of the body will result in a transformation of its angular-momentum eigenfunctions:

$$|jm\rangle \rightarrow |jm\rangle' = |j\rangle = R|jm\rangle = |jm'\rangle\langle jm'|R|jm\rangle, \qquad \text{(I-17)}$$

where $|jm\rangle'$ is the same function of the new body-frame coordinates $\bar{\lambda}'$ as $|jm\rangle$ is of the original body-frame coordinates, with the original body frame playing the role of the "space-fixed" frame. The expansion is valid because the reoriented-body wave function is still an eigenfunction of J^2 with the same eigenvalue, but no longer of J_z, and the $|jm\rangle$ form a complete set over m for fixed j. The expansion coefficients are by definition the D-functions:[4]

$$D_{m'm}^{j}(\Phi, \Theta, \Psi) \equiv \langle jm'|R|jm\rangle \qquad \text{(I-19)}$$

Corresponding to the two equivalent sets of Euler rotations taking frame 1 into frame 2, it can be shown[4,5] that the transformation operator R takes on the two forms:

$$R = e^{-i\Psi J_{z_2=\zeta_2}}\, e^{-i\Theta J_{y_2=\eta_1}}\, e^{-i\Phi J_{\zeta_1=z_1}}\,; \qquad \text{(I-20)}$$

$$R = e^{-i\Phi J_z}\, e^{-i\Theta J_y}\, e^{-i\Psi J_z}. \qquad \text{(I-21)}$$

The latter form is convenient since it contains only space-frame components of the angular momentum. In a representation in which J_z is diagonal, $J_z|jm\rangle = m\hbar|jm\rangle$, the D-functions are

$$D^j_{m'm}(\Phi,\Theta,\Psi) = \langle jm'|e^{-i\Phi J_z}\, e^{-i\Theta J_y}\, e^{-i\Psi J_z}|jm\rangle \qquad \text{(I-22)}$$
$$= e^{-i(m'\Phi + m\Psi)}\langle jm'|e^{-i\Theta J_y}|jm\rangle = e^{-i(m'\Phi + m\Psi)}d^j_{m'm}(\Theta)$$

in which the matrix formed from the matrix elements,

$$\langle jm'|e^{-i\Theta J_y}|jm\rangle \equiv d^j_{m'm}(\Theta) \qquad \text{(I-23)}$$

is not diagonal.

There has been considerable variation in the literature on the exact definition of these functions arising from different phase conventions for the angular-momentum operators and eigenfunctions and from different definitions of the Euler angles. The form adopted in this thesis is that of Rose.[4]

2. Rigid Symmetric Top

The Hamiltonian of an isolated rigid body in terms of Euler angles specifying its orientation with respect to an inertial frame derived from Euler's geometrical equations and the kinetic energy expressed in terms of the angular momentum is derived as follows. These equations are simply expressions for the body-axes components of the velocity field with respect to the space frame of points fixed in the body frame. The velocity field is given by $\vec{v} = \vec{\omega}\times\vec{r}$ ($\vec{v}' \equiv \vec{r}' \equiv \vec{0}$), or

$$\begin{pmatrix} V_x \\ V_y \\ V_z \end{pmatrix} = \begin{pmatrix} \dot{x} \\ \dot{y} \\ \dot{z} \end{pmatrix} = \begin{pmatrix} 0 & -\omega_z & \omega_y \\ \omega_z & 0 & -\omega_x \\ -\omega_y & \omega_x & 0 \end{pmatrix}\begin{pmatrix} x \\ y \\ z \end{pmatrix} \equiv \Omega \begin{pmatrix} x \\ y \\ z \end{pmatrix} \qquad \text{(I-24)}$$

in terms of the space-frame components. The body-frame components of $\vec{v}$, $\vec{r}$ and $\vec{\omega}$ are

$$\begin{pmatrix} x' \\ y' \\ z' \end{pmatrix} = \mathcal{R}(\Phi,\Theta,\Psi)\begin{pmatrix} x \\ y \\ z \end{pmatrix}, \quad \begin{pmatrix} v_1 \\ v_2 \\ v_3 \end{pmatrix} = \mathcal{R}\begin{pmatrix} v_x \\ v_y \\ v_z \end{pmatrix}, \quad \begin{pmatrix} \omega_1 \\ \omega_2 \\ \omega_3 \end{pmatrix} = \mathcal{R}\begin{pmatrix} \omega_x \\ \omega_y \\ \omega_z \end{pmatrix}; \tag{I-25}$$

whence

$$\begin{pmatrix} 0 & -\omega_3 & \omega_2 \\ \omega_3 & 0 & -\omega_1 \\ -\omega_2 & \omega_1 & 0 \end{pmatrix} \equiv \Omega' = \mathcal{R}\Omega\mathcal{R}^{-1}. \tag{I-26}$$

Here $\mathcal{R}$ is the product of the rotation matrices in eqn. (I-15). It can be noted in passing that

$$\begin{pmatrix} v_1 \\ v_2 \\ v_3 \end{pmatrix} = \mathcal{R}\begin{pmatrix} v_x \\ v_y \\ v_z \end{pmatrix} = \mathcal{R}\Omega\begin{pmatrix} x \\ y \\ z \end{pmatrix} = \mathcal{R}\Omega\mathcal{R}^{-1}\mathcal{R}\begin{pmatrix} x \\ y \\ z \end{pmatrix} = \Omega'\begin{pmatrix} x' \\ y' \\ z' \end{pmatrix}, \tag{I-27}$$

showing the form-invariance of this relation. With a little manipulation, one has

$$\frac{d}{dt}\left[\mathcal{R}^{-1}\begin{pmatrix} x' \\ y' \\ z' \end{pmatrix}\right] = \frac{d}{dt}\begin{pmatrix} x \\ y \\ z \end{pmatrix} = \Omega\begin{pmatrix} x \\ y \\ z \end{pmatrix} = \mathcal{R}^{-1}\Omega'\mathcal{R}\begin{pmatrix} x \\ y \\ z \end{pmatrix} = \mathcal{R}^{-1}\Omega'\begin{pmatrix} x' \\ y' \\ z' \end{pmatrix}. \tag{I-28}$$

Since $\begin{pmatrix} x' \\ y' \\ z' \end{pmatrix} \equiv$ const. in time, one has therefore,

$$\frac{d}{dt}\mathcal{R}^{-1}(\Phi,\Theta,\Psi) \equiv \frac{d}{dt}\left[\mathcal{R}_1^{-1}(\Phi)\mathcal{R}_2^{-1}(\Theta)\mathcal{R}_3^{-1}(\Psi)\right] = \mathcal{R}^{-1}\Omega'; \tag{I-29}$$

$$\frac{d\mathcal{R}_1^{-1}}{d\Phi}\mathcal{R}_2^{-1}\mathcal{R}_3^{-1}\dot{\Phi} + \mathcal{R}_1^{-1}\frac{d\mathcal{R}_2^{-1}}{d\Theta}\mathcal{R}_3^{-1}\dot{\Theta} + \mathcal{R}_1^{-1}\mathcal{R}_2^{-1}\frac{d\mathcal{R}_3^{-1}}{d\Psi}\dot{\Psi} = \mathcal{R}_1^{-1}\mathcal{R}_2^{-1}\mathcal{R}_3^{-1}\Omega'. \tag{I-30}$$

Multiplying on the left by $\mathcal{R}_1\mathcal{R}_2\mathcal{R}_3$ and applying the rule for differentiation of matrices with respect to parameters in their elements, one finds

$$\begin{pmatrix} 0 & -\cos\Theta & \sin\Theta\sin\Psi \\ \cos\Theta & 0 & \sin\Theta\cos\Psi \\ -\sin\Theta\sin\Psi & -\sin\Theta\cos\Psi & 0 \end{pmatrix}\dot{\Phi} + \begin{pmatrix} 0 & 0 & \cos\Psi \\ 0 & 0 & -\sin\Psi \\ -\cos\Psi & \sin\Psi & 0 \end{pmatrix}\dot{\Theta}$$
$$+ \begin{pmatrix} 0 & -1 & 0 \\ 1 & 0 & 0 \\ 0 & 0 & 0 \end{pmatrix}\dot{\Psi} = \Omega' \equiv \begin{pmatrix} 0 & -\omega_3 & \omega_2 \\ \omega_3 & 0 & -\omega_1 \\ -\omega_2 & \omega_1 & 0 \end{pmatrix}, \tag{I-31}$$

which reduces to

$$\omega_1 = -\sin\Theta\cos\Psi\dot{\Phi} + \sin\Psi\dot{\Theta}, \tag{I-32}$$

$$\omega_2 = \sin\Theta\sin\Psi\dot{\Phi} + \cos\Psi\dot{\Theta}, \tag{I-33}$$

$$\omega_3 = \cos\Theta\dot{\Phi} + \dot{\Psi}, \tag{I-34}$$

or more succinctly,

$$\begin{pmatrix}\omega_1\\ \omega_2\\ \omega_3\end{pmatrix} = \begin{pmatrix}\cos\Psi & \sin\Psi & 0\\ -\sin\Psi & \cos\Psi & 0\\ 0 & 0 & 1\end{pmatrix}\begin{pmatrix}-\sin\Theta & 0 & 0\\ 0 & 1 & 0\\ \cos\Theta & 0 & 1\end{pmatrix}\begin{pmatrix}\dot{\Phi}\\ \dot{\Theta}\\ \dot{\Psi}\end{pmatrix}. \tag{I-35}$$

These are Euler's geometrical equations.

Now suppose the isolated body has rotational kinetic energy given by

$$T = \tfrac{1}{2}\vec{\omega}\cdot\overleftrightarrow{\mathcal{I}}\cdot\vec{\omega} = \tfrac{1}{2}\vec{\omega}'\cdot\overleftrightarrow{\mathcal{I}}'\cdot\vec{\omega}' \equiv \tfrac{1}{2}\sum_{\mu}\sum_{\nu}\omega_{\mu}\mathcal{I}_{\mu\nu}\omega_{\nu} \tag{I-36}$$

where $\vec{\omega} = \begin{pmatrix}\omega_x\\ \omega_y\\ \omega_z\end{pmatrix}$, $\vec{\omega}' = \begin{pmatrix}\omega_1\\ \omega_2\\ \omega_3\end{pmatrix}$, and $\overleftrightarrow{\mathcal{I}}$ is the inertia tensor,

$$\overleftrightarrow{\mathcal{I}} = \int\rho(\vec{r})\,(r^2\hat{\hat{\mathcal{J}}} - \vec{r}\,\vec{r}\,)\,d\vec{r} \quad , \tag{I-37}$$

$\hat{\hat{\mathcal{J}}}$ being the unit dyadic. In particular,

$$\overleftrightarrow{\mathcal{I}} = \begin{pmatrix}\mathcal{I}_{xx} & \mathcal{I}_{xy} & \mathcal{I}_{xz}\\ \mathcal{I}_{yx} & \mathcal{I}_{yy} & \mathcal{I}_{yz}\\ \mathcal{I}_{zx} & \mathcal{I}_{zy} & \mathcal{I}_{zz}\end{pmatrix} \tag{I-38}$$

and

$$\overleftrightarrow{\mathcal{I}}' = \begin{pmatrix}\mathcal{I}'_{11} & \mathcal{I}'_{12} & \mathcal{I}'_{13}\\ \mathcal{I}'_{21} & \mathcal{I}'_{22} & \mathcal{I}'_{23}\\ \mathcal{I}'_{31} & \mathcal{I}'_{32} & \mathcal{I}'_{33}\end{pmatrix} \equiv \begin{pmatrix}\mathcal{I}'_1 & 0 & 0\\ 0 & \mathcal{I}'_2 & 0\\ 0 & 0 & \mathcal{I}'_3\end{pmatrix}. \tag{I-39}$$

In terms of body components, then,

$$T_R = \tfrac{1}{2}\sum_i \mathcal{I}'_i\,\omega_i^2 \quad . \tag{I-40}$$

Substitution from Euler's geometric equations results in

$$T_R = \tfrac{1}{2}\Big[\mathcal{I}_1' \,(-\dot{\Phi}\sin\Theta\cos\Psi + \dot{\Theta}\sin\Psi)^2 \qquad \text{(I-41)}$$
$$+ \mathcal{I}_2' \,(\dot{\Phi}\sin\Theta\sin\Psi + \dot{\Theta}\cos\Psi)^2$$
$$+ \mathcal{I}_3' \,(\dot{\Phi}\cos\Theta + \dot{\Psi})^2\Big]$$

An interesting point may be noted in passing by writing this as

$$T_R = \tfrac{1}{2}\,(A\,\mathcal{I}_1' + B\mathcal{I}_2' + C\,\mathcal{I}_3') \qquad \text{(I-42)}$$

and setting

$$\mathcal{I}_1' = \bar{\mathcal{I}}_1', \qquad \mathcal{I}_2' = \bar{\mathcal{I}}_1' + \bar{\mathcal{I}}_2', \qquad \mathcal{I}_3' = \bar{\mathcal{I}}_3' \;; \qquad \text{(I-43)}$$
$$\bar{\mathcal{I}}_1' = \mathcal{I}_1', \qquad \bar{\mathcal{I}}_2' = \mathcal{I}_2' - \mathcal{I}_1', \qquad \bar{\mathcal{I}}_3' = \mathcal{I}_3' \;. \qquad \text{(I-44)}$$

This results in an alternative form of T:

$$T_R = \tfrac{1}{2}\Big[\bar{\mathcal{I}}_1' \,(\sin^2\Theta\;\dot{\Phi}^2 + \dot{\Theta}^2) \qquad \text{(I-45)}$$
$$+ \bar{\mathcal{I}}_2' \,(\sin\Theta\sin\Psi\,\dot{\Phi} + \cos\Psi\,\dot{\Theta})^2$$
$$+ \bar{\mathcal{I}}_3' \,(\cos\Theta\,\dot{\Phi} + \dot{\Psi})^2\Big]$$

which is of the form,

$$T_R = \tfrac{1}{2}\,(\bar{A}\,\bar{\mathcal{I}}_1' + \bar{B}\,\bar{\mathcal{I}}_2' + \bar{C}\,\bar{\mathcal{I}}_3') \qquad \text{(I-46)}$$

but with the coefficients

$$\bar{A} = A + B, \qquad \bar{B} = B, \qquad \bar{C} = C \;. \qquad \text{(I-47)}$$

The dependence of the coefficients of the "1" component of inertia on $\Phi, \Theta, \Psi, \dot{\Phi}, \dot{\Theta}$ and $\dot{\Psi}$ is changed, and the numerical value of the "2" component is altered, but the structure of the Hamiltonian is unchanged. It is therefore important to be careful what is meant in discussing deviations from equality of the "1" and "2" components. One can note that $\mathcal{I}'_1 = \mathcal{I}'_2$ if and only if $\bar{\mathcal{I}}_2 = 0$, or that the second form is convenient for treating small deviations from axial symmetry. A third form of writing T_R is also possible:

$$T_R = \tfrac{1}{2}\,(\bar{\bar{A}}\,\bar{\bar{\mathcal{I}}}'_1 + \bar{\bar{B}}\,\bar{\bar{\mathcal{I}}}'_2 + \bar{\bar{C}}\,\bar{\bar{\mathcal{I}}}'_3) \qquad \text{(I-48)}$$

$$\bar{\bar{\mathcal{I}}}'_1 = \tfrac{1}{2}(\mathcal{I}'_1 + \mathcal{I}'_2) \qquad \bar{\bar{\mathcal{I}}}'_2 = \tfrac{1}{2}(\mathcal{I}'_1 - \mathcal{I}'_2) \qquad \bar{\bar{\mathcal{I}}}'_3 = \mathcal{I}'_3 \qquad \text{(I-49)}$$

$$\mathcal{I}'_1 = \bar{\bar{\mathcal{I}}}'_1 + \bar{\bar{\mathcal{I}}}'_2 \qquad \mathcal{I}'_2 = \bar{\bar{\mathcal{I}}}'_1 - \bar{\bar{\mathcal{I}}}'_2 \qquad \mathcal{I}'_3 = \bar{\bar{\mathcal{I}}}'_3 \qquad \text{(I-50)}$$

$\mathcal{I}'_1 = \mathcal{I}'_2$ if and only if $\bar{\bar{\mathcal{I}}}'_2 = 0$. Here,

$$\bar{\bar{A}} = A + B = \bar{A}, \quad \bar{\bar{B}} = A - B = A - \bar{B}, \quad \bar{\bar{C}} = C = \bar{C} \quad . \qquad \text{(I-51)}$$

This again alters the values of the inertia tensor components and the dependences of their coefficients in T_R on $\Phi, \Theta, \Psi, \dot{\Phi}, \dot{\Theta}$ and $\dot{\Psi}$, without changing the form of T_R, and provides a form that would also be convenient for treating small deviations from axial symmetry were it not for the fact that the value of $\bar{\bar{\mathcal{I}}}'_1$ now depends on the size of $\bar{\bar{\mathcal{I}}}'_2$.

Returning to the symmetric top problem, Φ, Θ, Ψ are now taken as generalized coordinates. Working with the form of T_R using the conventionally defined inertia tensor components $\mathcal{I}'_1$, $\mathcal{I}'_2$, $\mathcal{I}'_3$, one has for the isolated rigid body the Hamiltonian $T_R = H$, wherein the generalized momenta are given by

$$p_{\Phi} = \frac{\partial T_R(\Phi\Theta\Psi\dot{\Phi}\dot{\Theta}\dot{\Psi})}{\partial\dot{\Phi}}, \text{ etc.} \tag{I-52}$$

It can be shown by performing the indicated differentiations that

$$\begin{pmatrix} p_{\Phi} \\ p_{\Theta} \\ p_{\Psi} \end{pmatrix} = \begin{pmatrix} -\sin\Theta & 0 & \cos\Theta \\ 0 & 1 & 0 \\ 0 & 0 & 1 \end{pmatrix} \begin{pmatrix} \cos\Psi & -\sin\Psi & 0 \\ \sin\Psi & \cos\Psi & 0 \\ 0 & 0 & 1 \end{pmatrix} \begin{pmatrix} \mathcal{I}_1' & 0 & 0 \\ 0 & \mathcal{I}_2' & 0 \\ 0 & 0 & \mathcal{I}_3' \end{pmatrix} \begin{pmatrix} \cos\Psi & \sin\Psi & 0 \\ -\sin\Psi & \cos\Psi & 0 \\ 0 & 0 & 1 \end{pmatrix} \tag{I-53}$$

$$\times \begin{pmatrix} -\sin\Theta & 0 & 0 \\ 0 & 1 & 0 \\ \cos\Theta & 0 & 1 \end{pmatrix} \begin{pmatrix} \dot{\Phi} \\ \dot{\Theta} \\ \dot{\Psi} \end{pmatrix} \equiv \Theta^{\dagger}\Psi^{\dagger}\mathcal{I}'\Psi\Theta \begin{pmatrix} \dot{\Phi} \\ \dot{\Theta} \\ \dot{\Psi} \end{pmatrix}$$

$$= \widetilde{\Theta}\,\widetilde{\Psi}\,\mathcal{I}'\,\Psi\,\Theta \begin{pmatrix} \dot{\Phi} \\ \dot{\Theta} \\ \dot{\Psi} \end{pmatrix},$$

and hence,

$$\begin{pmatrix} \dot{\Phi} \\ \dot{\Theta} \\ \dot{\Psi} \end{pmatrix} = \Theta^{-1}\Psi^{-1}\mathcal{I}'^{-1}\widetilde{\Psi}^{-1}\widetilde{\Theta}^{-1} \begin{pmatrix} p_{\Phi} \\ p_{\Theta} \\ p_{\Psi} \end{pmatrix} = \widetilde{\Theta}\,\widetilde{\Psi}\,\mathcal{I}'^{-1}\,\Psi\,\Theta \begin{pmatrix} p_{\Phi} \\ p_{\Theta} \\ p_{\Psi} \end{pmatrix}, \tag{I-54}$$

where the properties $\Psi^{-1} = \widetilde{\Psi}$; $\widetilde{M^{-1}} = \widetilde{M}^{-1}$ for arbitrary nonsingular matrices M; and where

$$\widetilde{\Theta}^{-1} = \frac{1}{\sin\Theta} \begin{pmatrix} -1 & 0 & \cos\Theta \\ 0 & \sin\Theta & 0 \\ 0 & 0 & \sin\Theta \end{pmatrix}, \quad \mathcal{I}'^{-1} = \begin{pmatrix} \frac{1}{\mathcal{I}_1'} & 0 & 0 \\ 0 & \frac{1}{\mathcal{I}_2'} & 0 \\ 0 & 0 & \frac{1}{\mathcal{I}_3'} \end{pmatrix}. \tag{I-55}$$

T_R in terms of $p_{\Phi}, \cdots, \Psi$ can now be derived. From the Euler geometrical equations,

$$\begin{pmatrix}\omega_1\\ \omega_2\\ \omega_3\end{pmatrix} = \begin{pmatrix}\cos\Psi & \sin\Psi & 0\\ -\sin\Psi & \cos\Psi & 0\\ 0 & 0 & 1\end{pmatrix}\begin{pmatrix}-\sin\Theta & 0 & 0\\ 0 & 1 & 0\\ \cos\Theta & 0 & 1\end{pmatrix}\begin{pmatrix}\dot\Phi\\ \dot\Theta\\ \dot\Psi\end{pmatrix} = \Psi\,\Theta\begin{pmatrix}\dot\Phi\\ \dot\Theta\\ \dot\Psi\end{pmatrix}, \tag{I-56}$$

one can show that generally,

$$T_R = \frac{1}{2}\sum_i\sum_j \omega_i \mathcal{I}'_{ij}\,\omega_j = \frac{1}{2}(\omega_1\,\omega_2\,\omega_3)\begin{pmatrix}\mathcal{I}_{11}' & \mathcal{I}_{12}' & \mathcal{I}_{13}'\\ \mathcal{I}_{21}' & \mathcal{I}_{22}' & \mathcal{I}_{23}'\\ \mathcal{I}_{31}' & \mathcal{I}_{32}' & \mathcal{I}_{33}'\end{pmatrix}\begin{pmatrix}\omega_1\\ \omega_2\\ \omega_3\end{pmatrix} \tag{I-57}$$

$$= \frac{1}{2}(\dot\Phi\,\dot\Theta\,\dot\Psi)\,\tilde\Theta\,\tilde\Psi\,\mathcal{I}'\,\Psi\,\Theta\begin{pmatrix}\dot\Phi\\ \dot\Theta\\ \dot\Psi\end{pmatrix},$$

or in particular, for the case $\mathcal{I}'_{ij} = \mathcal{I}'_i\,\delta_{ij}$,

$$\begin{pmatrix}P_\Phi\\ P_\Theta\\ P_\Psi\end{pmatrix} = \tilde\Theta\,\tilde\Psi\,\mathcal{I}'\,\Psi\,\Theta\begin{pmatrix}\dot\Phi\\ \dot\Theta\\ \dot\Psi\end{pmatrix} \tag{I-58}$$

and

$$P_\Phi\,\dot\Phi + P_\Theta\,\dot\Theta + P_\Psi\,\dot\Psi = (\dot\Phi\,\dot\Theta\,\dot\Psi)\begin{pmatrix}P_\Phi\\ P_\Theta\\ P_\Psi\end{pmatrix}$$

$$= (\dot\Phi\,\dot\Theta\,\dot\Psi)\,\tilde\Theta\,\tilde\Psi\,\mathcal{I}'\,\Psi\,\Theta\begin{pmatrix}\dot\Phi\\ \dot\Theta\\ \dot\Psi\end{pmatrix} = 2T_R \tag{I-59}$$

or

$$T_R = \frac{1}{2}(\dot\Phi\,\dot\Theta\,\dot\Psi)\begin{pmatrix}P_\Phi\\ P_\Theta\\ P_\Psi\end{pmatrix}. \tag{I-60}$$

But

$$\begin{pmatrix}\dot\Phi\\ \dot\Theta\\ \dot\Psi\end{pmatrix} = \Theta^{-1}\,\tilde\Psi\,\mathcal{I}'^{-1}\,\Psi\,\tilde\Theta^{-1}\begin{pmatrix}P_\Phi\\ P_\Theta\\ P_\Psi\end{pmatrix}. \tag{I-61}$$

Hence

$$(\dot\Phi\,\dot\Theta\,\dot\Psi) = (P_\Phi\;P_\Theta\;P_\Psi)\;\Theta^{-1}\,\tilde\Psi\,\mathcal{I}'^{-1}\,\Psi\,\tilde\Theta^{-1}, \tag{I-62}$$

from which follows,

$$T_R = \frac{1}{2}\left(p_\Phi\ p_\Theta\ p_\Psi\right) \Theta^{-1}\widetilde{\Psi}\ \mathcal{I}'^{-1}\ \Psi\ \widetilde{\Theta}^{-1} \begin{pmatrix} p_\Phi \\ p_\Theta \\ p_\Psi \end{pmatrix} \tag{I-63}$$

$$= \frac{1}{2}\left(p_\Phi p_\Theta p_\Psi\right)\frac{1}{\sin^2\Theta}\begin{pmatrix} -1 & 0 & 0 \\ 0 & \sin\Theta & 0 \\ \cos\Theta & 0 & \sin\Theta \end{pmatrix}\begin{pmatrix} \cos\Psi & -\sin\Psi & 0 \\ \sin\Psi & \cos\Psi & 0 \\ 0 & 0 & 1 \end{pmatrix}\begin{pmatrix} \frac{1}{\mathcal{I}_1'} & 0 & 0 \\ 0 & \frac{1}{\mathcal{I}_2'} & 0 \\ 0 & 0 & \frac{1}{\mathcal{I}_3'} \end{pmatrix}\begin{pmatrix} \cos\Psi & -\sin\Psi & 0 \\ \sin\Psi & \cos\Psi & 0 \\ 0 & 0 & 1 \end{pmatrix}\begin{pmatrix} -1 & 0 & \cos\Theta \\ 0 & \sin\Theta & 0 \\ 0 & 0 & \sin\Theta \end{pmatrix}\begin{pmatrix} p_\Phi \\ p_\Theta \\ p_\Psi \end{pmatrix}$$

So far the order of the factors has been preserved, so that in the quantum context, in the coordinate representation wherein $p = -i\hbar\frac{\partial}{\partial q}$, $\left[p,\ f(q)\right] \neq 0$, operators take the form $\mathcal{O} = f(q)p$, $\mathcal{O}^\dagger = p^* f(q^*)$. The momenta canonically conjugate to the Euler angles are angular momentum components about the corresponding axes, and in the quantum coordinate representation employing the Euler angles are given by the differential operators $-i\hbar\frac{\partial}{\partial\Phi}$, $-i\hbar\frac{\partial}{\partial\Theta}$, $-i\hbar\frac{\partial}{\partial\Psi}$. In any representation they do not commute with functions of the angles.

For a general angle coordinate θ, the canonically conjugate angular momentum $p_\theta \equiv L_\theta$ satisfies

$$\left[p_\theta,\ f(\theta)\right] = -i\hbar\frac{df}{d\theta}. \tag{I-64}$$

Then $p_\Phi F(\Phi, \Theta, \Psi) = F(\Phi, \Theta, \Psi)p_\Phi - i\hbar\frac{\partial F}{\partial\Phi}$, etc. This complicates the explicit calculation of the operator for T_R in the form with all the p's on the right. The expressions become much simpler however in the case of axial symmetry, $\mathcal{I}_1' = \mathcal{I}_2' \equiv \mathcal{I}' \neq \mathcal{I}_3'$, for which direct calculation shows that

$$T_R = \frac{1}{2}\left\{\frac{1}{\mathcal{I}'}\left[\frac{1}{\sin^2\Theta}\left(L_\Phi - \cos\Theta L_\Psi\right)^2 + L_\Theta^2 - i\hbar\frac{\cos\Theta}{\sin\Theta}L_\Theta\right] + \frac{1}{\mathcal{I}_3'}L_\Psi^2\right\} \tag{I-65}$$

if

$$L_{\Theta} \equiv -i\hbar \frac{\partial}{\partial\Theta}, \quad L_{\Theta}^{2} = -\hbar^2 \frac{\partial^2}{\partial\Theta^2} , \tag{I-66}$$

or

$$T_R = \frac{1}{2} \left\{ \frac{1}{\mathcal{I}'} \left[\frac{1}{\sin^2\Theta} (L_{\Phi} - \cos\Theta\, L_{\Psi})^2 + L_{\Theta}'^{2} \right] + \frac{1}{\mathcal{I}_3'} L_{\Psi}^{2} \right\}, \tag{I-67}$$

identical to the classical form, if

$$L_{\Theta} \equiv -i\hbar \frac{\partial}{\partial\Theta}, \quad L_{\Theta}^{2} = -\hbar^2 \frac{1}{\sin\Theta} \frac{\partial}{\partial\Theta} (\sin\Theta \frac{\partial}{\partial\Theta}) \tag{I-68}$$

$$= -\hbar^2 \left(\frac{\partial^2}{\partial\Theta^2} + \cot\Theta \frac{\partial}{\partial\Theta} \right).$$

T_R may be expressed in terms of angular momentum components about the body axes, written in terms of the Euler angles, as follows: from the transformation properties of vectors or pseudovectors under proper rotations $\mathcal{R}(\Phi\Theta\Psi)$: $(x,y,z) \rightarrow (1,2,3)$ (space frame $\rightarrow$ body frame), which are assumed to be the same as for the coordinates,

$$\begin{pmatrix} 1 \\ 2 \\ 3 \end{pmatrix} = \mathcal{R}(\Phi\Theta\Psi) \begin{pmatrix} x \\ y \\ z \end{pmatrix} \tag{I-69}$$

one can set analogously to (I-14,15,16),

$$\begin{pmatrix} L_1 \\ L_2 \\ L_3 \end{pmatrix} = \mathcal{R}_3(\Psi) \begin{pmatrix} L_{\xi'} \\ L_{\eta'} \\ L_{\zeta'} \end{pmatrix} ; \quad \begin{pmatrix} L_{\xi'} \\ L_{\eta'} \\ L_{\zeta'} \end{pmatrix} = \mathcal{R}_2(\Theta) \begin{pmatrix} L_{\xi} \\ L_{\eta} \\ L_{\zeta} \end{pmatrix} ; \tag{I-70}$$

$$\begin{pmatrix} L_{\xi} \\ L_{\eta} \\ L_{\zeta} \end{pmatrix} = \mathcal{R}_1(\Phi) \begin{pmatrix} L_x \\ L_y \\ L_z \end{pmatrix}$$

Noting that the canonical momenta

$$L_{\Phi} = -i\hbar \frac{\partial}{\partial \Phi} \equiv L_{z=\zeta}(\Phi \Theta \Psi) = \begin{pmatrix} 0 \\ 0 \\ L_z \end{pmatrix} \tag{I-71}$$

$$L_{\Theta} = -i\hbar \frac{\partial}{\partial \Theta} \equiv L_{\eta=\eta'}(\Phi \Theta \Psi) = \begin{pmatrix} 0 \\ L_\eta \\ 0 \end{pmatrix}$$

$$L_{\Psi} = -i\hbar \frac{\partial}{\partial \Psi} \equiv L_{3=\zeta'}(\Phi \Theta \Psi) = \begin{pmatrix} 0 \\ 0 \\ L_3 \end{pmatrix}$$

are the angular momentum components about the specified axes, and hence pseudovectors, one may express L_{Φ}, L_{Θ}, L_{Ψ} in terms of L_x, L_y, L_z or of L_1, L_2, L_3, which can in turm be solved for $L_{x,y,z,1,2,3}$ in terms of L_{Φ}, L_{Θ}, L_{Ψ}. Arguments[4] based on compounding of rotations through infinitesmal angles give the same results. The results are:

$$L_x(\Phi\Theta\Psi) = -i\hbar\left(-\frac{\cos\Phi\cos\Theta}{\sin\Theta}\frac{\partial}{\partial\Phi} - \sin\Phi\frac{\partial}{\partial\Theta} + \frac{\cos\Phi}{\sin\Theta}\frac{\partial}{\partial\Psi}\right) \tag{I-72}$$

$$L_y(\Phi\Theta\Psi) = -i\hbar\left(-\frac{\sin\Phi\cos\Theta}{\sin\Theta}\frac{\partial}{\partial\Phi} + \cos\Phi\frac{\partial}{\partial\Theta} + \frac{\sin\Phi}{\sin\Theta}\frac{\partial}{\partial\Psi}\right)$$

$$L_z(\Phi\Theta\Psi) = -i\hbar\frac{\partial}{\partial\Phi}$$

$$L_{\pm}(\Phi\Theta\Psi) = -i\hbar e^{\pm i\Phi}\left[-\frac{1}{\sin\Theta}\left(\cos\Theta\frac{\partial}{\partial\Phi} - \frac{\partial}{\partial\Psi}\right) \pm i\frac{\partial}{\partial\Theta}\right]$$

$$L_1(\Phi\Theta\Psi) = -\,L_x(-\Psi\,-\Theta\,-\Phi) \tag{I-73}$$

$$L_2(\Phi\Theta\Psi) = -\,L_y(-\Psi\,-\Theta\,-\Phi)$$

$$L_3(\Phi\Theta\Psi) = -\,L_z(-\Psi\,-\Theta\,-\Phi) = -\,i\hbar\frac{\partial}{\partial\Psi}$$

$$L_{\pm'}(\Phi\Theta\Psi) = -\,L_{\pm}(-\Psi\,-\Theta\,-\Phi)$$

$$L_x^2(\Phi\Theta\Psi)+L_y^2(\Phi\Theta\Psi)+L_z^2(\Phi\Theta\Psi) = L_1^2(\Phi\Theta\Psi)+L_2^2(\Phi\Theta\Psi)+L_3^2(\Phi\Theta\Psi) \quad \text{(I-74)}$$

$$\equiv L^2(\Phi\Theta\Psi) = -\hbar^2\left[\frac{\partial^2}{\partial\Theta^2}+\frac{\cos\Theta}{\sin\Theta}\frac{\partial}{\partial\Theta}+\frac{1}{\sin^2\Theta}\left(\frac{\partial^2}{\partial\Phi^2}+\frac{\partial^2}{\partial\Psi^2}\right)-\frac{2\cos\Theta}{\sin^2\Theta}\frac{\partial^2}{\partial\Phi\partial\Psi}\right]$$

Here $L_\pm = L_x \pm iL_y$, $L_{\pm'} = L_1 \pm iL_2$. From these expressions it can be shown that

$$\left[L_x(\Phi\Theta\Psi),\ L_y(\Phi\Theta\Psi)\right] = +\,i\hbar L_z(\Phi\Theta\Psi) \text{ et cycl.,} \quad \text{(I-75)}$$

but that

$$\left[L_1(\Phi\Theta\Psi),\ L_2(\Phi\Theta\Psi)\right] = -\,i\hbar L_3(\Phi\Theta\Psi) \text{ et cycl.} \quad \text{(I-76)}$$

In terms of these quantities, T_R becomes

$$T_R = \tfrac{1}{2}\left[\frac{1}{\mathcal{I}'} L^2(\Phi\Theta\Psi) + \left(\frac{1}{\mathcal{I}'_3} - \frac{1}{\mathcal{I}'}\right) L_3^2(\Phi\Theta\Psi)\right] \quad \text{(I-77)}$$

The D-functions defined above are eigenfunctions of $L_3(\Phi\Theta\Psi)$, $L_z(\Phi\Theta\Psi)$, $L^2(\Phi\Theta\Psi)$, and hence of T_R. This is easy to prove for L_z and L_3. In the representation in which L_z is diagonal it was noted that

$$D^j_{m'm}(\Phi\Theta\Psi) = e^{-i(m'\Phi+m\Psi)}\, d^j_{m'm}(\Theta) \quad \text{(I-78)}$$

with the immediate consequences,

$$L_z(\Phi\Theta\Psi)D^{I*}_{MK}(\Phi\Theta\Psi) = -i\hbar\frac{\partial}{\partial\Phi}D^{I*}_{MK}(\Phi\Theta\Psi) = \hbar M D^{I*}_{MK}(\Phi\Theta\Psi) \quad \text{(I-79)}$$

$$L_3(\Phi\Theta\Psi)D^{I*}_{MK}(\Phi\Theta\Psi) = i\hbar\frac{\partial}{\partial\Psi}D^{I*}_{MK}(\Phi\Theta\Psi) = \hbar K D^{I*}_{MK}(\Phi\Theta\Psi)\,. \quad \text{(I-80)}$$

The following relations can be derived from the commutation relations:[4,7]

$$L^2(\Phi\Theta\Psi)D^{I*}_{MK}(\Phi\Theta\Psi) = \hbar^2 I(I+1)D^{I*}_{MK}(\Phi\Theta\Psi) \quad \text{(I-81)}$$

$$L_{\pm}(\Phi\Theta\Psi)D_{MK}^{I*}(\Phi\Theta\Psi) = \hbar C_{\pm}\sqrt{(I\mp M)(I\pm M+1)}\; D_{M\pm1\,K}^{I*}(\Phi\Theta\Psi) \tag{I-82}$$

$$L_{\pm'}(\Phi\Theta\Psi)D_{MK}^{I*}(\Phi\Theta\Psi) = \hbar C'_{\pm}\sqrt{(I\pm K)(I\mp K+1)}\; D_{M\,K\mp1}^{I*}(\Phi\Theta\Psi) \tag{I-83}$$

where $C_{\pm}$, $C'_{\pm}$ are phase factors, $|C_{\pm}| = |C'_{\pm}| = 1$, of which mention will be made below. Then also,

$$T_R D_{MK}^{I*}(\Phi\Theta\Psi) = \frac{\hbar^2}{2}\left(\frac{I(I+1)-K^2}{\mathcal{I}'} + \frac{K^2}{\mathcal{I}'_3}\right) D_{MK}^{I*}(\Phi\Theta\Psi) \quad . \tag{I-84}$$

3. General Classical Rotor

Suppose there is a body of unspecified content which moves essentially in the manner of a fluid (possibly a rigid or elastic solid), that can have its content and motion specified by a mass density $\rho_M(\vec{r},t)$ and a velocity field $\vec{v}(\vec{r},t)$. In the center of mass frame the net linear momentum

$$\vec{p} = \int \rho_M(\vec{r},t)\vec{v}(\vec{r},t)\; d\vec{r} = \vec{0} \;, \tag{I-85}$$

where the integration is carried out throughout all space for which $\rho_M(\vec{r},t) > 0$, that is, throughout the body. For convenience the origin may be taken at the mass centroid, which in the absence of external forces acting on the body's material will be unaccelerated.

Now a number of convenient definitions will be introduced. With the origin at the mass centroid, for convenience, define an instantaneous local angular velocity field vector $\vec{\omega}(\vec{r},t)$:

$$\vec{v}(\vec{r},t) = \vec{\omega}(\vec{r},t) \times \vec{r} \tag{I-86}$$

and analogously

$$\mathscr{p}(\vec{r},t) = \rho_M(\vec{r},t)\vec{v}(\vec{r},t) \tag{I-87}$$

$$\vec{\ell}(\vec{r},t) = \vec{r}\times\vec{\mathscr{p}} = \rho_M(\vec{r},t)\vec{r}\times\vec{v}(\vec{r},t) \tag{I-88}$$

$$= \rho_M\vec{r}\times(\vec{\omega}\times\vec{r}) = \rho_M(\vec{r}\vec{r}\cdot\vec{\omega} - \vec{\omega}\vec{r}\cdot\vec{r})$$

$$= \rho_M(\vec{r},t)[\vec{r}\vec{r} - r^2\hat{\hat{\mathscr{I}}}]\cdot\vec{\omega}(\vec{r},t)$$

where $\hat{\hat{\mathscr{I}}} = \hat{i}\hat{i} + \hat{j}\hat{j} + \hat{k}\hat{k}$ is the unit dyadic. (In general, I mean by $\vec{v}$, a vector; $\vec{\vec{v}}$, a dyadic; $\hat{v}$, a unit vector, etc.) Define in conjunction with the local instantaneous angular momentum density a local instantaneous inertia moment density

$$\vec{\vec{\mathscr{I}}}(\vec{r},t) = \rho_M(\vec{r},t)(\vec{r}\vec{r} - \hat{\hat{\mathscr{I}}}r^2) \tag{I-89}$$

Then $\vec{\ell}(\vec{r},t) = \vec{\vec{\mathscr{I}}}(\vec{r},t)\cdot\vec{\omega}(\vec{r},t)$. Define a nonrelativistic kinetic energy density

$$t(\vec{r},t) \equiv \frac{1}{2}\rho_M(\vec{r},t)[\vec{v}(\vec{r},t)]^2 = \frac{1}{2}\vec{\omega}\cdot\vec{\vec{\mathscr{I}}}\cdot\vec{\omega} = \frac{1}{2}\vec{\omega}\cdot\vec{\ell} \quad . \tag{I-90}$$

Now, with the otherwise arbitrary body so localized and constituted as to make all the relevant integrals converge, the gross rotational parameters may be defined and separated from the residual or "intrinsic" velocity fields. Define an arbitrary net rotational component to the overall internal motion of the body:

$$\vec{v}_R(\vec{r},t) = \vec{\Omega}(t)\times\vec{r} \tag{I-91}$$

where $\vec{\Omega}$ is now independent of $\vec{r}$. Let $\vec{\omega}(\vec{r},t) = \Omega(t) + \vec{\omega}'(\vec{r},t)$ and $\vec{v}(\vec{r},t) = \vec{\omega}\times\vec{r} = (\vec{\Omega}+\vec{\omega}')\times\vec{r} = \vec{v}_R + \vec{\omega}'\times\vec{r} \equiv \vec{v}_R + \vec{v}'$. $\vec{v}'$ and $\vec{\omega}'$ are the residual velocity field and its associated residual local instantaneous angular velocity field. Then

$$\vec{\ell} = \rho_M\vec{r}\times(\vec{v}_R + \vec{v}') = \vec{\vec{\mathscr{I}}}\cdot\vec{\omega} = \vec{\vec{\mathscr{I}}}\cdot(\vec{\Omega}+\vec{\omega}') \ , \tag{I-92}$$

and the total angular momentum, possibly a function of time but independent of time in the absence of external torques, and the associated inertia dyadic may be defined:

$$\vec{L}(t) = \int \vec{\ell}(\vec{r},t)\,d\vec{r} = \int \overleftrightarrow{\mathcal{I}}\cdot\vec{\omega}\,d\vec{r} = \int \overleftrightarrow{\mathcal{I}}\,d\vec{r}\cdot\vec{\Omega} + \int \overleftrightarrow{\mathcal{I}}\cdot\vec{\omega}'\,d\vec{r} \tag{I-93}$$
$$\equiv \overleftrightarrow{I}(t)\cdot\vec{\Omega}(t) + \int \overleftrightarrow{\mathcal{I}}(\vec{r},t)\cdot\vec{\omega}'(\vec{r},t)\,d\vec{r} \quad .$$

At this point the net instantaneous rotational velocity vector of this arbitrary body may be defined by choosing

$$\vec{\Omega}(t) \equiv \vec{\Omega}_R(t), \tag{I-94}$$

so that

$$\int \overleftrightarrow{\mathcal{I}}(\vec{r},t)\cdot\vec{\omega}'(\vec{r},t) \equiv \vec{O} \quad . \tag{I-95}$$

Then

$$\vec{L} = \overleftrightarrow{I}(t)\cdot\vec{\Omega}_R(t) \;;\quad \overleftrightarrow{I}(t) \equiv \int \rho_M(\vec{r},t)(\vec{r}\vec{r} - \hat{\hat{\mathcal{I}}}r^2)\,d\vec{r}\,. \tag{I-96}$$

Even if L is constant in time, as for an isolated body, both $\overleftrightarrow{I}$ and $\vec{\Omega}_R$ still may be time-dependent.

The total kinetic energy is

$$T = \int t(\vec{r},t)\,d\vec{r} = \frac{1}{2}\int \rho_M(\vec{r},t)[\vec{v}(\vec{r},t)]^2 d\vec{r} = \frac{1}{2}\int \rho_M(\vec{\omega}\times\vec{r})^2 d\vec{r} \tag{I-97}$$
$$= \frac{1}{2}\int \rho_M\,\vec{\omega}\cdot[\vec{r}\times(\vec{\omega}\times\vec{r})]\,d\vec{r} = \frac{1}{2}\int \rho_M\,\vec{\omega}\cdot[(\vec{r}\vec{r} - \hat{\hat{\mathcal{I}}}r^2)\cdot\vec{\omega}]\,d\vec{r}$$
$$\equiv \frac{1}{2}\int \vec{\omega}\cdot\overleftrightarrow{\mathcal{I}}\cdot\vec{\omega}\,d\vec{r} = \frac{1}{2}\vec{\Omega}(t)\cdot\overleftrightarrow{I}(t)\cdot\vec{\Omega}(t)$$
$$+ \frac{1}{2}\int[\vec{\omega}'\cdot\overleftrightarrow{\mathcal{I}}\cdot\vec{\Omega} + \vec{\Omega}\cdot\overleftrightarrow{\mathcal{I}}\cdot\vec{\omega}']\,d\vec{r} + \frac{1}{2}\int \vec{\omega}'\cdot\overleftrightarrow{\mathcal{I}}\cdot\vec{\omega}'\,d\vec{r} \quad .$$

The second term is

$$\frac{1}{2}\left[\int \vec{\omega}'\cdot\overleftrightarrow{\mathcal{I}}\,d\vec{r}\cdot\vec{\Omega} + \vec{\Omega}\cdot\int \overleftrightarrow{\mathcal{I}}\cdot\vec{\omega}'\,d\vec{r}\right] \tag{I-98}$$

For the special choice $\vec{\Omega} = \vec{\Omega}_R$, for which $\int \overleftrightarrow{\mathcal{I}}\cdot\vec{\omega}'\,d\vec{r} \equiv \vec{O}$, and since $\overleftrightarrow{\mathcal{I}}$ is a symmetric dyadic, one finds that $\vec{\omega}'\cdot\overleftrightarrow{\mathcal{I}} \equiv \overleftrightarrow{\mathcal{I}}\cdot\vec{\omega}'$, or $\int \vec{\omega}'\cdot\overleftrightarrow{\mathcal{I}}\,d\vec{r} \equiv \vec{O}$. That is, with the rotational component to the motion that is related in the conventional way to the angular momentum, the cross terms in the kinetic energy expression vanish. Then,

$$T = T_R + T_i \;; \tag{I-99}$$
$$T_R = \frac{1}{2}\vec{\Omega}_R(t)\cdot\overleftrightarrow{I}(t)\cdot\vec{\Omega}_R(t) \tag{I-100}$$
$$T_i = \frac{1}{2}\int \vec{\omega}'(\vec{r},t)\cdot\overleftrightarrow{\mathcal{I}}(\vec{r},t)\cdot\vec{\omega}'(\vec{r},t)\,d\vec{r}$$

provide rotational and intrinsic components to the kinetic energy. All these quantities may be time-dependent; even in the absence of external forces, T may change, with an accompanying change in net potential energy of the body configuration so that $T(t)+V(t)$ remains constant. Even with T identically constant, T_R and T_i can undergo compensating changes, and even if T_R and T_i are constant in time, $\vec{\Omega}_R, \vec{\vec{I}}$ and $\vec{\omega}'$, $\vec{\vec{\mathcal{J}}}$ need not be.

The Euler angles Φ, Θ, Ψ connecting orthogonal reference frames with coincident origins at the mass centroid but different orientations are convenient for the discussion of kinematics and mechanics of any bodies which display approximately time-invariant surface configurations, apart from orientations, such as the rotational nuclei under discussion, and may be conveniently introduced at this point into T_R just as with the rigid body above. But now the kinetic energy is divided into rotational and residual parts, and the inertia moments and angular velocities are related to a quite general velocity field. In this way the concept of a rotation is generalized to a universal formal aspect of internal motion, from the usual conception which corresponds to time-independent inertia dyadic and net angular velocity.

A pure rotational band, however, is the signature of the presence of the more specialized uniform rotational motion: $\vec{\Omega}_R \equiv$ constant in time. In choosing $\vec{\Omega}_R^{(c)}$ constant in time for an arbitrary system for which $\vec{\Omega}_R$ as defined above is time-dependent, but using a Hamiltonian $H_o = H_R + H_i$ is tantamount to neglect of the now non-vanishing cross terms $\int \vec{\mathcal{J}} \cdot \vec{\omega}'^{(c)} d\vec{\pi}$ which provide those terms responsible for "rotational-particle" and rotation-vibration coupling, and also to taking $T_i^{(c)} = \frac{1}{2} \int \vec{\omega}'^{(c)} \cdot \overleftrightarrow{\mathcal{J}} \cdot \vec{\omega}'^{(c)} d\vec{\pi}$ with respect to $\vec{\omega}'^{(c)}$, not $\vec{\omega}'(t)$. The smallness of these mixing cross terms is the measure of the "extent" of a pure time-constant rotational component in the true motion.

D. Collective Models

1. History

Many features of nuclear data for heavy nuclei, in particular characteristic level energy and spin sequences, fast E2 transitions, and large static quadrupole moments, suggest the existence of modes of motion in which the entire nucleus contributes in a collective fashion. Bohr[6], and Bohr and Mottelson[8] introduced a phenomenological model for collective motion in which they represented the nucleus as an incompressible charged fluid body whose boundary is given by

$$R = R_0\left[1 + \sum_{\lambda=2}^{\infty} \sum_{\mu=-\lambda}^{\infty} \alpha_{\lambda\mu} Y_\lambda^\mu(\theta,\phi)\right] \tag{I-101}$$

and for which the flow pattern is irrotational:

$$\nabla \times \vec{v} \equiv \vec{0} \quad , \quad \vec{v}(\vec{r}) = -\nabla\phi(\vec{r}) \quad . \tag{I-102}$$

With small values of the deformation parameters $\alpha_{\lambda\mu}$ which allow the simple-harmonic approximation to the potential energy function, the Hamiltonian was constructed as follows:

$$\begin{aligned} T &= \frac{1}{2}\sum_\lambda \sum_\mu B_\lambda |\dot{\alpha}_{\lambda\mu}|^2 = \frac{1}{2}\sum_\lambda \sum_\mu \frac{1}{B_\lambda}|\pi_{\lambda\mu}|^2 \\ V &\approx \frac{1}{2}\sum_\lambda \sum_\mu C_\lambda |\alpha_{\lambda\mu}|^2 \\ \pi_{\lambda\mu} &\equiv \frac{\partial T}{\partial \dot{\alpha}_{\lambda\mu}} = B_\lambda \dot{\alpha}_{\lambda\mu}^* \\ H_c &= T + V = \sum_\lambda \sum_\mu \left(\frac{1}{2B_\lambda}|\pi_{\lambda\mu}|^2 + \frac{C_\lambda}{2}|\alpha_{\lambda\mu}|^2\right) \end{aligned} \tag{I-103}$$

The motion consists of simple-harmonic oscillations, or phonons in the quantized version, with energy $\hbar\omega_\lambda = \hbar\sqrt{\frac{C_\lambda}{B_\lambda}}$, where C_λ is related to the Coulomb repulsion and the surface tension, B_λ to the effective moments of inertia. The terms with $\lambda = 0$ and $\lambda = 1$, corresponding to radial compressional oscillations and (to first order) translations, respectively, are excluded from the low-energy phenomena of interest, so that the lowest-order non-vanishing terms are associated with the quadrupole surface deformations, $\lambda = 2$.

The empirical data suggested definite regions of the periodic table, $A \sim 25$, $150 \lesssim A \lesssim 190$ and $A \gtrsim 225$, not too near the "magic-number" nuclei, where the nuclei displayed well-developed rotatianal structures characteristic of appreciably nonspherical equilibrium shapes. For an irrotational flow the moment of inertia about an axis of symmetry is small, or may vanish altogether, and to the extent that the real nuclear flow pattern approximates irrotational flow, the energies of states corresponding to rotation about a symmetry axis will tend to be large. The well-developed low-lying rotational bands then imply the large static deformations. In this case it was found convenient to choose a body-fixed principal-axis frame and to redefine the surface parameters (considering only $\lambda = 2$ terms):

$$\begin{aligned} a_{2\nu} &= \sum_{\mu=-2}^{2} \alpha_{2\mu}\, D^{2}_{\mu\nu}(\Phi,\Theta,\Psi) \\ \alpha_{2\mu} &= \sum_{\nu=-2}^{2} a_{2\nu}\, D^{2*}_{\mu\nu}(\Phi,\Theta,\Psi) \\ a_{20} &= \beta\cos\gamma \\ a_{2\pm2} &= \frac{1}{\sqrt{2}}\beta\sin\gamma \end{aligned} \qquad \text{(I-104)}$$

Then the expression

$$R = R_0\left[1+\sum_{\mu} a_{2\mu} Y_2^{\mu}(\theta', \varphi')\right] \qquad \text{(I-105)}$$

describes the nuclear surface in the body frame, and θ', φ' are the new spherical coordinates, as shown in Fig. I.1. For convenience the new constants $a_{\lambda\mu}$ are replaced by certain

The Rare Earth Rotational Region

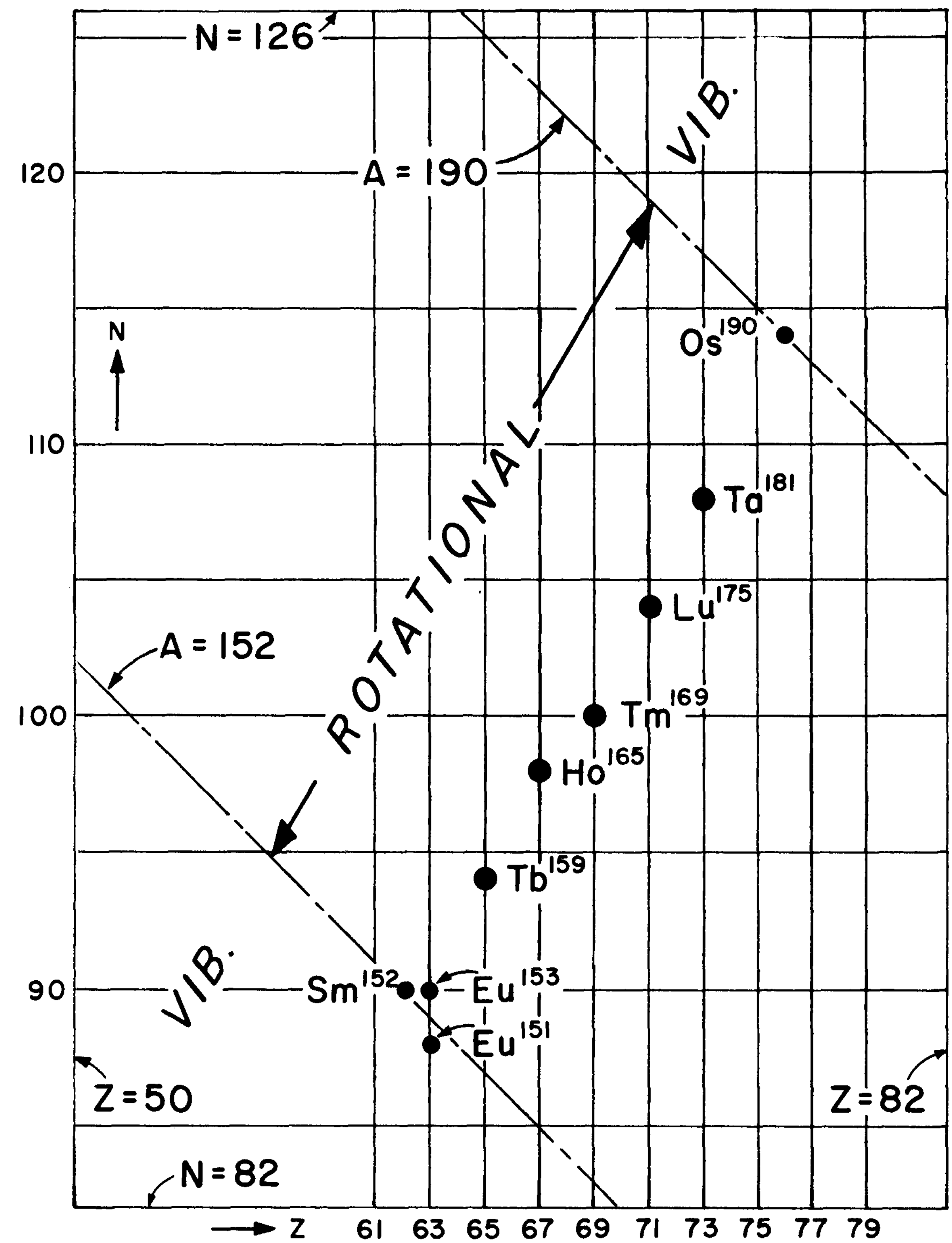

FIG I-2

functions of them, which for $\lambda = 2$ are the five independent parameters $\Phi, \Theta, \Psi, \beta, \gamma$, the three Euler angles specifying the orientation and the other two the shape of the most general quadrupole surface deformation. To first order in the deformation parameters this surface is an ellipsoid with, in general, three mutually unequal semiaxes. For the general λ-surface such shape and orientation parameters are denoted by $\beta_{\lambda\mu}$. Possible motions associated with the quadrupole surface are the rotations, and shape oscillations involving changes in the parameters β and γ known as beta- and gamma-vibrations. With the assumptions of rigidity against gamma-vibrations, the small-amplitude simple-harmonic approximation of the potential energy function for beta-vibrations, and irrotational incompressible flow, it was found that the Hamiltonian separated into several parts:

$$V = \tfrac{1}{2} C_2 \beta^2$$
$$T = \tfrac{1}{2} B_2 (\dot{\beta}^2 + \beta^2 \dot{\gamma}^2) + \tfrac{1}{2} \sum_i q_i^2 \mathcal{I}_i' = T_V + T_R \; . \qquad \text{(I-106)}$$

Here,

$$\mathcal{I}_i' = 4 B_2 \beta^2 \sin^2\left(\gamma - \frac{2\pi i}{3}\right) = \mathcal{I}_{i_{RIG}}' \frac{\varepsilon_i^2}{4} \qquad \text{(I-107)}$$

are the irrotational principal inertia moments,

$$\varepsilon_3 = 1 - \left(\frac{R_2}{R_1}\right)^2 \qquad \text{et. cycl.} \qquad \text{(I-108)}$$

are the eccentricities of the (approximately) elliptical sections perpendicular to the 3-, 1-, and 2-axes respectively, and

$$q_i = \frac{\hbar L_i}{\mathcal{I}_i'} \qquad \text{(I-109)}$$

are the operators for the body-frame components of angular momentum in terms of the Euler angles. The Hamiltonian operator in β-γ-Φ-Θ-Ψ- space became

$$H_c = \frac{\hbar^2}{2B_2}\left\{\frac{1}{\beta^4}\frac{\partial}{\partial\beta}\left(\beta^4\frac{\partial}{\partial\beta}\right)+\frac{1}{\beta^2}\left[\frac{1}{\sin 3\gamma}\frac{\partial}{\partial\gamma}\left(\sin 3\gamma\frac{\partial}{\partial\gamma}\right)\right]\right\}+\frac{1}{2}\sum_i\frac{\hbar^2 L_i^2(\Phi\Theta\Psi)}{\mathcal{J}_i'}+\frac{1}{2}C_2\beta^2 \quad \text{(I-110)}$$

The Schrödinger equation was separated into equations in terms of the coordinates β, γ, and the rotational coordinates Φ, Θ, Ψ. The total wave function was written in the form

$$\Psi(\beta,\gamma;\Phi\Theta\Psi)=f(\beta)\,\Phi(\gamma;\Phi\Theta\Psi),$$
$$\Phi_{IM}^{\tau}(\gamma;\Phi\Theta\Psi)=\sum_{K=-I}^{I} g_{IK}^{\tau}(\gamma)\,\mathcal{D}_{MK}^{I}(\Phi\Theta\Psi) \quad \text{(I-111)}$$

A suitable choice of phase for the $\mathcal{D}$-functions is discussed below. It was noted that for the case of axial symmetry, $\gamma = 0$ or π, only one K would contribute to an energy eigenfunction, and that the $\mathcal{D}$-functions satisfied (I-79,80,81).

With restriction to right-handed coordinate axes, it was noted that there are 24 different sets of $\beta_{2\mu}$ corresponding to a given set of $\alpha_{2\mu}$, all mutually related through repeated applications of three basic transformations: reversal of the "2" and "3" axes, rotation of 90° about the "3" axis plus reversal of the sign of γ, and cyclic permutation of axes plus subtraction of $2\pi/3$ from γ. Single-valuedness of the wave function in $\alpha_{2\mu}$ required invariance of $\Psi(\beta_{2\mu})$ under these transformations, which when taken together with the symmetry properties of the $\mathcal{D}_{MK}^{I}$-functions implied certain restrictions on the "partial" functions $f(\beta)$ and $g(\gamma)$; e.g., that $g(\gamma)$ be some function of $\cos 3\gamma$ with the range of γ restricted to $0 \leq \gamma \leq \pi/3$.

For odd-A nuclei the unpaired nucleon was treated as an entity separate from the even-even core:

$$H = H_c + H_p + H_i \quad \text{(I-112)}$$

where to the collective core Hamiltonian are added two terms. $H_p = T_p + V_p$ is a shell model Hamiltonian with a spherical well potential with $\vec{\ell}\cdot\vec{s}$ term, but in later work of Nilsson[9], Gottfried[10], Lemmer[11], Davidson and Chi[12], and others it is taken as various deformed wells with harmonic oscillator or more realistic radial shapes, $\vec{\ell}\cdot\vec{s}$ and ℓ^2 terms, or even non-local potentials, and these were taken to depend on the intrinsic particle coordinates $\vec{r}'$ and, parametrically, on the shape parameters β, γ. H_1 denoted an explicit coupling term taken of form

$$H_1 = -k(r)\sum_{\mu} \alpha_{2\mu} Y_2^{\mu}(\theta,\phi) \qquad \text{(I-113)}$$

to first order in $\alpha_{2\mu}$, which arises from expansion of $V_p(\vec{r}, \alpha_{2\mu})$ about $\alpha_{2\mu} = 0$.

In the regions of nearly spherical nuclei, between the magic number nuclei and the rotational regions (Fig. I-2), the odd nucleon was considered as coupled weakly to the surface configuration and strongly to any specified space quantization axis, so that

$$H = H_c(\alpha_{2\mu}) + H_p(\vec{r}) + H_1(\vec{r}, \alpha_{2\mu}) \qquad \text{(I-114)}$$

and the only collective-intrinsic coupling was contained in H_1, which was treated as a perturbation. In the deformed regions, the particle was considered to be strongly coupled to body-fixed axes. H_1 was put in the form $H_1(\vec{r}', \beta_{2\mu})$, and a deformed potential well was used. In the "adiabatic limit" such a well will rotate slowly compared to the particle motion, and non-adiabatic effects such as centrifugal stretching of the nuclear core, which determines the well shape, and the Coriolis force can be treated as perturbations. The total angular momentum was divided into collective and intrinsic odd-particle angular momenta:

$$\vec{I} = \vec{R} + \vec{j} \tag{I-115}$$

$$\vec{I} = \vec{I}(\Phi\Theta\Psi); \quad \vec{I}\times\vec{I} = -i\vec{I} \tag{I-116}$$

$$\vec{j} = \vec{\ell} + \vec{s} = -i\vec{\pi}' \times \nabla' + \tfrac{1}{2}\sigma'; \quad \vec{j}\times\vec{j} = +i\vec{j} \tag{I-117}$$

$$T_R = \frac{1}{2}\sum_i \frac{\hbar^2 R_i^2}{\mathcal{I}_i'} \tag{I-118}$$

In the representation in which the angular momentum components on the "3" axis, I_3 and j_3, are diagonal and have expectation values K and Ω respectively, for irrotational flow the problem separated into equations in $\beta-\gamma$; Φ, Θ, Ψ ; and intrinsic (body-frame) odd-particle coordinates $\vec{\pi}'$, with the total wave function becoming:

$$\Psi_{IM}^{\tau} = \sum_K \sum_\Omega \Phi_{IK\Omega}^{\tau}(\beta,\gamma)\chi_\Omega(\vec{\pi}')\mathcal{D}_{MK}^{I}(\Phi\Theta\Psi) \ . \tag{I-119}$$

Symmetry conditions for this case required a function of the form

$$\Psi_{IM}^{\tau s} = \sum_{\Omega\geq 0}\sum_{K=-I}^{I}\Phi_{jK\Omega}^{\tau}(\beta,\gamma)\Big[\chi_\Omega(\vec{\pi}';\beta\gamma;\Phi\Theta\Psi)\mathcal{D}_{MK}^{I}(\Phi\Theta\Psi) + (-1)^{I-j}\chi_{-\Omega}(\vec{\pi}';\beta\gamma;\Phi\Theta\Psi)\mathcal{D}_{M-K}^{I}(\Phi\Theta\Psi)\Big] \tag{I-120}$$

for which $K-\Omega = 0, \pm 2, \pm 4, \ldots$ only. In the adiabatic limit of slow rotation, $\chi_\Omega(\vec{\pi}')$ will be undisturbed and β and γ will remain constant. Nonadiabatic effects, centrifugal stretching which changes the inertial moments with increasing $\vec{R}$ as well as the values of β and γ, and the Coriolis interaction or "rotational-particle coupling", can be treated as perturbations. They have effects both on a single pure rotational band because of the wave function symmetrization, and in the case of several rotational bands based on intrinsic or vibrational states, arising from band mixing. In the case of axial symmetry where only one K-term contributes, the Hamiltonian was found to be:

$$H = H_o + U \tag{I-121}$$

where

$$H_o = T_v + V + H_p + H_i + T_R{}^o \tag{I-122}$$

$$T_R{}^o = \frac{\hbar^2}{4}\left(\frac{1}{\mathcal{I}_1'} + \frac{1}{\mathcal{I}_2'}\right)\left(I^2 - I_3^2 + j^2 - j_3^2\right) + \frac{\hbar^2}{2\mathcal{I}_3'}\left(I_3 - j_3\right)^2 \; ; \tag{I-123}$$

$$U = U_1 + U_2 + U_3 \quad ;$$

$$U_1 = -\frac{\hbar^2}{\mathcal{I}_1'} I_1 j_1 - \frac{\hbar^2}{\mathcal{I}_2'} I_2 j_2 \qquad \text{(Coriolis interaction);} \tag{I-124}$$

$$\left.\begin{aligned} U_2 &\approx \left[\frac{\hbar^2}{4}\left(\frac{1}{\mathcal{I}_1'} - \frac{1}{\mathcal{I}_2'}\right) + \frac{\sqrt{3}}{2} k C_j \beta \sin\gamma\right]\left(j_1^2 - j_2^2\right) \\ U_3 &= \frac{\hbar^2}{4}\left(\frac{1}{\mathcal{I}_1'} - \frac{1}{\mathcal{I}_2'}\right)\left(I_1^2 - I_2^2\right) \end{aligned}\right\} \text{(Effects of nonaxiality);}$$

$$H_i = \tfrac{1}{2} k C_j \beta \cos\gamma \left(3 j_3^2 - j^2\right) \tag{I-125}$$

The approximations for U_2 and H_i are valid provided one spherical-well wave function predominates in $\chi_\Omega = \sum_j C_j \chi_{j\Omega}$. H_i is an explicit collective-intrinsic coupling term appropriate for small β, $V \approx \frac{1}{2} C_2 \beta^2$ is a deformation energy, T_v is the vibrational kinetic energy operator, and H_p is the odd-nucleon Hamiltonian. In the adiabatic limit $H \approx H_o$, whose eigenfunctions, the zero-order pure rotational band functions, were given by

$$H_0 \Phi_{IMK\Omega}^{\tau s} = E_{\beta\gamma}^{\circ} \Phi_{IMK\Omega}^{\tau s} \qquad (\text{"s" for symmetrization}), \qquad (I\text{-}126)$$

$$\Phi_{IMK\Omega}^{\tau s} = \phi_{IK\Omega}^{\tau}(\beta,\gamma)\left[\chi_{\Omega}\, \mathcal{D}_{MK}^{I} + (-1)^{I-j}\chi_{-\Omega}\, \mathcal{D}_{M-K}^{I}\right] \qquad (I\text{-}127)$$

$$H_0 = T_v + W(\beta,\gamma) \qquad (I\text{-}128)$$

where W is independent of $\frac{\partial}{\partial\beta}$ and $\frac{\partial}{\partial\gamma}$, which is equivalent to neglect of the vibrational kinetic energy in H_0. Upon substituting $V = \frac{1}{2}C_2\beta^2$ and $\mathcal{I}_i' = 4B_2\beta^2\sin^2(\gamma - \frac{2\pi i}{3})$ from the irrotational flow model into the terms of W, it was noted that a crude estimate of equilibrium deformation β_0, γ_0 could be calcuted as those values of β and γ for which $\langle\Phi|W-H_p|\Phi\rangle$ is a minimum. It was found that, where one j predominates in χ_Ω, $\gamma_0 = 0$ if $3\Omega^2 < j(j+1)$ (axially symmetric prolate spheroid), or $\gamma_0 = \pi$ if $3\Omega^2 > j(j+1)$ (axially symmetric oblate spheroid), and that if $\gamma = \gamma_0$ then β_0 is a root of the equation

$$C_2\beta - \frac{1}{2}kC_j\left|3\Omega^2 - j(j+1)\right| - \frac{\hbar^2}{3B_2\beta^3}\left[I(I+1) + j(j+1) - 2\Omega^2\right] = 0 \quad (I\text{-}129)$$

which has just one positive root. Then

$$W(\beta,\gamma) \approx W(\beta_0,\gamma_0) + \frac{1}{2}C_\beta(\beta-\beta_0)^2 + \frac{1}{2}C_\gamma(\gamma-\gamma_0)^2 \qquad (I\text{-}130)$$

where

$$C_\beta \approx C_\beta^\circ + \frac{\hbar^2}{B_2\beta_0^4}\left[I(I+1) + j(j+1) - 2\Omega^2\right]$$

$$C_\gamma \approx \frac{1}{2}kC_j\beta_0\left|3\Omega^2 - j(j+1)\right| + \frac{2\hbar^2}{3B_2\beta_0^2}\left[I(I+1) + j(j+1) - 2\Omega^2\right]. \qquad (I\text{-}131)$$

The latter terms in C_β and C_γ, small for large equilibrium deformations, are in the nature of vibration-rotation interactions. Neglecting these, the potential for vibrations, W, is approximately harmonic:

$$\phi(\beta,\gamma) \approx \phi_\beta(\beta)\,\phi_\gamma(\gamma) \;;$$

$$H_0\,\phi(\beta,\gamma) \approx \left[W(\beta_0,\gamma_0)+E_\beta+E_\gamma\right]\phi(\beta,\gamma) \qquad (\beta-\beta_0,\ \gamma-\gamma_0\ \text{small});$$

$$E_\beta = \frac{2\hbar^2}{B_2\beta_0^2}+\hbar\sqrt{\frac{C_\beta}{B_2}}\left(n_\beta+\tfrac{1}{2}\right), \qquad n_\beta = 0,1,2,\ldots; \tag{I-132}$$

$$E_\gamma=\hbar\sqrt{\frac{C_\gamma}{B_2\beta_0^2}}\,(n_\gamma+1), \quad n_\gamma=0,2,4,\ldots \text{ (no odd } n_\gamma \text{ because of symmetry)}$$

The matrix elements of U with respect to $\Phi^{TS}_{IMK\Omega}$ were expressed in terms of

$$\langle\Omega|\,j_{\pm}'\,|\Omega\pm1\rangle=\sqrt{(j\mp\Omega)(j\pm\Omega+1)}\quad\text{, others 0;}$$
$$\langle K\,|\,I_{\pm}'\,|\,K\pm1\rangle=\sqrt{(I\pm K)(I\mp K+1)}\quad\text{, others 0.} \tag{I-133}$$

It was found that U_1 connects the state $|K,\Omega\rangle$ with $|K\pm1,\Omega\pm1\rangle$ and $|K\mp1,\Omega\pm1\rangle$; U_2, $|K,\Omega\rangle$ with $|K,\Omega\pm2\rangle$; and U_3, $|K,\Omega\rangle$ with $|K\pm2,\Omega\rangle$. The effects of U were small in the strong-coupling limit of large β_0, and were treated as perturbations.

Kerman[14] considered the perturbations arising from small nonaxiality (U_2, U_3) and from the R.P.C. (rotation-particle coupling, or Coriolis interaction, U_1) term, along the following lines: the Hamiltonian was written in the form

$$H = H_p+T_R^0+t_R = H^0+t_R \tag{I-134}$$

where t_R is the R.P.C. term for the case of axial symmetry, written in a slightly different manner:

$$t_R = -\frac{\hbar^2}{2\mathcal{J}'}\left(I_+'j_-'+I_-'j_+'\right) \quad . \tag{I-135}$$

H_p is the deformed-well single-particle Hamiltonian above plus the term $\frac{\hbar^2}{2\mathcal{J}'}\,j^{\,2}$, and for which

$$\left\langle \psi^{s}_{IMK\Omega} \right| H^{\circ} \left| \psi^{s}_{IMK\Omega} \right\rangle = \mathcal{E}^{\circ}_{\Omega} + \frac{\hbar^2}{2\mathcal{I}_3'}(K-\Omega)^2 + \frac{\hbar^2}{2\mathcal{I}'}\left[I(I+1) - K^2 - \Omega^2\right] \equiv E^{\circ}_{IK\Omega} \quad . \tag{I-136}$$

For the case of an isolated band with $K = \Omega$, and including vibration-rotation interaction, he gave

$$E_{IK\Omega=K} \approx \mathcal{E}^{\circ}_{K} + \mathcal{E}^{(1)}_{K}\left[I(I+1) + \delta_{K\frac{1}{2}} a(-1)^{I+\frac{1}{2}}(I+\tfrac{1}{2})\right] - \mathcal{E}^{(2)}_{K}\left[I(I+1) + \delta_{K\frac{1}{2}} a(-1)^{I+\frac{1}{2}}(I+\tfrac{1}{2})\right]^2 . \tag{I-137}$$

For slight nonaxiality he listed the additional perturbations in the following forms:

$$H' = H_1' + H_2' + H_3' + V' \; (\vec{\pi}') ; \tag{I-138}$$

$$\begin{aligned} H_1' &= \frac{-\hbar^2}{4}\left(\frac{1}{\mathcal{I}_1'} - \frac{1}{\mathcal{I}_2'}\right)(I_{+'} j_{+'} + I_{-'} j_{-'}) \\ H_2' &= \frac{\hbar^2}{8}\left(\frac{1}{\mathcal{I}_1'} - \frac{1}{\mathcal{I}_2'}\right)(j_{+'} j_{+'} + j_{-'} j_{-'}) \\ H_3' &= \frac{\hbar^2}{8}\left(\frac{1}{\mathcal{I}_1'} - \frac{1}{\mathcal{I}_2'}\right)(I_{+'} I_{+'} + I_{-'} I_{-'}) \end{aligned} \tag{I-139}$$

$V'\;(\vec{\pi}')$ = axially asymmetric component of particle potential.

Of these potentials H_1' is related to $U_1 - t_R$, H_2' to the first term in U_2, and H_3' to U_3. He noted that these, in contrast to t_R, do not preserve $K-\Omega$ as a good quantum number. The zero-order (axially symmetric) energy expressions were taken with $\mathcal{I}'$ set equal to the harmonic mean of $\mathcal{I}_1'$ and $\mathcal{I}_2'$. In second-order perturbation theory H_3' produced a negative $I^2(I+1)^2$ term, H_1' and H_3' renormalized $\mathcal{I}'$, and H_2' and $V'(\vec{\pi}')$ renormalized $\mathcal{E}^{\circ}_{K}$. These assertions hold as a consequence of the formal structure of the Hamiltonian, irrespective of assumptions about the actual values of $\mathcal{I}_i'$. It was noted that centrifugal distortion, which changes $\mathcal{I}_i'$, will have the same general effects on $\mathcal{I}'$, ε_{Ω}^{0}, and will produce the same type of vibration-rotation interaction term as H'.

The possibility, besides K = 1/2 decoupling due to symmetry, of band mixing involving excited odd-A single-particle states resulting from the Coriolis interaction was considered. An exact diagonalization in the presence of two zero-order pure bands of the Coriolis term was carried out, and expressions for energy perturbations and admixed wave-function amplitudes in terms of the quantity $A_K \equiv \left| \langle \chi_K | \frac{\hbar^2}{2\mathcal{I}'} j_-' | \chi_{K+1} \rangle \right|$ were presented. The effects were a renormalization of $\mathcal{I}'$ and the introduction of an $[I(I+1)]^2$ term that under certain conditions (small inertia moment of the inter-acting band compared to the ground-state band) can be positive.

It was noted that an effect of R.P.C. in a more "self-consistent" type of calculation provided an explanation of the moment of inertia associated with the rotation, on a perturbation approach, as the effect of t_R, introduced to represent the presence of rotation, operating in the second order of perturbation theory over all the particles comprising the nuclear state with the non-rotating self-consistent deformed potential. The change in the total nuclear energy due to the impressed rotation, which is the sum of the perturbations on all the single-particle or shell-model energies, turns out to be of the form[15,16], (coefficient) $x\omega^2$, where ω is the assumed angular velocity of the body-frame (the "cranking" frequency), and the coefficient is interpreted as the corresponding inertia moment. It has been shown[17] that substitution into the "cranking formula" for the inertia moments of unmixed deformed shell-model states yields the rigid-body values. This is true for any system of fermions, interacting or not, so long as they are uncorrelated. Mixing due to Coriolis (or other) perturbations reduces the calculated effective inertia moments to values more nearly in line with experiment, and provides a qualitative cause for the observed lower $\mathcal{I}'$ values in odd-A nuclei than in adjacent even-even nuclei, where the admixed intrinsic states produce smaller energy denominators because of the even-even energy gap.

In this regard theoretical work appears to indicate that the use of two main types of residual interactions in the framework of independent-particle models, the Bardeen-Cooper-Schreiffer type pairing interactions (e.g., ref. 18,19,20) and the Elliott or quadrupole force[21] can reproduce most gross dynamical nuclear properties. The former is diagonal in the seniority angular momentum coupling scheme and can be defined by matrix elements which are non-zero only between the $|j,m\rangle, |j,-m\rangle$ pairs of shell-model states and appreciable only between pairs in the same major oscillator shell, and favors spherical equilibrium shapes, in fact allowing spherical shapes for some non-magic nuclei that would otherwise have small but definite calculated asphericities, in disagreement with experiment. The latter favors larger deformations and, acting in conjuction with the pairing force, produces the sudden onset of deformations at the correct values of A. These two residual interactions permit electromagnetic transition B-values, static electromagnetic moments, energy gaps in even-even nuclei, moments of inertia, etc. to be calculated in wide ranges of nuclei with some success. In particular, the pairing interaction gives calculated inertia moments in good agreement with experimental values[1], reproducing the rather wide fluctuations in values for odd-A nuclei rather well.

Alaga et al[22] gave intensity rules for gamma transitions between members of pure rotational bands, for the axially symmetric case, without R.P.C. mixing but including the first-order decoupling energy correction $\Delta E_{dec} = \frac{\hbar^2}{2\mathcal{I}'} a(-1)^{I+\frac{1}{2}}(I+\frac{1}{2})\,\delta_{K\frac{1}{2}}$ and the vibration-rotation interaction energy, which for the irrotational-flow model is

$$\Delta E_{VR} = -2\left[\frac{3}{(\hbar\omega_\beta)^2} + \frac{1}{(\hbar\omega_\gamma)^2}\right]\frac{\hbar}{\mathcal{I}'}\,E^{\circ\;2}_{IMK\Omega=K} \qquad (I\text{-}140)$$

as part of the "zero-order" energies. This topic is dealt with below. Kerman[14] also considered interband and intraband B-value modifications due to Coriolis mixing of bands. Bohr and Mottelson[23], in a paper presenting details of Alaga rule modifications, noted that (as of 1962) experimental accuracy of measured B-values was $\sim$ 5-10%, and had not produced evidence of deviations from the large collective leading terms in intraband E2 transition probabilities, for which estimated deviations due to mixing are $\lesssim$ 1%.

Because of the outstanding success of the shell model of the nucleus and because of the theoretical justifiability of the model in spite of the strong, short-range nature of the nucleon-nucleon interaction (essentially an effect of the Pauli principle, which acts to inhibit most free-nucleon scattering processes), the nucleon intrinsic states in the rotational region have been calculated on a deformed-well shell model by many authors. In the absence of complete self-consistent calculations for heavy finite nuclei, recourse had to be taken to assumed one-body potentials, adjusted to reproduce observed nuclear shell structure, ground state spins, and other pertinent properties, and to be consistent with requirements on the true self-consistent potential resulting from the observed characteristics of the nucleon-nucleon interaction. Of the different deformed shell models developed the most readily employed is the Nilsson[9,24] model, for which tables of eigenvalues and eigenfunctions have been published. This model uses a (rather unrealistic) simple-harmonic axially symmetric anisotropic local potential with $\vec{\ell}\cdot\vec{s}$ and ℓ^2 terms, the latter to represent the momentum-dependence required in the true self-consistent potential. The more sophisticated calculations (using more realistic one-body potentials) do not give substantially altered energy levels as functions of the deformation β, although they do give somewhat different spherical-shell model components in the eigenfunctions, which may, for example, account for some of the B(E1) values in odd-A nuclei that even Coriolis mixing of the Nilsson wave functions cannot reproduce[25]. An approximation to self-consistency was obtained by calculating the sum of single-particle energies for all the nucleons as a function of the deformation and using for equilibrium deformation that which minimized the sum of the single-particle energies. The calculated deformations agreed for the Nilsson model quite well with the values of the deformation obtained from measurements of spectroscopic quadrupole moments Q together with the relation of these and the intrinsic moments Q_0 (moments with respect to a principal-axis body frame) characteristic of the rotational model, and also gave correct ground-state spins, in the region $150 < A < 190$.

In the core-plus-single-nucleon picture the polarization of the even-even core by this nucleon was accounted for by minimizing the total energy of the odd number of nucleons to produce the equilibrium deformation and using this as the deformation of the even-even core and as the shape of the Nilsson potential for the odd-nucleon intrinsic state.

2. Theoretical justification

The core-plus-nucleon model is useful for classifying nuclear states, as abundant evidence shows[1,24], indicating that it is a fairly close representation of low-energy nuclear behavior. There have been three main approaches[26] to relating the model to more fundamental considerations.

In the first method[27,28,29,30] collective coordinates are introduced by a variational procedure. Letting $\psi(\vec{\pi}_i,\alpha)$ be a wave function for the n-body problem, for example a Hartree-Fock type of self-consistent function that depends parametrically on certain quantities α, the function

$$\phi(\vec{\pi}_i) = \int \psi(\vec{\pi}_i,\alpha)\,\chi(\alpha)\,d\alpha \qquad \text{(I-141)}$$

is formed, for which the variation equation

$$\delta\left[\langle\phi|H|\phi\rangle - \mathcal{E}\langle\phi|\phi\rangle\right] = 0 \tag{I-142}$$

yields a Schrödinger type equation in α, all of whose eigenstates have the same intrinsic structure, $\psi(\vec{\pi}_i, \alpha)$. The $\chi(\alpha)$ is chosen so that ϕ will be an eigenstate of total linear and angular momentum operators expressed in terms of α and $-i\hbar\frac{\partial}{\partial\alpha}$, a property not possessed by the straight Hartree-Fock solutions. In the case of linear momentum the Hartree-Fock solutions of H contain components from "ghost levels", various "excited states" of the center-of-mass motion,

$$\langle\psi_{H.F.}|H|\psi_{H.F.}\rangle = E_0 + \frac{\sum_{i=1}^{N} p_i^2}{2\sum_{i=1}^{N} m_i} \quad . \tag{I-143}$$

For any ξ, $\psi_{H.F.}(\vec{\pi}_i + \vec{\xi})$ is degenerate with $\psi_{H.F.}(\vec{\pi}_i)$.

Then a solution comprising a linear combination of these,

$$\phi(\vec{\pi}_i) = \int \psi_{H.F.}(\vec{\pi}_i + \vec{\xi})\,\chi(\vec{\xi})\,d\vec{\xi} \tag{I-144}$$

will usually remove the degeneracy; the choice

$$\chi(\vec{\xi}) = e^{-i\vec{P}\cdot\vec{\xi}} \tag{I-145}$$

causes ϕ to be an eigenstate of the total angular momentum; the lowest energy eigenvalue will correspond to P=0. The "ghost states" of center-of-mass motion are eliminated. The energies

$$E_P = \frac{\langle\phi|H|\phi\rangle}{\langle\phi|\phi\rangle} \tag{I-146}$$

can be shown for small values of

$$P = \langle\phi|\mathcal{P}|\phi\rangle \,, \qquad \mathcal{P} \equiv \sum_i \vec{P}_i \tag{I-147}$$

to be given by

$$E_P = \left[\langle\psi|H|\psi\rangle - \frac{\langle\psi|H\mathcal{P}^2|\psi\rangle - \langle\psi|H|\psi\rangle\langle\psi|\mathcal{P}^2|\psi\rangle}{2\langle\psi|\mathcal{P}^2|\psi\rangle}\right] \tag{I-148}$$

$$+\frac{1}{2}P^2\left[\frac{\langle\psi|H\mathcal{P}^2|\psi\rangle - \langle\psi|H|\psi\rangle\langle\psi|\mathcal{P}^2|\psi\rangle}{\langle\psi|\mathcal{P}^2|\psi\rangle^2}\right] + \ldots \approx \langle H\rangle + \frac{P^2}{2M}$$

where
$$\frac{1}{M} = \frac{\langle H P^2\rangle - \langle H\rangle\langle P^2\rangle}{\langle P^2\rangle^2} \tag{I-149}$$
takes the role of the mass parameter as calculated from the self-consistent solutions.

For angular momentum, one has
$$\phi_{IM}(\vec{r}) = \int \chi(\Theta_j)\,\psi_K[\vec{r}_i{}'(\vec{r}_i;\Theta_j)]\,d\Omega_{\Theta_j} \quad . \tag{I-150}$$
The choice
$$\chi(\Theta_j) = \mathcal{D}^{I}_{MK}(\Theta_j) \tag{I-151}$$
removes the angular momentum ghost states, splitting the self-consistent degeneracy with respect to orientation, and produces the set of non-rotating ground-state and rotational excited state eigenfunctions of the angular momentum operators I^2, I_z, I_3 expressed in terms of the Euler angles comprising a rotational band. For slow rotations expansion of $\frac{\langle\phi|H|\phi\rangle}{\langle\phi|\phi\rangle}$ in powers of
$$I(I+1) = \frac{\langle\phi|J^2|\phi\rangle}{\langle\phi|\phi\rangle} \quad , \quad \vec{J} = \sum_{i=1}^{N}\vec{J}_i \tag{I-152}$$
yields the result
$$E_I = E_{I=0} + \frac{I(I+1)}{2\mathcal{I}'} + \ldots . \tag{I-153}$$
in which, as calculated with the straight Hartree-Fock solutions in analogy to the mass parameter above, the reciprocal moment of inertia is
$$\frac{1}{\mathcal{I}'} = \frac{\langle H J^2\rangle - \langle H\rangle\langle J^2\rangle}{\langle J^2\rangle^2} \quad . \tag{I-154}$$
When such approximations to self-consistent solutions as are available for nuclear intrinsic states are substituted into this formula, the resulting values tend to be in qualitative agreement with experiment. It can also be shown that the quantities
$$Q \equiv \frac{\langle\phi_{I,M=I}|\mathcal{Z}_{20}|\phi_{II}\rangle}{\langle\phi_{II}|\phi_{II}\rangle} \quad , \quad Q_0 \propto \langle\psi_K|\mathcal{Z}'_{20}|\psi_K\rangle \tag{I-155}$$

are related by $Q = c(I,K)Q_0$, wherein $c(I,K)$ turns out to be the usual value

$$c(I,K) = \frac{3K^2 - I(I+1)}{(I+1)(2I+3)} \quad . \tag{I-156}$$

The second method[31] consists in noting that for any system of N particles, each of mass m, there exists a decomposition of the total kinetic energy $T = \sum_i \frac{P_i^2}{2m}$, resulting from a canonical transformation, into terms depending explicitly on the total angular momentum $\vec{I}$, on a certain non-conserved angular momentum $\vec{j}$, and on the total linear momentum $\vec{P}$:

$$T = \frac{P^2}{2M} + \frac{1}{2}\sum_\mu \sum_\nu Q_{\mu\nu}(\xi)(I_\mu - j_\mu)(I_\nu - j_\nu) + \frac{1}{2}\sum_\sigma \sum_\tau D_{\sigma\tau}(\xi)\pi_\sigma \pi_\tau \quad , \tag{I-157}$$

where $M = mN$, ξ_ρ, π_ρ are new canonically conjugate intrinsic generalized coordinates and momenta (3N-6 in number), $\vec{j}\,(\xi, \pi)$ plays the role of the intrinsic angular momentum $Q_{\mu\nu}(\xi)$ of the reciprocal inertia tensor, and where the last term is the intrinsic energy. The transformation equations may be written

$$\vec{r}_i = \vec{R} + \vec{\vec{\mathcal{R}}}(\Theta_j) \cdot \vec{r}_i{}' \tag{I-158}$$

$$\vec{r}_i{}' = \vec{r}_i{}'(\xi_\rho) \quad \text{or} \quad \xi_\rho = \xi_\rho(\vec{r}_i{}')$$

where $\vec{R}$ is the usual center-of-mass coordinate vector, $\vec{\vec{\mathcal{R}}}$ is the rotation dyadic, and not all the $\vec{r}_i{}'$ are independent but are subject to $\sum_i \vec{r}_i{}' = \vec{0}$ from the definition of the center-of-mass frame and three other conditions,

$$F_0(\vec{r}_i{}') \equiv 0 \tag{I-159}$$

which are related to the "$\vec{r}_i{}'$" or "body-frame" orientation relative to the system, specified by the Euler angles Θ_i. A superficial disadvantage of this approach is that the ξ_ρ are rather complicated combinations of the $\vec{r}_i{}'$, not readily physically interpretable in usual shell-model terms. The coupling term in T, containing both collective and intrinsic coordinates, which no non-inertial body frame can remove, have their roots in the associated Coriolis forces. The calculation of such parameters as inertia moments, electromagnetic B-values, etc. for the system requires detailed solutions for the intrinsic structure, which of course are not available for large n. Here, models of the intrinsic structure must be used.

A variation of this procedure is to transform only the N_c particles of an even-even core, leaving the N_e extra-core nucleons expressed in the space frame. This gives

$$T = \frac{P_c^2}{2mN_c} + H_i(\Pi_\rho, \xi_\rho) + \sum_e \left\{ \frac{P_e^2}{2m} + \sum_{i=1}^{N_e} V\left[\vec{r}_e - \vec{r}_i{}'(\xi)\right] + \sum_e \sum_s V_{es}(\vec{r}_e, \Theta_s) \right\} \qquad (\text{I-160})$$
$$+ \frac{1}{2} \sum_\mu \sum_\nu Q_{\mu\nu} \left[I_\mu - j_\mu - \sum_e j_{e\mu}\right]\left[I_\nu - j_\nu - \sum_e j_{e\nu}\right]$$

where $j_e = \ell_e + \frac{1}{2}\sigma_e$ refers to the extra-core nucleons, Θ_s are the Euler angles for the core-frame orientation, $\vec{j}$ is the core intrinsic angular momentum, and $\vec{I}$ is still the total system angular momentum. Typically $\vec{j}$ will be $\vec{0}$ for non-vibrating even-even cores. This method ameliorates the interpretation difficulties for the intrinsic state of the odd nucleon in odd-A core-plus-nucleon models, but still leaves the calculation of core properties a formidable problem. In (I.160) the extra-core particle energy terms are particle kinetic energy, a potential depending essentially on particle-core relative positions, and a "particle-rotational coupling" potential. The "zero-order" Coriolis coupling results from the presence of $\vec{j}_e$, residing with the odd nucleon(s), and nonadiabatic effects of rotation on the intrinsic state from the "rotational-particle coupling" potential.

It is possible to separate out multipole vibrational coordinates by this method, recovering Hamiltonians resembling the Hamiltonians of the vibrational model.

The third method is a variation on the second which seeks to circumvent the necessity of using ξ_ρ by introducing redundant variables, as follows: in transforming from $\vec{\pi}_i$ to $\vec{\pi}_i'$, α, the conditions of constraint $F_s(\vec{\pi}_i') \equiv 0$, $s = 1, \ldots, f$ are ignored and the values of F_s treated as dynamical variables, possessing canonically conjugate momenta G_s:

$$F_s, \vec{\pi}_i \rightarrow \alpha_j, \vec{\pi}_i' \; ; \quad G_s, \vec{p}_i \rightarrow \Pi_s, \vec{p}_i' \; ; \quad [F_s, G_t] = -i\hbar\delta_{st} \text{ etc.} \tag{I-161}$$

Then $H = H(F_s, \vec{\pi}_i, G_s, \vec{p}_i)$, which is actually independent of F_s, G_s, becomes $\tilde{H}(\vec{\pi}_i', \alpha_s, \vec{p}_i', \Pi_s)$, which commutes with F_s, G_s and has eigenfunctions $\tilde{\psi}(\vec{\pi}_i', \alpha_s)$. But if $\psi(\vec{\pi}_i)$ is an eigenfunction of H, then

$$\tilde{\psi}(\vec{\pi}_i', \alpha_s) \equiv U(F_s)\,\psi(\vec{\pi}_i) \quad , \tag{I-162}$$

where U is an arbitrary function of F_s, are degenerate. If it should turn out that

$$\tilde{H} = H_1(\Pi_s, \alpha_s) + H_2(\vec{p}_i', \vec{\pi}_i') + H_3(\alpha_s, \vec{\pi}_i') \quad , \tag{I-163}$$

with the coupling term, independent of Π_s, $\vec{p}_i'$, small, then zero-order wave functions, eigenfunctions of

$$H_0 \equiv H_1 + H_2 \tag{I-164}$$

can be written in the form

$$\tilde{\psi}_n^0(\alpha_s, \vec{\pi}_i') = \chi_n(\alpha_s)\,\phi_n(\vec{\pi}_i') \quad . \tag{I-165}$$

The development of this method is in a very nascent state.

The foregoing indicates that the kinds of terms occurring in sinple models for collective and intrinsic motions and coupling between them also arise from more fundamental theoretical considerations. Hence the experimental determination of the magnitude of these phenomenological terms is of paramount importance for quantitative understanding of nuclear structure.

The criterion of "validity" of the rotational model, whether the Euler angles are considered as dynamical variables that are linear combinations of the intrinsic particle coordinates or as parameters of transformation coefficients to a rotating frame chosen to minimize coupling terms in the Hamiltonian, is the success of the description of a component of the total nuclear motion as a rotation, as measured by the degree of separability of the Hamiltonian. Since the separation is never complete, except in such physically unattainable limiting cases as perfectly rigid solids or incompressible, nonviscous fluids, there is always some coupling between the assumed zero-order modes of motion, here the rotation, and the other modes of motion or "degrees of freedom", such as core vibrations, "intrinsic" motions, residual two-body interactions, or, ultimately, the entire rest of the motion of the real system not accounted for by any of the terms in the adopted provisionally-complete model Hamiltonian. The criterion is a relative concept, then, so that trying to describe a vibrational nucleus in terms of rotational-model variables may be logically valid procedure, but highly impracticable and uninformative. The use of "vibrational variables" would result in a much better approximate separation, and show that what is actually happening is almost a pure vibration.

In this spirit one can "subtract off" phenomenological concepts such as "rotation", "vibration", "single-particle excitation", study the properties of these modes and the magnitudes and effects of possible couplings between them, and see if all the observable effects can be accounted for, leaving the effects of the unknown, neglected residual terms in the true Hamiltonian below the level of current measurement capabilities.

E. On the Core-Plus-Nucleon Model

1. $\mathcal{I}_\nu'$ Constant

To display certain higher-order phenomena in rotational nuclei a simple axially-symmetric quadrupole core-plus-odd-nucleon model formalism will be set down. The Hamiltonian may be written

$$H = H_p + T_R \qquad \text{(I-166)}$$

where T_R is the collective core rotational kinetic energy,

$$T_R = \sum_{\nu=1}^{3} \frac{R_\nu^2}{2\mathcal{I}_\nu'} \qquad \text{(I-167)}$$

in terms of the core angular momentum $\vec{R}$, and H_p is the energy of the odd particle in the deformed core potential. For axial symmetry the inertia moments are

$$\mathcal{I}_1' = \mathcal{I}_2' \equiv \mathcal{I}' \neq \mathcal{I}_3' \qquad \text{(I-168)}$$

and the particle can be represented approximately by a Nilsson state. Setting

$$\vec{R} = \vec{I} - \vec{j} \qquad \text{(I-169)}$$

where $\vec{I}$ and $\vec{j}$ are the total and intrinsic angular momenta respectively, results in:

$$H = H_\rho + T_R^\circ + t_R \equiv H^\circ + t_R \qquad \text{(I-170)}$$

where

$$H_\rho = H_p + \frac{\hbar^2 j^2}{2\mathcal{I}'} \qquad \text{(I-171)}$$

and T_R° and t_R are given by

$$T_R^\circ = \frac{\hbar^2}{2\mathcal{I}'}\left[I^2 - I_3^2 - j_3^2\right] + \frac{\hbar^2}{2\mathcal{I}_3'}\left(I_3 - j_3\right)^2 \quad ; \qquad \text{(I-172)}$$

$$t_R = -\frac{\hbar^2}{2\mathcal{I}'}\left(I_{+1}j_{-1} + I_{-1}j_{+1}\right) . \tag{I-173}$$

t_R is the "rotational-particle coupling" or Coriolis term, which will be treated as a perturbation. In the absence of this term the zero-order unsymmetrized eigenfunctions of H° are

$$|IMK\Omega\rangle = \sqrt{\frac{2I+1}{8\pi^2}}\,|\chi_\Omega D^{I*}_{MK}\rangle \tag{I-174}$$

and satisfy the relations

$$I^2 D^{I*}_{MK} = \hbar^2 I(I+1) D^{I*}_{MK} \qquad I_z D^{I*}_{MK} = \hbar M D^{I*}_{MK}$$
$$I_3 D^{I*}_{MK} = \hbar K D^{I*}_{MK} \qquad j_3 \chi_\Omega = \hbar\Omega\chi_\Omega \tag{I-175}$$

and therefore,

$$H_p\chi_\Omega = \mathcal{E}^\circ_\Omega\chi_\Omega \;; \quad \mathcal{E}^\circ_{-\Omega} = \mathcal{E}^\circ_\Omega$$
$$T^\circ_R D^{I*}_{MK} = E^\circ_{IK\Omega} D^{I*}_{MK} \tag{I-176}$$
$$H^\circ|IMK\Omega\rangle = \left(E^\circ_{IK\Omega} + \mathcal{E}^\circ_\Omega\right)|IMK\Omega\rangle$$

where $\mathcal{E}^\circ_\Omega$ are single-particle energies, and

$$E^\circ_{IK\Omega} = \frac{\hbar^2}{2\mathcal{I}'}\left[I(I+1) - K^2 - \Omega^2\right] + \frac{\hbar^2}{2\mathcal{I}_3'}(K-\Omega)^2 \tag{I-177}$$

are the energies of pure rotational bands based on these states. The Ω and K-dependent parts can be subsumed in $\mathcal{E}^\circ$.

Because of the large values for the reciprocal inertia moment for rotation about a symmetry axis, the low-lying levels will have $K=\Omega$. Following Preston[32], the intrinsic state can be expressed as a sum over spherical-well states:

$$\chi_\Omega = \sum_\ell{}' \sum_\Lambda a_{\ell\Lambda\Omega}\chi_{\ell\Lambda\Omega} = \sum_j C_{j\Omega}\chi_{j\Omega} \; , \tag{I-178}$$

where the states $\chi_{\ell\Lambda\Omega}$ are diagonal in the ℓ^2, $\ell_3=\Lambda$, s^2, $s_3=\Sigma$ representation, $\chi_{j\Omega}$ in the ℓ^2, s^2, j^2, $j_3=\Omega$ representation, and the two are connected by

$$\chi_{j\Omega} = \sum_{\Lambda}{}' \sum_{\Sigma} \chi_{\ell\Lambda\Omega} \langle \ell\Lambda s\Sigma | \ell s j\Omega \rangle \quad , \tag{I-179}$$

from which it can be shown that

$$C_{j\Omega} = \sum_{\ell} \sum_{\Lambda}{}' \langle \ell\Lambda s\Sigma | \ell s j\Omega \rangle \, a_{\ell\Lambda\Omega} \quad . \tag{I-180}$$

The parities of the functions $\chi_{\ell\Lambda\Omega}$ are given by

$$\pi_{\chi} = (-1)^{\ell} \tag{I-181}$$

so that sums over ℓ are restricted to only even or odd ℓ values. Axial symmetry requires that K and Ω be good quantum numbers (constants of motion).

Symmetry with respect to the equatorial plane requires invariance in form of the wave function under a rotation of the body-frame through 180° about the 2-axis; going from the $\vec{\mathcal{R}}'$-frame (1-2-3-axes), reached from the space frame via the Euler rotations Φ, Θ, Ψ, to an $\vec{\mathcal{R}}''$ -frame (1'-2'-3'-axes), which is reached from the old body frame via Euler rotations $0, \pi, \pi$, or directly from the space frame via Euler rotations $\pi+\Phi, \pi-\Theta, 2\pi-\Psi$. Let R_1 denote the resulting transformation on the wave function. Then, if χ_{jm} represent the usual angular momentum eigenfunctions,

$$\begin{aligned} \chi_{jm}(\vec{\mathcal{R}}') &= \sum_{m'} D^{j}_{m'm}(\Phi\Theta\Psi)\chi_{jm'}(\vec{\mathcal{R}}) \\ \chi_{jm}(\vec{\mathcal{R}}'') &= \sum_{m'} D^{j}_{m'm}(0\pi\pi)\chi_{jm'}(\vec{\mathcal{R}}') \\ &= \sum_{m'} D^{j}_{m'm}(\pi+\Phi, \pi-\Theta, 2\pi-\Psi)\chi_{jm'}(\vec{\mathcal{R}}) \quad . \end{aligned} \tag{I-182}$$

Taking χ_{jm} in the Euler angle representation and noting that $D^{j}_{mm'}(0\pi\pi) = (-1)^{j+m-m'}\delta_{m,-m'}$, or working directly with the explicit D-functions, it may be shown that

$$D^{I^*}_{MK}(\pi+\Phi, \pi-\Theta, 2\pi-\Psi) = (-1)^I D^{I^*}_{M-K}(\Phi\Theta\Psi) \quad . \tag{I-183}$$

Hence

$$\begin{aligned} R_1|IMK\Omega\rangle &= D^{I^*}_{MK}(\pi+\Phi, \pi-\Theta, 2\pi-\Psi)\chi_\Omega(\vec{\pi}'') \\ &= (-1)^I D^{I^*}_{M-K}(\Phi\Theta\Psi)\sum_j C_{j\Omega}\sum_{\Omega'} D^{j}_{\Omega'\Omega}(0\pi\pi)\chi_{j\Omega'}(\vec{\pi}') \\ &= (-1)^I D^{I^*}_{M-K}(\Phi\Theta\Psi)\sum_j C_{j\Omega}(-1)^{-j}\chi_{j-\Omega}(\vec{\pi}') \quad , \end{aligned} \tag{I-184}$$

where use has been made of the fact that $(-1)^{2(j-\Omega)} \equiv +1$.

Now[32] from the property of the Nilsson functions' amplitudes, $a_{\ell\Lambda\Omega} = a_{\ell-\Lambda-\Omega}$, it may be shown that $C_{j\Omega} = \pi_\chi(-1)^{j-\frac{1}{2}}C_{j-\Omega}$, so that

$$R_1|IMK\Omega\rangle = (-1)^{I-\frac{1}{2}}\pi_\chi D^{I^*}_{M-K}(\Phi\Theta\Psi)\chi_{-\Omega}(\vec{\pi}') \quad . \tag{I-185}$$

Since the symmetrized wave function is to obey

$$R_1\psi^s = \psi^s \quad , \tag{I-186}$$

and $R_1^2 = 1$, the required normalized symmetrized function is

$$\psi^s = \frac{1}{\sqrt{2}}(\psi + R_1\psi) \tag{I-187}$$

or

$$\psi^s \equiv |IMK\Omega^s\rangle = \sqrt{\frac{2I+1}{16\pi^2}}\left[D^{I^*}_{MK}\chi_\Omega + (-1)^{I-\frac{1}{2}}\pi_\chi D^{I^*}_{M-K}\chi_{-\Omega}\right] . \tag{I-188}$$

It can be shown that

$$T_R^0|IMK\Omega^s\rangle = E^0_{IK\Omega}|IMK\Omega^s\rangle \quad , \tag{I-189}$$

and that although

$$\langle IMK\Omega|\,t_R\,|IMK\Omega\rangle = 0 \tag{I-190}$$

or there is no "decoupling" without symmetrization, yet

$$\begin{aligned} &\langle IMK\Omega^s|\,t_R\,|IMK\Omega^s\rangle \\ &= -\frac{2I-1}{16\pi^2}\frac{\hbar^2}{2\mathcal{I}'}\left\langle D^{I^*}_{MK}\chi_\Omega + (-1)^{I-\frac{1}{2}}\pi_\chi D^{I^*}_{M-K}\chi_{-\Omega}\middle| I_+j_{-1} + I_-j_{+1}\middle| D^{I^*}_{MK}\chi_\Omega + (-1)^{I-\frac{1}{2}}\pi_\chi D^{I^*}_{M-K}\chi_{-\Omega}\right\rangle \\ &= \frac{-\hbar^2}{2\mathcal{I}'}\pi_\chi(-1)^{I-\frac{1}{2}}K^+_{I,|K|}\,\delta_{|K|\frac{1}{2}}\,\delta_{\Omega K}\,\mathrm{re}\langle\chi_\Omega|\,j_{+1}\,|\chi_{-\Omega}\rangle \end{aligned} \tag{I-191}$$

$$=\frac{\hbar^2}{2\mathcal{I}'}\pi_\chi(-1)^{I+\frac{1}{2}}(I+\tfrac{1}{2})\,\mathcal{Re}\langle\chi_\Omega|\,j_{+'}|\chi_{-\Omega}\rangle$$, as given in ref. 33,

where

$$K^{\pm}_{jm}\equiv\sqrt{(j\pm m)(j\mp m+1)} \tag{I-192}$$

and

$$\langle\chi_{-\Omega}|\,j_{-'}|\chi_\Omega\rangle=\langle\chi_\Omega|\,j_{+'}|\chi_{-\Omega}\rangle^* \quad . \tag{I-193}$$

Here, primes on quantities denote reference to the body frame. It can be shown that[34]

$$\mathcal{Re}\langle\chi_\Omega|\,j_{+'}|\chi_{-\Omega}\rangle=-\sum_j|C_{j\frac{1}{2}}|^2(-1)^{j+\frac{1}{2}}(j+\tfrac{1}{2})\pi_\chi\,\delta_{\Omega\frac{1}{2}}\,;$$
$$\therefore\ a=-\sum_j|C_{j\frac{1}{2}}|^2(-1)^{j+\frac{1}{2}}(j+\tfrac{1}{2})\,. \tag{I-194}$$

This is the usual decoupling and occurs for an isolated rotational band only if $K=\Omega=\pm 1/2$. The Coriolis term can cause mixing of states from other bands into a given band, as is discussed below.

2. Inclusion of Core Distortion

Higher-order effects depend on higher-order terms in the Hamiltonian[23*]. A possible mechanism for these is centrifugal distortion of the core. As above,

$$T_R=\sum_{\nu=1}^{3}\frac{R_\nu^2}{2\mathcal{I}'_\nu}=\frac{1}{2\mathcal{I}'}(R^2-R_3^2)+\frac{1}{2\mathcal{I}'_3}R_3^2\,, \tag{I-195}$$

and

$$R^2-R_3^2=I^2-I_3^2-j_3^2+j^2-(I_{+'}j_{-'}+I_{-'}j_{+'}),\ R_3^2=(I_3-j_3)^2, \tag{I-196}$$

from which follows

$$T_R=T_R^0+t_R-\frac{\hbar^2 j^2}{2\mathcal{I}'} \quad . \tag{1-197}$$

Centrifugal core distortion can be introduced by permitting the $\mathcal{I}'$, $\mathcal{I}_3'$ to depend on the magnitude of the core angular

---

*Relevant formulae of the Rayleigh-Schrödinger scheme appear in appendix 3.

momentum, in analogy to the classical situation in the presence of centrifugal force $\vec{\omega}\times(\vec{\omega}\times\vec{\pi}')=(\vec{\omega}\vec{\omega}-\hat{\hat{\mathcal{I}}}\omega^2)\cdot\vec{\pi}'\propto\omega^2$.
The dependence can be expressed as a phenomenological power-series expansion of $\mathcal{I}'$, $\mathcal{I}_3'$, in powers of R^2:

$$\frac{1}{\mathcal{I}'}=\frac{1}{\mathcal{I}^0}\sum_{\mu=0}^{\infty}B^{(\mu)}R^{2\mu} \tag{I-198}$$

$$\frac{1}{\mathcal{I}_3'}=\frac{1}{\mathcal{I}_3^0}\sum_{\mu=0}^{\infty}B_3^{(\mu)}R^{2\mu} \tag{I-199}$$

where $B^{(\mu)}$, $B_3{}^{(\mu)}$ assume the role of adjustable parameters . Upon substitution into T_R there results, after some manipulation,

$$T_R=\frac{1}{2\mathcal{I}^0}\sum_{\mu=0}^{\infty}\left[A^{(\mu)}+\frac{\mathcal{I}^0}{\mathcal{I}_3^0}R_3^2A_3^{(\mu+1)}\right](R^2-R_3^2)^{\mu+1}+\frac{1}{2\mathcal{I}_3^0}A_3^{(0)}R_3^2 \quad , \tag{I-200}$$

where

$$A^{(\mu)}=\sum_{\nu=\mu}^{\infty}\binom{\nu}{\mu}B^{(\nu)}R_3^{2(\nu-\mu)} \quad , \tag{I-201}$$

$$A_3^{(\mu)}=\sum_{\nu=\mu}^{\infty}\binom{\nu}{\mu}B_3^{(\nu)}R_3^{2(\nu-\mu)} \quad , \tag{I-202}$$

and therefore

$$\left[A^{(\mu)}+\frac{\mathcal{I}^0}{\mathcal{I}_3^0}R_3^2A_3^{(\mu+1)}\right]=B^{(\mu)}+\sum_{\nu=\mu+1}^{\infty}\left[\binom{\nu}{\mu}B^{(\nu)}+\frac{\mathcal{I}^0}{\mathcal{I}_3^0}\binom{\nu}{\mu+1}B_3^{(\nu)}\right]R_3^{2(\nu-\mu)} \tag{I-203}$$

and

$$A_3^{(0)}=\sum_{\nu=0}^{\infty}B_3^{(\nu)}R_3^{2\nu}=1+B_3^{(1)}R_3^2+B_3^{(2)}R_3^4+\ldots \tag{I-204}$$

Noting that $R_3^\nu=(I_3-j_3)^\nu$ is diagonal in the $|\psi_{IMK\Omega}^{s}\rangle$ representation and that for low-lying states,

$$\langle IMK\Omega^s|\,I_3\,|IMK\Omega^s\rangle\equiv K=\Omega\equiv\langle IMK\Omega^s|\,j_3\,|IMK\Omega^s\rangle \quad , \tag{I-205}$$

there follows

$$R_3^{\nu}|IMK\Omega^s\rangle=0 \quad , \tag{I-206}$$

so that the terms of T_R giving non-vanishing energy contributions are simply,

$$T_R = \frac{1}{2\mathcal{I}^0}\sum_{\mu=0}^{\infty} B^{(\mu)}(R^2-R_3^2)^{\mu+1}, \qquad B^{(0)}=1\,. \tag{I-207}$$

The leading term is the problem in the absence of R^2 dependence of $\mathcal{I}'$, and, similarly to this case, one has

$$\begin{aligned}\langle IMK\Omega^s|\,R^2-R_3^2\,|IMK\Omega^s\rangle &= \langle \chi_\Omega|j^2|\chi_\Omega\rangle + I(I+1)-K^2-\Omega^2\\ &+\pi_\chi(-1)^{I+\frac{1}{2}}(I+\tfrac{1}{2})\,\delta_{|K|\frac{1}{2}}\,\delta_{\Omega K}\,\mathrm{re}\langle\chi_{\frac{1}{2}}|j_{+1}|\chi_{-\frac{1}{2}}\rangle\,,\end{aligned} \tag{I-208}$$

where $K=\Omega$ and $\langle\chi_\Omega|j^2|\chi_\Omega\rangle$ can be included with the single-particle energies $\mathcal{E}^0_\Omega$.

The only "first-order" effect is the usual decoupling produced by

$$I_{+1}j_{-1}+I_{-1}j_{+1}\equiv \mathcal{C} \tag{I-209}$$

In second-order, the first stretching correction occurs, involving the matrix element $\langle IMK\Omega^s|(R^2-R_3^2)^2|IMK\Omega^s\rangle$. Noting the relation

$$\begin{aligned}(R^2-R_3^2)^2 &= (I^2-I_3^2-j_3^2)^2+j^4+\mathcal{C}^2+2(I^2-I_3^2-j_3^2)\,j^2\\ &+2(I^2+j^2)\mathcal{C}-\left[(I_3^2+j_3^2)\mathcal{C}+\mathcal{C}(I_3^2+j_3^2)\right],\end{aligned} \tag{I-210}$$

the terms that arise from this matrix element are as follows:

$$\langle IMK\Omega^s|(I^2-I_3^2-j_3^2)^2|IMK\Omega^s\rangle = \left[I(I+1)-K^2-\Omega^2\right]^2, \tag{I-211}$$

which is a usual vibration-rotation type coupling term;

$$\langle IMK\Omega^s|\,j^4\,|IMK\Omega^s\rangle = \langle\chi_\Omega|j^4|\chi_\Omega\rangle\,, \tag{I-212}$$

calculated with the help of the relations

$$\langle\chi_{-\Omega}|j^4|\chi_{-\Omega}\rangle=\sum_j |C_{j-\Omega}|^2[j(j+1)]^2=\sum_j |C_{j\Omega}|^2[j(j+1)]^2=\langle\chi_\Omega|j^4|\chi_\Omega\rangle, \tag{I-213}$$

and which can be subsumed in the intrinsic energy; and thirdly

$$\langle IMK\Omega^s|\mathcal{C}^2|IMK\Omega^s\rangle = [I(I+1)-K^2][\langle\chi_\Omega|j_{+1}j_{-1}|\chi_\Omega\rangle + \langle\chi_{-\Omega}|j_{+1}j_{-1}|\chi_{-\Omega}\rangle]$$
$$= 2[I(I+1)-K^2][\langle\chi_\Omega|j^2|\chi_\Omega\rangle - \Omega^2], \tag{I-214}$$

the latter equality holding for half-integral K only. The effect of this term is a renormalization of the inertia constant, as well as of the single-particle energies. It also produces, for $K=\pm1$ bands, the higher-order decoupling effect given by Bohr and Mottelson[23]. Continuing,

$$\langle IMK\Omega^s|2(I^2-I_3^2-j_3^2)j^2|IMK\Omega^s\rangle = 2[I(I+1)-K^2-\Omega^2]\langle\chi_\Omega|j^2|\chi_\Omega\rangle. \tag{I-215}$$

This term contributes to the inertia constant renormalization (but not to the single-particle energies, provided $K=\Omega$).

$$\langle IMK\Omega^s|2(I^2+j^2)\mathcal{C}|IMK\Omega^s\rangle$$
$$= 2I(I+1)\langle IMK\Omega^s|\mathcal{C}|IMK\Omega^s\rangle + 2\langle IMK\Omega^s|j^2\mathcal{C}|IMK\Omega^s\rangle \tag{I-216}$$
$$= \pi_\chi(-1)^{I-\frac{1}{2}}(I+1)\delta_{|K|\frac{1}{2}}\delta_{\Omega K}\left[2I(I+1)\,re\langle\chi_{\frac{1}{2}}|j_{+1}|\chi_{-\frac{1}{2}}\rangle + 2\,re\langle\chi_{\frac{1}{2}}|j^2j_{+1}|\chi_{-\frac{1}{2}}\rangle\right].$$

This renormalizes and includes a small additive $I(I+1)$-dependent part in the decoupling parameter a. Finally,

$$\langle IMK\Omega^s|-[(I_3^2+j_3^2)\mathcal{C} + \mathcal{C}(I_3^2+j_3^2)]|IMK\Omega^s\rangle$$
$$= -\pi_\chi(-1)^{I-\frac{1}{2}}(I+\tfrac{1}{2})\delta_{|K|\frac{1}{2}}\delta_{\Omega K}\,re\langle\chi_{\frac{1}{2}}|j_{+1}|\chi_{-\frac{1}{2}}\rangle. \tag{I-217}$$

Thus, with renormalization of $\mathcal{E}_\Omega^0$, $\mathcal{I}'$, a, the rotational energies to this order are of the form

$$E_{Rot} = AI(I+1) + BI^2(I+1)^2 + \dots + (-1)^{I+\frac{1}{2}}(I+\tfrac{1}{2})[A_1 + B_1I(I+1) + \dots] \quad (|K|=\tfrac{1}{2}) \tag{I-218}$$

as noted by Bohr and Mottelson[23].

In third order the matrix element to be considered is $\langle \psi^{s}_{IMK\Omega} | (R^2 - R_3^2)^3 | \psi^{s}_{IMK\Omega} \rangle$. It can be shown that

$$
\begin{aligned}
(R^2-R_3^2)^3 &= (I^2 - I_3^2 - j_3^2 + j^2 - \mathcal{C})^3 \\
&= (I^2+j^2)^3 - 3(I^2+j^2)^2(I_3^2+j_3^2) - 3(I^2+j^2)\mathcal{C} + 3(I^2+j^2)(I_3^2+j_3^2)^2 \\
&\quad + 3(I^2+j^2)\mathcal{C}^2 + (I_3^2+j_3^2)^3 + \mathcal{C}^3 + 3(I^2+j^2)\left[(I_3^2+j_3^2)\mathcal{C} + \mathcal{C}(I_3^2+j_3^2)\right] \\
&\quad - (I_3^2+j_3^2+\mathcal{C})\left[(I_3^2+j_3^2)\mathcal{C} + \mathcal{C}(I_3^2+j_3^2)\right] - (I_3^2+j_3^2)^2 - (I_3^2+j_3^2)\,\mathcal{C}^2 \,.
\end{aligned}
\tag{I-219}
$$

There are many terms contributing to renormalizations of all the foregoing constants plus some new contributions. Of particular interest are the terms $(I^2 + j^2)^3$, which will give rise to an $I^3(I+1)^3$ energy correction term, and the $\mathcal{C}^3$ term, the calculation of whose characteristic effect follows:

$$
\begin{aligned}
\mathcal{C}^3 |IMK\Omega^s\rangle = \sqrt{\frac{2I+1}{16\pi^2}} \Big| & K^+_{I,K-2} K^+_{I,K-1} K^+_{IK} D^{I*}_{M,K-3}\, j_{-1}^{3} \chi_\Omega + \ldots + K^-_{I,K+2} K^-_{I,K+1} K^-_{IK} D^{I*}_{M,K+3}\, j_{+1}^{3} \chi_\Omega \\
& + \pi_\chi (-1)^{I-\frac{1}{2}} \left[K^+_{I,-K-2} K^+_{I,-K-1} K^+_{I,-K} D^{I*}_{M,-K-3}\, j_{-1}^{3} \chi_{-\Omega} + \ldots + K^-_{I,-K+2} K^-_{I,-K+1} K^-_{I,-K} D^{I*}_{M,-K+3}\, j_{+1}^{3} \chi_{-\Omega} \right] \Big\rangle ,
\end{aligned}
\tag{I-220}
$$

where $K^{\pm}(jm) = K^{\mp}(j,-m) = \sqrt{(j \pm m)(j \mp m + 1)}$. Then, after some manipulation,

$$
\begin{aligned}
\langle IMK\Omega^s | \mathcal{C}^3 | IMK\Omega^s \rangle &= \sqrt{\frac{2I+1}{16\pi^2}} \langle D^{I*}_{MK} \chi_\Omega + (-1)^{I-\frac{1}{2}} \pi_\chi D^{I*}_{M-K} \chi_{-\Omega} | \mathcal{C}^3 | IMK\Omega^s \rangle \\
&= \frac{1}{2} \pi_\chi (-1)^{I-\frac{1}{2}} (I-\tfrac{1}{2})(I+\tfrac{1}{2})(I+\tfrac{3}{2})\, \delta_{|K|\frac{3}{2}}\, \delta_{\Omega K}\, \mathrm{re} \langle \chi_{\frac{3}{2}} | j_{+1}^{3} | \chi_{-\frac{3}{2}} \rangle
\end{aligned}
\tag{I-221}
$$

$$+ \text{ terms proportional to } \delta_{|K|\frac{1}{2}} .$$

This term, besides producing renormalization of the $I(I+1)$-dependent part of the decoupling parameter a for $|K| = 1/2$ bands, gives rise to a higher-order decoupling effect present in $|K| = 3/2$ bands, with the consequence that the alternating elevation and depression of levels can occur for these bands even in the absence of any Coriolis mixing, that is, in a manner that does not result in any admixtures in the zero-order wave functions.

3. Band Mixing

Another mechanism that can similarly affect $K = 3/2$ bands arises from the action of the Coriolis term in the presence of more than one rotational band, a situation that pertains if H_ρ has more than one eigenvalue $\mathcal{E}_\Omega^\circ$. Because of the properties of the D^{I*}_{MK} only states of equal I from the two bands are coupled by the Coriolis perturbation. This coupling first occurs in second-order perturbation theory:

$$E_n^{(2)} = \sum_{i \neq n} \frac{\langle n | H' | i \rangle \langle i | H' | n \rangle}{E_n^\circ - E_i^\circ} , \tag{I-222}$$

where $H = H^\circ + H'$ and $H^\circ |n\rangle = E_n^\circ |n\rangle$ gives the zero-order eigenstates. The perturbed wave functions are, to first order,

$$|\psi_n\rangle = |n\rangle + \sum_{j \neq n} \frac{|j\rangle\langle j | H' | n\rangle}{E_n^\circ - E_j^\circ} . \tag{I-223}$$

If, to improve convergence, the device of employing first- instead of zero-order energies in the second-order energy denominators is employed, the Coriolis decoupling of $|K| = 1/2$ bands that might be admixed with bands under consideration will be mirrored in the perturbed energies, as follows: the uncoupled bands are described by the equations (assuming $K = \Omega$ in all cases)

$$\begin{aligned} T_R^\circ |IMK\Omega^s\rangle &= E_{IK}^\circ |IMK\Omega^s\rangle , \\ H_\rho |IMK\Omega^s\rangle &= \mathcal{E}_\Omega^\circ |IMK\Omega^s\rangle ; \end{aligned} \tag{I-224}$$

$$E_{IK}^\circ = \frac{\hbar^2}{2}\left[\frac{1}{\mathcal{I}'} I(I+1) + \left(\frac{1}{\mathcal{I}_3'} - \frac{1}{\mathcal{I}'}\right)K^2\right] \tag{I-225}$$

for the K-band, and

$$\bar{T}_R^\circ |IM\bar{K}\bar{\Omega}^s\rangle = E_{I\bar{K}}^\circ |IM\bar{K}\bar{\Omega}^s\rangle , \tag{I-226}$$

$$\begin{aligned} H_\rho |IM\bar{K}\bar{\Omega}^s\rangle &= \mathcal{E}_{\bar{\Omega}}^\circ |IM\bar{K}\bar{\Omega}^s\rangle ; \\ E_{I\bar{K}}^\circ &= \frac{\hbar^2}{2}\left[\frac{1}{\bar{\mathcal{I}}'} I(I+1) + \left(\frac{1}{\bar{\mathcal{I}}_3'} - \frac{1}{\bar{\mathcal{I}}'}\right)\bar{K}^2\right] \end{aligned} \tag{I-227}$$

for the $\bar{K}$-bands. The total Hamiltonian describing these states is

$$H = H_p + T_R = H_\rho + T_R' = H_\rho + T_R^\circ + t_R = H^\circ + t_R \tag{I-228}$$

for the K-band, as previously, and the same except that t_R is replaced by

$$\bar{t}_R = -\frac{\hbar^2}{2\mathcal{I}'}\left(I_{+'}j_{-'} + I_{-'}j_{+'}\right) \tag{I-229}$$

and $\mathcal{I}'$, $\mathcal{I}_3'$ by the inertia moments $\bar{\mathcal{I}}'$, $\bar{\mathcal{I}}_3'$, for the $\bar{K}$-bands.

The perturbation problem is, for the K-band,

$$H^\circ |IMK\Omega^s\rangle = \left(\varepsilon_\Omega^\circ + E_{IK}^\circ\right)|IMK\Omega^s\rangle \ ; \tag{I-230}$$

$$H\ |\psi_{IMK\Omega}^{s}\rangle = \left(\varepsilon_\Omega^\circ + E_{IK}\right)|\psi_{IMK\Omega}^{s}\rangle \ . \tag{I-231}$$

To first order the perturbed wave functions are

$$|\psi_{IMK\Omega}^{s}\rangle \approx |IMK\Omega^s\rangle + \sum_{\bar{K}}{}' \frac{|IM\bar{K}\bar{\Omega}^s\rangle\langle IM\bar{K}\bar{\Omega}^s|t_R|IMK\Omega^s\rangle}{\varepsilon_\Omega^\circ - \varepsilon_{\bar{\Omega}}^\circ + E_{IK}^\circ - E_{I\bar{K}}^\circ} \tag{I-232}$$

where the sum is over all bands specified by the $\bar{K}$, except the band specified by K. In the case of two bands, K, the ground-state band, and $\bar{K}$, the upper band, this becomes

$$\begin{aligned} |\psi_{IMK\Omega}^{s}\rangle &\approx |IMK\Omega^s\rangle + \frac{\langle IM\bar{K}\bar{\Omega}^s|t_R|IMK\Omega^s\rangle}{\varepsilon_\Omega^\circ - \varepsilon_{\bar{\Omega}}^\circ + E_{IK}^\circ - E_{I\bar{K}}^\circ}|IM\bar{K}\bar{\Omega}^s\rangle \\ &\equiv |IMK\Omega^s\rangle + \frac{C_{IK\bar{K}}}{-\delta E_{IK\bar{K}}^\circ}|IM\bar{K}\bar{\Omega}^s\rangle \ ; \end{aligned} \tag{I-233}$$

$$\begin{aligned} |\psi_{IM\bar{K}\bar{\Omega}}^{s}\rangle &\approx |IM\bar{K}\bar{\Omega}^s\rangle - \frac{\langle IMK\Omega^s|\bar{t}_R|IMK\Omega^s\rangle}{\varepsilon_\Omega^\circ - \varepsilon_{\bar{\Omega}}^\circ + E_{IK}^\circ - E_{I\bar{K}}^\circ}|IMK\Omega^s\rangle \\ &\equiv |IM\bar{K}\bar{\Omega}^s\rangle - \frac{\bar{C}_{I\bar{K}K}}{-\delta E_{IK\bar{K}}^\circ}|IMK\Omega^s\rangle \ . \end{aligned} \tag{I-234}$$

The quantities $C_{IK\bar{K}}$, $\bar{C}_{I\bar{K}K}$ are given by:

$$\begin{aligned} C_{IK\bar{K}} &= \langle IM\bar{K}\bar{\Omega}^s|t_R|IMK\Omega\rangle \\ &= -\frac{\hbar^2}{2\mathcal{I}'}\frac{1}{2}\Big\{K_{IK}^+\Big[\left(\langle\bar{\chi}_{\bar{\Omega}}|j_{-'}|\chi_\Omega\rangle + \pi_\chi\pi_{\bar{\chi}}\langle\bar{\chi}_{-\bar{\Omega}}|j_{+'}|\chi_{-\Omega}\rangle\right)\delta_{\bar{K},K-1} \\ &\quad + (-1)^{I-\frac{1}{2}}\pi_\chi\left(\langle\bar{\chi}_{\bar{\Omega}}|j_{+'}|\chi_{-\Omega}\rangle + \pi_{\bar{\chi}}\pi_\chi\langle\bar{\chi}_{-\bar{\Omega}}|j_{-'}|\chi_\Omega\rangle\right)\delta_{\bar{K},-K+1}\Big] \\ &\quad + K_{IK}^-\Big[\left(\langle\bar{\chi}_{\bar{\Omega}}|j_{+'}|\chi_\Omega\rangle + \pi_{\bar{\chi}}\pi_\chi\langle\bar{\chi}_{-\bar{\Omega}}|j_{-'}|\chi_{-\Omega}\rangle\right)\delta_{\bar{K},K+1} \\ &\quad + (-1)^{I-\frac{1}{2}}\pi_\chi\left(\langle\bar{\chi}_{\bar{\Omega}}|j_{-'}|\chi_{-\Omega}\rangle + \pi_{\bar{\chi}}\pi_\chi\langle\bar{\chi}_{-\bar{\Omega}}|j_{+'}|\chi_\Omega\rangle\right)\delta_{\bar{K},-K-1}\Big]\Big\} , \end{aligned} \tag{I-235}$$

and for the upper band ($\bar{C}_{I\bar{K}K}$), the same except that $\not{t}_R$ is replaced by $\bar{\not{t}}_R$ and K, $\bar{K}$; $\chi_\Omega, \bar{\chi}_{\bar{\Omega}}$: and $\pi_\chi, \pi_{\bar{\chi}}$ are interchanged throughout. Noting that $K^\pm(j,-m) = K^\pm(j,m\pm 1) = K^\mp(j,m)$, $\pi_\chi^2 = \pi_{\bar{\chi}}^2 = 1$, and $\langle \chi_\Omega | j_{\pm'} | \bar{\chi}_{\bar{\Omega}} \rangle = \langle \bar{\chi}_{\bar{\Omega}} | j_{\mp'} | \chi_\Omega \rangle^*$, by a little manipulation $\bar{C}_{I\bar{K}K}$ can be put in a form identical to $C_{IK\bar{K}}$ except that $\mathcal{I}'$ is replaced by $\bar{\mathcal{I}}'$ and $\langle \bar{\chi}_{\bar{\Omega}} | j_{\pm'} | \chi_\Omega \rangle$ is now $\langle \bar{\chi}_{\bar{\Omega}} | j_{\pm'} | \chi_\Omega \rangle^*$. Then apart from the possible slight difference in $\mathcal{I}'$ and $\bar{\mathcal{I}}'$, the admixing amplitudes for the two bands are equal in magnitude provided quantities such as $[\langle \bar{\chi}_{\bar{\Omega}} | j_{-'} | \chi_\Omega \rangle + \pi_\chi \pi_{\bar{\chi}} \langle \bar{\chi}_{-\bar{\Omega}} | j_{+'} | \chi_{-\Omega} \rangle] \delta_{\bar{\Omega},\Omega-1}$ are real. That this is the case can be illustrated as follows: supposing $\bar{\Omega}\,(=\bar{K}) = \Omega - 1$ $(\Omega = K)$, and setting

$$\chi_\Omega = \sum_j C_{j\Omega} \chi_{j\Omega} \;, \quad \bar{\chi}_\Omega = \sum_j \bar{C}_{j\Omega} \chi_{j\Omega} \;, \tag{I-236}$$

one has

$$\begin{aligned} &[\langle \bar{\chi}_{\bar{\Omega}} | j_{-'} | \chi_\Omega \rangle + \pi_{\bar{\chi}} \pi_\chi \langle \bar{\chi}_{-\bar{\Omega}} | j_{+'} | \chi_{-\Omega} \rangle] \, \delta_{\bar{\Omega},\Omega-1} \\ &\quad = \langle \bar{\chi}_{\Omega-1} | j_{-'} | \chi_\Omega \rangle + \pi_{\bar{\chi}} \pi_\chi \langle \bar{\chi}_{-\Omega+1} | j_{+'} | \chi_\Omega \rangle \\ &\quad = \sum_j \bar{C}_{j\Omega-1} C_{j\Omega} [\langle \chi_{j\Omega-1} | j_{-'} | \chi_{j\Omega} \rangle + \langle \chi_{j-\Omega+1} | j_{+'} | \chi_{j-\Omega} \rangle] \end{aligned} \tag{I-237}$$

where use was made of

$$\begin{aligned} C_{j-\Omega} &= \langle \ell -\Lambda \tfrac{1}{2} -\Sigma | \ell \tfrac{1}{2} j -\Omega \rangle a_{\ell -\Lambda -\Omega} = \langle \ell -\Lambda \tfrac{1}{2} -\Sigma | \ell \tfrac{1}{2} j -\Omega \rangle a_{\ell\Lambda\Omega} \\ &= (-1)^{\ell + \frac{1}{2} - j} \langle \ell \Lambda \tfrac{1}{2} \Sigma | \ell \tfrac{1}{2} j \Omega \rangle a_{\ell\Lambda\Omega} = \pi_\chi (-1)^{-j+\frac{1}{2}} C_{j\Omega} \;, \end{aligned} \tag{I-238}$$

and the fact that the $a_{\ell\Lambda\Omega}$ are real[9], and hence also $C_{j\Omega}$. Also required were

$$\begin{aligned} &\langle \chi_{j\Omega-1} | j_{-'} | \chi_{j\Omega} \rangle + \langle \chi_{j-\Omega+1} | j_{+'} | \chi_{j-\Omega} \rangle \\ &\quad = K^+_{j\Omega} [\langle \chi_{j\Omega-1} | \chi_{j\Omega-1} \rangle + \langle \chi_{j-\Omega+1} | \chi_{j-\Omega+1} \rangle] = 2 K^+_{j\Omega} \end{aligned} \tag{I-239}$$

and the reality of $K^+_{j\Omega}$.

The perturbed energies are

$$\begin{aligned} E_{IK} &= E^\circ_{IK} + \langle IMK\Omega^s | \not{t}_R | IMK\Omega^s \rangle + \frac{|\langle IM\bar{K}\bar{\Omega}^s | \not{t}_R | IMK\Omega^s \rangle|^2}{\mathcal{E}^\circ_\Omega - \mathcal{E}^\circ_{\bar{\Omega}} + E^\circ_{IK} - E^\circ_{I\bar{K}}} \\ &\equiv E^\circ_{IK} + \langle IMK\Omega^s | \not{t}_R | IMK\Omega^s \rangle + C^2_{IK\bar{K}} / (-\delta E^\circ_{IK\bar{K}}) \end{aligned} \tag{I-240}$$

$$E_{I\bar K} = E^{\circ}_{I\bar K} + \langle IM\bar K\bar\Omega^{s}|\mathcal{H}_R|IM\bar K\bar\Omega^{s}\rangle - \frac{|\langle IMK\Omega^{s}|\mathcal{H}_R|IM\bar K\bar\Omega^{s}\rangle|^2}{\varepsilon^{\circ}_{\Omega} - \varepsilon^{\circ}_{\bar\Omega} + E^{\circ}_{IK} - E^{\circ}_{I\bar K}}$$

$$\equiv E^{\circ}_{I\bar K} + \langle IM\bar K\bar\Omega^{s}|\mathcal{H}_R|IM\bar K\bar\Omega^{s}\rangle - \bar C_{I\bar K K}^{\,2}\big/(-\delta E_{IK\bar K}) \; . \qquad \text{(I-241)}$$

For the case $|\bar K| = 1/2$, $|K| \neq 1/2$, the diagonal term in E_{IK} is zero. The diagonal term in $E_{I\bar K}$, the Coriolis decoupling in the upper band, is found analogously to (I-191) to be

$$\langle IM\bar K\bar\Omega^{s}|\mathcal{H}_R|IM\bar K\bar\Omega^{s}\rangle = -\frac{\hbar^2}{2\bar{\mathcal{I}}'}\pi_{\bar\chi}(-1)^{I-\frac{1}{2}}\delta_{|\bar K|\frac{1}{2}}\delta_{\bar\Omega\bar K}K^{+}(I\bar K)\,\mathrm{re}\langle\bar\chi_{\bar\Omega}|j_{+'}|\bar\chi_{-\bar\Omega}\rangle$$
$$= +\frac{\hbar^2}{2\bar{\mathcal{I}}'}(-1)^{I+\frac{1}{2}}(I+\tfrac{1}{2})\,\delta_{|\bar K|\frac{1}{2}}\,\bar a \qquad \text{(I-242)}$$

where the decoupling parameter is

$$\bar a = \pi_{\bar\chi}\,\delta_{\bar\Omega\bar K}\,\mathrm{re}\langle\bar\chi_{\bar\Omega}|j_{+'}|\bar\chi_{-\bar\Omega}\rangle \; , \qquad \text{(I-243)}$$

and the first-order upper-band decoupling correction is

$$E^{(1)}_{I\bar K} \equiv \langle IM\bar K\bar\Omega^{s}|\mathcal{H}_R|IM\bar K\bar\Omega^{s}\rangle = \frac{\hbar^2}{2\bar{\mathcal{I}}'}\,\bar a\,(-1)^{I+\frac{1}{2}}(I+\tfrac{1}{2}) \; . \qquad \text{(I-244)}$$

Replacing $E^{0}_{I\bar K}$ by $E^{0}_{I\bar K} + E^{(1)}_{I\bar K}$ in the second-order energy denominator to improve convergence results in

$$E_{IK} = E^{\circ}_{IK} + \frac{|\langle IM\bar K\bar\Omega^{s}|\mathcal{H}_R|IMK\Omega^{s}\rangle|^2}{-\delta E_{IK\bar K} - \frac{\hbar^2}{2\bar{\mathcal{I}}'}\bar a(-1)^{I+\frac{1}{2}}(I+\frac{1}{2})} \qquad \text{(I-245)}$$

$$= E^{\circ}_{IK} + |\langle IM\bar K\bar\Omega^{s}|\mathcal{H}_R|IMK\Omega^{s}\rangle|^2\left\{\frac{1}{-\delta\varepsilon^{\circ}_{K\Omega\bar K\bar\Omega} + \frac{\hbar^2}{2}\left(\frac{1}{\mathcal{I}} - \frac{1}{\bar{\mathcal{I}}}\right)I(I+1) - \frac{\hbar^2}{2\bar{\mathcal{I}}}\bar a(-1)^{I+\frac{1}{2}}(I+\frac{1}{2})}\right\}$$

where

$$\varepsilon^{\circ}_{\Omega} + E^{\circ}_{IK} = \varepsilon^{\circ\prime}_{K\Omega} + \frac{\hbar^2}{2\mathcal{I}}I(I+1) \; ,$$
$$\varepsilon^{\circ\prime}_{K\Omega} \equiv \hbar^2\left(\frac{1}{\mathcal{I}_3} - \frac{1}{\mathcal{I}}\right)K^2 + \varepsilon^{\circ}_{\Omega} \; ; \qquad \text{(I-246)}$$

and

$$\delta\varepsilon^{\circ}_{K\Omega\bar K\bar\Omega} \equiv \varepsilon^{\circ\prime}_{\bar K\bar\Omega} - \varepsilon^{\circ\prime}_{K\Omega} \qquad \text{(I-247)}$$

is the zero-order band-head separation. Neglecting the second term of the denominator, to first order in small quantities,

$$E_{IK} \approx E^{\circ}_{IK} - \frac{|\langle IMK\Omega^{s}|\mathcal{H}_R|IMK\Omega^{s}\rangle|^2}{\delta\varepsilon^{\circ}_{K\Omega\bar K\bar\Omega}} + \frac{|\langle IM\bar K\bar\Omega^{s}|\mathcal{H}_R|IMK\Omega^{s}\rangle|^2}{(\delta\varepsilon^{\circ}_{K\Omega\bar K\bar\Omega})^2}\,\bar a\,\frac{\hbar^2}{2\bar{\mathcal{I}}'}(-1)^{I+\frac{1}{2}}(I+\tfrac{1}{2}) . \qquad \text{(I-248)}$$

The third term mirrors the upper-band decoupling in the ground-state band perturbations, and can be reduced to a more familiar form as follows:

for the case $\bar{K} = K-1$, $K = 3/2$, $\bar{\Omega} = \bar{K}$, $\Omega = K$,

$$\begin{aligned}
&|\langle IM\bar{K}\bar{\Omega}^s|t_R|IMK\Omega^s\rangle|^2 \\
&= \left[-\frac{\hbar^2}{2\mathcal{I}'}K^+(I,K)\cdot\frac{1}{2}\left(\langle\bar{\chi}_{\bar{\Omega}}|j_{-'}|\chi_\Omega\rangle+\pi_\chi\pi_{\bar{\chi}}\langle\bar{\chi}_{-\bar{\Omega}}|j_{+'}|\chi_{-\Omega}\rangle\right)\right]^2 \\
&= \left[-\frac{\hbar^2}{2\mathcal{I}'}K^+(I,\tfrac{3}{2})\langle\bar{\chi}_{\frac{1}{2}}|j_{-'}|\chi_{\frac{3}{2}}\rangle\right]^2 \\
&= \left(\frac{\hbar^2}{2\mathcal{I}'}\right)^2(I-\tfrac{1}{2})(I+\tfrac{3}{2})\langle\chi_{\frac{3}{2}}|j_{+'}|\bar{\chi}_{\frac{1}{2}}\rangle^2 \quad ,
\end{aligned} \tag{I-249}$$

where use was made of (I-184):

$$\begin{aligned}
\mathcal{R}_1\chi_\Omega(\vec{\pi}') &= \chi_\Omega(\vec{\pi}'') = \sum_j\sum_{\Omega'}C_{j\Omega}D^j_{\Omega'\Omega}(0,\pi,0)\chi_{j\Omega'}(\vec{\pi}') \\
&= (-1)^{\Omega-\frac{1}{2}}\pi_\chi\chi_{-\Omega}(\vec{\pi}') \; , \\
\mathcal{R}_1\chi^*_\Omega(\vec{\pi}') &= \chi^*_\Omega(\vec{\pi}'') = \sum_j\sum_{\Omega'}C^*_{j\Omega}D^j_{\Omega'\Omega}(0,\pi,0)\chi^*_{j\Omega'}(\vec{\pi}') \\
&= (-1)^{\Omega-\frac{1}{2}}\pi_\chi\chi^*_{-\Omega}(\vec{\pi}') \; ,
\end{aligned} \tag{I-250}$$

in which $\mathcal{R}_1$ is a body-frame rotation of 180° about the "2" axis, from which follows

$$\langle\bar{\chi}_{-\Omega}|\chi_{-\Omega}\rangle = \pi_{\bar{\chi}}\pi_\chi\langle\mathcal{R}_1\bar{\chi}_\Omega|\mathcal{R}_1\chi_\Omega\rangle = \pi_{\bar{\chi}}\pi_\chi\langle\bar{\chi}_\Omega|\chi_\Omega\rangle \quad , \tag{I-251}$$

the second equality valid because $\mathcal{R}_1$ is unitary; and also of the reality of $\langle\bar{\chi}_{\frac{1}{2}}|j_{-'}|\chi_{\frac{3}{2}}\rangle$ (for Nilsson wave functions).

Therefore,

$$\begin{aligned}
&\frac{1}{(\delta\mathcal{E}^\circ_{K\bar{K}})^2}\left|\langle IM\bar{K}\bar{\Omega}^s|t_R|IMK\Omega^s\rangle\right|^2\bar{a}\frac{\hbar^2}{2\bar{\mathcal{I}}'}(-1)^{I+\frac{1}{2}}(I+\tfrac{1}{2}) \\
&= \bar{a}\frac{\hbar^2}{2\bar{\mathcal{I}}'}\left[\frac{\frac{\hbar^2}{2\mathcal{I}'}\langle\chi_{\frac{3}{2}}|j_{+'}|\bar{\chi}_{\frac{1}{2}}\rangle}{(\delta\mathcal{E}^\circ)^2}\right]^2(-1)^{I+\frac{1}{2}}(I-\tfrac{1}{2})(I+\tfrac{1}{2})(I+\tfrac{3}{2}) \equiv C(-1)^{I+\frac{1}{2}}(I-\tfrac{1}{2})(I+\tfrac{1}{2})(I+\tfrac{3}{2}) .
\end{aligned} \tag{I-252}$$

This is the expression given in the paper of Diamond, Elbek and Stephens[35]. It is seen that the sign of C is the same as the sign of $\bar{a}$, and that the form of the alternating term is identical in its I-dependence to the form of the term arising from centrifugal stretching.

If one has $\bar{K} = -K+1 = -1/2$, the squared quantity turns out to be the same.

4. Inclusion of Vibrations

The nature of β and γ-vibrational states in odd-A deformed nuclei will now be considered. For this purpose it is necessary to consider the particular kind of collective model that has been more or less successful in describing observed rotational and vibrational nuclear phenomena.

The energy is taken as a function of the nuclear shape, specified by the equation of the surface, $R = R_0\sum_{\lambda=0}^{\infty}\sum_{\mu=-\lambda}^{\lambda}\alpha_{\lambda\mu}Y_\lambda^\mu(\theta\varphi)$. The $\alpha_{\lambda\mu}$ are given the role of generalized coordinates. As is generally the case with mechanical systems, the kinetic energy is a homogeneous quadratic form in the generalized velocities:

$$T = \frac{1}{2}\sum_{\lambda\mu} B_\lambda(\dot{\alpha}_{\lambda\mu})^2 = \frac{1}{2}\sum_\lambda B_\lambda \sum_\mu (-1)^\mu \dot{\alpha}_{\lambda\mu}\dot{\alpha}_{\lambda-\mu} \quad . \tag{I-253}$$

The relation $\alpha_{\lambda-\mu} = (-1)^\mu\alpha^*_{\lambda\mu}$ follows from the requirement that R be real. In the approximation of small $|\alpha_{\lambda\mu}|$, B_λ are approximately independent of $\alpha_{\lambda\mu}$, and in that approximation,

$$V = \frac{1}{2}\sum_\lambda C_\lambda \sum_\mu (-1)^\mu \alpha_{\lambda\mu}\alpha_{\lambda-\mu} \quad . \tag{I-254}$$

For the quadratic deformations, $\lambda = 2$, the generalized momenta $\pi_{2\mu} = \partial T/\partial\dot{\alpha}_{2\mu} = B_2(-1)^\mu\dot{\alpha}_{2-\mu}$ and the Hamiltonian $H_2 = \frac{1}{2B_2}\sum_\mu(-1)^\mu\pi_{2\mu}\pi_{2-\mu} + \frac{C_2}{2}\sum_\mu(-1)^\mu\alpha_{2\mu}\alpha_{2-\mu}$ may be written down. The problem is that of a five-dimensional harmonic oscillator, and has for its solution the energy eigenvalues $E = \hbar\omega\sum_\mu(n_\mu+\frac{1}{2}) = \hbar\omega(N+\frac{5}{2})$, $\omega = \sqrt{\frac{C_2}{B_2}}$ and eigenstates $\Psi_N = \prod_{\mu=-2}^{2} H_{n_\mu}(\alpha_{2\mu})e^{-\frac{B_2\omega}{2\hbar}\sum_\nu|\alpha_{2\nu}|^2}$. Low-lying positive-parity quadrupole vibrations about a spherical equilibrium shape for an even-even nucleus, described by this model, are the 0+ ground state, a 2+ first excited state, a 0+ 2+

4+ triplet at twice the energy of the 2+ , etc. In regions between closed-shell configurations and the rotational regions of the periodic table, the "vibrational regions", such sequences of levels are frequently encountered. For odd-A nuclei in these regions the Hamiltonian consists of a collective part $H_c(\alpha_{2\mu}, \pi_{2\mu})$ for the core, an intrinsic part $H_p = \sum_i (p_i^2 + V(\vec{r}_i))$ for the particles (generally only extra-core particles), where

$$V(r\theta\phi) = V_{SPH}\left(\frac{r}{1+\sum_\mu \alpha_{2\mu} Y_2^\mu(\theta\phi)}\right) = V_{SPH}(r) - \sum_\mu \alpha_{2\mu} Y_2^\mu(\theta\phi)\left(r\frac{\partial V(r\theta\phi;\alpha_{2\mu})}{\partial r}\right)\Bigg|_{\alpha_{2\mu}\equiv 0} + \ldots, \tag{I-255}$$

and only the spherical shell-model potential is included in H_p , and the interaction terms, of the form $-\sum_i K(r_i)\sum_\mu \alpha_{2\mu} Y_2^\mu(\theta_i\phi_i)$. This treatment in which $V_{sph}(r)$ is used in H_p and for calculating the interaction term between the core and the particles is the so-called "weak-coupling" case.

To describe the situation in the rotational region a transformation to body-frame coordinates is expedient. Here $\alpha_{\lambda\mu}$ will not be small, so that $V(r, \theta, \phi)$ can no longer be expanded as above to advantage. The C_2 and the B_2 may be $\alpha_{\lambda\mu}$-dependent, and in the case of odd-A nuclei, the interaction term will not be "small". All these effects lead to gross distortions of the simple vibrational sequences, out of which ultimately emerges, for strong deformations, the rotational picture whose simplest description is in terms of body-frame coordinates.

Following somewhat the precepts set out by J. P. Davidson[217], the general nuclear surface is given in terms of body coordinates

$$R = R_0 \sum_{\lambda=0}^{\infty} \sum_{\mu=-\lambda}^{\lambda} a_{\lambda\mu} Y_\lambda^\mu (\theta' \varphi') \tag{I-256}$$

whence because of the relation $Y_\lambda^\mu(\theta', \varphi') = \sum_\nu D_{\nu\mu}^\lambda (\Phi\Theta\Psi) Y_\lambda^\nu(\theta\varphi)$, the $a_{\lambda\mu}$ obey the relations

$$a_{\lambda\mu}^* = \sum_\nu D_{\nu\mu}^\lambda (\Phi\Theta\Psi) \alpha_{\lambda\nu}^* , \quad \alpha_{\lambda\mu}^* = \sum_\nu D_{\mu\nu}^{\lambda *} (\Phi\Theta\Psi) a_{\lambda\nu}^* , \tag{I-257}$$

showing that $\alpha_{\lambda\mu}^*$ are spherical tensors. Then the terms in the vibrational Hamiltonian become

$$\begin{aligned} V_\lambda &= \tfrac{1}{2} C_\lambda \sum_\mu \alpha_{\lambda\mu}^* \alpha_{\lambda\mu} = \tfrac{1}{2} C_\lambda \sum_\nu \sum_\rho \sum_\mu D_{\mu\nu}^{\lambda *} D_{\mu\rho}^\lambda a_{\lambda\nu}^* a_{\lambda\rho} \\ &= \tfrac{1}{2} C_\lambda \sum_\nu \sum_\rho \delta_{\nu\rho} a_{\lambda\nu}^* a_{\lambda\rho} = \tfrac{1}{2} C_\lambda \sum_\nu |a_{\lambda\nu}|^2 \equiv V_\lambda' \end{aligned} \tag{I-258}$$

$$\begin{aligned} T_\lambda = \tfrac{1}{2} B_\lambda \sum_\mu \dot{\alpha}_{\lambda\mu}^* \dot{\alpha}_{\lambda\mu} = \tfrac{1}{2} B_\lambda \sum_\nu \sum_\rho \sum_\mu \big[& \dot{D}_{\mu\nu}^{\lambda *} \dot{D}_{\mu\rho}^\lambda a_{\lambda\nu}^* a_{\lambda\rho} \\ & + \dot{D}_{\mu\nu}^{\lambda *} D_{\mu\nu}^\lambda a_{\lambda\nu}^* \dot{a}_{\lambda\rho} + D_{\mu\nu}^{\lambda *} \dot{D}_{\mu\rho}^\lambda \dot{a}_{\lambda\nu}^* a_{\lambda\rho} + D_{\mu\nu}^{\lambda *} D_{\mu\rho}^\lambda \dot{a}_{\lambda\nu}^* \dot{a}_{\lambda\rho} \big] . \end{aligned} \tag{I-259}$$

The first term of T_λ describes a rotation, the last, a vibration, and the middle two, the vibration-rotation interaction . The $\dot{D}_{\mu\nu}^{\lambda *}$ have to be evaluated. One has

$$\dot{D}_{\mu\nu}^{\lambda *} (\Phi\Theta\Psi) = \frac{\partial D_{\mu\nu}^{\lambda *}}{\partial \Phi} \dot{\Phi} + \frac{\partial D_{\mu\nu}^{\lambda *}}{\partial \Theta} \dot{\Theta} + \frac{\partial D_{\mu\nu}^{\lambda *}}{\partial \Psi} \dot{\Psi} . \tag{I-260}$$

From the expression[4] $D_{\mu\nu}^{\lambda *}(\Phi\Theta\Psi) = e^{i(\mu\Phi + \nu\Psi)} d_{\mu\nu}^\lambda(\Theta)$, there follow

$$\begin{aligned} &\frac{\partial D_{\mu\nu}^{\lambda *}}{\partial \Phi} = i\mu D_{\mu\nu}^{\lambda *} ; \qquad \frac{\partial D_{\mu\nu}^{\lambda *}}{\partial \Psi} = i\nu D_{\mu\nu}^{\lambda *} ; \\ &\frac{\partial D_{\mu\nu}^{\lambda *}}{\partial \Theta} = e^{i(\mu\Phi + \nu\Psi)} \frac{d\, d_{\mu\nu}^\lambda(\Theta)}{d\Theta} . \end{aligned} \tag{I-261}$$

The evaluation of $d\, d_{\mu\nu}^\lambda(\Theta)/d\Theta$ is most readily accomplished by recourse to the definition and transformation properties of certain angular momentum components in the Euler-angle configuration space; using the notation given with the definitions of the Euler angles,

$$-i\frac{\partial}{\partial\Theta}\left[D_{MK}^{I*}(\Phi\Theta\Psi)\chi_\Omega(\vec{\pi}')\right] \equiv I_\eta(\Phi\Theta\Psi)\left[D_{MK}^{I*}(\Phi\Theta\Psi)\chi_\Omega(\vec{\pi}')\right]$$

$$= \left[-\sin\Phi\, I_x(\Phi\Theta\Psi)+\cos\Phi\, I_y(\Phi\Theta\Psi)\right]\left[D_{MK}^{I*}(\Phi\Theta\Psi)\chi_\Omega(\vec{\pi}')\right] \qquad \text{(I-262)}$$

$$= \frac{1}{2i}\left[e^{-i\Phi}I_+(\Phi\Theta\Psi)-e^{i\Phi}I_-(\Phi\Theta\Psi)\right]\left[D_{MK}^{I*}(\Phi\Theta\Psi)\chi_\Omega(\vec{\pi}')\right].$$

If $\chi_\Omega(\vec{\pi}')$ is independent of Φ, Θ, Ψ, which in strongly deformed nuclei will be approximately the case, this becomes

$$\frac{1}{2i}\left[e^{-i\Phi}(I_+D_{MK}^{I*})\chi_\Omega - e^{i\Phi}(I_-D_{MK}^{I*})\chi_\Omega\right]$$
$$= \frac{1}{2i}\left[e^{-i\Phi}K_{IM}^{-}D_{M+1}^{I*} - e^{i\Phi}K_{IM}^{+}D_{M-1\,K}^{I*}\right]\chi_\Omega \quad , \qquad \text{(I-263)}$$

where as before $K_{jm}^{\pm} \equiv \sqrt{(j\pm m)(j\mp m+1)}$. From this it follows that

$$\frac{d\, d_{MK}^{I}(\Theta)}{d\,\Theta} = \frac{1}{2}\left[K_{IM}^{-}\, d_{M+1\,K}^{I}(\Theta) - K_{IM}^{+}\, d_{M-1\,K}^{I}(\Theta)\right]. \qquad \text{(I-264)}$$

Also,

$$I_\eta(\Phi\Theta\Psi)\left[D_{MK}^{I*}\chi_\Omega\right] = I_{\eta'}(\Phi\Theta\Psi)\left[D_{MK}^{I*}\chi_\Omega\right]$$
$$= (\sin\Psi I_1+\cos\Psi I_2)\left[D_{MK}^{I*}\chi_\Omega\right] = \frac{1}{2i}\left[e^{i\Psi}I_{+'}-e^{-i\Psi}I_{-'}\right]\left[D_{MK}^{I*}\chi_\Omega\right], \qquad \text{(I-265)}$$

which in an analogous way, under Φ, Θ, Ψ -independence of χ_Ω leads to the alternative relation,

$$\frac{d\, d_{MK}^{I}(\Theta)}{d\,\Theta} = \frac{1}{2}\left[K_{IK}^{+}\, d_{MK-1}^{I}(\Theta) - K_{IK}^{-}\, d_{MK+1}^{I}(\Theta)\right], \qquad \text{(I-266)}$$

whence,
$$\dot{D}_{\mu\nu}^{\lambda*} = i(\mu\dot{\Phi}+\nu\dot{\Psi})D_{\mu\nu}^{\lambda*} + \tfrac{1}{2}\dot{\Theta}\left(e^{-i\Phi}K_{\lambda\mu}^{-}D_{\mu+1\,\nu}^{\lambda*} - e^{i\Phi}K_{\lambda\mu}^{+}D_{\mu-1\,\nu}^{\lambda*}\right)$$
$$= i(\mu\dot{\Phi}+\nu\dot{\Psi})D_{\mu\nu}^{\lambda*} + \tfrac{1}{2}\dot{\Theta}\left(e^{i\Psi}K_{\lambda\nu}^{+}D_{\mu\,\nu-1}^{\lambda*} - e^{-i\Psi}K_{\lambda\nu}^{-}D_{\mu\,\nu+1}^{\lambda*}\right), \qquad \text{(I-267)}$$

or more succinctly,

$$\dot{D}^{\lambda *}_{\mu\nu} = \left(D^{\lambda *}_{\mu+1\,\nu} \; D^{\lambda *}_{\mu\nu} \; D^{\lambda *}_{\mu-1\,\nu} \right) \begin{pmatrix} 0 & \frac{1}{2} e^{-i\Phi} K^{-}_{\lambda\mu} & 0 \\ i\mu & 0 & i\nu \\ 0 & -\frac{1}{2} e^{i\Phi} K^{+}_{\lambda\mu} & 0 \end{pmatrix} \begin{pmatrix} \dot{\Phi} \\ \dot{\Theta} \\ \dot{\Psi} \end{pmatrix} \tag{I-268}$$

$$= \left(D^{\lambda *}_{\mu\nu+1} \; D^{\lambda *}_{\mu\nu} \; D^{\lambda *}_{\mu\nu-1} \right) \begin{pmatrix} 0 & -\frac{1}{2} e^{-i\Psi} K^{-}_{\lambda\nu} & 0 \\ i\mu & 0 & i\nu \\ 0 & \frac{1}{2} e^{i\Psi} K^{+}_{\lambda\nu} & 0 \end{pmatrix} \begin{pmatrix} \dot{\Phi} \\ \dot{\Theta} \\ \dot{\Psi} \end{pmatrix}$$

From the Euler geometrical equations in this form,

$$\begin{pmatrix} \dot{\Phi} \\ \dot{\Theta} \\ \dot{\Psi} \end{pmatrix} = \begin{pmatrix} -\frac{\cos\Psi}{\sin\Theta} & \frac{\sin\Psi}{\sin\Theta} & 0 \\ \sin\Psi & \cos\Psi & 0 \\ \frac{\cos\Psi}{\tan\Theta} & -\frac{\sin\Psi}{\tan\Theta} & 1 \end{pmatrix} \begin{pmatrix} \Omega_1 \\ \Omega_2 \\ \Omega_3 \end{pmatrix} \tag{I-269}$$

one can get $\dot{D}^{\lambda *}_{\mu\nu}$ in terms of the body components of the angular velocity of the body frame as seen from the space frame. Substituting into the rotational term of the Hamiltonian gives

$$T^R_\lambda = \frac{1}{2} B_\lambda \sum_\mu \sum_\nu \sum_\rho (\Omega_1 \Omega_2 \Omega_3) \begin{pmatrix} -\frac{\cos\Psi}{\sin\Theta} & \sin\Psi & \frac{\cos\Psi}{\tan\Theta} \\ \frac{\sin\Psi}{\sin\Theta} & \cos\Psi & -\frac{\sin\Psi}{\tan\Theta} \\ 0 & 0 & 1 \end{pmatrix} \begin{pmatrix} 0 & -i\mu & 0 \\ -\frac{1}{2} e^{i\Psi} K^{-}_{\lambda\rho} & 0 & \frac{1}{2} e^{-i\Psi} K^{+}_{\lambda\rho} \\ 0 & -i\rho & 0 \end{pmatrix}$$

$$\times \begin{pmatrix} D^{\lambda}_{\mu\rho+1} D^{\lambda *}_{\mu\nu+1} & D^{\lambda}_{\mu\rho+1} D^{\lambda *}_{\mu\nu} & D^{\lambda}_{\mu\rho+1} D^{\lambda *}_{\mu\nu-1} \\ D^{\lambda}_{\mu\rho} D^{\lambda *}_{\mu\nu+1} & D^{\lambda}_{\mu\rho} D^{\lambda *}_{\mu\nu} & D^{\lambda}_{\mu\rho} D^{\lambda *}_{\mu\nu-1} \\ D^{\lambda}_{\mu\rho-1} D^{\lambda *}_{\mu\nu+1} & D^{\lambda}_{\mu\rho-1} D^{\lambda *}_{\mu\nu} & D^{\lambda}_{\mu\rho-1} D^{\lambda *}_{\mu\nu-1} \end{pmatrix} \begin{pmatrix} 0 & -\frac{1}{2} e^{-i\Psi} K^{-}_{\lambda\nu} & 0 \\ i\mu & 0 & i\nu \\ 0 & \frac{1}{2} e^{i\Psi} K^{+}_{\lambda\nu} & 0 \end{pmatrix} \tag{I-270}$$

$$\times \begin{pmatrix} -\frac{\cos\Psi}{\sin\Theta} & \frac{\sin\Psi}{\sin\Theta} & 0 \\ \sin\Psi & \cos\Psi & 0 \\ \frac{\cos\Psi}{\tan\Theta} & -\frac{\sin\Psi}{\tan\Theta} & 1 \end{pmatrix} \begin{pmatrix} \Omega_1 \\ \Omega_2 \\ \Omega_3 \end{pmatrix} a^*_{\lambda\nu} \, a_{\lambda\rho}$$

$$\equiv \frac{1}{2} B_\lambda \sum_\mu \sum_\nu \sum_\rho \Omega^+ A^+ B^+_{\lambda\mu\rho} \mathcal{D}_{\lambda\mu\rho\nu} B_{\lambda\mu\nu} A \Omega \, a^*_{\lambda\nu} \, a_{\lambda\rho}$$

$$= \frac{1}{2} B_\lambda \Omega^+ A^+ \Big[\sum_\mu \sum_\rho B^+_{\lambda\mu\rho} \sum_\nu \mathcal{D}_{\lambda\mu\rho\nu} B_{\lambda\mu\nu} \, a^*_{\lambda\nu} \, a_{\lambda\rho} \Big] A \Omega .$$

At this point generally one can set to advantage, with no loss of generality,

$$a^*_{\lambda\rho} = \beta_\lambda \epsilon_{\lambda\rho}, \quad \beta_\lambda \text{ real}, \quad \sum_\rho |\epsilon_{\lambda\rho}|^2 = 1 \ . \tag{I-271}$$

$\sum_\nu \sum_\rho \sum_\mu A^+ B^+_{\lambda\mu\rho} \mathcal{D}_{\lambda\mu\rho\nu} B_{\lambda\mu\nu} A \, a_{\lambda\rho} \, a^*_{\lambda\nu}$ must be diagonalized by a suitable choice of $\epsilon_{\lambda\rho}$, which is tantamount to specifying (Φ, Θ, Ψ) $(\Phi_\lambda, \Theta_\lambda, \Psi_\lambda)$, in general different for each λ, for rotation to a principal-axis body frame. Symmetry requirements on the wave functions, which are connected with the non-uniqueness in the choice of body frames will be treated below. For the case of a constant rotating shape, the β_λ, $\epsilon_{\lambda\rho}$ may be chosen independent of time. It is also necessary if T^R is to have meaning as a rotational Hamiltonian that the Φ, Θ, Ψ-dependence of the various matrices be eliminated upon performing the μ, ρ, ν sums. The manner of the emergence of a rotational term from the surface-energy model of collective motion, with the $a^*_{\lambda\mu}$ (or β_λ, $\epsilon_{\lambda\rho}$)-dependence of elements of the inertia tensor implied in the phenomenological "centrifugal stretch" calculation, is thus displayed.

The vibrational term of T is much easier to treat.

$$\begin{aligned} T^V_\lambda &= \tfrac{1}{2} B_\lambda \sum_\mu \sum_\nu \sum_\rho D^\lambda_{\mu\rho} D^{\lambda *}_{\mu\nu} \, \dot{a}_{\lambda\rho} \, \dot{a}^*_{\lambda\nu} \\ &= \tfrac{1}{2} B_\lambda \sum_\nu \sum_\rho \dot{a}_{\lambda\rho} \, \dot{a}^*_{\lambda\nu} \sum_\mu D^\lambda_{\mu\rho} D^{\lambda *}_{\mu\nu} \\ &= \tfrac{1}{2} B_\lambda \sum_\nu |\dot{a}_{\lambda\nu}|^2 \end{aligned} \tag{I-272}$$

With $a^*_{\lambda\rho} = \beta_\lambda \epsilon_{\lambda\rho}$, as above, and noting $\sum_\nu \mathcal{Re}\, \epsilon^*_{\lambda\nu} \dot{\epsilon}_{\lambda\nu} = \sum_\nu \frac{1}{2} \frac{d}{dt} \epsilon_{\lambda\nu} \epsilon^*_{\lambda\nu} = 0$, one has

$$T^V_\lambda = \tfrac{1}{2} B_\lambda \left[\dot{\beta}^2_\lambda + \beta^2_\lambda \sum_\nu |\dot{\epsilon}_{\lambda\nu}|^2 \right] \ . \tag{I-273}$$

For a rigid quadrupole surface the conventional choice of parameters is $a_{2,\pm1} = 0$, $a_{2,\pm2} = \frac{\beta \sin\gamma}{\sqrt{2}}$, $a_{20} = \beta\cos\gamma$, whence

$$T_2^{V} = \frac{1}{2} B_2\left(\dot{\beta}^2 + \beta^2\dot{\gamma}^2\right) . \tag{I-274}$$

For a specific situation, for example a rigid body or a non-viscous incompressible fluid in irrotational flow or, as experimental data in the rotational regions seem to indicate, the somewhat intermediate case of actual deformed nuclei, whenever the rotational term has Euler-angle-independent and time-independent inertia tensor components these two terms comprise the collective part of the zero-order rotational model Hamiltonians commonly expounded. For quadrupole deformations,

$$T_2^{V} + T_2^{R} = \frac{1}{2} B_2\left(\dot{\beta}^2 + \beta^2\dot{\gamma}^2\right) + \sum_{\nu} \frac{R_\nu^2}{2\mathcal{I}_\nu} . \tag{I-275}$$

The collective potential energy is generally given a form suitable for small deviations about an equilibrium shape specified by the equilibrium values β_0, $\gamma_0 = 0$:

$$V_2 = \frac{1}{2} C_2^{\beta}(\beta - \beta_0)^2 + \frac{1}{2} C_2^{\gamma}\gamma^2 , \tag{I-276}$$

The model Hamiltonian is of the form

$$H_2 = \left[T_2^{V} + \frac{1}{2} C_2^{\beta}(\beta-\beta_0)^2 + \frac{1}{2}C_2^{\gamma}\gamma^2\right] + \left[H_{p'}^{(0)} + \bar{T}_R^{o(0)}\right] + t_R^{(0)} + \sum_{p} V_{V.P.}^{(p)} + T_{R.V.P.} + T_2^{V.R.} . \tag{I-277}$$

The first three terms constitute the zero-order vibrational Hamiltonian, $H_V^{(0)}$. The next two terms are the zero-order rotational and particle terms considered above (e.g.,(I-170), H^O), denoted here by $H_o^{(0)}$. $t_R^{(0)}$, as before ((I-170), t_R) refers to the Coriolis term $-\frac{\hbar^2}{2\mathcal{J}^{(0)}}\left[I_{+'}j_{-'}+I_{-'}j_{+'}\right]$ (primes mean that $I_{\pm'}$ etc. are referred to body-frame axes.) $H_p'^{(0)}$ is given by $H_p'^{(0)} = \sum_p \left[T_p + V_p(\beta_o, \gamma_o; \vec{\pi}_p', \vec{l}_p', \vec{s}_p')\right] + \frac{\hbar^2}{2\mathcal{J}^{(0)}}\vec{j}'^2$ as before, but with equilibrium values of β and γ. Superscripts $^{(0)}$ denote that quantities are calculated using the equilibrium values of β and γ ; e.g. $\mathcal{J}_\nu^{(0)} = \mathcal{J}_\nu(\beta_o, \gamma_o)$. $\overline{T}_R^{o\,(o)} = T^{R\,(o)} - \frac{\hbar^2 j^2}{2\mathcal{J}^{(0)}}$, as before, where $T^{R\,(o)} = \sum_\nu \frac{R_\nu^2}{2\mathcal{J}_\nu^{(0)}}$. The perturbations neglected in the zero-order Hamiltonian, aside from the Coriolis term $t_R^{(0)}$, are the vibration-rotation terms arising from the $\alpha_{\lambda\mu}$-to-$a_{\lambda\mu}$ transformation, $T_2^{v.r}$; terms correcting for the use of equilibrium values β_o, γ_o in $H_p'^{(0)}$, $V_{v.p.}^p$; and terms correcting for the use of β_o , γ_o in the inertia moments $\mathcal{J}_\nu^{(o)}$. The neglected vibration-rotation terms $T_2^{v.r}$, which may be expected to produce the most significant perturbations, would be present in the absence of any significant β- and γ-dependence of $\mathcal{J}_\nu$, or in the case of the use of exact $\mathcal{J}_\nu(\beta, \gamma)$ in the rotation terms $\overline{T}_R^o + t_R$. The vibrational potential term $(1/2)C_2^\beta(\beta - \beta_o)^2$ has been altered from that in the spherical case in a somewhat ad hoc manner to suit expected conditions.

Then, with neglect of vibration-rotation interactions and β, γ-dependence of $\mathcal{J}_\nu$, the zero-order plus Coriolis terms of the Hamiltonian for a spheroidal-core-plus-particles model with vibrations is

$$H_2^{(0)} = \frac{1}{2}B_2(\dot{\beta}^2 + \beta^2\dot{\gamma}^2) + \frac{1}{2}C_2^\beta(\beta-\beta_o)^2 + \frac{1}{2}C_2^\gamma\gamma^2 + H_p'^{(0)} + \overline{T}_R^{o(o)} + t_R \quad (I\text{-}278)$$

Quantization* in $\beta-\gamma-\Phi-\Theta-\Psi$ space leads to

$$T_2^{\,v} = \frac{-\hbar^2}{2B_2}\left[\frac{1}{\beta}+\frac{\partial}{\partial\beta}\beta^4\frac{\partial}{\partial\beta}+\frac{1}{\beta^2\sin 3\gamma}\frac{\partial}{\partial\gamma}\left(\sin 3\gamma\frac{\partial}{\partial\gamma}\right)\right] \equiv T_\beta + \frac{T_\gamma}{\beta^2} \quad \text{(I-279)}$$

The separation of the $H_2^{(0)}$ eigenvalue problem, without the Coriolis term, depends on the assumed β- and γ-dependence of $\mathcal{I}_\nu$. For example** the use of irrotational moments $\mathcal{I}_\nu^{\,irr} = 4B_2\beta^2\sin^2(\gamma-2\pi\nu/3)$ allows a separation of $H_2^{(0)}$ with exact $\mathcal{I}_\nu(\beta,\gamma)$ used in $\overline{T}_R^{\,0}+\not{t}_R$. The nature of the vibrational functions will depend on the method of handling $\mathcal{I}_\nu(\beta,\gamma)$ and the kind of exact or approximate separations resulting.

As examples, following Davidson[217] somewhat, with T_β and T_γ as given above, and noting that in general the inertia moments $\mathcal{I}_\nu$ are functions of β and γ, separations in irrotational and "quasi-rigid" situations will be examined. One has***

$$\left[T_\beta+\frac{T_\gamma}{\beta^2}+V_\beta+V_\gamma+\sum_\nu\frac{(I_\nu-j_\nu)^2}{2\mathcal{I}_\nu(\beta,\gamma)}+H_p(\vec{r}_p^{\,\prime};\beta,\gamma)\right]\Psi = E\,\Psi \quad . \quad \text{(I-280)}$$

Here $V_\beta = (1/2)C_2^\beta(\beta-\beta_0)^2$, $V_\gamma = (1/2)C_2^\gamma\gamma^2$, typically. Approximating H_p by $H_p^{(0)}(\vec{r}_p^{\,\prime}) \equiv H_p(\vec{r}_p^{\,\prime};\beta_0,\gamma_0)$, and calling the approximate E,Ψ, E^0 and Ψ^0, for the irrotational flow case one can make separations as follows[217]:

$$\Psi^0(\beta,\gamma,\Phi,\Theta,\Psi,\vec{r}_p^{\,\prime}) = \Psi_1^0(\beta,\vec{r}_p^{\,\prime})\,\Psi_2^0(\gamma,\Phi,\Theta,\Psi) \quad \text{(I-281)}$$

$$\frac{\left(\beta^2T_\beta+\beta^2V_\beta+\beta^2H_p^{(0)}(\vec{r}_p^{\,\prime})-\beta^2E^0\right)\Psi_1^0}{\Psi_1^0} = -\frac{\left(T_\gamma+B^2V_\gamma+\sum_\nu\frac{(I_\nu-j_\nu)^2}{2\mathcal{J}_\nu^{irr}(\gamma)}\right)\Psi_2^0}{\Psi_2^0} \equiv \frac{\hbar^2\Lambda}{2B_2} \quad \text{(I-282)}$$

*See e.g. J.P.D.[217], p. 114

**See e.g. M. A. Preston[32], p. 237

***See e.g. J.P.D.[217], equation (II-14)

Here $\mathcal{J}_\nu^{irr}(\gamma) = \frac{\mathcal{I}_\nu^{irr}(\beta,\gamma)}{\beta^2} = 4B_2\sin^2(\gamma - 2\pi\nu/3)$. If $\beta^2 V_\gamma$ is approximated by $\beta_0^{\,2}V_\gamma$, then each fraction is a function of only its own independent variables and $\hbar^2\Lambda/2B_2$ must be a constant. Treating the rotational terms as in the rotational formalism expounded above leads to

$$\left[T_\beta + V_\beta + H_p^{\prime(0)}(\vec{\pi}_p^{\,\prime}) - \frac{\hbar^2\Lambda}{2B_2\beta^2}\right]\Psi_1^{\circ} = E^{\circ}\,\Psi_1^{\circ} \tag{I-283}$$

$$\left[T_\gamma + V_\gamma + \bar{\tilde{T}}_R^{\circ(0)} + \tilde{\mathcal{Z}}_R^{(0)}\right]\Psi_2^{\circ} = -\frac{\hbar^2\Lambda}{2B_2}\Psi_2^{\circ} \quad . \tag{I-284}$$

As before, the prime on H_p denotes that the term proportional to $\vec{j}^{\,2}$ has been transferred thereto, and the bar on $\bar{\tilde{T}}_R^{\circ(0)}$, that it has been removed therefrom. The $^{\circ}$ denotes absence of the Coriolis term $\tilde{\mathcal{Z}}_R^{(0)}$, the $^{(0)}$, the use of equilibrium deformation values of the inertia moments, and the $\sim$, the use of $\mathcal{J}_\nu(\gamma_0) = \frac{\mathcal{I}_\nu(\beta_0,\gamma_0)}{\beta_0^{\,2}} \equiv \mathcal{J}_\nu^{(0)}$ in all the rotational expressions, which appears to be a feature in this kind of separation. The first equation separates again, with $E^{\circ} = E_{\beta\Lambda} + \epsilon$; with ϵ the separation constant:

$$\Psi_1^{\circ}(\beta, \vec{\pi}_p^{\,\prime}) = \phi(\beta)\,\chi(\vec{\pi}_p^{\,\prime}) \tag{I-285}$$

$$\frac{\left[T_\beta + V_\beta - \frac{\hbar^2\Lambda}{2B_2\beta^2} - E^{\circ}\right]\phi}{\phi} = -\frac{\left[H_p^{\prime(0)}(\vec{\pi}_p^{\,\prime})\right]\chi}{\chi} \equiv -\epsilon \tag{I-286}$$

$$\left[T_\beta + V_\beta - \frac{\hbar^2\Lambda}{2B_2\beta^2}\right]\phi = E_{\beta\Lambda}\,\phi \tag{I-287}$$

$$H_p^{\prime(0)}(\vec{\pi}_p^{\,\prime})\,\chi = \epsilon\,\chi\,.$$

These give the equations for β-vibrations and the single-particle motions. The second equation separates only if the Coriolis term $\tilde{\mathcal{Z}}_R^{(0)}$ is neglected, whence

$$\Psi_2^{\,o}(\gamma,\Phi,\Theta,\Psi) = g(\gamma)\,\mathcal{D}(\Phi,\Theta,\Psi) \tag{I-288}$$

$$\frac{\left[T_\gamma + \beta_0^2 V_\gamma + \frac{\hbar^2\Lambda}{2B_2}\right] g}{g} = -\frac{\tilde{T}_R^{\,o(o)}\,\mathcal{D}}{\mathcal{D}} = -\tilde{E}_R^{\,o(o)} \tag{I-289}$$

$$(T_\gamma + \beta_0^2 V_\gamma)\, g = E_\gamma\, g \tag{I-290}$$

$$\tilde{T}_R^{\,o(o)}\,\mathcal{D} = \tilde{E}_R^{\,o(o)}\,\mathcal{D} \;.$$

Here $E_\gamma + \tilde{E}_R^{o(o)} = -\hbar^2\Lambda/2B_2$, and the vibrational and the rotational energies are reflected in E^0 via $E_{\beta\Lambda}$. The wave function is of the form $\Psi^{\,o} = \phi(\beta)\,g(\gamma)\,\mathcal{D}(\Phi,\Theta,\Psi)\,\chi(\vec{\pi}_p{}')$, and the usual kind of vibration-rotation-particle picture emerges.

In the "quasi-rigid" case, one may take $\mathcal{I}_{1,2}(\beta,\gamma) \approx \mathcal{I}_{1,2}(\beta_0,\gamma_0) \equiv \mathcal{I}_{1,2}(\beta_0, 0) \equiv \mathcal{I}^{(0)}$; $\mathcal{I}_3(\beta,\gamma) \approx \mathcal{I}_3(\beta_0,\gamma) \equiv \mathcal{I}_3^{(0)}(\gamma)$. For a rigid axially-symmetric body, $\mathcal{I}^{(0)\,\mathrm{rig}} = 3B_2^{\mathrm{rig}}\beta_0^{\,2}$, and $\mathcal{I}_3^{(0)}$ is approximately independent of γ. (In the irrotational case $\mathcal{I}^{(0)} = 3B_2^{\mathrm{irr}}\beta^2 \approx 3B_2^{\mathrm{irr}}\,\beta_0^{\,2}$, $B_2^{\mathrm{irr}} \ll B_2^{\mathrm{rig}}$, and $\mathcal{I}_3^{(0)}(\gamma) \approx 4B_2^{\mathrm{irr}}\beta_0^{\,2}\gamma^{\,2} \equiv 4B_2^{\gamma}\gamma^2$ and is typically very small, and zero at equilibrium.) Again using $H_p^{(0)}(\vec{\pi}_p{}') \equiv H_p(\vec{\pi}_p{}'; \beta_0, \gamma_0)$, but $T_\gamma/\beta^2 \approx T_\gamma/\beta_0^{\,2}$ and the equilibrium inertia moments, one has

$$\left[T_\beta + \frac{T_\gamma}{\beta_0^2} + V_\beta + V_\gamma + \sum_\nu \frac{(I_\nu - j_\nu)^2}{2\mathcal{I}_\nu^{(0)}} + H_p^{(0)}(\vec{\pi}_p{}')\right]\Psi^{\,o} = E^{\,o}\,\Psi^{\,o}, \tag{I-291}$$

or, as previously, with $\bar{T}_R^{\,0\,(0)} = \frac{1}{2\mathcal{I}^{(0)}}(I^2 - I_3^2 - j_3^2) + \frac{1}{2\mathcal{I}_3^{(0)}(\gamma)}(I_3 - j_3)^2$, $t_R^{(0)} = -\frac{1}{2\mathcal{I}^{(0)}}(I_{+'}j_{-'} + I_{-'}j_{+'})$, $H_p'^{\,(0)} = H_p^{(0)} + \frac{1}{2\mathcal{I}^{(0)}}\vec{j}^{\,2}$, this equation separates if $t_R^{(0)}$ is neglected, but due to the use of $T_\gamma/\beta_0^{\,2}$ in lieu of T_γ/β^2, in a somewhat different manner:

$$\Psi^{\,o}(\beta,\gamma,\Phi,\Theta,\Psi,\vec{\pi}_p{}') = \Psi_a(\beta,\gamma)\,\Psi_b(\Phi,\Theta,\Psi,\vec{\pi}_p{}') \tag{I-292}$$

$$\frac{\left[T_\beta+V_\beta+\frac{T_\gamma}{\beta_0^2}+V_\gamma+\frac{(K-\Omega)^2}{2\mathcal{I}_3^{(0)}(\gamma)}\right]\Psi_a}{\Psi_a}+\frac{1}{2\mathcal{I}^{(0)}}\left[I(I+1)-K^2-\Omega^2\right]+\epsilon_\Omega=E^\circ \qquad \text{(I-293)}$$

$$\left[T_\beta+V_\beta+\frac{T_\gamma}{\beta_0^2}+V_\gamma+\frac{(K-\Omega)^2}{2\mathcal{I}_3^{(0)}(\gamma)}\right]\Psi_a=E_{vK\Omega}\Psi_a . \qquad \text{(I-294)}$$

Here the vibrational energy appears explicitly: $E_{vK\Omega}+E^{o(0)}_{IK\Omega}+\epsilon_\Omega=E^O$, along with the usual rotational and particle equations. Further separation is possible immediately:

$$\Psi_a(\beta,\gamma)=\phi(\beta)\,g(\gamma) \qquad \text{(I-295)}$$

$$\left[T_\beta+V_\beta\right]\phi=E_\beta\phi\ ; \qquad \text{(I-296)}$$

$$\left[\frac{T_\gamma}{\beta_0^2}+V_\gamma+\frac{(K-\Omega)^2}{2\mathcal{I}_3^{(0)}(\gamma)}\right]g=E_{\gamma K\Omega}\,g$$

$$E_{\gamma K\Omega}+E_\beta=E_{vK\Omega}. \qquad \text{(I-297)}$$

Now $T_\beta=\frac{-\hbar^2}{2B_2}\frac{1}{\beta^4}\frac{\partial}{\partial\beta}\beta^4\frac{\partial}{\partial\beta}=-\frac{\hbar^2}{2B_2}\left(\frac{4}{\beta}+\frac{\partial^2}{\partial\beta^2}\right)=-\frac{\hbar^2}{2B_2}\frac{4}{\beta_0+\beta'}\frac{\partial}{\partial\beta'}+\frac{\partial^2}{\partial\beta'^2}\approx\frac{-\hbar^2}{2B_2}\left(\frac{4}{\beta_0}\frac{\partial}{\partial\beta'}+\frac{\partial^2}{\partial\beta'^2}\right)$; for small equilibrium deformations, and acting on not-too-rapidly varying functions, this operator is approximated by $-\frac{\hbar^2}{2B_2}\frac{\partial^2}{\partial\beta'^2}$, whence the β-vibration resembles that of a one-dimensional oscillator (J.P.D., equation II-25) which, with a harmonic potential $(1/2)C_2^\beta(\beta-\beta_0)^2=(1/2)C_2^\beta\beta'^2$, has the energy spectrum $E_\beta=\hbar\omega_\beta(n_\beta+1/2)$, $n_\beta=0,1,2,3,\ldots$ Also, for small deviations from axial symmetry, one has T_γ/β_0^2 $=\frac{-\hbar^2}{2B_2\beta_0^2}\frac{1}{\sin 3\gamma}\frac{\partial}{\partial\gamma}\sin 3\gamma\frac{\partial}{\partial\gamma}\approx\frac{-\hbar^2}{2B_2\beta_0^2}\frac{1}{\gamma}\frac{\partial}{\partial\gamma}\gamma\frac{\partial}{\partial\gamma}$ characteristic of a two-dimensional oscillator. With a harmonic potential (1/2) $\times C_2^\gamma\gamma^2$ and neglect of γ-dependence of $\mathcal{I}_3^{(0)}$, this can be shown to have the spectrum (J.P.D., equation II-26): $E_\gamma=\hbar\omega_\gamma(n_\gamma+1)$, $n_\gamma=(1/2)\left|K-\Omega\right|+2N$, $N=0,1,2,3,\ldots$:

$$\left(\frac{T_\gamma}{\beta_0^2}+V_\gamma\right)g=\left(E_\gamma-\frac{(K-\Omega)^2}{2\mathcal{I}_3^{(0)}}\right)g\ . \qquad \text{(I-298)}$$

From symmetry considerations $K-\Omega$ turns out to be even; for the lowest vibrational states, $K=\Omega \pm 2$, $(K-\Omega)^2 = 4$, and the energy in the g-equation is $E_\gamma - 2/\mathcal{I}_3^{(0)}$; $\mathcal{I}_3^{(0)}$ will not differ very much between the two γ-vibrational states with $|K-\Omega| = 2$, or $N = 0$, $n_\gamma = 1$, and energy differences will depend primarily on C_2^γ, which would reflect core polarizabilities for the two cases. The approximation of T_γ/β_0^2 is still present, causing neglect of β- and γ-band coupling (as does neglect of the Coriolis term). The zero-order problem is again separated in the usual way.

Experimental data indicate that for real nuclei, in which the inertia moments are between the rigid and irrotational values and not closely approximating either one, this kind of separation does occur, to a good degree of approximation.

As to the question of inclusion of centrifugal stretching in the present context, with vibrations included, one may set

$$\begin{aligned} \beta_0 &= \beta_0^{\circ}(1 + b_1 R^2 + b_2 R^4 + \dots) \\ \gamma_0 &= \gamma_0^{\circ}(1 + c_1 R^2 + c_2 R^4 + \dots) \; ; \end{aligned} \tag{I-299}$$

$$\begin{aligned} \mathcal{I}_\nu(\beta,\gamma) \approx \mathcal{I}_\nu(\beta_0,\gamma_0) &\equiv \mathcal{I}_\nu\left[\beta_0^{\circ}(1+b_1R^2+\dots),\ \gamma_0^{\circ}(1+c_1R^2+\dots)\right] \\ &= \mathcal{I}_\nu(\beta_0^{\circ},\gamma_0^{\circ})\left[1 + a_1^{(\nu)}R^2 + a_2^{(\nu)}R^4 + \dots\right] \end{aligned} \tag{I-300}$$

Also,

$$\mathcal{I}_\nu(\beta,\gamma) = \mathcal{I}_\nu(\beta_0,\gamma_0) + (\beta-\beta_0)\left.\frac{\partial \mathcal{I}_\nu}{\partial\beta}\right|_{\beta_0\gamma_0} + (\gamma-\gamma_0)\left.\frac{\partial \mathcal{I}_\nu}{\partial\gamma}\right|_{\beta_0\gamma_0} + \dots$$

$$\equiv \mathcal{I}_\nu(\beta_0,\gamma_0)+(\beta-\beta_0)\mathcal{I}_\nu^\beta(\beta_0,\gamma_0)+(\gamma-\gamma_0)\mathcal{I}_\nu^\gamma(\beta_0,\gamma_0)+\dots \qquad \text{(I-301)}$$

$$=\mathcal{I}_\nu(\beta_0^\circ,\gamma_0^\circ)(1+a_1^{(\nu)}R^2+\dots)+[\beta-\beta_0^\circ(1+b_1R^2+\dots)]\mathcal{I}_\nu^\beta(\beta_0^\circ,\gamma_0^\circ)(1+a_1^{(\beta\nu)}R^2+\dots)$$

$$+[\gamma-\gamma_0^\circ(1+c_1R^2+\dots)]\mathcal{I}_\nu^\gamma(\beta_0^\circ,\gamma_0^\circ)(1+a_1^{(\gamma\nu)}R^2+\dots)+\dots$$

Thus β- and γ-dependent perturbations are introduced, in addition to the R^{2n} terms of the previous pure rotational situation. With $\mathcal{I}_1(\beta_0^\circ,\gamma_0^\circ)=\mathcal{I}_2(\beta_0^\circ,\gamma_0^\circ)\equiv\mathcal{I}(\beta_0^\circ,\gamma_0^\circ)\equiv\mathcal{I}^{00}\neq\mathcal{I}_3(\beta_0^\circ,\gamma_0^\circ)\equiv\mathcal{I}_3^{00}$, there are effects on various terms in the model Hamiltonian. $V_\beta+V_\gamma$ becomes

$$\tfrac{1}{2}C_{2\beta}[\beta-\beta_0^\circ(1+b_1R^2+\dots)]^2+C_{2\beta}'[\beta-\beta_0^\circ(1+b_1R^2+\dots)]^3+\dots$$
$$+\tfrac{1}{2}C_{2\gamma}[\gamma-\gamma_0^\circ(1+c_1R^2+\dots)]^2+C_{2\gamma}'[\gamma-\gamma_0^\circ(1+c_1R^2+\dots)]^3+\dots$$
$$+C_{2\beta\gamma}'[\beta-\beta_0^\circ(1+b_1R^2+\dots)]^2[\gamma-\gamma_0^\circ(1+c_1R^2+\dots)]$$
$$+C_{2\gamma\beta}'[\beta-\beta_0^\circ(1+b_1R^2+\dots)][\gamma-\gamma_0^\circ(1+c_1R^2+\dots)]^2+\dots \qquad \text{(I-302)}$$

$$=\tfrac{1}{2}C_{2\beta}(\beta-\beta_0^\circ)^2+\tfrac{1}{2}C_{2\gamma}(\gamma-\gamma_0^\circ)^2+R^4\left[\frac{C_{2\beta}}{2}\beta_0^{\circ 2}b_1^2+\frac{C_{2\gamma}}{2}\gamma_0^{\circ 2}c_1^2\right]+R^2(\beta-\beta_0^\circ)[-C_{2\beta}\beta_0^\circ b_1]$$
$$+R^2(\gamma-\gamma_0^\circ)[-C_{2\gamma}\gamma_0^\circ c_1]+R^6[-C_{2\beta\beta}'\beta_0^{\circ 3}b_1^3-C_{2\beta\gamma}'\beta_0^\circ b_1c_1^2-C_{2\gamma\beta}'\beta_0^\circ\gamma_0^\circ b_1c_1^2-C_{2\gamma\gamma}'\gamma_0^{\circ 3}c_1^3]$$
$$+R^4(\beta-\beta_0^\circ)[-C_{2\beta}\beta_0^\circ b_2-3C_{2\beta\beta}'\beta_0^{\circ 2}b_1^2]+R^4(\gamma-\gamma_0^\circ)[-C_{2\gamma}\gamma_0^\circ c_2-3C_{2\gamma\gamma}'\gamma_0^{\circ 2}c_1^2]$$
$$+\{R^2(\beta-\beta_0^\circ)^2;\ R^2(\beta-\beta_0^\circ)(\gamma-\gamma_0^\circ);\ R^2(\gamma-\gamma_0^\circ)^2;\ (\beta-\beta_0^\circ)^3;\dots;(\gamma-\gamma_0^\circ)^3\ \text{terms}\}+\dots$$
$$\equiv\tfrac{1}{2}C_{2\beta}(\beta-\beta_0^\circ)^2+\tfrac{1}{2}C_{2\gamma}(\gamma-\gamma_0^\circ)^2+\sum_{\rho=2}^{\infty}\sum_{\sigma\tau}A_{\rho\sigma\tau}R^{2\rho}(\beta-\beta_0^\circ)^\sigma(\gamma-\gamma_0^\circ)^\tau.$$

$\sum_\nu \frac{R_\nu^2}{2\mathcal{I}_\nu(\beta\gamma)}$ becomes

$$\sum_\nu\frac{R_\nu^2}{2}\,1\Big/\left\{\mathcal{I}_\nu(\beta_0^\circ,\gamma_0^\circ)[1+a_1^{(\nu)}R^2+\dots]+\mathcal{I}_\nu^\beta(\beta_0^\circ,\gamma_0^\circ)[1+a_1^{(\nu\beta)}R^2+\dots](\beta-\beta_0)+\dots\right\}$$

$$=\sum_\nu\frac{R_\nu^2}{2\mathcal{I}_\nu(\beta_0^\circ,\gamma_0^\circ)}\,1\Big/\left\{1+a_1^{(\nu)}R^2+\dots+\frac{\mathcal{I}_\nu^\beta(\beta_0^\circ,\gamma_0^\circ)}{\mathcal{I}_\nu(\beta_0^\circ,\gamma_0^\circ)}\left[(\beta-\beta_0^\circ)(1+a_1^{(\nu\beta)}R^2+\dots)-\beta_0^\circ[b_1R^2+\dots]\right][1+a_1^{(\nu\beta)}R^2+\dots]+\dots\right\} \qquad \text{(I-303)}$$

The bracket can be shown to be

$$[\;] = 1\Big/\Big\{1+R^2\Big[a_1^{(\nu)} - \frac{\mathcal{Z}_\nu^\beta}{\mathcal{Z}_\nu}\beta_0^\circ b_1 - \frac{\mathcal{Z}_\nu^\gamma}{\mathcal{Z}_\nu}\gamma_0^\circ c_1\Big] + (\beta-\beta_0^\circ)\Big[\frac{\mathcal{Z}_\nu^\beta}{\mathcal{Z}_\nu}\Big] + (\gamma-\gamma_0^\circ)\Big[\frac{\mathcal{Z}_\nu^\gamma}{\mathcal{Z}_\nu}\Big]$$
$$+R^4\Big[a_1^{(\nu)} - \frac{\mathcal{Z}_\nu^\beta}{\mathcal{Z}_\nu}\beta_0^\circ b_1 a_1^{(\nu\beta)} - \frac{\mathcal{Z}_\nu^\gamma}{\mathcal{Z}_\nu}\gamma_0^\circ c_1 a_1^{(\nu\gamma)} + (\mathcal{Z}_\nu^{\beta\beta}; \mathcal{Z}_\nu^{\beta\gamma}; \mathcal{Z}_\nu^{\gamma\gamma}\text{ terms})\Big] + R^2(\beta-\beta_0^\circ)\Big[\frac{\mathcal{Z}_\nu^\beta}{\mathcal{Z}_\nu}a_1^{(\nu\beta)}\Big]$$
$$+R^2(\gamma-\gamma_0^\circ)\Big[\frac{\mathcal{Z}_\nu^\gamma}{\mathcal{Z}_\nu}a_1^{(\nu\gamma)}\Big] + (\beta-\beta_0^\circ)^2\Big[\mathcal{Z}_\nu^{\beta\beta}\text{terms}\Big] + (\beta-\beta_0^\circ)(\gamma-\gamma_0^\circ)\Big[\frac{\mathcal{Z}_\nu^\beta\mathcal{Z}_\nu^\gamma}{\mathcal{Z}_\nu^2}\Big] \qquad \text{(I-304)}$$
$$+(\gamma-\gamma_0^\circ)^2\Big[\mathcal{Z}_\nu^{\gamma\gamma}\text{terms}\Big] + \ldots\Big\} \equiv 1\Big/\Big\{\sum_{\rho\sigma\tau=0}^{\infty}\alpha_{\rho\sigma\tau}^{(\nu)}R^{2\rho}(\beta-\beta_0^\circ)^\sigma(\gamma-\gamma_0^\circ)^\tau\Big\}$$

which may be inverted:

$$[\;] = \sum_{\rho\sigma\tau=0}^{\infty} B_{\rho\sigma\tau}^{(\nu)} R^{2\rho}(\beta-\beta_0^\circ)^\sigma(\gamma-\gamma_0^\circ)^\tau, \quad B_{000}^{(\nu)} \equiv 1. \qquad \text{(I-305)}$$

Here $\rho+\sigma+\tau$ gives the "order" of the correction terms. The $\alpha_{\rho\sigma\tau}^{(\nu)}$ or $B_{\rho\sigma\tau}^{(\nu)}$ depend on $b_1, b_2, \ldots; c_1, c_2, \ldots$; and through $\mathcal{Z}_\nu(\beta, \gamma)$, on $a_1^{(\nu)}, a_2^{(\nu)}, \ldots; a_1^{(\nu\beta)}, a_2^{(\nu\beta)}, \ldots; a_1^{(\nu\gamma)}, a_2^{(\nu\gamma)}, \ldots;$ $a_j^{(\nu\beta\gamma)}, a_j^{(\nu\gamma\beta)}, a_j^{(\nu\gamma\gamma)}, a_j^{(\nu\beta\beta)}, \ldots$, the "model parameters", as do the $A_{\rho\sigma\tau}$.

The particle potential $V_p(\vec{\pi}_p'; \beta, \gamma)$ becomes

$$V_p(\vec{\pi}_p'; \beta,\gamma) = V_p(\vec{\pi}_p'; \beta_0, \gamma_0) + \frac{\partial V_p}{\partial\beta}\Big|_{\beta_0\gamma_0}(\beta-\beta_0) + \frac{\partial V_p}{\partial\gamma}\Big|_{\beta_0\gamma_0}(\gamma-\gamma_0) + \ldots \qquad \text{(I-306)}$$
$$\equiv V_p(\vec{\pi}_p'; \beta_0, \gamma_0) + V_p^\beta(\vec{\pi}_p'; \beta_0, \gamma_0)(\beta-\beta_0) + V_p^\gamma(\vec{\pi}_p'; \beta_0, \gamma_0)(\gamma-\gamma_0) + \ldots$$

This, in an analogous way, becomes

$$V_p(\vec{\pi}_p'; \beta, \gamma) = V_p(\vec{\pi}_p'; \beta_0^\circ, \gamma_0^\circ)\sum_{\rho\sigma\tau=0}^{\infty} C_{\rho\sigma\tau}R^{2\rho}(\beta-\beta_0^\circ)^\sigma(\gamma-\gamma_0^\circ)^\tau; \; C_{000} = 1. \qquad \text{(I-307)}$$

Two things are at once apparent: the number of model parameters inherent in the quantities $A_{\rho\sigma\tau}, B_{\rho\sigma\tau}, C_{\rho\sigma\tau}$ is rather too large to permit a meaningful disentanglement of effects mirrored in "experimental" values of these quantities, and the perturbation terms are all of like form, and occur additively in factors multiplying the zero-order terms.

Thus the same situation with regard to these perturbations pertains as before, with β_0, γ_0 replaced by β_0^o, γ_0^o, except for the appearance of new rotation-vibration cross terms. The $(\vec{I}\cdot\vec{j})^3$ perturbation requires a second-order perturbation term R^4 on the eigenstates of $\overline{T}_R^{o(o)}$, and produces $K = 3/2$-band decoupling in the third order of perturbation theory. Third-order R^6 corrections to $V_v(\beta - \beta_0^o, \gamma - \gamma_0^o)$ and $V_p(\vec{\eta}_p; \beta_0^o, \gamma_0^o)$ will contribute to this, and higher-order cross terms of form $R^6(\beta - \beta_0^o)^\sigma(\gamma - \gamma_0^o)^\tau$ will cause "renormalizations" by mixing in vibrational states. To this order, $(\beta - \beta_0^o)^3$, $(\beta - \beta_0^o)^2(\gamma - \gamma_0^o)$, $(\beta - \beta_0^o)^2R^2$, $(\beta - \beta_0^o)^4$, $(\beta - \beta_0^o)^3(\gamma - \gamma_0^o)$, $(\beta - \beta_0^o)^2(\gamma - \gamma_0^o)^2$, $(\beta - \beta_0^o)^3R^2$, $(\beta - \beta_0^o)^2(\gamma - \gamma_0^o)R^2$, and $(\beta - \beta_0^o)^2R^4$ terms are added to a harmonic β-potential; analogous terms to a harmonic γ-potential and to rotational terms, but with a $(\beta - \beta_0^o)$ factor replaced by $(\gamma - \gamma_0^o)$, R^2 or R_3^2. These contribute to vibration-rotation interactions and vibrational anharmonicities. The main vibration-rotation interaction terms are still those neglected in the $\alpha_{\lambda\mu}$-to-$a_{\lambda\nu}$ transformation. Various "collective-particle" couplings arising from non-adiabaticity are included in V_p, but probably will be minor compared to the Coriolis coupling. At best the situation is exceedingly complex, but essentially unaltered in its important fundamental aspects.

The symmetry properties in the presence of the vibrational wave function are treated quite readily. Following arguments in Preston[32], wave functions of principal-axis body-frame coordinates must be invariant under three kinds of rotations of the body frame: R_1, a rotation of 180° about the "2"-axis (the "1"-axis would do as well); R_2, a 90° rotation about the "3"-axis; and R_3, a cyclic permutation of axes. This requirement arises from the fact that a principal-axis frame (of the same handedness as the space frame) may be chosen in 24 different ways for the same body orientation, all of which are connected by transformations comprised of a product of powers of R_1, R_2 and R_3, and the necessity for the wave function to be invariant under transformations among these 24 body frames in order to be single valued. In addition, for axial symmetry, invariance (except for overall phase changes) is required for arbitrary rotations of the body frame about the symmetry axis, taken customarily as the "3"-axis.

5. R_1-Invariance

In the case of even-even nuclei the unsymmetrized wave function is of the form, for axial symmetry,

$$|IMKn_\beta n_\gamma\rangle = f_{IK}^{n_\beta n_\gamma}(\beta,\gamma)\, D_{MK}^{I*}(\Phi,\Theta,\Psi) . \qquad \text{(I-308)}$$

The effect of R_1, transforming from 1,2,3 axes to, say, new body-frame 1',2',3' axes, can be written in two ways:

$$\begin{aligned} R_1|IMKn_\beta n_\gamma\rangle &= f_{I-K}^{n_\beta n_\gamma}(\beta',\gamma')\, D_{M-K}^{I*}(\Phi,\Theta,\Psi) \\ &\equiv f_{I-K}^{n_\beta n_\gamma}(\beta,\gamma)\, D_{M-K}^{I*}(\Phi,\Theta,\Psi) , \end{aligned} \qquad \text{(I-309)}$$

wherein the K-component of angular momentum in the new frame is of course reversed, and the corresponding reversal of the nuclear orientation with respect to the new body frame is given by changing β and γ but keeping Φ, Θ, Ψ the same, and noting that as it turns out, $\beta = \beta'$, $\gamma = \gamma'$; and

$$R_1 \left| IMKn_\beta n_\gamma \right\rangle = f_{IK}^{n_\beta n_\gamma}(\beta,\gamma) D_{MK}^{I*}(\Phi',\Theta',\Psi') \tag{I-310}$$

$$= f_{IK}^{n_\beta n_\gamma}(\beta,\gamma) D_{MK}^{I*}(\pi+\Phi, \pi-\Theta, 2\pi-\Psi) = f_{IK}^{n_\beta n_\gamma}(\beta,\gamma)(-1)^I D_{M-K}^{I*}(\Phi,\Theta,\Psi),$$

where the vibrational function is retained but the Euler angles for a rotation to the new orientation in the new body frame, (Φ', Θ', Ψ'), are used. Comparison yields the result

$$f_{I-K}^{n_\beta n_\gamma}(\beta,\gamma) = (-1)^I f_{IK}^{n_\beta n_\gamma}(\beta,\gamma) \, . \tag{I-311}$$

Thus if $K = 0$, I can only be an even integer. Since $R_1{}^2 = 1$, the function invariant under R_1 is

$$(1+R_1)\left| IMKn_\beta n_\gamma \right\rangle = \left| IMKn_\beta n_\gamma{}^s \right\rangle$$
$$= f_{IK}^{n_\beta n_\gamma}(\beta,\gamma)\left[D_{MK}^{I*}(\Phi\Theta\Psi) + (-1)^I D_{M-K}^{I*}(\Phi\Theta\Psi)\right] \tag{I-312}$$

which, as required, vanishes if $K = 0$ and I is odd. Also, applying (I-310) twice, one finds $R_1{}^2 \left| IMKn_\beta n_\gamma \right\rangle = (-1)^{2I} \left| IMKn_\beta n_\gamma \right\rangle$, from which, because $R_1{}^2 = 1$, I can only be an integer. For the corresponding odd-A case, the unsymmetrized wave function is

$$\left| IMK\Omega n_\beta n_\gamma \right\rangle = f_{IK\Omega}^{n_\beta n_\gamma} D_{MK}^{I*}(\Phi\Theta\Psi)\chi_\Omega(\vec{r}_p{}') \tag{I-313}$$

where the intrinsic function is taken as a Nilsson state:

$$\chi_\Omega(\vec{r}_p{}') \equiv \chi_\Omega(\theta_p', \varphi_p') = \sum_j C_{j\Omega}\chi_{j\Omega}(\theta_p', \varphi_p') = \sum_j C_{j\Omega}\sum_m D_{m\Omega}^j(\Phi\Theta\Psi)\chi_{jm}(\theta_p, \varphi_p);$$
$$C_{j-\Omega} = (-1)^{\frac{1}{2}-j}\pi_\chi C_{j\Omega} \, . \tag{I-314}$$

Here $\chi_{jm}(\theta',\varphi')$, $\chi_{jm}(\theta,\varphi)$ are the usual angular-momentum eigenstates in the body and space frames respectively. Then the effects of R_1, which do not affect any space-frame functions, are expressible alternatively as

$$R_1|IMK\Omega n_\beta n_\gamma\rangle = f^{n_\beta n_\gamma}_{IK\Omega}(\beta,\gamma)D^{I*}_{MK}(\pi+\Phi,\pi-\Theta,2\pi-\Psi)\sum_j C_{j\Omega}\sum_m D^{j}_{m\Omega}(\pi+\Phi,\pi-\Theta,2\pi-\Psi)\chi_{jm}(\theta_p,\varphi_p)$$

$$= f^{n_\beta n_\gamma}_{IK\Omega}(\beta,\gamma)(-1)^I D^{I*}_{M-K}(\Phi,\Theta,\Psi)\sum_j(-1)^{j-\frac{1}{2}}\pi_\chi C_{j-\Omega}\sum_m(-1)^{-j}D^{j}_{m-\Omega}(\Phi,\Theta,\Psi)\chi_{jm}(\theta_p,\varphi_p) \quad \text{(I-315)}$$

$$= (-1)^{I-\frac{1}{2}}\pi_\chi f^{n_\beta n_\gamma}_{IK\Omega}(\beta,\gamma)D^{I*}_{M-K}(\Phi,\Theta,\Psi)\chi_{-\Omega}(\theta_p',\varphi_p')\ ;$$

and

$$R_1|IMK\Omega n_\beta n_\gamma\rangle = f^{n_\beta n_\gamma}_{I-K-\Omega}(\beta',\gamma')D^{I*}_{M-K}(\Phi,\Theta,\Psi)\chi_{-\Omega}(\theta_p',\varphi_p') \quad \text{(I-316)}$$

where again[32] $\beta'=\beta$, $\gamma'=\gamma$. Comparison gives

$$f^{n_\beta n_\gamma}_{I-K-\Omega}(\beta,\gamma) = (-1)^{I-\frac{1}{2}}\pi_\chi f^{n_\beta n_\gamma}_{IK\Omega}(\beta,\gamma). \quad \text{(I-317)}$$

Applying twice and noting that $R_1{}^2 = 1$ leads to the conclusion that $f^{n_\beta n_\gamma}_{IK}(\beta,\gamma) = (-1)^{2I-1}f^{n_\beta n_\gamma}_{IK}(\beta,\gamma)$, or that $2I-1$ is an even integer or I a half-integer. The required R_1-invariant function is then

$$(1+R_1)|IMK\Omega n_\beta n_\gamma\rangle \equiv |IMK\Omega n_\beta n_\gamma^S\rangle = f^{n_\beta n_\gamma}_{IK\Omega}(\beta,\gamma)\left[D^{I*}_{MK}\chi_\Omega + (-1)^{I-\frac{1}{2}}\pi_\chi D^{I*}_{M-K}\chi_{-\Omega}\right]. \quad \text{(I-318)}$$

6. R_2-Invariance

With the help of the relations[32] $R_2 D^{I*}_{MK}(\Phi,\Theta,\Psi) = \sum_{K'} D^{I}_{K'K}(0,0,\frac{\pi}{2})D^{I*}_{MK'}(\Phi,\Theta,\Psi) = D^{I*}_{MK}(\Phi,\Theta,\Psi-\frac{\pi}{2}) = e^{-iK\frac{\pi}{2}}D^{I*}_{MK}(\Phi,\Theta,\Psi)$, one has analogously to the above, for even-even nuclei,

$$R_2|IMKn_\beta n_\gamma\rangle = f^{n_\beta n_\gamma}_{IK}(\beta,\gamma)D^{I*}_{MK}(\Phi,\Theta,\Psi-\tfrac{\pi}{2}) = e^{-iK\frac{\pi}{2}}f^{n_\beta n_\gamma}_{IK}(\beta,\gamma)D^{I*}_{MK}(\Phi,\Theta,\Psi);$$

$$R_2|IMKn_\beta n_\gamma\rangle = f^{n_\beta n_\gamma}_{IK}(\beta',\gamma')D^{I*}_{MK}(\Phi,\Theta,\Psi) = f^{n_\beta n_\gamma}_{IK}(\beta,-\gamma)D^{I*}_{MK}(\Phi,\Theta,\Psi); \quad \text{(I-319)}$$

whence

$$f_{IK}^{n_\beta n_\gamma}(\beta, -\gamma) = e^{-iK\frac{\pi}{2}} f_{IK}^{n_\beta n_\gamma}(\beta, \gamma). \qquad \text{(I-320)}$$

Applying twice leads to the conclusion that $f_{IK}^{n_\beta n_\gamma}(\beta, \gamma) = e^{-iK\pi} f_{IK}^{n_\beta n_\gamma}(\beta, \gamma)$ or that K is an even integer. Applying four times gives $f_{IK}^{n_\beta n_\gamma}(\beta, \gamma) = (-1)^{-2K} f_{IK}^{n_\beta n_\gamma}(\beta, \gamma) \equiv + f_{IK}^{n_\beta n_\gamma}(\beta, \gamma)$, which is automatically in accord with the property $R_2^4 = 1$. As to R_2-invariance, for the axially symmetric case under discussion this is automatically achieved for $(1 + R_1) \left| IMKn_\beta n_\gamma \right\rangle$:

$$\begin{aligned} R_2 \left| IMKn_\beta n_\gamma^s \right\rangle &= R_2 (1 + R_1) \left| IMKn_\beta n_\gamma \right\rangle \\ &= R_2 \left| IMKn_\beta n_\gamma \right\rangle + (-1)^I R_2 \left| IM{-K}n_\beta n_\gamma \right\rangle \\ &= e^{-i\pi\frac{K}{2}} \left[\left| IMKn_\beta n_\gamma \right\rangle + (-1)^{I-K} \left| IM{-K}n_\beta n_\gamma \right\rangle \right]. \end{aligned} \qquad \text{(I-321)}$$

But since K must be even, $(-1)^{-K} \equiv +1$ and

$$R_2 \left| IMKn_\beta n_\gamma^s \right\rangle = e^{-i\pi\frac{K}{2}} \left| IMKn_\beta n_\gamma^s \right\rangle . \qquad \text{(I-322)}$$

Since K is a constant of motion, the only effect of R_2 is an admissible overall phase change. For odd-A nuclei,

$$\begin{aligned} R_2 \left| IMK\Omega n_\beta n_\gamma^s \right\rangle &= R_2 (1 + R_1) \left| IMK\Omega n_\beta n_\gamma^s \right\rangle \\ &= R_2 \Big\{ f_{IK\Omega}^{n_\beta n_\gamma}(\beta, \gamma) \Big[D_{MK}^{I*}(\Phi, \Theta, \Psi) \sum_j C_{j\Omega} \sum_m D_{m\Omega}^{j}(\Phi, \Theta, \Psi) \chi_{jm}(\theta_p, \phi_p) \\ &\quad + (-1)^{I-\frac{1}{2}} \pi_\chi D_{M-K}^{I*} \sum_j C_{j-\Omega} \sum_m D_{m-\Omega}^{j}(\Phi, \Theta, \Psi) \chi_{jm}(\theta_p, \phi_p) \Big] \Big\} \\ &= f_{IK\Omega}^{n_\beta n_\gamma}(\beta, \gamma) e^{-i(K-\Omega)\frac{\pi}{2}} \left[D_{MK}^{I*} \chi_\Omega + (-1)^{I-\frac{1}{2}+K-\Omega} \pi_\chi D_{M-K}^{I*} \chi_{-\Omega} \right]. \end{aligned} \qquad \text{(I-323)}$$

But, from writing $R_2 \left| IMK\Omega n_\beta n_\gamma \right\rangle$ in the alternative way,

$$R_2\left|IMK\Omega n_\beta n_\gamma\right\rangle = f_{IK\Omega}^{n_\beta n_\gamma}(\beta,-\gamma)\, D_{MK}^{I*}(\Phi,\Theta,\Psi)\sum_j C_{j\Omega}\sum_m D_{m\Omega}^{j}(\Phi,\Theta,\Psi)\,\chi_{jm}(\theta_p,\phi_p),$$

and comparing with the first term above to find

$$f_{IK\Omega}^{n_\beta n_\gamma}(\beta,-\gamma) = e^{-i(K-\Omega)\frac{\pi}{2}} f_{IK\Omega}^{n_\beta n_\gamma}(\beta,\gamma), \qquad \text{(I-324)}$$

one concludes in the same way as with the even-even case that $K-\Omega$ is even, whence the automatic R_2-symmetry, apart from an overall phase change:

$$R_2\left|IMK\Omega n_\beta n_\gamma^s\right\rangle = e^{-i(K-\Omega)\frac{\pi}{2}}\left|IMK\Omega n_\beta n_\gamma^s\right\rangle. \qquad \text{(I-325)}$$

7. R_3-Invariance

This leads in analogous fashion to symmetry restrictions on the vibrational wave functions, which turn out to be connected to periodicity in the variable γ, causing restriction of a meaningful range to 0° to 30°.

An important consequence ensues: for vibrational states in odd-A nuclei,

$$\begin{aligned}
&\left\langle f_{IK\Omega}^{n_\beta n_\gamma} D_{MK}^{I*}\chi_\Omega \right| I_{-}j_{+}\left| f_{IK\Omega}^{n_\beta n_\gamma} D_{M-K}^{I*}\chi_\Omega\right\rangle \\
&= \left\langle f_{IK\Omega}^{n_\beta n_\gamma}\middle| f_{IK\Omega}^{n_\beta n_\gamma}\right\rangle \left\langle D_{MK}^{I*}\chi_\Omega \middle| D_{M,-K+1}^{I*}\chi_{\Omega+1}\right\rangle K_{I,-K}^{-}K_{j,-\Omega}^{+} \qquad \text{(I-326)}\\
&= \left\langle f_{IK\Omega}^{n_\beta n_\gamma}\middle| f_{IK\Omega}^{n_\beta n_\gamma}\right\rangle K_{IK}^{+}K_{j\Omega}^{-}\,\delta_{K,-K+1}\,\delta_{\Omega,-\Omega+1} \\
&= K_{IK}^{+}K_{j\Omega}^{-}\,\delta_{K\frac{1}{2}}\,\delta_{\Omega\frac{1}{2}},
\end{aligned}$$

with a similar expression for $\left\langle fD\chi\right| I_{+}j_{-}\left|fD\chi\right\rangle$. Then if the ground-state band has $\Omega\neq 1/2$, even if $K=1/2$ the Coriolis decoupling vanishes, so that there is no decoupling in $K=1/2$ γ-vibrational states. If $\Omega=1/2$, then γ-vibrational states have $K\neq 1/2$ ($K=3/2$ or $5/2$) and there is no decoupling;

for a β-vibrational state ($n_\gamma=0$, $n_\beta=1$, $K-\Omega=0$) based on an $\Omega=1/2$ configuration there would be decoupling.

F. Electromagnetic Transition B-Values

From the Wigner-Eckart theorem for spherical tensor operators $\mathcal{O}_{\lambda\mu}$

$$\langle j_f m_f | \mathcal{O}_{\lambda\mu} | j_i m_i \rangle = \langle j_i m_i \lambda\mu | j \lambda j_f m_f \rangle \langle j_f \| \mathcal{O}_\lambda \| j_i \rangle$$

$$\begin{aligned}\langle j_f m_f | \mathcal{O}^*_{\lambda\mu} | j_i m_i \rangle &= (-1)^\mu \langle j_f m_f | \mathcal{O}_{\lambda-\mu} | j_i m_i \rangle \\ &= (-1)^\mu \langle j_i m_i \lambda - \mu | j_i \lambda j_f m_f \rangle \langle j_f \| \mathcal{O}_\lambda \| j_i \rangle ,\end{aligned} \tag{I-327}$$

it is apparent that $\mathcal{O}_{\lambda\mu}$ describes an absorption process ($m_i + \mu = m_f$) and $\mathcal{O}^*_{\lambda\mu}$, an emission process ($m_i = \mu + m_f$), each involving a photon of multipolarity λ , μ and the initial and final nuclear states having angular-momentum parameters j_i , m_i and j_f , m_f respectively. Being spherical tensor components these operators transform under the space-to-body-frame rotations according to

$$\begin{aligned}&\mathcal{O}'_{\lambda\mu} = \sum_\nu D^\lambda_{\nu\mu} \mathcal{O}_{\lambda\nu} ; \quad \mathcal{O}_{\lambda\nu} = \sum_\mu D^{\lambda *}_{\nu\mu} \mathcal{O}'_{\lambda\mu} ; \\ &\mathcal{O}'^*_{\lambda\mu} = \sum_\nu D^{\lambda *}_{\nu\mu} \mathcal{O}^*_{\lambda\nu} ; \quad \mathcal{O}^*_{\lambda\nu} = \sum_\mu D^\lambda_{\nu\mu} \mathcal{O}'^*_{\lambda\mu} ;\end{aligned} \tag{I-328}$$

wherein the arguments of all the D-functions are the Euler angles Φ , Θ , Ψ for rotations taking the space frame into the body frame. This fact is of use in calculating electromagnetic transition moments between nuclear states with "laboratory operators": using symmetrized wave functions,

$$\begin{aligned}\langle I_f M_f K_f \Omega^s_f | \mathcal{O}_{\lambda\mu} | I_i M_i K_i \Omega^s_i \rangle &= \sum_\sigma \langle I_f M_f K_f \Omega^s_f | D^{\lambda *}_{\mu\sigma} \mathcal{O}'_{\lambda\sigma} | I_i M_i K_i \Omega^s_i \rangle \\ \equiv \frac{\sqrt{(2I_f+1)(2I_i+1)}}{16\pi^2} \iint & \left[D^{I_f *}_{M_f K_f} \chi^f_{\Omega_f} + (-1)^{I_f - \frac{1}{2}} \pi_{\chi_f} D^{I_f *}_{M_f - K_f} \chi^f_{-\Omega_f} \right]^* \sum_\sigma D^{\lambda *}_{\mu\sigma} \mathcal{O}'_{\lambda\sigma} \left[D^{I_i *}_{M_i K_i} \chi^i_{\Omega_i} \right. \\ &\left. + (-1)^{I_i - \frac{1}{2}} \pi_{\chi_i} D^{I_i *}_{M_i - K_i} \chi^i_{-\Omega_i} \right] d\Omega_{\Phi\Theta\Psi} \, d\vec{r}'_p\end{aligned} \tag{I-329}$$

$$= \frac{\sqrt{(2I_f+1)(2I_i+1)}}{16\pi^2} \sum_{\sigma} \Big[\langle D^{I_f *}_{M_f K_f} | D^{\lambda *}_{\mu\sigma} | D^{I_i *}_{M_i K_i} \rangle \langle \Omega_f | \mathcal{O}'_{\lambda\sigma} | \Omega_i \rangle + (-1)^{-I_f+\frac{1}{2}} \pi_{\chi_f}$$

$$\times \langle D^{I_f *}_{M_f -K_f} | D^{\lambda *}_{\mu\sigma} | D^{I_i *}_{M_i K_i} \rangle \langle -\Omega_f | \mathcal{O}'_{\lambda\sigma} | \Omega_i \rangle + (-1)^{I_i-\frac{1}{2}} \pi_{\chi_i} \langle D^{I_f *}_{M_f K_f} | D^{\lambda *}_{\mu\sigma} | D^{I_i *}_{M_i -K_i} \rangle$$

$$\times \langle \Omega_f | \mathcal{O}'_{\lambda\sigma} | -\Omega_i \rangle + (-1)^{-I_f+I_i} \pi_{\chi_f} \pi_{\chi_i} \langle D^{I_f *}_{M_f -K_f} | D^{\lambda *}_{\mu\sigma} | D^{I_i *}_{M_i -K_i} \rangle \langle -\Omega_f | \mathcal{O}'_{\lambda\sigma} | -\Omega_i \rangle \Big] .$$

Using the properties

$$\langle -\Omega_f | \mathcal{O}'_{\lambda -\sigma} | -\Omega_i \rangle = (-1)^{-\lambda} \pi_{\chi_f} \pi_{\chi_i} \langle \Omega_f | \mathcal{O}'_{\lambda\sigma} | \Omega_i \rangle \qquad \text{(I-330)}$$

for the Nilsson wave functions $|\Omega\rangle \equiv \chi_\Omega = \sum_j C_{j\Omega} \chi_{j\Omega}$, and

$$\langle D^{I' *}_{M'K'} | D^{\lambda *}_{\mu\sigma} | D^{I *}_{MK} \rangle \equiv \int D^{I'}_{M'K'} D^{\lambda *}_{\mu\sigma} D^{I *}_{MK} \, d\Omega_{\Phi\Theta\Psi} \qquad \text{(I-331)}$$

$$= \frac{8\pi^2}{2I'+1} \langle I M \lambda \mu | I \lambda I' M' \rangle \langle I K \lambda \sigma | I \lambda I' K' \rangle$$

results in

$$\langle I_f M_f K_f \Omega_f^s | \mathcal{O}_{\lambda\mu} | I_i M_i K_i \Omega_i^s \rangle = \sqrt{\frac{2I_i+1}{2I_f+1}} \langle I_i M_i \lambda \mu | I_i \lambda I_f M_f \rangle \Big[\langle I_i K_i \lambda \sigma | I_i \lambda I_f K_f \rangle \qquad \text{(I-332)}$$

$$\times \langle \Omega_f | \mathcal{O}'_{\lambda \Delta K} | \Omega_i \rangle + (-1)^{I_i - \frac{1}{2}} \pi_{\chi_i} \langle I_i -K_i \lambda K_f + K_i | I_i \lambda I_f K_f \rangle \langle \Omega_f | \mathcal{O}'_{\lambda K_i + K_f} | -\Omega_i \rangle \Big]$$

The last term in the brackets may be equivalently replaced by $(-1)^{I_f - \frac{1}{2}} \pi_{\chi_f} \langle I_i K_i \lambda - K_f - K_i | I_i \lambda I_f - K_f \rangle \langle -\Omega_f | \mathcal{O}'_{\lambda - K_f - K_i} | \Omega_i \rangle$. The first intrinsic matrix element vanishes unless $\Delta\Omega = \Delta K$, the second unless $\Omega_f + \Omega_i = K_f + K_i$, where $\Delta K \equiv K_f - K_i$, $\Delta\Omega = \Omega_f - \Omega_i$. Performing the necessary incoherent sums over magnetic substates, an average over the initial and a sum over the final substates, there results

$$\frac{1}{2I_i+1} \sum_{M_i} \sum_{\mu} \sum_{M_f} \left| \langle I_f M_f K_f \Omega_f^s | \mathcal{O}_{\lambda\mu} | I_i M_i K_i \Omega_i^s \rangle \right|^2 = \Big| \langle I_i K_i \lambda \Delta K | I_i \lambda I_f K_f \rangle \qquad \text{(I-333)}$$

$$\times \langle \Omega_f | \mathcal{O}'_{\lambda \Delta K} | \Omega_i \rangle + (-1)^{I_i - \frac{1}{2}} \pi_{\chi_i} \langle I_i -K_i \lambda K_i + K_f | I_i \lambda I_f K_f \rangle \langle \Omega_f | \mathcal{O}'_{\lambda K_f + K_i} | -\Omega_i \rangle \Big|^2 .$$

(This agrees with Preston[32], equation 13-14 and Davidson[217], equation IV-24, where $T^B_{\lambda\nu} \equiv \mathcal{O}^*_{\lambda-\nu}$.) It should be noted that replacing K_f by $-K_f$ and Ω_f by $-\Omega_f$ in this expression multiplies it by $\left|(-1)^{2I_i - I_f - 1/2}\pi_{\chi_f}\right|^2 \equiv +1$, leaving it invariant. Then, arbitrarily setting $K_i \geq 0$, if a K_f turns out to be negative the above substitution may be made; thus all K's may be taken ≥ 0. (This may require use of an $\Omega_f < 0$ on occasion.)

An example of this kind of calculation is the derivation of the relation between intrinsic and spectroscopic (laboratory) quadrupole moments. Using unsymmetrized wave functions for the moment,

$$\begin{aligned}
\langle IMK\Omega|\mathcal{O}_{\lambda\mu}|IMK\Omega\rangle &= N_I\langle D^{I*}_{MK}\chi_\Omega|\sum_\sigma D^{\lambda*}_{\mu\sigma}\mathcal{O}'_{\lambda\sigma}|D^{I*}_{MK}\chi_\Omega\rangle \\
&= N_I\sum_\sigma\langle D^{I*}_{MK}|D^{\lambda*}_{\mu\sigma}|D^{I*}_{MK}\rangle\langle\chi_\Omega|\mathcal{O}'_{\lambda\sigma}|\chi_\Omega\rangle \\
&= \sum_\sigma\langle IM\lambda\mu|I\lambda IM\rangle\langle IK\lambda\sigma|I\lambda IK\rangle\langle\chi_\Omega|\mathcal{O}'_{\lambda\sigma}|\chi_\Omega\rangle \\
&= \langle IM\lambda 0|I\lambda IM\rangle\langle IK\lambda 0|I\lambda IK\rangle\langle\chi_\Omega|\mathcal{O}'_{\lambda 0}|\chi_\Omega\rangle\,\delta_{\mu 0},
\end{aligned} \tag{I-334}$$

whence

$$\langle IIK\Omega|\mathcal{O}_{\lambda 0}|IIK\Omega\rangle = \langle II\lambda 0|I\lambda II\rangle\langle IK\lambda 0|I\lambda IK\rangle\langle\chi_\Omega|\mathcal{O}'_{\lambda 0}|\chi_\Omega\rangle. \tag{I-335}$$

For $\lambda = 2$, using $\langle jm20|j2jm\rangle = \left[3m^2 - j(j+1)\right]/\sqrt{j(j+1)(2j-1)(2j+3)}$, there results the familiar relation:

$$Q \equiv \langle IIK\Omega|\mathcal{O}_{20}|IIK\Omega\rangle = \frac{3K^2 - I(I+1)}{(I+1)(2I+3)}\,Q_0\,, \quad Q_0 \equiv \langle\chi_\Omega|\mathcal{O}'_{20}|\chi_\Omega\rangle. \tag{I-336}$$

For electromagnetic emission processes the necessary operators are of the form $\mathcal{O}^*_{\lambda\mu} = (-1)^\mu\mathcal{O}_{\lambda-\mu}$. The calculation proceeds in the same way, using the relations,

$$\langle D^{I'*}_{M'K'}|D^{\lambda}_{\mu\nu}|D^{I*}_{MK}\rangle = \frac{8\pi^2}{2I+1}\langle I'M'\lambda\mu|I'\lambda IM\rangle\langle I'K'\lambda\nu|I'\lambda IK\rangle,$$

$$\langle -\Omega_f|\mathcal{O}'^{*}_{\lambda-\nu}|-\Omega_i\rangle = (-1)^{\lambda}\pi_{\chi_i}\pi_{\chi_f}\langle\Omega_f|\mathcal{O}'^{*}_{\lambda\nu}|\Omega_i\rangle, \tag{I-337}$$

and producing the results:

$$\langle I_fM_fK_f\Omega^s_f|\mathcal{O}^{*}_{\lambda\mu}|I_iM_iK_i\Omega^s_i\rangle = \sqrt{\frac{2I_i+1}{2I_f+1}}(-1)^{\mu}\langle I_iM_i\lambda-\mu|I_i\lambda I_fM_f\rangle$$

$$\times\sum_{\nu}(-1)^{-\nu}\Big[\langle I_iK\lambda-\nu|I_i\lambda I_fK_f\rangle\langle\Omega_f|\mathcal{O}'^{*}_{\lambda\nu}|\Omega_i\rangle + (-1)^{I_i-\frac{1}{2}}\pi_{\chi_i}$$

$$\times\langle I_i-K_i\lambda-\nu|I_i\lambda I_fK_f\rangle\langle\Omega_f|\mathcal{O}'^{*}_{\lambda\nu}|-\Omega_i\rangle\Big] \tag{I-338}$$

$$= \sqrt{\frac{2I_i+1}{2I_f+1}}\langle I_fM_f\lambda\mu|I_f\lambda I_iM_i\rangle\sum_{\nu}\Big[\langle I_fM_f\lambda\nu|I_f\lambda I_iK_i\rangle\langle\Omega_f|\mathcal{O}'^{*}_{\lambda\nu}|\Omega_i\rangle$$

$$+(-1)^{I_i-\frac{1}{2}}\pi_{\chi_i}\langle I_fK_f\lambda\nu|I_f\lambda I_i-K_i\rangle\langle\Omega_f|\mathcal{O}'^{*}_{\lambda\nu}|-\Omega_i\rangle\Big]$$

and finally,

$$B(\lambda, I_iK_i\rightarrow I_fK_f) \equiv \frac{1}{2I_i+1}\sum_{M_i}\sum_{\mu}\sum_{M_f}\left|\langle I_fM_fK_f\Omega^s_f|\mathcal{O}^{*}_{\lambda\mu}|I_iM_iK_i\Omega^s_i\rangle\right|^2$$

$$= \Big|\langle I_iK_i\lambda\Delta K|I_i\lambda I_fK_f\rangle\langle\Omega_f|\mathcal{O}'^{*}_{\lambda-\Delta K}|\Omega_i\rangle + (-1)^{I_i+\frac{1}{2}}\langle I_i-K_i\lambda K_f+K_i|I_i\lambda I_fK_f\rangle$$

$$\times\langle\Omega_f|\mathcal{O}'^{*}_{\lambda-K_i-K_f}|-\Omega_i\rangle\Big|^2 \tag{I-339}$$

$$\equiv\langle I_iK_i\lambda\Delta K|I_i\lambda I_fK_f\rangle^2\left|\langle\Omega_f|\mathcal{O}'^{*}_{\lambda-\Delta K}|\Omega_i\rangle\right|^2\left|1+(-1)^{I_i+\frac{1}{2}}\frac{\langle I_i-K_i\lambda K_i+K_f|I_i\lambda I_fK_f\rangle}{\langle I_iK_i\lambda\Delta K|I_i\lambda I_fK_f\rangle}R^{(\lambda)}_{fi}\right|^2.$$

This expression, which forms the basis for the Alaga rules, also is invariant under the replacement of K_f,Ω_f by their negatives, permitting all K's to be taken ≥ 0.

According to this result, if $|\Delta K| > \lambda$ then the B-value vanishes; the radiative decay of this multipolarity is strictly forbidden, and the transition is said to be K-forbidden. It either must go via the multipolarity λ by virtue of band-mixing state impurities or impure K-mixtures due to nonaxiality, or else via a higher multipolarity $\lambda' : \lambda' \leq |\Delta K|$. If $|\Delta K| \leq \lambda < K_i + K_f$ (having set K_i and $K_f \geq 0$), the second term in $B(\lambda, i \to f)$ vanishes, and $B(\lambda, i \to f) \propto \langle I_i K_i \lambda \Delta K | I_i \lambda I_f K_f \rangle^2$, or the simple Alaga rules pertain. If $\lambda \geq K_i + K_f$, the extra symmetry term contributes "symmetrization corrections" to these simple rules, even for pure K-bands. This is the case with dipole transitions within and between $K = 1/2$ bands, and for quadrupole transitions within and between $K = 1/2$ bands or between a $K = 1/2$ band and a $K = 3/2$ band, for example, between $1/2 + \gamma$-vibrational or $1/2 + [411]$ bands and the $3/2 + [411]$ ground-state band in Tb^{159}.

The relation $B(\lambda, f \to i)/B(\lambda, i \to f) = (2I_i + 1)/(2I_f + 1)$ holds even for symmetry-modified cases provided $\pi_{\chi_i} \pi_{\chi_f} = +1$; e.g. E2, M1, etc. but not E1, etc. In particular,

$$B(E2, i \to f) = \langle I_i K_i 2 \Delta K | I_i 2 I_f K_f \rangle^2 \left| \langle \Omega_f | \mathcal{O}'^{*}_{E2,-\Delta K} | \Omega_i \rangle \right|^2 \times \left| 1 + (-1)^{I_i + \frac{1}{2}} \left[d_1 \delta_{K_i \frac{1}{2}} \delta_{K_f \frac{1}{2}} + d_2 \delta_{K_i \frac{3}{2}} \delta_{K_f \frac{1}{2}} + d_3 \delta_{K_i \frac{1}{2}} \delta_{K_f \frac{3}{2}} \right] \mathcal{R}^{E2}_{fi} \right|^2 ; \tag{I-340}$$

$$B(M1, i \to f) = \langle I_i K_i 1 \Delta K | I_i 2 I_f K_f \rangle^2 \left| \langle \Omega_f | \mathcal{O}'^{*}_{M1,-\Delta K} | \Omega_i \rangle \right|^2 \times \left| 1 + (-1)^{I_i + \frac{1}{2}} \left[d_1' \delta_{K_i \frac{1}{2}} \delta_{K_f \frac{1}{2}} \right] \mathcal{R}^{M1}_{fi} \right|^2 ;$$

where $d_1, \ldots, d_1'$ are given in Table (I-1) and $\mathcal{R}^{(\lambda)}_{fi}$ is given by

$$\mathcal{R}^{(\lambda)}_{fi} = \frac{\langle \Omega_f | \mathcal{O}'^{*}_{\lambda - K_i - K_f} | -\Omega_i \rangle}{\langle \Omega_f | \mathcal{O}'^{*}_{\lambda - \Delta K} | \Omega_i \rangle} . \tag{I-341}$$

For pure Nilsson states, $|\Omega\rangle = \sum_j C_{j\Omega} | j \Omega \rangle$, using the Wigner-Eckart theorem,

Table I-1

	$I_f =$	I_i-2	I_i-1	I_i	I_i+1	I_i+2	Agrees with:
$d_1 = \dfrac{\langle I_i \;\; -1/2 \;\; 2 \;\; 1 \mid I_i \;\; 2 \;\; I_f \;\; 1/2\rangle}{\langle I_i \;\; 1/2 \;\; 2 \;\; 0 \mid I_i \;\; 2 \;\; I_f \;\; 1/2\rangle} =$		$-\frac{2}{\sqrt{6}}$	$-\frac{2}{\sqrt{6}} I_i$	0	$-\frac{2}{\sqrt{6}}(I_i+1)$	$\frac{2}{\sqrt{6}}$	
$d_2 = \dfrac{\langle I_i \;\; -3/2 \;\; 2 \;\; 2 \mid I_i \;\; 2 \;\; I_f \;\; 1/2\rangle}{\langle I_i \;\; 3/2 \;\; 2 \; -1 \mid I_i \;\; 2 \;\; I_f \;\; 1/2\rangle} =$		$-\frac{1}{2}$	$\frac{1}{2}\,\frac{2I_i-1}{I_i-2}$	$\frac{1}{2}(I_i+1)$	$-\frac{1}{2}\,\frac{2I_i+3}{I_i+3}$	$\frac{1}{2}$	J.P.D.[217] Eqn. III-23
$d_3 = \dfrac{\langle I_i \;\; -1/2 \;\; 2 \;\; 2 \mid I_i \;\; 2 \;\; I_f \;\; 3/2\rangle}{\langle I_i \;\; 1/2 \;\; 2 \;\; 1 \mid I_i \;\; 2 \;\; I_f \;\; 3/2\rangle} =$		$-\frac{1}{2}$	$-\frac{1}{2}\,\frac{2I_i+1}{I_i+2}$	$-\frac{1}{2}(I_i+1)$	$\frac{1}{2}\,\frac{2I_i+1}{I_i-1}$	$\frac{1}{2}$	
$d_1 = \dfrac{\langle I_i \;\; -1/2 \;\; 1 \;\; 1 \mid I_i \;\; 1 \;\; I_f \;\; 1/2\rangle}{\langle I_i \;\; 1/2 \;\; 1 \;\; 0 \mid I_i \;\; 1 \;\; I_f \;\; 1/2\rangle} =$		---	$-\frac{1}{\sqrt{2}}$	$-\frac{1}{\sqrt{2}}(2I_i+1)$	$\frac{1}{\sqrt{2}}$	---	J.P.D.[217] Eqn. III-22

$$\mathcal{R}_{fi}^{(\lambda)} = \pi_{\chi_i} \frac{\sum_{j_f}\sum_{j_i} (-1)^{j_i+\frac{1}{2}} \langle j_i -\Omega_i \lambda K_i+K_f | j_i \lambda j_f \Omega_f \rangle C^{f*}_{j_f\Omega_f} C^{i}_{j_i\Omega_i} \langle j_f \| \mathcal{O}'^{*}_{\lambda} \| j_i \rangle}{\sum_{j_f}\sum_{j_i} \langle j_i \Omega_i \lambda \Delta K | j_i \lambda j_f \Omega_f \rangle C^{f*}_{j_f\Omega_f} C^{i}_{j_i\Omega_i} \langle j_f \| \mathcal{O}'^{*}_{\lambda} \| j_i \rangle} \tag{I-342}$$

and can in general be expected to take on arbitrary values.

The quantity $|\langle \Omega_f | \mathcal{O}'^{*}_{\lambda-\Delta K} | \Omega_i \rangle|^2$ for intraband E2 transitions, $K > 1/2$, is to be associated with $(5/16\pi)e^2 Q_0{}^2$, if $\mathcal{O}'^{*}_{\lambda-\Delta K}$ is an electromagnetic multipole operator $[r^{\lambda} Y_{\lambda}^{-\Delta K}(\theta,\varphi)]^{*}$.

The presence of band mixing will cause modification of the Alaga rules as follows: for pure-band unsymmetrized wave functions the electric multipole matrix elements can be written as

$$\langle I_f M_f K_0 \Omega_0^s | \mathcal{O}^{*}_{\lambda\mu} | I_i M_i K \Omega^s \rangle = \sqrt{\frac{2I_i+1}{2I_f+1}} \langle I_f M_f \lambda \mu | I_f \lambda I_i M_i \rangle \Big[\langle I_f K_0 \lambda -\Delta K | I_f \lambda I_i K \rangle$$
$$\times \langle \Omega_0 | \mathcal{O}'^{*}_{\lambda-\Delta K} | \Omega \rangle + (-1)^{I_i-\frac{1}{2}} \pi_{\chi_i} \langle I_f K_0 \lambda -K-K_0 | I_f \lambda I_i -K \rangle \langle \Omega_0 | \mathcal{O}'^{*}_{\lambda-K-K_0} | -\Omega \rangle \Big] ;$$

(I-343)

$$\langle I_f M_f K_0 \Omega_0^s | \mathcal{O}_{\lambda\mu} | I_i M_i K \Omega^s \rangle = \sqrt{\frac{2I_i+1}{2I_f+1}} \langle I_i M_i \lambda \mu | I_i \lambda I_f M_f \rangle \Big[\langle I_i K \lambda \Delta K | I_i \lambda I_f K_0 \rangle$$
$$\times \langle \Omega_0 | \mathcal{O}'_{\lambda \Delta K} | \Omega \rangle + (-1)^{I_f-\frac{1}{2}} \pi_{\chi_f} \langle I_i K \lambda -K-K_0 | I_i \lambda I_f -K \rangle \langle -\Omega_0 | \mathcal{O}'_{\lambda-K-K_0} | \Omega \rangle \Big]$$

where K, Ω and K_0, Ω_0 refer to the upper and lower bands in the case of interband transitions, and $\Delta K = K_0 - K$. Now suppose two bands are mixed by some perturbation. Only states of equal I can be mixed, because of angular momentum conservation. Suppose the lower and upper band states are given respectively by

$$|IM_0^s\rangle = |IMK_0\Omega_0^s\rangle - \frac{C^{0}_{IK_0K}}{\delta E^{0}_{I\Delta K}} |IMK\Omega^s\rangle$$
$$|IM^s\rangle = |IMK\Omega^s\rangle + \frac{C_{IKK_0}}{\delta E^{0}_{I\Delta K}} |IMK_0\Omega_0^s\rangle \, . \tag{I-344}$$

For corresponding pairs of states the admixture coefficients are equal and opposite if inertia moments in the two bands are equal. Then, for intraband transitions in the lower band one has:

$$\langle I_f M_{f0}^{\ s} | \mathcal{O}^*_{\lambda\mu} | I_i M_{i0}^{\ s} \rangle = \langle I_f M_f K_0 \Omega_0^s | \mathcal{O}^*_{\lambda\mu} | I_i M_i K_0 \Omega_0^s \rangle$$
$$+ \frac{C^0_{I_i K_0 K}}{\delta E^0_{I_i \Delta K}} \langle I_f M_f K_0 \Omega_0^s | \mathcal{O}^*_{\lambda\mu} | I_i M_i K \Omega^s \rangle + \frac{C^{0*}_{I_f K_0 K}}{\delta E^0_{I_f \Delta K}} \langle I_f M_f K \Omega^s | \mathcal{O}^*_{\lambda\mu} | I_i M_i K_0 \Omega_0^s \rangle$$
$$+ \frac{C^0_{I_i K_0 K} C^{0*}_{I_f K_0 K}}{\delta E^0_{I_i \Delta K} \delta E^0_{I_f \Delta K}} \langle I_f M_f K \Omega^s | \mathcal{O}^*_{\lambda\mu} | I_i M_i K \Omega^s \rangle . \qquad \text{(I-345)}$$

In these expressions δE^0 is always taken non-negative. The leading term is the collectively enhanced pure-band matrix element. The second and third terms are small interband matrix elements multiplied by small coefficients, and the fourth, an upper-band collective matrix element multiplied by the product of two small coefficients. All three are thus roughly of second order in smallness with respect to the leading term (in rotational regions where mixing amplitudes do appear to be small), and result in fairly negligible corrections to the intraband (symmetry-modified) Alaga ratios.

For interband transitions, however, one has

$$\langle I_f M_{f0}^{\ s} | \mathcal{O}^*_{\lambda\mu} | I_i M_i^{\ s} \rangle = \langle I_f M_f K_0 \Omega_0^s | \mathcal{O}^*_{\lambda\mu} | I_i M_i K \Omega^s \rangle$$
$$+ \frac{C_{I_i K K_0}}{\delta E^0_{I_i \Delta K}} \langle I_f M_f K_0 \Omega_0^s | \mathcal{O}^*_{\lambda\mu} | I_i M_i K_0 \Omega_0^s \rangle - \frac{C^{0*}_{I_f K_0 K}}{\delta E^0_{I_f \Delta K}} \langle I_f M_f K \Omega^s | \mathcal{O}^*_{\lambda\mu} | I_i M_i K \Omega^s \rangle$$
$$- \frac{C_{I_i K K_0} C^{0*}_{I_f K_0 K}}{\delta E^0_{I_i \Delta K} \delta E^0_{I_f \Delta K}} \langle I_f M_f K \Omega^s | \mathcal{O}^*_{\lambda\mu} | I_i M_i K_0 \Omega_0^s \rangle . \qquad \text{(I-346)}$$

The final term is a matrix element of the order of magnitude of the leading term times the product of two small coefficients and may to first order be neglected. The second and third terms are collective matrix elements times small coefficients, and may represent appreciable corrections to the smaller zero-order interband matrix element. The lowest-order effect of these terms on the B-value is given, with the help of $\langle f|\mathcal{O}|i\rangle^* = \langle i|\mathcal{O}^\dagger|f\rangle$, by

$$
\begin{aligned}
B(\lambda, i\to f) &= \frac{1}{2I_i+1}\sum_{M_i}\sum_{\mu}\sum_{M_f}\left|\langle I_f M_{f0}^{s}|\mathcal{O}^*_{\lambda\mu}|I_i M_i^{s}\rangle\right|^2 \\
&= \frac{1}{2I_i+1}\sum_{M_i}\sum_{\mu}\sum_{M_f}\Big\{\left|\langle I_f M_f K_0 \Omega_0^s|\mathcal{O}^*_{\lambda\mu}|I_i M_i K\Omega^s\rangle\right|^2 \\
&\quad + 2\,\mathrm{re}\Big[\frac{C^*_{I_i K K_0}}{\delta E^0_{I_i \Delta K}}\langle I_i M_i K\Omega^s|\mathcal{O}_{\lambda\mu}|I_f M_f K_0\Omega_0^s\rangle\langle I_f M_f K_0\Omega_0^s|\mathcal{O}^*_{\lambda\mu}|I_i M_i K_0\Omega_0^s\rangle \\
&\quad - \frac{C^0_{I_f K_0 K}}{\delta E^0_{I_f \Delta K}}\langle I_f M_f K_0\Omega_0^s|\mathcal{O}^*_{\lambda\mu}|I_i M_i K\Omega^s\rangle\langle I_i M_i K\Omega^s|\mathcal{O}_{\lambda\mu}|I_f M_f K\Omega^s\rangle\Big] + \dots\Big\},
\end{aligned}
\qquad (\text{I-347})
$$

which may be evaluated with the aid of (I-343). The leading term is the unmixed B-value $B(\lambda, I_i K \to I_f K_0)$. The correction terms turn out to have the same M_i, μ, M_f-dependence, so the sums may be done immediately in analogous fashion to the leading-term sums. The result is twice the real part of terms which are comprised of the mixing amplitudes times brackets containing terms that are products of various combinations of inter- and intraband Clebsch-Gordon coefficients and corresponding intrinsic matrix elements. These would need to be evaluated for each individual case.

II. History of Studies on the Structure of Tb

Most of the previous investigations of Tb^{159} were based on studies of the beta decay of Gd^{159} and the electron-capture decay of Dy^{159} and, subsequent to the discovery of the process, by Coulomb excitation of Tb with light projectiles.

A. Gadolinium Decay

In 1938 Pool and Quill[36] observed 18-hour and 3.5-minute activities as a result of fast and slow neutron irradiation of natural gadolinium. Subsequent studies by several groups[37,38,39,40] identified the 3.5-minute activity as associated with mass 161, the 18-hour activity with mass 159, and from absorption measurements showed that the radiation associated with the latter activity contained $\sim$0.9-MeV beta rays and $\sim$55-keV and 350-keV gamma rays. Jordan, Cork, and Burson[41] irradiated 99.9% pure Gd_2O_3 in a reactor for 55 hours and observed the resulting beta and gamma singles spectra and beta-gamma and gamma-gamma coincident spectra utilizing a 180^o electron photographic spectrometer and NaI scintillation spectrometers. Among the observed internal conversion lines, some having greater than eighteen-hour "half-lives", some the 9.3-hour half-life attributed to Eu^{152}, were six lines that decayed with the 18-hour half-life of Gd^{159} resulting from the Gd^{158}(24.87% nat. abund.[42]) (n, γ) reaction: L_i, L_{iii}, M, N lines due to a 57.5 ± .3-keV transition, for which intensities $I(L_i) >> I(L_{iii})$ suggest M1, and weak K and L lines from a 364 ± 3-keV transition for which $I(K)/I(L) \gtrsim 5$, the uncertainty not permitting an assignment of multipolarity. Tb 44-keV X-rays and some gamma radiation at 57 1/2 keV and ≈364 keV were observed, as well as impurity gamma rays of 49 keV due to Dy^{161} produced by Gd^{160}(21.90% nat. abund.[42]) (n, γ) $Gd^{161} \xrightarrow[3.7\ \text{min.}]{} Tb^{161} \xrightarrow[6.8\ \text{da.}]{} Dy^{161}$, 122 keV from 9.3-hour Eu, and ~860 keV and ~970 keV with a ~10-hour "half-life", probably from Eu. Gamma-gamma coincident observations showed no 364-keV gamma rays in coincidence with the Tb X-ray region of the spectrum, indicating that the 57.5-keV and 364-keV gamma rays are not in cascade. Beta-gamma coincident measurements with Na I and anthracene detectors and a ~2μsec. resolving time, utilizing a critical absorption technique, indicated a ~1.1-MeV beta group decaying with 18-hour half-life in coincidence with the X-rays, and a ~.9-MeV in coincidence with the 364-keV gamma rays.

N. Marty[43] noted that the recently discovered Coulomb excitation process, applied to Tb^{159}, indicated a 136-keV level, and undertook to investigate why no beta branch to this level was seen in Gd^{159} decay. Eu-free Gd_2O_3 was neutron-irradiated, and subsequent gamma and beta radiations observed. Gamma rays observed were a 364-keV and a weak 57-keV, the latter obscured by Tb X-rays, 46-keV gamma rays from Dy^{161} produced as above, and Eu X-rays arising from

Gd^{152}(0.200% nat. abund.[42]) (n, γ)$Gd^{153} \xrightarrow[E.C.]{} Eu^{153}$. A gamma-internal conversion electron coincidence measurement showed no 364-keV gamma rays coincident with 57-keV internal conversion electrons. Fermi-Kurie analysis of the beta rays indicated a beta group at 940 ± 10 keV, ~80%, log ft = 6.6 and a beta group at ~630 ± 30 keV, ~20%. Analysis of the beta rays in coincidence with the 364-keV gamma ray gave the result 598 ± 8 keV, 16%, log ft = 6.5. It was noted that the log ft values suggest $\Delta I = 0$ or 1, $\Delta\pi = -1$ for the beta decays. 56 ± 1 but no 79-keV transition internal conversion lines were seen, from which it was concluded that the beta branch to the 136-keV level, if it exists, is less than 5% of the high-energy beta group. From the strength of the 57-keV internal conversion lines, in order to account for the log ft values and the absence of a beta group to the presumed 7/2+ 136-keV level, the Gd^{159} ground state was assigned $I^{\pi} = 1/2-$. The K conversion coefficient $\alpha_K(364)$ for the 364-keV transition was estimated from the data to be $\sim 10^{-2}$, suggesting E1, or M1 + E2 with E2 predominating. The division of the high-energy beta branch between the 0 and 57-keV levels, from the strength of the 57-keV internal conversion lines, was estimated to be more than 90% in favor of the ground-state transition.

Barloutaud and Ballini[44] investigated the gamma rays from Gd^{159} decay, whose half-life they gave as 18 ± 0.2 h., subsequent again to neutron-irradiation of Gd_2O_3. In gamma singles they observed 45-keV, 75-keV, and 365-keV X or gamma radiation (and a Gd^{153} decay 105-keV gamma ray). Gamma-gamma coincident spectra, obtained with fast-slow electronics for which "fast" signal pulses were 20 nsec. long, showed a 230-keV gamma ray in coincidence with the X-ray region of the spectrum, and $\sim$45-keV X-rays and $\approx$80-keV gamma rays in coincidence with the 230-keV gamma radiation. They proposed levels at 58 ± 1, 139 ± 2, and 364 ± 4 keV, with the 364-keV level decaying to the ground state producing the 365-keV gamma rays, or to the 139 ± 2-keV level, producing cascade $\approx$80 and 230-keV gamma rays. They noted that with the spins of the first two excited Tb^{159} levels required by the rotational interpretation suggested by the Coulomb excitation results, the fact that the 364-keV level decays to both the 7/2+ and the 3/2+ members of the ground-state band in observable amounts suggests that the decay to the 7/2+ member cannot be pure E2, or it would not compete with the predominately M1 ground-state decay, and that therefore this level has spin greater than 3/2 (and even parity). Then the beta decay results ($\Delta I = 0$ or 1 from log ft values) require the Gd^{159} ground-state spin to be greater than 1/2, firmly reestablishing the mystery of the missing beta branch to the 7/2+ Tb^{159} ground-state band member.

To attempt further to resolve the difficulty, Ballini and Barloutaud[45] conducted another Gd^{159} decay study. Gamma rays of 365, $\sim$300, and 225 ± 10 keV were seen with intensity ratios $100/0.5/2.5 \pm 1$, the latter number coming out $\sim$1.5 from the gamma-gamma coincident data, in agreement.

Internal conversion lines corresponding to 222-keV and 364-keV transitions were observed, from which it was calculated that $\alpha_K(364) = (15 \pm 10) \times \alpha_K(222)$, suggesting that the 222-keV transition is M1 or E2 or E3. Gamma-gamma coincident spectra showed 45-keV X-rays, ~ 58 and ≈ 80-keV gamma rays in coincidence with gamma radiation within a 220 to 230-keV gate, the 58-keV gamma ray being detected by using absorbers to differentially disfavor the X-radiation. Beta spectra in coincidence with the 58-keV region showed a group in coincidence with the 58-keV gamma rays occuring with an intensity of about 20% of the beta group to the ground state, and of maximum energy several dozen keV less. These data were noted to corroborate the decay scheme consisting of a 364-keV level decaying to 0, 58, and 139-keV levels, with the 139-keV level decaying to the 0 and 58-keV levels, and the 58-keV level going to the ground state, in which the 58 and 364-keV levels as well as the ground state are fed by the Gd beta decay. Marked deviations from the intensities predicted by the then formulated Alaga rules were noted.

Quidort[46] measured the mean life of the 364-keV level, obtaining the result $\tau \leq 5 \times 10^{-10}$ sec., suggesting the 364 -keV transition to be E1 or E2, and if the latter then probably collectively enhanced since the B(E2) value comes out $0.02 \times 10^{-48} e^2 \ cm^4$, large for a single-particle transition.

Nielsen, Nielson, and Skilbreid[47], noting the discrepancies between the beta and gamma-ray transition ratios and the Alaga rules, were next to take up the Gd^{159} decay problem, with improved equipment. Samarium and europium are frequent contaminants of gadolinium which are difficult to separate. To insure purity, subsequent to neutron irradiation in the pile at Saclay, a $GdCl_3$ sample was run through an electromagnetic mass separator. Gamma rays, beta rays, and conversion lines were observed in singles and coincidence, using scintillation gamma-ray detectors and two six-gap beta spectrometers. From a study of intensities of gamma rays and internal conversion lines certain definite conclusions were reached. As measured against a standard Cs^{137} beta-661-keV gamma source ($\alpha_K = 0.095$) in the same geometry, the intensities of the 364-keV gamma and K-conversion lines yielded the result $\alpha_K = 0.0083$, implying that the 364-keV transition is E1 (for which the Sliv and Band[48] value is α_K (E1, 365) = 0.0090). The 225-keV K line was not seen; from the 225-keV gamma intensity the maximum possible α_K (225) was small enough to allow the conclusion that the 225-keV transition was E1. With the interpretation as decays to the 3/2+ and 7/2+ members of the ground-state band, respectively, the 364-keV level spin is determined as 5/2-. From an estimate of the K X-ray to 57-keV (unresolved) gamma-ray intensity ratio it was calculated that $\alpha_K (57) \approx 6$, indicating dipole, suggesting M1, for this transition. 79-keV K and L lines were observed with the result $\alpha_K/\alpha_L = 6 \pm 1$, indicating a dipole transition here. Because of the 79-keV gamma-ray intensity E1 was ruled out in favor of predominant M1 character.

Fermi analysis of the beta groups in coincidence with the gamma rays showed there to be in coincidence with gamma rays $\geq$ 80 keV a beta group of 600-keV end point occurring in 13% of the decays, and in coincidence with gamma rays $\geq$ 20 keV, also two groups too close in energy to perform a subtraction analysis, but under the assumption of $\Delta E = 57$ keV for the end-point energies, with best fit by a 24% branch of 890 keV with the remaining 63%, not in coincidence with any gamma radiation, to the ground-state, with end-point energy 950 ± 10 keV.

The nature of the decay scheme was proved, except for the order of the 57 and 225-keV transitions, by conversion electron-gamma ray coincidence observations; 225-keV and 300-keV gamma rays were seen in coincidence with the 57-keV L line and the 225-keV gamma ray in coincidence with the 79-keV K and L lines. The assumption that the 225-keV transition arises from decay of the 364-keV level to the ground-state band 136-keV level fixes the 57-225 keV order.

From comparison of the 57 L and 79 K and L-line intensities with the 225-keV gamma-ray intensity, using theoretical conversion coefficients, it was concluded that both the 225-keV and the 79-keV transitions occur in 0.26% of all decays. As a check it was found that 0.95 225-keV gamma rays accompany each 79-keV transition, in agreement. Comparison of 300-keV gamma and 57-keV L intensities indicated the 300-keV transition occurred in 0.10% of the decays. From the K-line intensity and the measured α_K the 364-keV transition was found to occur in 9.4% of the decays, the same order of magnitude as is implied by the beta Fermi analyses. It was noted that the intensities agreed with the results of Ballini and Barloutaud[45].

In their discussion of the results the following points were noted. Assuming the ground-state band rotational structure, the multipolarities fix the 364-keV level as 5/2-, which then could be the Nilsson level 5/2- [532] . The absence of a beta branch to the 7/2+ 136-keV level suggests that out of the possible 5/2±, 3/2- states for Gd^{159}, its ground state is 3/2-. Then the Tb^{161} 3/2+ [411] $\xrightarrow[\beta]{}$ Dy^{161*} 3/2- and the Gd^{159} 3/2- [532] $\xrightarrow[\beta]{}$ Tb^{159} g.s. connect the same Nilsson states; as expected, the observed log ft values are almost identical, 6.7 and 6.8 respectively. Assuming 3/2- for Gd the Alaga rules predict a ratio of reduced transition probabilities for beta groups to the 0 and 57-keV levels in Tb of 1.5, compared to the experimental 2.0. The E1 B-value ratios for transitions from the 364-keV 5/2- to the 0, 57, 136-keV ground-state band levels are predicted by the Alaga rules to be 1/0.43/0.07, in disagreement with the experimental values from their work, 1/0.016/0.11.

A thin-lens beta spectrometer of 1.7% resolution and NaI scintillation spectrometers were employed in a Gd decay study by Malik, Nath, and Mandeville[49]. Isotopically enriched $Gd^{159}{}_2O_3$ was neutron irradiated in a reactor for 12 hours, the irradiation time chosen to minimize competing activities. In gamma singles X-ray-plus-58-keV, weak 80-keV, weak backscatter-plus-136-keV, moderate 225-keV, weak 305-keV and strong 361-keV gamma rays were observed. Internal conversion lines corresponding to 56-keV LM..., 80-keV LM..., 136-keV K, 361-keV K, 361-keV LM... and conversion lines not previously seen corresponding to 225-keV K and 305-keV K conversions were seen in beta-singles spectra. A measurement of $\alpha_K(361)$ compared with measurements on Cs^{137} 662-keV and Hg^{203} 279-keV standard transitions yielded $\alpha_K(361) = (3.9 \pm 0.8) \times 10^{-2}$, in disagreement with Nielsen et al.[47] The 361-keV K/LM... ratio was found to be 4 ± 1, from which the K/L ratio was set at 5 ± 1, which, using Rose's tables[50], indicated 70% E2 + M1, giving $\alpha_K(\text{theor.}) = 4.1 \times 10^{-2}$. (It can be interjected that the above conclusions regarding this transition were not ultimately confirmed.)

Fast-slow gamma-gamma coincident measurements with a 30-nsec. resolving time gave spectra in coincidence with radiation within various differential discriminator settings with the following features: in coincidence with the X-ray region, X + 56-, 80-, 136-, 225- and 305-keV gamma rays; with 136-keV, X and 225-keV gamma rays; with 225-keV, X + 56-, 80-, 136-keV gamma rays; with 305-keV, X + 56-keV gamma rays; and with 361-keV, no gamma rays. Studies of beta rays in coincidence with X + 56-, 80-, 136-, 225-, 305- and 361-keV gamma rays showed a 580±10-keV beta group, 20%; in coincidence with X + 56-keV gamma rays but no others a group at 880± 20-keV, 16%; and in coincidence with none of the gamma rays, the 940 ± 15-keV group, 74%, these branching fractions being in rough agreement with previous determinations. The (incorrect) conjecture was made that, with the Gottfried[10] model and a deformation parameter $\beta \approx 0.4$ suggesting probably 3/2-, possibly 1/2- for the Gd^{159} ground state, the 560-keV beta-group log ft value and the supposed E2 + M1 character of the 361-keV transition, the 361-keV level is 1/2+, but that otherwise the decay scheme is as given by Nielsen et al.[47]

Because of the persistent controversy over the multipolarity of the transitions from the 362-keV level, a lifetime measurement of the level was undertaken by Metzger and Todd[51], who noted that the previous result, $\tau \leq 5 \times 10^{-10}$ sec., could be long enough to include an E1 transition hindered by a factor $\sim 10^{5}$, by then a known characteristic of other E1 transitions in the rare-earth region, as well as being consistent with an M1+ E2 classification. Gd_2O_3 enriched to 92.87% Gd^{158} was irradiated about one day in the O.R.N.L. reactor to produce the Gd^{159}. No chemical separation was performed, so that there was 9-hour Eu^{152} present. A resonance fluorescence technique was used in which gamma radiation from the source was scattered from three pounds of Tb_4O_7. The resonant gamma scattering cross section could be written in terms of Γ, the radiation width of the excited level of interest (in the scatterer nuclei), Γ_0, the partial width to the ground state, and the effective temperatures of the scatterer and source, assuming Maxwellian thermal velocity distributions. From the assumption of $\Gamma / \Gamma_0 \approx 0.96$ for the 362-keV level, a measurement of the average resonant scattering cross section at two temperatures would yield Γ_0. These authors used a scatterer temperature of 317° K. and source temperatures of 317° K. and 1283° K. Scattered gamma rays were observed with a 35 x 40 mm. NaI detector at angles of 125° and 144° at both source temperatures. At the higher temperature the resonance scattering was about 5% of the total cross section, so that high statistical inaccuracies did not permit the angular dependence of the cross section to be observed; the result for the angular correlation coefficient was $a_2 = 0.1 \pm 0.4$. Thus no conclusion regarding multipolarity could be drawn, but the result was consistent with the theoretical value of the coefficient, 0.23, for a 3/2-5/2-3/2 spin sequence.

Γ_0 was detetermined from the 125° data since the resonant scattering differential cross section obeys the relation

$$\frac{d\sigma(125.3^\circ)}{d\Omega} = \frac{\sigma_{tot.}}{4\pi} \tag{II.1}$$

independent of a_2. The result was $\Gamma_0 = 3.33 \times 10^{-6}$ ev, or, allowing in the error estimate for geometrical errors as well as statistical uncertainties, a radiative decay mean life,

$$\tau_\gamma = (2.0 \pm 0.3) \times 10^{-10} \text{ sec.,} \tag{II.2}$$

and a total level mean life,

$$\tau_{level} = (1.9 \pm 0.3) \times 10^{-10} \text{ sec.,} \tag{II.3}$$

corresponding to a hindrance factor of 5×10^4.

The conversion coefficient $\alpha_K(362)$ was determined using a lens spectrometer to detect the internal conversion electrons. Direct comparison was made with the standard transitions, 265 keV in As^{75} ($\alpha_K=(6.2\pm 0.3)\times 10^{-3}$), and 412 keV in Hg^{198} ($\alpha_K=2.81\times 10^{-2}$), of measurements of gamma-ray and internal conversion electron intensities. The result was

$$\alpha_K(362)=(8.1\pm 2.0)\times 10^{-3}, \qquad \text{(II.4)}$$

in agreement with Nielsen et al.[47] and in disagreement with Malik et al.[49], implying the multipolarity for the ground-state transition, E1.

A measurement on the 362-keV level lifetime was performed by Gorodetzky, Manquenouille, Richert, and Knipper[52, 53], using the method of delayed coincidences, as part of a series of lifetime measurements in a variety of nuclei. Using Ne-102 phosphor to detect both beta and gamma rays, and with the characteristics $2\tau_0=7.5\times 10^{-10}$ sec. (width), $T_{\frac{1}{2}}=8\times 10^{-11}$ sec. (slope) for the Na^{22} prompt curve, the slope of the 590-keV beta-362-keV gamma coincident curve yielded the result,

$$T_{\frac{1}{2}}=(1.6\pm 0.16)\times 10^{-10}\ \text{sec.}, \qquad \text{(II.5)}$$

or

$$\tau_{\text{level}}=(2.3\pm 0.23)\times 10^{-10}\ \text{sec.}, \qquad \text{(II.6)}$$

for the level lifetimes, assuming an $\alpha_K=0.0083$ [47], in agreement within the uncertainty limits with the result of Metzger and Todd[51], and corresponding to a retardation compared to the Moskowski single-particle lifetime estimate $\tau_\gamma^{s.p.}(\text{E1}, 362)=5.6\times 10^{-15}$ sec. by a factor of 4.3×10^4.

Manquenouille[54] observed the branching ratios for the decay of the 362-keV level to the ground-state band and derived the B(E1)-value ratios 1/0.018/0.11, in essential agreement with previous work.

Vartapetyan et al.[55] measured the half-life of the 364-keV level using the beta-gamma delayed coincidence technique. Anthracene and NaI detectors, and a Ru^{103} prompt standard were employed. The fast-slow coincidence system resolving time was 6 nsec.; the half-life was determined from a measurement of the center-of-gravity shift of the coincidence resolving curve. Their result is

$$T_{\frac{1}{2}}(364) = (1.7 \pm 0.7) \times 10^{-10} \text{ sec.}, \qquad \text{(II.7)}$$

which corresponds to the mean life $(2.46 \pm 1.01) \times 10^{-10}$ sec., again in satisfactory agreement with the other results. Decay of this level to the ground-state band with emission of 364, 307, and 225-keV gamma rays was observed, for which the B(E1)-value ratios were determined to be 1/0.013/0.12, in essential agreement with the previous determinations. Similar branching ratios were observed in decay studies of the level structures of Tb^{157} and Tb^{155}. It was noted that information on hand indicated serious deviations of B(E1)-values from the Alaga rules in the three Tb isotopes and in Yb^{173}, Lu^{175}, and Hf^{177}.

Subba-Rao[56] employed a method to check the anomalous branching ratios from the 364-keV level in which the gamma-ray intensities were examined as a function of solid angle of the NaI crystals as seen from the source, and extrapolated to full solid angle to obtain the true intensities. The source was prepared by neutron irradiation of Gd_2O_3 enriched to 92.9% Gd^{158}. The gamma rays of 57, 79, 225, 306, and 364 keV were found to have intensities of 42 ± 8, 0.35 ± 0.10, 1.90 ± 0.20, 0.85 ± 0.15, 100, respectively, in essential agreement with the previous work.

Gamma-gamma coincident checks with discriminators set to accept radiation corresponding to 55 to 80 keV and ≥ 220 keV verified that there was a 227-keV gamma ray in coincidence with the 57- and 79-keV gamma rays. The 225-79-keV angular correlation function $W(\theta) = 1 + A_2P_2 + A_4P_4$ was measured with the results $A_2 = 0.014 \pm 0.030$, $A_4 = 0.010 \pm 0.055$, consistent with a 5/2-7/2-5/2 sequence for the 364; 136; and 57-keV levels, with $\delta(79) = \sqrt{E2/M1} = +0.13 \pm 0.06$. From an excitation B(E2)-value for the 136-keV level as determined by Sharp and Beuchner[57] and the intensity ratio observed for the cascade and crossover decays of this level, the mean life of the level was found to be $\sim 10^{-10}$ sec., too short to affect the correlation. From this B(E2)-value and the $\delta(79)$ it was concluded that $g_K - g_R = +1.43 \pm 0.10$, or, taking $\mu = 1.50$ n. m., that $g_R = 0.14 \pm 0.10$, $g_K = 1.57 \pm 0.15$. g_R is thus nowhere near the expected collective value, $\sim Z/A = 0.409$ for Tb^{159}. In this regard it may be mentioned that, as is noted below, some recalculations of rare-earth ion wave functions used in determining μ from the hyperfine structure splitting result in the value 1.9. I have verified the numbers 1.572 and 0.141 for g_K and g_R above, and find that with $\mu = 1.9$, the values become 1.839 and 0.409 respectively, with the same error limits for an equivalent error assigned to the new μ value, so that there is now a (possibly slightly fortuitous) excellent agreement between g_R and the collective estimate.

Returning to the reference, it was noted that if the Mottelson-Nilsson[24] assignments $\frac{3}{2}-[521]$, $\frac{5}{2}-[532]$ are given to the Gd^{159} ground state and Tb^{159} 364-keV level, then the beta transition between the levels should be allowed, and unhindered by the N but hindered by the n_z and Λ asymptotic selection rules[24], which circumstance is actually reflected in the observed log ft = 6.7 for the beta group in coincidence with the 364-keV gamma rays, which if allowed and unhindered would have log ft ~5.

In this connection Cabezas et al.[58] noted that if in Gd the ground-state spin is 3/2 then the log ft values for the beta decay to the Tb excited states shows the parity to be −.

K. Takahashi[59] prepared a Gd^{159} source in a new way. 99.999% pure Gd_2O_3 with unenriched gadolinium was irradiated with bremsstrahlung, causing the reaction $Gd^{160}(\gamma,n)$ Gd^{159}. The bremsstrahlung was kept under 13 MeV by magnetically determining the electron beam energy, to avoid the possibility of the $Gd^{158}(\gamma,p)Eu^{157}$(15.4 h.) reaction. NaI and anthracene were used for gamma-ray and electron detectors, and were calibrated for energy and efficiency with suitable sources. The higher-energy gamma-ray spectrum was found to contain the 364-keV gamma ray and a new, weak gamma ray at

595 keV, with an intensity 1.5% of the 364-keV intensity. In beta-gamma coincidence the 0.59-MeV beta group was observed in coincidence with the 364-keV gamma ray, and a new group with 0.35-MeV end-point energy and intensity about 1% of that of the 0.59-MeV group (in rough agreement with the gamma-ray intensity ratio), or an absolute intensity of about 0.2% of all decays, in coincidence with the 595-keV gamma-ray. Gamma-gamma coincidence measurements showed no cascade gamma radiation in coincidence with either of the above gamma rays. Weak gamma rays of ~140, ~80, ~60 keV, and 42-keV X-rays were seen in coincidence with 225-keV gamma rays, in agreement with previous work.

The interpretation of a new 595-keV level fed by the new beta branch and decaying to the Tb ground state was made, giving for the set of beta branches, 0.95 MeV, 63%, log ft = 6.7, first forbidden unhindered, to the $\frac{3}{2}+$ [411] ground state; 0.89 MeV, 24%, log ft = 7.0, first forbidden unhindered, to the 58-keV level; 0.59 MeV, 13%, log ft = 6.7, allowed hindered, to the 364-keV $\frac{5}{2}-$ [532] level (from Nielsen et. al.[47]); and 0.35 MeV, ~0.2%, log ft = 7.5, first forbidden unhindered, to the 595-keV level. It was conjectured that, with the Nilsson equilibrium deformation $\delta = 0.31$, the new level might be the $\frac{1}{2}+$ [411], which would be expected at about this energy. It was further noted that available evidence indicates that the $\frac{1}{2}+$ [411] and $\frac{3}{2}+$ [411] states appear in Eu^{153}, Tb^{155}, Tb^{159}, and Tm^{171} ($\delta = 0.30$, 0.30, 0.31, 0.28 respectively), separated by about the same energies, 607, 660, 595, and 668 keV respectively.

A measurement of the Tb^{159} 136-keV level lifetime using a Gd source was performed by Govil and Khurana[60], who used a delayed coincidence technique, setting a gate on the 228-keV gamma ray from the 364-keV level, detecting it with a NaI crystal, and using a plastic scintillator to detect the 79 -keV gamma ray, but they obtained only an upper limit estimate because of the adverse effects of combined low counting rate and poor resolution at low energy on the data.

B. Dysprosium Decay

Ketelle[61] in 1949 first observed activities in Dy upon ion-exchange separation of the products resulting from neutron irradiation of Dy_2O_3 in a reactor. Among these was a 140 ± 10 da. e.c. activity due to Dy^{157} or Dy^{159} as well as 138 min. Dy^{165} and an 81 h. activity. The mass assignments for the activities were determined by Butement[40, 62, 63]. Neutron-irradiated Dy_2O_3 was observed, starting 60 days after irradiation, which allowed Dy^{166}(80.2 h.[42]) to decay, for a period of 400 days. Activities seen were 132 day., Dy^{159}; 140 min., Dy^{165}; and 82 h., Dy^{166}. Also, Tb_4O_7 was bombarded with 9-MeV deuterons; upon ion-exchange separation the product of the $Tb^{159}(d, 2n)Dy^{159}$ reaction, with a half life of 136 da., was seen. Absorption measurements with Cu and Al absorbers indicated that in both cases the 159 activity emitted 6.6-keV and 44-keV Tb L and K X-rays. The rate of positron emission was determined to be less than 0.1%.

In the next reported investigation of Dy^{159} decay, done in 1957 by Mihelich, Harmatz, and Handley[64], the 134-da. Dy source was produced by means of the $Tb^{159}(p, \gamma)Dy^{159}$ reaction, during the course of an investigation of the activities induced by proton bombardment of rare earths. Conversion electron lines were observed associated with the Dy^{159} decay corresponding to a 57.98-keV transition, with the following intensities: L_i, 1000; L_{ii}, ~ 140 (not completely resolved); L_{iii}, 125; M, 305; N, 80. From the L/L ratios it was concluded that this transition was M1 + E2.

In a continuation of the work, these authors[65] found evidence of similarities in the spectra associated with the decays $Dy^{155} \xrightarrow[e.c.,10h.]{} Tb^{155}$ (5.6 da.), $Dy^{157} \xrightarrow[e.c.,8h.]{} Tb^{157}$, and $Dy^{159} \xrightarrow[e.c.,134da.]{} Tb^{159}$ (stable), and listed the ground-state band rotational levels at 64.5 and 155.8 keV in Tb^{155}, 60.8 and 143.9 keV in Tb^{157}, and 58.0 and 137.5 keV in Tb^{159}, and gave values for the coefficients A, B under the assumption $E_I = E_o + AI(I+1) + BI^2(I+1)^2$. They found for the Tb^{157} 60.8-keV transition, $L_i/L_{ii}/L_{iii} = 1/\geq 0.14/0.12$ or $\delta^2 \equiv E2/M1 = 1/60$, and for the Tb^{159} 58.0-keV transition, $L_i/L_{ii}/L_{iii} = 1/0.18/0.12$ or $\delta^2 = 1/65$.

Ketelle and Brossi[66] used proton capture on ion-exchange purified Tb to produce Dy^{159}, on which they did a variety of measurements. They observed gamma rays of ~200, ~300, and 350 ± 10 keV in singles; K X-rays; inner bremsstrahlung with end point < 350 keV; 59; 200; and 290; but no 350-keV gamma rays in coincidence with K X-rays; and the same plus 350-keV gamma rays in coincidence with L X-rays. With the new gamma rays suggesting a new Tb level, the absence of K capture to this level implied a maximum difference between it and the Dy^{159} ground state of 50 keV. From various intensity measurements using both NaI and proportional counters, the latter to resolve the 58-keV gamma ray from the various X-rays, a number of conclusions were reached. With the source between two NaI crystals in a 4π geometry, a spectrum was obtained which had two broad peaks centered at 46 and 98 keV, due to various combinations of Dy and Tb X-rays and the Tb 58-keV gamma ray. From the size of the "98"-keV peak and the observed absolute K X-ray rate, K X-ray/gamma ray ratio, and the fluorescent yield, it was concluded that $\alpha_K(58) = 5 \pm 1.5$. From assumed K/L capture ratios, the above α_K, and the size of the "46"-keV peak, the capture branching ratio to the 0- and 59-keV levels was deduced. The capture branches were found to be e.c. to the ground state, 75%, log ft=7.2; e.c. to the 58 -keV level, 25%, log ft=7.8; e.c. to the assigned 350-keV level, $\sim 10^{-3}$%. Then the e.c. decay is first forbidden, implying for the Dy ground state 1/2- or 3/2- but not 5/2- because no beta group to the Tb 136-keV level was seen. The intensity ratios of the 350, 290, and 200-keV gamma rays were found to be 0.2/1.0/1.0, and the gamma radiation, prompt to a 1 μsec. resolving time coincidence circuit, implying multiploarity no higher than quadrupole and probable M1 and /or E2. On this basis the 350-keV level was assigned as 3/2+ or 5/2+ but not 7/2+ because then the electron capture to this level would be first forbidden unique or third forbidden and with the maximum available energy would not be seen. A delayed-coincidence measurement of the lifetime of the 58-keV level was made, with the resulting resolving curve exactly like the Na^{22} prompt curve in appearance, with the conclusion $T_{\frac{1}{2}}(58) \leq 10^{-9}$ sec. A least-squares analysis of the electromagnetic radiation rate associated with the Dy decay, observed with a high-pressure ionization chamber, yielded the half-life for Dy^{159} of 144.4 ± 0.2 da. (error std. dev.).

Greenwood and Brannen[67] next took up the study of Dy decay, again using proton capture to prepare the source. In gamma singles were seen Tb X-rays, the 58-keV gamma ray, and an 89-keV peak which, in the absence of 138-keV gamma radiation, was assigned as a Dy K X-ray-Tb 58-keV gamma-ray sum peak from K capture to the 58-keV level. From coincidence measurements with 10^{-7} sec. resolving time, with gates set to accept the X-rays, strong K capture X-ray- internal conversion X-ray coincidences confirmed the K capture to the 58-keV level, and a bulge on one of the X-ray peaks indicated the presence of the 58-keV gamma ray. Because of the uncertainty in the 58-keV intensity, these spectra only permitted the conversion coefficient estimate $\alpha_K(58) > 6$. From the absence of 136-keV radiation the upper limit to the decay branch to the 138-keV level was set at 0.1%. By the ingenious technique of adding a second coincidence counter to detect K_α escape X-rays, which causes the escape peaks only (in principle) to occur in the observed spectra, at the energies 15.7 keV (Tb K_α), 21.9 keV (Tb K_β), and 29.5 keV (Tb 58 keV), a reasonable separation of the X-ray and gamma-ray components was achieved, permitting deduction of the K-shell-vacancy-58-keV gamma-ray ratio with the result

$$\alpha_K(58) = 8.5^{+.7}_{-1.2} \quad . \tag{II-9}$$

The total decay energy was estimated, from electron capture theoretical energy dependences and the measured LM.../K capture probability ratio for capture to the 58-keV level of

0.17 ± 0.15, to be > 230 keV. From intensity and conversion coefficient data the e.c. branches to the 0- and 58-keV levels were estimated to be 63^{+3}_{-5} % and 37^{+5}_{-3} % respectively, in rough agreement with Ketelle and Brossi[66]. It was pointed out that under the assumption of a Dy^{159} disintegration energy greater than 230 keV, of the three possible Nilsson states, 3/2- [521] , 5/2+ [642] , 5/2- [523] , the last two would, according to the Alaga[68] β-decay rules, result in allowed hindered and first forbidden hindered transitions respectively, to all three of the 0-, 58-, and 136-keV levels, implying an expected capture branch to the last of at least a few percent. They are therefore to be rejected in favor of the 3/2- [521] state, which gives first forbidden unhindered transitions to the 0- and 58-keV levels but first forbidden unique hindered to the 138-keV level, in agreement with the failure to observe this branch. But then decay to the 364-keV level observed in Gd decay would be allowed. The upper limit to a possible branch to this level was set at 0.1%, implying that the total disintegration energy is less than 450 keV, in agreement with the estimate of Ketelle and Brossi[66].

Berlovich et al.[69,70], in an effort to check Coulomb-excitation determinations of g_R and g_K in which a B(M1) value derived from measured values of B(E2), δ^2, and cascade/crossover ratio λ for the second rotational state decay was used, determined B(M1, 58) by measuring the 58-keV level half life directly by observing the capture X-ray - 58-keV gamma-ray delayed coincidence in Dy^{159} decay. By

0.17 ± 0.15, to be > 230 keV. From intensity and conversion coefficient data the e.c. branches to the 0- and 58-keV levels were estimated to be 63^{+3}_{-5} % and 37^{+5}_{-3} % respectively, in rough agreement with Ketelle and Brossi[66]. It was pointed out that under the assumption of a Dy^{159} disintegration energy greater than 230 keV, of the three possible Nilsson states, 3/2- [521] , 5/2+ [642] , 5/2- [523] , the last two would, according to the Alaga[68] β-decay rules, result in allowed hindered and first forbidden hindered transitions respectively, to all three of the 0, 58, and 136-keV levels, implying an expected capture branch to the last of at least a few percent. They are therefore to be rejected in favor of the 3/2- [521] state, which gives first forbidden unhindered transitions to the 0- and 58-keV levels but first forbidden unique hindered to the 138-keV level, in agreement with the failure to observe this branch. But then decay to the 364-keV level observed in Gd decay would be allowed. The upper limit to a possible branch to this level was set at 0.1%, implying that the total disintegration energy is less than 450 keV, in agreement with the estimate of Ketelle and Brossi[66].

Berlovich et al.[69,70], in an effort to check Coulomb-excitation determinations of g_R and g_K in which a B(M1) value derived from measured values of B(E2), δ^2, and cascade/crossover ratio λ for the second rotational state decay was used, determined B(M1, 58) by measuring the 58-keV level half life directly by observing the capture X-ray - 58-keV gamma-ray delayed coincidence in Dy^{159} decay. By comparison with the standard Hg^{203} 279-keV transition (delay $(2.90 \pm 0.12) \times 10^{-10}$ sec.), they obtained the result

$$T_{\frac{1}{2}}(58) = (1.3 \pm 0.4) \times 10^{-10} \text{ sec.} \qquad \text{(II.10)}$$

Then assuming pure M1, which is approximately correct, and the value 1.5 n.m.[71] they found $g_R = 0.44 \pm 0.10$, $g_K = 1.37 \pm 0.08$, more reasonable values, which are in disagreement with the Coulomb-excitation results (e.g., $g_R = 0.25$, $g_K = 0.49$[72]), and conjectured that the determination of the M1-E2 mixing ratio from the Coulomb excitation work[72, 73] was at fault.

However in the same year there was a theoretical development bearing on the determination of g_R and g_K. I. Lindgren[74] reported new, accurate numerical calculations of radial wave functions for rare earth ions, which are required for the determination of μ from h.f.s. data observed by paramagnetic resonance. The accuracy of the calculated matrix elements was estimated to be 5%, and the results for calculated magnetic moment values were about 15% higher than previous values. For Tb^{159} the previously reported values were 1.50 n.m., 1.52 n.m.[71, 75]. The recalculated value was 1.90 n.m. It was noted that the theoretical value calculated[24] from the Nilsson model is + 2.2 n.m., and that for Ho^{165}, the paramagnetic resonance result, corroborated by optical alignment measurements, 3.3 n.m., is recalculated at 4.1 n.m., compared to the Nilsson model prediction of + 4.5 n.m. The effect of this, as noted previously, is to increase the estimates of g_K and g_R as determined from indirect Coulomb-excitation derived B(M1) and spectroscopically determined μ values, bringing g_R more closely in line with the collective estimate.

A careful study of Dy^{159} decay was carried out by Ryde, Persson, and Oelsner-Ryde[76]. The 144 da. Dy^{159} source was perpared by bombarding 99.9% pure Tb_4O_7 with 22-MeV deuterons. All possible products from Tb bombardment are stable or short-lived except 144 da. Dy^{159}, the main activity produced, and 72 da. Tb^{160} and >30y. Ho^{166}, which were removed by means of ion exchange. Some weak lines were seen in the gamma-ray spectra that could be attributed to the decay of the long-lived products of Y^{89} (100% nat. abund.) bombardment, $Zr^{88} \xrightarrow[85da.]{} Y^{88} \xrightarrow[105da.]{} Sr^{88}$. Conversion electron data were obtained with a double-focusing beta spectrometer and a G.M. detector.

Internal and external conversion lines and gamma-ray lines were obtained in the singles mode as noted in Fig.II-1, which incorporates some conclusions of the work of Persson[77] as well. Extensive observations of internal conversion and gamma-ray line intensities relative to the 348-keV internal conversion and gamma intensities, and of the latter relative to the 58-keV intensity and the X-ray and auger yields permitted deduction of "absolute" intensities of the various transitions, with respect to the total number of decays, and of the e.c. decay branching ratios. The percentage for the weak decay branch to the 137.5-keV level was found by comparing the population of this level as deduced from the strength of the 80-and 138-keV transitions by which it decays plus Sliv and Band[48] theoretical conversion coefficients with the population implied by the strength of the 211-keV transitions by which the 348-keV level decays through it, and attributing the excess population to the e.c. branch. The results are in essential agreement with previous work.

Gamma-gamma coincidence runs using a fast-slow coincidence system with $2\tau = 30$ nsec., requiring 50 h. each for accumulation of true coincidence, random coincidence (200 μsec. delay), and coincidence background spectra, in the latter of which gamma rays in the 100- to 400-keV range in coincidence with K X-rays were observed, showed 210- and 290- but no 348-keV gamma rays. The 211-, 289-, and 348-keV transitions were found to be M1 + E2 (but the mixing ratios could not be determined), so that the 348.1-keV level is 5/2+, probably the 5/2+ [413] Nilsson level. It was noted that in Eu^{153} a 103-keV 3/2+ [411] level decays to the ground state, 5/2 + [413], with a half life of 3.3×10^{-9} sec. With the same levels involved here, and assuming E_γ^3 energy dependence for M1 transitions and equal intrinsic matrix elements since both nuclei have similar deformations, the expected Tb^{159} 348-keV level half life was calculated to be $\sim 10^{-10}$ sec., or prompt to the coincidence circuit. Hence the absence of 348-keV gamma rays, allowing the deduction that K capture to this level is less than 6%, in agreement with the observation of Ketelle and Brossi[66], correspondingly implied an upper limit for the energy separation of the Dy^{159} ground state and the Tb^{159} 348-keV level of 58 keV, so that the total disintegration energy obeys 348 keV $< \mathcal{E} <$ 406 keV.

A weak beta decay branch to the 348-keV level was seen in the Gd decay study of Persson[77], who found log $ft = 8.2 \pm 0.5$. If the same value were assumed for the Dy e.c. decay to this level, it was calculated that a decay energy of 19 keV or a total disintegration energy of 367^{+10}_{-5} keV would result.

The transition multipolarities shown in Fig. II-1 were deduced from conversion coefficient values and K/L or L/L ratios determined from the data. The small value of the K conversion coefficient for the 58-keV transition, $\alpha_K = 4 \pm 1$, was noted to be in rough agreement with the values found by Ketelle and Brossi[66] and Greenwood and Brannen[67], 5.0 ± 1.5 and $8.5^{+0.7}_{-1.2}$ respectively.

The B-value ratios for decay of the 348-keV level to the ground-state band together with the values predicted by the Alaga rules, as determined by these authors, are listed on Fig. II-1. They suggest a predominance of M1 but, because of the unknown mixing ratios, do not permit a precise check of the Alaga rules; however it was noted that there probably is a discrepancy.

C. Coulomb Excitation

Natural terbium consists of 100% Tb^{159} [78]. Upper limits for the isotopes 155 through 162 were determined in 1957 by Collins et al.[79], who found in no case a limit exceeding 4×10^{-4}%. Thus Coulomb excitation of natural Tb is a suitable method of studying Tb^{159}.

In 1955 Mark and Paulissen[80] reported results of Coulomb excitation using 2.89-MeV protons as projectiles. The bombardment of Tb_4O_7 produced a ~77-keV gamma ray, not single, a 167-keV gamma ray, probably due to impurities, and suggestion of a low-energy gamma ray among the terbium X-rays. No conclusive information about the level structure was deduced for this element.

The first quantitative measurments from the Coulomb excitation of Tb were reported by Heydenburg and Temmer[81]. 3- and 6-MeV alpha particles from a van de Graaf, with energy known to ± 50 keV, were used as projectiles. Thick target yields were obtained relative to a Au^{197} source standardized in strength by the National Bureau of Standards. As a check on the method it was found that the B-value obtained for the 136-keV transition in Ta^{181} implied a lifetime in agreement with the directly measured value. In Tb, gamma rays of 79 and 136 keV were observed with the same intensity ratio at the two energies, suggesting an origin from the same state. If the 79-keV radiation were from the excitation of an independent 79-keV level, the intensity ratio would change by a factor of three. The interpretation was made in terms of levels at 57 and 136 keV, and it was noted that the measured energy ratio, 2.39 ± 0.05, agreed with the theoretical ratio for an $I(I+1)$ level sequence with ground-state spin 3/2, 2.40. Using the value of the excitation parameter ξ appropriate for the excitation of a 136-keV level, the quantities $\epsilon\, B(E2)$ for the 136 and 79-keV transitions were calculated to be $0.041 \times 10^{-48}\ e^2 cm^4$ and $0.19 \times 10^{-48}\ e^2 cm^4$ respectively ($\pm$ 30%), but no evaluation of the factors ϵ, containing the conversion coefficients and the M1 competition correction to the branching ratio, was attempted.

It was noted that in the many nuclei studied in this work the variations in the $\epsilon\, B(E2)$ values to the second excited states of odd-A nuclei, computed from observed crossover gamma-ray yields, probably do not reflect variations in the B(E2) values but rather variations in the factors caused by the B(M1) values involved in the M1 fractions of the competing cascade gamma rays, which are proportional to $(g_\Omega - g_R)^2$, the former g-factor being prone to extreme variations. In Tb the fact that the 79-keV cascade gamma ray was ~ 5 times as intense as the 136-keV crossover gamma ray indicated the predominance of this M1 component. It was noted further that deformations derived from the intrinsic quadrupole moment Q_0, available when the ϵ factors could be evaluated, tended not to agree with the deformations implied by the values of the inertia parameters $\frac{\hbar^2}{2\mathcal{I}'}$ from the observed level spacings on the model assuming irrotational flow.

In 1956 a further study was reported by Heydenburg and Temmer[82] in which for Tb an attempt to measure the E2 and M1 components of the transitions among the first three levels of the ground-state band was made, because of the absence of reliable theoretical conversion coefficient data and of experimental information on the M1/E2 mixing ratios in the deformed regions. Alaga rules for the intraband E2 transitions were assumed and on this basis the theoretical E2 branching ratio λ^* for crossover/cascade gamma radiation was computed, assuming level energies $E_I = E_0 + AI_0(I_0 + 1)$:

$$\lambda^* = \left(\frac{E_{I_0+2} - E_{I_0}}{E_{I_0+2} - E_{I_0+1}}\right)^5 \frac{B(E2; I_0+2 \to I_0)}{B(E2; I_0+2 \to I_0+1)} = \left(\frac{(I_0+2)(I_0+3) - I_0(I_0+1)}{(I_0+2)(I_0+3) - (I_0+1)(I_0+2)}\right) \frac{\langle I_0 2 K 2 0 | I_0 2 2 I_0 K\rangle^2}{\langle I_0 2 K 2 0 | I_0 2 2 I_0 1 K\rangle^2}$$

$$= \left(\frac{2I_0+3}{I_0+2}\right)^5 \frac{(2I_0+1)(I_0+3)}{2I_0^2(2I_0+3)} \quad . \qquad \text{(II-11)}$$

Any discrepancy in the observed intensity ratio λ was ascribed to the competing M1 component in the cascade radiation, permitting an evaluation of the mixing parameter

$$\delta'^2(I_0+2 \to I_0+1) = \frac{\lambda}{\lambda^* - \lambda} \quad . \qquad \text{(II-12)}$$

If the Alaga rules hold for M1 transitions as well, it was pointed out that then the mixing ratio for the decay radiation of the first excited state is given by

$$\frac{\delta^2}{\delta'^2} = \left(\frac{I_0+1}{I_0+2}\right)^3 \frac{I_0+3}{I_0} = 1.093 \quad \text{for } I_0 = \frac{3}{2} \quad . \qquad \text{(II-13)}$$

The odd-A nuclei in the deformation region, Eu^{153} to

Lu^{175} (and also Eu^{151}) were studied in a gamma-gamma coincidence arrangement using slow coincidences ($\tau \sim 0.5\,\mu$sec.), and previously observed rotational decay schemes were confirmed. The branching ratios λ were deduced from gamma singles spectra for the purpose of obtaining values of g_Ω and g_R within the framework of the strong-coupling Bohr-Mottelson model, which can be done as follows: the model predicts the equations

$$Q_0 = \sqrt{\frac{16\pi}{15}\,\frac{(I_0+1)(I_0+2)}{I_0}\,B(E2, I_0 \to I_0+1)} \quad ; \qquad \text{(II-14)}$$

$$Q_0 = \sqrt{\frac{8\pi}{15}(2I_0+3)(I_0+2)\,B(E2, I_0 \to I_0+2)} \quad ; \qquad \text{(II-14a)}$$

$$\mu = \frac{I_0}{I_0+1}(g_\Omega I_0 + g_R) \quad ; \qquad \text{(II-15)}$$

where Q_0 and μ are the intrinsic quadrupole and magnetic dipole moments of the ground-state configuration; and

$$B(M1; I_0+2 \to I_0+1) = \frac{3}{4\pi}\left(\frac{e\hbar}{2Mc}\right)^2 (g_\Omega - g_R)^2 \frac{4I_0^2(I_0+1)}{(I_0+2)(2I_0+5)}, \qquad \text{(II-16)}$$

from which

$$\delta' = \pm\frac{0.933\,E_\gamma Q_0}{(g_\Omega - g_R)\sqrt{(I_0+1)(I_0+3)}} \quad , \qquad \text{(II-17)}$$

where E_γ is the cascade transition energy in MeV and Q_0 is in barns. In bases for which B(E2) values for both the first and second excited states were available it was found that the derived Q_0 values agreed. Where δ was independently available, as from K/L ratio determinations, it was found to be consistent with δ'.

In Tb^{159} the observed $\lambda = 0.13$ led to the value $\delta'^2 = 0.013$ ($= 1/77$). Including an arbitrary downward correction to point-nucleus M1 conversion coefficients in conformity with what Sliv and collaborators had by then found was necessary, but using Rose's values for E2 coefficients, $1+\alpha_{tot}$ was estimated at 4.3 for the 79-keV transition and 2.0 for the 136-keV transition, giving the value corrected for cascade and conversion, $B(E2; I_0 \rightarrow I_0 + 2) = 2.2$ barns^2 or $Q_0 = 8.7$ barns. With $\mu = +1.5$ n.m., this implied $g_\Omega = 0.34$, $g_R = 1.99$ if $\delta' < 0$, or $g_\Omega = 1.66$, $g_R = 0.01$ if $\delta' > 0$, neither g_R being near the characteristic value Z/A. It was noted that the uncertainty in $|\mu|$ (which turned out to be significant) as well as in the conversion coefficient data and the (especially M1) Alaga rules rendered any definite conclusions rather doubtful.

Huus, Bjerregaard, and Elbek[72] made a study of the internal conversion lines resulting from the Coulomb excitation of Tb_4O_7 with 1.75-MeV deuterons. The following lines were observed: 80.9-keV L, 81.9-keV M, 57.9-keV L, 58.6-keV M. L line yields permitted evaluation of the ϵB values: $\epsilon B(80) \sim 0.2$, $\epsilon B(58) \approx 0.45$. Because no crossover radiation was seen it was concluded that the 80-keV radiation was mostly M1; no conclusion about the factor ϵ was reached. For the 58-keV transition, it was estimated that $1/\delta^2 \gtrsim 50$ or that the decay fraction for L conversion is $\epsilon_L = 7.7$, leading to $B(E2) = 3.5 \times 10^{-48}$ cm^4, or $Q_0 = 8.3$ barns, in essential agreement with previous work.

In 1958 three papers containing information on Tb^{159} Coulomb excitation appeared. Precise measurements of transition energies using a bent-crystal spectrograph for some rotational nuclei were reported by Chupp et. al.[83]. Using protons from a high-current linear accelerator to bombard water-cooled targets which in the case of rare earths consisted of the metal evaporated onto Cu backings, this arrangement necessary due to the inherent inefficiency for gamma detection with the bent-crystal technique, energy measurements of the Coulomb-excitation gamma rays were obtained with accuracies from 1 part in 3000 at 50 keV to 1 part in 1000 at 150 keV. Higher energies could not be detected with sufficient statistical significance in reasonable running time. The results for Tb, when corrected for X.U. to keV conversion, were $E_1 = 57.99 \pm 0.01$ keV, $E_2 - E_1 = 79.51 \pm 0.02$ keV. Measurements were made for Ho^{165} and Ta^{181} rotational levels as well. In all cases the measured E_2 was less than the value predicted in the absence of a $BI^2(I+1)^2$ energy term. The vibration-rotation interaction in which $\mathcal{I}'$ increases with I, causing a depression of the second level of the order $E_{rot}{}^3/E_{vib}{}^2$, and effects of the Coriolis interaction as given by Kerman[14], which can raise or depress a level, by an amount characteristically of the order $E_{rot}{}^3/E_{sp}{}^2$, were noted as possible causes.

Because of the uncertainties in the rotational B-values and the problems of detector efficiency, conversion coefficient, mixing ratio, cascade/crossover ratio, and thick-target yield corrections involved in their determination from gamma-ray yields, Sharp and Beuchner[57] made a determination by a method that circumvents these difficulties: measurement of the elastic and inelastic yields of proton groups from the Coulomb excitation process. The problems in the method are the necessity for very thin targets and small solid angle detectors, with resulting poorer counting statistics in the observed spectra.

7.0-MeV protons from a van de Graaf generator were used to bombard targets of rare earth metals evaporated onto Formvar that were 10 keV thick to the protons. In Tb^{159} proton groups were observed corresponding to Q-values of 58 ± 10 keV and 138 ± 10 keV, corroborating the rotational level structure. The inelastic and elastic scattered proton groups were observed in position and intensity by counting tracks in nuclear emulsion used as the detector. From these and the theoretical Rutherford differential cross-section, which upon checking at 130° and 50° and at 6.0 and 7.0 MeV was found to hold to within the experimental errors, absolute B-values were derived, assuming pure E2 excitation:

$$B(E2\uparrow;58) = (3.56 \pm 0.32) \times e^{2} 10^{-48} \text{ cm}^{4}, \tag{II-18}$$

in disagreement with the value 2.4 reported as a result of analysis of Coulomb excitation yield measurements in the review article of Alder et. al.[1] but in agreement with the value 3.5 obtained by Huus et. al.[72]; and

$$B(E2\uparrow;138) = (1.27 \pm 0.13) \times e^2 10^{-48} cm^4, \qquad \text{(II-19)}$$

in agreement with the value 1.4 reported by Alder et. al.[1] The ratio of the B-values was thus noted to be 0.36 ± 0.05, compared to the prediction of the Alaga rules,

$$\frac{B(E2;\frac{3}{2}\rightarrow\frac{7}{2})}{B(E2;\frac{3}{2}\rightarrow\frac{5}{2})} = \frac{\langle \frac{3}{2}\,\frac{3}{2}\,2\,0|\frac{3}{2}\,2\,\frac{7}{2}\,\frac{3}{2}\rangle^2}{\langle \frac{3}{2}\,\frac{3}{2}\,2\,0|\frac{3}{2}\,2\,\frac{5}{2}\,\frac{7}{2}\rangle^2} = \frac{5}{9} \approx 0.56, \qquad \text{(II-20)}$$

showing strong disagreement for the intraband B(E2) values. They reported this to be a typical situation among the rare earths.

A careful analysis of Coulomb excitation data from proton bombardment of deformed odd-A nuclei from Eu^{151} to Ta^{181} (plus two Ag and one Au isotope) for the purpose of deriving B-values was carried out by Martin, Marmier, and de Boer[73]. Gamma-ray angular correlation data and thick-target gamma-ray yields were used to obtain ϵ B(E2) values and mixing ratios, and theoretical conversion coefficients of Sliv and Band[48] were employed in the elimination of ϵ. For terbium, 4.05 ± 0.05-MeV cyclotron-generated protons were used to bombard a Tb_4O_7 target. From the gamma singles spectrum the measured 138-keV crossover/79-keV cascade ratio was found to be $\lambda = 0.16$, compared to the result 0.13 of Heydenburg and Temmer[82]. Angular correlation measurements on the 138-keV (11% anisotropy) and 79-keV radiations yielded the result $\delta'^2 = 0.02 \pm 0.01$, which compares with 0.013 derived in ref.82, but is more reliable in that it does not make use of the Alaga rules. The excitation yields resulted in the values $\epsilon\, B(E2\uparrow;79) = 0.32 \times 10^{-48}\ e^2\,cm^4$ and $\epsilon\, B(E2\uparrow;138) = 0.051 \times 10^{-48}\ e^2 cm^4$. Correcting the latter value for conversion using the theoretical Sliv and Band coefficient $\alpha = 0.94$ resulted in $B(E2\uparrow) = 1.9 \times 10^{-48}\ e^2 cm^4$, or $B(E2\downarrow) = 0.95 \times 10^{-48}\ e^2 cm^4$, from which $Q_0 = 8.1$ barns, or $\beta = 0.38$.

The accuracy of the absolute magnitudes of the directly measured B(E2) values was estimated at ± 50%. It was noted that if the Alaga rules were to hold for the E2 moments then $B(E2\downarrow;79)$ would be $1.4 \times 10^{-48}\ e^2 cm^4$, and from the observed mixing ratio and cascade/crossover branching, B(M1;79) would be 0.3 n.m.^{2} which with $\mu = +1.5$ gives $g_R = 0.25$, $g_K = 1.49$ (but, however, more reasonable values with the new value of μ).

In 1960 two Coulomb excitation studies including terbium were reported. Nathan and Popov[84] employed the 20-MeV alpha particle beam from the Copenhagen cyclotron and a helium gas energy degrader to observe the Coulomb excitation at 14, 17, and 20 MeV of several elements in the rotational and vibrational regions. To facilitate the search for weaker excitations, only radiation in coincidence with backscattered ions, as detected with a ring CsI detector and a fast-slow coincidence system of 60 nsec. resolving time, was observed, in order to suppress the competing background. Thick metallic targets were used; a discriminator was set to accept only the higher part of the thick-target particle spectrum, to guard against detection of contaminating low-energy reaction products, if any. From the number of counts in the alpha and gamma counters, assuming the gamma photopeaks to be entirely the result of the excitation of known mulitpolarity, and upon doing thick-target integrations of the first-order (single-excitation) cross sections, values of ϵ B(E2) were deduced. At 14 and 17 MeV these tended to agree with previous Coulomb excitation results, but at 20 MeV some anomalies showed up, suggesting detectable double E2 processes at this energy. For Tb, transitions of 200 ± 10 keV, 360 ± 15 keV, and 560 ± 20 keV were observed, with ϵ B(E2) values 0.010, 0.013, and 0.019 respectively, in units 10^{-48} $e^2 cm^4$. These were interpreted as due to excitation of a 560-keV level and its subsequent decay to the 3/2+ ground state and the 363-keV 5/2- level seen in Dy^{159} decay. It was speculated that if the 560-keV state were one of the two gamma-vibrational states then it would be the 7/2+ state, with the 200-keV transition an E1, and the B(E2 $\uparrow$) to it would be small compared to the case of gamma-vibrational states in the adjacent even-even nuclei, a situation that it was noted obtains also in Ho^{165} where an observed 515-keV 3/2- state is almost certainly one of the gamma-vibrational states since the nucleus can have no low-lying 3/2- Nilsson states.

Olesen and Elbek[85] made another determination of B-values by observing inelastic projectile groups. Protons and deuterons from a 5-MeV van de Graaf were used to bombard pure rare-earth oxide targets evaporated onto aluminized

Formvar or pure carbon foils, of 50 to 100 $\mu gm/cm^2$ thickness. The projectiles were observed by counting tracks in photographic emulsion. In Tb, groups were found corresponding to levels at 59 ± 2 keV and 138 ± 2 keV, for which , from the excitation cross-section formulae, the B-values were calculated to be $B(E2\uparrow;59) = 2.81 \pm 0.08$ and $B(E2\uparrow;138) = 1.54 \pm 0.06$, in appropriate units, compared to 3.56 ± 0.32 and 1.27 ± 0.13 respectively, found by Sharp and Beuchner[57] by this technique. The ratio is then 0.516, much closer to the value from the Alaga rules, 0.556, than the ratio 0.36 of the values of ref. 57. It was pointed out that this is much more reasonable, since perturbations on the pure rotational states should not alter the intraband B(E2) values more than perhaps $\sim 2\%$.

D. Miscellaneous Measurements

The ground-state spin of Tb^{159}, $I_o = 3/2$, was first determined from h.f.s. measurements in 1934 by Schuler and Schmidt[86], and was corroborated by Baker and Bleaney[75] and Hutchison and Wong[87], who found $|\mu| = 1.5$ and $\mu = +1.52 \pm 0.08$ respectively (now revised to ~ 1.90).

A value of Q_o was determined by Fuller and Weiss[88] from an analysis of the giant dipole resonance profile, observed by exciting Tb^{159} (and Ta^{181}, Au^{197}) with high-energy bremsstrahlung and measuring the photoneutron yields. Using the value $r_o = 1.09$ f. in the theory they found $Q_o = +5.6 \pm 0.6$ barns, smaller than the results from B(E2) determinations.

Transitions in Tb^{159}

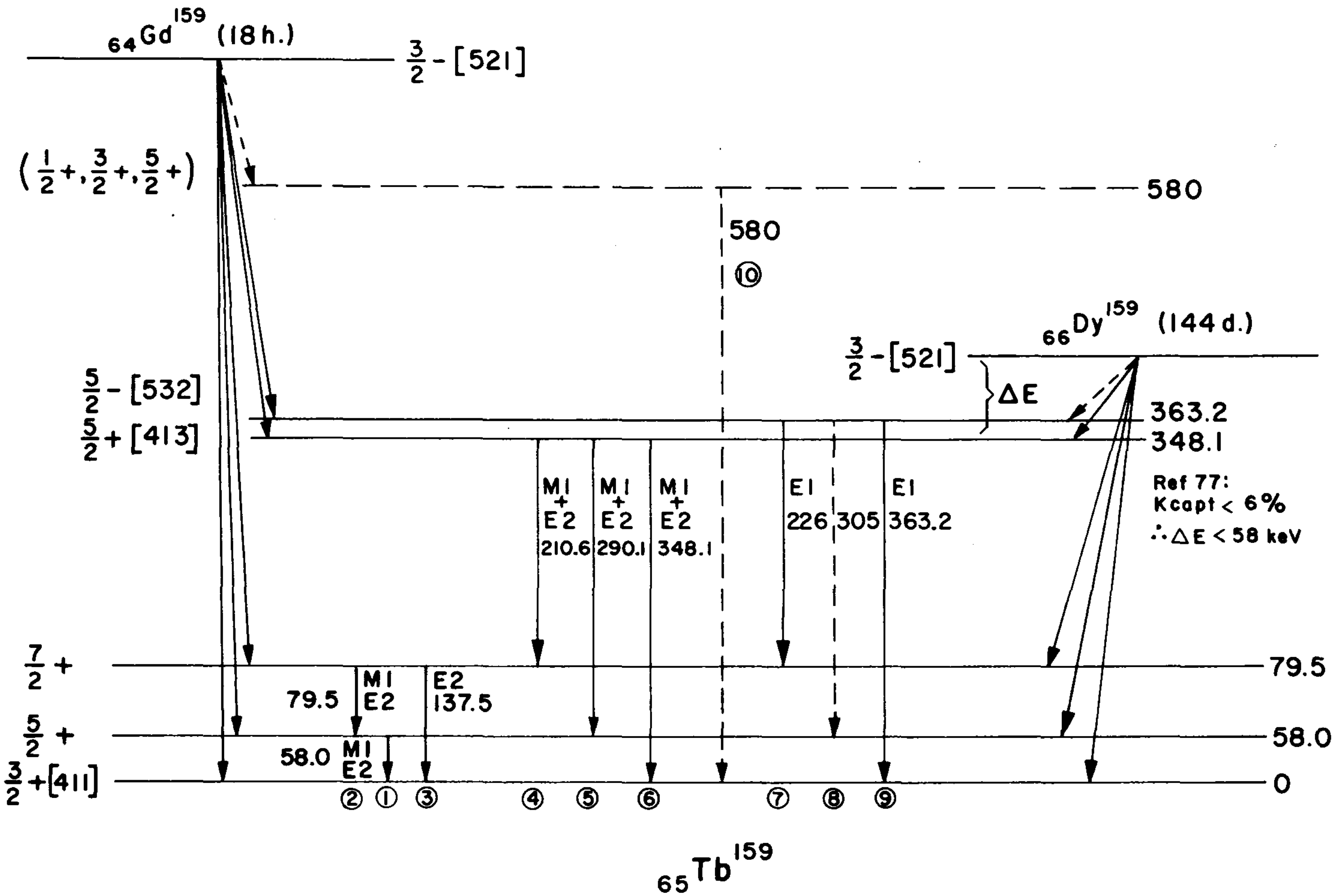

FIG II-1

Fig. II-1-Notes

Transition number:

1 Ref. 83: $E_\gamma = 57.99 \pm 0.01$ keV (xtal. diffraction)
Ref. 64: $E_\gamma = 57.98 \pm 0.09$ keV
(others)
Ref. 76.77: L_{iii}/L_i implies M1E2, $\delta^2 = 0.015 \pm 0.004$ (Tb^{157}, analogous 61-keV transition: $\delta^2 = 0.011 \pm 0.003$)
$\alpha_K = 4 \pm 1$ (from Dy decay).
Ref. 66: $\alpha_K(59) = 5.0 \pm 1.5$
Ref. 67: $\alpha_K(58) = 8.5 {}^{+.7}_{-1.2}$
Ref. 72: i.c. intensities imply $\delta^2 \lesssim 0.02$, B(E2↑) $= 3.5e^2 10^{-48}$ cm.^{4}, $Q_0 = 8.3$ barns.

2 Ref. 83: $E_\gamma = 79.51 \pm 0.02$ keV
Ref. 56: Gd decay 255-79 ang. correl. implies $\delta(79) \equiv \delta' \equiv \sqrt{E2/M1} = +0.13 \pm 0.06$
Ref. 73: 137.5-keV state decay crossover/cascade ratio is $\lambda = 0.16$
Ref. 82: Crossover/cascade ratio is $\lambda = 0.13$. Then Alaga rules imply $\delta'^2 = 0.013$. Estimate $\alpha_{tot}(79) = 3.3$, $\alpha_{tot}(136) = 2.0$, B(E2↑)$= 2.2e^2 10^{-48}$ cm^4, $Q_0 = 8.7$ barns.
Ref. 73: Ang. correl. measurements imply $\delta'^2 = 0.02$. Measured ϵB(E2,79) = 0.32, ϵB(E2,138) = 0.051, est. from Sliv & Band conv. coeff., B(E2↑) = 1.9 ± 50%, B(E2↓) = 0.95, $Q_0 = 8.1$, deformation parameter $\beta = 0.38$.
Ref. 57: Inelastic proton groups imply levels of 58 ± 10 keV, 138 ± 10 keV, B(E2,58↑) = 3.56 ± 0.32, B(E2,138↑) = 1.27 ± 0.13, ratio=0.36 ± 0.05 (Alaga rules give 5/9)
Ref. 85: Inelastic proton groups imply levels of 59 ± 2 keV, 138 ± 2 keV, B(E2,59↑) = 2.81 ± 0.08, B(E2,138↑) = 1.54 ± 0.06. ratio=0.516.

3 Ref. 83: $E_\gamma = 137.50 \pm 0.03$
Ref. 76,77: $\alpha_K > 0.06$
β-γ and γ-γ cascade relationships variously confirmed.

4 Ref. 76,77: $E_\gamma = 210.6 \pm 0.3$ keV (ext. conv., Gd decay). E.c., i.c. and γ lines observed in Gd and/or Dy decays.

5 Ref. 76,77: $E_\gamma = 290.1 \pm 0.3$ keV (ext. conv., Gd decay). E.c., i.c. and γ lines observed in Gd and/or Dy decays.
Ref. 56: 225-keV-79-keV cascade verified.

6 Ref. 76,77: $E_\gamma = 348.1 \pm 0.3$ keV (ext. conv., Gd decay). E.c., i.c. and γ lines observed in Gd and/or Dy decays.

Fig. II-1-Notes (Cont.)

Transition number:

4-6 Ref 76,77: 211 keV/290 keV/348 keV intensity ratios from Dy decay: gamma, 0.04 ± 0.02/--/1.0 ± 0.1 (348 γ = 1); K i.c., 0.5 ± 0.3/0.13 ± 0.04/1.0 ± 0.2; L i.c., 0.25 ± 0.15/ 0.35 ± 0.15/0.25 ± 0.10 (348K = 1). B-value ratios B(211)/ B(290)/B(348): experiment, 0.5 ± 0.3/0.3 ± 0.1/1 ± 0.1 if pure E2, 0.18 ± 0.09/0.22 ± 0.07/1 ± 0.1 if pure M1; Alaga rules, 0.83/1.5/1 if pure E2, 0.071/0.43/1 if pure M1. Suggests band impurities.

Ref 66: 200-keV/290-keV/350-keV intensity ratios = 0.2/1/1; 59-, 200-, 290-keV gamma rays observed in coincidence with K X-rays; same plus 350-keV gamma rays observed in coincidence with L X-rays.

7-9 Ref. 47: 225 γ-57L, 300 γ-57L, 225 γ-79K, 225 γ-79L cascades observed. B(E1)-value ratios, 364-keV/300-keV/ 225-keV = 1/0.016/0.11; Alaga rules, 1/0.43/0.07. 225-, 300-keV i.c. lines not observed, implying E1. β-γ cascade verified.

Ref. 54: B(E1)-value ratios: 1/0.018/0.11

Ref. 55: B(E1)-value ratios: 1/0.013/0.12. Similar results for Tb^{155}, Tb^{157}.

Ref. 51: $\alpha_K(362) = 0.0081 \pm 0.0020$

Ref. 47: $\alpha_K(364) = 0.0083$; $\alpha_{theor}(E1) = 0.0090$ ($Cs-Ba^{137}$ 662-keV standard).

Ref. 49: $\alpha_K(361) = 0.0039 \pm 0.0008$

10 Ref. 76,77: $E_\gamma = 580 \pm 5$ keV (Gd decay)

Ref. 84: $E_\gamma = 200 \pm 10$ keV, 360 ± 15 keV, 560 ± 20 keV (c.e., 17-MeV alpha particles). Suggests excitation of 560-keV level and subsequent decay to ground state and 363-keV 5/2- level.

The mass assignments for this isomeric activity and for the beta-unstable 2.5 h. activity produced by neutron-irradiation of dysprosium oxide, Dy^{165m} and Dy^{165} (and also the activities: 102 h., Yb^{175}; 6.6 d., Lu^{177}; following irradiation of ytterbium and lutetium oxides), were made by Inghram et. al.[103, 104] using a mass-spectroscopic isotope separation technique. They pointed out that failure to observe a growth of the 2.6 h.-activity after a short irradiation by Flammersfeld suggested that some Dy^{165m} decayed directly to Ho^{165}.

In a study of the Dy^{165} decay, Slatis[97] found the beta end-point energy to be 1.24 MeV and observed 0.42-MeV and 0.88-MeV beta components and, from a study of internal and external conversion, 0.36-MeV, 0.76-MeV, and 0.91-MeV electromagnetic transitions. In 1948 during a study of nuclear isomerism N. Hole[105] observed a 93-keV electron radiation accompanying dysprosium decay, which he attributed to L-conversion of a 102-keV transition in Ho. Two years later R. Caldwell[106] reported observations of K, L_1, L_2, M, and N conversion lines due to an 87.8$\pm$0.7-keV transition, and a sixth line, probably a K line due to a transition of greater than 300 keV, associated with the 2.6 h. Dy^{165} activity, and K, L_1, L_3, M, and N lines, with relative intensities 1.8, 14.3, 9.4, 6.3, and 3.0 respectively, due to a 109.0-keV transition associated with the 1.3-min. isomeric activity, for which the lifetime and the K/L ratio of 0.08 suggested a hexadecapole transition. In 1951 Wright and Deutsch,[107] attempting to measure nuclear excited-state half lives with a delayed-coincidence technique, using anthracene or stilbene scintillation detectors, observed a 91-keV level in Ho^{165} populated in Dy decay, and found the half life to be less than 5 nsec. The same year J. Kahn[108] observed a 102-keV gamma ray from Dy^{165m} decay, utilizing a gamma scintillation detector. The following year Mihelich and Church,[109] in the course of a study of the energies and intensities of low-energy transitions in neutron-induced beta activities in heavy elements, reported associated with 2.5 h. Dy^{165} activity, K, L_1, L_3, M_1, and N_5 lines due to a 95.1±0.05-keV transition, for which $K/L_1/L_3$ intensities were 6.4/1.0/<0.2, or K/L = 5.9±2.0, suggesting M1 or M1+E2.

Jordan et. al.[110] investigated the dysprosium activity with a 180° electron photographic spectrometer and scintillation coincidence spectrometer. K, L_2, L_3, M_2+M_3, and N lines with relative intensities 3,10, 10, 5, 1.5, K/L=0.15±0.05, due to a 108.0±0.2-keV transition in Dy, and a weak K line due to a 517±3-keV transition in Ho were observed associated with the 1.2-min. activity. For the former it was noted that the K/L ratio, comparing to an empirical relation of Goldhaber and Sunyar, suggested E3. Associated with 2.3 h. activity were the lines due to Ho transitions: K, L_1, M, N, intensities 60/7.8/~1.5/--, K/L=7.7±2.0 suggesting M1 due to a 94.4±0.2-keV transition; K, L_1, K/L>5 due to a 279.4±0.8-keV transition, K, L_1, K/L>5 due to a 361.2±1.0-keV transition, and K, L due to a 634±3-keV transition. Gamma-ray singles spectra showed lines due to K X-rays and 108-keV, 160-keV, 310-keV, and 515-keV gamma rays decaying with 1.2-min. half life. 360-keV gamma rays were found to be coincident with the 160-keV region. None of the higher transitions were in coincidence with the 108-keV transition, but seemed to be in coincidence with a beta ray. From the X-ray and 108-keV gamma ray intensities, neglecting X-rays from conversion of higher-energy transitions, it was estimated that $\alpha_K(108)\sim4$, corresponding to $\alpha_{tot}(108)\sim40$. Gamma rays from the 2.3 h. activity corresponding to the internal conversion lines and to 710-keV and 1020-keV transitions were observed. The 279-keV and 710-keV gamma rays, and the 361-keV and 634-keV gamma rays were found to be in coincidence; other possible cascade pairs were found not to be in coincidence. The decay-scheme proposal by this group, consistent with all the data, is shown in Fig. III.1.

In a study of isomeric transitions with a beta spectrometer, G. Weber[111] observed internal conversion lines in the Dy activities: K and L lines having a 1.25-min. half life, corresponding to a transition of 106.2 ± 1.4 keV, $K/L=0.15\pm0.03$, suggesting from the Goldhaber-Sunyar empirical curves, E3; and K and L lines with a 2.42 h. half life, transition energies 92.7 ± 0.8 keV, $K/L=2.7\pm0.5$, suggesting M1+E2.

E. Mayquez[112] measured the Dy^{165} activity half life, with the result $T_{1/2}=143.0\pm2.6$ min. ($=2.838\pm0.043$ h.).

Grenags and Meessen[113] obtained Dy^{165} from neutron-irradiation of Ho_2O_3, and did a study of the decay radiation. 630 keV-360 keV and 270 keV-710 keV cascades were observed, in agreement with Jordon et. al.[110] The resolution of the coincidence circuitry was shorter than the lifetime of the

360-keV state, indicating a lifetime $>2.5 \times 10^{-7}$ sec., in agreement with Kane et. al.,[114] who measured this half life by the method of delayed coincidences, with the result 6.65×10^{-6} sec. Measurements of the angular correlation coefficients for the 270-710 cascade, with both solid and liquid sources for which the results agreed within the experimental errors, gave $A_2=-0.040\pm0.007$, $A_4=-0.011\pm0.006$, which it was noted were consistent within the experimental errors with $11/2\rightarrow7/2\rightarrow7/2$ and $5/2\rightarrow(5/2$ or $3/2)\rightarrow7/2$ but not $3/2\rightarrow5/2\rightarrow7/2$ spin sequences.

Bonhoeffer et. al.[115] made a study of the radiations accompanying Dy^{165} decay using beta and gamma-ray spectrometers for which detectors were anthracene and NaI(Tl), and coincidence techniques. The results of the study, beta and gamma transition energies and intensities, cascade relationships, and proposed decay scheme, are shown in Fig. III.1.

Harmatz et. al.[65] measured energies, to $\sim$0.15%, and intensities of lines from the decay of proton-rich isotopes produced by proton irradiation of very pure rare-earth oxides, using an internal conversion permanent-magnet photographic spectrometer, and ion-exchange and chemical activity separation procedures. Their interpretation of holmium isotope results is shown in Fig. III.1.

The ground-state and isomeric activities of Dy^{165}, produced by neutron irradiation of Dy_2O_3, were studied with gamma scintillation and electron spectrometers by R. Tornau.[117] The results and the proposed decay scheme are displayed in Fig. III.1.

Hashizume et. al.[118] irradiated 99.9% pure Dy_2O_3 with neutrons and studied the resulting radioactivity with NaI(Tl) counters and gamma-gamma sum-coincidence techniques. The results and interpretation of this investigation are shown also in Fig. III.1.

T. von Egidy,[119] using a double-focusing beta spectrometer set for 0.11% resolution, studied the internal-conversion spectrum following Dy^{165} decay by a technique in which the source, produced by the Ho^{165} (n,γ) reaction was located within a reactor, the electrons emerging through an evacuated tube. Energy and conversion ratio calibrations were made with $Ca\text{-}Ba^{137}$ and $Au\text{-}Hg^{198}$ standard sources. The observed i. c. lines and comparisons with previous work and with Rose's theoretical conversion coefficients are listed in Fig. III.1.

Experimental M1 conversion coefficients had been found in some nuclei which disagreed with the theoretical value of Rose,[48] and of Sliv and Band[49] who used a surface-current nuclear model, a circumstance shown by Church and Weneser[120] and by Green and Rose[121] to be theoretically expected as a nuclear-structure effect, giving M1 coefficients in the form

$$\beta_\lambda \approx [1-(\lambda-1)C(Z,k)]^2 \beta_1 \; . \qquad \text{(III-1)}$$

Here $\lambda = M_e/M_\gamma$ =matrix-element ratio for electron and photon emission has the value 1 for the surface-current model. The λ-dependent structure effect is particularly pronounced in slow M1 transitions such as l-forbidden particle transitions, 2+ gamma-vibrational band$\rightarrow$2+ ground-state band transitions in even-even nuclei, or intraband M1 transitions in odd-A rotational nuclei. Because of this situation Novakov and Stepić[122] measured the M1 coefficients in some odd-A rotational nuclei, where the small B(M1) values result from the accidental circumstance, $g_R \approx g_K$. The deexcitation of the first excited state in Ho^{165} was among the transitions studied. From the X-ray and 94-keV gamma-ray intensities in the gamma-ray spectrum in coincidence with the high-energy portion of the beta-ray spectrum, the total K-conversion coefficient was found:

$$\alpha_K(94) = 2.5 \pm 0.2 \; . \qquad \text{(III-2)}$$

K/L ratios were determined using an iron-free double-focusing spectrometer of resolution 0.08%, with the results:

$$\text{(III-3)}$$

$$\frac{K}{L_1+L_2} = 6.75 \pm 0.20, \qquad \frac{L_1}{L_2} = 6.5 \pm 0.2,$$

$$\frac{L_1}{L_3} = 13.4 \pm 0.4, \qquad \frac{L_2}{L_3} = 2.0 \pm 0.1.$$

From these and α_K, α_L -values were calculated:

$$\alpha_{L_1}(94) = 0.320 \pm 0.025; \; \alpha_{L_2}(94) = 0.049 \pm 0.005; \qquad \text{(III-4)}$$

$$\alpha_{L_3}(94) = 0.024 \pm 0.004.$$

To obtain the $\alpha(M1) \equiv \beta$ components, the E2-M1 mixture was estimated from the conversion ratios to be 2% E2, and it was noted that a small uncertainty in this would not affect the K or L_1 results seriously. The values found were:

Theor. values, $\lambda=1$ (Sliv & Band) (III-5)

$$\beta_K(\lambda)=2.5\pm0.2 \qquad \beta_K(1)_{Th.}=2.65$$
$$\beta_{L_1}(\lambda)=0.323\pm0.025 \qquad \beta_{L_1}(1)_{Th.}=0.357$$
$$\beta_{L_2}(\lambda)=0.031\pm0.005 \qquad \beta_{L_2}(1)_{Th.}=0.0284$$
$$\beta_{L_3}(\lambda)=0.0045\pm0.0004 \quad \beta_{L_3}(1)_{Th.}=0.0048\ .$$

With C(Z,k)=0.0147, C(Z,k)=0.0154 from K and L_1 subshell tabulations and the experimental ratios:

$$\beta_K(\lambda)/\beta_K(1) = 0.94\pm0.07;\ \beta_{L_1}(\lambda)/\beta_{L_1}(1)= 0.90\pm0.07\ , \qquad \text{(III-6)}$$

it was calculated that $+2<\lambda<+5$, in agreement with the theoretical result of A. Reiner[123] for rotational collective M1 transitions, $+0.8<\lambda<+1.8$. That is, there was an observed structure effect, correctly predicted by the collective model. The three experimental L-subshell ratios were compared with theoretical ratios plotted as a function of E2 admixture, and gave slightly different, nonoverlapping results ranging from 1¾ % to ~3% E2, suggesting different values of C(Z,k) for the different L subshells, in agreement with a theoretical prediction to this effect by Church and Weneser.[124]

L. Persson et. al.,[125] in the course of a program of study of the level structures of deformed rare-earth nuclei, did a careful investigation of the Dy^{165} decay, using double-focusing and intermediate-image beta spectrometers, NaI(Tl) and bent-crystal diffraction gamma spectrometers, and a gamma ray external converter. The source was produced by neutron-irradiation of 99.9% pure Dy_2O_3 (natural isotopic composition, 28% Dy^{164}). Care was exercised to eliminate incorrect isotope assignment of any transition because of possible competing activations of principal impurities and other Dy isotopes: $Dy^{164}(n,\gamma)Dy^{165}(n,\gamma)Dy^{166}$(82 h.), Dy^{158}(0.1% nat. abund.) $(n,\gamma)Dy^{159}$(144 d.), $Ho^{165}(n,\gamma)$ Ho^{166m}(27 h.), $Tb^{159}(n,\gamma)$ Tb^{160}(73 d.), and $Y^{89}(n,\gamma)Y^{90}$(64 h.). In the study of the Dy^{165m} activity the source was retracted from the irradiating pile and positioned in the measuring apparatus by a fast-acting pneumatic device.

Results and comparisons with other work of crystal diffraction energy measurements presented by these authors are shown in Table III.1.

Dy decay gamma-ray spectra were obtained with the NaI(Tl) detector. No peaks above 1080 keV were observed. Only the K X-ray and 94.7-keV and 361.5-keV gamma-ray intensities were derived from the scintillation spectra, K/94.7-keV γ/361.5-keV γ =(0.930$\pm$0.037)/(0.370$\pm$0.022)/(0.100$\pm$0.012), which from the K fluorescent yield[126] corresponded to 1.000 $\pm$0.040 K-shell vacancies, or correcting for conversion in higher transitions, 0.970$\pm$0.050 vacancies due to the 94.7-keV transition, from which was calculated

$$\alpha_K(94.7) = 2.62\pm0.20 \ . \qquad \text{(III-7)}$$

Energies and relative intensities of other gamma rays were obtained from external conversion spectra (intensities could not be reliably extracted from the crystal-diffraction data). Photoelectron lines from a uranium converter, observed with a double-focusing spectrometer and G. M. detector, were converted to gamma intensities with the aid of theoretical photoelectron cross-section and (K+L+M)/K cross-section ratios from tables of White-Grodstein[127] and of Hultberg,[128] corrected for angular distribution effects using experimental and theoretical photoelectron angular distributions, and also for absorption in the source and converter, equipment dead-time, and source decay. The main background was Compton electrons from the converter. Source beta rays and i. c. electrons were shielded out with aluminum. Energy errors were mainly statistical and calibration errors; the calibration point was the 361.5-keV L_{1+2} photoelectron line. Intensity errors were $\sim$5% for the photoelectron cross-section. The results and comparisons given are shown in Table III.1. It was noted that, assuming the 715.7-keV and 621.0-keV transitions are between a 715.7-keV level and the first two members of the ground-state band in Ho, the Alaga rules for B-value ratios imply a 621.0 keV/715.7 keV gamma intensity ratio 0.186, while the experimental ratio was 0.15 ± 0.04.

Internal conversion spectra were obtained employing a thin target of oxide vacuum evaporated onto 2 mg./cm.^{2} aluminum foil, good thickness uniformity of which was achieved by mounting the foil on a spindle which was rotated just above the crucible opening at 2-300 r.p.m. No interfering radiations from activation of the backing were found by activating a plain aluminum foil. The lines were observed with the double-focusing spectrometer set for momentum-resolution 0.1%-0.5% and a G. M. detector with 4-keV cutoff, calibrated with B, F, and I lines from a near-monolayer Th(B+C'+C")source. The main energy errors were from magnetic field fluctuations. Intensities were normalized to the 361.5-keV gamma intensity with the aid of the measured $\alpha_K(94.7)$ and $\alpha_K(361.5)$. The results are displayed in Table III.1. The mixing ratio $\delta^2 \equiv I_\gamma^{E2}(94.7)/I_\gamma^{M1}(94.7)$ was calculated from the L ratios, $\delta^2=(I_{L_3}/I_{L_1}) \times [\beta_{M1}(L_1)/\alpha_{E2}(L_3)]$, using theoretical coefficients of Sliv and Band[48], after correcting the L_3 intensity for slight M1 admixture and the L_1 intensity for slight E2 admixture from the theoretical ratios of Sliv and Band interpolated for Z=67; $L_1/L_2/L_3$=0.115/0.81/0.81 (E2); =0.36/0.031/0.0048 (M1), with the result,

$$\delta^2(94.7) = (2.6 \pm 0.4)10^{-2}. \qquad \text{(III-8)}$$

The error excludes the nuclear-structure uncertainty in the deformed region.

Beta-ray branching in the Dy^{165} decay was deduced from a measurement of the total beta-ray and 94.7-keV K-line intensities with the double-focusing spectrometer (result, $I(94.7K)/I(\beta^-_{tot})=0.093 \pm 0.010$) and the conversion line and gamma-ray relative intensities.

The primary beta end-point energy was determined from a Kurie plot of the high-energy portion of the beta spectrum obtained with the double-focusing spectrometer, momentum resolution set at 0.8%, after subtraction of a hypothetical component of maximum energy 94.7-keV less than the energy of the ground state-ground state transition, with intensity ratio 0.173±0.020. The g.s.-g.s. transition, it was noted, is first-forbidden, unhindered, and the Kurie plot of the corrected high-energy portion of the spectrum was a straight line. The errors were uncertainties in the straight-line fit and in the spectrometer calibration. The result was

$$E_{max}(\beta^-) = 1285 \pm 10 \text{ keV}, \qquad \text{(III-9)}$$

which was compared with the result of Cranston et al.,[129] 1.28 MeV, and the predictions from nuclide mass tables of Cameron,[130] Everling et. al.,[131] and Seeger:[131a] 1857 keV, 1250±20 keV, and 1234 keV respectively.

The 361.5-keV K-conversion coefficient was measured against that of a $Ca\text{-}Ba^{137}$ 662-keV standard using the intermediate-image spectrometer and a NaI(Tl) counter. The Ca-Ba values used were $\alpha_K = 0.093 \pm 0.005$ (mean of determinations of Hultberg et. al.[132] and De Vries et. al.[133]); $K/LM... = 4.55 \pm 0.10$ (mean of determinations of Graves et al.[134] and Maerter and Birkhoff[135]). The main errors were from the 662-keV uncertainty, the ratio of photopeak efficiencies at the two energies, and absorption, dead-time, and solid-angle corrections. The result was

$$\alpha_K(361.5) = 0.22 \pm 0.04. \qquad \text{(III-10)}$$

Multipolarity assignments were made on the basis of comparison with theoretical conversion coefficients of Rose[50] (uncorrected for screening and finite-nucleus effects) and Sliv and Band[48] (corrected for these but subject to the structure-effect uncertainties of Church and Weneser[120]), and are listed in Table III.1.

From a study of the decay of the 94.7-keV gamma-ray peak in the NaI(Tl) spectra through ten half lives, the half life for the Dy^{165} decay was determined to be 139.0±0.5 min. No e.c. or gamma lines attributed to Ho^{165} decayed with a different half life, including the new 575.1-keV and 1055.6-keV K lines (deviation from 139-min. h.l. < 10%).

A discussion of the data was presented in which the following points were developed. The deformation of Ho^{165} was given from experimental information by Olesen and Elbek[85] as $\delta \equiv \Delta R/R_0 = 0.31$, in agreement with the theoretical calculation of Mottelson and Nilsson[24] in which the sum of the single-particle Nilsson states, filled in pairwise fashion, was minimized, $\delta \approx 0.30$. In connection with the proposed decay scheme (Fig. III.2), the log ft value for the g.s.-g.s. beta transition implies first-forbidden unhindered or $\Delta\pi$ = yes. Measured ground-state spins in Ho^{165} and Dy^{165} are both 7/2. For $\delta \approx 0.30$, the Nilsson model predictions for the ground states are 7/2-[523] and 1/2-[521] respectively, with a low-lying 7/2+[633] orbital in Dy^{165}. There is, then, in dysprosium evidently a level inversion, the 7/2+ state being the ground state, for which the change in asymptotic quantum numbers, $\Delta N=1, \Delta n_z=1, \Delta\Lambda=0$, implies an unhindered beta transition (Alaga et al.[22]). The 1/2- state is the 1.25-min. isomer, decaying partly to the Dy^{165} ground state by E3, partly to Ho^{165} by beta decay.

Of the first two excited states in the ground-state band, a discrepancy in the reported energies for the second was noted: 209$\pm$2 keV by Olesen and Elbek,[85] agreeing with other determinations, and 204.63$\pm$0.05 keV by Chupp et al.,[83] who mistook the Ho line for an anticipated background line from their copper target backing, and measured an unanticipated background line.

The absence of observable population of the 11/2- ground-state band member in the Dy^{165} decay is consistent with the anticipated log ft value for the transition which implies a branch $\sim$1% of the branch to the 9/2- member. Because if it terminated on the first excited state there would be an unexplained absence of a crossover transition to the ground state, the 361.5-keV transition was assigned as deexciting a 361.5-keV level, fed via a 633.5-keV decay of a 995.1-keV level, which is supported by observations of several authors of a 633 keV-361 keV cascade relationship. Of the possible assignments for the 361.5-keV level, 3/2+ and 11/2+ implied by the M2 transition multipolarity determined from α_K and K/L values and the 7/2- assignment for the ground state, the latter was rejected because of absence of a deexciting transition to the 94.7-keV level, and the former was identified with an anticipated 3/2+ [411] Nilsson state, implying for the M2 transition, $\Delta N=-1, \Delta n_z=-1, \Delta\Lambda=-2$, or an allowed status according to the asymptotic selection rules.[22] An unexplained anomaly was the total 361.5-keV transition intensity, 0.128±0.013, vs. the 633.5-keV intensity, 0.0650±0.0060, suggesting that the 361.5-keV level is fed by another means, which would not be beta decay from the Dy^{165} ground state because this would be second-forbidden, log ft ~13, very weak.

The 635.5 keV-361.5 keV and the 279.6 keV-715.5 keV transition pairs had been observed by other groups to be in cascade, deexciting the 995.1-keV level. A transition of 620 keV seen by Cranston et al.[129] corresponds to the 621.0-keV transition external conversion line observed here, differing in energy from the 715.7-keV transition by an estimated 94.7±0.5 keV, suggesting the cascade decay of the 995.1-keV level not through a 279.6-keV but through a 715.7-keV level, deexciting to the first two members of the ground-state band. The total intensity (361.5-keV gamma=1) of the 279.6-keV transition feeding this level, 0.650±0.060, vs. the total intensity of the 715.7-keV and 621.0-keV transitions deexciting it, 0.750±0.070, suggested that any direct beta branch to the level would be quite weak, < 0.210. The 621.0/715.7 intensity ratio agrees with the Alaga rules if the 715.7-keV state has spin 7/2.

Log ft for the beta branch to the 995.1-keV level, 5.7±0.2, indicates allowed, hindered, and hence positive parity for this state. Measured $\alpha_K(633.5)$ implies M1 or E3. The same parity assignment, positive, for the 995.1-keV and 361.5-keV levels from the nature of the 633.5 keV-361.5-keV cascade radiation, excludes E3. Observable direct decay of the 995.1-keV level to the 3/2+ 361.5-keV and 7/2- ground states but not to the

9/2- 94.7-keV state suggests an assignment of 5/2+. Then the M1 assignment for the 279.6-keV transition and the deexcitation of the 715.7-keV level to both of the first two members of the ground-state band implies an assignment for this level of 7/2+, which of the possible E1 and E2 assignments for the 715.7-keV transition, rules out E2.

A cascade of gamma rays, it was noted, of $\sim$500 keV observed by Hashizume et al.,[118] and 480-keV and 515-keV gamma rays seen by Cranston et al.[129] corresponded to lines of about equal intensity due to 478.7-keV and 514.2-keV transitions observed in the external-conversion spectra. Allowed beta decay from the Dy^{165m} 1/2- state to a Ho^{165} 516-keV level depopulated by a weak 156-keV transition to the 361.5-keV 3/2+ level and directly to the ground state was reported by Cranston et al.,[136] who gave the level a probable 3/2- assignment. This was noted to suggest that the 478.7-keV and 514.2-keV transitions deexcite the 995.1-keV state with a 3/2- 514.2-keV intermediate state (same energy within experimental errors). Of possible K=5/2 positive-parity Nilsson states, 5/2+ [402], 5/2+ [413] and K=7/2 positive-parity states, 7/2+ [404], only the last was assigned as the 715.7-keV level. Then beta decay to this state, while allowed, is strongly hindered by the asymptotic selection rules ($\Delta N=2$, $\Delta n_z=3, \Delta\Lambda=-1$), accounting for the weakness of the possible beta branch (log ft>7.3). It was noted that a similar large log ft value (7.8) for a 7.2+ [404]$\rightarrow$7/2+ [633] transition in Hf^{177} following Ta^{177} decay was observed by Harmatz et al.[137]

The near-equality in intensity of the 633.5-keV and 279.6-keV M1 transitions depopulating the 995.1-keV level suggested that the former but not the latter violates asymptotic selection rules, which, assuming [404] for the 715.7-keV level and [411] for the 361.5-keV level, suggests 5/2+ [413] for the 995.1-keV level; the alternative assignment would reverse the situation with regard to the selection rules.

It was noted that since no negative-parity K=3/2 Nilsson states are available, the 3/2- state would be either a K=1/2 [541] level descending from the next major shell, or else the K_{σ}-2 gamma-vibrational state as suggested by Nathan and Popov.[84]

The high-energy feature of the gamma scintillation spectrum, which had been interpreted as due to 995-keV and 1080-keV transitions by Cranston et al.,[129] 1000-keV and 1068-keV transitions by Kane et al.,[114] and 998-keV and 1055-keV transitions by Hashizume et al.[118] was found from the external-conversion spectra to consist of lines due to three transitions, 995.1 keV, 1055.6 keV, and 1080.1 keV which, since the total decay energy is only 1285 keV, probably originate from separate levels of these energies decaying directly to the ground state. No crossover transitions that would result if one of these transitions terminated on the 94.7-keV level were observed. Hashizume et al.[118] had observed cascades with a coincidence sum about the lower but not the upper part of the ~1040-keV gamma scintillation peak complex. With the assumption of log ft values for beta decay to the 1055.6-keV and 1080.1-keV levels of 7.0 and 6.4 implying allowed hindered or first-forbidden unhindered transitions, possible spins of the two states were noted to be 5/2 or 7/2 or 9/2. Available Nilsson levels are 5/2+ [402], 9/2- [514], and 5/2-[532]; the 1080.1-keV state could be a first rotational excited state based on the 995.1-keV 5/2+ [413] state, an assignment supported by the observation that the difference in log ft for beta decay to the 995.1-keV and 1080.1-keV levels is the same as the difference for beta decay to the first two members of the ground-state band, and the appropriate energy difference of the levels, 85 keV, for a spin-5/2 band in this region.

The remaining assignments were noted to be very conjectural. The placement of the 695.0-keV transition was on the basis of energy sums, correct to well within experimental errors, and would not have been seen in the sum-coincidence work of Hashizume et al.[118] because of the weakness of the transition and the relatively long half life of the 361.5-keV state. The 565.7-keV and 514.2-keV transitions add to 1079.9 keV, but since the 565.7 intensity is $\sim$4 times higher than the 514.2 intensity, and a corresponding cascade was not seen by Hashizume et al.,[118] the cascade decay of the 1080.1-keV level through an intermediate 514.2-keV state was ruled out. (I would interject here that the 478.2 keV-514.7 keV cascade depopulation of the 995.1-keV, with a weak superposed 565.7 keV-514.2 keV cascade depopulation of the 1080.1-keV level seems a definite possibility.)

Preliminary Coulomb excitation results of Diamond et al.[138] indicated population of a level at 575±15 keV, which could be identified with the level depopulated by one of the weak 565.7-keV and 575.1-keV transitions, of which the latter could be placed as shown in the level scheme, depopulating a first rotational excited member of the 361.5-keV band, providing also a placement of the 500.8-keV transition, as indicated.

The origins of the relatively high-intensity 545.5-keV transition and a weak 587.6-keV transition within the Ho level scheme were noted to be essentially unknown.

Transitions in Ho^{165}

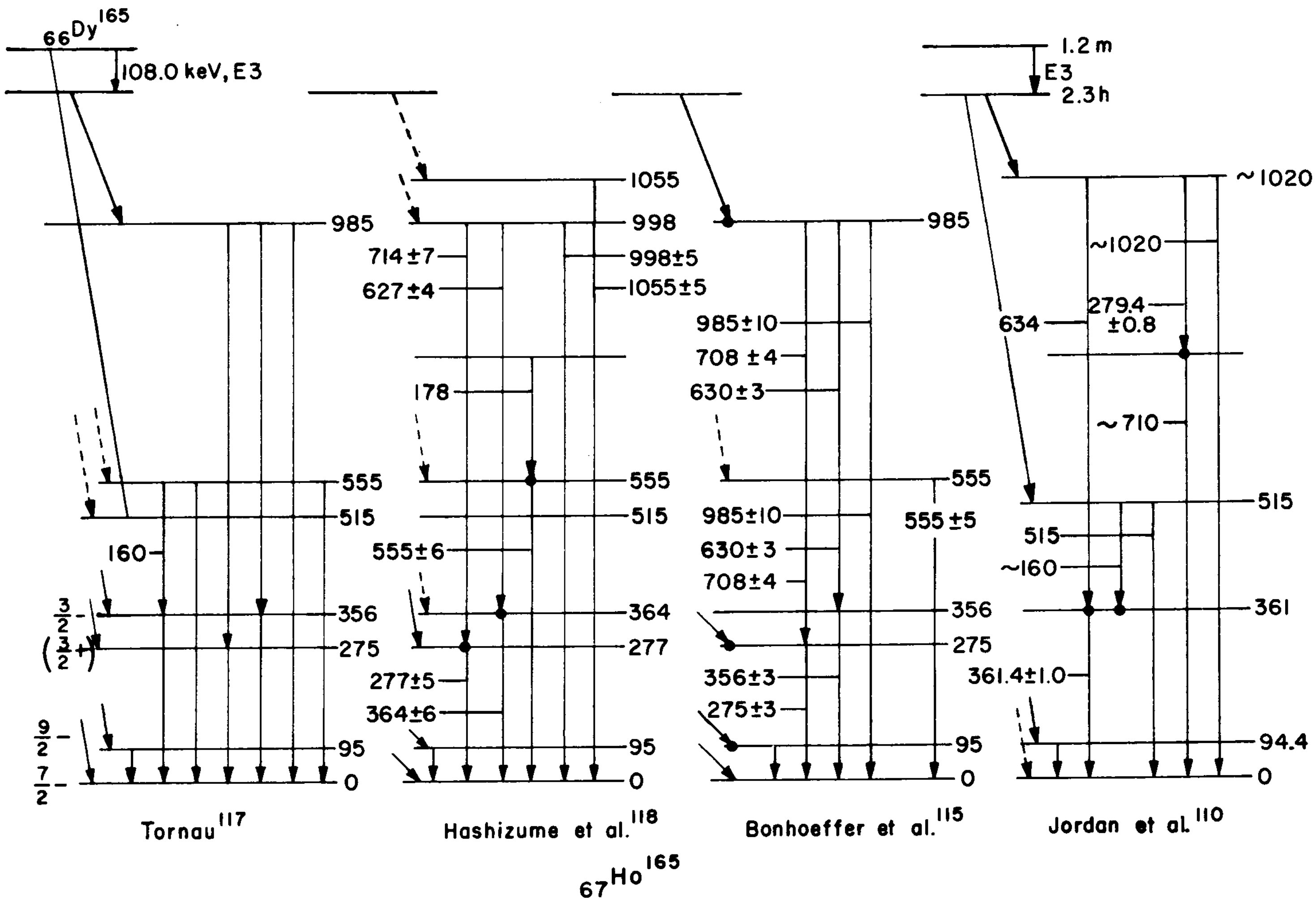

FIG III-1

Transitions in Ho^{165}

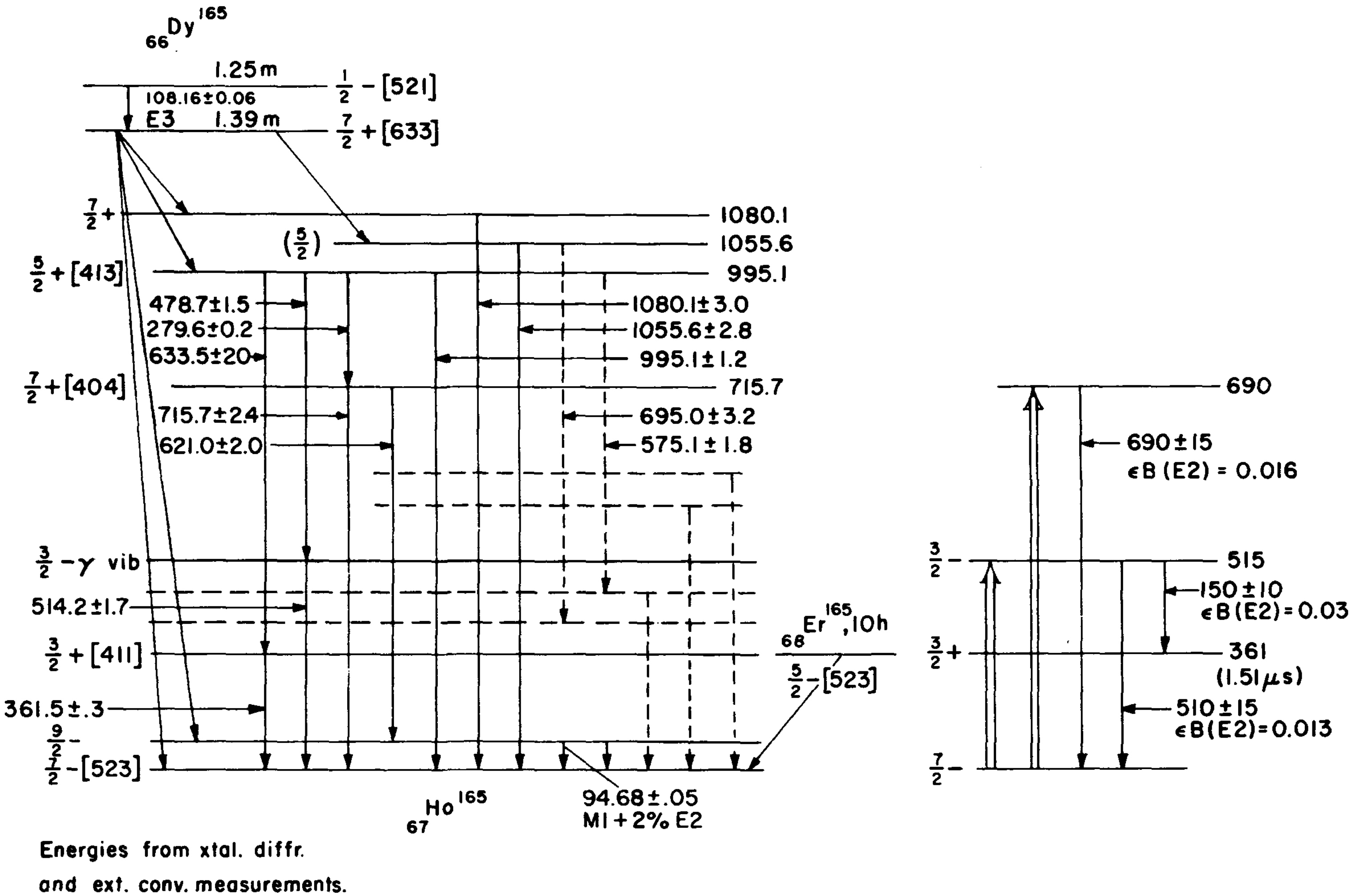

Persson et al.[125]

FIG III-2

Nathan & Popov[84]

Multipolarity Assignments (Persson et al.[125])

Trans. Energy, keV	Quantity	Experimental Value	Sliv & Band Theoretical Values, Z=67 M1	M2	M3	E1	E2	E3	Assigned Multipolarity
94.68±0.05	α_K	2.62±0.20	2.6	2.2	9.8	0.30	1.2	3.8	M1+E2
	K/L	$6.6^{+1.4}_{-1.2}$	6.6	3.8	0.95	6.2	0.7	0.07	δ^2=0.026±0.004
	Li/Lii/Liii	100±5/18.3±3.8/7.2±1.7	100/8.6/1.3	100/12/22	100/17/110	100/25/30	100/700/700	100/4200/5900	(L-ratios); agrees with Cranston et al.[129]; most M-
	L/M	$4.6^{+0.7}_{-0.6}$	---	---	---	---	---	---	conversion in lowest subshells,
	M/N...	$4.5^{+2.0}_{-1.2}$	---	---	---	---	---	---	in agreement with Rose's theoretical M1 M-shell coefficients.
279.6±0.2	α_K	0.125±0.035	0.12	0.51	1.7	0.028	0.061	0.19	M1(+E2).
	K/L	5.5	6.7	5.1	3.7	6.9	3.4	1.3	Agrees with Cranston et al.[129]
361.5±0.3	α_K	0.22±0.04	0.061	0.23	0.67	0.0094	0.029	0.086	M2
	K/L	4.7	6.7	5.5	4.0	6.9	4.1	1.9	Agrees with Cranston et al.[129] conversion data and half-life
								E4=0.24	of 1.51±0.01 μsec.
633.5±2.1	α_K	0.018±0.006	0.015	0.042	0.10	0.0027	0.0072	0.017	M1(+E2), or E3; E3 ruled out from decay scheme.
								E4=0.041	
715.7±2.4	α_K	0.008*	0.011	0.030	0.069	0.0021	0.0055	0.012	E1, or E2; E2 ruled out from decay scheme.

* Not well-resolved from beta continuum.

B. Coulomb Excitation

Heydenburg and Temmer,[81] in an early survey of Coulomb excitation of heavy nuclei by 6-MeV alpha particles, observed in Ho^{165} population of levels at 94 keV and 206 keV, and found $\epsilon B(E2)$-values 0.54 and 0.036 (10^{-48}cm.^{4}) respectively. The energy ratio was 2.19±0.04, compared to the theoretical ratio for a simple rotor, 2.22.

Huus et al.[72] studied internal conversion lines following the Coulomb excitation of Ho^{165} with 1.75-MeV deuterons and 1.75 and 1.90-MeV protons, and found K, L, M lines due to a 96-keV transition, K and L lines due to a 116-keV transition, and possibly a K line due to a 212-keV crossover transition, for which $\epsilon B(E2)$-values were ≈ 1.6 (96-keV K), 0.32 (96-keV L), ~ 0.074 (116-keV L). Quoted results were, 96-keV L: $K/L \approx 4.9$, $1/\delta^2 \sim 11$, $1/\epsilon \approx 7.7$, $B(E2\uparrow,\ 0 \to 96) \approx 2.5$, $Q_0 = 7.7$, $|g_K - g_R| = 0.51$; 116-keV L: $1/\delta^2 \sim 11$, direct/crossover=0.9, $1/\epsilon \approx 10$, $B(E2\uparrow,\ 0 \to 212) \approx 0.76$, $Q_0 = 8.4$. For a pure rotational band, the energy ratio should be 20/9 and the B-value ratio 35/9; measured values were 2.21 and ≈ 3.2 respectively, in agreement. K conversion peaks for decay of the second excited state were about as expected for a pure rotational band. Transition moments for the second excited state were noted to be somewhat uncertain because of possible inaccuracies in the yields, so that an apparent inconsistency with the result of Heydenburg and Temmer is probably not outside the experimental errors.

In order to test the Bohr-Mottelson model predictions for relative energies, B-values, and deexcitation radiation mixing ratios, Bernstein and Lewis[139] bombarded some heavy odd-A nuclei with alpha particles and observed the deexcitation internal conversion lines from the first two excited rotational states. In this work a primary limitation on the accuracy of yield measurements was knowledge of the target thickness. Targets were rare-earth oxides evaporated onto thick copper or aluminum backings. Thickness was determined by comparing the amount of background of atomic electrons produced in slowing the projectiles with a theoretical estimate of Huus et al.,[72] and was estimated to be good to $\pm 50\%$. Mixing ratios were deduced from experimental K/L ratios and extrapolations of Sliv corrections to Rose's point-nucleus theoretical E2 and M1 K and L conversion coefficients. B(E2↑) values for the first rotational state were found from gamma-ray deexcitation intensities of Heydenburg and Temmer,[81] the theoretical corrected total conversion coefficients, and the mixing ratios derived from observed K/L ratios. B(E2↑) values for the second excited state were found from conversion electron yields relative to yields from the first excited state and the cross-over gamma-ray yields of Heydenburg and Temmer.[81] Absolute B(E2↑) values were estimated to be good to $\pm 50\%$, relative values for the first and second excited state, to $\pm 20\%$ or better, and K/L ratios for the first excited state, to $\pm 10\%$, and for the cascade radiation, to $\pm 15\%$. Results for Ho^{165} are listed in Table III.2. It was noted that the Q_0 values calculated from first and from second excited state excitations essentially agreed, and that δ^2 values calculated from the cascade/crossover ratio and from the K/L ratio were in agreement within the experimental errors (somewhat large for K/L), indicating for Ho^{165} agreement with the rotational model predictions.

Goldring and Paulisson,[140] in order to check the agreement of B-value ratios with the pure rotational model predictions and the disagreement of deformations calculated from B-value-derived quadrupole moments, assuming uniform charge distribution, with those calculated from energy spacings, assuming irrotational flow inertia parameters, carefully measured gamma-ray yields following Coulomb excitation of several odd-A heavy nuclei bombarded with 3-MeV protons, using a 76^{o} half-angle geometry in which the target was placed between two NaI(Tl) crystals, one set to accept the $I_o+2 \rightarrow I_o+1$ cascade photopeak, the other, the $I_o+1 \rightarrow I_o$ photopeak. From the singles rate of the $I_o+1 \rightarrow I_o$ gamma radiation and the gamma-gamma coincidence rates from the two counters (the crossover depopulation of the second excited state representing a minor correction) the ratio of the populations of the first two excited states was deduced. Counter efficiencies were measured at 175 keV and 125 keV with sources calibrated in a 4π geometry, and interpolated for other energies. Rose's conversion coefficients corrected according to the findings of Sliv and the mixing ratios of Huus et al.[72] were used in the data reduction. Results for Ho^{165} were noted to be in rough accord with the collective model theoretical intraband B-value ratios as follows: (M1 conversion correction factor = p)

Observed if p = 1.0   0.8   0.6   Theoretical

$$\frac{B(E2\uparrow I_0\to I_0+2)}{B(E2\uparrow I_0\to I_0+1)} = 0.22;\ 0.195;\ 0.17;\ 0.257 \qquad \text{(III-11)}$$

$$\frac{\delta^2(I_0+1\to I_0)}{I_0(I_0+2)} = 0.6;\quad \frac{\delta^2(I_0+2\to I_0+1)}{(I_0+1)\ (I_0+3)} = 1.2\pm0.2. \qquad \text{(III-12)}$$

Here $\delta^2(I_0+1\to I_0)$ was taken from Huus et al.[72] and $\delta^2(I_0+2\to I_0+1)$ from the experimental data. The two quantities involving δ^2 should be equal and proportional to $(g_\Omega-g_R)^2/Q_0$. Discrepancies were noted to be probably inside the experimental errors for this and most of the other nuclei studied. (Definite discrepancies in B-value ratios for Re isotopes were noted.)

Extending their work, Heydenburg and Temmer[82] bombarded heavy odd-A nuclei with 6-MeV alpha particles and observed singles, X-X, X-gamma, and gamma-gamma coincident spectra using NaI(Tl) detectors. The cascade relations among the decay radiations of the first two excited states were proved from the X-X, X-γ, and γ-γ coincident data. ϵ B(E2) values were obtained from gamma-ray intensities. Theoretical M1 and E2 conversion coefficients of Rose, the M1 coefficients decreased by 25% in accordance with the findings of Sliv and coworkers, were used in the data reduction. M1/E2 mixture ratios were deduced from $\lambda^* = \left(\frac{2I_0+3}{I_0+2}\right)^5 \frac{(2I_0+1)(I_0+3)}{2I_0^2(2I_0+3)}$, the pure rotational band theoretical cascade/crossover ratio for pure E2 decay, as compared to the observed branching ratio λ, by ascribing the excess cascade radiation to the M1 fraction: $\delta'^2 = \lambda/(\lambda^*-\lambda)$; $\delta'^2 \equiv {}^2(I_0+2\to I_0+1)$. For $I_0>1/2$, $\delta^2 \equiv \delta^2(I_0+1\to I_0)$, the theoretical ratio of the mixing ratios in a pure band is

$$\left(\frac{\delta}{\delta'}\right)^2 = \left(\frac{I_0+1}{I_0+2}\right)^3 \ \frac{I_0+3}{I_0} = 1.017 \text{ for } I_0 = \frac{7}{2}\,. \qquad \text{(III-13)}$$

Other formulae used in the analysis by these authors are found on pp.116-117. Results for Ho^{165} are shown in Table III.2.

Martin et al.[73] Coulomb excited some odd-A heavy nuclei with 4.05-MeV protons and did careful measurements on the deexcitation radiation. Conclusions from analysis of gamma-ray intensities and of an angular distribution measurement for the cascade mixing are shown in Table III.2.

Olesen and Elbek[85] measured absolute B-values in a number of odd-A rare earth nuclei by observing the inelastic and elastic groups of scattered projectiles, describing the latter by the Rutherford cross section. Protons and deuterons of 4-1/2 MeV from an electrostatic generator passed through a 90° analyzing magnet, impinged on the target, and those scattered through 145° were recorded in thick photographic emulsion. For holmium, pure Ho_2O_3 (Spedding, Iowa State), vacuum evaporated at $2\text{-}300^{0}$ C. from a carbon crucible onto aluminized Formvar or pure carbon foils, the latter 50-100 μgm./cm.^{2}, constituted the target. Results and comparison to earlier work presented by these authors are shown in Table III.2.

To check rotational model predictions for B(M1↓) values as well as B(E2) values in ground-state bands, noting that studies of inelastic ion groups give only B(E2↑) values, Bernstein and Graetzer[144] made a study of internal conversion deexcitation radiation following Coulomb excitation of rare-earth isotopes. The first two excited states were populated by bombardment with 2-3.7-MeV protons. A 90^{o} electrostatic analyzer energy-calibrated to 0.05% by the $Li^{7}(p,n)$ threshold (1.881 MeV) defined the incident energy. Conversion electrons were collected by a wedge-gap spectrometer arranged to permit angular distribution measurements. Ratio-to-Rutherford yields were calculated with the aid of the intensity of elastically scattered protons detected with a CsI scintillation detector set at 155^{o}. The electrons were detected with anthracene, calibrated for efficiency as a function of energy by means of the Pr^{147} beta spectrum, which has a known linear Kurie-plot. The efficiency was constant over the energy region of interest. The spectrometer effective solid angle ($(0.9 \pm 0.1)\%$ of a sphere) was deduced from measurement with and without the interposed spectrometer of the internal conversion lines from a $Cs\text{-}Ba^{137}$ source. Targets were made by vacuum evaporation of the metals onto thick carbon backing. Theoretical conversion coefficients of Sliv and Band[48] were used where required in the analysis. Results of the study are shown in Table III.2.

Nathan and Popov[84] used cyclotron-generated 20-MeV alpha particles, energy degraded to 20, 17, and 14 MeV, as projectiles in a study of Coulomb excitation of heavy nuclei in which double Coulomb excitation effects were observed. Gamma rays were detected in coincidence with backscattered projectiles in order to cut down the background. The electronics were capable of 0.06 μsec. resolving time under ideal conditions, but the random coincidence vs. the singles counting rates indicated an effective resolving time of 0.3 μsec. Targets were 5 mg./cm.^{2} oxide on Pb backing. ϵB values were deduced from thick-target integrations of the Rutherford and single Coulomb excitation cross sections and observations of the gamma and back-scattered alpha counting rates. Energy determinations were good to $\sim$2%. Results for Ho^{165} are shown in Fig. III.2.

Table III-2

Coulomb Excitation Results for Ho^{165}

E_{trans}, keV	94	113	207	94	114	208	94	---	209±2	96	122	218	95	115	210
K/L	---	---	---	---	---	---	---	---	---	5.4	6.9	---	6.0±.5	5.8±.6	---
$\therefore \delta^2$	---	---	---	~ 0	---	---	---	---	---	.044	0	---	2.5^{+25}_{-2}%E2	5±3%E2	---
Meas. α_{tot}	---	---	---	2.4	1.3	0.2	---	---	---	2.6	1.3	---	---	---	---
B(E2↑, trans↓)	2.8	0.7	---	---	---	---	---	---	---	2.76	0.68	.028	---	---	---
B(E2↑)	2.8	0.7		2.5	0.52		2.41±.07	.63±.04		2.79	0.71		2.8±.4*	.65±.13*	
Q_o, b.	8.0	8.0		7.6	6.9			7.56		8.1	8.2		---	---	
	B(E2,94↑) and B(E2,113↑) from ref. 73, 82, 139 72 (2.5, 0.76) and 140: av.= 2.65±0.15, 0.66 ±0.10 resp. Av. ratio 0.25±0.04; Alaga=0.257. γ-intens. ratios imply $\delta^2(113)$= 0.05; 113K conv. rate implies 0.04 ±0.02. 94- and 207-keV γ-ray ang. distr. imply $\delta(113) > 0$.			Crossover/cascade ≡λ=0.16 implies $\delta^2(114)$=0.039. X-X, X-γ, γ-γ cascades verified. If μ_o=+3.3n.m. (ref. 141), then with above Q_o, g_Ω=1.10, g_R=0.39 if $\delta(113) > 0$, g_Ω= 0.78, g_R=1.49 if $\delta(113) < 0$.			B-values from inelastic proton groups. Ratio= 0.261; Alaga= 0.257. Q_o implies deform. β=0.327, 10% lower than the Nilsson value. No significant deviations from Alaga rules obs. in a number of odd-A rotational nuclei studied, from Eu^{153} to Lu^{175}.			Crossover/cascade implies $\delta^2(122)$= 0.023			*Various other ratios among obs. K- and L-conv. transitions quoted. B(E2↑, 95L↓) =0.328, B(E2↑, 114L↓) =0.055, B(E2↑, 210K↓) =0.0031. B(E2,95↑)/B(E2,210↑) =0.23±0.03; Alaga =0.257. %E2(95)/%E2(115) =0.57 Alaga ≈1.01.		
	Martin et al.[73]			Heydenb. and Temmer[82]			Olesen and Elbek[85]			Bernstein and Lewis[139]			Bernstein and Graetzer[144]		

C. Erbium Decay

The first mention of an Er^{165} observation was an erroneous assignment to this isotope of a 1.1-min activity seen by Pool and Quill[36] in 1938 following a fast-neutron irradiation of Er.

Er^{165} was prepared by Butement[147] in 1950 by the $Ho^{165}(p,n)Er^{165}$ reaction from bombardment of 99.97% pure Ho_2O_3 with 10-MeV protons. Chemical separation of the rare earths and ion-exchange separation of the Er fraction were done. An activity of 10.0 ± 0.1 h. half life was observed with a Geiger counter through 10 half lives. None of the resulting radiation was deflected by magnetic fields and was therefore assumed to be purely electromagnetic. Absorption measurements showed two component energies: 6.6 keV and 52 keV, and in a second measurement of the latter using Cu instead of Al, 47 keV. No higher-energy gamma radiation was found. The energies were noted to be correct for Ho K and L X-rays, suggesting 100% e.c. decay to the Ho^{165} ground state.

In the same year, Wilkinson and Hicks did ion-exchange separations of products produced by 3.8-MeV alpha-particle bombardment of very pure Dy_2O_3 in which they found in the Er fraction an activity of 11.2 ± 0.2 h. half life, and followed it through 6 half lives. Aluminum, beryllium, and lead absorption measurements showed that the radiation was mainly electromagnetic, with energies 7.2 and 52 keV, the average K and L X-ray energies for Ho, but in addition, weak components of 1.1-MeV gamma radiation and 80-keV electron radiation.

Intensities were: $e^{\pm}$/L X-ray/K X-ray/1.1-MeV γ-ray = $10^{-3}/\sim0.5/1/\sim0.2$. Of possible mass assignments of 161, 163, and 165 for the radioactivity, 161 was eliminated because the $Dy^{160}(\alpha,3n)Er^{161}$ production cross section was too small, and 165 was (erroneously) ruled out because of lack of activities of $>$1 h. half life observed following bombardment of Ho^{165}.

Zylicz et al.[149] studied singles and K X-ray-coincident inner bremsstrahlung spectra occurring in the Er^{165} electron-capture decay, and found agreement with theory for a Q-value 371±6 keV, concluding that the half life was 10.39±0.7 h., and the ft value $(4.33\pm0.17)\times10^{4}$ sec. for the ground-state branch.

The definitive work on this isotope was done by H. Ryde et al.[150] They noted that Butement[147] had seen only the Ho K and L X-rays, for which Grigoriev et al.[151] deduced from proportional counter measurements of the K/L ratio a total electron-capture decay energy of 82^{+10}_{-5} keV, and that the Mottelson-Nilsson[24] classifications of the Ho^{165} and Er^{165} ground states were 7/2- [523] and 5/2- [523] respectively, implying allowed unhindered e.c. decay in disagreement with a log ft value found by Soloviev.[152] The source was produced by irradiation of 99.9% pure Ho_2O_3 with 22-MeV deuterons. The main impurities, Er, Dy, and Y, were reduced to $<$ 0.005% by ion-exchange purifications before and after the irradiation. The main interfering activities were greatly attenuated, except for 27 h. Ho^{166} from $Ho^{165}(d,p)$ which has a much lower cross section than $Ho^{165}(d,2n)Er^{165}$.

From the K X-rays, the half life of Er^{165} was found to be 10.34±0.05 h., and from the inner bremsstrahlung, 10.3±0.3 h. From comparison of the experimental inner bremsstrahlung spectra, normalized to the rate of K-vacancy production as determined from K X-ray and K auger yields, with the theoretical radiative capture calculations for 1S, 2S and P and 3P electrons including screening corrections where important, the decay energy was deduced:

$$Q_{E.C.} = 370 \pm 10 \text{ keV}, \qquad \text{(III-14)}$$

which with the half life implied a log ft value of 4.61±0.02. (The errors reflected experimental but not interpretative theoretical uncertainties.) Thus the transition was noted to be allowed, unhindered ($\Delta\pi$=no, $\Delta I=0,1$, and no violation of asymptotic selection rules: $\Delta N=\Delta n_z=\Delta\Lambda=0$), supporting the assignment 5/2-[523] for the Er^{165} ground state. The Nilsson diagram for $\delta=0.31$, the same as found for the neighboring nuclei Ho^{165} and Er^{167} (Olesen and Elbek[85]), predicted 11/2-[505] with 5/2-[523] as a low-lying excited state.

The electron spectrum of Er^{165}, as obtained with an intermediate-image beta spectrometer of 4% resolution and 8% transmission, was searched for possible levels not expected to be seen in Dy^{165} decay, for example the 1/2+[411] band possibly recognized in Ho^{163}. No internal conversion lines were seen above the K auger region. No conversion lines were found in spectra of the auger region obtained with a double-focusing spectrometer. From the absence of the

94.7- keV L line, log ft for decay to that level was fixed at >10, suggesting a second-forbidden transition (log ft$\sim$13). It was observed that energetics probably ruled out population of the 361.5-keV 3/2+ [411] level, for which from scintillation gamma-ray spectra the partial half life was found to be >6000 y. Thus no information on the Ho^{165} level structure was obtained.

D. Miscellaneous Measurements

The ground-state spin of Ho^{165} was determined in 1935 by Schüler and Schmidt[152] from the hyperfine structure, and found to be 7/2.

Baker and Bleaney[141] calculated the static magnetic dipole and electric quadrupole moments of Ho^{165} utilizing the available data, with the results: $\mu = 3.29 \pm 0.17$ n.m., $Q \approx 2$ barns.

W. Leland,[154] in a mass-spectrographic study of isotopic abundances of some rare-earth elements, found that Ho was essentially monoisotopic, but because of Dy-contamination, could only assign upper limits to other Ho isotopes: $Ho^{161,2,3,4}$, $< 0.04\%$; $Ho^{166,7,8}$, $< 0.001\%$; Ho^{169}, $< 0.004\%$.

F. McGowan[155] obtained upper limits to the lifetimes of low-lying levels in several heavy nuclei by means of the delayed-coincidence technique. For the Ho^{165} 95-keV level, he found

$$T_{1/2}(95 \text{ keV lev.}) < 0.8 \text{ nsec.} \qquad \text{(III-15)}$$

From low-lying gamma-ray to X-ray intensity ratios obtained from NaI(Tl) scintillation spectra he obtained conversion-coefficient estimates in some of the nuclei. In Ho^{165} an upper limit only to the 95-keV K coefficient was obtained: $\alpha_K(95 \text{ keV}) \leq 2.9$, which was compared with a theoretical estimate, 1.40. T. Stribel[156] deduced this quantity from intensities of the X ray and gamma ray in NaI(Tl) scintillation spectra with the result $\alpha_K(95 \text{ keV}) = 2.90 \pm 0.30$, which he compared to theoretical estimates of Rose, 3.0(M1); 1.5(E2).

Some sources of uncertainty in h.f.s. determinations of magnetic moments of rare earths were discussed by Watson and Freeman.[157] The expression for the dominant orbital contribution to the "hyperfine field" contains the quantity $\langle 1/r^3 \rangle$, for the evaluation of which one would need accurate 4f electronic wave functions, which appeared to be unavailable. Corrections to Hartree-Fock wave functions corresponding to intermediate coupling, configuration mixing, relativistic effects, certain radial wave-function modifications, exchange effects, and environmental perturbations were noted as sources of possible significant errors in quantities calculated from the wave functions. By way of illustration discrepancies between calculated and measured values of a certain spin-orbit coupling parameter for rare-earth ions was cited. It was noted that values of $\langle 1/r^3 \rangle$ calculated from wave functions derived by different calculational or semi-empirical procedures differed by as much as $\sim$20%. It was further noted that the above-mentioned expression for the "hyperfine field" may be inaccurate because of significant contribution of other than the 4f electrons. For Ho^{165}, four values for μ were cited: +3.3 (estimate of B. Bleaney[158]); +4.1 (estimate of Judd and Lindgren[159]); +3.7, from optical measurements of h.f.s. involving 6s,p and 5d electrons, whose wave functions are similarly subject to uncertainties; +3.5, using $\langle 1/r^3 \rangle$ as calculated from Hartree-Fock wave functions.

B. Wybourne[160] examined the problem of calculating nuclear magnetic moments and quadrupole moments from measurements of h.f.s. by means of atomic-beam resonance measurements on neutral rare-earth atoms, and paramagnetic resonance measurements of rare-earth ions included as impurities in certain crystal lattices, and from comparison of intermediate-coupling calculations with data concluded that as much as 8% deviation from the usually assumed Russel-Saunders coupling of I and J occurs. They cited Ho^{165} as an example: calculation of the h.f.s. splitting constants from data of Goodman et al.,[161] assuming Russel-Saunders coupling, resulted in μ=4.23 n.m., Q=2.99 barns, while using the same data but an intermediate-coupling calculation, they found μ=4.39 n.m., Q=2.83 barns, the major part of the change being due to interaction of the nucleus with the electron spins.

He noted that h.f.s. interactions are measurable for rare-earth trivalent ions when in the known trichloride or ethylsulphate crystal lattice environments, for which other than paramagnetic resonance interactions can be evaluated from optical spectra. From h.f.s. splitting constants of $HoCl_3$ measured by Hutchison and Wong,[87] but using intermediate-coupling wave functions for rare-earth ions in the crystal field, he obtained μ=3.97 n.m., 9.6% lower than the neutral-atom atomic-beam value, and noted that the value of $\langle 1/r^3 \rangle$, obtained theoretically by Judd and Lindgren,[159] was mostly in doubt, and in particular that the Watson and Freeman[157] value for this quantity from Hartree-Fock wave functions was substantially different.

The specifically intermediate-coupling corrections to μ and Q values for the cases treated were $\sim$2-4%.

Tipler et al.[162] in effect produced monochromatic gamma rays of 0.6% energy resolution in a bremsstrahlung monochromator that worked by means of detection of post-bremsstrahlung electrons of appropriate energy, and studied the "elastic scattering" of the photons at 48 incident energies between 10.92 MeV and 19.06 MeV, in the dipole resonance region, from Ho^{165}, at a scattering angle of 135°. They found that agreement of scattering and photoabsorption data with a theoretical two-Lorentz-line form resulting in the case of an axially-symmetric hydrodynamic model of the nucleus was not very good, but that acceptable agreement was obtained with a three-line fit, which requires a vibrationally or statically assymmetric model. If static, the required deformation parameters for a good three-line fit were found to be $\beta_0=0.33$, $\gamma_0=20^{\circ}$. Zero-point gamma-vibration of a symmetrical static equilibrium shape was advanced as a possible mechanism for the three-line dipole resonance. The required amplitude of these vibrations was found to be $\sim 10^{\circ}$. It was noted that in this situation, because the gamma-vibrations are slow compared to dipole oscillations, the incident photons would see various "instantaneously-assymmetric" nuclear shapes. A zero-point beta-vibration, it was noted, would only broaden a resonance line, to first order. A choice between the static and vibrational cases could not be made on the basis of the data.

IV. History of Studies of the Structure of Lu^{175}

Both Hf^{175} and Yb^{175} decay as well as Coulomb excitation studies have contributed substantially to the knowledge of the Lu^{175} level structure.

A. Ytterbium and Hafnium Decays

Hf^{175} was discovered by Wilkinson and Hicks[148] as a product of deuteron- and proton-bombardment of Lu_2O_3. The Hf activity, having been chemically separated, was observed to have a half life of 70 ± 2 d., and associated X and gamma rays of energied estimated from their absorption in aluminum or lead to be 8.2, 55, 350 and ~ 1500 keV, the first ywo being Lu L and K X rays. Observed intensity ratios, $e^-/L/K/350\gamma/1500\gamma = 0.1/0.1/1/0.2/0.05$ (estimated correct to within a factor of ~ 2) permitted the conversion-coefficient estimate: $\alpha_K(350) = 0.4$.

Cork et al.[164,165,(166,167)] observed internal-conversion lines associated with neutron-induced activities in Yb, and made element assignments from K-L-M energy differences. A 4.2-d. activity assigned to Lu consisted ov various internal-conversion lines from 137.5-, 396.4-, 258.9 ± 0.1- and 282.6-keV transitions. Because of mass-assignment uncertainties in neutron-induced activities in natural Hf, Hedgran ant Thulin[168] employed electromagnetically-separated Hf isotopes. i.c. lines from 26- and 279-keV and an external-conversion line from a 342.2-keV transition were observed associated with the Hf^{175} electron-capture decay to Lu^{175}.

Burson et al.[169] studied n-induced activities in isotopically-enriched Hf and HfO_2 samples. A 70-d. activity was assigned to the Hf^{175} electron-capture decay from isotopic studies and K-L-M energy differences. 89.1-, 342.3-, 113.4- and 228.4-keV i.c. lines were observed. Burson and Rutledge[170] observed these same i.c. lines plus lines due to 318- and 431-keV transitions associated with the Hf^{175} decay. A substantially correct decay scheme was presented. Bashilev et al.[171] meausred the 89.1- and 342.3-keV internal-conversion coefficients from the Hf^{175} decay and found: 89.1 keV, K/L/M = 30/15/1.5; 342.3 keV, K/L/M = 100/20/5. Burford et al.[172] studied i.c. lines associated with activities induced by n-irradiation of HfO_2 with the Hf enriched to 7.85% Hf^{174}. Lines were assigned to Lu^{175} rather than the contaminating Hf^{181} via the relative half lives associated therewith. Results appear in Table IV-1. The 342.3-keV K/L ratio was larger than previously-reported values; these authors felt that K/L was probably ~ 5 or 6, suggesting M1 + E2, M1 49% to 79%, and that α_K was probably between 0.079 and 0.104, comparing well with a privately-communicated unpublished value due to McGowan, 0.095 ± 0.015, used by these authors in normalixing observed i.c. and e.c. line intensities. K/L(128.4) agreed with Burson and Rutdledge; K/L(89.1) was twice their value and three times that of Bashilev et al. 113-keV i.c. lines were not detected, providing an upper limit for this conversion coefficient. Spin-assignment arguments were as follows: from the 342-keV transition multipolarity the 342.3-keV level would have I = 5/2, 7/2 or 9/2, with 9/2 rejected because of theoretical unavailability of a 9/2 state in the subshell containing the 71st proton. The predominant M1 character of the 89.1-keV transition indicated by the conversion coefficient and K/L-ratio values thus implies spin 3/2, 5/2, 7/2 or 9/2 for the 431-keV level. 3/2 was excluded because detection of the 318-keV transition implied $\Delta I < 3$. 5/2 was excluded since otherwise the gamma intensity of the 431-keV transition would have been greater than that of the 89.1-keV transition. 9/2 was excluded since no 9/2 single-particle level was available. (however it could have been a 9/2 rotational member of a 342-keV $K = 7/2$ band). Spin 7/2 for both the 342- and 431-keV levels was excluded on the basis of 89.1-, 318- and 431-keV gamma-ray intensities. Then with spin 5/2 for the 342-keV level, the 431-keV level was noted to be possibly a spin-7/2 rotational state, accounting for the high 89.1-keV intensity. The rotational-inertia parameter would then approximately equal that of the ground-state band, and the 228-keV transition would be pure E2, consistent with its K/LM... value, 2.0 ± 0.5, and the K-line intensity relative to that of the 342.3-keV intensity, assuming 20% E2 for the latter.

N. Marty[173] measured intensities of 282- and 396-keV gamma rays seen in Yb^{175} decay and found $I_\gamma(282)/I_\gamma(396) = 0.58 \pm 0.05$, and observed an intense 113 ± 1-keV gamma ray and the Lu K X ray in coincidence with the 282-keV radiation. From coincident X- and gamma-ray entensities, the 113-keV coefficient was determined:

$$\alpha_K(113) = 2.35 \pm 0.4 \qquad \text{(IV-1)}$$

suggesting M1 (+E2). No important gamma rays were observed in coincidence with the 396-keV radiation. The interpretation is shown in Fig. IV-3.

To investigate why Cork et al.[165] did not see the 113-keV level of Lu^{175} in Yb^{175} decay, H. Waard[174] studied this (and the Yb^{177}) decays subsequent to neutron irradiation of Yb_2O_3. Gamma, beta and electron singles and gamma-beta and agmma-conversion electron coincidence spectra were obtained. Observations and interpretations for Yb^{175} decay are shown in Fig. IV-1 and Table IV-1.

Akerlind et al.[175] did an angular-correlation measurement of the Lu^{175} 281-keV-113-keV gamma-ray cascade following Yb^{175} decay, with the result

$$W(\theta) = 1 + (0.202 \pm 0.012) P_2(\cos\theta) + (-0.004) P_4(\cos\theta) \qquad \text{(IV-2)}$$

It was noted that possible spin sequences were $9/2 \rightarrow 9/2 \rightarrow 7/2$ and $7/2 \rightarrow 9/2 \rightarrow 7/2$, the transition being of mixed multipolarity in either case, and that A_4 and mixing ratios of Waard[174] strongly favored $9/2 \rightarrow 9/2 \rightarrow 7/2$.

Mize, Bunker and Starner[176] studied both 4.2 d. Yb^{175} and 70 d. Hf^{175} decays, observing electrons and gamma rays in singles and in coincidence. Contaminating radiations in the Yb_2O_3 and HfO_2 neutron-induced activities were separated on the basis of half lives. Results appear in Fig. IV-1. Cork et al.[177] studied n-induced activity in 99.8% pure Yb metal of natural-isotopic composition, making A and Z assignments to observed i.c. lines from half lives and K-L-M energy differences. An anomalously low amount of certain contamination Lu^{177} lines was noted as a puzzling feature suggesting a mass-assignment error. Results of the 4.2 d. half-life radiation studies appear in Fig. IV-1 and Table IV-1. Agreement of the spin assignment for the 397-keV level with results of Akerlind et al.[175] and disagreement of the parity assignment with that of Mize et al.[176] was noted.

Hatch et al.[178], using beta and gamma-scintillation in coincidence and a bent-crystal gamma spectrometer of resolution $\Delta E/E = 3\times10^{-5}$, studied Tm^{169} and Lu^{175} levels to examine vibration-rotation and Coriolis terms in the Bohr-Mottelson strong-coupling model. Yb_2O_3 (natural-isotopic Yb) and HfO_2 (enriched to 10% Hf^{174}) were n-irradiated to produce sources housed in 0.007 in. diameter capillary tubes for gamma-ray observations, or vacuum-evaporated onto mica to thicknesses of several light waves for the beta spectrometers. Results appear in Fig. IV-1 and Table IV-1. Conversion coefficients were deduced by normalizing Yb^{175} data to the 130.5-keV transition in Tm^{169} and the Hf^{175} data to the 133.2-keV transition in Ta^{181}, and assigning Sliv values of α_K for these two fiducial transitions. Sliv α_K and Rose α_L values were used to deduce multipolarities. The 396-keV line was found to be E1, in agreement with Mize et al. and in disagreement with Cork et al.[177], and in other respects previous results were confirmed. The ground-state-band energies measured were found to be given by

$$E_I = E_0 + AI(I+1) + BI^2(I+1)^2 \quad , \qquad \text{(IV-3)}$$

$$E_0 = -201.471 \text{ keV}, \; A = 12.913 \text{ keV}, \; B = -6.595 \text{ eV}. \qquad \text{(IV-4)}$$

T. Weidling[179] measured the angular correlation of the 283-113-keV gamma cascade in Lu^{175} in aqueous nitrate solutions of varying viscosities (obtained by addition of glycerine) of n-irradiated Yb. No viscosity-dependent correlation coefficient attenuation was observed. The result was

$$W(\theta) = 1 + (0.227 \pm 0.004) P_2(\cos\theta) , \qquad \text{(IV-5)}$$

implying E1 + (4 ± 2)%M2 for the 283-keV transition, M1 + (17 ± 3)%E2 for the 113-keV transition, in essential agreement with Hatch et al.H. Vartapetian[180] confirmed the E1 retardation implied by the observed M2 396-keV component by measuring the level half life. 70-keV beta-396-keV gamma and 70-keV beta-282-keV gamma cascades were used in the method of delayed coincidences. The result was

$$T_{\frac{1}{2}} (396 \text{ kev}) = (3.4 \pm 0.3) \text{ nsec.} \qquad \text{(IV-6)}$$

From relative gamma intensities of Mize et al.[176], partial gamma-ray mean lives were deduced:

$$\tau_{396\gamma} = 5.5 \text{ nsec.}, \ \tau_{282\gamma} = 1.3 \text{ nsec.} \qquad \text{(IV-7)}$$

It was noted that for single-particle states from the $g_{7/2}$ and $h_{11/2}$ shells, $\Delta j = 2$, the E1 component would be 0 for zero deformation, and that Chase and Willets[184] calculated an E1 retardation using Nilsson wave functions and a deformation $\delta = 0.28$, obtaining 1.4×10^{-4}, and the retardation implied by $\tau_{396\gamma}$, $\sim 10^{-6}$, is explained if a 17% M2 component is assigned to the 396-keV gamma radiation in essential agreement with Hatch et al.

Grace et al. measured Yb^{175} radiations from Yb in a magnetically-cooled ytterbium ethylsulfate crystal. 282-keV and 396-keV gamma-ray angular distributions were measured at temperatures from 0.014° K. where appreciable anisotropy in h.f.s. level populations was present to $\sim 1^\circ$ K. where emission was isotropic. The coefficient A_2 in the angular-distribution function $I(\theta) = 1 + A_2P_2(\cos\theta) + A_4P_4(\cos\theta)$ with respect to the nuclear alignment axis is given by

$$A_2 = B_2 U_2 F_2 (1+3\alpha\delta-3\beta\delta^2)/(1+\delta^2) \;, \tag{IV-8}$$

where B_2, a function of the tenperature, is a measure of the degree of nuclear alignment; U_2 is a function of the spins involved in the preceding beta decay; F_2, α and β are functions of the spins and gamma-ray multipolarity, and $\delta = \pm\sqrt{M2/E1}$. From observed anisotropies,

$$A_2(282) = -0.061 \pm 0.003, A_2(396) = +0.017 \pm 0.003, A_4\text{'s negligible.} \tag{IV-9}$$

With B_2, U_2 the same for both transitions and F_2, α, β known functions, a relation between $\delta(282)$ and $\delta(396)$ was deduced:

$$\frac{4.4+6.0\delta(282)+2.7\delta^2(282)}{3.0-18.7\delta(396)-0.2\delta^2(396)} \cdot \frac{1+\delta^2(396)}{1+\delta^2(282)} = \frac{A_2(282)}{A_2(396)} = \frac{0.061 \pm 0.003}{0.017 \pm 0.003} \;. \tag{IV-10}$$

Because of the experimental value of the A_2 ratio this was found to be inconsistent with averages of previous $|\delta(282)|$ and $|\delta(396)|$ values. The 282-114-keV gamma-gamma angular correlation was measured with a number of sources in order to test for effects of correlation coefficient attenuation; previous results were confirmed. It was noted that the discrepancy is not removed by assigning the 396-keV level as 7/2-, which is not favored by the correlation results in any case. It was concluded that the $|\delta(396)|$ value must be in error, and that using $\delta^2(114)$ of Weidling[179] and the angular-correlation result, $\delta(282) \sim -0.2$ to $+0.2$, the allignment results imply $\delta(396) = +0.10 \pm 0.03$. From the experimental temperature dependence of B_2 ad ascertained from A_2 measurements, as compared to the theoretical dependence on temperature, the h.f.s. splitting constant and the nuclear spin, the splitting constants and thence the magnetic moment was determined. From the 0.014° K. A_2 value the result was

$$\mu = 0.15 \pm 0.04 \text{ n.m.}, \qquad \text{(IV-11)}$$

the main error being from $\delta(282)$ uncertainty. The theoretical temperature dependence of the anisotropy was confirmed.

E. Klema[182] did measurements of gamma-gamma cascades in Lu^{175} at 19 angles, using sources in solid and dilute aqueous solution forms. The 89.36-343.40-keV cascade following Hf^{175} e.c. decay was found found to have the correlation:

$$W(\theta) = 1 + (0.001 \pm 0.004) P_2(\cos\theta). \qquad \text{(IV-12)}$$

It was noted that an unpublished upper limit of the 343-keV level lifetime due to McGowan, of 10^{-9} sec., is long enough to permit perturbations of the correlation pattern by extranuclear effects. The following interpretation was presented: the expression for A_2 contains two factors, one dependent on $\delta(343)$ which does not vanish for the experimental range of values of this quantity, and one dependent on $\delta(89)$. Taking the 343-keV gamma ray as M1+E2 (from conversion data of McGowan[183], Burford et al.[172] and Mize et al.[176]) and the 89-keV gamma ray as M1+E2 (from the α_L-values of Mize et al. who found $\delta^2(89) \sim 0.1$), values of $\delta(89)$ for which $A_2 = 0$ were calculated for all combinations of spin sequences consistent with a ground-state spin of 7/2 and spin differences of 0 or ±1 between the adjascent levels. Spin sequences compatable with existing information on $\delta(89)$ turned out to be $5/2 \rightarrow 5/2 \rightarrow 7/2$, $\delta = -0.392$ ($\delta^2 = 0.15$); $7/2 \rightarrow 5/2 \rightarrow 7/2$, $\delta = -0.100$ ($\delta^2 = 0.01$); $3/2 \rightarrow 5/2 \rightarrow 7/2$, $\delta = +0.193$ ($\delta^2 = 0.037$) (the first of these is the sequence of Mize et al., the second that of Burford et al. and Hatch et al. and suggested by theory, as pointed out by Chase and Willets). Previous experimental values of $\delta(89)$ were noted to be 0.1 (Mize et al.) and 0.03 (Hatch et al.).

For the 282.57-113.51-keV cascade following Yb^{175} beta decay, results were

$$W(\theta) = 1 + (0.221 \pm 0.004) P_2(\cos\theta) \qquad \text{(IV-13a)}$$

for liquid sources, in essential agreement with Weidling, and

$$W(\theta) = 1 + (0.210 \pm 0.003) P_2(\cos\theta) \qquad \text{(IV-13b)}$$

for dry sources. Using the value $\delta^2(113.81) = 0.18$ $(|\delta(114)| = 0.42)$ from previous conversion-coefficient observations of Burford et al.[172], Waard[174], Mize et al.[176], Cork et al.[177], Hatch et al.[178], Huus et al.[72] and Bernstein and Lewis[185], mixed-mixed cascades for spin sequences 7,9,11/2(E1-M2)9/2(E2-M1)7/2 were compared with the experimental correlation coefficients. The first and last sequences yielded $\delta(283)$ values in disagreement with previous results; the middle sequence gave the best fit, $A_2 = 0.221$, $A_4 = -0.0021$, $\delta(114) = +0.42$, $\delta(283) = +0.22$ or $\delta^2(283) = 0.05$, in fair agreement with previous results.

E. Berlovich[186] failed to detect a shift in beta-gamma vs. gamma-beta delayed-coincidence curves for the 114-keV transition in Lu^{175} following Yb^{175} decay, and set the upper limits: $T_{1/2}(114) \leq 2\text{x}10^{-10}$ sec., $\tau_\gamma \leq 6.8\text{x}10^{-10}$ sec., and under the assumption of M1 + 25%E2, $\tau_\gamma(E2) \leq 1.4\text{x}10^{-9}$ sec. or $Q_0 \geq 6.8$ b.

Daniels, Lamarche and LeBlank[187] measured Lu^{175} gamma rays following decay of Yb^{175} incorporated in a cerium magnesium mitrate crystal lattice, with nuclear alignment being achieved by magnetic cooling to 0.003°K. Some 32.4 d. Yb^{169} and 6.7 d. Lu^{177} were noticed, but 42 d. Yb^{175} was predominant. Spectra were obtained from 0.003° K. to 1.25° K. with and without mental values of $\delta(89)$ were noted to be 0.1 (Mize et al.) and 0.03 (Hatch et al.).

For the 282.57-113.51-keV cascade following Yb^{175} beta decay, results were

$$W(\theta) = 1 + (0.221 \pm 0.004) P_2(\cos\theta) \qquad \text{(IV-13a)}$$

for liquid sources, in essential agreement with Weidling, and

$$W(\theta) = 1 + (0.210 \pm 0.003) P_2(\cos\theta) \qquad \text{(IV-13b)}$$

for dry sources. Using the value $\delta^2(113.81) = 0.18$ ($|\delta(114)| = 0.42$) from previous conversion-coefficient observations of Burford et al.[172], Waard[174], Mize et al.[176], Cork et al.[177], Hatch et al.[178], Huus et al.[72] and Bernstein and Lewis[185], mixed-mixed cascades for spin sequences 7,9,11/2(E1-M2)9/2(E2-M1)7/2 were compared with the experimental correlation coefficients. The first and last sequences yielded $\delta(283)$ values in disagreement with previous results; the middle sequence gave the best fit, $A_2 = 0.221$, $A_4 = -0.0021$, $\delta(114) = +0.42$, $\delta(283) = +0.22$ or $\delta^2(283) = 0.05$, in fair agreement with previous results.

E. Berlovich[186] failed to detect a shift in beta-gamma vs. gamma-beta delayed-coincidence curves for the 114-keV transition in Lu^{175} following Yb^{175} decay, and set the upper limits: $T_{1/2}(114) \leq 2\text{x}10^{-10}$ sec., $\tau_\gamma \leq 6.8\text{x}10^{-10}$ sec., and under the assumption of M1 + 25%E2, $\tau_\gamma(E2) \leq 1.4\text{x}10^{-9}$ sec. or $Q_0 \geq 6.8$ b.

Daniels, Lamarche and LeBlank[187] measured Lu^{175} gamma rays following decay of Yb^{175} incorporated in a cerium magnesium mitrate crystal lattice, with nuclear alignment being achieved by magnetic cooling to 0.003°K. Some 32.4 d. Yb^{169} and 6.7 d. Lu^{177} were noticed, but 42 d. Yb^{175} was predominant. Spectra were obtained from 0.003° K. to 1.25° K. with and without an external magnetic field parallel to the crystal axis. Contrary to Grace et al.[181], no anisotropy was found for either the 396-keV or the 282-keV gamma rays. They noted that dispite relatively crude estimates of the spin Hamiltonian of Yb^{+++} in this lattice environment, it was possible to infer that an anisotropy should have been seen; Yb ions being at other than the expected Ce lattice sites or the Lu^{175} 396-keV level lifetime being long enough to permit precession in the atomic field were advanced as possible explanations, the latter possibility still allowing anisotropy to be predicted for the ethylsulfate lattice where precession does not affect the angular distributions. For this mechanism to be operative the required lifetime for the 396-keV level would be $\sim 10^{-10}$ sec.

H. Vartapetian[188] observed the beta-gamma cascade through the Lu^{175} 396-keV level following Yb^{175} decay using the method of delayed coincidences, and found:

$$T_{1/2}(396\ \text{kev}) = (3.4 \pm 0.3)\ \text{nsec.}, \qquad \text{(IV-14)}$$

in agreement with previous work. Using values from Mize et al., $I_\gamma(396)/I_\gamma(282) = 2.3$, $M2/E1(282) = 3$, $M2/E1(396) = 20$, he calculated $1/\tau_{\gamma E1}(396) = 1.5\text{x}10^8$ sec.$^{-1}$, retardation with respect to the Weisskopf estimate, $5\text{x}10^{-7}$, and $1/\tau_{\gamma E1}(282) = 7.7\text{x}10^7$ sec.$^{-1}$, retardation factor $7.2\text{x}10^{-7}$. The former of these was noted not to agree with the value calculated by Chase and Willets from Nilsson functions with the deformation $\delta = 0.28$, $1.4\text{x}10^{-4}$. It was noted that the measured $B(E1,282\downarrow)/B(E1,396\downarrow)$ ratio was equal to the theoretical value,10, unlike the case for Hf^{177} involving a transition between the same two states, for which the ratio was a thousand times the Alaga value, suggesting a sensitivity to the validity of the Bohr-Mottelson strong-coupling assumption. He calculated also $1/T_{\gamma M2}(396) \approx 0.8$ and $1/T_{\gamma M2}(282) \approx 0.5$ times the Weisskopf value.

Harmatz et al.[65] studied i.c. radiation from proton-rich rare-earth isotopes produced by proton bombardment of Er and Yb enriched isotopes (as oxides). For Lu^{173} the ground state was found to be 9/2-; a 7/2+ state (g.s. in Lu^{175}) at 124 keV, a state at 264 keV that is probably the 9/2+ rotational state, and possible states at 129 keV (7/2+ or 9/2+), 426 keV, 436 keV and $\geq$1638 keV were observed. Thus the 7/2+ and 9/2- states are reversed from their order in other Lu and Ta isotopes.

g-factors for some short-lived nuclear states were measured by Manning and Rogers[189] from the perturbations of gamma-gamma cascade patterns caused by applied magnetic fields. The cascade intermediate state with magnetic moment μ precesses with radian frequency $\omega = H_{eff}\mu/I\hbar$, from which $g = \mu/I$ can be ascertained once H_{eff}, the effective magnetic field at the nucleus, and the nuclear-state lifetime are known. For lifetimes $\tau \ll 1/\omega$, the perturbation was a rotation of the correlation pattern. Reductions in experimental pattern rotations due to local atomic-field fluctuations were taken into account in the data reduction. For Lu^{175}, previous 282-114-keV correlation coefficients[179,182] were confirmed, enviromental perturbations were found to be negligible ($G \approx 1$) and a pattern rotation upon field reversal corresponding to $G\omega\tau = -(3.0 \pm 1.0) \times 10^{-3}$ rad. was observed. The 114-keV level mean life was estimated from the B(E2) value and total conversion coefficient given by Alder et al.[1] and E2/M1 $= 0.22$, given by Martin et al.[73] Quoted results were $g =$

$(0.51 \pm 0.17)/\beta G$; $\beta \equiv H_{applied}/H_{eff} \approx 1$; or

$$g = 0.5 \pm 0.2 . \qquad \text{(IV-15)}$$

The value calculated for the Nilsson 7/2+[404] state at deformation $\delta = 0.28$, via:

$$\mu = \frac{1}{I+1}\left[\frac{1}{2}(g_s - g_l)K\sum_{l}(a_{l\Omega-\frac{1}{2}}^{2} - a_{l\Omega+\frac{1}{2}}) + (g_l - g_R)K\Omega + g_R I(I+1)\right], \qquad \text{(IV-16)}$$

was $g_{theor} = 0.41$.

Gnedich et al.[190] measured external-conversion line intensities for transitions deexciting the Lu^{175} 396-keV level, to check deviations from the Alaga rules found by Mize et al. and Hatch et al. Results, shown in Table IV-1, confirmed the previous findings.

Bozhko et al.[191] measured the Lu^{175} 113.8-keV level half life using beta-gamma delayed coincidences, employing Stilbene for both gamma and electron detection. The result was

$$T_{1/2}\,(114\ \text{kev}) = (3.6 \pm 0.6) \times 10^{-10}\ \text{sec.} \qquad \text{(IV-17)}$$

They reported that their measurements showed the gamma radiation to be M1 + 80% E2.

A 72 ± 5 msec. isomeric state of Yb^{175} at 495 ± 15 keV for which α_{Tot} and α_K suggested M3 was discovered by Hoffmann[192] during a study of n-induced rare-earth activities. For $|\Delta I| = 3$, a required 1/2- Nilsson state was noted to be available.

Because E1 transition moments are expected to provide rather good probes of spherical-shell-model function components in the deformed-model wave functions, which tend to differ appreciably for different Nilsson-type models according to the type of one-body potential well employed, Hauser et al.[193] measured E1 transition probabilities in Hf^{177} and Lu^{175} in the hope of making a choice between the models of Nilsson[9,24] and of Lemmer and Green[93] who obtained purer and less deformation-dependent spherical-model configurations with a non-local diffuse-surface velocity-dependent potential. It was noted that states connected by E1 moments are not admixed into each other by nuclear perturbations. From the beta-396γ delayed coincidence in Yb^{175} beta decay, the result was

$$T_{1/2}\,(396\ \text{kev}) = (3.1 \pm 0.3)\ \text{nsec.}, \tag{IV-18}$$

in agreement with Vartapetian[180]. Delayed 283-114-keV gamma-gamma coincident measurement gave the result:

$$T_{1/2}\,(114\ \text{kev}) \leq 1.5 \times 10^{-10}\ \text{sec.}, \tag{IV-19}$$

which is compatable with the Coulomb-excitation result of Blaugrund et al.[194], $(1.01 \pm 0.07)\text{x}10^{-10}$ sec.

Results were compared with the model in the following manner: for the strong-coupling case (permanent deformation), $K = \pm 1/2 \rightarrow K' = \mp 1/2$ transitions excluded,

$$T(E1) = \frac{16\pi}{9}\frac{1}{\hbar}\left(\frac{\omega}{c}\right)^3\left[e^2\left(1-\frac{Z}{A}\right)^2\frac{\hbar}{M\omega_0}\frac{3}{4\pi}\langle I1KK'-K|I'K'\rangle^2\right]G_{E1}^2\ \text{sec}^{-1}, \tag{IV-20}$$

$$G_{E1} = \sum_{\ell}\sum_{\ell'}\langle N'\ell'|r|N\ell\rangle\sqrt{\frac{2\ell+1}{2\ell'+1}}\langle \ell 1 0 0|\ell' 0\rangle\sum_{\Lambda\Lambda'}\sum_{\Sigma\Sigma'}\delta_{\Sigma\Sigma'}a'_{\ell'\Lambda'}a_{\ell\Lambda}\langle \ell 1\Lambda K'-K|\ell'\Lambda'\rangle. \tag{IV-21}$$

$a_{\ell\Lambda}$ is the amplitude of the spherical-wave-function component in the state, and $\langle \ell_3\rangle = \Lambda$, $\langle s_3\rangle = \Sigma$, $\langle j_3\rangle = \Omega$, $\langle I_{03}\rangle = K$, $K = \Omega = \Lambda + \Sigma$, and $\hbar\omega_0$ is the oscillator level specing. The transitions involved are $I, K = 9/2, 9/2 \rightarrow I', K' = (7,9,11)/2, 7/2$, and are K-allowed but forbidden by the asymptotic selection rules. The radial matrix elements $\langle N'\ell'|r|N\ell\rangle$ were available for the Nilsson but not the Lemmer and Green potential, so only the former could be checked against the data available for E1 transitions (in Hf^{177}, $Lu^{175,177}$, $Ta^{179,181}$). Calculations were made assuming the same deformation in the initial and final states (it was noted that changes in deformation to ~10% would not alter the results appreciably). From the 396-keV level half life, the percentage of M2, conversion coefficients and the relative gamma-ray intensities from the work of Hatch et al.[178], the partial E1 decay constants and hence values of G^2(E1)(exper.) were obtained: ${G_{E1}}^2$(396 trans) = 4.5×10^{-7}, ${G_{E1}}^2$(283 trans) = 3.2×10^{-6}, ${G_{E1}}^2$(145 trans) = 2.2×10^{-5}. It was noted that the B(E1) values calculated from the Nilsson wave functions were ~100 times too small for the ground-state transitions but were sensitive to the wave-function configuration mixtures, and that incorrect choice of deformations could not be responsible.

A few points resulting from the study were observed. Small variations in the experimental ratios of the transition probabilities (to a factor of ~7 in odd-p and ~2 or 3 in odd-n nuclei) suggested approximately constant intrinsic structure within a rotational band, except for Hf^{177} where band mixing in the first excited member of the ground-state band of a K= 9/2 state was stated to be a possible cause for an anomaly in G_{E1} for this member. The wave-function configuration seemed to be about the same in the four nuclei, but the 9/2- level energy and the deformation parameter decreased and the inertia moment increased appreciably with increasing A, suggesting that the core collective properties or the addition of two extra protons or neutrons do not alter the residual interactions enough to change the single-particle wave functions very much. The close-lying 5/2+ state (349 keV in Lu^{175}, 482 keV in Ta^{181}, unknown in Lu^{177} and Ta^{179} as yet) could have its first excited band member mixed in the 7/2+ ground state, and in the case of purer configurations, as in the Lemmer-Green model, result in the required $\sim$100 factor increase in G_{E1} for the ground-state transition.

In order to search for nuclear-structure effects in the internal-conversion process, which are best detected in the angular-correlation patterns, Thun et al.[195] studied electron-gamma, gamma-electron and gamma-gamma angular correlations in the 282-114-keV cascade in Lu^{175}. Transitions in Tl^{203} (279 keV, ℓ-forbidden M1), Tl^{201} (330 keV, ℓ-forbidden M1) were known to have normal K-conversion coefficients but anomalous bamma directional correlation patterns; in Ta^{181} (482 keV, asympt.-forbidden M1), an abnormal coefficient and correlation pattern, but in Sn^{150} (90 keV, slightly-retarded E1), no anomalous effects. Lu was chosen because structure-dependent anomalies tend to appear in retarded transitions such as the 282-keV E1 transition in the above-mentioned cascade.

The 282-114-keV gamma-gamma correlation coefficients were found to be $A_2 = 0.240 \pm 0.004$, $A_4 = 0.003 \pm 0.009$; the 282K-114γ coefficient, corrected for correlation in the β -114γ background, $A_2 = 0.015 \pm 0.030$; and the 282γ -114K correlation coefficient, corrected for the coincidence background, A_2 0.02 0.01. From the 114K-282γ coincidence and 282γ singles rates, there followed:

$$\alpha_K(114) = 1.6 \pm 0.3, \tag{IV-22}$$

in agreement with Hatch et al. (1.6) and Mize et al. (1.7 0.4). From the 114K and 282K singles rates the fraction of 114-keV transitions in coincidence with 282-keV transitions as determined from intensity ratios of Hatch et al., α_K above and the 282-keV K/LM... ratio of Mize et al., there followed

$$\alpha_K(282) = 0.030 \pm 0.007 . \tag{IV-23}$$

With exclusion of negative δ on the basis of correlation and 282-keV conversion results, comparison of $\alpha_K(114)$ with Sliv theoretical values gave:

$$\delta(114) \equiv \pm\sqrt{\frac{E2}{M1}} = +0.84^{+0.44}_{-0.34} . \tag{IV-24}$$

Essentially the same result followed from the independent method of comparing their values of $A_2(282\gamma\text{-}114K)/A_2(282\gamma\text{-}114\gamma)$ as a function of $\delta(114)$ with the measured value of this ratio, 0.133 ± 0.006, a method noted to be independent of $\delta(282)$. δ (282) was deduced from δ (114) and the 114γ-282γ correlstion coefficient; also from $\alpha_K(282)$; and lastly from theoretical values of $A_2(282K\text{-}114\gamma)/A_2(282\gamma\text{-}114K)$ as a function of $\delta(282)$ (this ratio being independent of δ (114)), compared to the measured value of the ratio, 0.06 ± 0.12. Possible ranges of δ (282)($|\delta| \sim 0.1$, either sign) from the first two methods overlapped, but no value of δ (282) gave an A_2 ratio near the experimental value, due to too small a result for $A_2(282K\text{-}114\gamma)$. It was concluded that conversion coefficients for both transitions were normal, but the correlation pattern involving 282-keV K-conversion electrons was anomalous, whereas the others were normal.

Bashandy and El-Nesr[196] studied beta and gamma radiations associated with the Yb^{175} beta decay. Yb^{169}, Yb^{175} and Yb^{177} activities from neutron-irradiated Yb_2O_3 were run through a mass spectrometer, and singles and beta-gamma coincidence measurements were carried out. Hf^{175} decay radiations from n-irradiated HfO_2 (Hf enriched to ~10% Hf^{174}) were studied, using electron-gamma and electron-electron cioncidences. The results of the study are shown in Table IV.1. Branching ratios in the decay scheme were derived from observed coincidence and singles counting rates. The 343.4-keV K-conversion coefficient was determined relative to a Hg^{198} 4.2-keV standard transition, and was found to agree within the errors with the theoretical M1 coefficients of Rose and of Sliv and Band. The 89.3-keV and 161.3-keV L coefficients and the 161.3-keV K coefficient were determined from gamma-electron coincidence intensities measured at 126° to minimize angular-correlation effects, the measured branching ratios, and the K/LM ratios of Hatch et al.

B. Deutch[197] measured the lifetime of the 343-keV level in Lu^{175} by a resonance-fluorescence technique employing a centrifuge to produce a source velocity. Under the assumption of a ground-state decay branch of 0.883, the result was

$$\tau_\gamma(343) = (4.7 \pm 0.4) \times 10^{-10}\,\text{sec}, \qquad \text{(IV-25)}$$

From this and the mixing ratio as determined in previous conversion and correlation work, the M1 component of the transition to the ground state was found to be hindered by a factor of 700 with respect to the single-particle estimate, which was noted to be 4000 times less than the hindrance of the 482-keV M1 transition in Ta^{181} between the same two Nilsson states.

Because nuclear-structure effects should be most apparent in hindered M1 transition coefficients, Novakov and Stepić measured M1 coefficients of heavy odd-A nuclei. L ratios for the 114-keV Lu^{175} transition were obtained. Comparison to the theoretical results of Church and Weneser showed that assumption of an equal structure effect (equal value of c(Z, k)) on all L-subshells was inconsistent with the data, yielding non-overlapping permissible E2-M1 mixture ratios from the different L ratios (ranging from ~11% to ~18½% E2). This was in accord with theoretical expectations, according to Church and Weneser.[124]

Lindskog et al. did lifetime measurements of first excited states in odd-A rotational nuclei using an electron-electron coincidence spectrometer. Coincidence-curve centroid-shift measurements against those of cascades involving known or negligible lifetimes were observed, using a time-to-pulse-height converter calibrated by delay cables with transition speeds measured with the aid of a Hewlett-Packard electronic counter as time standard. Instrumental effects were carefully accounted for. N-irradiated HfO_2, Hf enriched to 7.9% Hf^{174}, five months old to allow the 4.6 d. Hf^{181} to decay to ~2% of the 70 d. Hf^{175} strength, served as the source. The 229L-114L cascade and the fiducial $Pb^{212} \xrightarrow[\beta]{} Bi^{212*}(238.6) \xrightarrow[2\gamma L]{} Bi^{212}$g.s.(60 m.) cascade were observed, and effects of interfering coincidences from other subshells were taken into account. The result was:

$$T_{1/2}(114\ kev) = (9 \pm 1) \times 10^{-11}\ sec., \qquad \text{(IV-26)}$$

in agreement with previous results.[194,199] δ^2 for the 114-keV transition was computed from comparison of the mean of the L ratios of Cork et al.[177], Mize et al.[176] and Hatch et al.[178] with the theoretical coefficients of Rose[50], with the results: from L_1/L_2, $\delta^2 = 0.15 \pm 0.06$; from L_1/L_3, $\delta^2 = 0.20 \pm 0.04$; but from comparison of the mean of K/L values of Cork et al. and Blaugrund et al.[194], $\delta^2 = 0.52 \pm 0.11$, in disagreement, but from the K/L of Bernstein and Lewis[185], $\delta^2 = 0.24 \pm 0.05$, agreeing within the errors. (Thun et al.[195] found from angular-correlation measurements, $\delta = +0.84^{+0.44}_{-0.34}$ or $\delta^2 = 0.71^{+0.7}_{-0.6}$.) For the calculation of B values, the value $\delta^2 = 0.18 \pm 0.05$ was assumed; then Rose's theoretical E2 and M1 coefficients and the assumption that $\alpha_{MN...} = 1/3\alpha_L$ yielded $\alpha_{tot} = 2.5 \pm 0.1$. The level energy 113.81 ± 0.02 keV of Hatch et al. and, for obtaining g_K and g_R, the magnetic moment $\mu = 2.23 \pm 0.01$ n.m. of Reddoch[200], were used. Results appear in Table IV-2. (A discrepancy in the B(E2) value in Lu^{177} compared to those in Lu^{175}, Ta^{181} and other nearby nuclei was noted.) Berlovich et al.[201] measured the half lives of the 114-keV and 393-keV states of Lu^{175}, populated by Yb decay. They noted contradictions in some previous determinations: $T_{\frac{1}{2}}(114) = 1.4 \times 10^{-10}$ sec., Berlovich[186], using a time analyser; $T_{\frac{1}{2}} = (3.6 \pm 0.6) \times 10^{-10}$ sec., Bozhko et al.[191], using delayed coincidences; and $T_{\frac{1}{2}} = (1.01 \pm 0.07) \times 10^{-10}$ sec., Blaugrund et al.[194], from a microwave yechnique with Coulomb excitation. Interference from 30.6 d. Yb^{169} cascade decay through the Tm^{169} 118-keV level (6.2×10^{-11} sec. h.l.) and 139-keV level (2.9×10^{-10} h.l.) and of 6.9 d. Lu^{177} through a Hf^{177} 113-keV level ($4.2 \times 10^{-\cdot 0}$ sec. h.l.) were advanced as possible explanations. Accordingly, Yb enriched to 74% Yb^{174} (nat. abund. 32%) and containing 0.1% Yb^{176} was used in the preparation of the source, via neutron irradiation. From the high-energy beta-114-keV K-line delayed-coincidence-curve centroid shift the half life was deduced:

$$T_{1/2}(114\ kev) = (1.1 \pm 0.1) \times 10^{-10}\ sec. \qquad \text{(IV-27)}$$

From the 72-keV beta-396-keV gamma delayed-coincidence-curve final slope, the other half life was found:

$$T_{1/2}\,(396\ \mathrm{kev}) = (3.25 \pm 0.10) \times 10^{-9}\,\mathrm{sec.}, \qquad \text{(IV-28)}$$

in agreement with the result of Vartapetian[180], 3.4 ± 0.3 nsec. The partial transition probabilities were calculated from the half life (IV-28), the 396-keV/282-keV/144-keV gamma intensity ratios 23/10/13.6 from Mize et al.[176] and Hatch et al.[178], and the 396-keV and 282-keV E1/M2 ratios of 2 and 33 respectively, and were compared to the theoretical estimates from the Nilsson model. Results were $T_\gamma(396) = 1.2 \times 10^8$ sec.$^{-1}$, $T_\gamma(282) = 5.7 \times 10^9$ sec.$^{-1}$, $T_\gamma(144) = 8 \times 10^6$ sec.$^{-1}$, compared to theoretical estimates of 1.18×10^{10} sec.$^{-1}$, 9.76×10^8 sec.$^{-1}$, $1{,}32 \times 10^7$ sec.$^{-1}$, or hindrances of 105, 17 and 1.6 respectively. The common phenomenon of hindrance with respect to Nilsson-model estimates for deformed-region E1 transitions was noted. Collective model parameters were calculated with the results given in Table IV-2, in essential agreement with previous work.

It was noted that of the nuclei that had been investigated, Hf^{177}, Lu^{175} and Ir^{191}, the last, near the end of the deformation region, had a smaller Q_0 (4.25 b.) and a larger g_R ($0.46 \sim Z/A$) than the others, and that the tendency for g_R to be larger and in closer agreement with the value Z/A near the deformation-region boundary was theoretically understood in terms of perturbations in the collective model due to pairing correlations, as shown by Nilsson and Prior.[202]

Transitions in Lu^{175}

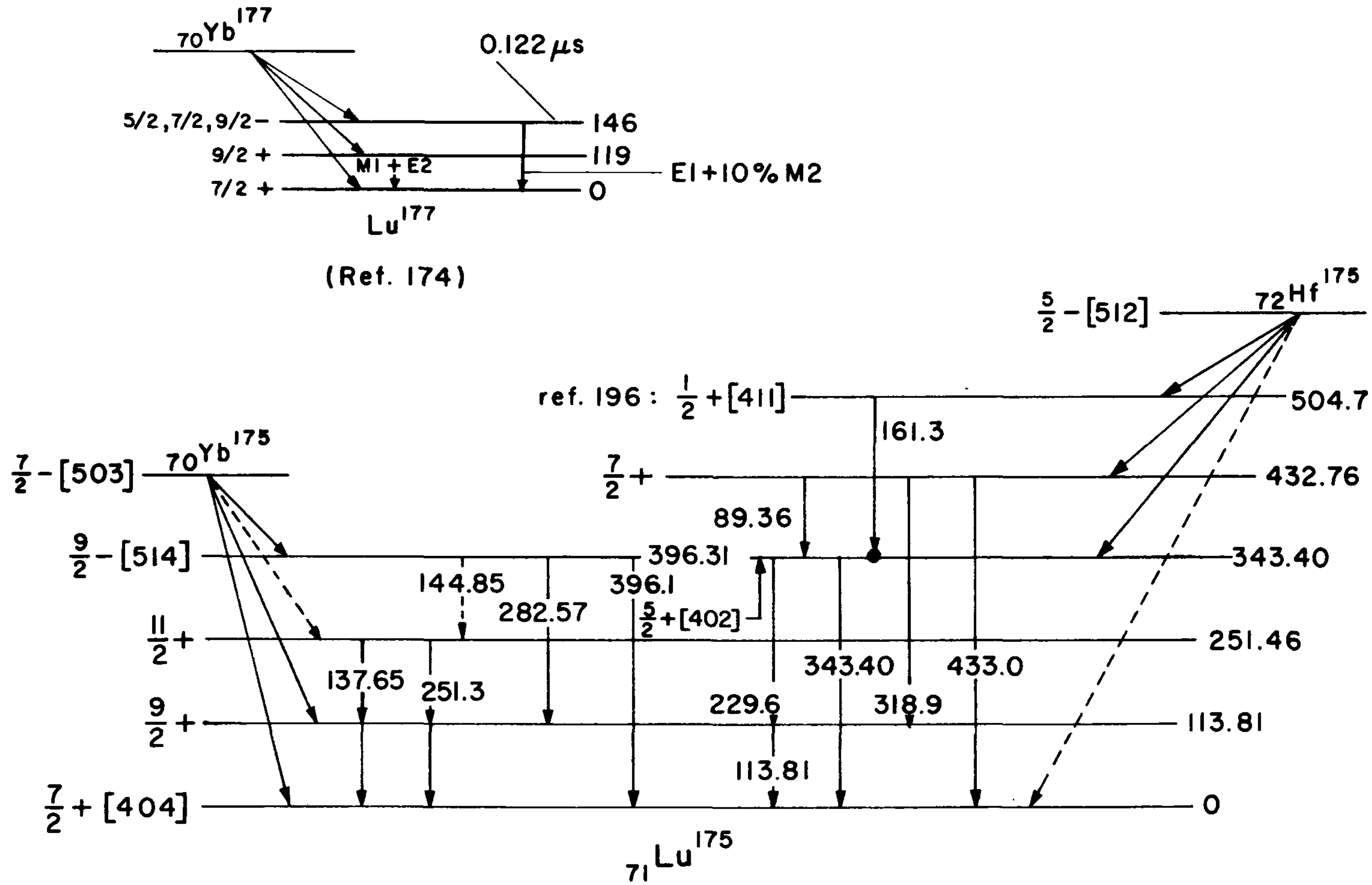

Energies: Hatch et al.[178]

FIG IV-1

Table IV-1 Transitions in Lu^{175}

Ref.	E ,keV	α_K	α_L	K/L *K/LMN	$L_i/L_{ii}/L_{iii}$	Multipolarity
174	113.0±0.3	2.25±0.5	---	2.5±0.5*	---	E2/M1=0.33±0.10
176	113.6±0.2	1.7±0.4	---	---	3/~1/~1	E2/M1=0.30±0.06
177	114.1	---	---	2.9±0.4	10/4.1/2.7	M1+E2
178	113.81±0.02	1.6	i,ii,iii=.39, .10,.13	---	39/10/13	
176	137.6±0.2	---	---	---	---	
177	137.8	---	---	~2	---	E2
178	137.65±0.05	1.0	---	---	---	M1+E2
176	144	---	---	---	---	E1: I.c. not seen.∴E1 or E2; β decay rules out E2.
177	145.0	---	---	---	---	
178	144.85±0.03	0.11	---	---	---	E1
190	145	---	---	---	---	
176	≈251	---	---	---	---	
178	251.3±0.5	---	---	---	---	(E2)
174	281±1	---	---	>4	---	M2/E1=0.04±0.02. 114-282 ang. correl.
176	282.4±0.2	0.038±0.01	---	≥5*	---	M2/E1=0.027±0.016 implies M2/E1=
177	282.9	---	---	~6	---	M1+E2 0.04±0.03.
178	282.57±0.13	0.030	0.0037	8	---	E1+2%M2
190	283	---	---	---	---	
174	395.1±0.3	---	---	5.9±0.7	---	M2/E1=0.26±0.07 K/MN=4.3±1
176	396.0±0.2	0.050±0.005	---	5.8±0.5*	---	M2/E1=0.20±0.03
177	397.0	---	---	5.4±0.3	---	E2
178	396.1±0.3	0.067	0.0085	7.9	---	E1+20%M2
190	396	---	---	---	---	
172	89.1	---	---	6.0±1	---	M1(+E2) L/M=3.5±0.9
176	89.3±0.2	---	---	---	10/1/1	E2/M1~0.1
178	89.36±0.01	2.2	i+ii=.43,iii=.022	---	---	M1+3%E2
196	89.3	---	0.495±0.050	---	---	M1+E2
172	113.4	<1	---	---	---	M1(+E2)
176	113.6±0.2	---	---	---	---	M1+E2
178	113.81±0.05	~2	---	---	(i+ii)/iii ~6	M1+10%E2

Ref.	E_{trans}, keV	α_K	α_L	K/L *K/LMN	$L_i/L_{ii}/L_{iii}$	Multipolarity
178	161.3±0.2	0.5	0.2	2.5	---	(E2)
196	161.3	0.311±0.032	0.198±0.015	1.5	---	Pure E2
172	228.4	---	---	2±0.5*	---	E2 Ref. 170: K/L~10
176	229.3±0.2	---	---	~2	---	E2
178	229.6±0.6	0.11	0.05	5.5	---	E2
172	318	---	---	---	---	
176	318.6±0.2	---	---	---	---	Ref. 170: K/L~2
178	318.9±0.6	---	---	---	---	(M1)
172	342.3	---	---	4.94±0.5*; ~6	---	Pure M1(from α_K) Ref. 170: K/L=
176	342.9±0.2	---	---	5.0±0.5*	---	E2/M1≤ 0.25 4.94±0.20; ref.
178	343.40±0.08	0.105	0.019	5.5	---	M1+ to 25%E2 171: K/L=5.0.
172	430	---	---	---	---	
176	432.2±0.2	---	---	---	---	
178	433.0±0.5	0.061	0.0095	6.4	---	M1+ to 25%E2

B. Coulomb Excitation

Heydenburg and Temmer[203] first observed Coulomb excitation in Lu^{175} during a survey with 3-MeV α-particle projectiles, observing the 113-keV line. Later[80] they reported, from a Coulomb-excitation survey using 6-MeV α particles, 114-keV and 250-keV lines and gave $\epsilon B(E2)$ values of 0.72 and 0.20 respectively (in the units $e^2 10^{-48}$cm.^{4}). A 180-keV line of Lu^{176} (2.6% nat. abund.) was observed as well. The agreement of the energy ratio, 2.19 ± 0.04, with that of the pure rotational model was noted. Huus et al.[72] observed the Lu^{175} 114-keV i.c. lines, and from the L-line yield obtained $\epsilon_L B(E2) = 0.36$. Quoted results were $K/L \approx 5.5$ or $1/\delta^2 \approx 20$, $1/\epsilon_L = 8.9$, $B(E2) = 3.2\ e^2 10^{-48}$cm.^{4}, $Q_0 = 8.8$ b., $|g_K - g_R| \sim 1.0$. They noted that pure-band intensity rules would imply a B(E2) value to the second excited state four times that of Heydenburg and Temmer, but in agreement within the experimental errors, and that a $\sim 20\%$ decrease in K/L would multiply $|g_K - g_R|$ by 1/1.8 giving better agreement with Heydenburg and Temmer, without altering B(E2) appreciably. Bernstein and Lewis observed i.c. lines from Coulomb excitation of the first two excited states of heavy odd-A nuclei by means of α particles, and for Lu^{175}, in conjunction with the gamma-ray results of Heydenburg and Temmer, confirmed rotational-model predictions. Mixing ratios were determined by comparison to Sliv corrections to Rose's point-nucleus E2 and M1 K and L conversion coefficients. B(E2) to the first excited state was determined from the Heydenburg and Temmer gamma-ray yield and the total conversion coefficient derived from theoretical coefficients and the mixing ratios; to the second excited state, from the conversion-electrin yield relative to that from the first excited state, and the crossover gamma yield of Heydenburg and Temmer. Absolute B values were estimated to be good to 50%, relative B values to the two excited states, to 20% or better, and K/L ratios, to 15% for the cascade radiation and 10% for the first-excited-state decay transition. Quoted results for Lu^{175} are shown in Table IV-2. The Q_o values calculated from excitation data on the first and second excited states were found essentially to agree, and the δ^2 values from K/L ratios and from branch ratios were found to agree within the (somewhat large) experimental errors, indicating accord with collective-model predictions.

To check agreement of B values with rotational-model predictions and the disagreement of deformations derived from Q_o values with those predicted for observed energy spacings using the irrotational-flow inertia moments, Goldring and Paulisson[140] measured gamma-ray yields following Coulomb excitation by 3-MeV protons, with the targed situated between two NaI(Tl) crystals in a 76^o half-angle geometry. One counter accepted the cascade decay photopeak, the other, the first-excited-state decay photopeak. From singles and coincidence rates (the crossover transition rate representing a minor correction), the population ratio for the two states was derived. M1/E2 ratios of Huus et al. and corrected Rose values of theoretical conversion coefficients were employed. Lu^{175} results, agreeing with theoretical intraband B-value ratios, are shown in Table IV-2.

Extending their earlier work, Heydenburg and Temmer[82] observed singles and X-X, X-γ and γ-γ coincident radiation from 6-MeV α-particle-induced Coulomb excitation of heavy odd-A nuclei. The cascade radiation mixing ratio was determined from the cascade/crossover ratio under the assumption that pure-band E2 intensity rules hold and the excess cascade radiation is the M1 component. Rose's E2 coefficients and Rose's M1 coefficients decreased 25% in accord with the findings of Sliv and coworkers were used. The results appear in Table IV-2.

Martin et al.[73] Coulomb excited some odd-A heavy nuclei with 4.05-MeV protons, and performed careful measurements of the deexcitation radiation. In Lu^{175} the first two excited states were populated. The results of intensity and angular-distribution measurements on the deexcitation gamma rays are given in Table IV-2.

Chupp et al.[83], in their precision determinations of deexcitation gamma-ray energies following Coulomb excitation by 3.7-MeV protons with a bent-crystal spectrograph, found the energy of the first excited state in Lu^{175} to be

$$E_\gamma = 113.79 \pm 0.04 \text{ keV}, \qquad \text{(IV-29)}$$

in agreement with the previous best value due to Hatch et al.[178], 113.81 $\pm$ 0.02 keV.

Elbek et al.[199] studied the inelastic scattering of 4 to $4\frac{1}{2}$-MeV protons and deuterons from thin evaporated metallic lutetium targets. In order to get data for both Lu^{175} and Lu^{176}, enrichment of the latter was performed in an electromagnetic mass separator, and the target material was collected on thin Formvar backing by reducing the ion energies with a retarding potential. Results for Lu^{175} were as follows:

$$\begin{aligned} &E_1 = 114 \pm 2 \text{ keV}; \quad E_2 = 251 \pm 2 \text{ keV}; \quad E_2/E_1 = 2.20 ; \\ &B(E2, I_0 \to I_0+1) = (2.34 \pm 0.10) e^2 10^{-48} \text{cm.}^4 ; \\ &B(E2, I_0 \to I_0+2) = (0.57 \pm 0.08) e^2 10^{-48} \text{cm.}^4 ; \\ &\frac{B(E2, 7/2 \to 11/2)}{B(E2, 7/2 \to 9/2)} = 0.244 ; \quad Q_0 = 7.45 \pm 0.35 \text{ barns.} \end{aligned} \tag{IV-30}$$

They were noted to be in accord with previous work. The ratio of the B-values was, within the experimental errors, equal to the value from the Alaga rules, 0.257. The spectroscopic quadrupole moment from h.f.s. measurements due to Steudel[204], $Q = Q_0 \dfrac{I_0(2I_0-1)}{(I_0+1)(2I_0+3)} = 5.6 \pm 0.5$ corresponding to $Q_0 = 12.0 \pm 1.1$, does not agree, however, with the above Q_0 from the B-values. It was noted that this class of discrepancies, present also in other nuclei, may be due to use of inadequate electronic wave functions in the h.f.s. data analysis.

To check predictions of the rotational model for B(M1) values as well as B(E2) values in ground-state bands, Bernstein and Graetzer[144] studied internal conversion deexcitation lines following Coulomb excitation of several rare-earth odd-A isotopes with 2 to 3.7-MeV protons. Conversion electrons were detected with a wedge-gap spectrometer arranged to permit angular distribution measurements. CsI scintillators detected scattered protons at 155°, to permit ratio-to-Rutherford yield measurements. Electrons were detected with anthracene, calibrated in efficiency with the Pr^{147} beta spectrum which has a known linear Kurie plot, and found to be constant over the energy region of interest. Targets were prepared by vacuum evaporation onto thin carbon backing.

Lu^{175} results are shown in Table IV-2. The following points were noted about the 258-keV transition i.c. line: it was too strong to come from the Lu^{176} target component, and was a K-line since if it were an L line the corresponding K line would be missing. Lack of an L line suggested M1 or E1 decay, and yield measurements at two incident energies suggested a parent level at 750 ± 100 keV. If the decay were M1 then $B(E2\uparrow, 750 \text{ keV})/B(E2\uparrow, 114 \text{ keV}) = 1/60$. If E1 (also compatible with $K/L \geq 5$), $B(E1\uparrow)$ would be much too large. Theoretical conversion coefficients of Sliv and Band were used in the data analysis.

To obtain information on the B(M1) values which are more sensitive indicators of the validity of the rotational model than B(E2) values, Blaugrund et al.[194] measured lifetimes of the first excited states of some heavy odd-A nuclei. As found from B(E2) values and mixing ratios derived from K/L or correlation measurements, because of uncertainties in the latter they were thought to be too imprecise to serve as collective model tests. The mean lives τ,

$$\frac{1}{\tau} = \frac{1}{\tau_{M1}} + \frac{1}{\tau_{E2}} = \frac{16\pi}{9}\frac{1}{\hbar}\left(\frac{E_\gamma}{\hbar c}\right)^3\left(\frac{e\hbar}{2Mc}\right)^2(1+\alpha_{tot})(1+\delta^2)B(M1), \qquad \text{(IV-31)}$$

would provide the required information. As noted under their Ho results, these authors used an r.f.-modulated 2.5-MeV proton beam to produce the excitation, and from analysis of the deexcitation data were able to detect lifetimes down to the 10-100 psec. range, too short for conventional delayed-coincidence techniques. In the work, K/L ratios were also determined.

Results for Lu^{175} are listed in Table IV-2.

To provide a test of the collective model, Goldring[205] obtained cascade transition B(M1) values in some heavy odd-A rotational nuclei from analysis of cascade/crossover ratio measurements and previous Coulomb-excitation B(E2) results. Targets of a few hundred μgm./cm.^{2} of rare-earth oxides evaporated onto carbon discs were bombarded by 3.1-3.4-MeV protons, and deexcitation radiation in coincidence with the inelastic proton group corresponding to the second excited state was detected. The protons were detected with a proton double-focusing magnetic spectrometer of $\sim$1-2% resolution set at a 135° scattering angle. This arrangement served to suppress the intense decay radiation from the first excited state. Gamma counter efficiencies were measured with sources at the beam spot position. Angular distribution effects were estimated from the counter solid angles and the single excitation formulae of Alder et al.[1] Summing effects were

Ref.	80, 203	72	139	140	82	73	199	144	205
E_{trans}	114	114.3	114	---	114	114	114±2†	114	---
$\epsilon_\gamma B(E2)$	0.72	---	---	---	---	0.72	---	---	---
$\epsilon_L B(E2)$	---	0.36	---	---	---	---	---	0.358	---
K/L	---	~5.5	4.3	---	---	---	---	4.40±0.5	---
$\therefore \delta^2$	---	1/20	0.11	---	---	---	---	---	---
$\therefore \alpha_{tot}$(theor)	---	---	2.3	---	2.1	2.66	---	---	---
$B(E2,114\downarrow), e^2 10^{-48} cm^4$	3.2	3.2	2.86	---	2.5	2.4*	---	2.4±0.5	---
$B(M1), \left(\frac{e\hbar}{2Mc}\right)^2$	---	---	---	---	---	0.08(18%E2)	---	---	---
Q_o, b.	---	8.8	8.2	---	7.6	7.5	---	---	---
E_{trans}	---	---	139	---	136	140	---	137	---
$\epsilon_\gamma B(E2)$	---	---	---	---	---	0.13	---	---**	---
K/L	---	---	5.5	---	---	---	---	4.30±0.4	---
$\therefore \delta^2$	---	---	0.08	---	---	0.22±0.04	---	---	---
$\therefore \alpha_{tot}$(theor)	---	---	1.4	---	2.0	1.4	---	---	---
δ^2 (from $\frac{crossov.}{casc.}$)	---	---	0.11	0.27	0.135	0.30	---	---	0.21±0.03##
B(M1)	---	---	---	---	---	0.09(8%E2)	---	---	.0903±.0014††
E_{trans}	250	---	253	---	250	254	251±2†	251	---
$\epsilon_\gamma B(E2)$	0.20	---	---	---	---	0.12	---	---	---
K/L	---	---	---	---	---	---	---	2.9±0.4	---
Crossov./Casc.	---	---	---	.90±.15	---	0.95	---	---	.932±.055
α_{tot}(theor)	---	---	---	---	0.1	0.13	---	---	---
$\delta^2(114)/\delta^2(140)$	---	---	1.38#	---	---	---	---	---	---
$B(E2,254\uparrow)$	---	---	0.75	---	0.78	0.45*	---	0.56±0.1	---
Rat., 254/114	---	---	0.26	2.23	0.31	0.19*	0.244	0.23±0.025	---
Q_o, b.	---	---	8.3	---	8.5	6.4	7.45±0.35	---	6.50±0.59

* Av. of ref. 72, 73, 82, 139, 146 quoted: B(E2,114)=2.8±0.3, B(E2,254)=0.7±0.2, ratio=0.25±0.4 (Alaga=0.257).

Alaga=1.018 †† From crossover/cascade, δ^2, ref. 199 B(E2).

† Inelastic proton groups ** $\epsilon_K B(E2)$=0.012, $\epsilon_L B(E2)$=0.044

Ref. 73, 144

Table IV-2 (Cont.)

Transitions in Lu^{175}

Ref.	198	201	83	194
E_{trans}	113.81 (ref.178)	Same	113.79±0.04	113.81 (ref.178)
$T_{1/2}$	$9\pm1\times10^{-11}$ sec.	$11\pm1\times10^{-11}$ sec.	---	$14.6\pm1.0\times10^{-11}$ sec.
K/L	---	---	---	3.2±0.3
α_{tot}	2.5±0.1	---	---	2.74
2	0.18±0.05	0.25	---	0.18±0.06
B(E2)	$1.41\pm0.05=240B_{sp}$	---	---	---
Q_o, b.	6.5±1.0	7.45	---	---
B(M1)	$.071\pm.009=1/22B_{sp}$	0.067	---	0.060±0.005*

* From τ, δ^2, α_{tot}; previous B(E2) value and crossover/cascade imply 0.085±0.03.

estimated and allowed for in the analysis. The Lu^{175} results are shown in Table IV-2.

C. Miscellaneous Measurements

In 1936 Gollnow[206] deduced the Lu^{175} ground-state spin to be 7/2, from results of a h.f.s. study, and quoted the results

$$Q = +\,5.98 \text{ barns}; \quad \mu \sim +\,2.6 \text{ n.m.} \tag{IV-32}$$

P. Klinkenberg[207] listed for Lu^{175} the values, as of 1955, for the static electromagnetic moments,

$$Q = +\,5.9 \text{ barns}; \quad \mu = +\,2.9 \pm 5.0 \text{ n.m.} \tag{IV-33}$$

I. Kamei[208], in a more accurate calculation taking account of a certain polarization correction omitted by Gollnow as well as core-shielding corrections, obtained the value for the Lu^{175} spectroscopic quadrupole moment:

$$Q = +\,5.7 \text{ barns} \pm 5\% \;. \tag{IV-34}$$

Murakawa and Kamei[209] did calculations to derive spectroscopic quadrupole moments using tentative improved shielding corrections for 5d electrons, and for Lu^{175} obtained the value

$$Q = +3.6 \pm 0.2 \text{ barns, or } Q_0 = 8 \text{ barns,} \tag{IV-35}$$

compared to the Coulomb-excitation value then available of Huus et al.[72], $Q_0 = 9$ barns, and an unpublished value due to Goodman[210], $Q_0 = 7.8$ barns.

Chase and Wilets[184] noted the interpretation of the then known Lu^{175} levels in terms of the Nilsson model, in which 0, 114, and 251-keV levels are rotational states on the 7/2+ [404] ground state, the 342.9 and 432.2-keV levels populated in Hf^{175}-decay are the ground member and first rotational member of the 5/2+ [402] band, and the 396-keV level is the 9/2- [514] Nilsson state. Yb^{175} and Hf^{175} ground states were assigned as 7/2- [503] and 5/2- [512] respectively. Slowness of the Hf decay to the Lu^{175} ground state and of Yb decay to the Lu^{175} 5/2+ state were noted to be effects of the asymptotic selection rules.

A. Steudel[204], from h.f.s. studies, derived the quadrupole moment for Lu^{175},

$$Q = 5.6 \pm 0.5 \text{ barns.} \qquad \text{(IV-36)}$$

A year later, in 1958, from a study of h.f.s. in six lines with a Fabrey-Perot interferometer, he obtained the results[211];

$$Q = 5.6 \pm 0.6 \text{ barns;} \qquad \mu = +2.0 \pm 0.2 \text{ n.m.} \qquad \text{(IV-37)}$$

Blaise et al.[212] observed h.f.s. with a Fabrey-Perot spectrometer from a Lu sample enriched in Lu^{176} (g.s. spin found to be 7, in accord with previous work), and found for Lu^{175},

$$\mu = +2.0 \pm 0.2 \text{ n.m.} \qquad \text{(IV-38)}$$

in agreement with Steudel, and

$$Q = (4.0 \pm 0.5)\ \frac{0.1}{1-R}\ \text{barns}$$
$$= (5.6 \pm 0.6)\ \frac{0.1}{1-R'}\ \text{barns}; \qquad \text{(IV-39)}$$

where the factors R, R' are so-called Sternheimer corrections for 6p and 5d electrons, respectively.

Because of the inherent uncertainties of indirect h.f.s. determinations of μ and Q values, due to lack of adequate knowledge of the ionic wave functions, G. Ritter[213] studied radio frequency transitions between h.f.s. levels of the $5d6s^2\ {}^2D_{3/2}$ ground-state and the ${}^2D_{5/2}$ metastable state configurations of Lu by an atomic beam resonance method, providing a more or less direct measurement of the Lu^{175} moments based on the interaction of I with an external magnetic field. Computer analysis of the data yielded, among other parameters having to do with electronic properties of the Lu atoms, the quantities, extracted from runs at high external magnetic fields,

$$g_I = (+3.50 \pm 0.16) \times 10^{-4}, \text{ or}$$
$$\mu_I = (+2.25 \pm 0.10)\ \text{n.m.} \qquad \text{(IV-40)}$$

from atoms in the ground state, and

$$g_I = (+3.13 \pm 0.24) \times 10^{-4}, \text{ or}$$
$$\mu_I = (+2.01 \pm 0.15)\ \text{n.m.} \qquad \text{(IV-41)}$$

from atoms in the metastable state. It was noted that the discrepancy was not fully understood, and that the weighted mean, 215 ± 0.19 n.m., was to be taken as the best value, or with diamagnetic shielding corrections,

$$\mu_I = (+2.17 \pm 0.19) \text{ n.m.} \qquad \text{(IV-42)}$$

The quadrupole moment, without the Sternheimer (induced quadrupole moment) correction, was found to be 5.74 barns from the atomic ground-state data and 5.63 barns from the metastable state data, or a mean of

$$Q = +5.68 \pm 0.06 \text{ barns (uncorr.)}. \qquad \text{(IV-43)}$$

These were compared with the values of μ_I, + 2.6 ± 0.5 n.m. (Gollnow[206]); + 2.0 ± 0.2 n.m. (Steudel[211]), and of Q, + 5.9 barns (Gollnow), + 5.6 ± 0.6 barns (Steudel), and + 5.15 ± 0.3 barns (Kamei[208]) (the figure in the Kamei article is actually + 5.7 ± 5%).

Reddoch and Ritter[214] did a nuclear magnetic resonance determination of the Lu^{175} magnetic moment. No resonance was observed in Lu compound solutions, probably due to environmental perturbations caused by the large quadrupole moment. To minimize these perturbations a solid of cubic symmetry was selected. Several such compounds showed no resonance either, but resonance was observed in LuB_{12} and in LuSb, formed by heating the oxide in vacuum and the metal in a sealed quartz tube with boron and with antimony respectively. Lattice characteristics were determined from X-ray powder diffraction patterns. Various environmental frequency shifts were investigated and found to be negligible. Diamagnetic shielding corrections due to inner electrons and paramagnetic corrections due to configuration impurity of the electronic ground state were applied in data reduction. The frequency was observed relative to a deuterium NMR standard frequency. The result for the Lu moment was

$$\mu = +2.230 \pm 0.011 \text{ n.m.} \qquad \text{(IV-44)}$$

compared to the atomic beam resonance result, 2.17 ± 0.19 n.m.

Because of the discrepancy between the Alaga rules and the observed intensities of E1 transitions terminating on members of the ground-state band in Yb^{173}, Lu^{175}, and Hf^{177} found by Gnedlich et al.[190], Yoshida and Lin[215] calculated these ratios on the basis of the Nilsson model[9,24] but including Kerman coupling[14]

$$H' = \kappa\left(-\frac{\hbar^2}{\mathcal{J}}\vec{I}\cdot\vec{j} + \frac{\hbar^2}{2\mathcal{J}}j^2\right), \qquad \text{(IV-45)}$$

treating κ as a free parameter. The asymptotic selection rules for transitions with $\Delta K = 0, \pm 1$ were noted:

$\|\Delta K\|$	operator	$\Delta\Lambda$	Δn_z	ΔN
1	$x \pm iy$	1	0	± 1
0	z	0	± 1	± 1

(IV-46)

The E1 gamma-ray intensity ratios were calculated including H', which mixed other Nilsson states into the 9/2- and 7/2+ states of Lu^{175} provided they satisfied the selection rules; the states considered were the 7/2,9/2- [514] state predicted at 4.4 MeV and the 9/2,9/2- [505] state at 6.8 MeV coupled to the 396-keV state, for which transitions to the ground state are asymptotically unhindered. For transitions from an initial state

$$|I_1K_1\rangle + \sum_{K'} a_{K'} |I_1K'\rangle \qquad (K' = K_1 \pm 1) \qquad \text{(IV-47)}$$

to a final state $|I_2 K_2\rangle$ the result was

$$\frac{I_{\gamma_2}}{I_{\gamma_1}} = \left(\frac{E_{\gamma_2}}{E_{\gamma_1}}\right)^3 \left[\frac{\langle I_1K_1 1 \Delta K|I_2{+}1\, K_2\rangle G_{E1}(K_1\to K_2) + \sum_{K'} a_{K'}\langle I_1K'1K_2{-}K'|I_2{+}1\,K_2\rangle G_{E1}(K'\to K_2)}{\langle I_1K_1 1 K_2{-}K_1|I_2K_2\rangle G_{E1}(K_1\to K_2) + \sum_{K'} a_{K'}\langle I_1K'1K_2{-}K'|I_2K_2\rangle G_{E1}(K'\to K_2)}\right]^2 \qquad \text{(IV-48)}$$

where the mixing amplitude was

$$a_{K'} = \langle I_1K_1|H'|I_1K'\rangle / (E_{I_1K_1} - E_{I_1K'}) ; \qquad \text{(IV-49)}$$

$I_{\gamma_3}/I_{\gamma_1}$ = same, except $E_{\gamma_2} \to E_{\gamma_3}$ and $(I_2 + 1) \to (I_2 + 2)$. With $\kappa = 6.0$, the resulting branching ratios were in very good agreement with the experimental data, as was also found to be the case for the other two nuclei. The ground-state transition B(E1) value with mixing came out closer to the experimental value; it was noted that the large changes in the branching ratios were caused by the rather small mixing amplitudes, in Lu^{175}, of the [514] and [505] states mentioned above in the 9/2- state, -0.0294 and +0.0143 respectively. The results were: $_{70}Yb^{173}$, 7/2+ [633], 351-keV state to 0, 79, and 180-keV members of the 5/2- [512] ground-state band, B(E1) ratios 100/1600/290 (experiment), 100/1510/290 (Nilsson model with Coriolis coupling, $\kappa = 6.9$), 100/14/0.43 (Alaga rules); $_{71}Lu^{175}$, 9/2-

[514] , 396-keV state to 0, 114, and 251-keV members of the 7/2+ [404] ground-state band, 100/71/7.5 (experiment), 100/71/7.1 (κ = 6.0), 100/8.3/0.11 (Alaga rules); $_{72}Hf^{177}$, 9/2+ [624] , 321-keV state to 0, 113, and 250-keV members of the 7/2- [514] ground-state band, 100/9700/80 (experiment), 100/9700/119 ($\kappa = 4.4$), 100/61/0.025 (Alaga rules). Also the B(E1, 9/2- $\rightarrow$ 7/2 +) theoretical value for Lu^{175} was found to be closer to experimental values in the presence of the Coriolis mixing than without it.

V. Experimental Apparatus and Procedure

A. Beam and Geometry

The beam used in this experiment was generated by the Heavy Ion Linear Accelerator of Yale University. O^{16} ions were accelerated to the terminal energy of about 10.6 MeV/amu and magnetically steered by a series of triplet quadrupole lenses and two 45° bending magnets into a target room constructed of special radiation-shielding concrete, in which neutron, gamma and X-ray fluxes were negligible, permitting personnel to work inside the room while the beam at an energy below the Coulomb barrier impinged on a high-Z target. Inside the low-level cave the beam was passed through three apertures of Pb foil, backed by tantalum, arranged so that no beam particle not scattered by an aperture could hit anything but the target. Energy degradation was accomplished by a series of graded aluminum foils that could be moved into the path of the beam at a point prior to the final 45° steering magnet, so placed in order to prevent forward-scattered debris from the foil from contaminating the degraded beam at the target. The energy was ascertained from the final bending-magnet current. The calibration was checked by Rutherford scattering of the beam from a thin Au foil into a silicon semi-conductor detector which was calibrated with a ThB alpha-ray source, and found to be in agreement with the current readings. The spread in energy of the degraded beam was of the order of a percent. The degradation resulted in substantial loss of average beam current at the target, frequently to values of the order of 100 namp. during the beam bursts, which in the HILAC, a pulsed machine, occur for 2 msec. duration at a repetition rate of ten pulses per second. Nevertheless the limitation was the instantaneous counting rate acceptable by the gamma counters while avoiding a significant percentage of "pileup" pulses. The semiconductor backscattered ion detectors were also running at instantaneous counting rates close to the limit acceptable to the electronics. Generally a substantial fraction and frequently all of the available beam intensity was used.

B. Target Chamber

A cross section of the target chamber appears in Fig. V-1. Upon entering the chamber the beam passed through a 1/2" i.d. by 2-3/8" long Pb-lined aperture, past the 1/2" by 1/2" opening in the detector mosaic, to be stopped within the target. The target was retained opposite a 1/32" thick by 1"diameter "window" area in the aluminum target plate by a retaining ring, and both were insulated from the chamber by a sheet of Teflon, the ring being bolted in place with Nylon screws. A signal lead was taken from the retaining ring, in electrical contact with the target, through a vacuum-tight BNC-type connector, for the purpose of providing a beam-monitoring signal.

In the chamber the junction-counter mosaic is mounted on a printed-circuit board, attached mechanically and electrically at eighteen points by means of 2-56 screws to heads soldered onto vacuum-tight ceramic feed-through connectors providing separate bias leads for 16 pairs of detectors, a common signal lead, and a spare terminal, and is positioned so that the sensitive detector surfaces are 1" from the target surface. The laboratory scattering angles to the centers of the 20 innermost detector positions, used in these experiments, ranged from 129.0° to 153.4°, with corresponding center-of-mass angles for O^{16} on Tb^{159} of 132.9° and 155.7° respectively. The laboratory solid angle of the 20 junction detectors totaled 1.300 sterad. or 10.34% of a sphere, with a corresponding effective center-of-mass total solid angle for O on

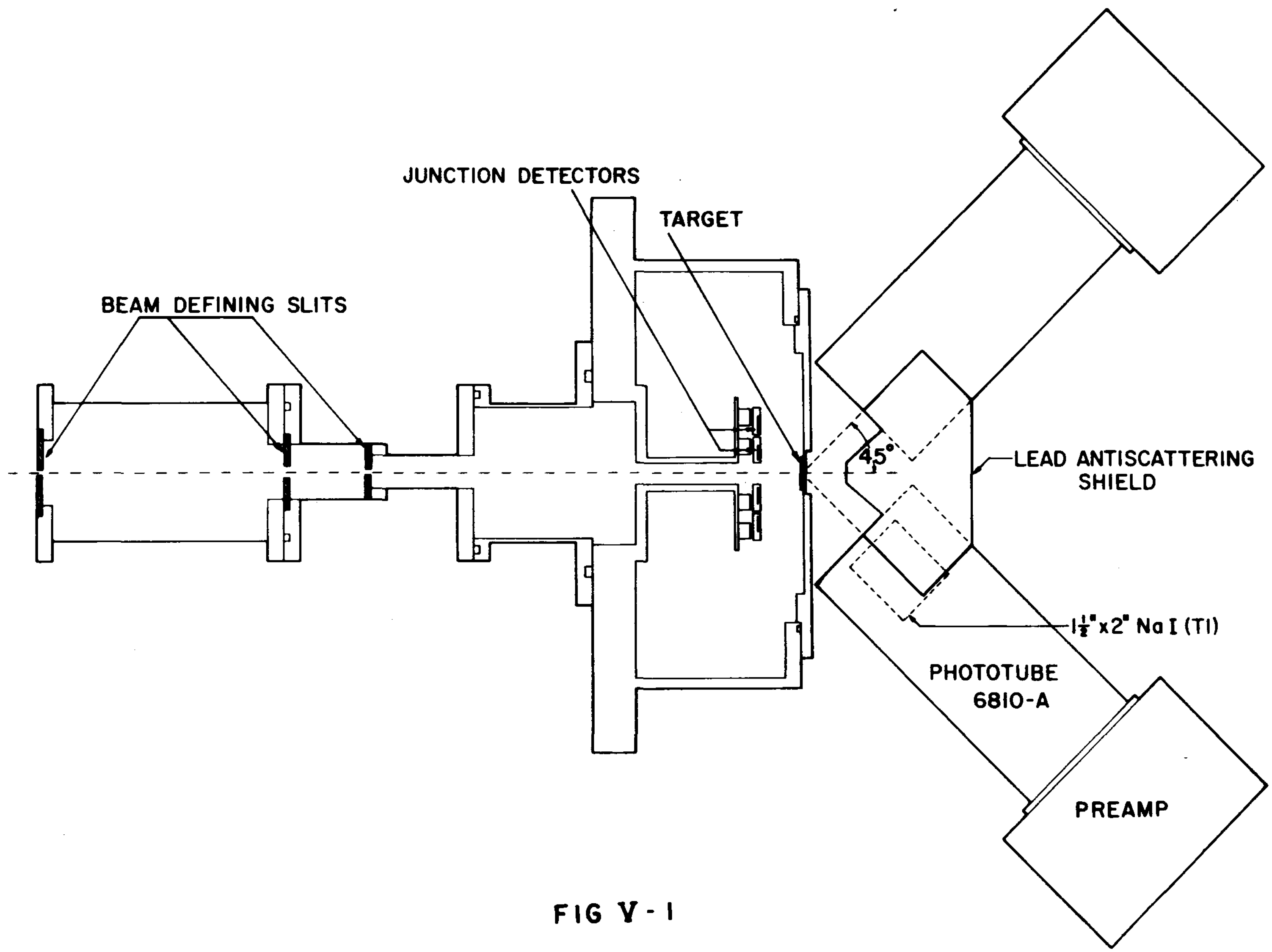
JUNCTION DETECTORS
TARGET
BEAM DEFINING SLITS
45°
LEAD ANTISCATTERING SHIELD
$1\frac{1}{2}$" x 2" Na I (Tl)
PHOTOTUBE 6810-A
PREAMP

FIG V - I

Tb of 1.125 sterad. or 8.95% of a sphere. 60% of the laboratory or 59% of the effective center-of-mass solid angle was associated with the inner ring of detectors.

The gamma-ray detector crystals and lead shielding cans are shown as employed in the gamma-gamma coincidence arrangement, with anti-Compton lead shield between the crystals, in Fig. III.1. Each crystal faces the beam spot on the target at a distance of three inches. In the gamma-heavy ion coincidence experiments the single gamma counter was placed facing directly into the target window, thereby achieving a larger solid angle as viewed from the target.

C. Detectors

The backscattered heavy ion detectors consisted of a mosaic of NPS 10x1Q-5000-25 phosphorus or lithium drifted 5KΩ-cm silicon junction detectors, rated for 25v. bias, with sensitive areas 10x10 mm., supplied by Solid State Radiations, Inc., Culver City, Calif. They were arranged in a circuit configuration suitable for integration into the physical apparatus and the fast-slow coincidence electronics. Miniature low-capacity switches were employed to permit switching out junction detectors in pairs in case of failure of a member of a pair during a run, to avoid drawing excessive bias current through the bias resistor to the pair, thereby decreasing its bias and loading the entire array with the resulting increased capacity, and to avoid injecting into the particle spectrum excessive noise from the offending detector. The detector signals were amplified by a voltage fed back preamplifier with low-noise cascode input stage designed by R. Berringer and constructed at this laboratory, with an added cathode-follower stage to split the signal into suitable "fast" and "slow" components. The gain was set at 10 to minimize voltage excursions from statistical pileup of the fast-rise, very slowly decaying signals. The "slow" signal, with its rise-time lengthened by RC integration to 1/4 μsec., was amplified by a second Berringer preamplifier with gain set at 100 and a 1 μsec. RC clipping at the input. The resulting linear pulse signals for 8.8-MeV alpha rays from a Th B alpha source were 130 mv. high with 20 junction detectors operating in parallel. A typical thick-target backscattered heavy-ion spectrum in singles and in coincidence with all resulting gamma radiation is shown in Fig. V-2. A theoretical thick-target Rutherford scattering calculation confirmed the shape of the singles spectrum; as expected the higher-energy portion of the spectrum, corresponding to scattering events nearer the target surface with the corresponding higher instantaneous projectile energies, was primarily associated with the deexcitation radiation.

Voltage fed back preamplifiers were used because gain stability was not a critical factor at the relatively poor overall array resolution, and because the entire array capacity would have been excessively large for a charge fed back preamplifier to handle properly.

The use of the low bias voltage was dictated by a combination of modest needs and economic considerations. In a period of approximately two years well over 100 detectors were purchased in order to maintain a working 20-detector array. The losses were due partly to various difficulties which caused a junction that worked well by itself not to perform properly within the array, such as loose base contacts causing an effective series resistance to produce a phenomenon of "double peaking" from the reduced effective gain of the offending detector (a signal from any detector for a given energy incident projectile involves collection of the same "deposited" charge across the same entire array capacity, theoretically producing the same sized current pulse,

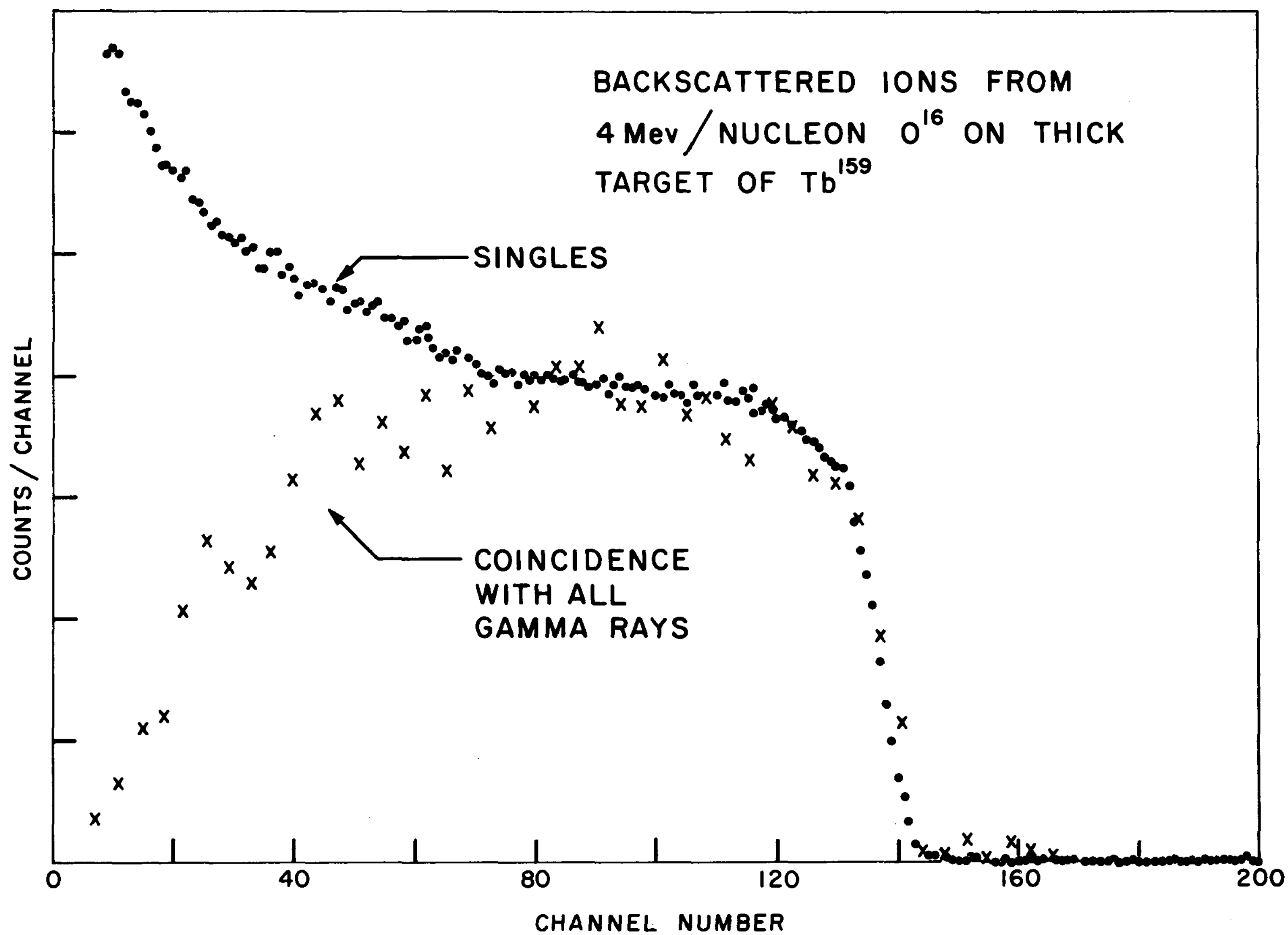
BACKSCATTERED IONS FROM
4 Mev / NUCLEON O16 ON THICK
TARGET OF Tb159
SINGLES
COINCIDENCE
WITH ALL
GAMMA RAYS
COUNTS / CHANNEL
0
40
80
120
160
200
CHANNEL NUMBER

FIG V-2

or voltage pulse across the external series resistor), and partly to deterioration due to radiation damage.

Detectors for gamma rays were 1-3/4" by 2" NaI(Tl) crystals supplied by the Harshaw Chemical Co., mounted on RCA 6810-A 14-stage photomultiplier tubes. Linear and logic pulses were taken from the tenth dynode and the anode respectively. The dynode voltages are those recommended by the manufacturer for low light level, high gain, low noise service. The auxiliary high-voltage setting was determined by adjusting the bucking voltage between the h.v. power supply and the bleeder chain with only the main supply attached to zero prior to connecting the auxiliary supply.

The bleeder chain, consisting of Corning Type C metal oxide film resistors with temperature coefficient ± 250 p.p.m. per deg. C., was temperature-regulated by containing it in transformer oil within a water-cooled brass can. This procedure substantially reduced gain drifts that were observed to occur in correlation with daily temperature cycles. The overall system gain stability was frequently better than 1/2-channel drift in eight hours for a gamma-ray source photopeak, at given counting rate, in the upper half of a 200-channel multichannel analyzer display. In the absence of automatic gain compensation, during long runs every 4 to 8 hours a check and minute adjustment of the gain were performed with a source placed in a fixed geometric relationship to the counter. The magnitude of the drift in tenths of a channel could be rapidly and reliably ascertained by noting how points of the analyzer c.r.t. display on opposite sides of the photopeak were geometrically related. Adjustments of any number of tenths of a channel were easily and quickly executed.

The photomultiplier anode signals were saturated for NaI light pulses from incident gamma rays of $\gtrsim 550$ keV. Thus, over much of the spectrum, timing errors in the "fast" delay-line-clipped signals arising from variable durations prior to "firing" of the 404-A input diode due to different initial slopes of the input pulse leading edge were minimized. However, with the wide dynamic range ($\sim$50 keV to $\sim$1-1/2 MeV) of pulses employed, variations in relative timing for various combinations of large and small anode pulses presented a limitation on the permissible narrowness on the coincidence resolving curves that still gave effectively 100% efficiency for the extreme range of possible situations, large (small) pulses in one leg of the fast circuitry coincident with small (large) pulses in the other leg, as discussed below.

The glass envelopes of the photomultipliers were coated with Aquadag and Al foil, electrically grounded for electrostatic shielding; Mu-metal shields for magnetic shielding, light-tight aluminum cans which clamped the NaI crystal housings to the p.m. tube heads, and finally tin-lined 1/8" thick cylindrical Pb housings. The best resolution typically obtained with these counters was approximately 8-1/2% f.w.h.m. for $Cs\text{-}Ba^{137}$ 661.6-keV gamma radiation. Proper optical coupling(using Dow-Corning high-viscosity silicone oil) and the elimination of electrical noise sources such as "open" solder joints to coaxial cable shields proved to be of particular and persistent concern in this regard.

D. Electronics

A block diagram of the fast-slow coincidence electronics system is displayed in Fig. V.3. The linear signals from the second semiconductor detector preamplifier or the cathode follower output from the 6810-A tenth dynode, each of order 1 v. x 1-1/2 μsec. x 1/4 μsec. rise time, are sent through approximately 200' of RG114/U cable from the cave to the experimenters' area at the other end of the accelerator, where electronics racks, kicksorters, and the accelerator control consoles are located, there to be amplified, delayed, and sent into linear gates whose two outputs are routed to multichannel analyzers or to integral or differential discriminators. Logic signals from the semiconductor array were generated by delay-line clipping the fast-rise output pulses from the first preamplifier with a 30' shorted length of RG62/U cable, amplifying with a series of Hewlett-Packard HP400-AR and BR wide-band distributed amplifiers, with an interposed noise and overload discriminator to avoid overloading the final two amplifiers and to cut out the otherwise troublesome high noise-pulse counting rate, and passing through a 404-A limiter identical to the limiters for the 6810-A anode signals. In the gamma-O^{16} ion coincidence mode a length of RG114/U cable was interposed in the gamma-ray fast side to compensate the signal delay inherent in the Hewlett-Packard amplifiers. The limiter outputs were cabled to the experimenters' room without appreciable deterioration in shape. There, across 180Ω terminations, they were 1/2 v. high

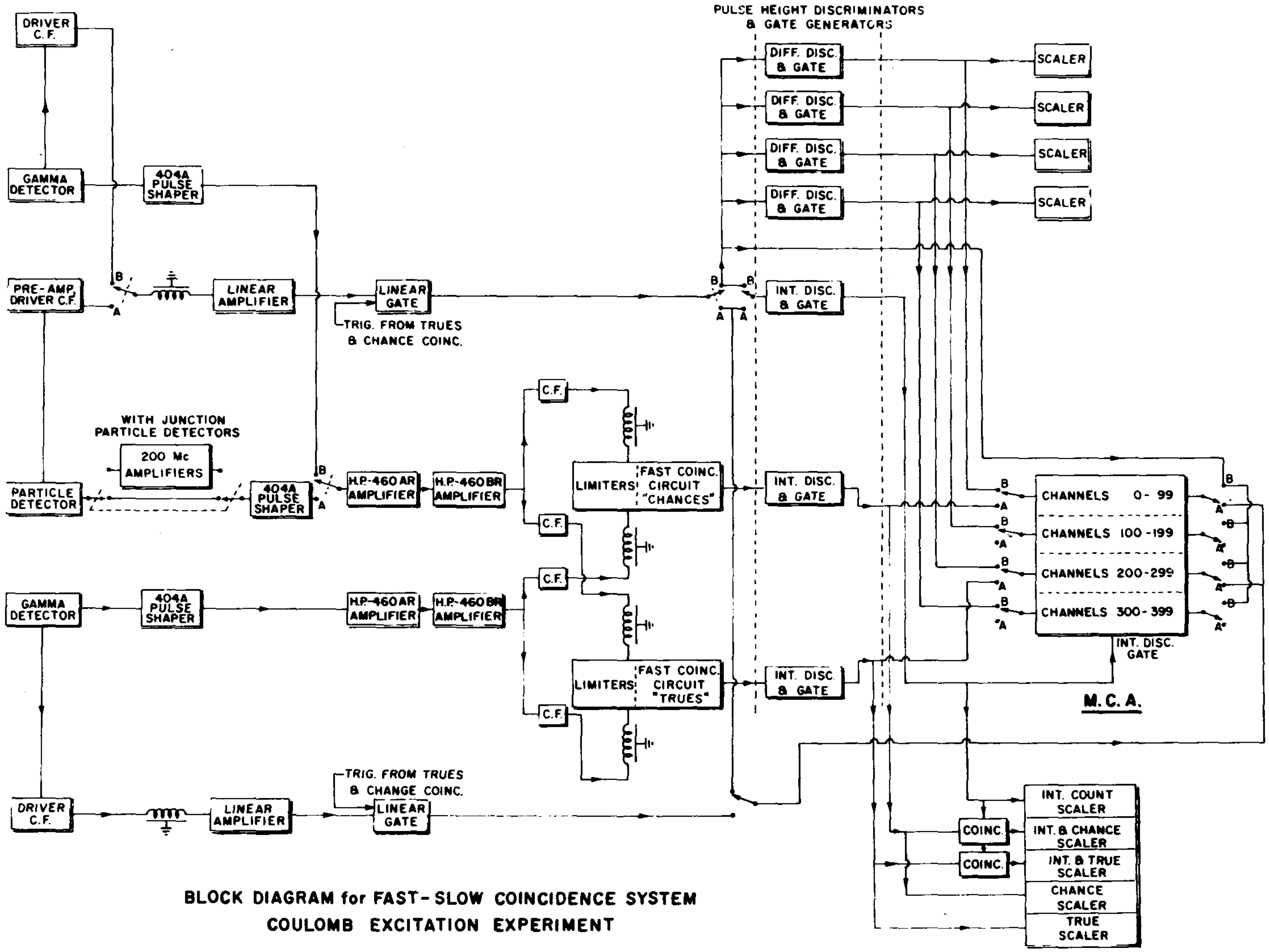

BLOCK DIAGRAM for FAST-SLOW COINCIDENCE SYSTEM
COULOMB EXCITATION EXPERIMENT

FIG V-3

x 10 nsec. f.w.h.m., and of Gaussian form. Subsequent to division into true and accidental legs and further amplification by means of Hewlett-Packard amplifiers they were fed through 7788 pulse-shaper and cathode follower circuits to inputs of "true" and "chance" 6BN6 gated-beam tubes, at which point in order to produce the required coincidence resolving curve widths they had been adjusted to 2 v. x 20 nsec., as illustrated in the diagram. The 6BN6 outputs were 0.02 v. for a pulse on one input grid, 0.6 v. for coincident pulses on both grids, which were amplified to 60 v. for the full-sized coincidence pulses and sent to Schmidt discriminators set to cut off at 20 v., well above the noncoincident pulse sizes, that in turn activated gate and trigger pulse generators which drove multichannel analyzer routing circuits, the high-level linear gates, and scalers.

These high-level gates, which are logically redundant, were nevertheless required to avoid difficulties with the analyzer gating when the analyzer inputs were accepting the instantaneous singles counting rates occurring in this experiment. Tests in a "self-coincidence" mode indicated that the gating efficiency with this arrangement was 100%. In all calibrations the gates were operated in a self-coincidence mode instead of being simply switched out of the circuit, in order to avoid introducing a relative gain change of a fraction of a percent; and singles runs were done also in the "self-coincidence" mode.

Additional gating was available in the analyzers to accept outputs of additional gate generators that could be actuated by differential or integral discriminators set on the gamma or particle spectra, and to accept a beam-pulse-correlated gate. Discriminating out of the lower half of the particle spectrum was done to avoid the possibility of accepting nuclear-reaction protons or alpha particles arising from low-Z contaminants such as oxygen or pump oil, although tests indicated negligible differences between the results with particle discriminated and straight particle spectra for gating. Gamma-gamma coincident spectra (except as obtained with the Victoreen two-dimensional analyzer) were gated by setting differential discriminators on suitable photopeaks in the "gating counter" spectrum. Tests of the integral and differential discrimination indicated 100% efficiency within the discriminator acceptance range, 0% outside the range, with sharp edges.

"True," "accidental" and "particle" integral discriminators, and gamma ray differential discriminators, had their outputs monitored with scalers, singly and in various coincidence combinations obtained by using passive diode coincidence circuits ahead of the appropriate scalers to accept outputs from a pair of the gate generators.

For gamma-gamma coincidence runs coincidence resolving curves to determine the proper relative delay of the two legs were obtained by observing Na^{22} annihilation radiation from a source between the two gamma counters arranged back-to-back. Spectra for fixed time intervals of each counter in "true" coincidence with all the radiation in the other counter were obtained, from which the total number of counts in ten-channel slices centered on the 511-keV photopeaks and Compton events equivalent to other suitable energies were computed and plotted as a function of the artifically inserted relative delay, obtained by using measured lengths of C-22 cable (Trans-Radio Ltd., London, $v/c \approx 0.95$, similar to RG114/U) between the pulse-splitter cathode followers and subsequent Hewlett-Packard amplifiers ahead of the coincidence circuits, for which reciprocal signal speed is approximately 1 nsec. per foot. The counting rate in the low (high) effective energy portion of a spectrum begins to drop off initially because of failure to accept true coincidences between the above pulses and the ones corresponding to the high(low) effective energy portions of the spectrum in the other, "gating" counter. Variations in the 404-A limiter relative "firing" times, dependent on relative pulse sizes of the anode signals from each photomultiplier, and in sign on which counter produced the smaller pulse, cause the shifts in the positions of the coincidence resolving curves, which were adjusted wide enough to include overlap of the flat portions for the complete range of energy combinations of interest, by means of the pulse shapers in front of the 6BN6 circuits, as mentioned above. The width was 35 nsec. "f.w.h.m." For the gamma-particle coincidence runs the timing curve was obtained by counting the number of gates generated by the "true coincidence" discriminator for a fixed number of gate signals from the "particle" discriminator, with the beam hitting the target, immediately prior to the actual run.

E. Targets

Odd-A rare earths mostly occur in nature monoisotopically.[78,7] In earlier runs discs of the metallic element cut from 1" to 1½" diameter ingots (Michigan Chemical Corp., Saint Louis, Michigan) were machined to thickness 10 mils, as thin as practicable without breakage, washed in acetone, thoroughly rinsed in ethanol, then immediately placed under vacuum in the target chamber. In the more recent work the metal, procured in the form of shavings, was vacuum evaporated onto ¼-mil tantalum to a thickness sufficient to stop the beam ($\sim$40 mg/cm^2 Tb$\approx$2 mils), for the purpose of minimizing self-absorption in the target.

The Tb targets were prepared from Tb metal of $\geq$99.9% purity with typically oxygen as the main contaminant, plus traces of Si, Ca, Fe, Cu, Ni, Al, Ta, but no detectable Dy, Y, Gd, or Eu (hence less than 500 p.p.m.), as determined by emission spectrographic analysis. The vacuum evaporation would be expected to increase the Ta content, to $\sim$1%; however, no evidence for the strong Ta lines at 136 and 301 keV was detected in the gamma spectra.

F. Experimental Procedure

A week prior to a run the electronics was turned on and allowed to stabilize during checkout procedures, in which counter resolutions, coincidence timing, pulse shapes and noise levels at most points in the system, particle-detector array response, gating efficiencies, multichannel analyser operation and calibration were all checked with the apparatus set up exactly as during a run. Immediately prior to the run a calibration of the gamma detectors with eight gamma-ray sources was performed, at a counting rate similar to the instantaneous counting rate during the beam bursts. During the data acquisition calibration checks were run every 4 to 12 hours, with the source spectrum being stored at a preset counting rate in the portion of the multichannel analysers containing the "accidentals" spectra, subsequent to printing and clearing the latter. (They had to be added together again later.) Bombardment was on a 24-hour basis, 50 hours of actual beam usually being required for each coincidence spectrum. Because of inefficiencies due to machine failures, apparatus failures and periodic gain checks, this usually entailed an entire week of running. At no time during a run was the full-energy beam permitted to reach the target area, to avoid the possibility of activation background in the target or the consequences of neutron irradiation of the iodine in the NaI crystals. The beam current was kept as constant as feasible by monitoring the beam trace derived from the insulated target, in order to minimize the effect of counting-rate-dependent gain changes.

VI. Treatment of Experimental Data

A. Ground-State Bands: Alder-Winther Calculation

1. Description of the A-W Theory

Time-dependent perturbation theory formulae may be stated as follows:

$$\begin{aligned} &H(\vec{r},t) = H_0(\vec{r}) + H'(\vec{r},t) \\ &H_0(\vec{r})u_n(\vec{r}) = E_n u_n(\vec{r}) \\ &H(\vec{r},t)\Psi(\vec{r},t) = i\hbar \frac{\partial \Psi(\vec{r},t)}{\partial t} . \end{aligned} \qquad \text{(VI-1)}$$

Substituting in the trial solution,

$$\Psi(\vec{r},t) = \sum_n a_n(t) u_n(\vec{r}) e^{-i\omega_n t}, \quad \omega_n \hbar = E_n , \qquad \text{(VI-2)}$$

results in

$$\frac{da_\ell(t)}{dt} = \frac{1}{i\hbar} \sum_n \langle u_\ell | H' | u_n \rangle a_n e^{i\omega_{\ell n} t}, \quad \omega_{\ell n} \equiv \omega_\ell - \omega_n . \qquad \text{(VI-3)}$$

Replacement of H' by λH' and expansion of a_n in powers of λ:

$$a_n(t) = \sum_{\nu=0}^{\infty} a_n^{(\nu)}(t) \lambda^\nu \qquad \text{(VI-4)}$$

results, on equating coefficients of powers of λ to zero, in the relations,

$$\begin{aligned} &\frac{da_\ell^{(0)}}{dt} = 0 \\ &\frac{da_\ell^{(\nu+1)}}{dt} = \frac{1}{i\hbar} \sum_n \langle u_\ell | H' | u_n \rangle a_n^{(\nu)} e^{i\omega_{\ell n} t}, \quad \nu = 0,1,2,\ldots, \end{aligned} \qquad \text{(VI-5)}$$

with the formal solution,

$a_\ell^{(0)} = \text{const.}$ (the initial conditions);

$$a_\ell^{(\nu+1)}(t) = \frac{1}{i\hbar}\sum_n \int_{-\infty}^{t} \langle u_\ell(\vec{\pi})| H'(\vec{\pi},t')|u_n(\vec{\pi})\rangle a_n^{(\nu)}(t') e^{i\omega_{\ell n}t'} dt'. \qquad \text{(VI-6)}$$

Upon setting $a_n^{(0)} = \delta_{nN}$ one obtains the familiar "first-order result",

$$a_\ell^{(1)}(t) = \frac{1}{i\hbar}\int_{-\infty}^{t} \langle u_\ell | H'(\vec{\pi},t')|u_N\rangle e^{i\omega_{\ell N}t'} dt' \qquad \text{(VI-7)}$$

which is essentially equation II A-6 in Alder et al.[1],

$$a_\ell^{(1)}(\infty) \equiv b_{if} = \frac{1}{i\hbar}\int_{-\infty}^{\infty} \langle f | \mathcal{H}(t)| i\rangle e^{i\omega t} dt. \qquad \text{(VI-7a)}$$

The general formal iteration solution is

$$a_\ell^{(\nu+1)}(t) = \left(\frac{1}{i\hbar}\right)^{\nu+1} \sum_{n_0}\cdots\sum_{n_\nu} \int_{-\infty}^{t}\int_{-\infty}^{t'}\cdots\int_{-\infty}^{t^{(\nu)}} \langle u_\ell | H'(\vec{\pi},t)|u_{n_0}\rangle\langle u_{n_0}|H'(\vec{\pi},t'')|u_{n_1}\rangle \cdots \qquad \text{(VI-8)}$$
$$\langle u_{n_{\nu-1}}|H'(\vec{\pi},t^{(\nu+1)})|u_{n_\nu}\rangle a_{n_\nu}^{(0)} e^{i[\omega_{\ell n_0}t' + \omega_{n_0 n_1}t'' + \cdots + \omega_{n_{\nu-1}n_\nu}t^{(\nu+1)}]} dt^{(\nu+1)} \cdots dt'' dt'.$$

The crux of the Alder-Winther procedure consists of avoiding the restriction to any finite order of perturbations by employing an approximate form for $H'(\vec{\pi},t)$ which allows this expression to be evaluated in a tractable form; essentially a "sudden approximation", in which the time-dependent Hamiltonian can be accurately represented by zero for all time except a (brief) interval, when it is constant in time (but not space, in general). It was convenient to work in the interaction representation:

$$\Psi(\vec{\pi},t) = e^{-\frac{i}{\hbar}H_0(\vec{\pi})t}\Phi(\vec{\pi},t) \qquad \text{(VI-9)}$$
$$\overline{H'}(\vec{\pi},t) = e^{\frac{i}{\hbar}H_0(\vec{\pi})t} H'(\vec{\pi},t) e^{-\frac{i}{\hbar}H_0(\vec{\pi})t}$$

The problem then assumes the form:

$$i\hbar \frac{\partial \Phi(\vec{r},t)}{\partial t} = \overline{H}'(\vec{r},t)\,\Phi(\vec{r},t). \qquad \text{(VI-10)}$$

The formal solution is

$$\Phi(\vec{r},t) = \Phi(\vec{r},t_0) + \frac{1}{i\hbar}\int_{t_0}^{t} \overline{H}'(\vec{r},t)\Phi(\vec{r},t')\,dt' \;; \qquad \text{(VI-11)}$$

and an iteration solution of this integral equation is

$$\Phi(\vec{r},t) = \Phi(\vec{r},t_0)\Big[1 + \frac{1}{i\hbar}\int_{t_0}^{t} \overline{H}'(r,t')\,dt' + \dots + \Big(\frac{1}{i\hbar}\Big)^{\nu}\int_{t_0}^{t}\int_{t_0}^{t'}\dots\int_{t_0}^{t^{(\nu-1)}} \overline{H}(\vec{r},t')\dots \qquad \text{(VI-12)}$$
$$\overline{H}'(\vec{r},t^{(\nu)})\,dt^{(\nu)}\dots dt' \equiv T e^{\frac{1}{i\hbar}\int_{t_0}^{t}\overline{H}'(\vec{r},t')\,dt'}\,\Phi(\vec{r},t_0)\,.$$

$\Phi(\vec{r},t_0)$ specifies the initial conditions at time t_0. For a scattering problem one lets $t_0 \to -\infty$, $t \to +\infty$. Expanding,

$$\Psi = e^{-\frac{i}{\hbar}H_0 t}\Phi = e^{-\frac{i}{\hbar}H_0 t}\sum_n a_n(t) u_n(\vec{r}) = \sum_n a_n e^{-\frac{i}{\hbar}H_0 t} u_n$$
$$= \sum_n a_n e^{-\frac{i}{\hbar}E_n^0} u_n = \sum_n a_n u_n e^{-i\omega_n t} \;; \quad \text{or} \qquad \text{(VI-13)}$$
$$\Phi(\vec{r},t) = \sum_n a_n(t) u_n(\vec{r})\,,$$

the time-dependent expansion coefficients are the same and one finds the same equations governing them as before; but also noting that $\Phi(\vec{r},t_0) = \sum_n u_n(\vec{r}) a_n(t_0) \equiv \sum_n a_n^{(0)} u_n(\vec{r})$, one finds with the help of (VI-12),

$$a_\ell(t) = \langle u_\ell | \Phi(\vec{r},t)\rangle = \langle u_\ell | T e^{\frac{1}{i\hbar}\int_{t_0}^{t}\overline{H}'(\vec{r},t')\,dt'} | \Phi(\vec{r},t_0)\rangle$$
$$= \langle u_\ell | T e^{\frac{1}{i\hbar}\int_{t_0}^{t}\overline{H}'(\vec{r},t)\,dt'} \sum_n | u_n\rangle \langle u_n | \Phi(\vec{r},t_0)\rangle \qquad \text{(VI-14)}$$
$$= \sum_n \langle u_\ell | T e^{\frac{1}{i\hbar}\int_{t_0}^{t}\overline{H}'(\vec{r},t')\,dt'} | u_n\rangle\, a_n^{(0)},$$

which reduces, for the special initial conditions $a_\ell^{(0)} = \delta_{\ell n}$, to A.W. equation 3.10. This equation forms the basis for the Alder-Winther multiple excitation calculation. A.W. note that if $\left|\frac{1}{i\hbar}\int_{-\infty}^{\infty}\bar{H}'(t')\,dt'\right| << 1$, as is the case for an interaction turned on for a brief enough period in relation to its overall strength in comparison to zero-order energy terms, that is, brief compared to the "periods" of the unperturbed system motions, then $T e^{\frac{1}{i\hbar}\int_{t_0}^{t}\bar{H}'(\vec{\pi},t')dt'} \approx e^{\frac{1}{i\hbar}\int_{t_0}^{t}\bar{H}'(\vec{\pi},t')dt'}$. An indication of how this comes about is had by considering the situation where $H'(\vec{\pi},t) = \mathcal{H}'(\vec{\pi})$ if $0 \le t \le \tau$, taking $-\infty \le t_0 \le \tau \le$ observation time $=$ upper limit in time integral $\le +\infty$; and 0 otherwise, with the proviso that also $\bar{\mathcal{H}}'(\vec{\pi},t) = e^{\frac{i}{\hbar}H_0(\vec{\pi})t}\,\mathcal{H}(\vec{\pi})\,e^{-\frac{i}{\hbar}H_0(\vec{\pi})t}$ be actually time-independent. Then $T e^{\frac{1}{i\hbar}\int_{t_0}^{t}\bar{H}'(\vec{\pi},t')\,dt'}$ becomes

$$
\begin{aligned}
T e^{\frac{1}{i\hbar}\int_0^\tau \bar{\mathcal{H}}' dt'} &= 1 + \frac{1}{i\hbar}\int_0^\tau \mathcal{H}' dt' + \left(\frac{1}{i\hbar}\right)^2 \int_0^\tau \mathcal{H}' \int_0^{t'} \mathcal{H}' dt''\,dt' + \ldots \\
&= 1 + \frac{\mathcal{H}'\tau}{i\hbar} + \left(\frac{\mathcal{H}'}{i\hbar}\right)^2 \int_0^\tau \int_0^{t'} dt''\,dt' + \ldots = 1 + \frac{\mathcal{H}'\tau}{i\hbar} + \frac{1}{2!}\left(\frac{\mathcal{H}'\tau}{i\hbar}\right)^2 + \ldots \qquad \text{(VI-15)} \\
&= e^{\frac{\mathcal{H}'\tau}{i\hbar}} .
\end{aligned}
$$

This holds for the kind of square-wave interaction described, no matter what the duration; however for the result of the actual time-dependent interaction to be approximated well by that of this square-wave perturbation, the actual perturbing influence must occur within a span of time during which the target system configuration is essentially static, that is, very suddenly in terms of the nuclear dynamics. When this is the case,

$$
a_\ell(+\infty) \approx \sum_n \langle u_\ell | e^{\frac{1}{i\hbar}\int_{-\infty}^{\infty}\bar{\mathcal{H}}'(\vec{\pi},t')\,dt'} | u_n \rangle\, a_n(-\infty). \qquad \text{(A.W. 3.11)}
$$

That ξ is a measure of the suddenness of an interaction may be seen as follows[1,3]:

$$\xi \equiv \eta_i - \eta_f = \eta_i \left[\frac{1}{\sqrt{1-\frac{\Delta E'}{T_i}}} - 1 \right] \approx \frac{1}{2} \eta_i \frac{M_1+M_2}{M_2} \frac{\Delta E}{T_i} \quad . \qquad \text{(VI-16)}$$

Here $\Delta E \equiv M_2 \Delta E'/(M_1+M_2)$ is the target level energy in a scattering experiment, $T_i = (1/2)M_i v_i{}^2$ is the initial projectile kinetic energy, and $\eta_i \equiv Z_1 Z_2 e^2/(\hbar v_i)$. Taking for a measure of the "collision time" half the closest approach distance in a head-on collision divided by the initial velocity:

$$\tau = \frac{a}{v_i} \quad , \qquad \text{(VI-17)}$$

and for the "frequency" associated with the target-system motion in the excited state:

$$\omega = \frac{\Delta E}{\hbar} \quad , \qquad \text{(VI-18)}$$

one finds

$$\xi = \frac{Z_1 Z_2 e^2 (M_1+M_2)\Delta E}{M_1 M_2 \hbar v_i^3} = \frac{Z_1 Z_2 e^2 \omega}{\mu v_i^3} = \frac{a\omega}{v_i} = \tau\omega \, . \qquad \text{(VI-19)}$$

Hence "sudden" collision phenomena require $\xi \ll 1$.

For E2 excitation, A.W. use the interaction (A.W. equation 2.3; Alder et al.[1], equation II a.10,11)

$$H_E'(t) = 4\pi Z_1 e \sum_{\lambda=1}^{\infty} \sum_{\mu=-\lambda}^{\lambda} \frac{\overline{S_{\lambda\mu}(t)}}{2\lambda+1} \mathcal{M}^*(E\lambda,\mu),$$

which is the multipole expansion of $\rho(\vec{r})\left[\frac{1}{|\vec{r}-\vec{r}_p(t)|} - \frac{1}{r_p(t)}\right]$, with moments $\mathcal{M}(E\lambda,\mu) = \int \rho(\vec{r}) r^\lambda Y_\lambda^\mu(\theta\phi)\, d\vec{r}$. $\overline{S}_{\lambda\mu}(t)$ are certain path integrals. They write

$$\frac{1}{\hbar}\int_{-\infty}^{\infty} H'_{E2}(t)\,dt \equiv -\frac{4\pi Z_1 e}{5\hbar v_i a}\sum_{\mu} Y_2^{\mu}\left(\frac{\pi}{2},0\right) J_{2\mu}(\theta)\,\mathcal{M}^*(E2,\mu)$$

$$\equiv -\sqrt{9\pi}\sum_{\mu} Y_2^{\mu}\left(\frac{\pi}{2},0\right) J_{2\mu}(\theta)\mathcal{M}^*(E2,\mu)\frac{\sqrt{2I_0+1}\;\chi_{0\to 1}}{\langle I_0\|\mathcal{M}(E2)\|I_1\rangle} \qquad \text{(A.W. 3.33,3.35)}$$

where $J_{2\mu}(\theta)$ are tabulated functions of the c.m. scattering angle θ, and for most θ, especially for backward directions, $|J_{2,\pm 2}(\theta)| \ll |J_{20}(\theta)|$. This is further rewritten:

$$\frac{1}{\hbar}\int_{-\infty}^{\infty} H'_{E2}(t)\,dt = -\sqrt{9\pi}\,Y_2^{0}\left(\frac{\pi}{2},0\right) J_{20}(\pi)\mathcal{M}^*(E2,0)\frac{\sqrt{2I_0+1}\;\chi_{\text{eff}}(\theta)}{\langle I_0\|\mathcal{M}(E2)\|I_1\rangle}\,, \qquad \text{(A.W. 3.3b)}$$

where

$$\chi_{\text{eff}}(\theta) = \frac{\sum_{\mu} Y_2^{\mu}\left(\frac{\pi}{2},0\right) J_{2\mu}(\theta)\mathcal{M}^*(E2,\mu)}{Y_2^{0}\left(\frac{\pi}{2},0\right) J_{20}(\pi)\mathcal{M}^*(E2,0)}\,\chi_{0\to 1}\,. \qquad \text{(VI-20)}$$

The so-called "$\chi_{\text{eff}}(\theta)$ approximation" consists in taking

$$\chi_{\text{eff}}(\theta) \approx \frac{J_{20}(\theta)}{J_{20}(\pi)}\chi_{0\to 1} = \frac{3}{4}J_{20}(\theta)\chi_{0\to 1}\,. \qquad \text{(A.W. 3.37)}$$

These expressions are substituted into the expression

$$|\phi_m(\vec{r},t)\rangle \approx \sum_n e^{-\frac{i}{\hbar}\int_{t_0}^{t} H'_{E2}(\vec{r},t')\,dt'}|u_n(\vec{r})\rangle\langle u_n(\vec{r})|\phi_m(\vec{r},t_0)\rangle \qquad \text{(VI-21)}$$

appropriate for the sudden approximation, to obtain,

$$|\phi_m(\vec{r},+\infty)\rangle \approx \sum_n e^{-\frac{i}{\hbar}\int_{-\infty}^{\infty} H'_{E2}(\vec{r},t')\,dt'}|u_n\rangle\, a_{mn}(-\infty) \qquad \text{(VI-22)}$$

in terms of the initial amplitudes $a_{mn}(-\infty)$ which are taken to be $a_{mn}(-\infty) = \delta_{mN}$. The amplitudes of the initial unperturbed eigenstates $u_n(\vec{r})$ in $\phi_m(\vec{r},+\infty)$ (or $u_n(\vec{r})e^{-i\omega_n t_0}$ in $\Psi_n(\vec{r},t_0 \to \infty)$), $a_{mn}(+\infty)$, are the required "multiple-excitation" populations, which have been obtained in the sudden and the $\chi_{\text{eff}}(\theta)$ approximations where a few universally applicable formulae and tables suffice to cover the experimental ranges of energies and angles. For instance, in an obvious notation,

$$|\phi_m,+\infty\rangle_{\theta,\chi} = e^{i\chi_{\rm eff}(\theta)}\sqrt{\frac{15}{2}}\,\frac{J_{22}(\theta)}{J_{20}(\theta)}\,\frac{\sqrt{2I_0+1}}{\langle I_0\|\mathcal{M}(E2)\|I_1\rangle}\left[\mathcal{M}^*(E2,2)+\mathcal{M}^*(E2,-2)\right]|\phi_m,+\infty\rangle_{\pi,\chi_{\rm eff}(\theta)}$$

(A.W. 3.38-40)

$$\equiv e^{iA}|\phi_m,+\infty\rangle_{\pi,\chi_{\rm eff}(\theta)} \approx |\phi_m,+\infty\rangle_{\pi,\chi_{\rm eff}(\theta)}\ ,$$

since it can be shown that $|A| << 1$. This gives approximate final eigenvectors for any angle θ in terms of those for $\theta = 180^\circ$, by the simple substitution of $\chi_{\rm eff}(\theta)$ for χ, obtained from a short $\chi_{\rm eff}(\theta)/\chi$ tabulation, obviating the necessity for tables for every angle θ. The approximation is best at backward angles.

The level populations are obtained from the amplitudes $a_{mn}(+\infty)_{I_iM_i\to I_fM_f}$ via the relations

$$d\sigma = P_{I_fI_i}\,d\sigma_R\ ;$$

$$P_{I_fI_i} = \frac{1}{2I_i+1}\sum_{M_i}\sum_{M_f}\left|a_{mn}(+\infty)_{I_iM_i\to I_fM_f}\right|^2 . \qquad \text{(VI-23)}$$

For many cases $\frac{1}{\hbar}\int_{-\infty}^{\infty} H'_{E2}(\vec{\pi},t')\,dt'$ has to be diagonalized with respect to $u_n(\vec{\pi})$, the unperturbed target-system eigenstates. For angular-momentum eigenstates this becomes

$$\langle I_fM_f|\frac{1}{\hbar}\int_{-\infty}^{\infty} H'_{E2}(\vec{\pi},t')\,dt'|I_iM_i\rangle \approx \chi_{\rm eff}(\theta)(-1)^{I_f-I_i}\sqrt{5(2I_0+1)}\begin{pmatrix} I_f & 2 & I_i \\ -M_f & 0 & M_i\end{pmatrix}\frac{\langle I_f\|\mathcal{M}(E2)\|I_i\rangle}{\langle I_0\|\mathcal{M}(E2)\|I_1\rangle}\delta_{M_fM_i}, \qquad \text{(A.W. 4.6,7)}$$

where I_0, I_1 refer to a particular fiducial pair of states within the set of initial (i) and the set of final (f) states over which diagonalization is to be done. The advantage of this method is that the ξ- corrections can be incorporated into the procedure.

For pure rotational bands,

$$\langle I_m \| \mathcal{M}(E2) \| I_n \rangle = \sqrt{\frac{5}{16\pi}} (-1)^{I_m - K} \sqrt{(2I_m+1)(2I_n+1)} \begin{pmatrix} I_m & 2 & I_n \\ -K & 0 & K \end{pmatrix} e Q_0 \qquad \text{(A.W. 4.10)}$$

and

$$\langle I_0 \| \mathcal{M}(E2) \| I_1 \rangle \equiv \langle I_0 = K \| \mathcal{M}(E2) \| I_1 = I_0 = K \rangle = \sqrt{\frac{5}{16\pi}} \, e Q_0 \; .$$

It turns out that for this case, in the sudden approximation, closed expressions can be obtained for populations in bands including infinitely many states, bypassing the diagonalization which for practical reasons can handle only a relatively small number of the states. The (collective part of) the multipole moments become

$$\mathcal{M}(E2,\mu) = \frac{1}{2} e Q_0 Y_2^{\mu}(\Theta,\Phi) \, , \qquad \text{(A.W. 5.4)}$$

and within a rotational band, $K_f = K_i = K$,

$$\begin{aligned} a_{I_f M_f}(+\infty) &= \langle f | e^{i \frac{4}{5} \frac{\pi Z_1 e}{\hbar v_i a^2} \sum_{\mu} Y_2^{\mu}(\frac{\pi}{2},0) J_{2\mu}(\theta) \mathcal{M}^*(E2,\mu)} | i \rangle \\ &= \langle I_f M_f K \Omega | e^{i \frac{8\pi}{5} q \sum_{\mu} Y_2^{\mu}(\frac{\pi}{2},0) J_{2\mu}(\theta) Y_2^{\mu *}(\Theta,\Phi)} | I_i M_i K \Omega \rangle , \end{aligned} \qquad \text{(A.W. 5.7-9)}$$

where the parameter q has been introduced:

$$q \equiv \frac{Z_1 e^2 Q_0}{4\hbar v_i a^2} \quad . \qquad \text{(A.W. 5.11)}$$

(This is $\sqrt{45/16}\,\chi_{0\to 1}$, with $\chi_{0\to 1}$ associated with a rotational $0+ \to 2+$ transition in an even-even nucleus of the same Q_0.) This leads to the excitation amplitudes from a state of I_i, M_i to states of I_f, M_f,

$$a_{I_f M_f}(+\infty) = \sum_{I}{}' \sqrt{(2I_i+1)(2I_f+1)}\,(2I+1)(-1)^{M_i - K} \begin{pmatrix} I_f & I_i & I \\ -M_f & M_i & M_f - M_i \end{pmatrix} \begin{pmatrix} I_f & I_i & I \\ -K & K & 0 \end{pmatrix} A_{I, M_f - M_i}(\theta, q) ; \qquad \text{(A.W. 5.8)}$$

$$A_{IM}(\theta,q_r)=\frac{1}{\sqrt{4\pi(2I+1)}}\int_0^{2\pi}\int_0^{\pi}Y_I^M(\Theta,\Phi)e^{i\frac{8\pi}{5}q_r\sum_\mu Y_2^\mu(\frac{\pi}{2},0)J_{2\mu}(\theta)Y_2^{\mu*}(\Theta,\Phi)}\sin\Theta d\Theta d\Phi, \qquad \text{(A.W. 5.9)}$$

and total excitation probabilities,

$$P_{I_fI_i}=\frac{1}{2I_i+1}\sum_{M_i}\sum_{M_f}|a_{I_fM_f}|^2=(2I_f+1)\sum_I{}'\sum_M(2I+1)\begin{pmatrix}I_f & I_i & I\\ -K & K & 0\end{pmatrix}|A_{IM}(\theta,q_r)|^2. \qquad \text{(A.W. 3.42,5.9)}$$

The primes on the summations signify that only even-I terms contribute, as can be shown directly from A.W. equation 5.9. Θ, Φ are the Euler angles in the rotational model. This expression was used in the population calculations below, with the aid of tables of $A_{IM}(\theta,q)$, calculated in the $\chi_{eff}(\theta)$, here the "$q_{eff}(\theta)$" approximation for which $A_{IM}=0$ unless $M=0$:

$$A_{I0}(\theta,q_r)\approx A_{I0}[\pi,q_{r\,eff}(\theta)]=e^{\frac{3}{2}iq_{r\,eff}(\theta)}\int_0^1 P_I(x)e^{-2iq_{r\,eff}(\theta)x^2}dx; \qquad \text{(A.W. 5.14)}$$

$$q_{r\,eff}(\theta)=\frac{3}{4}J_{20}(\theta)q_r. \qquad \text{(A.W. 5.15)}$$

$q_{eff}(\theta)/q$, and $q(\theta)/q=\frac{3}{4}\sqrt{[J_{20}(\theta)]^2+3[J_{22}(\theta)]^2}$ which gives a better forward-angle approximation, are tabulated by A.W.

2. Ground-State Band Population Calculations

Values of q/Q_0 as a function of effective incident projectile kinetic energy were calculated from A.W. equation 5.57:

$$q_r/Q_0=7.6241\frac{\sqrt{M_1E_i^3}}{\left(1+\frac{M_1}{M_2}\right)^2Z_1Z_2^2}. \qquad \text{(A.W. 5.57)}$$

For Tb, $(1+M_1/M_2)^2=(1+16/159)^2=1.2114$; Ho, $(1+16/165)^2=1.2033$; Lu, $(1+16/175)^2=1.1912$. Representative values are listed below:

E_i, $\frac{MeV}{amu}$	$\frac{q}{Q_o}$, Tb^{159}	Ho^{165}	Lu^{175}
2	.13483	.12775	.11492
3	.24769	.23468	.21111
4.08	.39285	.37221	.33482

The nonrelativistic relation between laboratory and center-of-mass scattering angles for elastic scattering of a point projectile of mass M_1 from a stationary point target of mass M_2 is independent of incident kinetic energy:

$$\sin(\theta_{CM}-\theta_L) = \frac{M_1}{M_2}\sin\theta_L \quad . \tag{VI-24}$$

In Coulomb excitation the projectile kinetic energy is so much larger than the target excitation energy that the projectile deflection is practically that of elastic scattering. The ratio of the solid angles is

$$\frac{d\Omega_{CM}}{d\Omega_L} = \frac{\sin\theta_{CM}\,d\theta_{CM}}{\sin\theta_L\,d\theta_L} = \sqrt{1-\left(\frac{M_1}{M_2}\right)^2\sin^2\theta_L} + 2\frac{M_1}{M_2}\cos\theta_L + \frac{\left(\frac{M_1}{M_2}\right)^2\cos^2\theta_L}{\sqrt{1-\left(\frac{M_1}{M_2}\right)^2\sin^2\theta_L}} \quad . \tag{VI-25}$$

For a one-inch junction counter active surface-to-target distance and the array geometry in Fig. VI-1, various pertinent quantities have been computed and listed in Table VI-1. The Rutherford cross section is given by

$$\frac{d\sigma_R}{d\Omega_{CM}} = \frac{1}{4}a^2\sin^{-4}\frac{\theta_{CM}}{2} \quad , \tag{VI-26}$$

where a, half the distance of closest approach (center-to-center) in a head-on collision, is

$$a = \frac{Z_1Z_2e^2}{\mu v_i^2} = \frac{Z_1Z_2e^2}{2T_i} = \frac{Z_1Z_2e^2}{2\frac{M_2}{M_1+M_2}T_{iL}} = \frac{Z_1Z_2}{2}\left(1+\frac{M_1}{M_2}\right)\frac{r_o}{T_{iL}/m_oc^2} \quad . \tag{VI-27}$$

Fig VI-1 Junction-Array Geometry

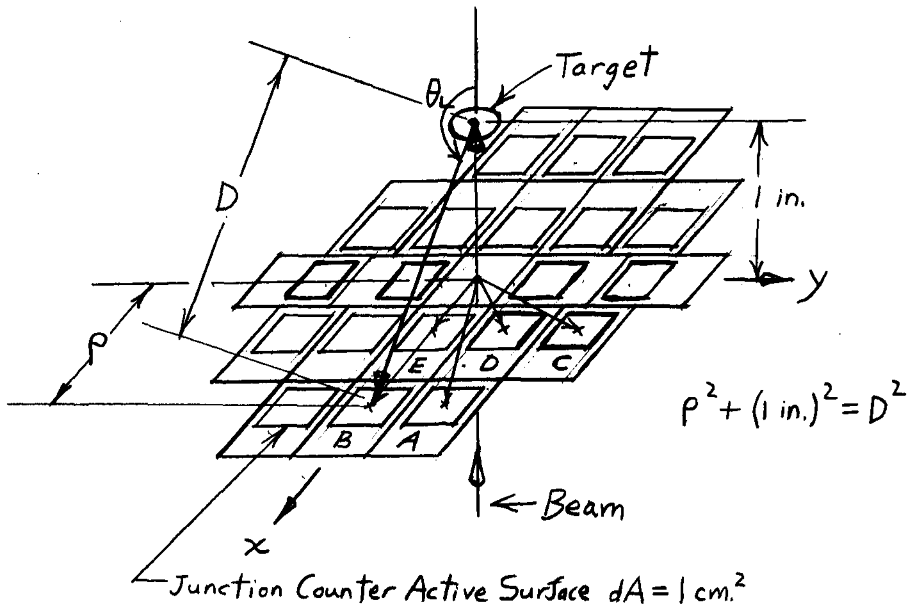

Position type (Four counters occupy each type of position.)	x, in.	y. in.	ρ, cm.	D, cm.
A	1.13	0.5	3.13862	4.03764
B	1.13	0	2.87020	3.83271
C	0.50	1	2.83981	3.81000
D	0.50	0.5	1.79605	3.11085
E	0.50	0	1.27000	2.83981

For one junction in a position,

Position	$d\Omega_L$, sterad.	θ_L, deg.
A	3.8588×10^{-2}	128° 59.'06
B	4.5115	131 30. 32
C	4.5926	131 40. 53
D	8.4371	144 44. 08
E	11.091	153 25. 93

For O^{16} on rare earths,

Tb: $16/159 = 0.10063$

Ho: $16/165 = 0.09697$

Lu: $16/175 = 0.09143$

8 inner junctions: $d\Omega_L$ = 6.2% of sphere
12 outer junctions: $d\Omega_L$ = 4.1% of sphere
20 junctions: $d\Omega_L$ = 10.3% of sphere

Table VI-1

Pos.	$\theta_{CM}-\theta_L$, Tb	Ho	Lu	$\frac{d\Omega_{CM}}{d\Omega_L}$, Tb	Ho	Lu	$\frac{q(\theta_{CM})}{q}$, Tb	Ho	Lu
A	$4^{o}29.4'$	$4^{o}19.4'$	$4^{o}\ 4.5'$	.8743	.8789	.8858	.8588	.8579	.8564
B	4 19.4	4 9.3	3 55.4	.8682	.8730	.8802	.8721	.8712	.8699
C	4 18.1	4 8.7	3 54.5	.8675	.8723	.8795	.8737	.8728	.8715
D	3 19.8	3 12.6	3 1.6	.8407	.8464	.8549	.9317	.9312	.9305
E	2 34.8	2 29.1	2 20.6	.8271	.8331	.8423	.9610	.9608	.9603

T_{iL}, MeV/amu	0	.5	1	1.5	2	2.5	3	3.5	4	4.5	5
$\overline{q}/Q_o$, Tb	0	.01536	.04345	.07983	.1229	.1718	.2258	.2845	.3476	.4148	.4858
Ho	0	.1454	.04114	.07558	.1164	.1626	.2138	.2694	.3291	.3928	.4600
Lu	0	.01307	.03697	.06792	.1046	.1462	.1921	.2421	.2958	.3530	.4134
$\overline{q}$ Tb, Q_o=8.1	0	.1244	.3520	.6466	.9955	1.391	1.829	2.305	2.816	3.360	3.935
Ho, Q_o=7.5	0	.1091	.3086	.5669	.8728	1.220	1.603	2.020	2.469	2.946	3.450
Ho, Q_o=8.0	0	.1163	.3291	.6047	.9310	1.301	1.710	2.155	2.633	3.142	3.680
Lu, Q_o=8.0	0	.1046	.2949	.5434	.8366	1.169	1.537	1.937	2.366	2.824	3.307

Here μ is the reduced mass; v_1, T_1 the initial relative speed and "relative kinetic energy" $(1/2)\mu v_1{}^2$; T_{1L} is the initial laboratory kinetic energy; and the classical electron radius and electron mass-energy equivalent are[218]:

$$r_0 = \frac{e^2}{m_0 c^2} = (2.81785 \pm 0.00004)\ \text{f.}\ ;$$

$$m_0 c^2 = (510.976 \pm 0.007)\ \text{keV}; \qquad \text{(VI-28)}$$

$$1\ \text{amu} = (931.141 \pm 0.010)\ \text{MeV} \quad (O^{16}\ \text{scale}).$$

From these values there follows the equation in **A.W.**:

$$a = 0.07199\left(1 + \frac{M_1}{M_2}\right)\frac{Z_1 Z_2}{T_{i,\text{MeV}}} \times 10^{-12}\ \text{cm.} \equiv \frac{a'}{T_{iL,\text{MeV}}}\ \text{f.}\ , \qquad \text{(A.W. 5.52)}$$

where a' is a "reduced Rutherford constant" for the problem which has the values:

O^{16} on Tb^{159}:	a' = 412.02	f.-MeV
Ho^{165}:	a' = 432.30	f.-MeV
Lu^{175}:	a' = 446.30	f.-MeV .

Using the c.m. = relative orbit scattering angle as argument, **A.W.** gives the formulae and numerical tables for $q_{eff}(\theta)/q$ (and $q(\theta)/q$) as functions of θ. Third-order-interpolated values for the five junction positions are listed in Table VI-1 and plotted in Fig. VI-2. For the range of angles of interest, roughly θ_L from 129° to 153° or θ_{CM} from 133° to 156° (to junction counter active surface centers), from **A.W.** Table 2, $(J_{22}(\theta)/J_{20}(\theta))^2 < 0.000477$. Hence, from **A.W.** Table 6, corrections to the $q(\theta)$ approximation for even I, Δ_I,

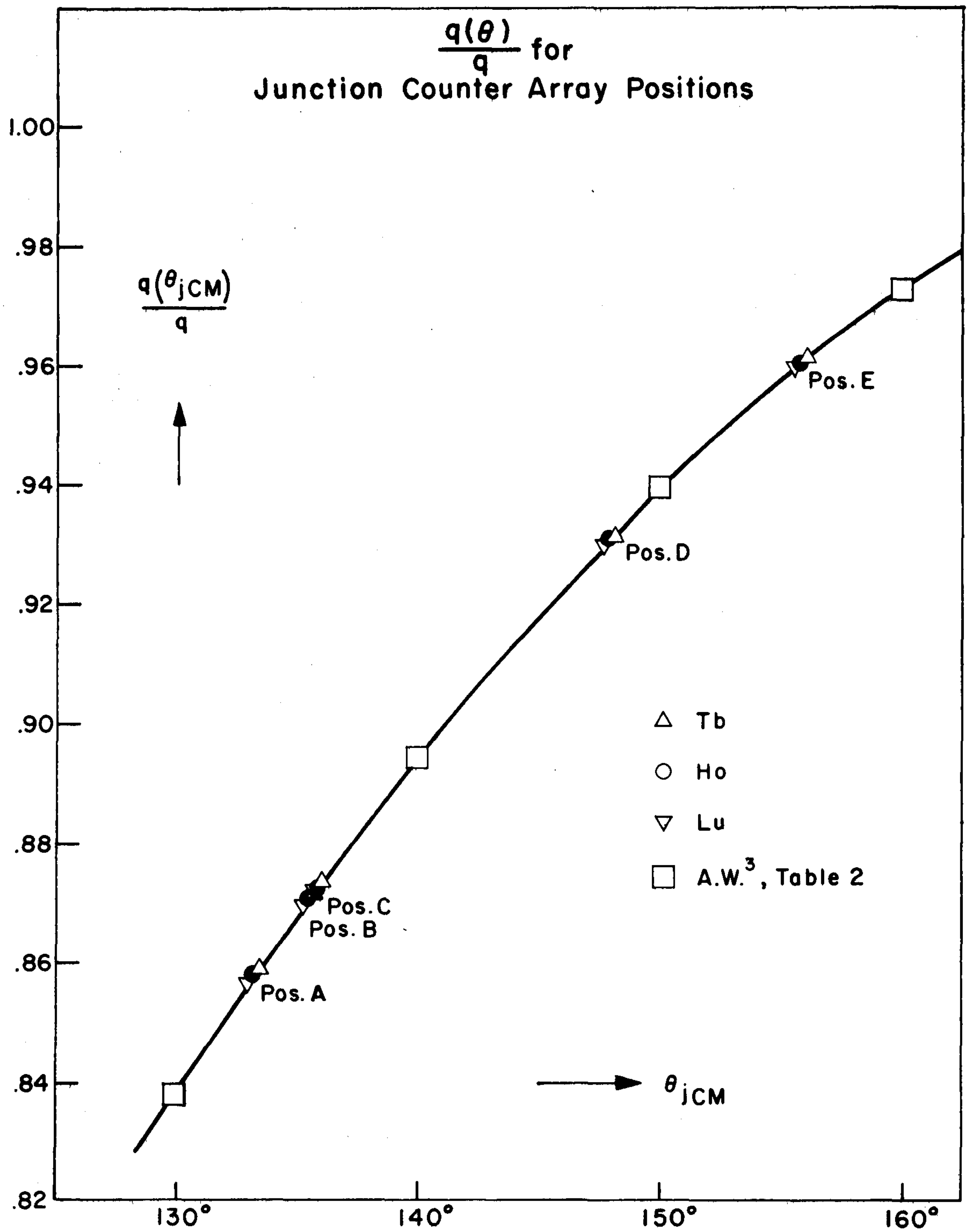
$\frac{q(\theta)}{q}$ for
Junction Counter Array Positions
1.00
.98
.96
.94
.92
.90
.88
.86
.84
.82
$\frac{q(\theta_{jCM})}{q}$
Pos. E
Pos. D
Pos. C
Pos. B
Pos. A
△ Tb
○ Ho
▽ Lu
□ A.W.[3], Table 2
θ_{jCM}
130°
140°
150°
160°

FIG VI - 2

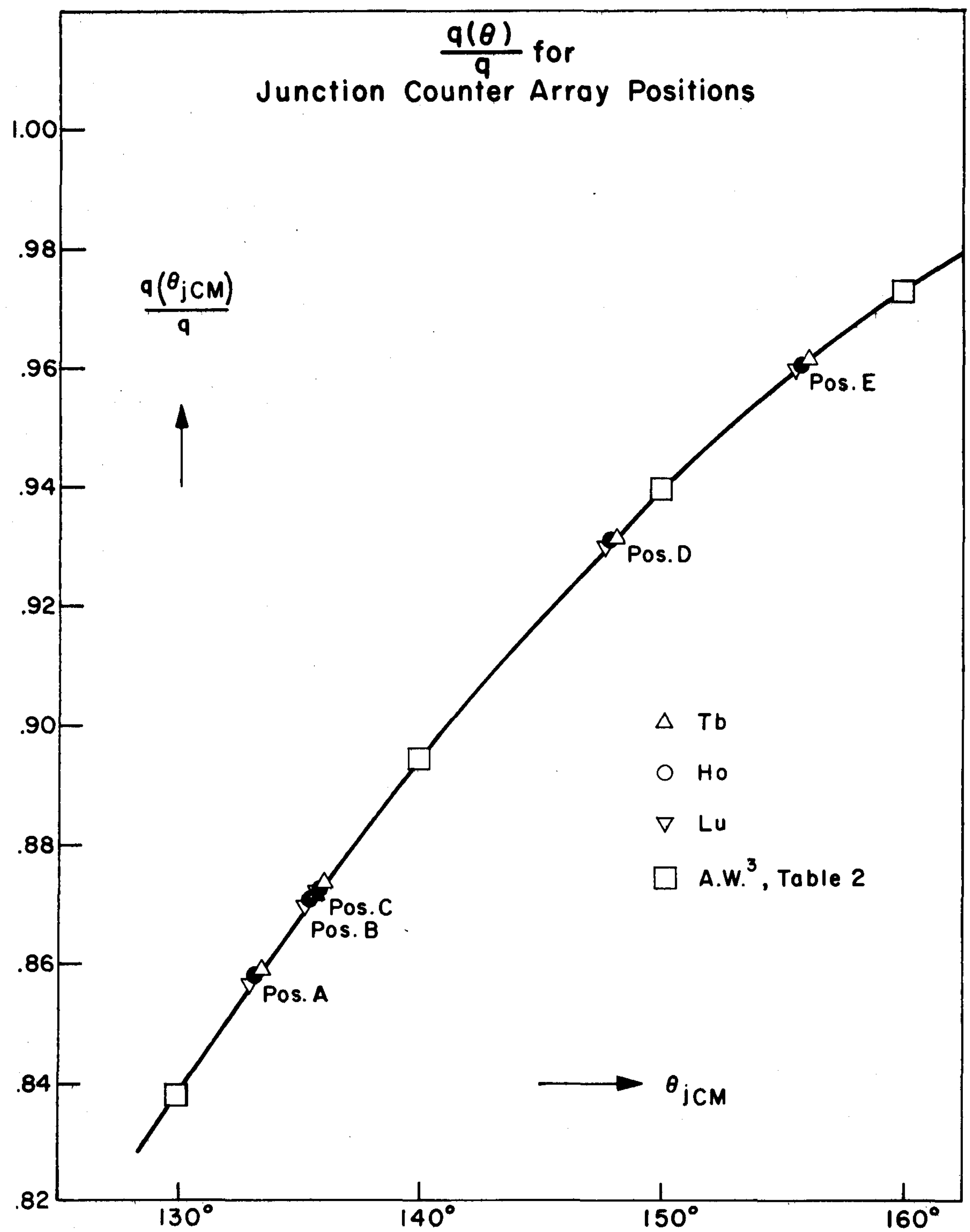

$\frac{q(\theta)}{q}$ for
Junction Counter Array Positions
$\frac{q(\theta_{jCM})}{q}$
1.00
.98
.96
.94
.92
.90
.88
.86
.84
.82
Pos. A
Pos. B
Pos. C
Pos. D
Pos. E
Tb
Ho
Lu
A.W.³, Table 2
θ_{jCM}
130°
140°
150°
160°

FIG VI - 2

$$P_{I0}(\theta, q_J, \xi=0) \approx P_I\left[q_J(\theta)\right] + \left(\frac{J_{22}(\theta)}{J_{20}(\theta)}\right)^2 \Delta_I\left[q_J(\theta)\right]\xi \qquad \text{(A.W. 5.61)}$$

in this range obey $|\Delta_0| < 1.9$, $|\Delta_2| < 1.2$, $|\Delta_4| < 0.21$; for the lower I-values, corrections to P_I are $\lesssim 0.5\%$, and considerably less for the most important larger, backward angles. Δ_I were not tabulated for odd I but corrections to the $q(\theta)$ approximation to odd-A P_{I_f} would be similarly inconsequential.

As to the "$\xi = 0$ approximation", A.W. defines a common ξ for a rotational band:

$$\xi = \frac{3\hbar a}{v_i \mathcal{I}} = \frac{6aA}{v_i \hbar} = 6\frac{Z_1 Z_2 e^2}{\mu v_i^2}\frac{A}{v_i \hbar} \quad . \qquad \text{(A.W. 5.35)}$$

With the help of A.W. equation 2.6, and for the case $E_I = E_0 + AI(I+1)$, $A = \hbar^2/2\mathcal{I}$. (For even-even nuclei, $K\pi = 0+$ bands, with the above E_I, $E_2 - E_0 = 6A$, and this ξ can be compared to $\xi_{1\to 2}$ in Alder et al.[1], $\xi_{1\to 2} \equiv \eta_f - \eta_i \approx \frac{Z_1 Z_2 e^2}{\hbar v_i}\frac{E_2 - E_1}{\mu v_i^2}$ --they are identical.) Using the expression of Alder et al.[1], $\xi \approx \frac{Z_1 Z_2 \sqrt{M_1}\, 6(1+\frac{M_1}{M_2}) A_{MeV}}{12.70\left[E_{iMeV} - \frac{1}{2}\{6(1+\frac{M_1}{M_2}) A_{MeV}\}\right]^{3/2}}$ (where the numerical factor 12.65, valid for a proton mass as unit mass, is replaced by 12.70, appropriate for 1 amu as unit mass), and the inertia parameters $A_{Tb} = 11.60$ keV, $A_{Ho} = 10.66$ keV, $A_{Lu} = 12.91$ keV, ground-state band ξ values were found to be:

T, $\frac{\text{MeV}}{\text{amu}}$	ξ, Tb	Ho	Lu
2	.06786	.06556	.08196
3	.03777	.03566	.04612
4.08	.02381	.02248	.02807

A.W. write for the first-order corrections to the sudden or $\xi = 0$ approximation,

$$P_{I_f I_i}(\theta, q, \xi) \approx P_{I_f I_i}(\theta, q, 0) + \Lambda_{I_f I_i}(\theta, q)\xi \; . \qquad \text{(A.W. 5.66)}$$

The $\Lambda_{I_f I_i}$ were tabulated only for $\theta = 180°$, $I_i = 0$ (A.W. Table 8). A.W. gave

$$\Lambda_{I_f 0}(\theta, q) \approx \left(\frac{q}{q(\theta)}\right)^2 \frac{f_0^0(\theta)}{f_0^0(\pi)} \Lambda_{I_f 0}[\pi, q(\theta)] \qquad \text{(A.W. 5.67)}$$

which was to be used with the aid of f-function tabulations (A.W. Table 7), and $\Lambda_{I_f}(q)$ from Table 8, and was stated to be accurate as long as $f_0^{0,2,4} >> f_2^{2,4}$; f_4^4; etc., as is the case at backward angles.

Unfortunately it was not possible to derive a simple procedure for calculating $\Lambda_{I_f I_i}$ for the odd-A case. From the $\xi = 0$ zero-order amplitude for population of a state with I_f, M_f of a band with a ground state I_i, M_i, which on performing the M sum is

$$a_{I_f M_f} = \sqrt{(2I_i+1)(2I_f+1)} \sum_I{}' (2I+1)(-1)^{M_i - K} \begin{pmatrix} I_f & I_i & I \\ -M_f & M_i & M_f - M_i \end{pmatrix} \begin{pmatrix} I_f & I_i & I \\ -K & K & 0 \end{pmatrix} A_{I, M_f - M_i}(\theta, q), \qquad \text{(A.W. 5.8)}$$

with A_{IM} given by A.W. equations 5.9,10, listed above, one finds the expression for $P_{I_f I_i}$ given above (A.W. equation 5.13), for the evaluation of which $A_I(q)$ tables constructed for the $q(\theta)$ approximation,

$$A_{I0}(\theta, q) \approx A_{I0}[\pi, q(\theta)] \equiv A_I[q(\theta)] \qquad \text{(A.W. 5.14)}$$

were used. To first order in ξ', the correction to be added to the zero-order amplitude $a_{I_f M_f}$ is given by A.W.:

$$a^{(1)}_{I_f M_f} = -\sqrt{\frac{16\pi}{5}}\, q\xi \sum_{II'} \sum_{M} \sum_{\mu=\pm 1} f_\mu(\theta)\left[1 + \frac{I_i(I_i+1)}{6} - \frac{I'(I'+1)}{6} + i\right]\sqrt{(2I_i+1)(2I_f+1)(2I+1)(2I'+1)}$$

$$\times \begin{pmatrix} 2 & I_i & I' \\ -\mu & M_i & \mu - M_i \end{pmatrix}\begin{pmatrix} 2 & I_i & I' \\ 0 & K & -K \end{pmatrix}\begin{pmatrix} I_f & I' & I \\ -M_f & -\mu + M_i & M \end{pmatrix}\begin{pmatrix} I_f & I' & I \\ -K & K & 0 \end{pmatrix} A_{IM}(\theta, q) + i\frac{8\pi}{15} q^2 \xi \quad \text{(A.W. 5.44)}$$

$$\times \sum_{II'} \sum_{M} \sum_{\ell m} (-1)^m f^\ell_m(\theta) \sqrt{(2I_i+1)(2I'+1)} \begin{pmatrix} \ell & I_i & I' \\ -m & M_i & m - M_i \end{pmatrix}\begin{pmatrix} \ell & I_i & I' \\ 0 & K & -K \end{pmatrix}\begin{pmatrix} I_f & I' & I \\ -M_f & m + M_i & M \end{pmatrix}\begin{pmatrix} I_i & I' & I \\ -K & K & 0 \end{pmatrix} A_{IM}(\theta, q),$$

where

$$f^\ell_m(\theta) = (2\ell+1)\begin{pmatrix} 2 & 2 & \ell \\ 0 & 0 & 0 \end{pmatrix}\left[12 - \ell(\ell+1)\right]\sum_{\mu\mu'}\begin{pmatrix} 2 & 2 & \ell \\ \mu & \mu' & m \end{pmatrix} f_{\mu\mu'} = \text{sph. tens.}, \quad \text{(A.W. 5.45)}$$

$$\left.\begin{aligned} f_{\mu\mu'} &= v_i^3 a^3 \int_{-\infty}^{\infty} \overline{S_{2\mu}}(t) \int_{-\infty}^{t} \overline{S_{2\mu'}}(t')\, dt'\, dt \\ f_\mu &= i\, v_i^2 a \int_{-\infty}^{\infty} t\, \overline{S_{2\mu}}(t)\, dt \end{aligned}\right\} \text{orbital integrals} \quad \begin{matrix}\text{(A.W. 5.42)} \\ \text{(A.W. 5.41)}\end{matrix}$$

$$f^\ell_{-m}(\theta) = f^\ell_m(\theta)\,. \quad \text{(A.W. 5.46)}$$

In the even-even case, $I_1 = 0$, A.W. 5.44 reduces to

$$a^{(1)}_{I_f 0} = i\frac{8\pi}{15} q^2 \xi \sqrt{(2I_f+1)}\, f^0_0(\pi) \sum_I (2I+1)\left[\begin{pmatrix} 0 & I_f & I \\ 0 & 0 & 0 \end{pmatrix}^2 + \begin{pmatrix} 2 & I_f & I \\ 0 & 0 & 0 \end{pmatrix}^2 + \begin{pmatrix} 4 & I_f & I \\ 0 & 0 & 0 \end{pmatrix}^2\right] A_{I0}(\pi, q), \quad \text{(A.W. 5.50)}$$

which leads to

$$P_I(\pi, q, \xi) = P_I(\pi, q, 0) + \Lambda_I(q)\xi \equiv P_I(q) + \Lambda_I(q)\xi\,, \quad \text{(A.W. 5.51)}$$

for which the Λ_I are tabulated; and

$$\begin{aligned} P_{I0}(\theta, q, \xi) &\approx P_{I0}(\theta, q, 0) + \Lambda_{I0}(\theta, q)\xi \quad \text{(A.W. 5.62,66,67)} \\ &\approx P_I[q(\theta)] + \left(\frac{q}{q(\theta)}\right)^2 \frac{f^0_0(\theta)}{f^0_0(\pi)} \Lambda_I[q(\theta)]\xi\,. \end{aligned}$$

The hope that substitution of this in

$$P_{I_f K}(\theta, q, 0) = (2I_f+1)\sum_I \begin{pmatrix} I_f & K & 0 \\ -K & K & 0 \end{pmatrix}^2 P_{I0}(\theta, q, 0) \quad \text{(A.W. 5.65)}$$

in place of $P_{I0}(\theta,q,0)$ would produce the required corrections as given by $a^{(1)}_{I_f I_i}$ turns out not to be realized. The error committed should not be in excess of a few percent for the lower-spin states, but the approximation may be out by tens of percent for the higher-spin observed band members.

The semi-classical approximation of the excitation theories used is quite close for heavy-ion projectiles, as is indicated by the condition $\eta \gg 1$; for example, 4.08 MeV/amu O^{16} on Tb^{159} has the smallest η_i among the cases studied,

$$\eta_i = \frac{Z_1 Z_2 e^2}{\hbar v_i} = \frac{Z_1 Z_2 \alpha}{\beta_i} = \frac{520/137.04}{0.09361} = 40.53 \gg 1. \qquad \text{(VI-29)}$$

From the relation

$$P_{I_f K}(\theta, q, \xi=0) \approx P_{I_f K}[q(\theta)] = (2I_f+1)\sum_I{}'(2I+1)\begin{pmatrix} I_f & K & I \\ -K & K & 0 \end{pmatrix}^2 P_I[q(\theta)] \qquad \text{(A.W. 5.65)}$$

and tables of $P_I(q)$ in A.W., values of odd-A $P_{I_f K}(q;\xi=0)$ can be calculated, and from these, the population cross sections obtained, via:

$$d\sigma_{I_f K} = P_{I_f K}[q(\theta)]\, d\sigma_R(\theta) \qquad (\theta \equiv \theta_{CM} = \theta_{rel.}) . \qquad \text{(VI-30)}$$

The results for $P_{I_f}(K=3/2, 7/2)$ are shown in Table A-1 (Appendix 3)* and Fig. VI-3 and 4.

Since the range of $q(\theta_j)$ is not great for the θ_j values corresponding to junction positions A to E, so that the effects of $P_{I_f K}(q)$ nonlinearity are minimal, the relation $f(\sum_i w_i x_i / \sum_i w_i) \approx \sum_i w_i f(x_i)/\sum_i w_i$, which is exact if $f(x) = a_0 + a_1 x$, was used to calculate average array angles, by identifying $w_j = d\sigma_R(\theta_j)$, $x_j = q(\theta_j)$, $f(x_j) = P_{I_f K}(q(\theta_j))$. Then the population probabilities are

$$P_f = \sum_j P_{I_f}[q(\theta_j)]\, d\sigma_R(\theta_j) \approx P_{I_f}(\bar{q}) \sum_j d\sigma_R(\theta_j) ; \qquad \text{(VI-31)}$$

$$\bar{q} \equiv \sum_j q(\theta_j)\, d\sigma_R(\theta_j) \Big/ \sum_j d\sigma_R(\theta_j). \qquad \text{(VI-32)}$$

Now $\bar{q} = Q_0 \cdot (\bar{q}/Q_0)$; $\bar{q}/Q_0 = (\bar{q}/q)\cdot(q/Q_0)$; and one has:

---

* Prefixes "A" on table, figure or equation numbers refer

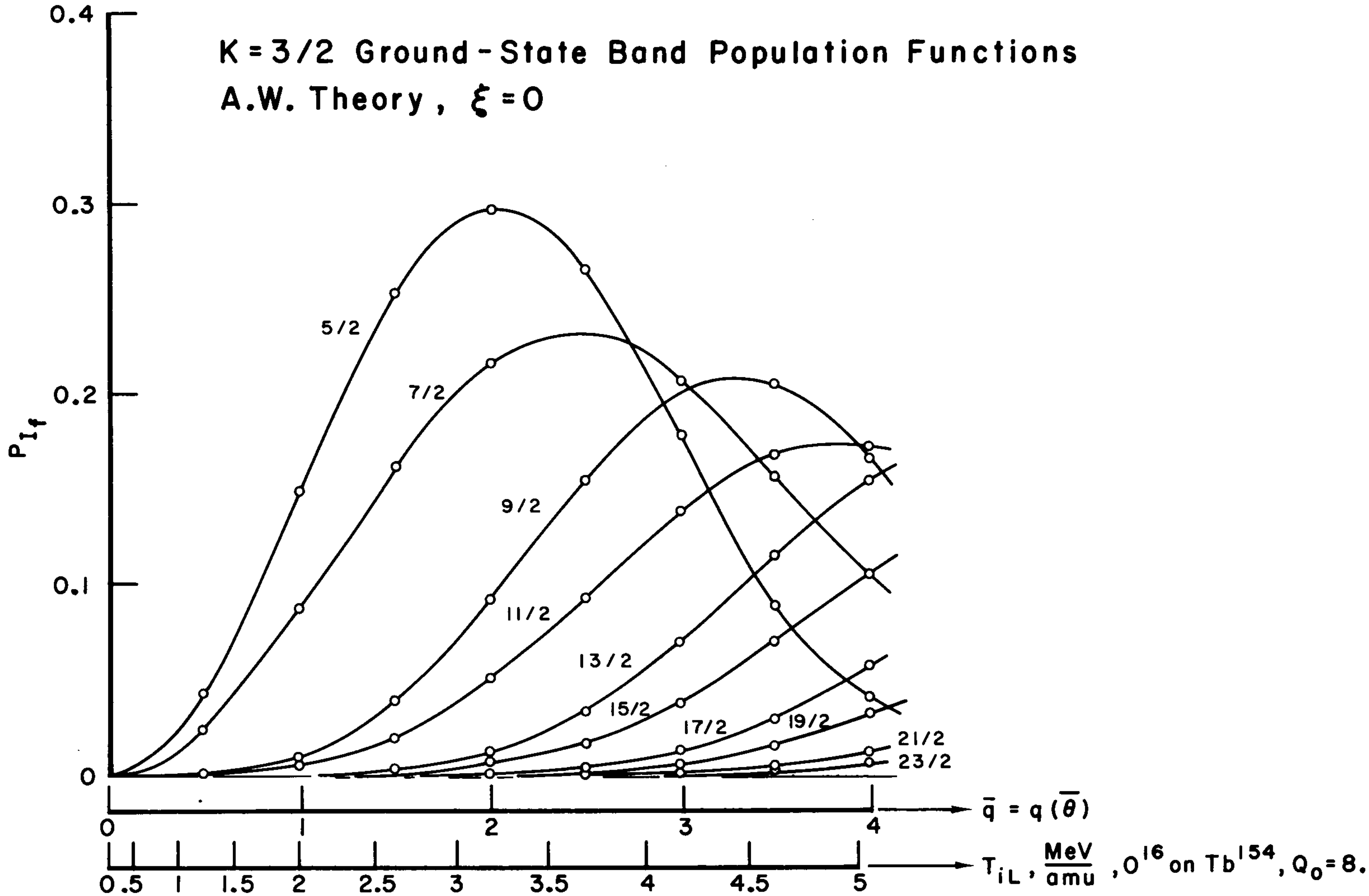

K = 3/2 Ground-State Band Population Functions
A.W. Theory , ξ = 0
P_{I_f}
0.4
0.3
0.2
0.1
0
5/2
7/2
9/2
11/2
13/2
15/2
17/2
19/2
21/2
23/2
$\bar{q} = q(\bar{\theta})$
0 1 2 3 4
T_{iL}, $\frac{MeV}{amu}$, O^{16} on Tb^{154}, Q_0 = 8.1
0.5 1 1.5 2 2.5 3 3.5 4 4.5 5

FIG VI-3

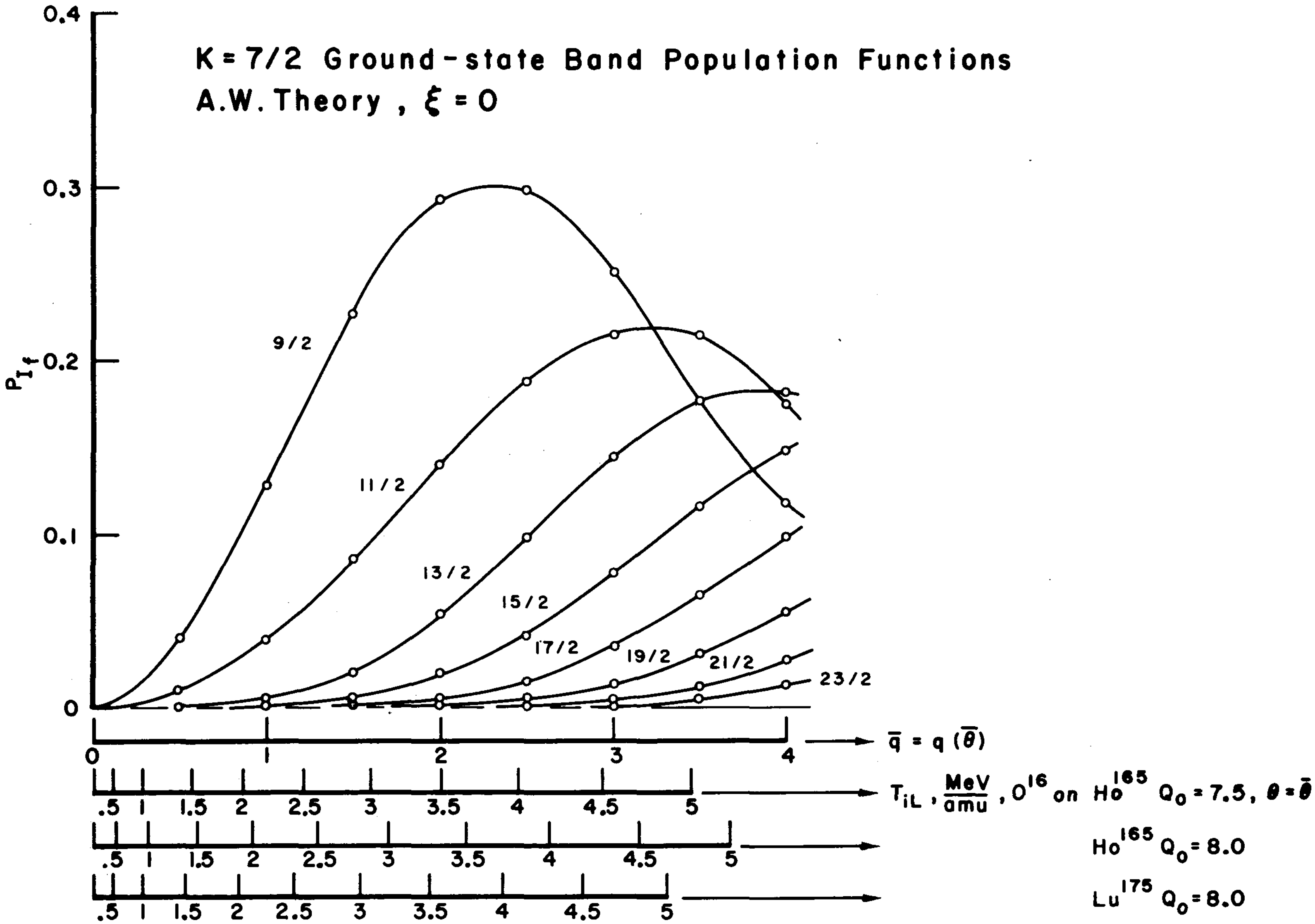

K = 7/2 Ground-state Band Population Functions
A.W. Theory , ξ = 0
P_{I_f}
0.4
0.3
0.2
0.1
0
9/2
11/2
13/2
15/2
17/2
19/2
21/2
23/2
0
1
2
3
4
$\bar{q} = q(\bar{\theta})$
.5
1
1.5
2
2.5
3
3.5
4
4.5
5
T_{iL}, $\frac{MeV}{amu}$, O^{16} on Ho^{165} Q_0 = 7.5, $\theta = \bar{\theta}$
Ho^{165} Q_0 = 8.0
Lu^{175} Q_0 = 8.0

FIG VI-4

$$\mathfrak{q}/Q_0 = 7.6241\left(\sqrt{M_1}\; E_{iMeV}^{3/2}\right)\Big/\left(1+\frac{M_1}{M_2}\right)^2 Z_1 Z_2^2 \quad ; \qquad \text{(A.W. 5.57)}$$

Element	$E_{iMeV}^{-3/2} q/Q_0$
Tb	7.4483×10^{-4}
Ho	7.0572×10^{-4}
Lu	6.3483×10^{-4}

To obtain $\bar{q}/q$ with the aid of (VI-32) and the $q(\theta_j)/q$ values in Table VI-1, the Rutherford cross sections are required as a function of θ_j and E_i. These were calculated from

$$d\sigma_R(\theta_j^{CM}, T_{iL}) = \frac{1}{4}\left(\frac{a'}{T_{iL,MeV}}\right)^2 \sin^{-4}\frac{\theta_j^{CM}}{2}\,\frac{d\Omega_{jCM}}{d\Omega_{jL}}\, d\Omega_{jL} \ , \qquad \text{(VI-33)}$$

where a' is the "reduced Rutherford constant" mentioned above. The weighted averages $\left[\sum_j q(\theta_j^{CM})\, d\sigma_R(\theta_j^{CM}, E_i)/q\right]\Big/\sum_j d\sigma_R(\theta_j^{CM}, E_i) = \bar{q}/q$ were obtained for each θ_{jCM}, E_i, and it turned out that $\bar{q}/q$ was independent of T_{iL}, as must be the case since

$$d\sigma_R(\theta_j, T_{iL}) = f(T_{iL})\, g(\theta_j) ; \qquad \text{(VI-34)}$$

$$\frac{\sum_j \frac{q(\theta_j)}{q}\, d\sigma_R(\theta_j, T_{iL})}{\sum_j d\sigma_R(\theta_j, T_{iL})} = \frac{f(T_{iL})\sum_j \frac{q(\theta_j)}{q}\, g(\theta_j)}{f(T_{iL})\sum_j g(\theta_j)} = \frac{\sum_j \frac{q(\theta_j)}{q}\, g(\theta_j)}{\sum_j g(\theta_j)} \qquad \text{(VI-35)}$$

The results are:

Experiment:	$\bar{q}/q$
O^{16} on Tb^{159}	0.91155
O^{16} on Ho^{165}	0.91093
O^{16} on Lu^{175}	0.91002

q/Q_0 was calculated from **A.W.** equation 5.57 as a function of

T_{iL} and thence $\bar{q}/Q_0$ as a function of T_{iL}. To obtain the necessary $\bar{q}$ values as a function of T_{iL} required for thick-target integration of the excitation probabilities, it was necessary to assume suitable values for Q_0. Comparison of calculated ground-state band gamma-ray intensities with the data would confirm the correctness or incorrectness of the choice, and of the other necessary initial choices for the deexcitation E2-M1 mixing ratios. A summary of experimental evidence on these parameters, and the choices employed, follow.

<u>Terbium-159</u>: Martin et.al.[73], from Coulomb-excitation yields, gamma-gamma angular correlations and Sliv and Band's theoretical conversion coefficients, found $\delta'^2(79.5) = 0.02 \pm 0.01$, $B(E2\uparrow,138) = 1.9 \pm 0.09 e^2 10^{-48} cm^4$ or $Q_0 = 8.1$ barns. (From the Alaga rules, $((I_0+2 \rightarrow I_0+1)/(I_0+1 \rightarrow I_0))^2 = \left(\frac{I_0+1}{I_0+2}\right)^3 \frac{I_0+3}{I_0}$.) This was probably the best determination of Q_0, and most other determinations tended to corroborate it.

Olesen and Elbek[85], from their inelastic projectile measurements, found $B(E2\uparrow,58) = 2.81 \pm 0.08$, $B(E2\uparrow,138) = 1.54 \pm 0.06$ (in units $e^2 10^{-48} cm^4$) and corresponding inelastic "reaction" Q-values corresponding to level energies 59 ± 2 and 138 ± 2 keV respectively. The B-value ratio, 0.516, compares favorably with the Alaga prediction, 0.556. To a degree this method is independent of the one above, and the results are probably superior to those found by the same technique by Sharp and Beuchner[57], $B(E2\uparrow,58) = 3.56 \pm 0.032$, $B(E2\uparrow,138) = 1.27 \pm 0.13$, ratio 0.36 and level energies 58 ± 10 and 138 ± 10 keV.

Huus et al.[72], from L and M conversion-line measurements following Coulomb excitation, estimated $\delta^2(58) \lesssim 0.02$ and gave $\epsilon_L B(E2,58) = 7.7$, $B(E2\uparrow,58) = 3.5$, $Q_o = 8.3$ barns, in essential agreement. Heydenburg and Temmer[82], from the observed crossover/cascade gamma-ray intensity ratio following Coulomb excitation and the assumption that the intraband Alaga rules are valid, deduced $\delta'^2(79) = 0.013$. Using this and theoretical E2 conversion coefficients and M1 coefficients with estimated Sliv-type corrections, $\alpha_{tot,theor}(79) = 3.3$, $\alpha_{tot,theor}(136) = 1.0$, they found $B(E2\uparrow,136) = 2.2$, $Q_o = 8.7$ b. Harmatz et al.[65] concluded from the L ratios from 58.0-keV transition radiation in Dy^{159} decay that $\delta^2(58) = 1/65 = 0.054$. Subba-Rao[56] observed the 225-79 keV gamma-gamma angular correlation following Gd^{159} decay and found $\delta'(79) = +0.13 \pm 0.06$, or $\delta'^2(79) = 0.017 \pm 0.015$. Ryde et al.[76], in their comprehensive work on Gd decay and their quoted prepublication results from Persson's Dy decay study, compared the 58-keV L ratios with the theoretical E2 and M1 coefficients and concluded that $\delta^2(58) = 0.015 \pm 0.004$.

From these results I adopt $Q_o = 8.1$ barns, $\delta^2(58) = 0.01$, 0.015 and 0.02.

Holmium-165: Huus et al.[72], from a study of conversion lines following Coulomb excitation of 96- and 121-keV levels, from the 96-keV K/L ratio concluded that $\delta^2(96) \sim 0.09$, and for the 116-keV transition, found also $\delta^2(116) \sim 0.09$. From measured $\epsilon B(E2)$ values for 96K, 96L and 116L decay radiations and estimates of ϵ_{e^-}, they obtained $(BE2\uparrow,96) \approx 2.3$ or $Q_o = 7.7$ b., and $B(E2\uparrow,212) \approx 0.76$ or $Q_o = 8.4$ b. (B-value ratio 3.2; Alaga rules, $35/9 = 3.89$). But Persson et al.[125], from L-ratios of 94.7-

keV conversion lines occuring in Dy^{165} decay, comparing with Sliv and Band's conversion coefficients, found $\delta^2(95) = 0.026 \pm 0.004$. Novakov and Stepić[122], also from conversion-line measurements following Dy decay, estimated $\delta^2(95) \approx 0.02$. Bernstein and Lewis[139], from their observed Coulomb-excitation K/L ratio, found $\delta^2(95) = 0.044$. From this, the conversion coefficients of Rose with Sliv-type corrections giving $\alpha_{tot,theor} = 2.6$, and $\epsilon B(E2)$-values of Heydenburg and Temmer[81], they calculated $B(E2\uparrow,96) = 2.76 \pm 50\%$ or $Q_0 = 8.1$ b. But from the crossover gamma-ray yield of Heydenburg and Temmer[81] and conversion-electron yields observed from the first and second excited states, they estimated $\delta^2(96) = 0.023$ and $B(E2\uparrow,218) = 0.71 \pm 50\%$ or $Q_0 = 8.2$ b., and noted that the δ^2 discrepancy was within the experimental error, which was somewhat large for the first value due to the K/L-determination uncertainty.

Olesen and Elbek[85] found from inelastic projectile measurements the values $B(E2\uparrow,94) = 2.41 \pm 0.07$, $B(E2\uparrow,209) = 0.63 \pm 0.04$, ratio 0.261, comparing favorably with the theoretical ratio 0.237. They therefore concluded that $Q_0 = 7.56$ b., a value lower than previous Coulomb-excitation and radioactive-decay results and corresponding to a deformation parameter β about 10% below the theoretical value from the Nilsson model. Heydenburg and Temmer[82], from Coulomb-excitation yields of 94-, 114- and 208-keV gamma rays, found $\delta^2(94) \sim 0$, $\delta'^2(114) = 0.039$, and from the estimates $\alpha_{tot}(94) = 2.4$, $\alpha_{tot}(114) = 1.3$, $\alpha_{tot}(208) = 0.2$ and their $\epsilon B(E2)$ measurements, deduced $B(E2\uparrow,94) = 2.5$ or $Q_0 = 7.6$ b., $B(E2\uparrow,208) = 0.52$ or $Q_0 = 6.9$ b., also lower than previous estimates.

Martin et al.[73], from their studies of Coulomb-excitation conversion lines, obtained results for B(E2↑,94), B(E2↑,207) and $\delta'^2(113)$ and averaged these with previous determinations:

	Martin et al.[73]	Huus et al.[72]	Goldring & Paulisson[140]	Heydenburg & Temmer[82]
B(E2↑,94)	2.8	2.5	--	2.5
B(E2↑,207)	0.70	0.76	--	0.52
Ratio*	0.25	0.3	0.20	0.21
$\delta'^2(114)$	0.05** 0.04 ± 0.02#	--	0.035	0.039

	Bernstein & Lewis[139]	Average	Q_0
B(E2↑,94)	2.79	2.65 ± 0.15	8.0 b.
B(E2↑,207)	0.71	0.66 ± 0.10	8.0 b.
Ratio*	0.25	0.25 ± 0.04	
$\delta'^2(114)$	0.044	--	

Bernstein and Graetzer[144] measured deexcitation 95-, 115- and 210-keV conversion lines following Coulomb excitation, and found that the 95-keV radiation was $2.5^{+3.5}_{-2.0}\%$ E2 which is $\delta^2(95) = 0.026^{+0.036}_{-0.020}$, and the 115-keV radiation, $(5 \pm 3)\%$ E2 (comparing well to the value $(4 \pm 2)\%$ E2 from the angular-correlation meas-

* Theory 0.257

** From I(207γ)/I(113γ) and assuming discrepancy from Alaga rules to be due to M1 components.

\# From gamma-ray angular-distribution measurements.

urements of Martin et al.[73]) which is $\delta'^2(115) = 0.053 \pm 0.031$. From measured $\epsilon_{95L}B(E2)$ and $\epsilon_{210K}B(E2)$ values and estimates of ϵ, they obtained $B(E2\uparrow,95) = 2.8 \pm 0.4$, $B(E2\uparrow,210) = 0.65 \pm 0.13$, in agreement with Olesen and Elbek's inelastic-projectile results. The ratio is 0.23 ± 0.03, comparing favorably with theory. $(\delta(95)/\delta'(115))^2$ is $0.57^{+0.65}_{-0.40}$, and is to be compared with the theoretical rotational value, 1.017.

In light of the foregoing results the provisional values $Q_o = 7.5$ and 8.0 b. and $\delta^2(95) = 0.040$ are employed.

Lutetium-175: H. de Waard[174], in a study of conversion lines and gamma rays following Yb^{175} decay, concluded that the first excited state of Lu^{175} at 113.0 ± 0.3 keV decayed via E2-M1 with $\delta^2 = 0.33 \pm 0.10$. Mize et al.[176], from conversion-line measurements following Yb and Hf decays, concluded that $\delta^2(113) = 0.30 \pm 0.06$. Cork et al.[177], from their conversion-line studies of the Yb^{175} decay, obtained results in essential agreement and concluded that the 114-keV radiation was E2 + M1. Hatch et al.[178], from a study of internal-conversion and gamma-ray lines from Hf and Yb decays, concluded that the 114-keV radiation was 20% E2 (Yb data) or 10% E2 (Hf data) ($\delta^2 = 0.25$, 0.11 respectively). Huus et al.[72], from their Coulomb-excitation work, estimated from the 114-keV K/L ratio $\delta^2(114) \approx 0.05$, and found $\epsilon_L B(E2)$ which with an estimate of ϵ_L gave $B(E2\uparrow,114) = 3.2$ or $Q_o = 8.8$ b. They noted that a ~20% lowering of their K/L ratio would give mixing in better accord with Heydenburg and Temmer's[82] results without altering the B(E2)-value very much. Heydenburg and Temmer[82] in their Coulomb-excitation study observed 114-, 136- and 250-keV decay transitions in the ground-state band and from the cascade/crossover ratio and assumed validity of the Alaga rules, found $\delta'^2(136) = 0.135$. From measured $\epsilon B(E2)$ values, $\delta'^2(136)$, and the theoretical conversion coefficients, $\alpha_{tot,theor}(114) = 2.1$, $\alpha_{tot,theor}(136) = 2.0$, $\alpha_{tot,theor}(250) = 0.1$, they obtained $B(E2\uparrow,114) = 2.5$ or $Q_0 = 7.6$ b., and $B(E2\uparrow,253) = 0.78$ or $Q_0 = 8.5$ b. Bernstein and Lewis[139], from their observations of Coulomb-excitation internal-conversion lines, found from the 114-keV K/L ratio, $\delta^2(114) = 0.11$, and from the measured $\alpha_{tot}(114) = 2.3$ and Heydenburg and Temmer's gamma-ray yields, $B(E2\uparrow,114) = 2.86$ or $Q_0 = 8.2$ b. They also found from the 139-keV K/L ratio the result $\delta'^2(139) = 0.08$, but from the crossover/cascade ratio estimate and the assumption of the validity of the Alaga rules, $\delta'^2(139) = 0.11$; and from the measured $\alpha_{tot}(139) = 1.4$, $B(E2,253\uparrow,139\downarrow) = 0.63$, $B(E2,253\uparrow,253\downarrow) = 0.12$ or $B(E2\uparrow,253) = 0.75$ corresponding to $Q_0 = 8.3$ b.

Martin it al.[73] presented results of intensity and angular-distribution measurements on deexcitation gamma radiation from Coulomb excitation, and averaged his results with previous results, as shown below:

	Martin et al.[73]	Huus et al.[72]	Goldring & Paulisson[140]	Heydenburg & Temmer[82]
$B(E2\uparrow,114)$	2.4	3.2	--	2.5
$B(E2\uparrow,254)$	0.45	--	--	0.78
Ratio*	0.19	--	0.23	0.31
$\delta'^2(140)$	{0.30** 0.22 ± 0.04##	--	0.27**	0.135**
$\delta^2(114)$	--	0.05***	--	--
Ratio#	--	--	--	--

	Bernstein & Lewis[139]	Hatch et al.[178]	Average	Q_0
$B(E2\uparrow,114)$	2.86	--	2.8 ± 0.3	7.5 b.
$B(E2\uparrow,254)$	0.75	--	0.7 ± 0.2	6.4 b.
Ratio*	0.26	--	0.25 ± 0.04	
$\delta'^2(140)$	0.08***	0.7**	--	
$\delta^2(114)$	0.11***	0.25***	--	
Ratio#	1.38	--	--	

Bernstein and Graetzer[144] measured deexcitation 114-, 137- and 251-keV conversion lines following Coulomb excitation and

---

* Theory 0.257.

Theory 1.018 .

** From $I(254\gamma)/I(140\gamma)$ and ascribing discrepancies from E2 Alaga rules to the M1 components.

From gamma-ray angular distributions.

*** From conversion data.

found the 114-keV radiation to be $(15 \pm 4)\%$ E2 + M1 which is $\delta^2(114) = 0.176 \pm 0.042$, and the 137-keV radiation, $(17 \pm 3)\%$ E2+M1 (comparing well with $(18 \pm 2.5)\%$ E2 or $\delta' = +0.22 \pm 0.04$ from the angular-correlation measurements of Martin et al.[73]) which is $\delta'^2(137) = 0.205 \pm 0.031$. From conversion-line intensity measurements and estimates of ϵ_{114L} and ϵ_{137K} they obtained $B(E2\uparrow,114) = 2.4 \pm 0.5$, agreeing with the inelastic-proton results of Elbek et al.[199], and $B(E2\uparrow,251) = 0.56 \pm 0.1$, ratio 0.23 ± 0.025, comparing favorably with theory, 0.257. For the ratio %E2(114)/%E2(137) they gave 0.86 ± 0.25, compared to theory, 1.017.

From a lifetime measurement of the 114-keV level with the result $\tau(114) = (14.6 \pm 1.0) \times 10^{-11}$ sec. using $\frac{1}{\tau} = \frac{16\pi}{9} \frac{1}{\hbar} \left(\frac{E_\gamma}{\hbar c}\right)^3 \left(\frac{e\hbar}{2Mc}\right)^2 \times (1 + \alpha_{tot})(1 + \delta^2) B(M1)$, the mixing $\delta^2 = 0.18 \pm 0.06$ estimated from the K/L ratios and the Sliv and Band $\alpha_{tot,theor}(114) = 2.74$, Blaugrund et al.[194] obtained $B(M1) = 0.060 \pm 0.005$. But from $\alpha_{tot,theor}$ and the inelastic-projectile B(E2) values due to Elbek et al.[199] ($B(E2\uparrow,114) = 2.34 \pm 0.10$ or $Q_0 = 7.31 \pm 0.50$; $B(E2\uparrow,251) = 0.57 \pm 0.08$ or $Q_0 = 7.51 \pm 0.16$, average $Q_0 = 7.45 \pm 0.35$, B-value ratio 0.244, level energies 114 ± 2- and 251 ± 2-keV) plus the mixing ratio above, they found $B(M1) = 0.085 \pm 0.030$. However, from the $B(E2\uparrow,114)$ of Elbek et al.[199], the measured $I(114\gamma)/I(137\gamma) = 0.937 \pm 0.55$ (compared to 0.50, Heydenburg and Temmer[82]; 0.95, Martin et al.[73]; 0.90, Goldring and Paulisson[140]), and the value $\delta'^2(114)$ suggested by the work of Martin et al.[73] and Bernstein and Graetzer[144], they obtained $B(M1,137) = 0.0903 \pm 0.0014$ and a value for B(E2,137) corresponding to $Q_0 = 6.50 \pm 0.60$, in poor agreement. They noted that this suggests their δ^2 may be wrong, although still perhaps within the error limits.

T. Weidling[179], from the 113-282 keV angular correlation following Yb decay, found the 113-keV radiation to be M1+ $(17\pm 3)\%$E2, which is $\delta^2 = 0.20\pm 0.03$, agreeing with Hatch et al.[178] E. Klema[182] obtained from this data the result $\delta^2(113) = 0.18$. Thun et al.[195], from gamma-gamma and electron-gamma 114-282-keV angular-correlation measurements, found $\delta^2(114) = 0.71^{+0.7}_{-0.6}$, and obtained $\alpha_K(114) = 1.6\pm 0.2$, in agreement with Hatch et al. (1.6) and Mize et al. (1.7 ± 0.4).

Lindskog et al.[198] measured the 114-keV level half-life, obtaining $(9\pm 1)\times 10^{-11}$ sec., compared to $(10.1\pm 0.7)\times 10^{-11}$ sec. (Blaugrund[194]) and $(10\pm 3)\times 10^{-11}$ sec. (Elbek et al.[199]). From comparison of Rose's conversion coefficients with the mean of L ratios of Cork et al.[177], Hatch et al.[178] and Mize et al.[176], they obtained $\delta^2 = 0.15\pm 0.06$ from L_i/L_{ii}, 0.20 ± 0.04 from L_i/L_{iii}, and adopted the value $\delta^2(114) = 0.18\pm 0.05$. They noted that the mean of the K/L ratios of Cork et al.[177] (2.9 ± 0.4) and Blaugrund et al.[194] (3.2 ± 0.3) gives $\delta^2(114) = 0.52\pm 0.11$ in disagreement, but that the K/L ratio of Bernstein and Lewis[139] (4.3 ± 0.4) gives $\delta^2 = 0.24\pm 0.05$, in closer accord. From this and Rose's theoretical coefficients the estimate $\alpha_{tot,theor}(114) = 2.5\pm 0.1$ was made. Then the half-life gave $B(M1,114) = (7.1\pm 0.9)\times 10^{-2}(e\hbar/2Mc)^2 = 1/22\times$s.p. and $B(E2,114) = 1.41\pm 0.45 = 240\times$s.p. or $Q_0 = 6.5\pm 1.0$ b.

In light of these various results, I use as tentative values $\delta^2(114) = 0.20$ and $Q_0 = 8.0$ b.

Values of $\overline{q}$ appropriate for these choices are displayed in Table VI-1 and Fig. VI-5.

Range-energy curves had to be constructed for Tb, Ho and Lu. Following L. Northcliff[223] in his discussion of heavy-ion range-energy relationships, the theory of ion energy loss in matter for nonrelativistic ions, neglecting atomic shell effects, can be formulated in terms of the relation

$$-\frac{dE}{dx} = \frac{4\pi Z_{1\,eff}^{2} e^{4}}{m_e v^{2}} NB \qquad \text{(VI-36)}$$

in which Z_{1eff} is the effective charge of the ion of nuclear charge number Z_1, travelling with speed v, $v_K \ll v \ll c$, in a medium with N atoms per cubic centimeter and characterized by a dimensionless quantity, the stopping number B. m_e and e are the electron rest-mass and charge respectively, and -dE/dx is the average energy loss per unit path length. Although the general theory of stopping treats of a problem of prohibitive complexity, empirical measurements by many groups have provided relatively accurate semi-empirical relations for $\gamma \equiv \overline{Z}_{1\ inst}/Z_1$ as a function of v, Z_1 and Z_2 = charge number of stopping material nuclei; and for $\mathcal{L} \equiv B/Z_2$ as a function of v, Z_2 (with a slight dependence on Z_{1eff}) which appear to be valid for all ion-absorber combinations. Data for specific combinations were interpolated with the aid of the range-energy relation in the form given by Northcliff,

$$-\frac{dE}{dX} = \frac{3.072\times10^{-4}}{\beta^{2}} \frac{Z_1^2 Z_2}{M_2} \gamma^{2}(\beta, Z_1, Z_2, \rho)\mathcal{L}(\beta, \gamma Z_1, Z_2) \frac{\text{MeV}}{\text{mg cm}^{-2}}, \qquad \text{(VI-37)}$$

where X is the path length in mg. cm.$^{-2}$, E the ion energy in

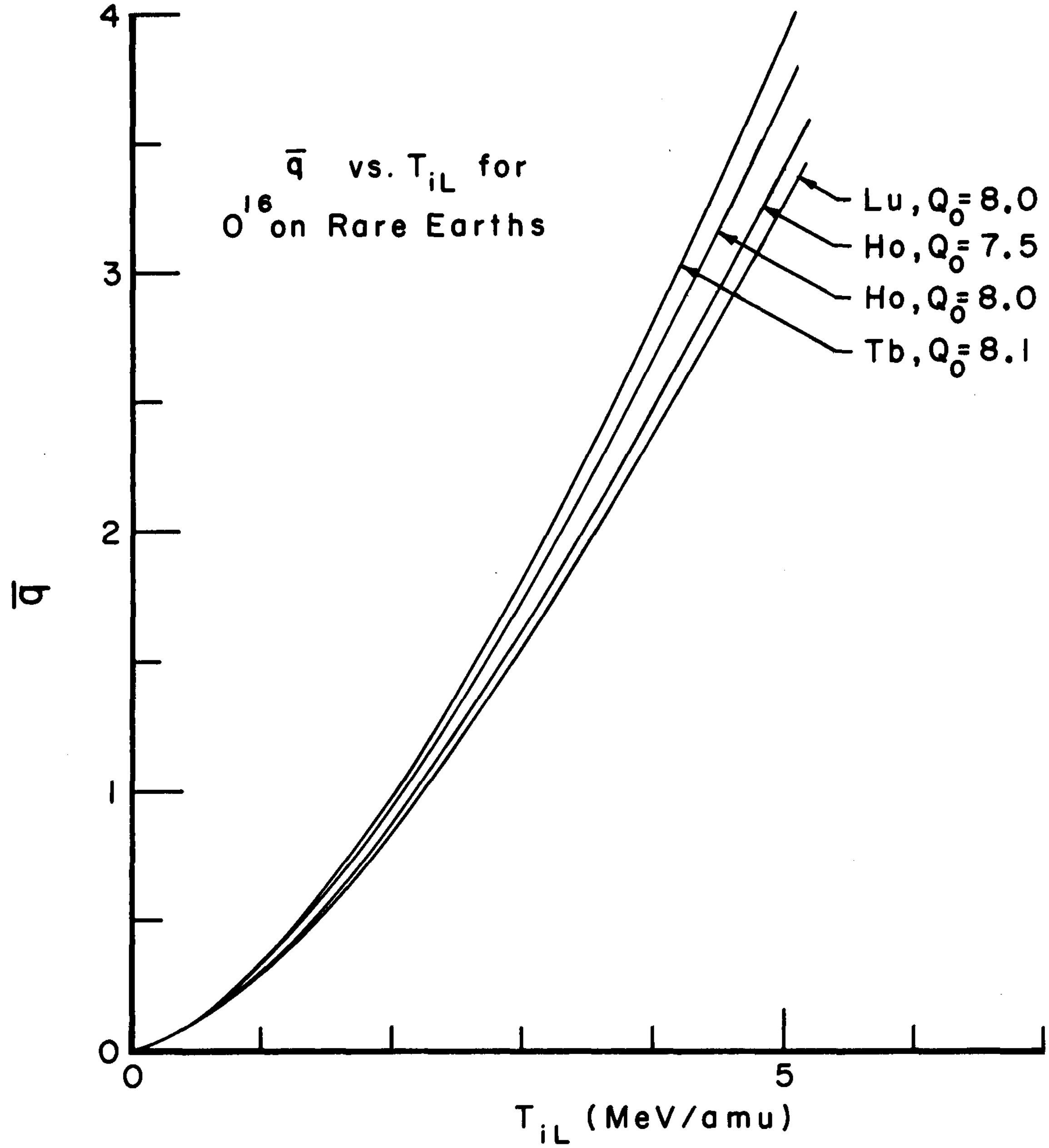
q̄ vs. T_iL for
O^16 on Rare Earths
Lu, Q_0 = 8.0
Ho, Q_0 = 7.5
Ho, Q_0 = 8.0
Tb, Q_0 = 8.1
q̄
T_iL (MeV/amu)
0
1
2
3
4
5

FIG VI - 5

MeV, $\beta = v/c$ and ρ is the stopping-material density in gm. cm.$^{-3}$. The function γ expresses the speed-dependent effective charge arising from capture and loss of projectile atomic electrons, an important process for heavy ions ($2 < Z_1 \lesssim 10$) in the range of energies of interest (1-10 MeV/amu). According to this relation the same kind of ion moving at the same speed in different media will experience relative stopping rates proportional to $(Z_2/M_2)\gamma^2(Z_2,\rho)\mathcal{L}(\gamma Z_1, Z_2)$ or, when the dependence of γ on Z_2 and ρ is negligible, as is usually the case, to $Z_2\mathcal{L}(Z_2)/M_2$.

Ranges are given by

$$R(E) = \int_0^E dE/-\frac{dE}{dX} \text{ mg. cm.}^{-2} \qquad \text{(VI-38)}$$

Depth in a target material corresponding to different energies E_2 from the incident energy E_1 at the surface ($\Delta R = 0$) to 0 are obtained from the relation

$$0 \leq \Delta R(E_1, E_2) \equiv R(E_1) - R(E_2) = -\frac{1}{3.072\times 10^{-4}} \frac{1}{Z_1^2} \frac{M_2}{Z_2} \int_{E_2}^{E_1} \frac{\beta^2 dE}{\gamma^2(\beta)\mathcal{L}(\beta, Z_2)}. \qquad \text{(VI-39)}$$

Ranges in specific stopping materials were constructed by interpolating ratios of Z_2R/M_2 for selected stopping materials for which experimental range data are available, for each β or E, as follows:

$$\frac{R(E,Z_2)}{R(E,Z_2')} = \frac{Z_2'}{M_2'} \frac{M_2}{Z_2} \frac{\int_0^E \frac{\beta^2 dE}{\gamma^2(\beta)\mathcal{L}(\beta, Z_2)}}{\int_0^E \frac{\beta^2 dE}{\gamma^2(\beta)\mathcal{L}(\beta, Z_2')}} \equiv \frac{Z_2'}{M_2'} \frac{M_2}{Z_2} \mathcal{R}(E, Z_2, Z_2'). \qquad \text{(VI-40)}$$

Data of E.L. Hubbard[224] were used for Z_2' and certain other Z_2 values which were used to generate $\mathcal{R}(E; Z_2, Z_2')$ as a function of

Z_2, which was then interpolated for $Z_2 = 65$, 67, 71 to obtain the necessary rare-earth curves, using $R(E,Z_{2re}) = \frac{Z_2'}{M_2'}\frac{M_{2re}}{Z_{2re}} \times \mathcal{R}(E;Z_{2re},Z_2')R(E,Z_2')$. Arbitrarily $Z_2' = 47$ (Ag) was chosen. The Hubbard data and other pertinent quantities are tabulated in Table A-2. For M_2, atomic weights which are averages of M_2 over the natural isotopic compositions of the stopping materials were used. A plot of $\left[R(E,Z_2)\frac{Z_2}{M_2}\right] \Big/ \left[R(E,Ag)\left(\frac{Z_2}{M_2}\right)_{Ag}\right]$ versus Z_2 for various E_{iL}, from the Hubbard data, appears in Fig. A-1. It was apparent that interpolation between the odd-Z materials $_{47}$Ag and $_{79}$Au would be suitable. This was done, with resulting range-energy data tabulated in Table A-3.

The situation for thick-target integration of the A.W. theory is illustrated in Fig. A-2. With the aid of $P_{I_fK}(q)$, $q = 0.0(0.5)5.0$, $\bar{q} \equiv q(\bar{\theta}_{CM})$ for each Q_o, Z_1M_1, Z_2M_2 combination as a function of T_{iL}, $T_{iL} = 0.5(0.5)5.0$ MeV/amu; the range-energy data $R(E;Z_1M_1;Z_2M_2)$ for $E = 0.0(1.0)5.0(1.25)7.5$; and $\sum_j d\sigma_R(\theta_{jCM}; T_L;Z_1M_1,Z_2M_2)$, $T_L = 0.5(0.5)5.0$ MeV/amu, the thin-target contributions to relative level populations at depths ℓ in the target were calculated:

$$P_f \equiv d\sigma_{I_fK}(\ell,T_{iL}) \approx P_{I_fK}\left\{\bar{q}\left[E_2(\ell,T_{iL})\right]\right\}\sum_j d\sigma_R\left[\theta_{jCM}; E_2(\ell,T_{iL})\right]\frac{\text{barn}}{\text{nucl.}} \quad \text{(VI-41)}$$

Under the assumption that scattering produced negligible attenuation of incident beam current in the energy range of interest, these were integrated to form the thick-target relative populations:

$$\mathcal{P}_f(T_{iL};\ell_{cut}) = \int_0^{\ell_{cut}} d\sigma_{I_fK}(\ell,T_{iL})\,d\ell \;\frac{\text{barn}}{\text{nucl.}} - \text{cm.} \qquad \text{(VI-42)}$$

In practice, depths were expressed in mg. cm.$^{-2}$ and P_f were obtained in barn/nucl.-mg./cm.^{2} For relative cross-section comparisons, this unit is sufficient; for absolute excitation probabilities, multiplication by $N \frac{\text{nuclei}}{\text{cm.}^3} \times 10^{-24} \frac{\text{cm.}^2}{\text{barn}} \Big/ \rho \frac{\text{mg.}}{\text{cm.}^3}$ is necessary, and for comparison to laboratory line intensities, a good beam integration is needed.

In going from E_2 to E_3 (Fig. A-2) by means of the Q-equation, the angles $\overline{\theta}_L$ corresponding to $\overline{q}$ are required. They are (Fig. VI-2):

Element	$\overline{q}/q$	$\overline{\theta}_{CM}: q(\overline{\theta}_{CM}) = \overline{q}$
Tb	.91155	143.6°
Ho	.91093	143.45°
Lu	.91002	143.2°

The Q-equation is simply a consequence of momentum and energy conservation in a non-relativistic situation of collision of a projectile with a target to yield new (possibly identical) projectile and target, in which through changes in internal configurations of the colliding bodies an amount of energy Q (possibly less than zero) is liberated. The equation as commonly stated in terms of laboratory parameters reads[222]

$$Q = -E_1\left(1 - \frac{M_1}{M_4}\right) + E_3\left(1 + \frac{M_3}{M_4}\right) - \frac{2}{M_4}\sqrt{M_1 M_3 E_1 E_3}\ \cos\theta_L \qquad \text{(VI-43)}$$

where E_1, E_2, E_3, E_4 are the kinetic energies of the original projectile and target and final projectile and target, in the 1(2,4)3 reaction, and M_1 to M_4 are their masses. In the case of Coulomb excitation $M_1 = M_3 \equiv m$, $M_2 = M_4 \equiv M$, and $Q \ll E_j$ may be ignored. With the definitions

$$\mathcal{E} \equiv \frac{E_3}{E_1} \quad ; \qquad \delta \equiv \frac{Q}{E_1} \;, \tag{VI-44}$$

the Q-equation becomes:

$$\sqrt{\mathcal{E}} = \frac{m/M}{1+m/M} \cos\theta_L \pm \sqrt{\left(\frac{m/M}{1+m/M}\cos\theta_L\right)^2 + \frac{\delta+1-m/M}{1+m/M}} \;. \tag{VI-45}$$

For Coulomb excitation, $\delta < 0$, $|\delta| << 1$, so that with $\theta_L > 90^o$, in order to have $|\mathcal{E}| < 1$, the upper sign is required. It can be noted that $\mathcal{E}$ is independent of E_1 provided $\delta = 0$. Values of the average array laboratory angles corresponding to the c.m. angles for the cases studied, and corresponding $\delta = 0$ $\mathcal{E}$-values, are:

Process	$\bar{\theta}_{CM}$	$\bar{\theta}_L$	$\mathcal{E}(\delta=0)$
O^{16} on Tb^{159}	143.6°	139.88°	.69995
O^{16} on Ho^{165}	143.45°	139.87°	.70974
O^{16} on Lu^{175}	143.2°	139.82°	.72468

For $\delta \neq 0$ the radical may be written in the form

$$\sqrt{(\delta)} = \sqrt{(\delta=0)}\left[1 + C_\delta \delta + \tfrac{3}{2} C_\delta \delta^2 + \ldots\right] ,$$
$$C_\delta = \frac{1}{2} \frac{1}{1+m/M} \frac{1}{\sqrt{(\delta=0)}} \tag{VI-46}$$

from which values of C_δ are:

Process	O^{16} on Tb^{159}	Ho^{165}	Lu^{175}
C_δ	.5522	.5506	.5477

Now $-\delta \propto \Delta E$ for an excited level. If, say, $\Delta E = 400$ keV, then with $E_1 = 4$ MeV/amu $= 64$ MeV, one has $\delta = -0.00625$, $1 + C_\delta \delta \sim 1 - 0.55 \times 0.00625 = 1 - 0.0034$, entailing an error for the $Q=0$ case of less than 0.4%. The $Q=0$ approximation was used in the calculations.

For the gamma-ray-ion coincidence runs the integral discriminator was set to accept the thick-target scattered-ion spectrum from maximum energy down to a cutoff energy set at half the "average maximum backscatter energy", which may be taken as $\mathcal{E}(\bar{\theta}_L)T_{1L}$, T_{1L} being the incident laboratory beam energy. $\mathcal{E}$, being independent of effective incident energy E_2, is therefore independent of depth ℓ in the target at which scattering occurs.

From the range-energy curves and the Q-equation, pertinent parameters of the thick-target ion-scattering processes were calculated at various incident beam energies and target depths, as required. Target depths for zero emergent ion energies and ion energies at the cutoff setting, for O^{16} on Tb^{159}, are shown as a function of incident beam energy in Fig. VI-6. From these data $\mathcal{P}_f$, the thick-target relative final-state population probabilities in barn/nucl.-mg./cm.^{2} were calculated from (VI-42) in the form:

$$\mathcal{P}_{I_f}(T_{iL}, \ell_{cut}) = \int_0^{\ell_{cut}} P_{I_f K}\left\{\bar{q}\left[E_2(\ell, T_{iL})\right]\right\} \sum_j d\sigma_R\left[\theta_{j\,CM}, E_2(\ell, T_{iL})\right] d\ell \qquad \text{(VI-42a)}$$

(wherein ℓ's are expressed in mg./cm.^{2}). From P_I tables in A.W. and Graetzer et al.[225], $P_{I_f, K=3/2}$ values were obtained at appropriate $\bar{q}(E) = \bar{q}\left[E_2(\ell, T_{1L} = 4.08 \text{ MeV/amu})\right]$ for O^{16} on Tb^{159},

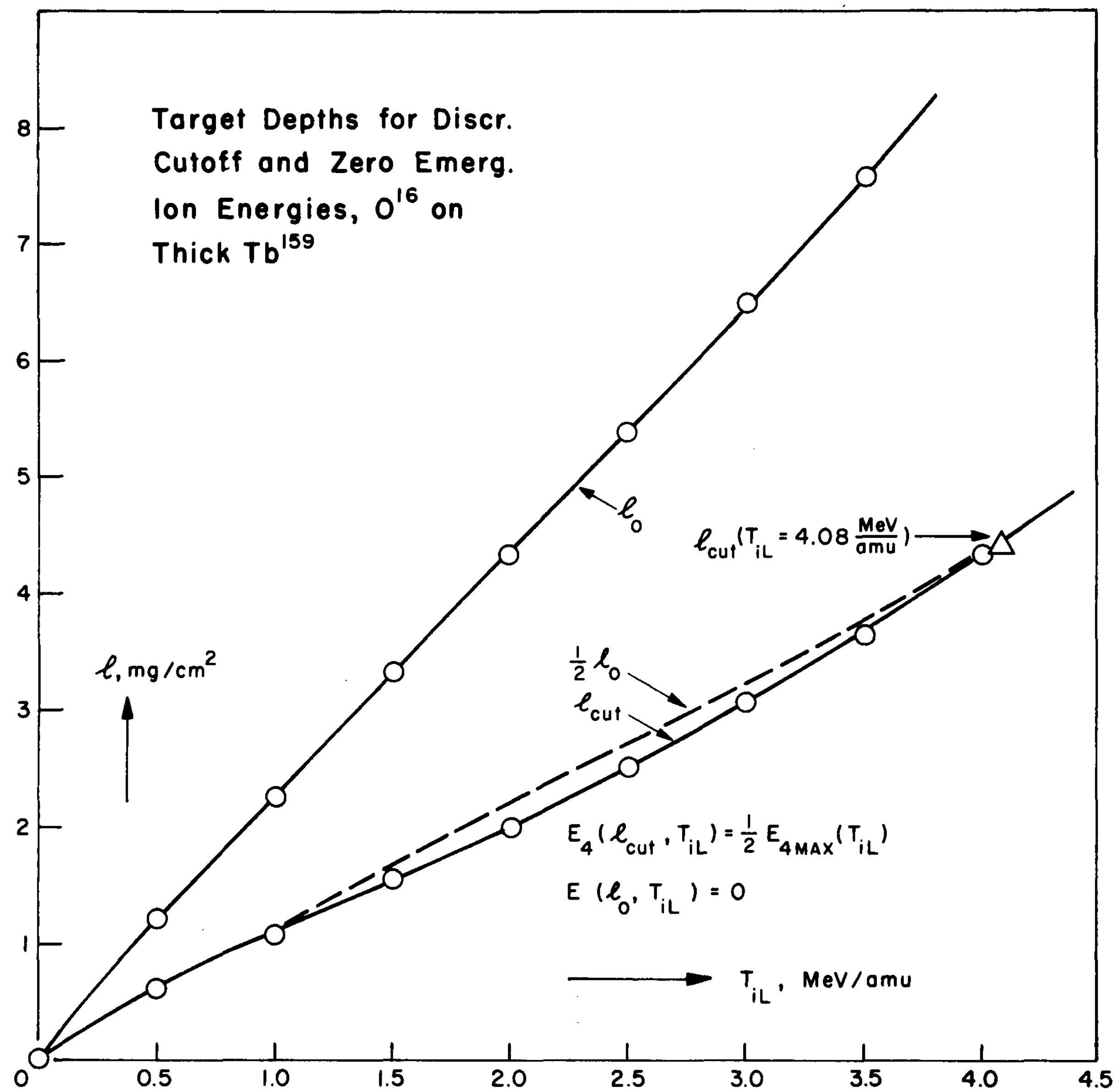

Target Depths for Discr.
Cutoff and Zero Emerg.
Ion Energies, O^{16} on
Thick Tb^{159}
ℓ_0
$\ell_{cut}(T_{iL} = 4.08 \frac{MeV}{amu})$
ℓ, mg/cm^2
$\frac{1}{2}\ell_0$
ℓ_{cut}
$E_4(\ell_{cut}, T_{iL}) = \frac{1}{2} E_{4MAX}(T_{iL})$
$E(\ell_0, T_{iL}) = 0$
T_{iL}, MeV/amu
0
0.5
1.0
1.5
2.0
2.5
3.0
3.5
4.0
4.5
1
2
3
4
5
6
7
8

FIG VI-6

providing in effect $P_{I_f 3/2}$ as a function of ℓ. These were multiplied by $\sum_j d\sigma_R\left[\Theta_{jCM}; E_2(\ell, T_{iL} = 4.08\ \mathrm{MeV/amu})\right]$, with the results shown in Table VI-2. Semi-log plots of $\sum_j d\sigma_R\ (\bar{q}_j)$ and $P_{I_f 3/2} \sum_j d\sigma_R$ barn/nucl. as functions of ℓ mg./cm.^{2} are shown in Fig. VI-7 and VI-8 respectively.

It can be noted that so far the only connection of the level populations to their energies in the ground-state band is through the dependence of q on Q_O, which in turn is related to the energy levels through the inertia moments consistent with that nuclear flow pattern which sustains the shape implied by Q_O in rotation with the necessary number of units of angular momentum. These relative populations as a function of ℓ were integrated from 0 to ℓ_{cut} to provide the thick-target populations, in barn/nucl.-mg./cm.^{2} A semi-log plot of these populations against the Tb ground-state band energies found in this work is shown in Fig. VI-9.

The same procedure was done for 4.08 MeV/amu O^{16} on Ho^{165}, $Q_O = 7.5$ and 8.0, and Lu^{175}, $Q_O = 8.0$. $\sum_j d\sigma_R$ and $\bar{q}$ evaluated at appropriate $E_2(\ell)$ appear in Table A-4. $P_{I_f, K=7/2}\left\{\bar{q}\left[E(\ell)\right]\right\}$ for appropriate $\bar{q}$ values were obtained and multiplied by $\sum_j d\sigma_R\left[\theta_{jCM}, E_2(\ell; T_{iL} = 4.08\tfrac{\mathrm{MeV}}{\mathrm{amu}})\right]$ with results shown in Tables VI-3 and 4. Plots of $P_{I_f, K=7/2} \sum_j d\sigma_R$ as functions of ℓ are shown in Fig. VI-10 and 11, and of resulting $\mathcal{P}_{I_f} = \int_0^{\ell_{cut}} P_{I_f K} \sum_j d\sigma_R\, d\ell$, the thick-target populations, versus the level energies found in this work, in Fig. VI-12 and 13.

Unlike the situation in even-even nuclei, there is no simple correlation within odd-A ground-state bands between one gamma-ray intensity and the populations of the band levels

Table VI-2

O^{16} on Tb^{159}, Q_o=8.1, Thick-Target Integration

$\ell_{\text{mg./cm.}^2}$	$I_f =$ 5/2	7/2	9/2	11/2	13/2	15/2	17/2	19/2	21/2	23/2
	$100\, P_{I_f, K=3/2} \sum_j d\sigma_R (\theta_{jcm}) =$									
0	2.664	2.900	2.619	1.748	.8282	.4447	.1302	.0620	.01197	.0040
.15	2.744	2.947	2.621	1.740	.8125	.4347	.1255	.0595	.01114	.00448
1.15	3.326	3.281	2.627	1.676	.7067	.3691	.0962	.0450	.00698	.00276
2.15	3.922	3.615	2.587	1.592	.6014	.3087	.0720	.0332	.00438	.00188
3.15	4.604	3.940	2.503	1.490	.5106	.2513	.0525	.0239	.00271	.00118
4.15	5.285	4.262	2.388	1.380	.4118	.2025	.0374	.0166	.00166	.00074
ℓ_{cut}=4.43	5.484	4.341	2.329	1.332	.3807	.1863	.0331	.0147	.00132	.00057
Thick-target relative populations, $100\,\rho_{I_fK}$*	17.76	16.09	11.30	6.975	2.666	1.366	.3292	.1524	.02208	.00900

$$*\rho_{I_fK} = \int_0^{\ell_{cut}} P_{I_fK} \sum \delta\sigma_R \, d\ell$$

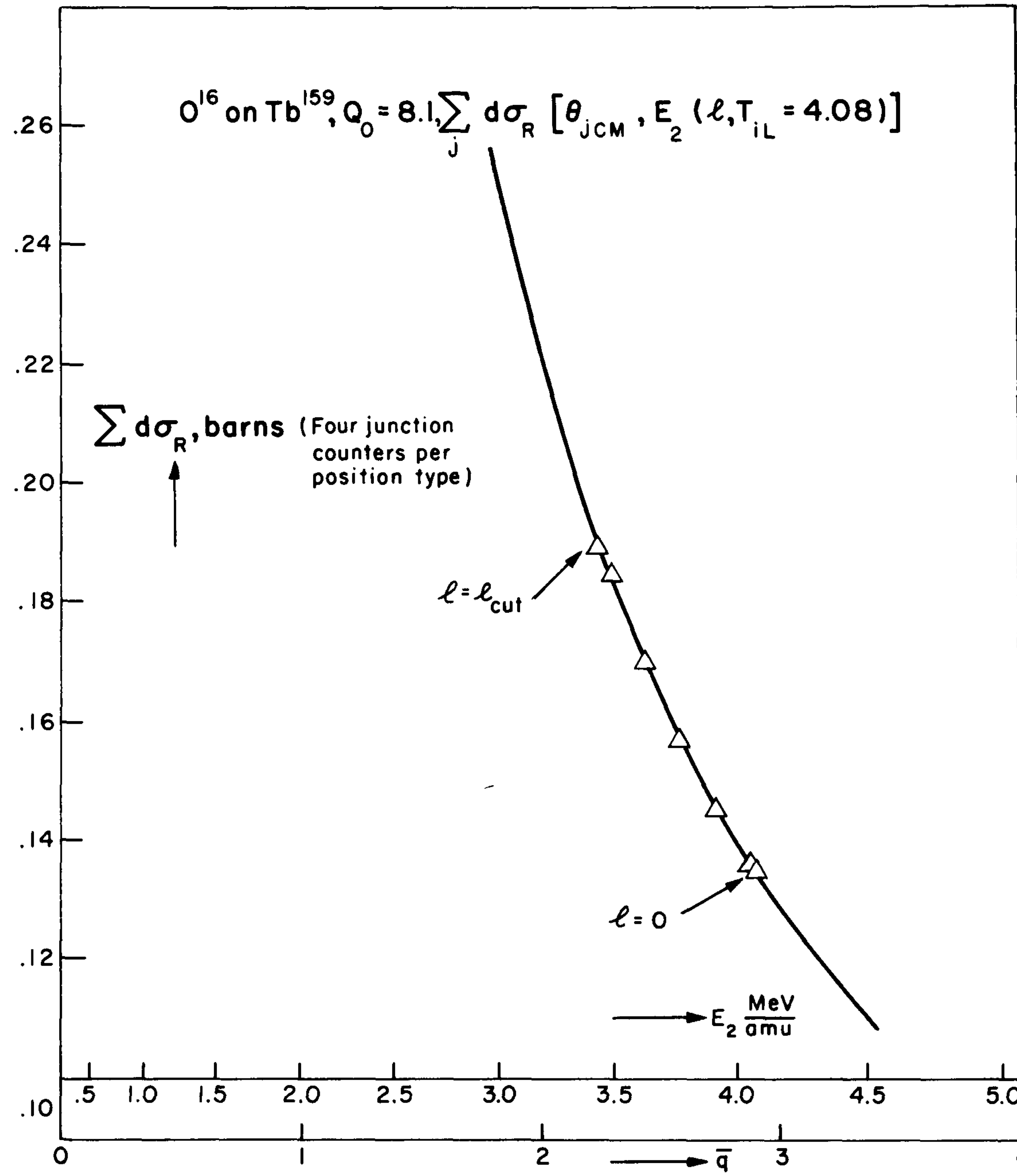

O^{16} on Tb^{159}, $Q_0 = 8.1$, $\sum_j d\sigma_R\,[\theta_{jCM}, E_2(\ell, T_{iL} = 4.08)]$
$\sum d\sigma_R$, barns (Four junction counters per position type)
$\ell = \ell_{cut}$
$\ell = 0$
$E_2\,\frac{MeV}{amu}$
$\bar{q}$
.26
.24
.22
.20
.18
.16
.14
.12
.10
.5
1.0
1.5
2.0
2.5
3.0
3.5
4.0
4.5
5.0
0
1
2
3
4

FIG VI-7

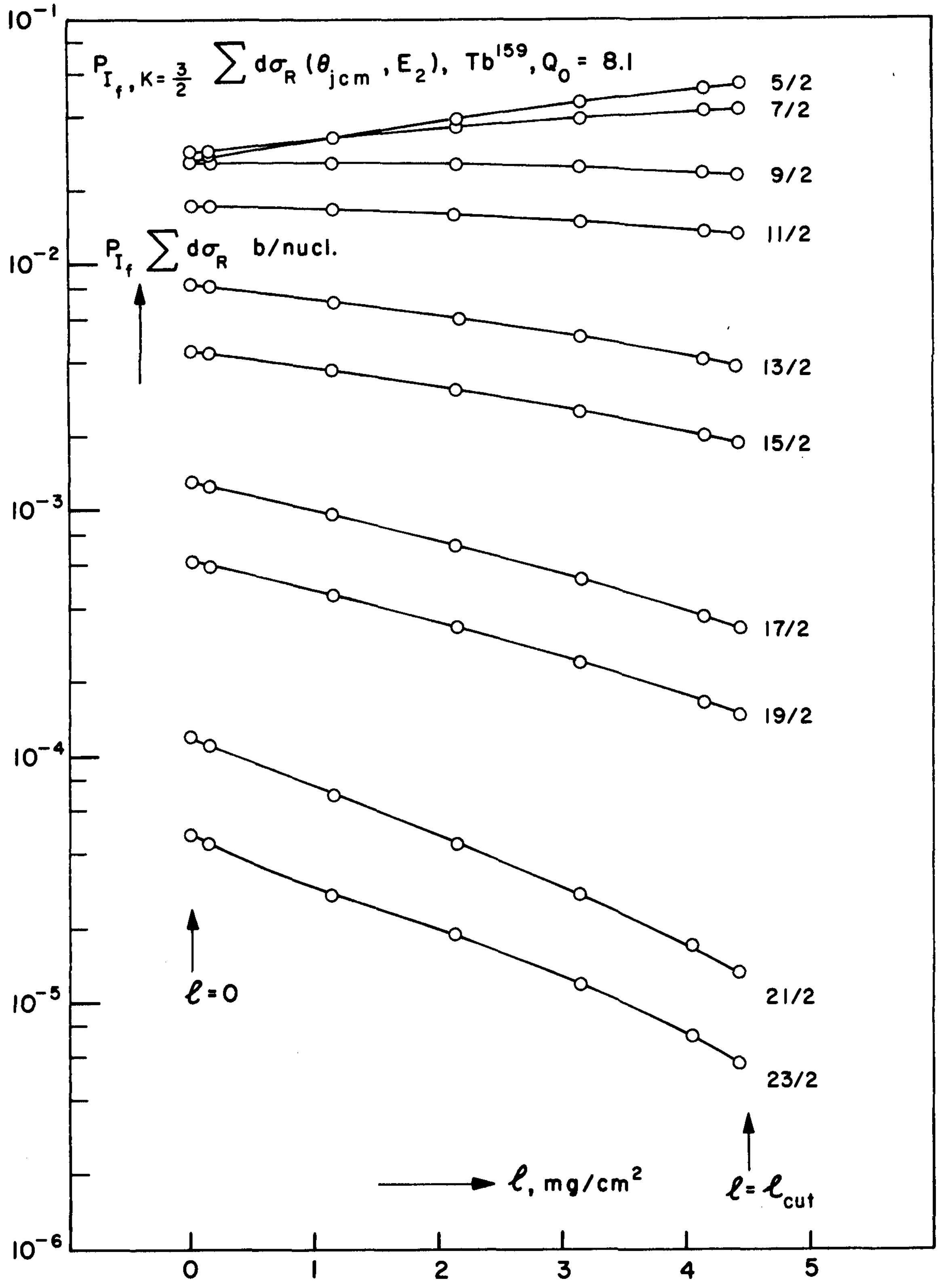

$P_{I_f, K=\frac{3}{2}} \sum d\sigma_R(\theta_{jcm}, E_2)$, Tb^{159}, $Q_0 = 8.1$
$P_{I_f} \sum d\sigma_R$ b/nucl.
5/2
7/2
9/2
11/2
13/2
15/2
17/2
19/2
21/2
23/2
$\ell = 0$
ℓ, mg/cm^2
$\ell = \ell_{cut}$
10^{-1}
10^{-2}
10^{-3}
10^{-4}
10^{-5}
10^{-6}
0
1
2
3
4
5

FIG VI-8

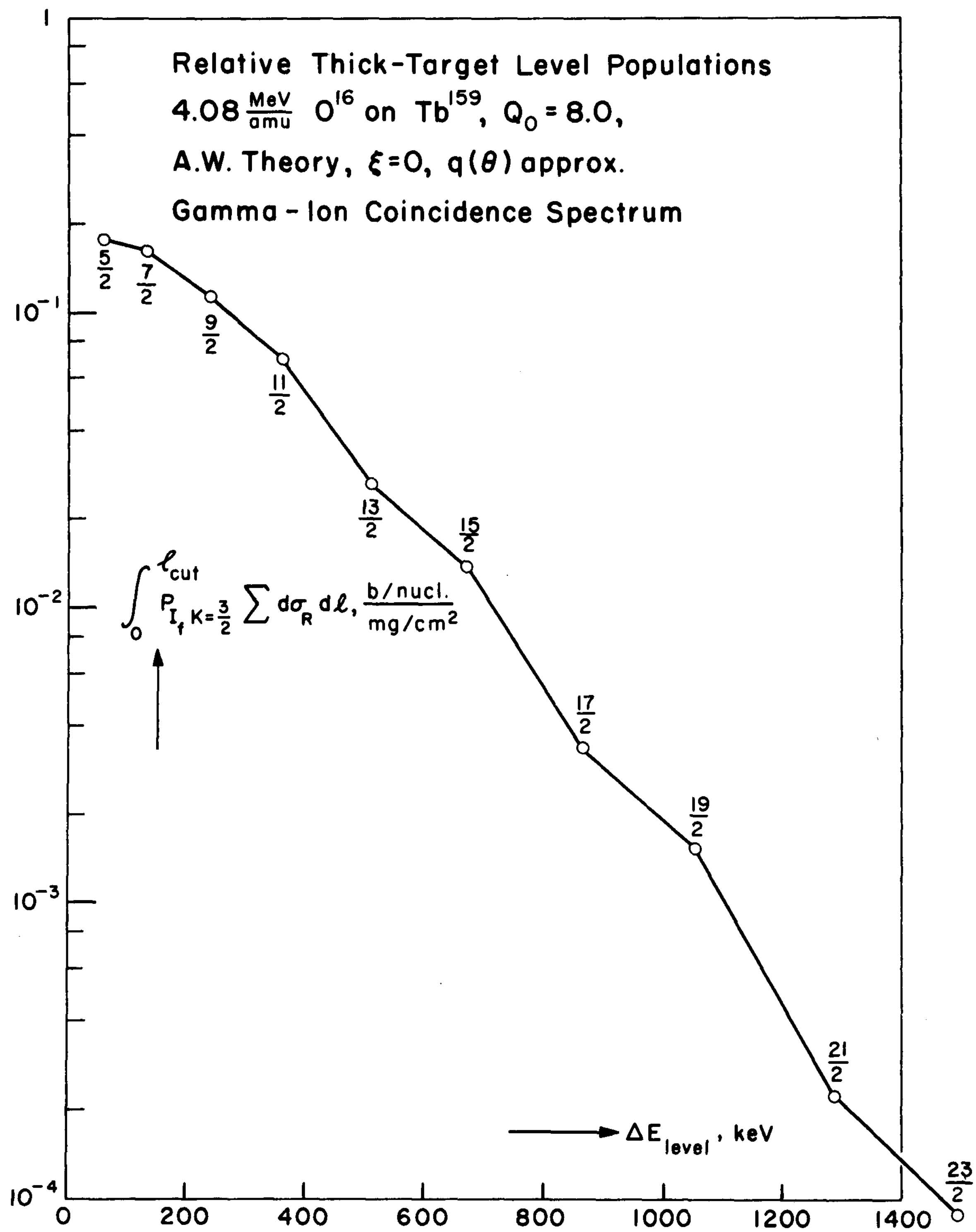
Relative Thick-Target Level Populations
4.08 $\frac{MeV}{amu}$ O^{16} on Tb^{159}, $Q_0 = 8.0$,
A.W. Theory, $\xi = 0$, $q(\theta)$ approx.
Gamma - Ion Coincidence Spectrum
$\int_0^{\ell_{cut}} P_{I_f K=\frac{3}{2}} \sum d\sigma_R \, d\ell$, $\frac{b/nucl.}{mg/cm^2}$
ΔE_{level}, keV
1
10^{-1}
10^{-2}
10^{-3}
10^{-4}
0
200
400
600
800
1000
1200
1400
$\frac{5}{2}$
$\frac{7}{2}$
$\frac{9}{2}$
$\frac{11}{2}$
$\frac{13}{2}$
$\frac{15}{2}$
$\frac{17}{2}$
$\frac{19}{2}$
$\frac{21}{2}$
$\frac{23}{2}$

FIG VI-9

O^{16} on Ho^{165}, Thick-Target Integration

$100 P_{I_f J} \sum d\sigma_R(\theta_{jcm})$ ($Q_0 = 7.5$)

ℓ mg./cm.^{2}	I_f = 9/2	11/2	13/2	15/2	17/2	19/2	21/2	23/2
0	4.221	2.742	1.467	.6394	.2342	.08016	.02115	.00657
.15	4.276	2.740	1.457	.6296	.2284	.07763	.02020	.00635
1.17	4.654	2.777	1.332	.5624	.1899	.06216	.01546	.00464
2.19	5.025	2.787	1.270	.4970	.1551	.04875	.01115	.00349
3.21	5.402	2.780	1.169	.4337	.1232	.03704	.00827	.00252
4.23	5.742	2.761	1.062	.3760	.0974	.02841	.00607	.00196
ℓ_{cut} = 4.58	5.818	2.731	1.011	.3514	.0878	.02543	.00525	.00182
Thick-target relative populations, 100 I_fK*	23.17	12.70	5.765	2.259	.7094	.2252	.0353	.0166

$100 P_{I_f J} \sum d\sigma_R(\theta_{jcm})$ ($Q_0 = 8.0$)

ℓ mg./cm.^{2}								
0	4.045	2.906	1.701	.7949	.3172	.1147	.03272	.01029
.15	4.111	2.918	1.690	.7834	.3097	.1113	.03131	.00981
1.17	4.555	2.981	1.608	.7048	.2601	.08938	.02428	.00726
2.19	4.998	3.023	1.499	.6262	.2143	.07054	.01764	.00532
3.21	5.432	3.039	1.398	.5495	.1733	.05466	.01259	.00396
4.23	5.893	3.045	1.287	.4785	.1366	.04115	.00921	.00294
ℓ_{cut} = 4.58	6.016	3.025	1.235	.4482	.1231	.0365	.00807	.00262
Thick-target relative populations, 100 ρ_{I_fK}*	25.69	13.78	6.852	2.844	.9797	.3258	.0833	.0256

$* \rho_{I_f K} = \int_0^{\ell_{cut}} P_{I_f K} \sum \delta\sigma_R \, d\ell$

Table VI-4

O^{16} on Lu^{175}, Thick-Target Integration

	$I_f =$ 9/2	11/2	13/2	15/2	17/2	19/2	21/2	23/2
$\ell = 0$	4.825	2.948	1.488	.6219	.2148	.07112	.01802	.00547
$100 P_{I_f} \sum_j d\sigma_R(\theta_{jCM})$	4.881	2.952	1.464	.6116	.2093	.06980	.01722	.00520
	5.260	2.965	1.377	.5445	.1729	.04585	.01288	.00400
$(Q_0 = 8.0)$	5.651	2.964	1.276	.4793	.1394	.04272	.00956	.00300
	5.987	2.938	1.161	.4169	.1110	.03280	.00709	.00223
	6.298	2.888	1.039	.3557	.0861	.02493	.00507	.00177
$\ell = \ell_{cut}$	6.387	2.865	.9859	.3323	.0771	.02220	.00435	.00160
Thick-target relative populations, $100 \rho_{I_f K}$*	27.21	14.13	5.989	2.271	.6748	.2064	.0472	.0148

$$* \rho_{I_f K} = \int_0^{\ell_{cut}} P_{I_f K} \sum \delta\sigma_R \, d\ell$$

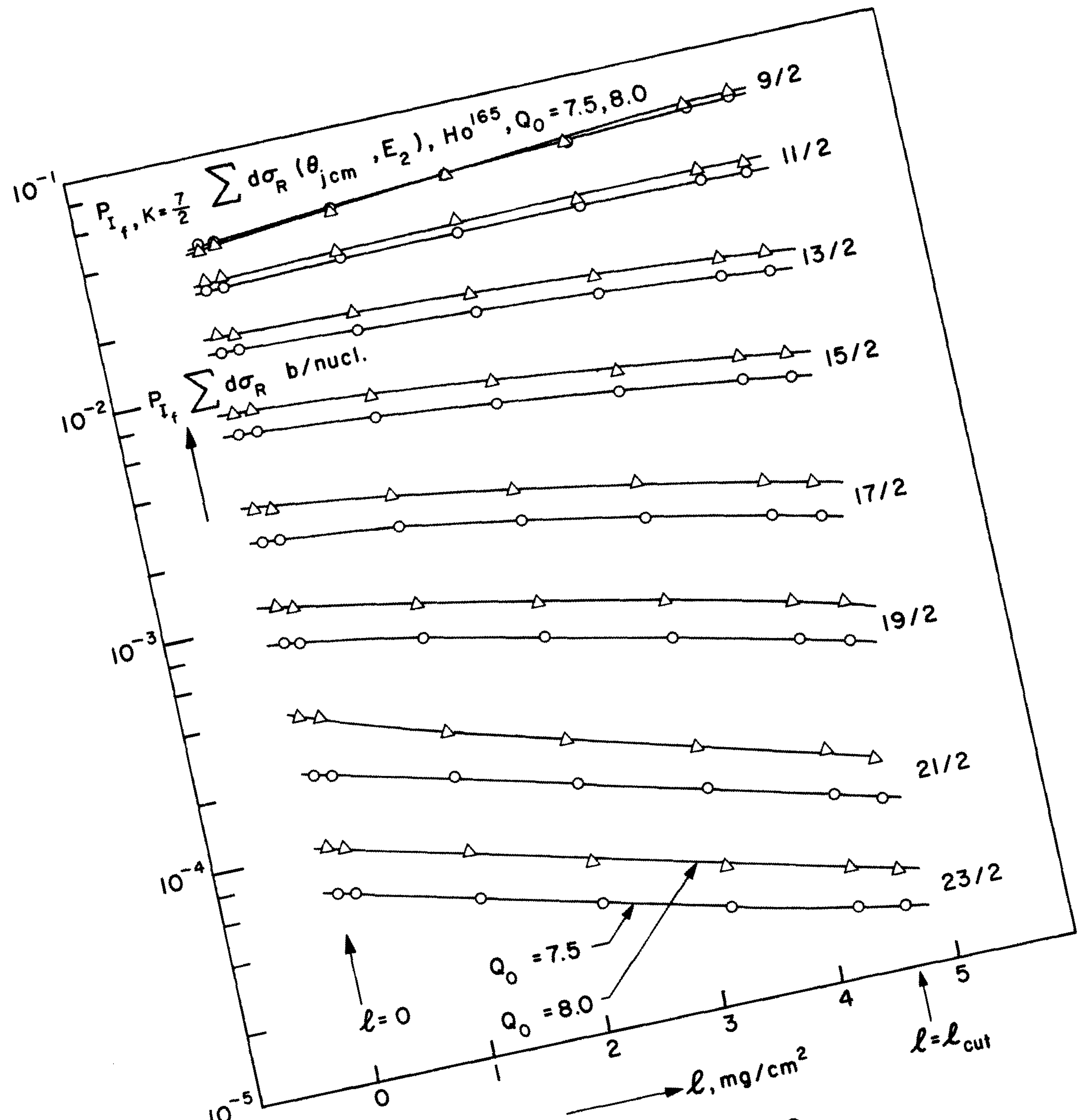

$P_{I_f, K=\frac{7}{2}} \sum d\sigma_R (\theta_{jcm}, E_2)$, Ho^{165}, $Q_0 = 7.5, 8.0$
$P_{I_f} \sum d\sigma_R$ b/nucl.
9/2
11/2
13/2
15/2
17/2
19/2
21/2
23/2
10^{-1}
10^{-2}
10^{-3}
10^{-4}
10^{-5}
$Q_0 = 7.5$
$Q_0 = 8.0$
$\ell = 0$
$\ell = \ell_{cut}$
0
1
2
3
4
5
ℓ, mg/cm^2

FIG VI - 10

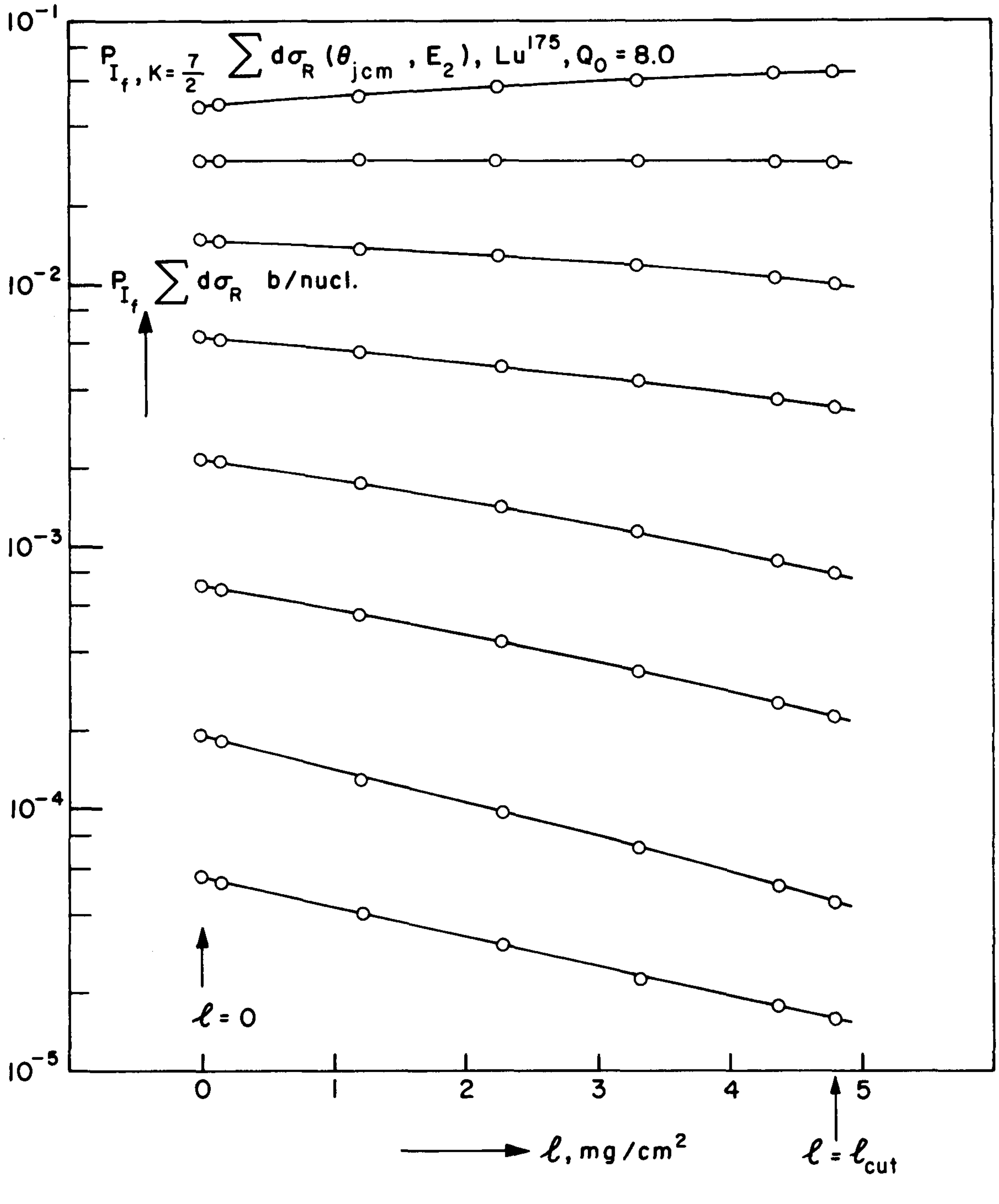

$P_{I_f, K=\frac{7}{2}} \sum d\sigma_R (\theta_{jcm}, E_2)$, Lu^{175}, $Q_0 = 8.0$
$P_{I_f} \sum d\sigma_R$ b/nucl.
10^{-1}
10^{-2}
10^{-3}
10^{-4}
10^{-5}
$\ell = 0$
0
1
2
3
4
5
ℓ, mg/cm^2
$\ell = \ell_{cut}$

FIG VI - 11

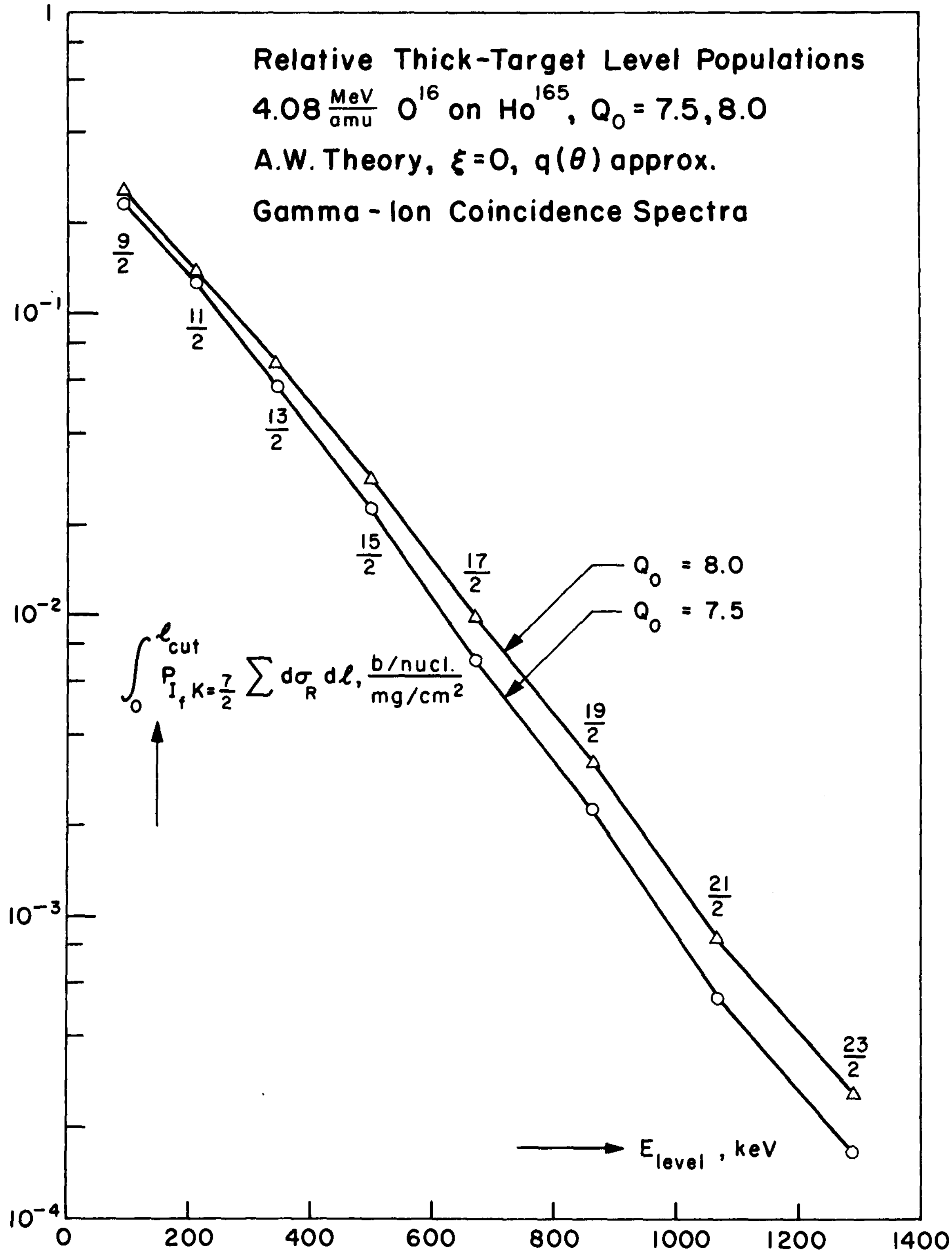

Relative Thick-Target Level Populations
$4.08 \frac{MeV}{amu}$ O^{16} on Ho^{165}, $Q_0 = 7.5, 8.0$
A.W. Theory, $\xi = 0$, $q(\theta)$ approx.
Gamma - Ion Coincidence Spectra
$\int_0^{\ell_{cut}} P_{I_f K=\frac{7}{2}} \sum d\sigma_R \, d\ell, \frac{b/nucl.}{mg/cm^2}$
Q_0 = 8.0
Q_0 = 7.5
E_{level}, keV
$\frac{9}{2}$
$\frac{11}{2}$
$\frac{13}{2}$
$\frac{15}{2}$
$\frac{17}{2}$
$\frac{19}{2}$
$\frac{21}{2}$
$\frac{23}{2}$
1
10^{-1}
10^{-2}
10^{-3}
10^{-4}
0
200
400
600
800
1000
1200
1400

FIG VI-12

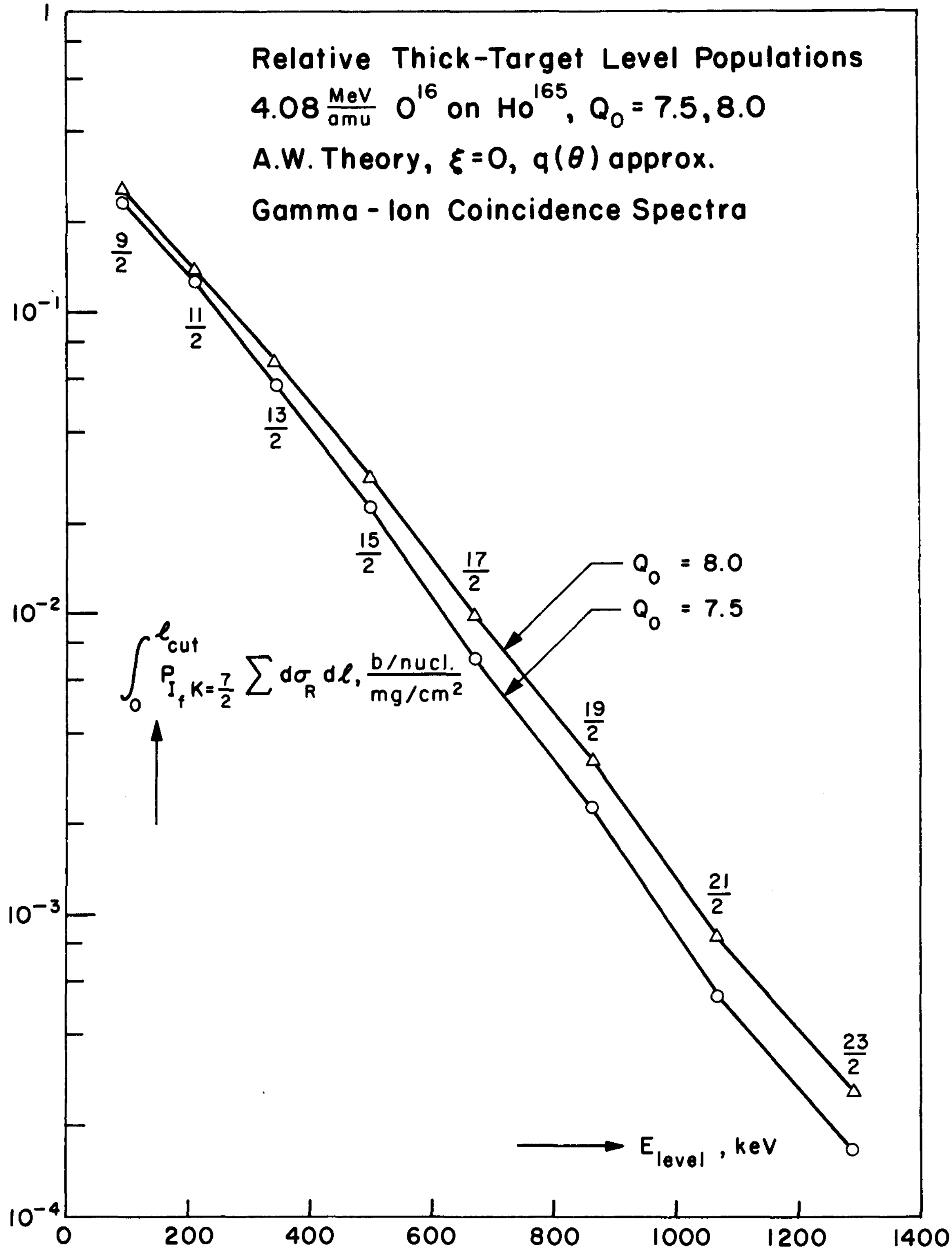

Relative Thick-Target Level Populations
4.08 $\frac{MeV}{amu}$ O^{16} on Ho^{165}, Q_0 = 7.5, 8.0
A.W. Theory, ξ = 0, $q(\theta)$ approx.
Gamma - Ion Coincidence Spectra
Q_0 = 8.0
Q_0 = 7.5
$\int_0^{\ell_{cut}} P_{I_f K=\frac{7}{2}} \sum d\sigma_R \, d\ell, \frac{b/nucl.}{mg/cm^2}$
E_{level}, keV
9/2
11/2
13/2
15/2
17/2
19/2
21/2
23/2
1
10^{-1}
10^{-2}
10^{-3}
10^{-4}
0
200
400
600
800
1000
1200
1400

FIG VI - 12

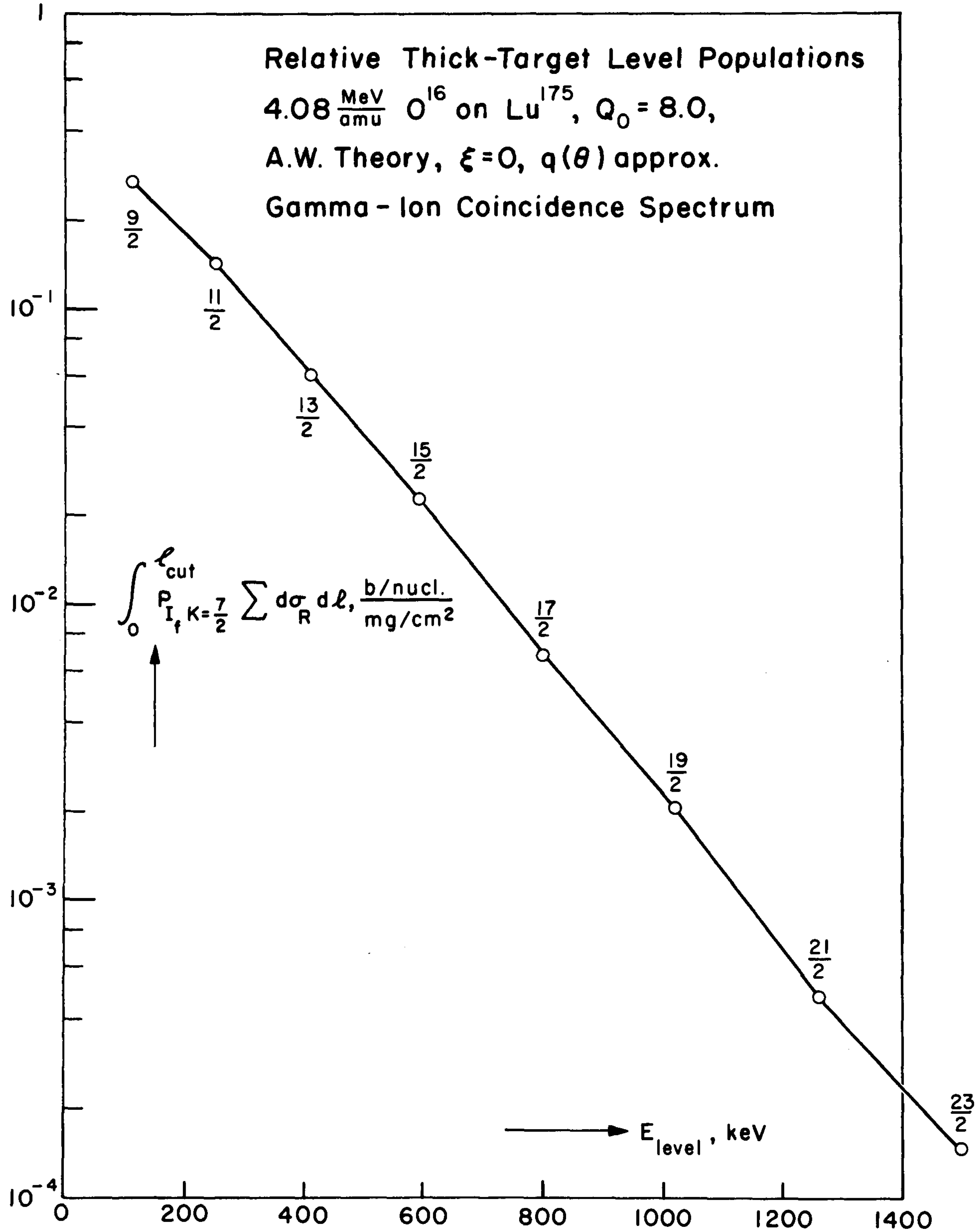
Relative Thick-Target Level Populations
4.08 MeV/amu O^{16} on Lu^{175}, $Q_0 = 8.0$,
A.W. Theory, $\xi=0$, $q(\theta)$ approx.
Gamma - Ion Coincidence Spectrum
$\int_0^{\ell_{cut}} P_{I_f K=\frac{7}{2}} \sum d\sigma_R \, d\ell, \frac{b/nucl.}{mg/cm^2}$
E_{level}, keV
9/2
11/2
13/2
15/2
17/2
19/2
21/2
23/2
1
10^{-1}
10^{-2}
10^{-3}
10^{-4}
0
200
400
600
800
1000
1200
1400

FIG VI-13

above the final state of that particular radiative transition. This derives from the possibility of E2 decay to either of the two next lower levels rather than uniquely to one level below, with the concomitant rapidly rising number of alternative paths available for decay of the higher levels to the ground state. The value of the branching ratio for $\Delta I = -1$ to $\Delta I = -2$ transitions is affected by an M1 component in the former decays, and of course, somewhat by internal conversion.

It is possible to show that the duration of the excitation process is very short compared to the mean life of any level against radiative or internally-converted decay. From the relativistic relation between projectile rest mass, kinetic energy and speed, for 4.08 MeV/amu O^{16} one has $T/M_0c^2 = 4.380\times10^{-3}$ or $\beta^2 = .008817$, $\beta \equiv v/c = .094$, $v = 2.8\times10^9$ cm./sec. Half the closest approach in head-on collisions, $a = Z_1Z_2e^2/(\mu v^2) = Z_1Z_2\frac{m_0}{\mu}\frac{r_0}{\beta^2}$, with m_0 = electron rest mass, μ = O^{16}-ion reduced mass, r_0 = classical electron radius, turns out to be as follows:

Process	a	$\tau_c = \frac{4a}{v}$
4.08 MeV/amu O^{16} on Tb^{159}	6.27 f.	8.91×10^{-22} sec.
Ho^{165}	6.44 f.	9.16×10^{-22} sec.
Lu^{175}	6.79 f.	9.65×10^{-22} sec.

A rough measure of the "collision time" is taken as $\tau_c \sim 4a/v$, and has the values above. So the projectile is near the target nucleus for $\sim10^{-12}$ nanosec. Any decay of any of the observed levels via gamma emission or internal conversion takes place in a time $> 10^{-3}$ nanosec. Hence any interference between excitation and deexcitation processes is negligible, and the full multiple-excitation thick-target populations may be taken as the initial conditions for the deexcitation problem.

Let the levels be numbered in order of increasing energy: 0 (ground state), 1,2,3,... Let P_i be the relative amount of population of the i^{th} excited level by thick-target multiple Coulomb excitation; P'_i the relative amount of population by deexcitation of a higher level. Define $\mathcal{P}_i = P_i + P'_i$ = total relative population of the level due to all causes. Set t_{ij} = transition probability for a level i→level j transition, given that level i is populated, and $I_{ij} = \mathcal{P}_i t_{ij}$ = relative intensity of the i→j transition. $t^{E2}_{i+1,i}$, $t^{M1}_{i+1,i}$, $t^{E2}_{i+2,i}$ will be taken as known, from the Alaga rules and the mixing ratios, and any other t_{ij} will be set equal to zero.

One has obviously,

$$\sum_{j \neq i} t_{ij} = 1 . \tag{VI-47}$$

Also,

$$P'_i = \sum_{j \neq i} I_{ji} \quad , \tag{VI-48}$$

whence in the present context,

$$I_{i,i-\mu} = \mathcal{P}_i t_{i,i-\mu} \quad (\mu = 1,2 \; ; \; i \geq \mu) \; ; \tag{VI-49}$$

$$\mathcal{P}_i = P_i + I_{i+1,i} + I_{i+2,i} \qquad (i \geq 0) \; ; \tag{VI-50}$$

from which,

$$-\mathcal{P}_{i+2}\, t_{i+2,i} - \mathcal{P}_{i+1}\, t_{i+1,i} + \mathcal{P}_i = P_i \ , \qquad \text{(VI -51)}$$

which can be written in matrix form to advantage:

$$(\mathcal{P}_0\ \mathcal{P}_1\ \mathcal{P}_2\ \mathcal{P}_3\ \mathcal{P}_4 \ldots)\begin{pmatrix} 1 & 0 & 0 & 0 & 0 & \ldots \\ -t_{10} & 1 & 0 & 0 & 0 & \ldots \\ -t_{20} & -t_{21} & 1 & 0 & 0 & \ldots \\ 0 & -t_{31} & -t_{32} & 1 & 0 & \ldots \\ 0 & 0 & -t_{42} & -t_{43} & 1 & \ldots \\ \vdots & \vdots & \vdots & \vdots & \vdots & \end{pmatrix} \qquad \text{(VI-51a)}$$

$$= (P_0\ P_1\ P_2\ P_3\ P_4\ \ldots)$$

or

$$\|\mathcal{P}\|\ \|t\| = \|P\| \ . \qquad \text{(VI-51b)}$$

In this way the problem of deducing I_{ij} from P_i given by multiple Coulomb excitation theory is reduced, with the aid of $I_{ij} = \mathcal{P}_i t_{ij}$, essentially to that of inverting $\|t\|$. Now if $\|t\|$ is cut off at any finite rank the determinant is $+1$, so that the infinite matrix is non-singular and can be inverted. Calling this inverse matrix $\|t\|^{-1} = \|u\|$, it turns out that $\|u\|$ is of the form

$$\|u\| = \begin{pmatrix} 1 & 0 & 0 & 0 & 0 & \ldots \\ 1 & 1 & 0 & 0 & 0 & \ldots \\ 1 & u_{21} & 1 & 0 & 0 & \ldots \\ 1 & u_{31} & u_{32} & 1 & 0 & \ldots \\ 1 & u_{41} & u_{42} & u_{43} & 1 & \ldots \\ \vdots & \vdots & \vdots & \vdots & \vdots & \end{pmatrix} \qquad \text{(VI-52)}$$

(In general, in the presence of transitions of all multipolarities, $t_{ij} \neq 0$, $i,j \geq 0$, and $t_{ii} \equiv 1$. Then $\|\mathcal{P}\|\,\|t\| = \|P\|$ reads

$$P_K = \mathcal{P}_K + \sum_{j=K+1}^{\infty} \mathcal{P}_j t_{jK} \,, \tag{VI-51c}$$

with the solution $\|\mathcal{P}\| = \|P\|\,\|u\|$:

$$\mathcal{P}_K = P_K + \sum_{j=K+1}^{\infty} P_j u_{jK} \quad . \tag{VI-53}$$

Two points emerge: first, if $t_{i,i+\nu} \equiv 0$, $\nu > \nu_0$, ν_0 = finite positive integer, it is still true in general and in the present case that $u_{i,i+\nu} \neq 0$ for arbitrarily large ν, i.e., that in $\|u\|$ the triangular block of u_{ij} is all "full"; and second, $u_{ii} \equiv 1$, which via (VI-53), $k=0$, reflects the fact that $\mathcal{P}_0 = \sum_{j=0}^{\infty} P_j$, i.e., that all states depopulate ultimately to the ground state.

Now for the ground-state bands in question, for which pure-rotational-band expressions are expected to be quite accurate, one has[1,2,32] the radiative transition probabilities per unit time for a transition from state i to state j:

$$T_\lambda^{(\gamma)} = \frac{8\pi(\lambda+1)}{\lambda[(2\lambda+1)!!]^2} \frac{1}{\hbar}\left(\frac{\omega}{c}\right)^{2\lambda+1} B(\lambda; I_i \to I_f)$$

$$T^{(\gamma)}(E2) = \frac{4\pi}{75}\frac{1}{\hbar}\left(\frac{\Delta E_{ij}}{\hbar c}\right)^5 B(E2; i \to j) \tag{VI-54}$$

$$T^{(\gamma)}(M1) = \frac{16\pi}{9}\frac{1}{\hbar}\left(\frac{\Delta E_{ij}}{\hbar c}\right)^3 B(M1; i \to j)$$

with, in cases where symmetry modifications do not apply,

$$B(E\lambda, i \to j) = \langle K|\mathcal{M}(E\lambda,0)|K\rangle^2 \langle I_i K \lambda 0 | I_j K\rangle^2 ;$$

$$B(E2, i \to j) = \frac{5}{16\pi} e^2 Q_0^2 \langle I_i K 2 0 | I_j K\rangle^2 \tag{VI-55}$$

$$B(M1, i\to j) = \frac{3}{4\pi}\left(\frac{e\hbar}{2Mc}\right)^2 (g_K - g_R)^2 K^2 \langle I_i K 1 0 | I_j K\rangle^2 ;$$

whence

$$T^{(\gamma)}_{I+2\to I} = T^{(\gamma)E2}_{I+2\to I} = \frac{1}{60}\,\frac{e^2Q_0^2}{\hbar}\left(\frac{\Delta E_{I+2,I}}{\hbar c}\right)^5 \langle I+2\ K\ 2\ 0 | I\ K\rangle^2$$

$$T^{(\gamma)}_{I+1\to I} = T^{(\gamma)E2}_{I+1\to I} + T^{(\gamma)M1}_{I+1\to I} = \frac{1}{60}\,\frac{e^2Q_0^2}{\hbar}\left(\frac{\Delta E_{I+2,I}}{\hbar c}\right)^5 \langle I+1\ K\ 2 0 | I K\rangle^2$$
$$+\frac{4}{3}\,\frac{1}{\hbar}\left(\frac{e\hbar}{2Mc}\right)^2 (g_K - g_R)^2 \left(\frac{\Delta E_{I+1,I}}{\hbar c}\right)^3 K^2 \langle I+1\ K\ 1\ 0 | I K\rangle^2 . \qquad \text{(VI-56)}$$

The mixing ratios for the $I+1\to I$ transitions are therefore

$$\delta^2_{I+1,I} = \frac{T^{(\gamma)E2}_{I+1\to I}}{T^{(\gamma)M1}_{I+1\to I}} = \frac{\frac{1}{60}\,\frac{e^2Q_0^2}{\hbar}\left(\frac{\Delta E_{I+1\to I}}{\hbar c}\right)^5 \langle I+1\ K\ 2 0 | I\ K\rangle^2}{\frac{4}{3}\,\frac{1}{\hbar}\left(\frac{e\hbar}{2Mc}\right)^2 (g_K-g_R)^2\left(\frac{\Delta E_{I+1,I}}{\hbar c}\right)^3 K^2 \langle I+1\ K 1 0 | I\ K\rangle^2}$$

$$= \frac{1}{80}\,\frac{e^2Q_0^2/\left(\frac{e\hbar}{2Mc}\right)^2}{(g_K-g_R)^2}\left(\frac{\Delta E_{I+1,I}}{\hbar c}\right)^2\left[\frac{\langle I+1\ K\ 2 0|I K\rangle}{K^2\langle I+1\ K 1 0|I K\rangle}\right]^2 = \left(\frac{Q_0\Delta E_{I+1,I}/(\hbar^2/M)}{g_K - g_R}\right)^2 \frac{3}{20}\,\frac{1}{I(I+2)} . \qquad \text{(VI-57)}$$

For a band with ground-state spin I_0 and spin for level i of $I_0 + i$, certain quantities may be defined:

$$F_i^{(1)\gamma} \equiv \frac{T^{(\gamma)M1}_{i\to i-1}}{\frac{3}{4}\,\frac{1}{\hbar}\left(\frac{e\hbar}{2Mc}\right)^2 (g_K-g_R)^2\left(\frac{\Delta E_{i,i-1}}{\hbar c}\right)^3} = K^2\langle I_0+i\ K\ 1\ 0 | I_0+i-1\ K\rangle^2$$
$$= K^2\,\frac{(I_0+i+K)(I_0+i-K)}{(I_0+i)(2I_0+2i+1)} ; \qquad \text{(VI-58)}$$

$$F_i^{(2)\gamma} \equiv \frac{T^{(\gamma)E2}_{i\to i-1}}{\frac{1}{60}\,\frac{e^2Q_0^2}{\hbar}\left(\frac{\Delta E_{i,i-1}}{\hbar c}\right)^5} = \langle I_0+i\ K\ 2 0 | I_0+i-1\ K\rangle^2$$
$$= 3K^2\,\frac{(I_0+i+K)(I_0+i-K)}{(I_0+i-1)(I_0+i)(I_0+i+1)(2I_0+2i+1)} ; \qquad \text{(VI-59)}$$

$$F_i'^{\gamma} \equiv \frac{T^{(\gamma)E2}_{i\to i-2}}{\frac{1}{60}\,\frac{e^2Q_0^2}{\hbar}\left(\frac{\Delta E_{i,i-2}}{\hbar c}\right)^5} = \langle I_0+i\ K\ 2 0 | I_0+i-2\ K\rangle^2$$
$$= \frac{3}{2}\,\frac{(I_0+i+K)(I_0+i-K)(I_0+i-1+K)(I_0+i-1-K)}{(I_0+i-1)(I_0+i)(2I_0+2i-1)(2I_0+2i+1)} \qquad \text{(VI-60)}$$

$$\delta_i^{(0)2} \equiv \frac{1}{20}\left(\frac{Q_0\Delta E_{i,i-1}/(\hbar/M)}{g_K-g_R}\right)^2 = \frac{(I_0+i-1)(I_0+i+1)}{3}\ \delta^2_{i\to i-1} . \qquad \text{(VI-61)}$$

Then,

$$F_i^{\gamma} \equiv \frac{T^{(\gamma)}_{i\to i-1}}{\frac{1}{60}\frac{e^2Q_0^2}{\hbar}\left(\frac{\Delta E_{i,i-1}}{\hbar c}\right)^5} = F_i^{(2)\gamma} + \frac{1}{\delta_i^{(0)2}} F_i^{(1)\gamma}\,, \tag{VI-62}$$

and, noting that in the presence of internal conversion, level-depopulation probabilities per unit time take the form $T_{ij} = T_{ij}^{(\gamma)}(1+\alpha_{tot}^{ij})$, and calling α_λ, β_λ the $E\lambda$ and $M\lambda$ conversion coefficients respectively, one has

$$t_{i,i-1} = \frac{T_{i\to i-1}}{T_{i\to i-1}+T_{i\to i-2}} \equiv \frac{1}{1+R_i}\;;$$
$$t_{i,i-2} = \frac{T_{i\to i-2}}{T_{i\to i-1}+T_{i\to i-2}} = 1 - t_{i,i-1} = \frac{1}{1+1/R_i}\;; \tag{VI-63}$$

where

$$R_i \equiv \frac{T_{i\to i-2}}{T_{i\to i-1}} = \frac{T^{E2}_{i\to i-2}}{T^{E2}_{i\to i-1}+T^{M1}_{i\to i-1}} = \frac{\left(\frac{\Delta E_{i,i-2}}{\Delta E_{i,i-1}}\right)^5 F_i'^{\gamma}\left(1+\alpha_2^{i,i-2}\right)}{F_i^{(2)\gamma}\left(1+\alpha_2^{i,i-1}\right)+\frac{1}{\delta_i^{(0)2}}F_i^{(1)\gamma}\left(1+\beta_1^{i,i-1}\right)}$$
$$\equiv R_i^{(E)} R_i^{(F)}\;; \tag{VI-64}$$

$$R_i^{(E)} = \left(\frac{\Delta E_{i,i-2}}{\Delta E_{i,i-1}}\right)^5,$$

$$R_i^{(F)} = 1\Big/\left\{\frac{F_i^{(2)\gamma}}{F_i'^{\gamma}}\,\frac{1+\alpha_2^{i,i-1}}{1+\alpha_2^{i,i-2}} + \frac{1}{\delta_i^{(0)2}}\,\frac{F_i^{(1)\gamma}}{F_i'^{\gamma}}\,\frac{1+\beta_1^{i,i-1}}{1+\alpha_2^{i,i-2}}\right\}$$
$$\equiv 1\Big/\left\{\frac{1}{R_{iE2}} + \frac{1}{\delta_i^{(0)2}}\,\frac{1}{R'}\right\}\;; \tag{VI-65}$$

$$R_{iE2}^{(F)} = \frac{1+\alpha_2^{i,i-2}}{1+\alpha_2^{i,i-1}}\,\frac{F_i'^{\gamma}}{F_i^{(2)\gamma}} = \frac{1+\alpha_2^{i,i-2}}{1+\alpha_2^{i,i-1}}\,\frac{\langle I_0+i\;K\;2\;0|I_0+i-2\;K\rangle^2}{\langle I_0+i\;K\;2\;0|I_0+i-1\;K\rangle^2}$$
$$= \frac{1+\alpha_2^{i,i-2}}{1+\alpha_2^{i,i-1}}\,\frac{(2I_0+i-1)(i-1)(I_0+i+1)}{2I_0^2(2I_0+2i-1)}\,, \qquad (K=I_0)\;;$$
$$R' = \frac{1+\alpha_2^{i,i-2}}{1+\beta_1^{i,i-1}}\,\frac{F_i'^{\gamma}}{F_i^{(1)\gamma}} = \frac{1+\alpha_2^{i,i-2}}{1+\beta_1^{i,i-1}}\,\frac{\langle I_0+i\;K\;2\;0|I_0+i-2\;K\rangle^2}{K^2\langle I_0+i\;K\;1\;0|I_0+i-1\;K\rangle^2} \tag{VI-66}$$
$$= \frac{1+\alpha_2^{i,i-1}}{1+\beta_1^{i,i-1}}\,\frac{3}{(I_0+i-1)(I_0+i+1)}\,R_{iE2}^{(F)} = \left(\frac{\delta_{i,i-1}}{\delta_i^{(0)}}\right)^2\frac{1+\alpha_2^{i,i-1}}{1+\beta_1^{i,i-1}}\,R_{iE2}\,,$$

the last equality holding because of (VI-61). Then,

$$\frac{1}{\mathcal{R}_i^{(F)}} = \frac{1}{\mathcal{R}_{i\,E2}^{(F)}}\left[1 + \frac{1}{\delta_{i,i-1}^2}\,\frac{1+\beta_1^{i,i-1}}{1+\alpha_2^{i,i-1}}\right] \quad . \tag{VI-67}$$

For the cases of interest here,

$$\begin{aligned} I_0 = 3/2: \quad \frac{1}{\mathcal{R}_{i\,E2}^{(F)}} &= \frac{1+\alpha_2^{i,i-1}}{1+\alpha_2^{i,i-2}}\,\frac{18(i+1)}{(i-1)(i+2)(2i+5)} \quad , \\ I_0 = 7/2: \quad \frac{1}{\mathcal{R}_{i\,E2}^{(F)}} &= \frac{1+\alpha_2^{i,i-1}}{1+\alpha_2^{i,i-2}}\,\frac{98(i+3)}{(i-1)(i+6)(2i+9)} \quad . \end{aligned} \tag{VI-68}$$

To obtain $\mathcal{R}_i^{(E)}$ and the conversion coefficients α_2, β_1 and mixing ratios δ_i^2 in $\mathcal{R}_i^{(F)}$, it was necessary to assume energies for the ground-state band intraband transitions. These energies are listed in Table A-5.

The internal-conversion coefficient tables of Rose[50] were used, in which K, L_I and L_{II} coefficients corrected for static finite nuclear-size effects and electron screening, L_{III} coefficients corrected for screening (these being not much affected by finite-size effects), and unscreened, point-nucleus total M-shell coefficients are given. (Differences between these and the Sliv coefficients which take into account an additional nuclear current interaction in the special case of a surface current are of the order of 5%.) Values of the total K, L and M coefficients for the relevant ground-state band energies for Z = 65, 67 and 71 were interpolated from the tables and extrapolated to form estimated total N-shell coefficients. The atomic configurations of Tb, Ho and Lu are

Tb: $1s^2 2s^2 2p^6 3s^2 3p^6 3d^{10} 4s^2 4p^6 4d^{10} 4f^9 5s^2 5p^6 6s^2$;

Ho: $1s^2 2s^2 2p^6 3s^2 3p^6 3d^{10} 4s^2 4p^6 4d^{10} 4f^{11} 5s^2 5p^6 6s^2$;

Lu: $1s^2 2s^2 2p^6 3s^2 3p^6 3d^{10} 4s^2 4p^6 4d^{10} 4f^{14} 5s^2 5p^6 5d^1 6s^2$;

that is, the N-shell is filled or nearly so, and there are a few electrons in the O and P shells; accordingly, as an approximation, extrapolated total N-shell coefficients were added, the neglected O and P shell contributions being balanced somewhat by the assumption of a full N-shell for Tb and Ho.

Resulting values for the total K, L, M, and estimated N coefficients for the relevant ground-state band energies are given in Table A-6 and for Ho are illustrated in Fig. A-3. The matrices to be inverted for pure M1 and for pure E2 deexcitation radiation, as calculated with the aid of (VI-63) ff., are displayed in Table A-7.

By means of the formulae $\delta^2_{i,i-1} \times \frac{(I_0+i-1)(I_0+i+1)}{3} = \frac{1}{20}\left(\frac{Q_0 \Delta E_{i,i-1}/(\hbar^2/M)}{g_K - g_R}\right)^2 = \delta_i^{(0)2} \equiv \delta_0^2 \Delta E^2_{i,i-1}$, the band energies, and the values for $\delta_1^2 \equiv \delta^2_{I_0+1 \to I_0}$ chosen as explained above, values of $1/\delta_i^2$ were calculated. With the aid of the theoretical conversion coefficients and (VI-63,4,5,7 and 8), values of $\mathcal{R}_i$, $t_{i,i-1}$ and $t_{i,i-2} = 1 - t_{i,i-1}$ were calculated for the various cases of interest. These are tabulated in Table A-8, and graphs of $t_{i,i-1}$ are displayed in Fig. A-4.

The matrices $\|t\|$ for the E2 and mixed decay situations were inverted, with results shown in Table A-9. From the relations $\mathcal{P}_j = \sum_i P_i u_{ij}$, "uncorrected" values of $\mathcal{P}_j$, in which contributions from decay from states higher than the highest observed state are neglected, were calculated and are tabulated in Table A-10. From graphical extrapolations of partial terms $P_i u_{ij}$ in the higher $\mathcal{P}_j$, corrections for the decay from the unobserved higher states were estimated and added on to yield "corrected" ρ_j values. Results are tabulated in Table A-10. From these relative total level populations ρ_i the intensity of the transition from level i to level j is given by

$$I_{ij}^{\text{trans.}} = I_{ij}^{e^-} + I_{ij}^{\gamma} = \rho_i t_{ij} = I_{ij}(1 + \alpha_{ij}^{tot}), \qquad \text{(VI-69)}$$

in which for the present situation, $t_{ij} = t_{ij}^{E2} + t_{ij}^{M1}$, the total transition conversion coefficient α_{ij}^{tot} is given by

$$\alpha_{i,i-1}^{tot} = \frac{\beta_1^{i,i-1} + \delta_i^2(\alpha_2^{i,i-1})}{1 + \delta_i^2} \qquad \text{(VI-70)}$$

Calculated intraband gamma-ray intensities I_{ij} were obtained with the aid of these expressions for the fourteen cases, Tb, $Q_0 = 8.1$, $\delta_1^2 = 0$, 0.01, 0.015, 0.02, ∞; Ho, $Q_0 = 7.5$, 8.0, $\delta_1^2 = 0$, 0.04, ∞; and Lu, $Q_0 = 8.0$, $\delta_1^2 = 0$, 0.20, ∞, with the results shown in Table VI-5 and Fig. VI-14 to 16.

Because of the large number of gamma rays in the deexcitation spectra, it was felt to be more practical, rather than to attempt a progressive gamma-ray "stripping", to correct the calculated gamma-ray intensities above for instrumental effects, and with the aid of standard gamma-ray response spectra taken in the identical geometry to that of the experiments, generate "theoretical laboratory spectrum profiles" to compare to the data. The instrumental effects that influence the photopeak heights in the observed spectra are the attenuation of the target gamma emission caused by the target, the aluminum back plate of the target chamber, the graded X-ray shields, and the detector crystal container front walls; the total

Table VI-5

Ground-State Band Predicted Deexcitation Gamma-Ray Intensities

Terbium, $Q_0 = 8.1$

i	$\delta_1^2 = 0$ (M1)	0.01	0.015	0.02	∞ (E2)
	$I_{i,i-1}$				
0	---	---	---	---	---
1	I.c. too great for accuracy, and obscured by X rays; omit.				
2	.04521	.06587	.06350	.06138	.009167
3	.07291	.05655	.05655	.05296	.003752
4	.05009	.03309	.03309	.03004	.001283
5	.02568	.01302	.01302	.01137	.0003469
6	.01146	.004930	.004930	.004182	.00009701
7	.003755	.001270	.001270	.001047	.00002370
8	.001340	.0003899	.0003899	.0003172	.000005243
9	.0002726	.00006515	.00006515	.00005249	.0000009905
10	.00008182	.00001661	.00001661	.00001339	.0000001713
	$I_{i,i-2}$				
0	---	---	---	---	---
1	---	---	---	---	---
2	0	.005908	.008506	.01092	.09458
3	0	.01354	.01878	.02335	.09687
4	0	.01640	.02185	.02635	.07195
5	0	.01011	.01267	.01457	.02726
6	0	.006353	.007904	.008909	.01796
7	0	.001858	.002176	.002383	.003360
8	0	.0009615	.001102	.001191	.001563
9	0	.0001500	.0001683	.0001801	.0002244
10	0	.00006582	.00007233	.00007736	.00009186

Holmium, $Q_0 = 7.5$

i	$\delta_1^2 = 0$ (M1)	0.04	∞ (E2)
	$I_{i,i-1}$		
0	---	---	---
1	.1082	.1051	.07135
2	.07519	.06617	.01969
3	.04087	.03145	.004993
4	.01782	.01174	.001225
5	.006280	.003479	.0002670
6	.002058	.0009864	.00006387
7	.0004522	.0002126	.00001118
8	.0001578	.00005515	.000002735
	$I_{i,i-2}$		
0	---	---	---
1	---	---	---
2	0	.01040	.08241
3	0	.01156	.05024
4	0	.007344	.02157
5	0	.003124	.006963
6	0	.001171	.002259
7	0	.0003297	.0005372
8	0	.0001042	.0001656

Table VI-5 (cont.)

Holmium, $Q_0 = 8.0$

i	$\delta_1^2 = 0$ (M1)	0.04	∞ (E2)
	$I_{i,i-1}$		
0	---	---	---
1	.1220	.1180	.0804
2	.08616	.07549	.02210
3	.05030	.03852	.006009
4	.02325	.01519	.001568
5	.008842	.004873	.0003768
6	.003036	.001444	.00009292
7	.0008459	.0003319	.00001750
8	.0002475	.00009019	.000004237
	$I_{i,i-2}$		
0	---	---	---
1	---	---	---
2	0	.01186	.09251
3	0	.01416	.06045
4	0	.009506	.02760
5	0	.004375	.009828
6	0	.001714	.003287
7	0	.0005148	.0008408
8	0	.0001628	.0002565

Lutetium, $Q_0 = 8.0$

i	$\delta_1^2 = 0$ (M1)	0.20	∞ (E2)
	$I_{i,i-1}$		
0	---	---	---
1	.1352	.1231	.1174
2	.08904	.05949	.02456
3	.04405	.02017	.005434
4	.01835	.005911	.001272
5	.006171	.001389	.0002557
6	.001918	.0003394	.00005727
7	.0004899	.00006410	.000009491
8	.0001429	.00001604	.000002408
	$I_{i,i-2}$		
0	---	---	---
1	---	---	---
2	0	.04148	.1060
3	0	.03207	.05510
4	0	.01568	.02220
5	0	.005363	.006714
6	0	.001760	.002095
7	0	.0004227	.0004599
8	0	.0001292	.0001493

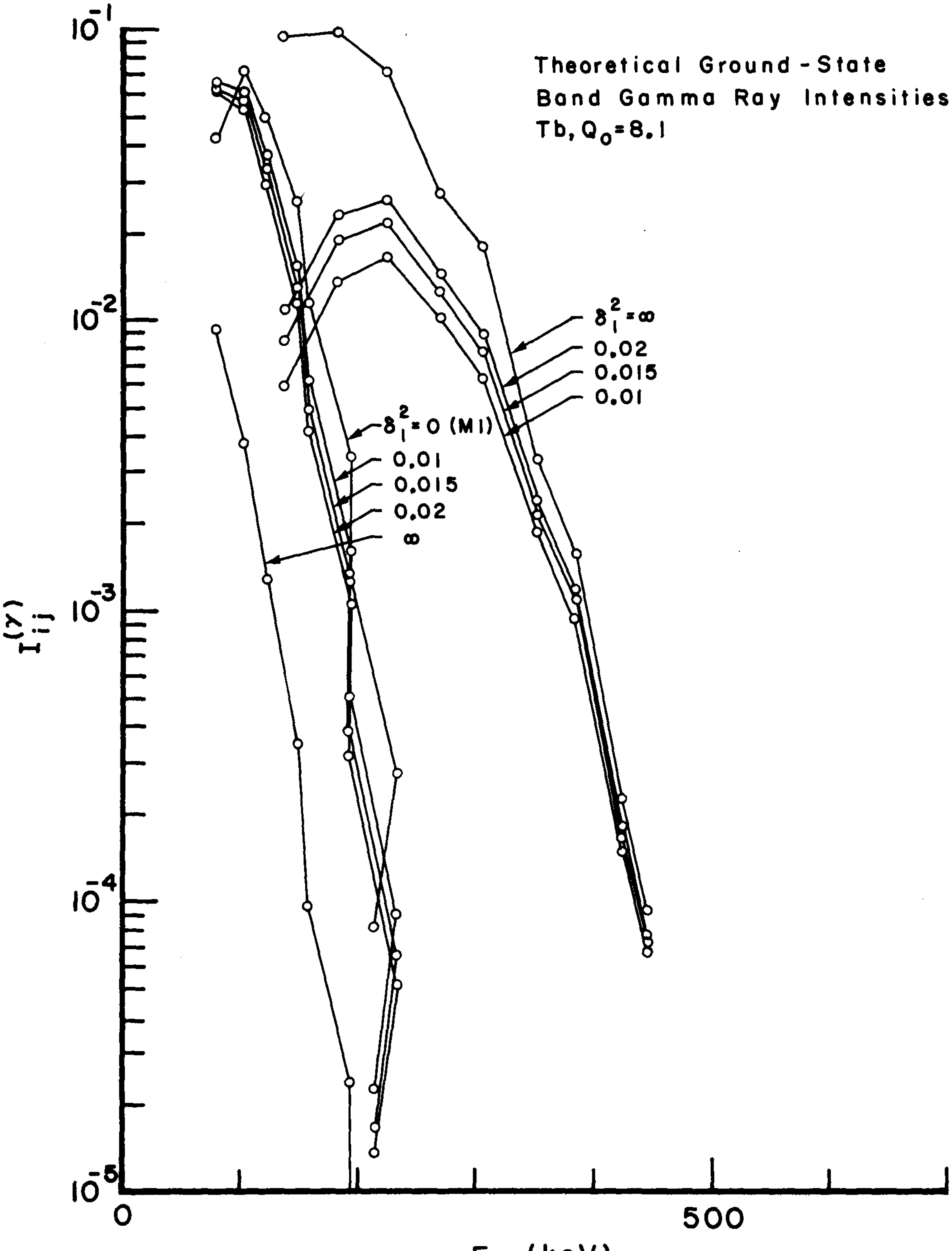

Theoretical Ground-State
Band Gamma Ray Intensities,
Tb, Q_0=8.1
$\delta_1^2=\infty$
0.02
0.015
0.01
$\delta_1^2=0$ (M1)
0.01
0.015
0.02
∞
10^{-1}
10^{-2}
10^{-3}
10^{-4}
10^{-5}
$I_{ij}^{(\gamma)}$
0
500
E_γ (keV)

FIG VI-14

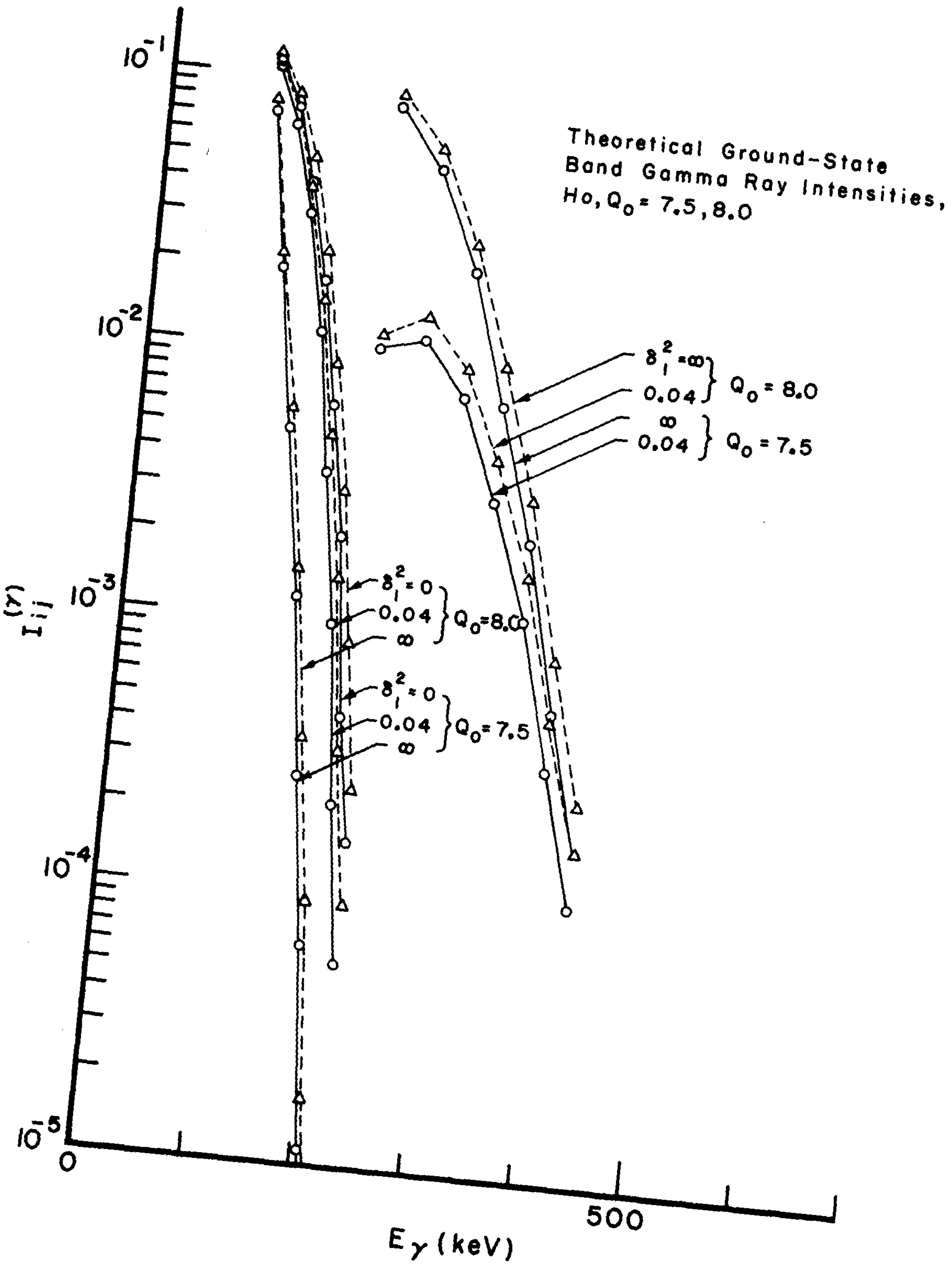
Theoretical Ground-State
Band Gamma Ray Intensities,
Ho, Q_0 = 7.5, 8.0
$\delta_1^2 = \infty$
0.04
Q_0 = 8.0
∞
0.04
Q_0 = 7.5
$\delta_1^2 = 0$
0.04
∞
Q_0 = 8.0
$\delta_1^2 = 0$
0.04
∞
Q_0 = 7.5
$I_{ii}^{(\gamma)}$
10^{-1}
10^{-2}
10^{-3}
10^{-4}
10^{-5}
0
500
E_γ (keV)

FIG VI - 15

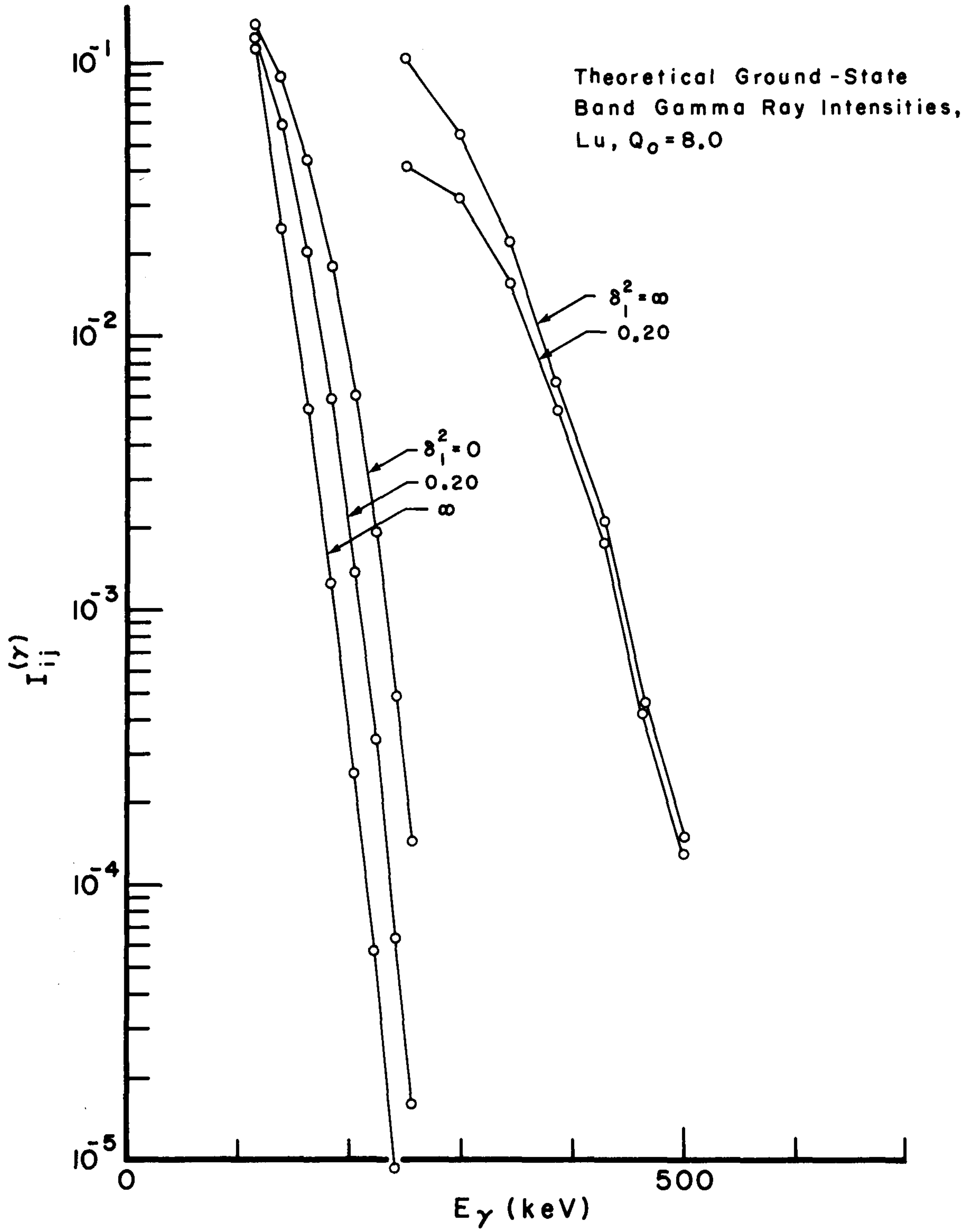

Theoretical Ground-State Band Gamma Ray Intensities, Lu, Q_0 = 8.0
$\delta_1^2 = \infty$
0.20
$\delta_1^2 = 0$
0.20
∞
10^{-1}
10^{-2}
10^{-3}
10^{-4}
10^{-5}
$I_{ij}^{(\gamma)}$
0
500
E_γ (keV)

FIG VI-16

efficiency for gamma-ray absorption of the 1-1/2 in. diameter by 2 in. NaI(Tl) crystals; the photopeak-to-total ratio characteristic of the crystals and geometry employed, and the resolution (f.w.h.m.) of the Gaussian photopeaks; all of these being distinct functions of the detected gamma-ray energies. These were calculated by the methods discussed in Appendix 4, yielding predicted laboratory photopeak intensities, and then, from the measured resolution function, the relative photopeak heights for the various transitions. Spectrum profiles were constructed with the aid of interpolated NaI standard response "shapes" derived from the thin-source spectra as explained in the appendix. Results are discussed in Section VII.

B. Higher Bands: Single Excitation Calculation

The relatively large gap in energy between the nuclear ground state and the lowest member of a rotational band built on an excited non-rotational state, compared to the low-lying rotational level spacings, is expected to retard considerably multiple-excitation processes. Furthermore, the difference in "frequencies" of nuclear motions associated with this gap render the $\xi = 0$ approximation suspect. The Lutgen-Winther[226] theory, in which the interband transition is treated as a perturbation but the subsequent intraband excitations in the sudden approximation, indicates that the effect of multiple processes in this approximation consists of a redistribution of band-member populations which leaves the total band population unchanged, thus leaving the sum of interband deexcitations invariant. This allows comparison of the sum of the observed interband deexcitation intensities with the sum of the intensities calculated on the basis of single-excitation processes alone. Experimental data indicate that multiple processes, where observed at all in higher bands of odd-A nuclei, tend to be quite weak. For these reasons it was decided to do single-excitation calculations for the higher states in Tb, Ho and Lu, after the manner of Alder et al.[1]

Previous work, mostly with radioactive decay, indicates the following low-lying states, with their Nilsson specifications: Tb, ground state 3/2+[411], 348.1 $\pm$ 0.3-keV[76,77] 5/2+[413], 363.2 $\pm$ 0.3-keV[76,77] 5/2-[532], 580-keV K = 1/2 vibrational state, and possibly[35] a 971-keV 1/2+[411] state; Ho, 7/2-[523] ground state, 361.5± 0.3-keV[84,125] 3/2+[411], 514.2-keV vibrational state, 715.7-keV[125] 7/2+[404], 995.1-keV[125] 5/2+[413], a 1055.6-keV[125] possibly I = 5/2 state which could be the 5/2+[402] state, possibly 545.5-keV and 565.7-keV states[125], which could be the first members of the 1/2+[411] band because of their small spacing, characteristic of the decoupling observed in other instances of this band, i.e., the Tm^{169} ground state, and predicted from the Nilsson model, and a 687-keV[84] vibrational state; and Lu, 7/2+[404] ground state, 343.40-keV[169,178] 5/2+[402], 504.7-keV[169,178] 1/2+[411], 396.31-keV[169,178] 9/2-[514], and a 486-keV vibrational state discovered from the present work. The location of these states on the Nilsson diagram is shown in Fig. VI-17. Conspicuous for its absence is the 7/2-[523] state expected in Tb, and probably observed[59] in Tb^{155}.

In Coulomb-excitation experiments the bands most strongly populated are those based on the collective vibrational states with their somewhat enhanced interband B(E2) values, and next, especially in gamma ray-backscattered ion coincidence experiments, those low-lying single-particle states connected to the ground state via non-vanishing E2 matrix elements. Single-particle states connected to the ground state by E1 (or M1) matrix elements are expected to be very weakly populated since dipole matrix elements between these states in distorted nuclei violate the "asymptotic selection rules"[8], generally, and are quite small. E1 excitation, like bremsstrahlung, and unlike excitations via other multipolarities, is strongest in the

Nilsson States

From
Mottelson & Nilsson[24]

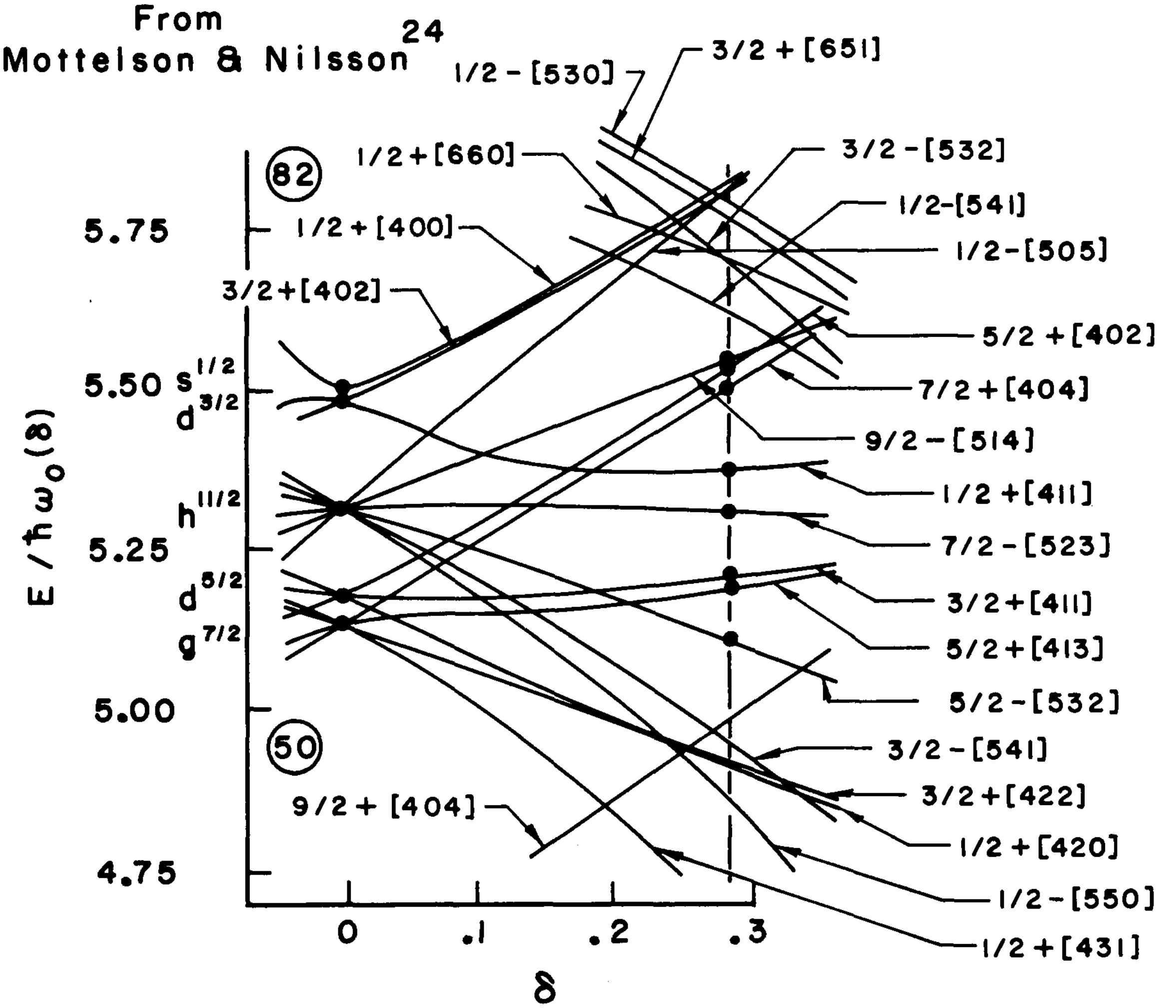

Occurence in Odd Z Nuclei

	Tb^{151}	Ho^{165}	Lu^{175}
5/2-[532]	363 keV		
5/2+[413]	348	995	
3/2+[411]	G.S.	361	
7/2-[523]	---	G.S.	
1/2+[411]	(971)	(545)	504
7/2+[404]		716	G.S.
5/2+[402]		(1056)	343
9/2-[514]			396

FIG VI-17

forward direction where the Rutherford cross section is large, and so might be seen in "singles" gamma-ray spectra despite a small B(E1) value. With this possible exception, the only states expected to be readily observable via Coulomb excitation are the 5/2+[413], 1/2+[411] and vibrational states in Tb^{159}; the vibrational states only in Ho^{165}; and the 5/2+[402], 1/2+[402], 1/2+[411] and vibrational states in Lu^{175}.

E2 single-excitation calculations were made for these states on the assumption that the intrinsic part of the matrix elements $\langle\Omega_f|\mathcal{O}^{*\prime}_{\lambda\nu}|\Omega_i\rangle$ had "single-particle strengths", in the sense:

$$|\langle\Omega_f|\mathcal{O}^{*\prime}_{\lambda-\Delta K}|\Omega_i\rangle|^2 = B_{SP}(\lambda)\,, \qquad \text{(VI-71)}$$

where the so-called "single-particle estimate" for radiative transitions between particle states is[1,2], for $\lambda = E2$,

$$B_{SP}(E2) = \frac{5e^2}{4\pi}\left(\frac{3}{5}\right)^2 R_o^4 = \frac{3916}{3125\,\pi} A^{\frac{4}{3}} e^2\, 10^{-52}\, cm^4, \qquad \text{(ABHMW II A.58)}$$

wherein $R_o = 1.2A^{1/3}$ f. is the effective nuclear radius for the single-particle estimate calculation and A is the mass number of the nucleus undergoing the radiative decay. The resulting calculated deexcitation radiation intensities were compared with the observed intensities to yield estimates of the values for some of the intrinsic matrix elements.

The excitation cross section from the time-dependent perturbation calculation is given by Alder et al.[1]:

$$\begin{aligned} d\sigma_{E2} &= \frac{4\pi Z_1^2 e^2}{\hbar^2}\, a^2 \sin^{-4}\frac{\theta_{CM}}{2}\, \frac{B(E2\uparrow)}{125}\sum_{\mu}|S_{E2,\mu}|^2 d\Omega \\ &= \left(\frac{Z_1 e}{\hbar v_i}\right)^2 a^{-2} B(E2\uparrow)\, df_{E2}(\theta_{CM},\xi). \end{aligned} \qquad \text{(ABHMW II A.21,28)}$$

Here $S_{E2,\mu}$ are certain projectile-path integrals, and half the distance of closest approach in a head-on collision a is in 10^{n} cm., $(Z_1 e/\hbar v_1)^2$ in units of $(1/e)^2$, B(E2) in units of $e^2 10^{-4n}$cm.^{4}, and $d\sigma_{E2}$ in units of 10^{2n}cm.^{2}, with n arbitrary. The functions $df_{E2}(\theta_{CM},\xi)$ are tabulated in Alder et al.[1] ξ is given in the form suitable for numerical calculation,

$$\xi = \frac{Z_1 Z_2 \sqrt{M_1}\,\Delta E'}{12.70\,[T_{iL}-(\Delta E'/2)]^{3/2}}\left[1+\frac{5}{32}\left(\frac{\Delta E'}{T_{iL}}\right)^2+\,\ldots\right], \qquad \text{(ABHMW II C.13)}$$

$$\Delta E' = \left(1+\frac{M_1}{M_2}\right)\Delta E\ , \qquad \text{(ABHMW II C.4)}$$

Where, as mentioned before, the numerical factor 12.65 in the expression as given in ref. 1 where masses are expressed in units of the proton mass is replaced by 12.70, appropriate for masses expressed in amu. ΔE is the excited-state level energy and T_{iL} the projectile incident laboratory kinetic energy.

These cross-section expressions were calculated in a semiclassical manner in which the effect of the projectile, which is assumed to traverse the classical trajectory, is totally specified by its time-dependent classical Maxwell field at the target nucleus. The changes resulting from calculating with a quantized Maxwell field occur in the form of the functions $df_E(\theta_{CM}, \eta_i, \xi)$ that reduce to the semiclassical ones in the limit $\eta_i \rightarrow \infty$. The semiclassical functions are accurate to within a fraction of a percent for the present cases of heavy-ion bombardment, and were employed. The calculations were performed using the forms for $d\sigma_{E2}$,

$$d\sigma_{E2} = (T_{1L}-\Delta E')\frac{M_1}{Z_2{}^2}\frac{4.820}{(1+M_1/M_2)^2}\,B(E2\uparrow)\,df_{E2}(\theta_{CM},\xi)\,, \qquad \text{(VI-72)}$$

in which T_{1L} and $\Delta E' \equiv (1+M_1/M_2)\Delta E$ are in MeV, B(E2) in $e^2 10^{-48}$cm.^{4}, M_1, M_2 in amu, producing $d\sigma_{E2}$ in barns.

For a thick target the yield (of level population) is defined as

$$Y = N\int_{E_{icut}}^{T_{1L}} d\sigma_{E\lambda}(E)\,w(E)\,dE \ , \tag{VI-73}$$

where E is the effective incident kinetic energy at depth ℓ in the target, and $w(E) = -d\ell/dE$ is the differential range-energy function. This may be further written in the forms

$$Y = N\,\frac{\text{nuclei}}{\text{cm}^3} \times 10^{-24}\frac{\text{cm}^2}{\text{barn}}\int_{E_{1cut}}^{T_{1L}} \sum_j \frac{d\sigma_{E2}[E(\xi),\theta_{jcM}]}{d\Omega_{cM}}\ \delta\Omega_{jcM}\,\frac{\text{barn}}{\text{nucl.}}\left(-\frac{1}{dE/d\ell}\right)\frac{\text{mg cm}^{-2}}{\text{MeV amu}^{-1}}\,dE\,\frac{\text{MeV}}{\text{amu}} \times$$

$$(1/\rho \ \text{mg/cm}^3) \tag{VI-74}$$

$$\approx \frac{10^{-24}N}{\rho}\left(\overline{\frac{1}{-dE/d\ell}}\right)\frac{\text{nuclei}}{\text{barn}} - \frac{\text{amu}}{\text{MeV}}\int_{E_{icut}}^{T_{1L}}\sum_j \frac{d\sigma_{E2}}{d\Omega_{cM}}\ \delta\Omega_{jcM}\,dE\,\frac{\text{barn/nucl.}}{\text{MeV/amu}}$$

$$\equiv \frac{10^{-24}N}{\rho}\ P$$

where

$$P \equiv \int_{E_{icut}}^{T_{1L}}\sum_j \frac{d\sigma_{E2}}{d\Omega_{cM}}\ d\Omega_{j,cM}\,dE\left(-\overline{\frac{d\ell}{dE}}\right)\frac{\text{barn}}{\text{nucl.}}\ \frac{\text{mg}}{\text{cm}^2} \ , \tag{VI-75}$$

the actual quantities calculated, can be compared directly with the $P_{I_f K}$ barn/nucl.-mg./cm.^{2} from the ground-state multiple Coulomb excitation calculations. This formula was used for the computations. $\overline{(1/(-dE/d\ell))}$ is an average of the reciprocal of the rate of energy loss in (MeV/amu)/(mg./cm.^{2}) over the projectile path in the target from $\ell = 0$ to $\ell = \ell_{cut}$, the discriminator cutoff depth. Placement of an average energy loss factor outside the integral was done to facilitate the integration. θ_{jCM}, $d\Omega_{jCM}$ are the center-of-mass system scattering angles and junction-counter solid angles for counter array positions A to E. The intratarget kinematics are the same as in the ground-state band calculations.

In order to use (VI-75) to perform the thick-target integrations various quantities had to be calculated. E_{ieff}, the effective ion incident energy within the target, was obtained as a function of ξ for various level energies E_{lev} by means of the formulae,

$$E_{i\,eff} = \frac{1}{2}E'_{lev} + \left(\frac{CE_{lev}}{\xi}\right)^{2/3}$$
$$C = \frac{Z_1 Z_2 \sqrt{M_1}\left(1+\frac{M_1}{M_2}\right)}{12.70}\ ; \quad E'_{lev} = \left(1+\frac{M_1}{M_2}\right)E_{lev}\ . \qquad \text{(VI-76)}$$

Values of $df_{E2}(\bar{\theta}_{CM},\xi)/d\Omega_{CM}$ were interpolated from Alder et al., Table II.8 for the center-of-mass angles corresponding to junction counter positions A to E for given values of ξ , and from these, $\sum_j (df(\theta_{jCM},\xi)/d\Omega_{CM})\,\delta\Omega_{jCM}$ for four junction counters per position type (twenty in all) were calculated. The quantities $\sum_j \frac{d\sigma_{E2}[E_{ieff}(\xi),\theta_{jCM}]}{d\Omega_{CM}}\,\delta\Omega_{jCM}$ were calculated as functions of ξ from the formula (Alder et al.[1], equations II.15 to 17):

$$\sum_j \frac{d\sigma_{E2}}{d\Omega_{CM}}\,\delta\Omega_{jCM} = \left(E_{ieff} - E'_{lev}\right)\mathcal{C}\ B(E2\uparrow)\sum_j \frac{df_{E2}}{d\Omega_{CM}}\,\delta\Omega_{jCM}\ \text{barns}, \qquad \text{(VI-77)}$$

in which, with energies in MeV and B(E2) values in $e^2 10^{-48}\text{cm.}^4$, the values of $\mathcal{C}$ are as follows:

$$\mathcal{C}_{Tb} = .015068$$
$$\mathcal{C}_{Ho} = .014277 \qquad \text{(VI-78)}$$
$$\mathcal{C}_{Lu} = .012843\ .$$

Predicted intensities on the provisional basis of $B(E2) = B_{sp}(E2)$ required the quantities $\mathcal{C}\, B_{sp}$:

$$B_{sp}(E2) = 2.9702\; A_2^{4/3}\, e^2\, 10^{-53}\, cm^4; \tag{VI-79}$$

	$B_{sp}(E2)$	$\mathcal{C}\, B_{sp}(E2)$
Tb	$2.5585\; e^2 10^{-50} cm.^4$	$3.8552\; e^2 10^{-52} cm.^4$
Ho	2.6880	3.8377
Lu	2.9074	3.7340

Results are given in Table A-15 (Appendix 4). Plots of $\sum_j \frac{d\sigma_{E2}}{d\Omega_{cM}} \delta\Omega_{jcM}$ versus E_{ieff} along with the pertinent integration ranges are shown in Fig. VI-18, 19 and 20. Values of $\int_{E_{icut}}^{T_{iL}} \sum_j \frac{d\sigma_{E2}}{d\Omega_{cM}} \delta\Omega_{jcM} dE$ were obtained and are listed in Table VI-6.

The average range-energy curve slopes, $-\overline{d\ell/dE}$, were obtained as follows: what are required are weighted averages with respect to the weight functions $\sum \frac{d\sigma_{E2}}{d\Omega}\delta\Omega$. Within the range of the thick-target integrations, both $-d\ell/dE \equiv \delta R/\delta E \equiv f(x)$ and $\sum \frac{d\sigma_{E2}}{d\Omega}\delta\Omega \equiv g(x)$ are approximately linear. Thus, taking them as linear and using the notation in Fig. A- 9 which contains a plot of the interpolated rare-earth range-energy curves in differential form, the weighted averages are given by

$$\bar{f} = \frac{\int_{x_0}^{x_1} f(x)\, g(x)\, dx}{\int_{x_0}^{x_1} g(x)\, dx} = \frac{y_0' y_0 + \frac{1}{2}(y_0 \delta y' + y_0' \delta y) + \frac{1}{3}\delta y' \delta y}{y_0 + \frac{1}{2}\delta y} . \tag{VI-80}$$

With the aid of the data in Fig. VI-18-20 and A- 9 , values for $\bar{f} \equiv -\overline{d\ell/dE}$ for each state were calculated, as shown in Table A-16. These were multiplied by $\int_{E_{icut}}^{T_{iL}} \sum \frac{d\sigma_{E2}}{d\Omega}\delta\Omega\, dE$ to produce values of the relative single-excitation level populations P_{sp}

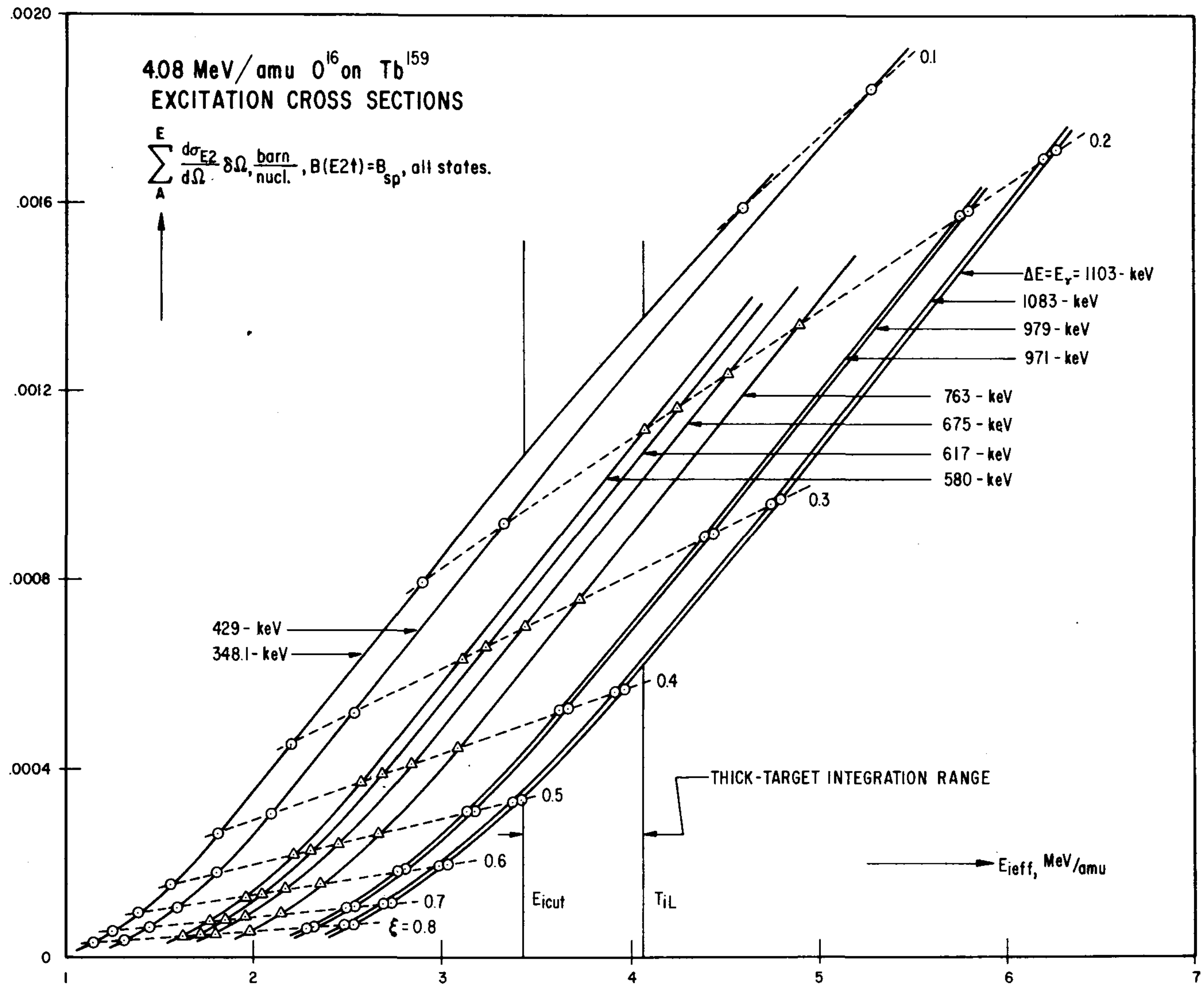
4.08 MeV/amu O16 on Tb159
EXCITATION CROSS SECTIONS
$\sum_A^E \frac{d\sigma_{E2}}{d\Omega} \cdot \delta\Omega, \frac{barn}{nucl.}, B(E2\uparrow)=B_{sp}$, all states.
0.1
0.2
0.3
0.4
0.5
0.6
0.7
ξ = 0.8
ΔE=Eγ= 1103-keV
1083-keV
979-keV
971-keV
763-keV
675-keV
617-keV
580-keV
429-keV
348.1-keV
THICK-TARGET INTEGRATION RANGE
Eicut
TiL
Eieff, MeV/amu
.0020
.0016
.0012
.0008
.0004
0
1
2
3
4
5
6
7

FIG VI-18

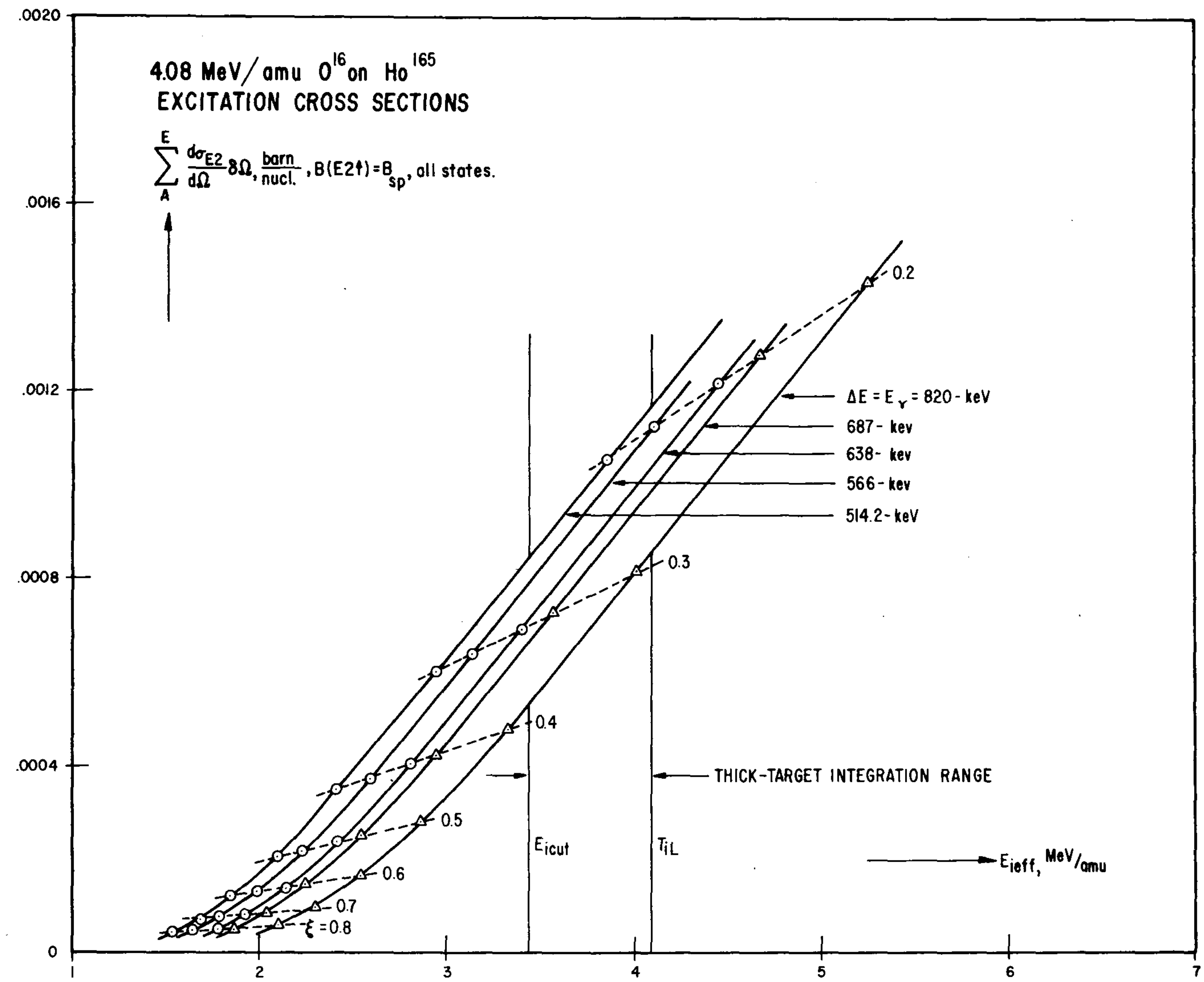

4.08 MeV/amu O16 on Ho165
EXCITATION CROSS SECTIONS
$\sum_A^E \frac{d\sigma_{E2}}{d\Omega} 8\Omega, \frac{\text{barn}}{\text{nucl.}}, B(E2\uparrow)=B_{sp}$, all states.
.0020
.0016
.0012
.0008
.0004
0
1
2
3
4
5
6
7
0.2
ΔE = Eγ = 820-keV
687-kev
638-kev
566-kev
514.2-keV
0.3
0.4
0.5
0.6
0.7
ξ = 0.8
THICK-TARGET INTEGRATION RANGE
Eicut
TiL
Eieff, MeV/amu

FIG VI-19

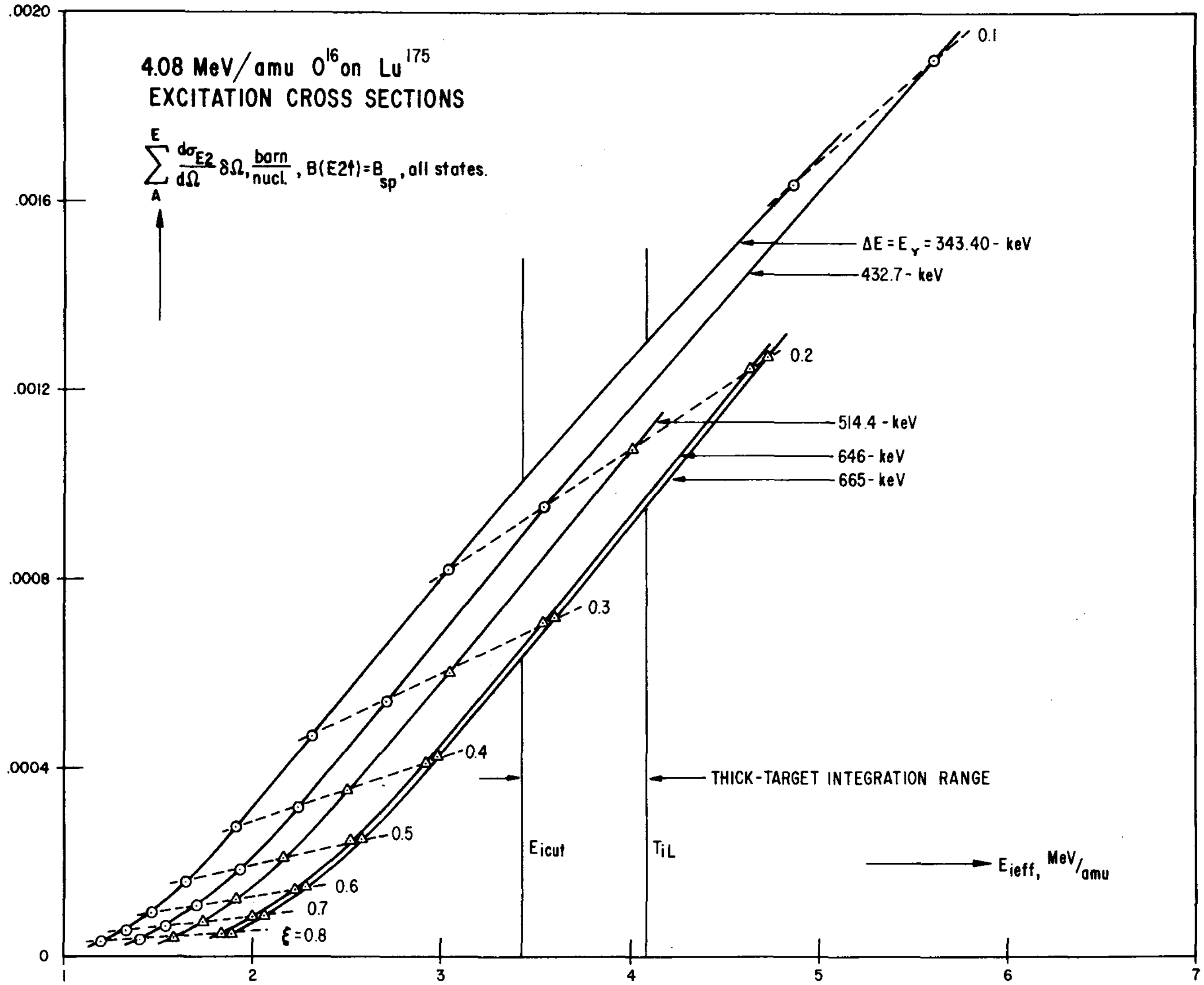

4.08 MeV/amu O16 on Lu175
EXCITATION CROSS SECTIONS
$\sum_{A}^{E} \frac{d\sigma_{E2}}{d\Omega} \delta\Omega, \frac{\text{barn}}{\text{nucl.}}, B(E2\uparrow)=B_{sp}$, all states.
.0020
.0016
.0012
.0008
.0004
0
1
2
3
4
5
6
7
0.1
$\Delta E = E_\gamma$ = 343.40 - keV
432.7 - keV
0.2
514.4 - keV
646 - keV
665 - keV
0.3
0.4
THICK-TARGET INTEGRATION RANGE
0.5
0.6
0.7
ξ = 0.8
E_{icut}
T_{iL}
E_{ieff}, MeV/amu

FIG VI-20

in (mg./cm.^{2})/(MeV/amu) listed in Table VI-6, appropriate for single-particle values for B(E2) to all of the member states of a band, and which hence must be multiplied by Clebsch-Gordon coefficients in the case of the population of rotational bands. (A few P_{sp} values were obtained by interpolating the present P_{sp} versus E_{lev} results.)

The excitation and subsequent deexcitation ratios were calculated on the assumption, expected to be fairly accurate in the rotational region, of pure unmixed bands.

In terbium, the assumed states which can be reached by single E2 Coulomb excitation from the ground state are illustrated in Fig. VI-21. The energies are suggested by the present work, the conversion-electron observations of Diamond et al.[35] and model systematics. As per the figure, the 5/2+[413] states disobey the Λ and n_z asymptotic selection rules[24] for E2 and M1 decays to the ground state; the 1/2+[411] states disobey Λ and n_z selection rules for E2 decays but are asymptotically allowed for one of the single-particle M1 operators. Other states predicted by the Nilsson model and previously observed in source work which are not coupled to the ground state by non-vanishing E2 matrix elements are the 363.2-keV 5/2-[523] which violates Λ and n_z asymptotic rules for E1, M2 and E3 operators, and the as-yet-unobserved 7/2-[523] state for which E1 transitions are K-forbidden but M2 and E3 transitions to the ground-state band are allowed both by K and by asymptotic rules.

The rotational populations found by multiplying P_{sp} by the

Table VI-6a

$$\int_{E_{icut}}^{T_{iL}} \sum \frac{d\sigma_{E2}}{d\Omega} \delta\Omega \, dE \ \frac{\text{barn}}{\text{nucl.}} \cdot \frac{\text{MeV}}{\text{amu}}$$

Terbium	Level Energy
7.783×10^{-4}	348.1 keV
7.236	429
6.113	580
5.859	617
5.491	675
4.921	763
3.707	971
3.652	979
3.120	1087
3.056	1103
Holmium	
6.575×10^{-4}	514.2 keV
6.209	566
5.703	638
5.372	687
4.482	820
Lutetium	
7.624×10^{-4}	343.40 keV
6.935	432.7
6.278	514.2
5.348	646
5.219	665

Table VI-6b

Single E2 Coulomb Excitation Level Populations for $B(E2\uparrow) = B_{sp}$,

All States

	E_{lev}	P_{sp}*
Terbium	348.1 keV	.005486
	429	.005100
	580	.004311
	617	.004133
	675	.003875
	763	.003473
	971	.002618
	979	.002579
	1083	.002204
	1103	.002159
Holmium	514.2 keV	.004740
	566	.004476
	638	.004111
	687	.003875
	820	.003234
Lutetium	343.4 keV	.005668
	432.7	.005158
	514.4	.004671
	646	.003980
	665	.003885

$$* \quad P_{sp} = \int_{E_{icut}}^{T_{iL}} \sum \frac{d\sigma_{E2,sp}}{d\Omega} \delta\Omega \, dE \left(- \frac{d\ell}{dE} \right) \quad \frac{\text{barn}}{\text{nucl.}} - \frac{\text{mg.}}{\text{cm.}^2}$$

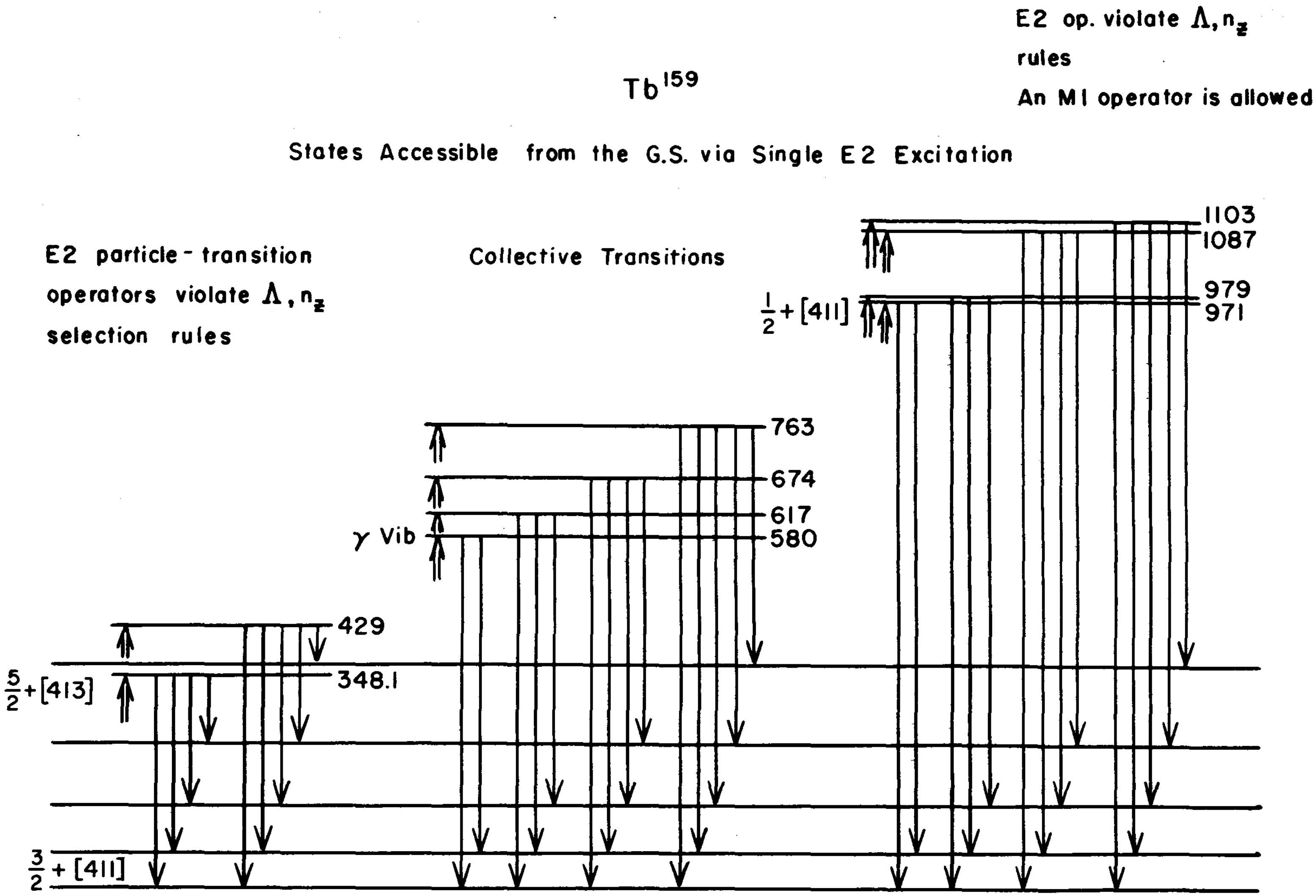
Tb159
States Accessible from the G.S. via Single E2 Excitation
E2 op. violate Λ, n_z
rules
An M1 operator is allowed
E2 particle-transition
operators violate Λ, n_z
selection rules
Collective Transitions
1103
1087
979
971
1/2 + [411]
763
674
617
580
γ Vib
429
348.1
5/2 + [413]
3/2 + [411]

FIG VI - 21

C.G. coefficients (which is equivalent to setting the intrinsic part of the matrix elements $|\langle\Omega_f|\mathcal{O}'^{*}_{\lambda-\Delta K}|\Omega_i\rangle|^2 = B_{sp}(E\lambda)$), and where applicable, i.e., only for the interband $K = 3/2 \rightarrow K = 1/2$ E2 transitions in Tb, by the symmetry-correction factors, are shown in Table VI-7. For the pure vibrational state, the symmetry-correction factor $\mathcal{R}$ becomes infinite but the factor $\langle\Omega_{v_f},\Omega_f|\mathcal{O}'^{*}_{\lambda,-\Delta K}|\Omega_{v_i},\Omega_i = \Omega_f\rangle = \langle\Omega_{v_f}|\Omega_{v_i}\rangle\langle\Omega_f|\mathcal{O}'^{*}_{\lambda-\Delta K}|\Omega_f\rangle$ is zero and cannot be set equal to B_{sp}. Then the correct procedure is to use the symmetry-unmodified form for the excitation ($f\rightarrow i$) B-values but with the $K_i = -1/2$ C.G. coefficients. This follows because e.g. for the radiative decays, $B(\lambda,i\rightarrow f) = |\langle I_i \tfrac{1}{2}\lambda 1|I_f \tfrac{3}{2}\rangle\langle 0,\tfrac{3}{2}|\mathcal{O}'^{*}_{\lambda,-1}|2,-\tfrac{3}{2}\rangle + (-1)^{I_i+\frac{1}{2}}\langle I_i -\tfrac{1}{2}\lambda 2|I_f\tfrac{3}{2}\rangle\langle 0,\tfrac{3}{2}|\mathcal{O}'^{*}_{\lambda-2}|-2,\tfrac{3}{2}\rangle|^2$ holds in this case, and $\langle 0,\tfrac{3}{2}|\mathcal{O}'^{*}_{\lambda,-1}|2,-\tfrac{3}{2}\rangle = \langle 0,\tfrac{3}{2}|\mathcal{O}'^{*}_{\mathrm{coll}\ \lambda,2} + \mathcal{O}'^{*}_{\mathrm{intr}\ \lambda,-3}|2,-\tfrac{3}{2}\rangle = \langle 0|\mathcal{O}'^{*}_{\mathrm{coll}\ \lambda,2}|2\rangle\langle\tfrac{3}{2}|-\tfrac{3}{2}\rangle + \langle 0|2\rangle\langle\tfrac{3}{2}|\mathcal{O}'^{*}_{\mathrm{intr}\ \lambda,-3}|-\tfrac{3}{2}\rangle = 0$, but $\langle 0,\tfrac{3}{2}|\mathcal{O}'^{*}_{\lambda,-2}|-2,\tfrac{3}{2}\rangle = \langle 0,\tfrac{3}{2}|\mathcal{O}'^{*}_{\mathrm{coll}\ \lambda,-2} + \mathcal{O}'^{*}_{\mathrm{intr}\ \lambda,0}|2,-\tfrac{3}{2}\rangle = \langle 0|\mathcal{O}'^{*}_{\mathrm{coll}\ \lambda-2}|-2\rangle\langle\tfrac{3}{2}|\tfrac{3}{2}\rangle + \langle 0|-2\rangle\langle\tfrac{3}{2}|\mathcal{O}'^{*}_{\mathrm{intr}\ \lambda,0}|\tfrac{3}{2}\rangle = \langle 0|\mathcal{O}'^{*}_{\mathrm{coll}\ \lambda,-2}|-2\rangle$, whence $B(\lambda, i\rightarrow f) = \langle I_i -\tfrac{1}{2}\lambda 2|I_f\tfrac{3}{2}\rangle^2|\langle 0|\mathcal{O}'^{*}_{\mathrm{coll}\ \lambda,-2}|-2\rangle|^2$, or in effect, $|\mathcal{R}| = \infty$. On this argument vibrational M1 transitions ($\lambda = 1$) are forbidden since $\langle 0|\mathcal{O}'^{*}_{\lambda,-2}|-2\rangle = 0$ if $\lambda < 2$. Here the multipole operator $\mathcal{O}'^{*}_{\lambda\mu}$ is divided into collective and intrinsic parts, and $\mu = \mu_{\mathrm{coll}} + \mu_{\mathrm{intr}}$, $|\mu_{\mathrm{coll}}| = 2$, $K_f = \Omega_{v_f} + \Omega_f = 0 + 3/2 = 3/2$, $K_i = \Omega_{v_i} + \Omega_i = 2 - 3/2 = 1/2$. For Ho and Lu vibrational states, $B(\lambda,i\rightarrow f) = |\langle I_i\tfrac{3}{2}\lambda 2|I_f\tfrac{7}{2}\rangle\langle 0,\tfrac{7}{2}|\mathcal{O}'^{*}_{\lambda-2}|-2,\tfrac{7}{2}\rangle + (-1)^{I_i+\frac{1}{2}}\langle I_i -\tfrac{3}{2}\lambda 5|I_f\tfrac{7}{2}\rangle\langle 0,\tfrac{7}{2}|\mathcal{O}'^{*}_{\lambda-5}|2,-\tfrac{7}{2}\rangle|^2 = \langle I_i\tfrac{3}{2}\lambda 2|I_f\tfrac{7}{2}\rangle^2|\langle 0|\mathcal{O}'^{*}_{\mathrm{coll}\ 2-2}|-2\rangle|^2$; or $|\langle I_i\tfrac{11}{2}\lambda -2|I_f\tfrac{7}{2}\rangle\langle 0,\tfrac{7}{2}|\mathcal{O}'^{*}_{\lambda 2}|2,\tfrac{7}{2}\rangle + (-1)^{I_i+\frac{1}{2}}\langle I_i -\tfrac{11}{2}|\mathcal{O}'^{*}_{\lambda 9}|I_f\tfrac{7}{2}\rangle\langle 0,\tfrac{7}{2}|\mathcal{O}'^{*}_{\lambda-9}|-2,-\tfrac{7}{2}\rangle|^2 = \langle I_i\tfrac{11}{2}\lambda -2|I_f\tfrac{7}{2}\rangle^2|\langle 0|\mathcal{O}'^{*}_{\mathrm{coll}\ 22}|2\rangle|^2$; the usual Alaga rules. It may be noted that in Tb the M1 matrix elements are not symmetry-corrected and also are not K-forbidden in the presence of symmetrixed wave functions; they vanish because of a complete separation of vibrational and intrinsic motions.

Table VI-7

Tb E2$\uparrow$ Transitions

<u>3/2+[411] → 5/2+[413]</u>

$\langle 3/2\ 3/2\ 2\ 1 | 5/2\ 5/2\rangle^2 = 3/7$

$\langle 3/2\ 3/2\ 2\ 1 | 7/2\ 5/2\rangle^2 = 4/7$

Sum = 1

<u>3/2+[411] → 1/2+ Vib.; 1/2+[411]</u>

$\langle 3/2\ 3/2\ 2\ -1 | 1/2\ 1/2\rangle^2 = 1/10$

$\langle 3/2\ 3/2\ 2\ -1 | 3/2\ 1/2\rangle^2 = 2/5$

$\langle 3/2\ 3/2\ 2\ -1 | 5/2\ 1/2\rangle^2 = 27/70$

$\langle 3/2\ 3/2\ 2\ -1 | 7/2\ 1/2\rangle^2 = 4/35$

Sum = 1

For these cases there are symmetry corrections involving the following C.G. coefficients:

$\langle 3/2\ 3/2\ 2\ -2 | 1/2\ 1/2\rangle^2 = 2/5$

$\langle 3/2\ 3/2\ 2\ -2 | 3/2\ 1/2\rangle^2 = 2/5$

$\langle 3/2\ 3/2\ 2\ -2 | 5/2\ 1/2\rangle^2 = 6/35$

$\langle 3/2\ 3/2\ 2\ -2 | 7/2\ 1/2\rangle^2 = 1/35$

Sum = 1

Table VI-8

Tb E2$\uparrow$ Transitions

keV	P_{sp} , barn/nucl.	$\mathcal{F}$	$P = \mathcal{F} P_{sp}$ $(\lvert\mathcal{R}\rvert \neq \infty)$
.1	5.485×10^{-3}	3/7	2.351×10^{-3}
	5.100	4/7	2.914
	4.311	$1/10\,\lvert 1 + 2\mathcal{R}\rvert^2$	$4.311\,\lvert 1 + 2\mathcal{R}\rvert^2$
	4.133	$2/5\,\lvert 1 - \mathcal{R}\rvert^2$	$1.653\,\lvert 1 - \mathcal{R}\rvert^2$
	3.875	$27/70\,\lvert 1 + 2/3\mathcal{R}\rvert^2$	$1.495\,\lvert 1 + 2/3\mathcal{R}\rvert^2$
	3.473	$4/35\,\lvert 1 - 1/2\mathcal{R}\rvert^2$	$0.3969\,\lvert 1 - 1/2\mathcal{R}\rvert^2$
	2.618	$1/10\,\lvert 1 + 2\mathcal{R}\rvert^2$	$0.2618\,\lvert 1 + 2\mathcal{R}\rvert^2$
	2.579	$2/5\,\lvert 1 - \mathcal{R}\rvert^2$	$1.0316\,\lvert 1 - \mathcal{R}\rvert^2$
	2.204	$27/70\,\lvert 1 + 2/3\mathcal{R}\rvert^2$	$0.8501\,\lvert 1 + 2/3\mathcal{R}\rvert^2$
	2.159	$4/35\,\lvert 1 - 1/2\mathcal{R}\rvert^2$	$0.246\,\lvert 1 - 1/2\mathcal{R}\rvert^2$

$$\mathcal{R} \equiv \mathcal{R}_{if} \equiv \frac{\langle \Omega_f \,|\, O'^{*}_{\lambda,-K_i-K_f} \,|\, -\Omega_i \rangle}{\langle \Omega_f \,|\, O'^{*}_{\lambda,-\Delta K} \,|\, \Omega_i \rangle} = \frac{\langle \frac{3}{2} \,|\, O'^{*}_{2,-2} \,|\, -\frac{1}{2} \rangle}{\langle \frac{3}{2} \,|\, O'^{*}_{2,-1} \,|\, \frac{1}{2} \rangle} ,$$

single-particle states ;

$$\equiv \frac{\langle \Omega_{V_f} \Omega_f \,|\, O'^{*}_{\lambda,-K_f-K_i} \,|\, -\Omega_{V_i} - \Omega_i \rangle}{\langle \Omega_{V_f} \Omega_f \,|\, O'^{*}_{\lambda,-\Delta K} \,|\, \Omega_{V_i} \Omega_i \rangle} = \frac{\langle 0, \frac{3}{2} \,|\, O'^{*}_{2,-2} \,|\, -2, \frac{3}{2} \rangle}{\langle 0, \frac{3}{2} \,|\, O'^{*}_{2,-1} \,|\, 2, -\frac{3}{2} \rangle}$$

$= \infty \cdot e^{i\varphi}$, vibrational states ,

$\Omega_V + \Omega = K$ (see text) .

For the calculation of deexcitations, provisional values had to be chosen for the E2-M1 mixing ratios, since M1 processes, not suppressed by a factor $\sim\beta^2$ as they are for excitation, favorably compete. For the $i \rightarrow f$ radiative decays, in the notation of Section I,

$$B(\lambda, i\rightarrow f) = \langle I_i K_i \lambda \Delta K | I_f K_f\rangle^2 \left|\langle \Omega_f | \mathcal{O}'^{*}_{\lambda-\Delta K} | \Omega_i\rangle\right|^2 \left| 1 + (-1)^{I_i+\frac{1}{2}} \frac{\langle I_i -K_i \lambda K_f + K_i | I_f K_f\rangle}{\langle I_i K_i \lambda \Delta K | I_f K_f\rangle} \mathcal{R}^{(\lambda)}_{if} \right|^2,$$

$$\mathcal{R}^{(\lambda)}_{if} = \langle \Omega_f | \mathcal{O}'^{*}_{\lambda-K_i-K_f} | -\Omega_i\rangle \Big/ \langle \Omega_f | \mathcal{O}'^{*}_{\lambda-\Delta K} | \Omega_i\rangle ; \tag{VI-81}$$

$$\left.\begin{aligned}
&B(E2, i\rightarrow f) = \langle I_i K_i 2 \Delta K | I_f K_f\rangle^2 \left|\langle \Omega_f | \mathcal{O}'^{*}_{2,-\Delta K} | \Omega_i\rangle\right|^2 \left| 1 + X^{(2)}_{if}\right|^2, \\
&B(M1, i\rightarrow f) = \langle I_i K_i 1 \Delta K | I_f K_f\rangle^2 \left|\langle \Omega_f | \mathcal{O}'^{*}_{1,-\Delta K} | \Omega_i\rangle\right|^2 \left| 1 + X^{(1)}_{if}\right|^2, \\
&X^{(2)}_{if} = (-1)^{I_i+\frac{1}{2}} \left[d_1 \delta_{K_i\frac{1}{2}} \delta_{K_f\frac{1}{2}} + d_2 \delta_{K_i\frac{3}{2}} \delta_{K_f\frac{1}{2}} + d_3 \delta_{K_i\frac{1}{2}} \delta_{K_f\frac{3}{2}} \right] \mathcal{R}^{(2)}_{if}, \\
&X^{(1)}_{if} = (-1)^{I_i+\frac{1}{2}} d_1' \, \delta_{K_i\frac{1}{2}} \delta_{K_f\frac{1}{2}} \mathcal{R}^{(1)}_{if} ;
\end{aligned}\right\} \tag{VI-82}$$

$$\left.\begin{aligned}
&T^{(\gamma)}_{\lambda} = \frac{8\pi(\lambda+1)}{\lambda[(2\lambda+1)!!]^2} \frac{1}{\hbar} \left(\frac{\Delta E_{if}}{\hbar c}\right)^{2\lambda+1} B(\lambda, i\rightarrow f) \text{ sec}^{-1}, \\
&T^{(\gamma)}_{E2} = \frac{1}{150} \left(\frac{\Delta E_{if}}{\hbar c}\right)^5 B(E2, i\rightarrow f), \\
&T^{(\gamma)}_{M1} = \frac{2}{9} \left(\frac{\Delta E_{if}}{\hbar c}\right)^3 B(M1, i\rightarrow f); \\
&\delta^2_{E2M1} = \frac{T^{(\gamma)}_{E2}}{T^{(\gamma)}_{M1}} = \frac{3}{100} \left(\frac{\Delta E}{\hbar c}\right)^2 \frac{B(E2, i\rightarrow f)}{B(M1, i\rightarrow f)} ;
\end{aligned}\right\} \tag{VI-83}$$

and for the $i \rightarrow f$ transitions in the present case,

$$\delta^2_{if} = \frac{3}{100} \left(\frac{\Delta E_{if}}{\hbar c}\right)^2 \frac{\langle I_i K_i 2 \Delta K | I_f K_f\rangle^2}{\langle I_i K_i 1 \Delta K | I_f K_f\rangle^2} \frac{\left|\langle \Omega_f | \mathcal{O}'^{*}_{2-\Delta K} | \Omega_i\rangle\right|^2}{\left|\langle \Omega_f | \mathcal{O}'^{*}_{1-\Delta K} | \Omega_i\rangle\right|^2} \frac{\left|1 + X^{(2)}_{if}\right|^2}{\left|1 + X^{(1)}_{if}\right|^2} . \tag{VI-84}$$

Calculations are made for δ^2 values $0, \infty$, and either multiples of the "single-particle estimates"[1]

$$\delta^2_{sp} = \frac{3}{100} \left(\frac{\Delta E}{\hbar c}\right)^2 \frac{B_{sp}(E2)}{B_{sp}(M1)} = \frac{3}{100} \left(\frac{\Delta E}{\hbar c}\right)^2 \cdot \frac{8}{75} \left(\frac{M_p c R_0^2}{\hbar}\right)^2 = \frac{2}{625} \left(\frac{\Delta E}{\hbar c/R_0} \cdot \frac{M_p c^2}{\hbar c/R_0}\right)^2 \ll 1, \tag{VI-85}$$

wherein M_p is the proton mass (for single-proton transitions) or experimental values, where available. For the cases in Tb with E2 symmetry modifications, trial values $\mathcal{R}_{if} = 0, \pm 1, \pm i, e^{i\phi}\infty$ (ϕ arbitrary) were used. Predicted decay fractions and relative gamma-ray intensities were computed via:

$$t_{if}^{(\gamma)} = \frac{T_{ifE2}^{(\gamma)} + T_{ifM1}^{(\gamma)}}{\sum_f \left[(1+\alpha_2^{if}) T_{ifE2}^{(\gamma)} + (1+\beta_1^{if}) T_{ifM1}^{(\gamma)}\right]} \,, \quad I_{if}^{(\gamma)} = t_{if}^{(\gamma)} P_i \,. \qquad \text{(VI-86)}$$

The computations in effect use

$$\begin{aligned} B(E2, i\to f) &= C_E \langle I_i K_i 2 \Delta K | I_f K_f \rangle^2 \left|1 + x_{if}^{(2)}\right|^2 B_{sp}(E2), \\ B(M1, i\to f) &= C_M \langle I_i K_i 1 \Delta K | I_f K_f \rangle^2 \left|1 + x_{if}^{(1)}\right|^2 B_{sp}(M1); \end{aligned} \qquad \text{(VI-87)}$$

$$\delta_{if}^2 = \frac{C_E}{C_M} \frac{\langle I_i K_i 2\Delta K | I_f K_f\rangle^2}{\langle I_i K_i 1\Delta K | I_f K_f\rangle^2} \frac{\left|1 + x_{if}^{(2)}\right|^2}{\left|1 + x_{if}^{(1)}\right|^2} \delta_{sp}^2 \,; \qquad \text{(VI-88)}$$

$$C_E = \frac{|\langle \Omega_f | \mathcal{O}'^{*}_{2\,-\Delta K} | \Omega_i \rangle|^2}{B_{sp}(E2)} \,, \quad C_M = \frac{|\langle \Omega_f | \mathcal{O}'^{*}_{1\,-\Delta K} | \Omega_i \rangle|^2}{B_{sp}(M1)} \,; \qquad \text{(VI-89)}$$

and provisionally set $C_E = 1$, $C_M = 0$ ($\delta^2 = \infty$); $C_E = 1$, $C_M = 1$ ($\delta^2 = \delta_{sp}^2$); etc.; $C_E = 0$, $C_M = 1$ ($\delta^2 = 0$).

The experimental information on the terbium interband decay mixing ratios is extremely scant. The 348.1-keV level is populated in Dy^{159} decay. Ketelle and Brossi[66] first reported transitions from this level to the first three ground-state band members from their gamma-gamma and gamma-X ray coincidence studies, and gave the intensity ratios 350-keV/290-keV/200-keV = 1.0/1.0/0.2, but no multipolarity determinations. Ryde et al.[76], from gamma-ray, beta-ray, gamma-gamma coincidence and gamma-beta coincidence measurements gave the level energy as 348.1 keV and found 211-, 289- and 348-keV transitions to the ground-state band all to be M1 + E2, but could not determine

δ^2. This however fixed $I\pi = 5/2+$ and suggested the Nilsson classification 5/2+[413]. They noted that if the transitions were pure E2 the B-value ratios would be $1.0 \pm 0.1/0.3 \pm 0.1/0.5 \pm 0.3$, compared to Alaga ratios 1/1.5/0.83; and if pure M1, $1.0 \pm 0.1/0.22 \pm 0.07/0.18 \pm 0.09$ compared to Alaga ratios 1/0.43/0.071. Diamond et al.[35] found that the 348-keV state was populated by E2 Coulomb excitation, but could not determine the E2-M1 mixing of the decay radiations. Thus there is essentially no definitive experimental value for the δ^2 in the decay of this band.

For the 580-keV band, Diamond et al. concluded from Doppler broadening of internal conversion decay lines and $\alpha_{tot}(K)$ estimates that the decay radiation was fast enough to be predominantly M1. As per remarks above, vibrational B(M1) values vanish, and any M1 components must be due to band mixing, or to vibrational-intrinsic coupling terms in the transition operators.

For the 1/2+[411] band decay as suggested in the work of Diamond et al., other than that the i.c. line shapes suggest fast predominantly M1 decay, no experimental information is available.

From (VI-85), for Tb, with $R_0 = 1.2\, A_2^{1/3}$ f., the single-particle estimate for mixing is

$$\delta^2_{if\,sp}(\mathrm{Tb}) = 3.2875 \times 10^{-9}\, \Delta E^2_{if,\,keV} \,. \qquad \text{(VI-90)}$$

Values of $t^{(\gamma)}_{if}$ were calculated via formulae given previously, in the form

$$\frac{T^{(\gamma)}_{if\,E2}}{T^{sp}_{i_0 f_0\,E2}} = \frac{B(E2, i \rightarrow f)}{B_{sp}(E2)} \left(\frac{\Delta E_{if}}{\Delta E_{i_0 f_0}} \right)^5 ,$$

$$\frac{T^{(\gamma)}_{if\,M1}}{T^{sp}_{i_of_o\,E2}} = \frac{1}{\delta^2_{i_of_o sp}} \frac{B(M1, i\rightarrow f)}{B_{sp}(M1)} \left(\frac{\Delta E_{if}}{\Delta E_{i_of_o}}\right)^3, \qquad \text{(VI-91)}$$

with the aid of (VI-87) to provide pure-band B/B_{sp} values; and

$$t^{(\gamma)}_{if} = \frac{T^{(\gamma)}_{if\,E2}/T^{sp}_{i_of_o\,E2} + T^{(\gamma)}_{if\,M1}/T^{sp}_{i_of_o\,E2}}{\sum_f\left[(1+\alpha_2^{if})T^{(\gamma)}_{if\,E2}/T^{sp}_{i_of_o\,E2} + (1+\beta_1^{if})T^{(\gamma)}_{if\,M1}/T^{sp}_{i_of_o\,E2}\right]} \qquad \text{(VI-92)}$$

$$= \frac{\langle I_iK_i2\Delta K|I_fK_f\rangle^2|1+x^{(2)}_{if}|^2\left(\frac{\Delta E_{if}}{\Delta E_{i_of_o}}\right)^5 + \frac{1}{\delta^2_{i_of_o sp}}\frac{C_M}{C_E}\langle I_iK_i1\Delta K|I_fK_f\rangle^2|1+x^{(1)}_{if}|^2\left(\frac{\Delta E_{if}}{\Delta E_{i_of_o}}\right)^3}{\sum_f\left[(1+\alpha_2^{if})\langle I_iK_i2\Delta K|I_fK_f\rangle^2|1+x^{(2)}_{if}|^2\left(\frac{\Delta E_{if}}{\Delta E_{i_of_o}}\right)^5 + (1+\beta_1^{if})\frac{1}{\delta_{i_of_o sp}}\frac{C_M}{C_E}\langle I_iK_i1\Delta K|I_fK_f\rangle^2|1+x^{(1)}_{if}|^2\left(\frac{\Delta E_{if}}{\Delta E_{i_of_o}}\right)^3\right]}.$$

Values of the pure-band decay branching fractions $t^{(\gamma)}_{if}$ and of $I^{(\gamma)}_{if} = P_i\, t^{(\gamma)}_{if}$ were calculated for various assumed E2/M1 ratios of the decay radiation and intrinsic intraband matrix elements of single-particle strength, and corrected for instrumental effects, just as with the ground-state band transitions. Resulting predicted photopeak intensities appear in Fig. VI-24. $t^{(\gamma)}_{if}$ and $I^{(\gamma)}_{if}$ are listed in Tables A-17 to 21.

In holmium the assumed states which can be reached by single E2 excitation from the ground state are illustrated in Fig. VI-22. The energies are suggested by the work of Diamond et al.[35] and model systematics. There are no low-lying negative-parity Nilsson states in Ho isotopes, so that all intrinsic excitations are strongly inhibited. Of the single-particle states identified in previous source work, the 3/2+[411] state at 361.5 keV has K-forbidden (vanishing) E1 matrix elements but K- and asymptotically-allowed M2 and E3 matrix elements to the 7/2-[523] ground-state band. The transitions from the 7/2+[404] state at 715.7 keV violate Λ and n_z asymptotic rules for E1 and E3, and either Λ or Λ and n_z rules for various

Ho^{165}

States Accessible from the G.S. via Single E2 Excitation

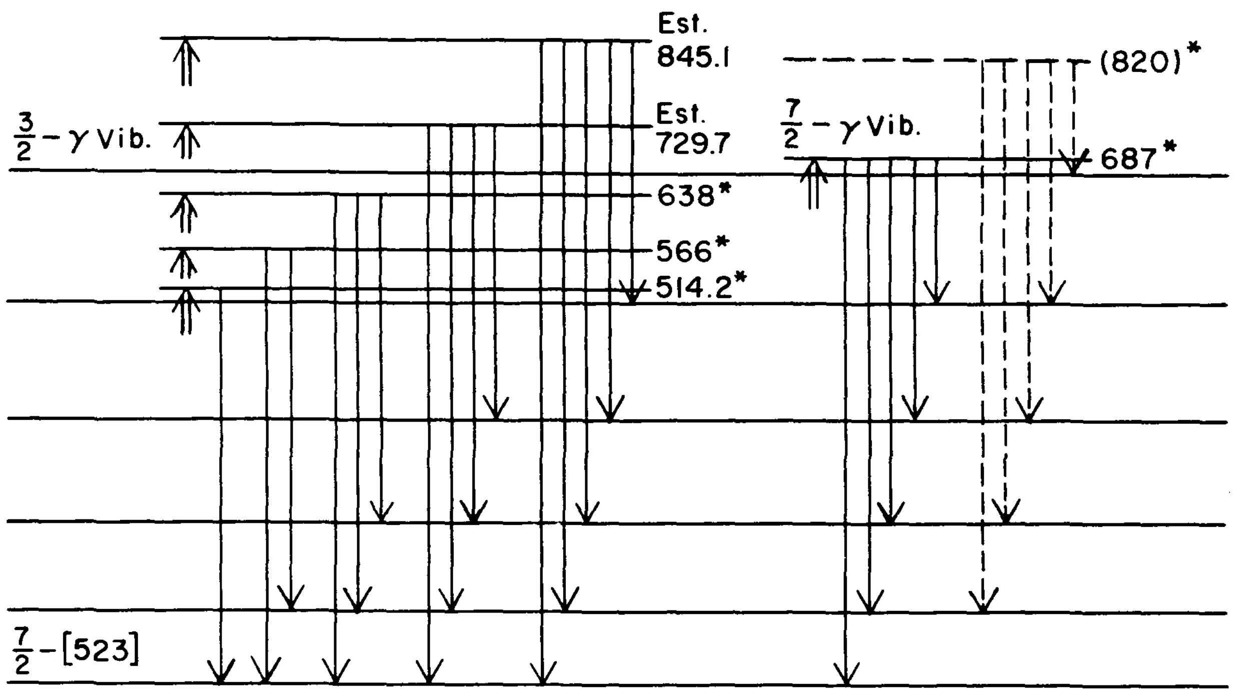

*Ref. 35

FIG VI-22

M2 single-particle transition operators. 5/2+[413] 995-keV$\rightarrow$ ground-state band transitions violate Λ and n_z rules for E1 and E3 operators and all the M2 operators except one, zs_+, for which the transitions are asymptotically allowed. 5/2+[402] 1055.6-keV$\rightarrow$ground-state band transitions violate the n_z rule for E1 operators, but certain of the M2 and E3 operators are asymptotically allowed. None of these transitions is expected to be seen following Coulomb excitation.

A list of the necessary Clebsch-Gordon coefficients for excitation of pure bands is found in Table VI-9 along with a list of the pure-band relative excitation populations P_i. Again values of $\ddagger_{if}^{(\gamma)}$ and $I_{if}^{(\gamma)}$ were calculated and corrected for instrumental effects. Results are given in Tables A-22 and 23. Plots of predicted photopeak intensities I_p $(B_{intr} = B_{sp})$ appear in Fig. VI-24.

For lutetium with its positive-parity ground state, the possible low-lying states are the vibrational states and the 343.40-keV 5/2+[402] state observed in source work and predicted by the Nilsson model, and the 504.7-keV 1/2+[411] state seen in source work, which has vanishing K-forbidden E2 matrix elements to the ground-state. The situation is illustrated in Fig. VI-23. Other states are the 9/2-[514] state which violates Λ and n_z rules for E1 and E3 operators for transitions to the ground-state band but has an asymptotically-allowed M2 operator (this state corresponds to a well-known 404-keV state in Ta^{181}), and an unobserved 7/2-[523] state which would be somewhat high in energy and would have asymptotically-forbidden E1, M2 and E3

Table VI-9

Ho E2↑ Transitions

<u>7/2-[523] → 3/2- γ Vib.</u>

$\langle 7/2\ 7/2\ 2\ {-2} \mid 3/2\ 3/2 \rangle = 1/2$

$\langle 7/2\ 7/2\ 2\ {-2} \mid 5/2\ 3/2 \rangle = 1/3$

$\langle 7/2\ 7/2\ 2\ {-2} \mid 7/2\ 3/2 \rangle = 2/15$

$\langle 7/2\ 7/2\ 2\ {-2} \mid 9/2\ 3/2 \rangle = 1/33$

$\langle 7/2\ 7/2\ 2\ {-2} \mid 11/2\ 3/2 \rangle = 1/330$

Sum 1

<u>7/2-[523] → 11/2- γ Vib.</u>

$\langle 7/2\ 7/2\ 2\ 2 \mid 11/2\ 11/2 \rangle = 1$

E_{lev}, keV	P_{sp}, barn/nucl.	$\mathcal{F}$	$P = \mathcal{F} P_{sp}$
514.2	4.740×10^{-3}	1/2	2.640×10^{-3}
566	4.476	1/3	1.492
638	4.111	2/15	0.5482
Est. 729.7#	3.669*	1/33	0.1112
Est. 845.1#	3.113	1/330	0.009433
687	3.874	1	3.874
(820)	(3.234)**	0	0

* Est. by extrapolation of P_{sp} vs. E_{lev} curve.

** If E2 were not impossible on angular-momentum grounds.

\# From $E_I = E_0 + AI(I+1) + BI^2(I+1)^2$, and $E_{3/2} = 514.2$ keV, $E_{5/2} = 566$ keV, $E_{7/2} = 638$ keV, which implies $A = 10.437$ keV, $B = 6.1905$ eV.

Lu^{175}

States Accessible from the G.S. via Single E2 Excitation

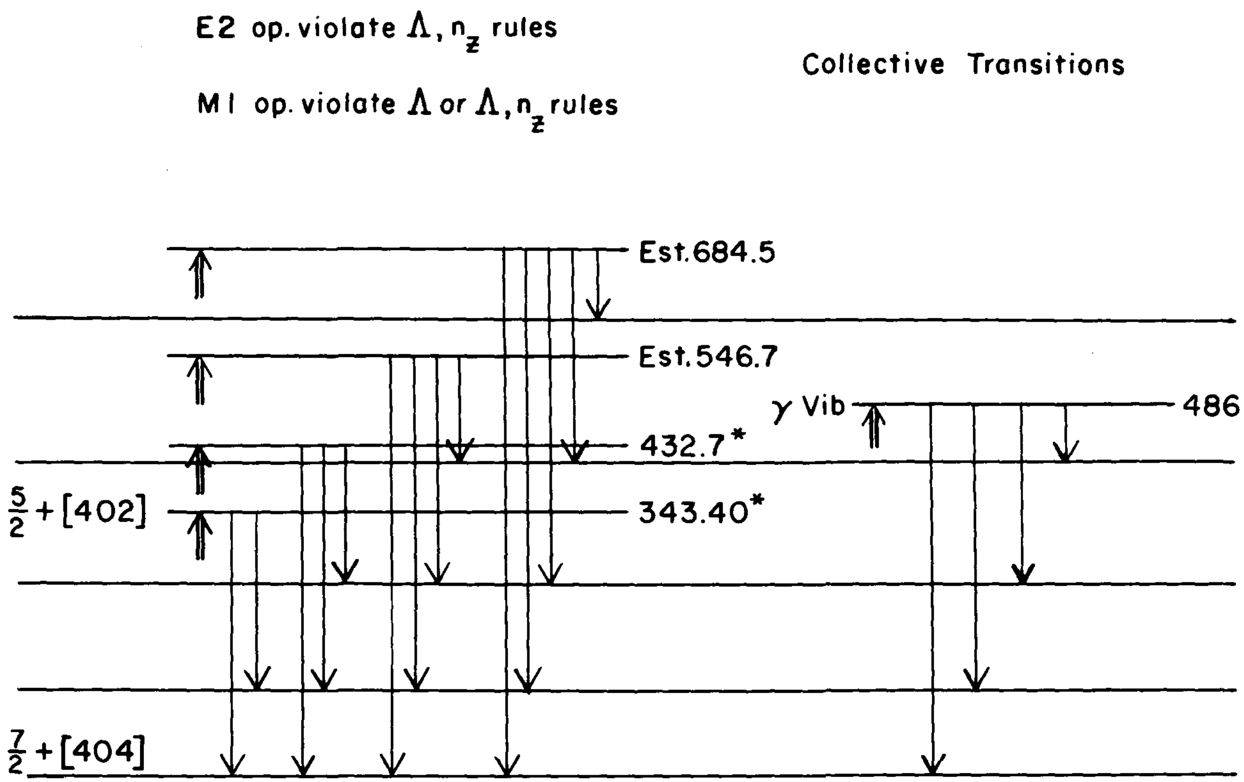

* Ref. 178

FIG VI-23

transitions to the ground-state band.

The necessary Clebsch-Gordon coefficients are the same as in the holmium cases with the same state spins; the $K = 7/2 \rightleftarrows K = 5/2$ transition C.G. coefficients and the pure-band excitation populations P_i are listed in Table VI-10.

A number of observations exist pertinent to the mixing ratios for transitions from the first two members of the 5/2+[402] band, populated in Hf^{175} decay, to the 7/2+[404] ground-state band. Wilkinson and Hicks[148] first observed this decay, found a ~350-keV transition, and obtained the rough measured value $\alpha_K(350) \sim 0.4$. Burson and Rutledge[170] reported a 342-keV $\alpha_K/\alpha_L = 4.95 \pm 0.25$. Bashilev et al.[171], from internal- and external-conversion measurements on transitions from the 342-keV state to the first two ground-state band levels, found $\alpha_K/\alpha_{LM}(342.3) = 4.94 \pm 0.5$ ($K/L \approx 6$), $\alpha_K/\alpha_{LM}(228.4) = 2.0 \pm 0.5$, and concluded that the 342-keV transitions are M1 + E2, M1 being between 49% and 79% (δ^2 from 1.04 to 0.27). Mize et al.[176] and Hatch et al.[78] made observations on transitions between the first two levels of the 5/2+ and of the ground-state bands. For the 343-keV transition Mize et al. from α_K/α_{LM} concluded that $\delta^2 \leq 0.25$; Hatch et al., that $0 \leq \delta^2 \leq 0.33$. For the 229-keV transition to the 114-keV ground-state band level Mize et al. and Hatch et al. found from i.c. coefficient measurements that the transition is predominantly E2. For transitions from the 432-keV first rotationally-excited upper-band member to the ground state, Hatch et al. found from i.c. coefficient measurements that again, $0 \leq \delta^2 \leq 0.33$. E. Klema, from the upper-intraband-interband

Table VI-10

Lu E2 Transitions

$7/2+[404] \rightarrow 5/2+[402]$

$\langle 7/2\ 7/2\ 2\ -1 \mid 5/2\ 5/2\rangle^2 = 5/12$

$\langle 7/2\ 7/2\ 2\ -1 \mid 7/2\ 5/2\rangle^2 = 2/5$

$\langle 7/2\ 7/2\ 2\ -1 \mid 9/2\ 5/2\rangle^2 = 7/44$

$\langle 7/2\ 7/2\ 2\ -1 \mid 11/2\ 5/2\rangle^2 = 4/165$

Sum = 1

E_{lev}^{*}, keV	P_{sp}, barn/nucl.	$\mathcal{F}$	$P = \mathcal{F} P_{sp}$
343.40*	5.668×10^{-3}	5/12	2.362×10^{-3}
432.76*	5.158	2/5	2.063
Est. 546.70	4.505	7/44	0.7167
Est. 684.51	3.78	4/165	0.009164
514.4	4.671		
646	3.980		
665	3.885		
486 ± 2	$(4.835 \pm 0.15) \times 10^{-3}$	1#	4.835

* These are precision energies due to Hatch et al.[178], who also observed ground-state band level energies of 113.81 ± 0.02 keV and 251.46 ± 0.07 keV. From the formula $E_I = E_0 + AI(I+1) + BI^2(I+1)^2$ and the value of $A_{g.s.}/B_{g.s.}$, estimates for A and B for the upper band were calculated and used to estimate the higher upper-band energies. The resulting values of A and B were approximately equal to those of the ground-state band; the equivalent spacing for a fictitious $7/2+ \rightarrow 5/2+$ transition in the upper band is 89.36 ± 0.01 keV, which is only 0.1% different from the corresponding ground-state band value of 89.26 keV as found by Hatch et al.

\# Assuming a $K = 11/2$ γ-vibrational band.

89.4 keV-343.4 keV gamma-gamma angular correlation, concluded that 3/2,5/2,7/2→5/2→7/2 spin sequences were compatible with the data, and that for the 7/2→5/2→7/2 rotational sequence, $\delta = -0.1$ ($\delta^2 = 0.01$). B.Deutsch measured the 343-keV transition mean life and found $\tau_\gamma(343) = (4.7 \pm 0.4)\times 10^{-10}$ sec., and concluded with the help of previous mixing determinations that B(M1,343) $= 1/700\ B_{sp} = 1/4000$ times the corresponding B(M1) value in Ta^{181}, indicating a strong dipole inhibition but suggesting also a certain amount of remaining uncertainty.

On the basis of these observations, besides 0 and ∞, trial values for δ^2 for the 343-keV transition of 0.1 and 0.25 are employed. Predicted $\ddagger_{if}$ and I_{if} values are presented in Tables A-24 and 25 for $B_{intr} = B_{sp}$. Plots of corresponding photopeak intensities appear in Fig. VI-24.

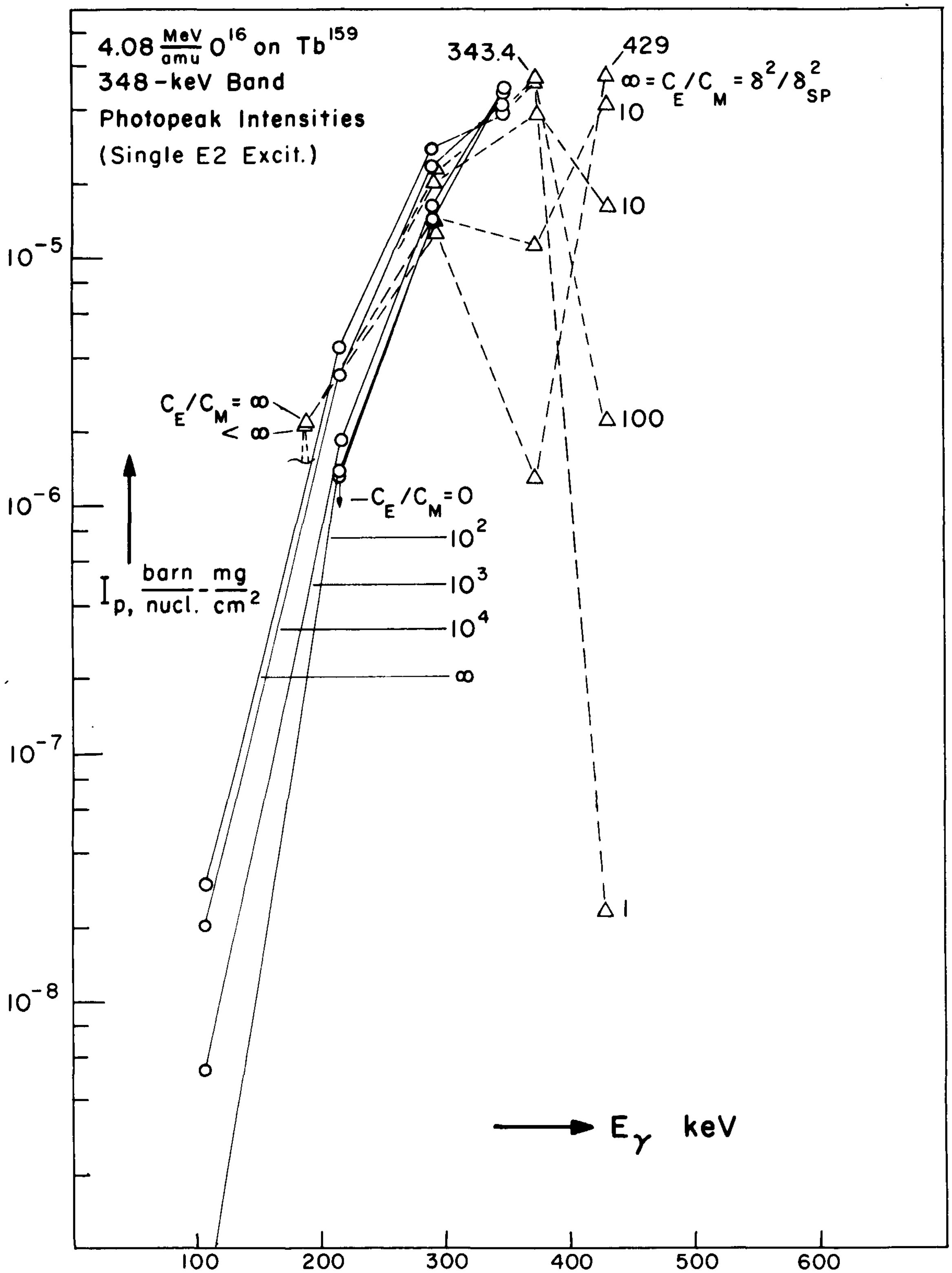
4.08 MeV/amu O16 on Tb159
348-keV Band
Photopeak Intensities
(Single E2 Excit.)
343.4
429
∞ = CE/CM = δ2/δ2SP
10
10
100
1
CE/CM = ∞
< ∞
−CE/CM = 0
102
103
104
∞
10−5
10−6
10−7
10−8
Ip, barn/nucl. - mg/cm2
Eγ keV
100
200
300
400
500
600

FIG VI - 24a

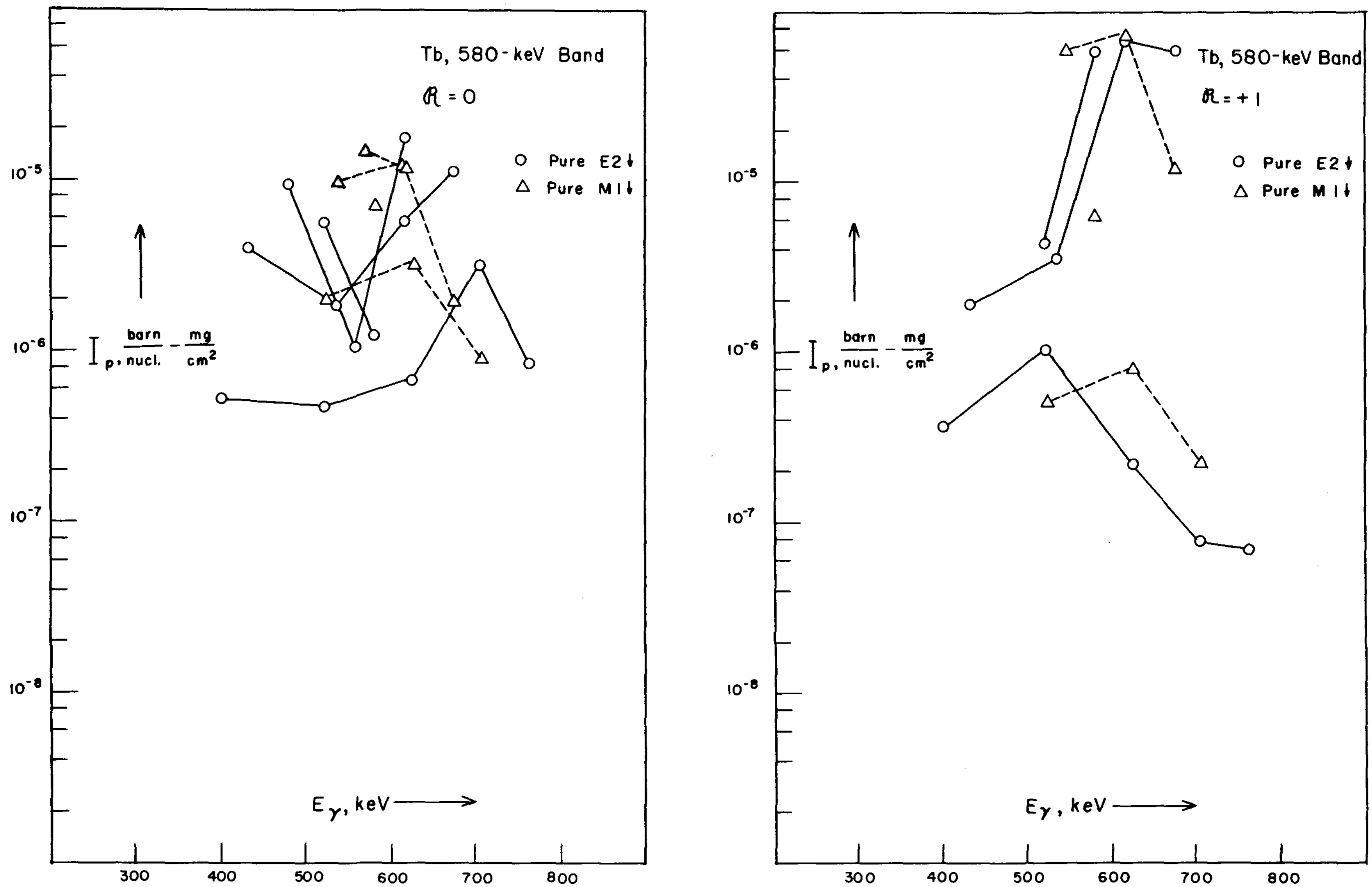

Tb, 580-keV Band
R = 0
Pure E2↓
Pure M1↓
10^{-5}
10^{-6}
10^{-7}
10^{-8}
$I_p, \frac{barn}{nucl.} - \frac{mg}{cm^2}$
E_γ, keV
300
400
500
600
700
800
Tb, 580-keV Band
R = +1
Pure E2↓
Pure M1↓
10^{-5}
10^{-6}
10^{-7}
10^{-8}
$I_p, \frac{barn}{nucl.} - \frac{mg}{cm^2}$
E_γ, keV
300
400
500
600
700
800

FIG VI-24b

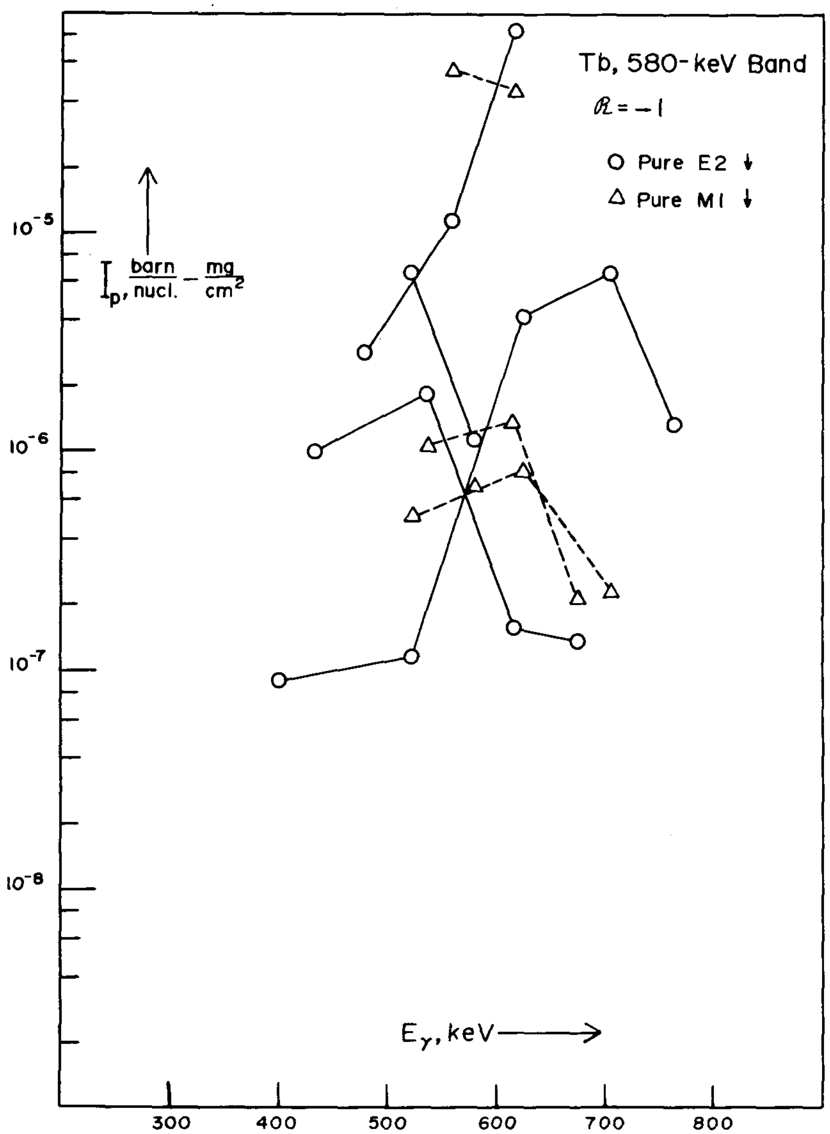

Tb, 580-keV Band
$\mathcal{R} = -1$
Pure E2
Pure M1
$I_p, \frac{barn}{nucl.} - \frac{mg}{cm^2}$
10^{-5}
10^{-6}
10^{-7}
10^{-8}
E_γ, keV
300
400
500
600
700
800

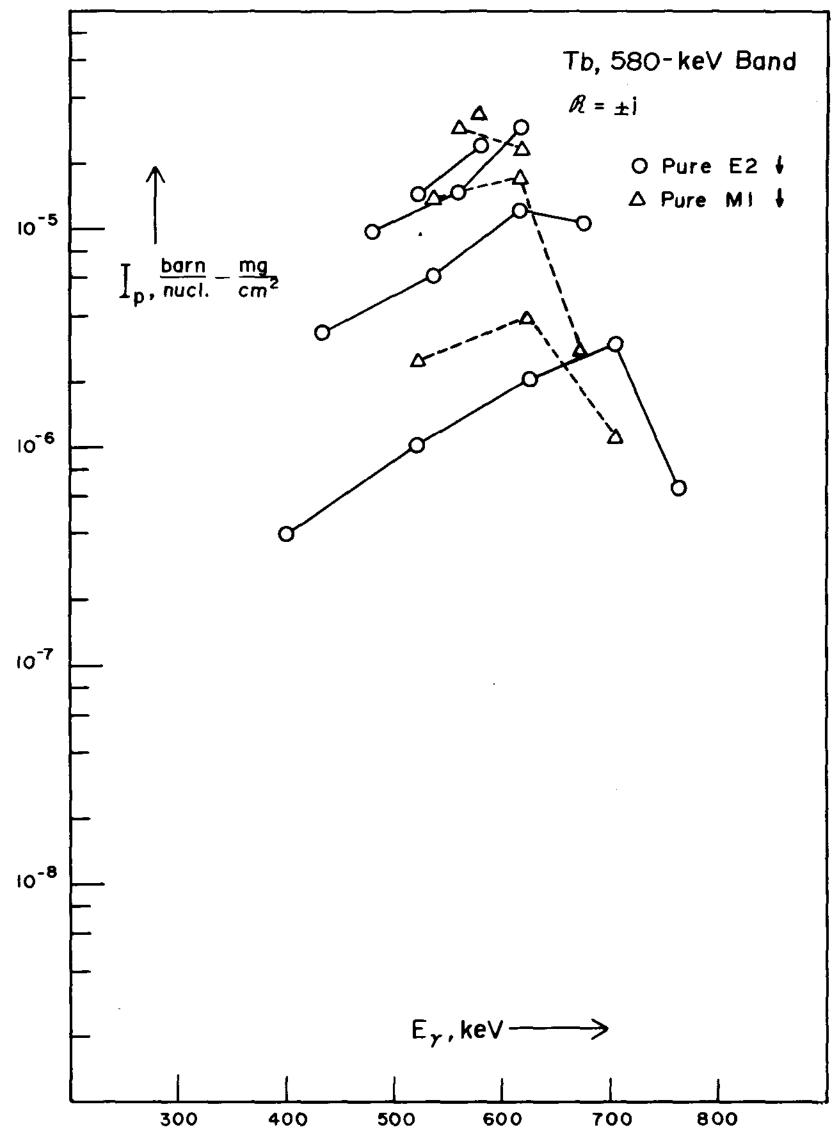

Tb, 580-keV Band
$\mathcal{R} = \pm i$
Pure E2
Pure M1
$I_p, \frac{barn}{nucl.} - \frac{mg}{cm^2}$
10^{-5}
10^{-6}
10^{-7}
10^{-8}
E_γ, keV
300
400
500
600
700
800

FIG VI-24c

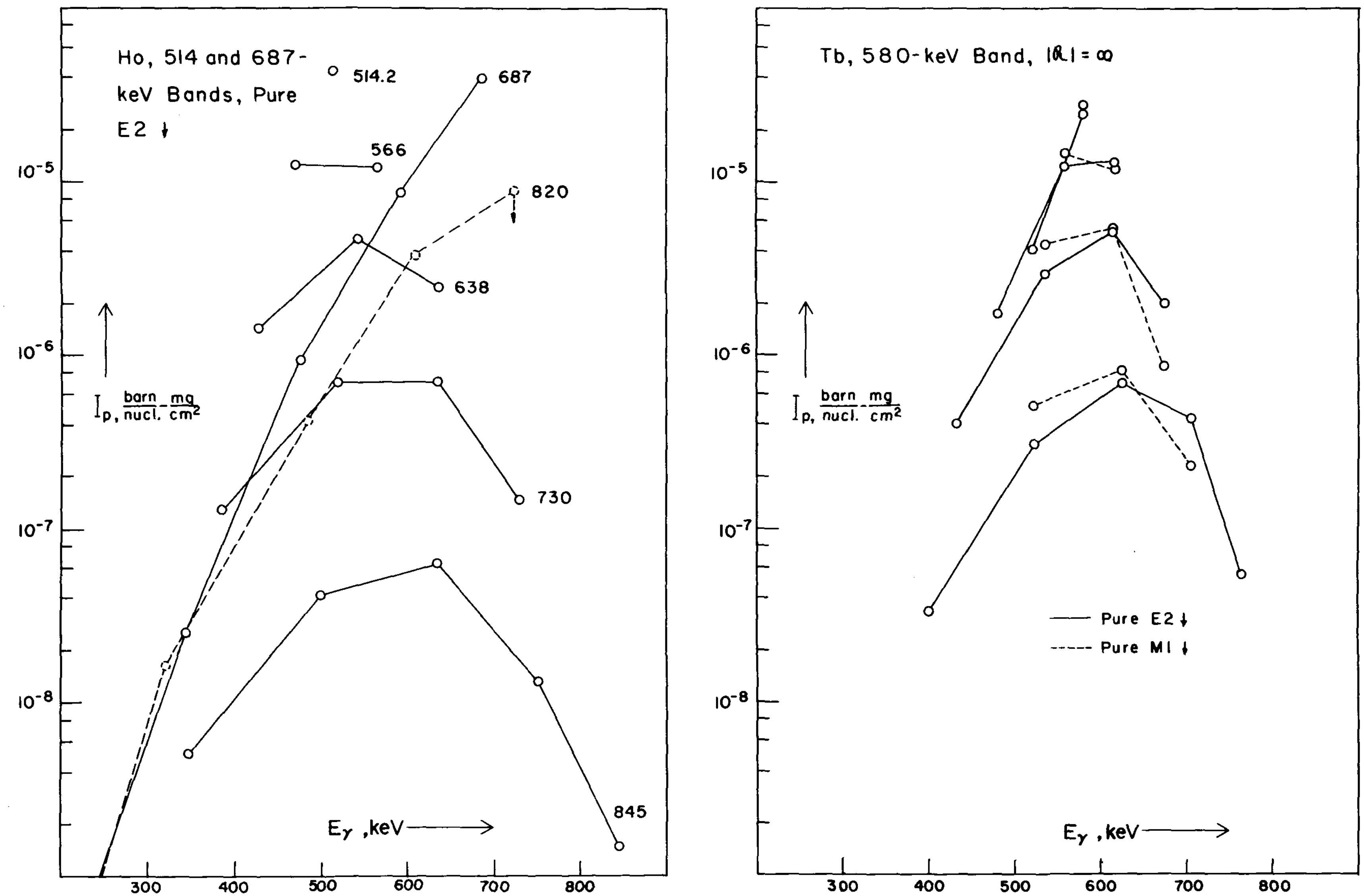
Ho, 514 and 687-keV Bands, Pure E2 ↓
514.2
687
566
820
638
730
845
$I_p, \frac{barn}{nucl.} \frac{mg}{cm^2}$
E_γ, keV
Tb, 580-keV Band, $|\Delta| = \infty$
Pure E2 ↓
Pure M1 ↓
10^{-5}
10^{-6}
10^{-7}
10^{-8}
300
400
500
600
700
800

FIG VI-24 d

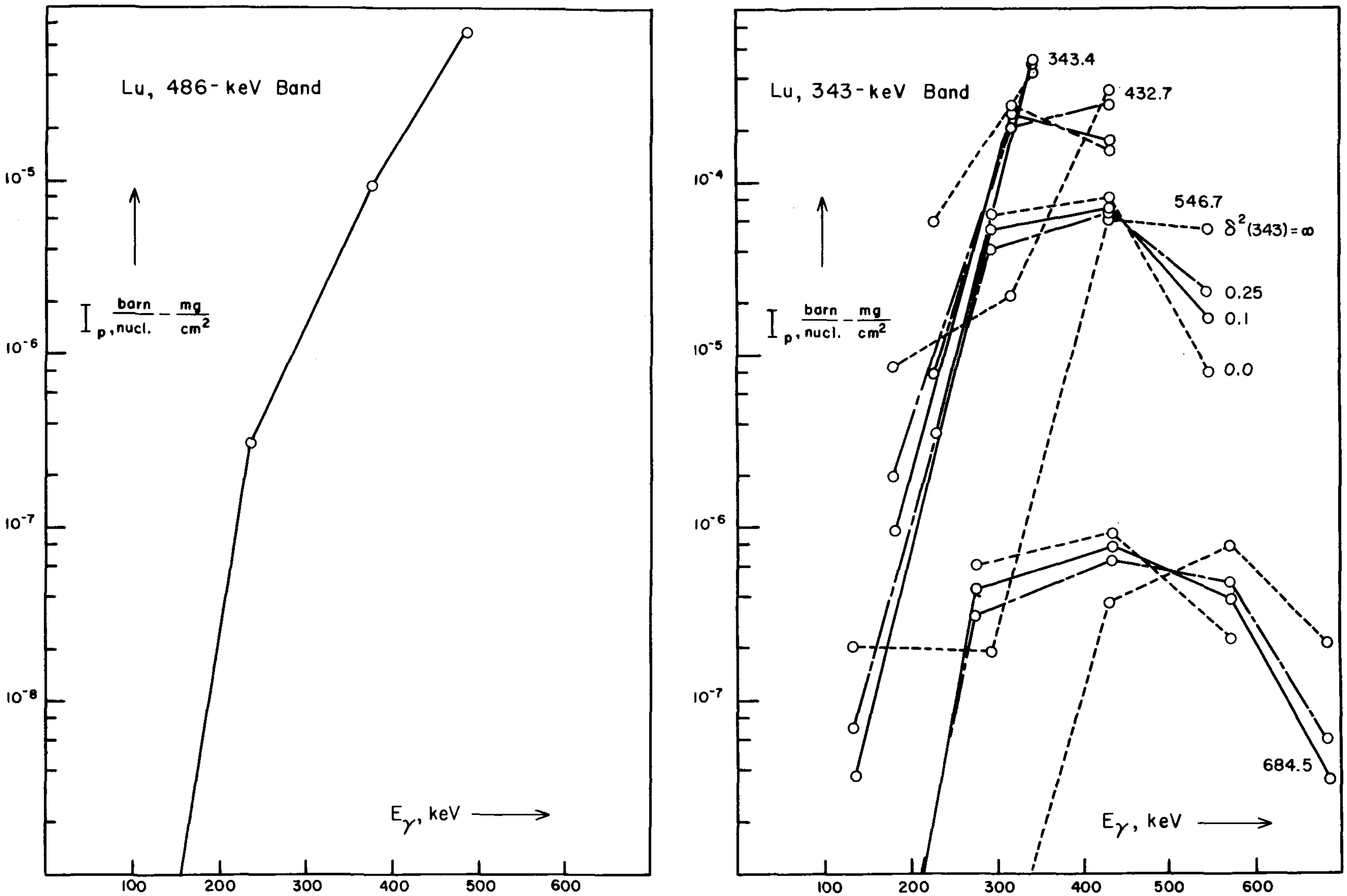

Lu, 486-keV Band
$I_{p}, \frac{barn}{nucl.} - \frac{mg}{cm^2}$
10^{-5}
10^{-6}
10^{-7}
10^{-8}
E_γ, keV
100
200
300
400
500
600
Lu, 343-keV Band
343.4
432.7
546.7
$\delta^2(343) = \infty$
0.25
0.1
0.0
684.5
10^{-4}
10^{-5}
10^{-6}
10^{-7}

FIG VI-24e

VII. Experimental Results and their Interpretation

A. Terbium

Spectra obtained in coincidence with backscattered oxygen ions are displayed in Fig. VII-1. Since an accidental coincidence spectrum identical to a singles spectrum in appearance is present in addition to any true coincidences, in order to allow for this with minimum deterioration of counting statistics the singles spectrum was renormalized to the random coincidence counting rate and subtracted off. As anticipated on the basis of the theory of Alder and Winther[3], for the relatively large values of the parameter $q_{eff}(\theta)$ associated with backward scattering angles of heavy-ion projectiles just below the Coulomb barrier, considerable high-order multiple excitation of the ground-state band occurred. A gamma-ray singles spectrum obtained with a cooled germanium semiconductor detector are displayed in Fig. VII-2. Features discernable above background are a number of the ground-state band transitions, 348-keV and 580-keV gamma rays discussed below and 511-keV annihilation radiation. (On the spectrum shown there is a non-repeating 332-keV feature.) Coincident spectra with the Ge detector could not be obtained because of the prohibitively low gamma-ray counting rate arising from the inherent detection inefficiency of the device.

Analysis of the energies of the gamma rays attributed to the ground-state band leads to the interesting result that there exists the phenomenon, similar to the well-known "decoupling" phenomenon due to non-zero diagonal matrix elements of the

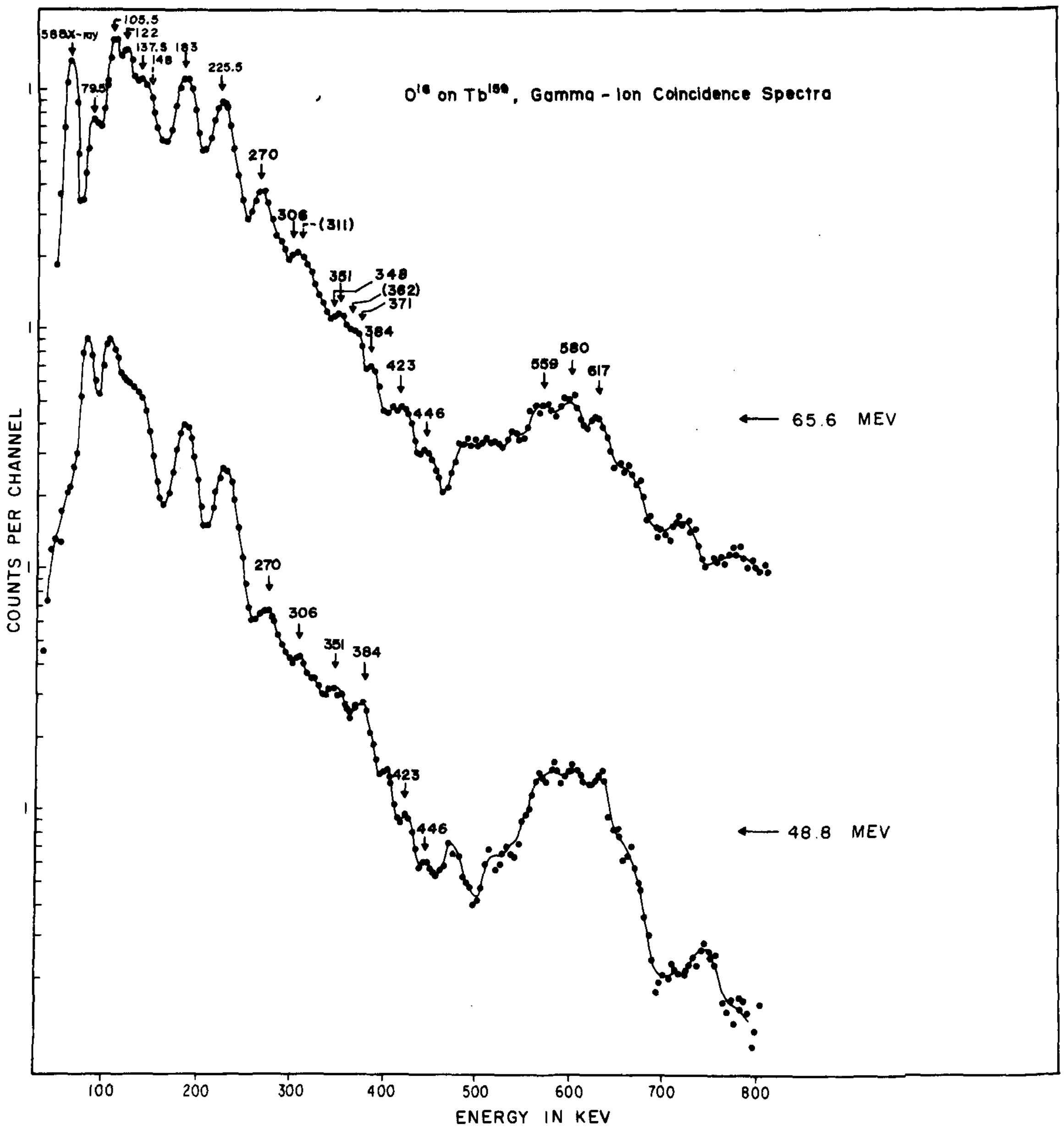

O^{16} on Tb^{159}, Gamma - Ion Coincidence Spectra
Sb X-ray
79.5
105.5
122
137.5
148
183
225.5
270
306
(311)
351
348
(362)
371
384
423
446
559
580
617
65.6 MEV
270
306
351
384
423
446
48.8 MEV
COUNTS PER CHANNEL
ENERGY IN KEV
100
200
300
400
500
600
700
800

FIG VII-1

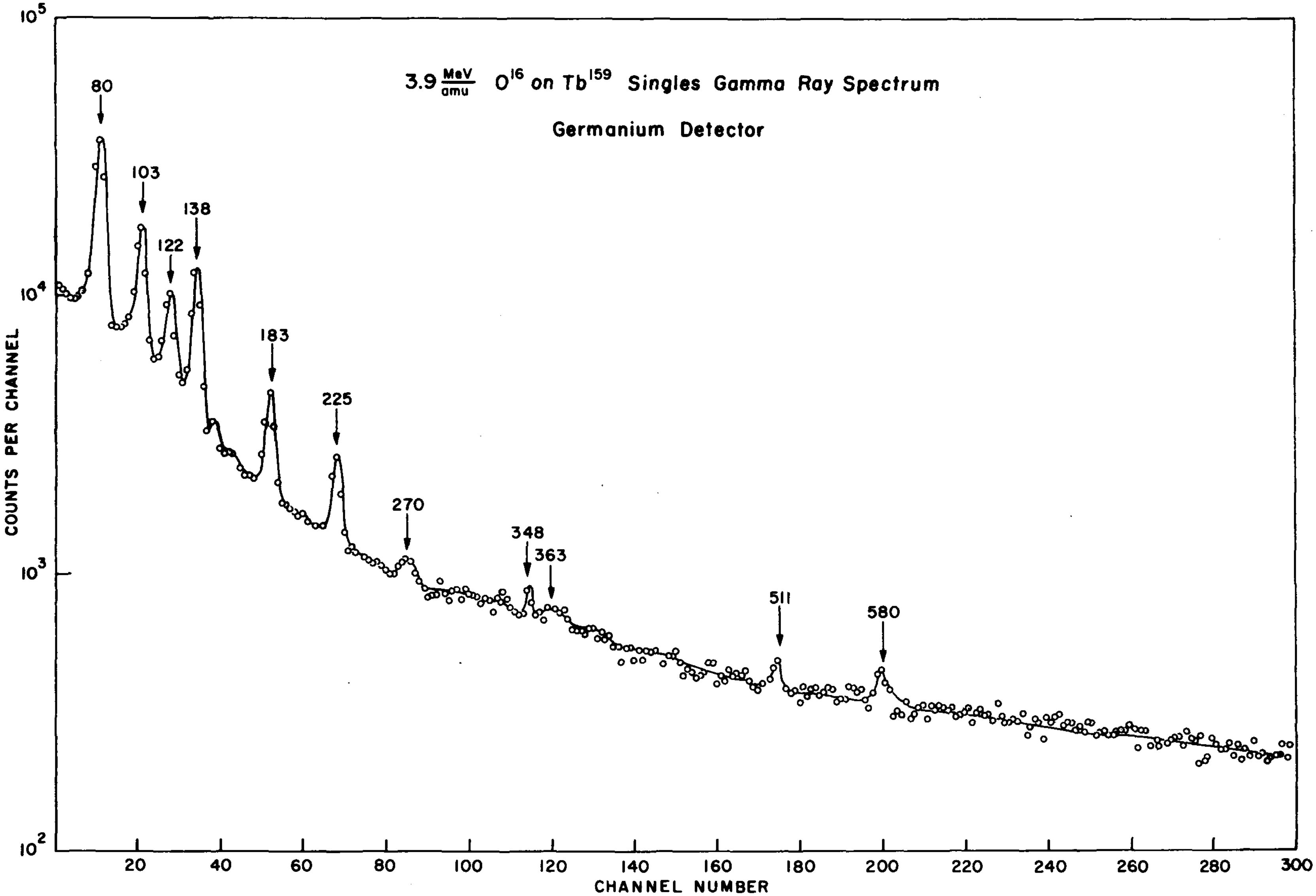

3.9 MeV/amu O^{16} on Tb^{159} Singles Gamma Ray Spectrum
Germanium Detector
80
103
122
138
183
225
270
348
363
511
580
COUNTS PER CHANNEL
CHANNEL NUMBER
10^5
10^4
10^3
10^2
20
40
60
80
100
120
140
160
180
200
220
240
260
280
300

FIG VII - 2

Coriolis perturbation in $K = 1/2$ rotational bands and characterized by energy corrections of alternating sign. Possible origins were discussed in Section I. With the energies of component states assumed to be of the form

$$E_I = E_0 + AI(I+1) + BI^2(I+1)^2 + C(-1)^{I+\frac{1}{2}}(I-\tfrac{1}{2})(I+\tfrac{1}{2})(I+\tfrac{3}{2}) \qquad \text{(VII-1)}$$

where the ground state has spin $I_0 = K = 3/2$ and $I = I_0$, I_0+1, $I_0+2, \ldots$, it can be shown that

$$y \equiv \frac{E_{I+1} - E_I}{2(I+1)} = A + (-1)^{I+\frac{1}{2}}\frac{C}{4} + \left[\frac{B}{2} - (-1)^{I+\frac{1}{2}}\frac{C}{4}\right]\chi \qquad \text{(VII-2)}$$

where

$$\chi \equiv [2(I+1)]^2. \qquad \text{(VII-3)}$$

If these quantities are calculated and plotted they should fall two straight lines, corresponding to odd and even values of $I+\frac{1}{2}$. Such a plot, derived from the observed energies, is calculated in Table VII-1 and appears in Fig. VII-3. Fitting these data to two straight lines by least squares (formulae in Appendix I) yielded the values for the intercepts $\alpha_\pm$ and slopes $\beta_\pm$ listed in Fig. VII-3, which are related to A, B and C as follows:

$$\begin{aligned}
\alpha_\pm &= A \pm \tfrac{1}{4}C \\
\beta_\pm &= \tfrac{1}{2}B \mp \tfrac{1}{4}C \\
A &= \tfrac{1}{2}(\alpha_+ + \alpha_-) \\
B &= \beta_+ + \beta_- \\
C &= -2(\beta_+ - \beta_-) .
\end{aligned} \qquad \text{(VII-4)}$$

Table VII-1

Tb^{159} Ground-State Band Parameters

I	$[2(I+1)]^2 \equiv x$	Assumed $E_I - E_{I_0}$, keV	$E_{I+1} - E_I$	$\frac{E_{I+1}-E_I}{2(I+1)} \equiv y$	Weight w *
$K=3/2=I_0$	25	0	58.00±0.01	11.6000	5000
5/2	49	58.00±0.01	79.50±0.02	11.3571	3400
7/2	81	137.50±0.02	103.5±1	11.5000	90
9/2	121	241±1	122±1	11.0909	110
11/2	169	363±1	148±3	11.3846	42
13/2	225	511±3	158±4	10.5333	37
15/2	289	669±4	193±5	11.3529	34
17/2	361	862±5	191±6	10.0526	31
19/2	441	1053±6	237±6	11.0476	34
21/2	529	1285±6	214±7	9.3044	33
23/2	625	1499±7	-----	--------	----

$$* \quad \frac{E_{I+1} - E_I \pm \delta(E_{I+1} - E_I)}{2(I+1)} \equiv y \pm \delta y \quad ; \quad w = \frac{10}{|\delta y|}$$

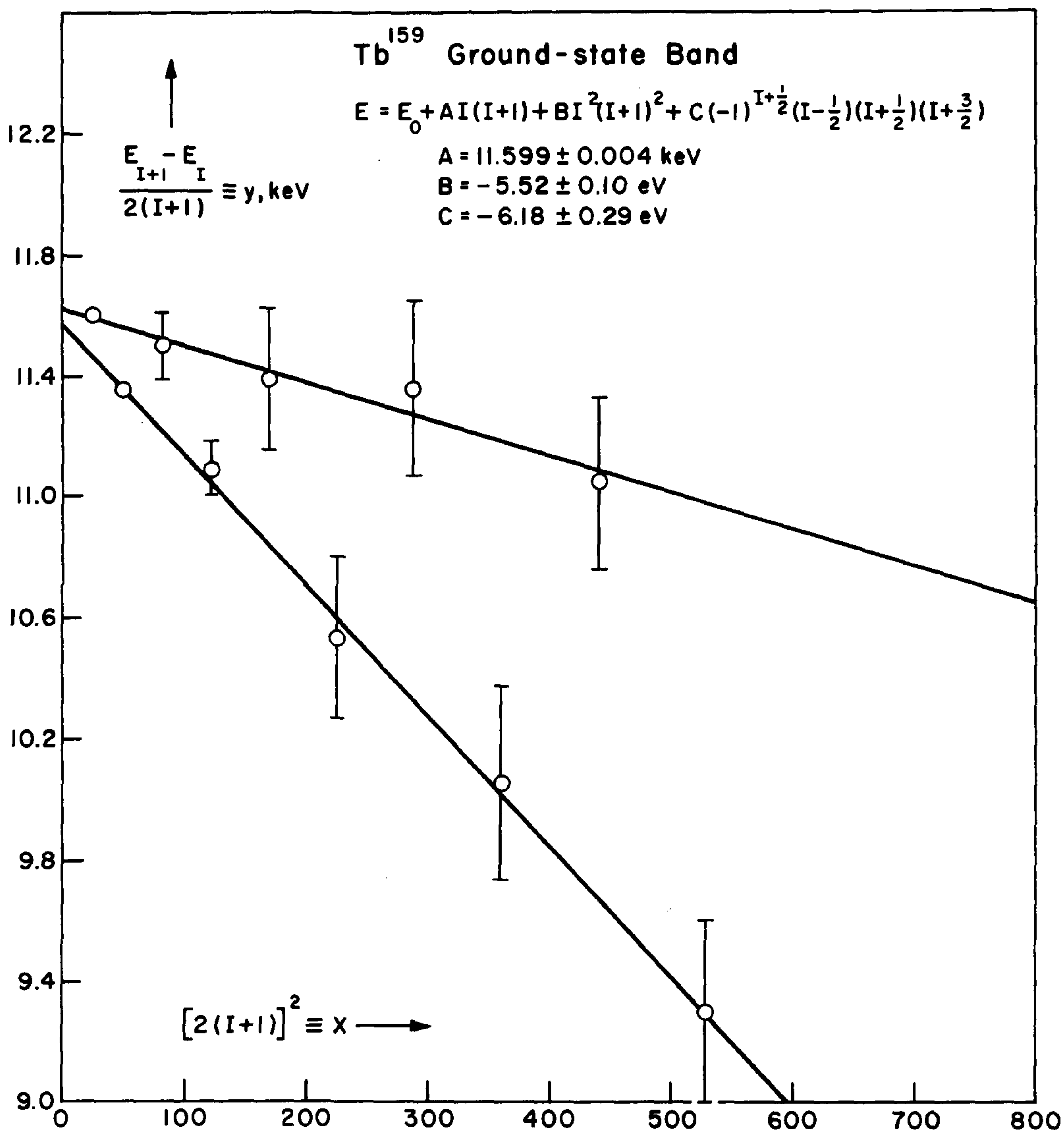

Tb159 Ground-state Band
E = E0 + AI(I+1) + BI2(I+1)2 + C(-1)I+1/2(I-1/2)(I+1/2)(I+3/2)
A = 11.599 ± 0.004 keV
B = -5.52 ± 0.10 eV
C = -6.18 ± 0.29 eV
(E_I+1 - E_I)/2(I+1) ≡ y, keV
[2(I+1)]2 ≡ x
12.2
11.8
11.4
11.0
10.6
10.2
9.8
9.4
9.0
0
100
200
300
400
500
600
700
800

FIG VII - 3

The final results are

$$A = 11.599 \pm 0.004 \text{ keV}$$
$$B = -5.52 \pm 0.10 \text{ eV} \qquad \text{(VII-5)}$$
$$C = -6.18 \pm 0.29 \text{ eV}$$

which agree within the quoted error limits with the findings of Diamond et al.[35] An alternative display of the data, calculated and displayed in Table VII-2 and Fig. VII-4, is based on the observation that

$$\frac{E_I - E_K}{I(I+1)-K(K+1)} = A + B[I(I+1)+K(K+1)+C(-1)^{I+\frac{1}{2}}\frac{(I-\frac{1}{2})(I+\frac{1}{2})(I+\frac{3}{2})}{I(I+1)-K(K+1)} - \frac{6C}{I(I+1)-K(K+1)} \qquad \text{(VII-6)}$$

which apart from the small I-dependent correction on the end takes, when plotted against $I(I+1)+K(K+1)$, the form of a straight line of slope A, y-intercept B, plus an I-dependent alternating correction term.

Diamond et al.[35] mention the possible mechanism for this suggested by Mottelson: band-mixing induced by the Coriolis perturbation of a (decoupled) $|K|=1/2$ band into the $K=3/2$ ground-state band, leading to the formula for C:

$$C = a_\nu \frac{\hbar^2}{2\mathcal{J}'}\left[\frac{\frac{\hbar^2}{2\mathcal{J}'}\langle \psi_{\frac{3}{2}} | j_{+'} | \psi_{\frac{1}{2}}\rangle}{\delta\varepsilon^0}\right]^2 . \qquad \text{(VII-7)}$$

This situation results in corrections to the interband transition moments $\langle I'M'K^s | \mathcal{M}(E2,\mu) | IM\bar{K}^s\rangle$, as noted in Section I, from which, with neglect of the term $\langle \psi_{I'M'K}^s | \mathcal{M} | \psi_{IM\bar{K}}^s\rangle$ for the pure-band intrinsic E2 transition moment, the modification of the collective moment, embodied in the term $\frac{1}{\delta E^0_{IK\bar{K}}}\left[C_{IK\bar{K}}\langle \psi_{I'M'K}^s | \mathcal{M} | \psi_{IMK}^s\rangle - C_{I'K\bar{K}}\langle \psi_{I'M'\bar{K}}^s | \mathcal{M} | \psi_{IM\bar{K}}^s\rangle\right]$ with the C's denoting Coriolis matrix elements, leads to the

The final results are

$$A = 11.599 \pm 0.004 \text{ keV}$$
$$B = -5.52 \pm 0.10 \text{ eV} \qquad \text{(VII-5)}$$
$$C = -6.18 \pm 0.29 \text{ eV}$$

which agree within the quoted error limits with the findings of Diamond et al.[35] An alternative display of the data, calculated and displayed in Table VII-2 and Fig. VII-4, is based on the observation that

$$\frac{E_I - E_K}{I(I+1)-K(K+1)} = A + B[I(I+1)+K(K+1)] + C(-1)^{I+\frac{1}{2}}\frac{(I-\frac{1}{2})(I+\frac{1}{2})(I+\frac{3}{2})}{I(I+1)-K(K+1)} - \frac{6C}{I(I+1)-K(K+1)} \qquad \text{(VII-6)}$$

which apart from the small I-dependent correction on the end takes, when plotted against $I(I+1)+K(K+1)$, the form of a straight line of slope A, y-intercept B, plus an I-dependent alternating correction term.

Diamond et al.[35] mention the possible mechanism for this suggested by Mottelson: band-mixing induced by the Coriolis perturbation of a (decoupled) $|K|=1/2$ band into the $K=3/2$ ground-state band, leading to the formula for C:

$$C = a_\upsilon \frac{\hbar^2}{2\mathcal{J}'}\left[\frac{\frac{\hbar^2}{2\mathcal{J}'}\langle \psi_{\frac{3}{2}} | j_{+'} | \psi_{\frac{1}{2}} \rangle}{\delta\varepsilon^0}\right]^2 . \qquad \text{(VII-7)}$$

This situation results in corrections to the interband transition moments $\langle I'MK^s | \mathcal{M}(E2,\mu) | IM\bar{K}^s \rangle$, as noted in Section I, from which, with neglect of the term $\langle \psi^s_{IMK} | \mathcal{M} | \psi^s_{IM\bar{K}} \rangle$ for the pure-band intrinsic E2 transition moment, the modification of the collective moment, embodied in the term $\frac{1}{\delta E^0_{IK\bar{K}}}\left[C_{IK\bar{K}}\langle \psi^s_{I'MK} | \mathcal{M} | \psi^s_{IMK} \rangle - C_{I'K\bar{K}}\langle \psi^s_{I'M\bar{K}} | \mathcal{M} | \psi^s_{IM\bar{K}} \rangle\right]$ with the C's denoting Coriolis matrix elements, leads to the

Table VII-2

Tb^{159} Ground-State Band

I	$I(I+1)+K(K+1)$	$E_I - E_{I_0}$	$\frac{E_I - E_{I_0}}{I(I+1)-K(K+1)}$
3/2	7.5	0	0
5/2	12.5	58.00±0.01	11.6000±0.002
7/2	19.5	137.50±0.02	11.4580±0.002
9/2	28.5	241±1	11.4762±0.048
11/2	39.5	363±2	11.3438±0.062
13/2	52.5	511±3	11.3556±0.067
15/2	67.5	669±4	11.1500±0.067
17/2	84.5	862±5	11.1948±0.065
19/2	103.5	1053±6	10.9688±0.062
21/2	124.5	1285±6	10.9829±0.051
23/2	147.5	1499±7	10.7071±0.050

I	Theory,A,B	Exp.-Theory	Theory,A,B,C	Exp.-Theory
3/2	11.5575	-------	-------	-------
5/2	11.5299	+0.0701	11.5670	+0.0330
7/2	11.4912	-0.0332	11.4634	-0.0054
9/2	11.4415	+0.0347	11.4786	-0.0024
11/2	11.3807	-0.0369	11.3413	+0.0025
13/2	11.3098	+0.0467	11.3559	-0.0003
15/2	11.2261	-0.0761	11.1748	-0.0248
17/2	11.1322	+0.0626	11.1905	+0.0043
19/2	11.0273	-0.0585	10.9639	+0.0049
21/2	10.9113	+0.0716	10.9813	+0.0016
23/2	10.7842	-0.0771	10.7087	-0.0016

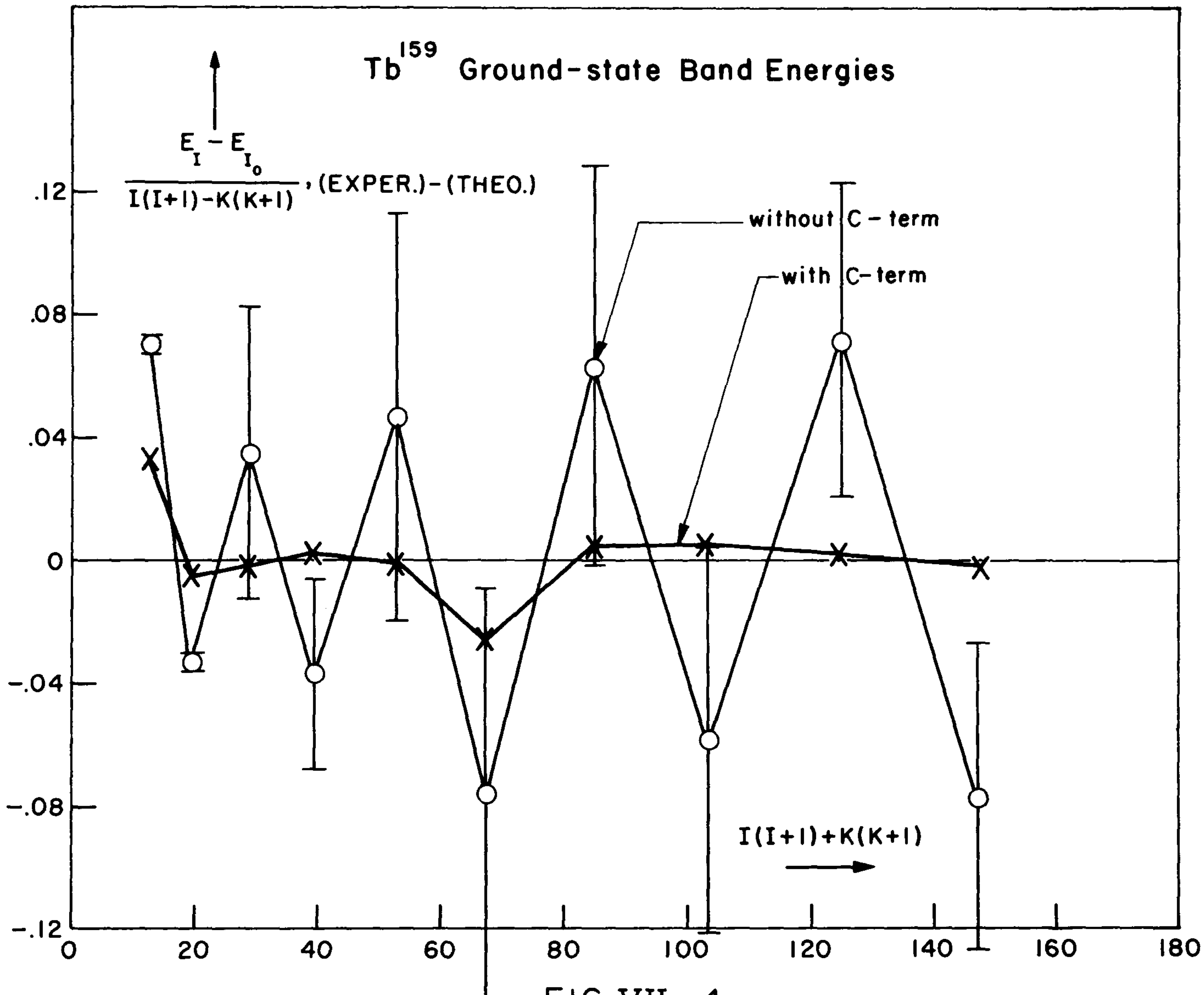

Tb159 Ground-state Band Energies
$\frac{E_I - E_{I_0}}{I(I+1)-K(K+1)}$, (EXPER.) - (THEO.)
without C - term
with C - term
I(I+1)+K(K+1)
.12
.08
.04
0
-.04
-.08
-.12
0
20
40
60
80
100
120
140
160
180

FIG VII - 4

estimate, with $\bar{K}=1/2$, $K=3/2$:

$$B(E2, \bar{K}=\tfrac{1}{2} \rightarrow K=\tfrac{3}{2}) = 6\,B(E2)_{Rot}\left[\frac{\frac{\hbar^2}{2\mathcal{J}'}\langle \psi_{\frac{3}{2}} | J_{+'} | \psi_{\frac{1}{2}} \rangle}{\delta E^{\circ}}\right]^2 \qquad \text{(VII-8)}$$

They note that if the upper $\bar{K}=1/2$ band is based on their assigned 971-keV 1/2+[411] Nilsson state and the intraband excitation moments of both bands, $|\langle \psi_{I'MK} | \mathcal{M} | \psi_{IMK} \rangle|$ and $|\langle \psi_{I'M\bar{K}} | \mathcal{M} | \psi_{IM\bar{K}} \rangle|$ are assumed equal, substitution of the ground-state band total excitation B-value and the value for the squared bracket as calculated from (VII-7) with $C = -8.0 \pm 2.0$ keV, $a_u = 0.81$, $\hbar^2/2$ $= 12$ keV, leads to a value of B(E2,3/2 → 1/2) in agreement, within experimental uncertainty, with the value estimated from their gamma-ray spectrum. Here a_u and $\mathcal{J}'$ are the decoupling and inertia parameters for the upper band. On the other hand they note that using these numbers plus the band-head separation $\delta E^{\circ} = 971$ keV and the ground-state band inertia parameter $\hbar^2/2$ $=11.61$ keV leads to

$$\langle \psi_{\frac{3}{2}} | J_{+'} | \psi_{\frac{1}{2}} \rangle = \sqrt{\frac{C}{\frac{\hbar^2}{2\mathcal{J}'} a_u}\;\frac{\delta E^{\circ}}{\frac{\hbar^2}{2\mathcal{J}'}}} = \sqrt{\frac{0.008 \pm 25\%}{0.81 \times 12} \times \frac{971}{11.61}} = 2.40 \pm 12\% \qquad \text{(VII-9)}$$

(which they gave, I believe erroneously, as 1.9), in disagreement with the theoretical value calculated from Nilsson wave functions, 0.56. It was noted that the only other $K=1/2$ Nilsson state in the $N=4$ shell near the terbium ground state and possessing an appreciable value of a has the wrong sign for a, giving, if admixed, a positive C.

Assuming their assignment to be correct, a possible way out of the dilemma would be the assignment of part of C to centrifugal stretching. If the matrix element does approximate the theoretical Nilsson value, then most of the value of C would be due to causes other than band mixing. (Alternatively, in connection with the possibility that the measured value of the matrix element is correct, it would be of interest to compare with calculations with wave functions from other versions of Nilsson-type models considered by Gottfried, Newton, Lemmer and Green and others, which are composed of somewhat different mixtures of spherical shell-model functions.)

As derived in Section I, centrifugal stretching can give rise to both B and C type terms in a pure band:

$$\begin{aligned} 1/\mathcal{J}' &= (1/\mathcal{J}^0)[1+B^{(1)}R^2+B^{(2)}R^4+\dots] \\ 1/\mathcal{J}_3' &= (1/\mathcal{J}_3^0)[1+B_3^{(1)}R^2+B_3^{(2)}R^4+\dots] \end{aligned} \qquad \text{(VII-10)}$$

$$T_R = \frac{1}{2\mathcal{J}'}(R^2-R_3^2) + \frac{1}{2\mathcal{J}_3'}R_3^2 = \frac{1}{2\mathcal{J}_0'}\sum_{\mu=0}^{\infty} B^{(\mu)}(R^2-R_3^2)^{\mu+1}, \quad \text{if } K=\Omega \qquad \text{(VII-11)}$$

The $\mu=2$ term, $B^{(2)}(R-R_3)^3$, contributes

$$\frac{\delta E_3}{\frac{B^{(2)}}{2\mathcal{J}_0}} \equiv \langle \psi^s_{IMK\Omega=K}|(R^2-R_3^2)^3|\psi^s_{IMK\Omega=K}\rangle = \langle\psi^s_{IMKK}|(I^2-I_3^2-j_3^2+j^2-\mathcal{C})^3|\psi^s_{IMKK}\rangle \qquad \text{(VII-12)}$$

of which of interest is

$$\begin{aligned} \langle\psi^s_{IMK\Omega}|\mathcal{C}^3|\psi^s_{IMK\Omega}\rangle &= \pi_{\chi_\Omega}(-1)^{I-\frac{1}{2}}(I-\tfrac{1}{2})(I+\tfrac{1}{2})(I+\tfrac{3}{2})\delta_{|K|\frac{3}{2}}\delta_{\Omega K}\, re\langle\chi_{\frac{3}{2}}|j_+^3|\chi_{-\frac{3}{2}}\rangle \\ &\equiv \frac{C}{B^{(2)}/2\mathcal{J}_0'}(-1)^{I+\frac{1}{2}}(I-\tfrac{1}{2})(I+\tfrac{1}{2})(I+\tfrac{3}{2})\delta_{|K|\frac{3}{2}}, \end{aligned} \qquad \text{(VII-13)}$$

or

$$C = -\pi_{\chi_\Omega}\delta_{\Omega K}\, re\langle\chi_{\frac{3}{2}}|j_+^3|\chi_{-\frac{3}{2}}\rangle\frac{B^{(2)}}{2\mathcal{J}_0}. \qquad \text{(VII-14)}$$

If most of C is due to stretching, then for $\pi_{\chi_\Omega}=-1$, corresponding to $\ell=3$ for the 2d shell, negative C implies that $re\langle\chi_{\frac{3}{2}}|j_+^3|\chi_{-\frac{3}{2}}\rangle$

and $B^{(2)}$ have opposite signs. It would be interesting to calculate this matrix element to discover the sign and size it predicts for $B^{(2)}$.

The term containing $(R^2-R_3^2)^2$ contributes an energy perturbation

$$\frac{\delta E_2}{B^{(1)}/2\mathcal{I}_0} \equiv \left\langle \Psi^{s}_{IMK\Omega=K} \middle| (R^2-R_3^2)^2 \middle| \Psi^{s}_{IMK\Omega=K} \right\rangle \tag{VII-15}$$

of which the contribution proportional to $I^2(I+1)^2$, from a term of the form $[I(I+1)-K^2-\Omega^2]^2 = I^2(I+1)^2 +$ const. gives the contribution:

$$\delta E_2 = \frac{B^{(1)}}{2\mathcal{I}_0} I^2(I+1)^2 = BI^2(I+1)^2. \tag{VII-16}$$

The measured B is negative; therefore if the sum is due to centrifugal distortion, $B^{(1)} < 0$. The classical meaning of this is that (for small R) increasing the core angular momentum R algebraically decreases $1/\mathcal{I}'$, or increases the inertia moment $\mathcal{I}'$ about the spin axis, which corresponds to the usual centrifugal flattening in the case of an elastic body. The signs of higher $B^{(\mu)}$ determine the ultimate behavior in the limit of high R^2 values, however; also, as is the case with classical rotating fluid bodies[90], axial symmetry may break down at high R.

The magnitude of $B^{(1)}$, if B is due entirely to centrifugal stretching, is

$$|B^{(1)}| = \frac{|B|}{1/2\mathcal{I}_0} \approx \frac{|B|}{A} = \frac{0.0055\ \text{keV}}{11.60\ \text{keV}} = 0.047, \tag{VII-17}$$

a not unreasonable value. Since $|C| \sim |B|$, there follows

$$\left|\frac{B^{(2)}}{B^{(1)}}\right| \sim \left| re \langle \chi_{\frac{1}{2}} | J_{+'}^{3} | \chi_{-\frac{1}{2}} \rangle \right| \qquad \text{(VII-18)}$$

provided most of C is also due to stretching. Unfortunately the possibilities of competing effects for both B (the neglected Euler angle-shape parameter cross terms in the body-frame Hamiltonian) and C (band mixing) render it impossible to reach any definite conclusions about this.

Interpolated gamma-ray response shapes and photopeak heights obtained as explained in Section VI were used to generate a predicted ground-state band spectrum for the case of 4.08 MeV/amu O^{16} on Tb^{159}, $Q_0 = 8.1$. Comparison with the upper spectrum in Fig. VII-1 after adding in the estimated 580-keV band gamma rays indicates that the parameters $Q_0 = 8$, $\delta^2 = 0.02$ are compatable with the observed data. The mixing ratio is estimated from the relative intensities of the $I \rightarrow I-1$ to $I \rightarrow I-2$ transitions between the lower-spin states in comparison to the pure-band calculated profiles, which in effect duplicates the method of Heydenburg and Temmer but in a multiple-excitation context. Higher-spin-state deexcitation intensities in principle would provide a sensitive check on the value of Q_0 because of the rapid decline of population of the higher band members with increasing q and the circumstance that $q \propto Q_0$. Unfortunately the fact of these transitions sitting on top of the 580-keV band Compton distributions and the effects of finite-ξ corrections negate this sensitivity.

Singles gamma-ray spectra at incident energies 1.0, 2.28, 3.05, 3.57 and 3.99 MeV/amu, displayed in Fig. VII-5, indicate

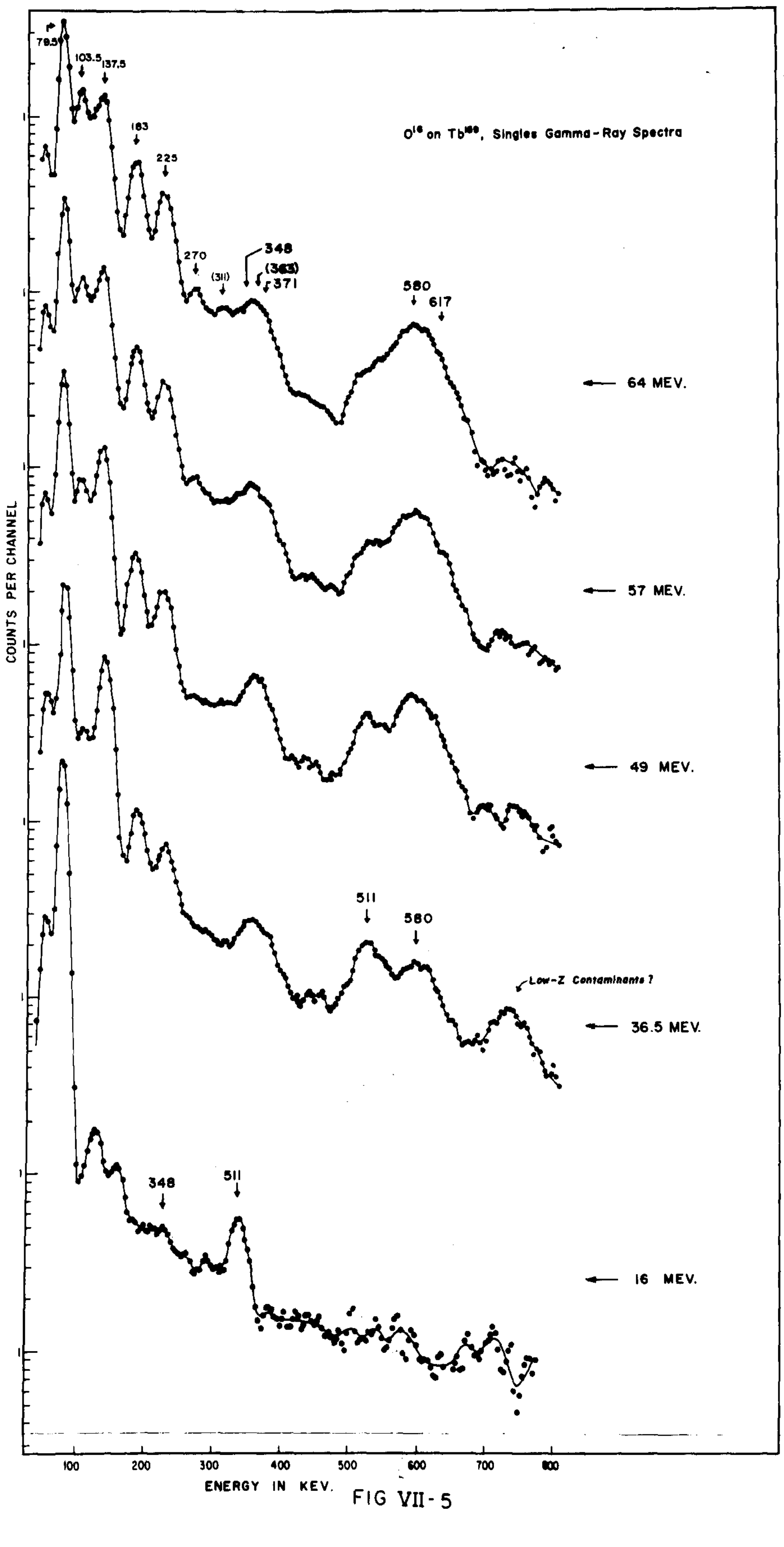

O^{16} on Tb^{159}, Singles Gamma-Ray Spectra
79.5
103.5
137.5
163
225
270
(311)
348
(363)
371
580
617
64 MEV.
57 MEV.
49 MEV.
511
580
Low-Z Contaminants ?
36.5 MEV.
348
511
16 MEV.
COUNTS PER CHANNEL
100
200
300
400
500
600
700
800
ENERGY IN KEV.

FIG VII-5

a relative enhancement of excitation by single as apposed to multiple processes, as is anticipated in the q(θ) approximation because of the smaller effective q values at the more forward scattering angles where the "ratio to Rutherford" for excitation is down but the Rutherford cross section is larber. The significant features of the spectra are indicated by the arrows.

There is a strong excitation of a level that decays emitting a gamma ray of about 350 keV, corroborating the assignment[35] of a single-particle level at 348 keV, and also suggestion of the presence of the expected 429-keV gamma ray. Strong population of levels decaying with 580- and 617-keV gamma radiation is consistent with these data, in corroboration of Diamond et al.[35]; substantially equal intensities within the employed bombarding energy range indicate the same multipolarity of excitation from the ground state of both the 580-keV and 617-keV levels (energy factor $(617/580)^5 = 1.362$).

The unassigned 362-keV transition seen by Diamond et al., which seems to be weakly present in our spectra, is probably from the 5/2-[532], 363.2-keV state seen by Ryde et al.[76] in Gd^{159} decay studies. The unassigned 311-keV transition[35] also aeems to be present, in coincidence and singles spectra, although the 306-keV ground-state band transition tends to obscure it. The origin of this transition remains in doubt. It is not any of the known gamma radiations of products of the O^{16} on O^{16}, N^{14} or C^{12} reactions followed by 1, 2, 3 or 4-nucleon emission, nor a Ta^{181} gamma ray. It was not seen in any background observations. 52 keV below the 363-keV level, it is not decay radiation from there to the 58.0-keV level of the ground-state band. There is no cogent reason for the existence of a weakly-excited level at this energy in Tb.

Intensities of the anticipated 371-keV and 429-keV decay radiation of the 429-keV member of the 348-keV band in comparison to the calculated decay intensity ratios in Fig. VI-24 (which apply to the singles spectra since decay ratios from one state are independent of the amount of population of that state) indicate a value $C_E/C_M \sim 1000$ or $\delta^2(429) \sim 1000\ \delta_{sp}{}^2(429) = 0.6$, or $\delta^2(348) \sim 0.4$. The relative absence of the 290-keV decay of the 348-keV state compared to the 348-keV decay, which indicates $C_E/C_M \gtrsim 1000$, also corroborates this estimate.

The intrinsic E2 matrix element connecting the ground-state and 348-keV bands, from the singles spectra and the calculated intensities, is estimated to be $\sim 1/3$ that connecting the ground-state and 580-keV bands. Although the intensity calculations were for a gamma-ion coincidence configuration, ratios of f_{E2} and of $\sum \frac{d f_{E2}}{d\Omega} \delta\Omega$ for 348- and 580-keV excitations are not substantially different, so that the estimate is valid.

A prominant feature is in the region centered at approximately 511 keV in the singles spectra: a transition that is enhanced relative to the 580-keV excitation with decreasing bombarding energy. If this were interpreted as indicative of a single-excitation process to a band containing states reached by multiple excitation and decaying with 580- and 617-keV radiation, then these transitions and the other related lines seen at Berkeley[35] could not be incorporated into a single rotational band of any spin appropriate to this nucleus. In any case excitation data suggested that the latter two radiations resulted from a direct E2 excitation process. A possible explanation arises from consideration of the (single) excitation functions $f_{E\lambda}(\eta_i=\infty,\xi)$. For small ξ, with increasing bombarding energy or decreasing ξ, $f_{E2}(\infty,\xi)$ increases faster than $f_{E1}(\infty,\xi)$; but just the reverse is true of the excitation cross sections $\sigma_{E\lambda}$. According to equation (II.c.13) of ref. 1, approximately, $\xi \propto E^{-3/2}$. Then from equation (II c.15), ref. 1, approximately, $\sigma_{E\lambda} \propto E^{-2\lambda-3} f_{E\lambda}(\eta_i,\xi)$. Therefore, approximately,

$$\sigma_{E\lambda} \propto \xi^{-\frac{2}{3}(2\lambda-3)} f_{E\lambda}(\xi) = \xi^{2-\frac{4}{3}\lambda} f_{E\lambda}(\xi) \qquad \text{(VII-19)}$$

or

$$\sigma_{E2}/\sigma_{E1} \propto \xi^{-\frac{4}{3}} f_{E2}/f_{E1}\,. \qquad \text{(VII-20)}$$

Computations indicate the correct amount of increased E1 over E2 excitation, as compared to the observed relative deexcitation intensities, at the three higher energies, the increase at 2.28 MeV/amu being, however, too large. There are physical reasons to anticipate a state populated by E1 excitation at about this energy. K. Takahashi[59] listed levels in Tb^{155} observed in the decay of Dy^{155}, as shown in Fig. VII-6, in addition to the levels observed in Tb^{159} from Gd^{159} and Dy^{159} decay and Coulomb excitation. He assigned a weak 595-keV gamma ray, seen also as a weak ~580-keV transition by Ryde et al.[76], as as 1/2+ [411], but with Diamond et al.[35] it is listed as gamma-vibrational. The levels in Tb^{155} and Tb^{159} are expected to be very similar;

States in Tb^{155} and Tb^{159}

(K. Takahashi, ref. 59)

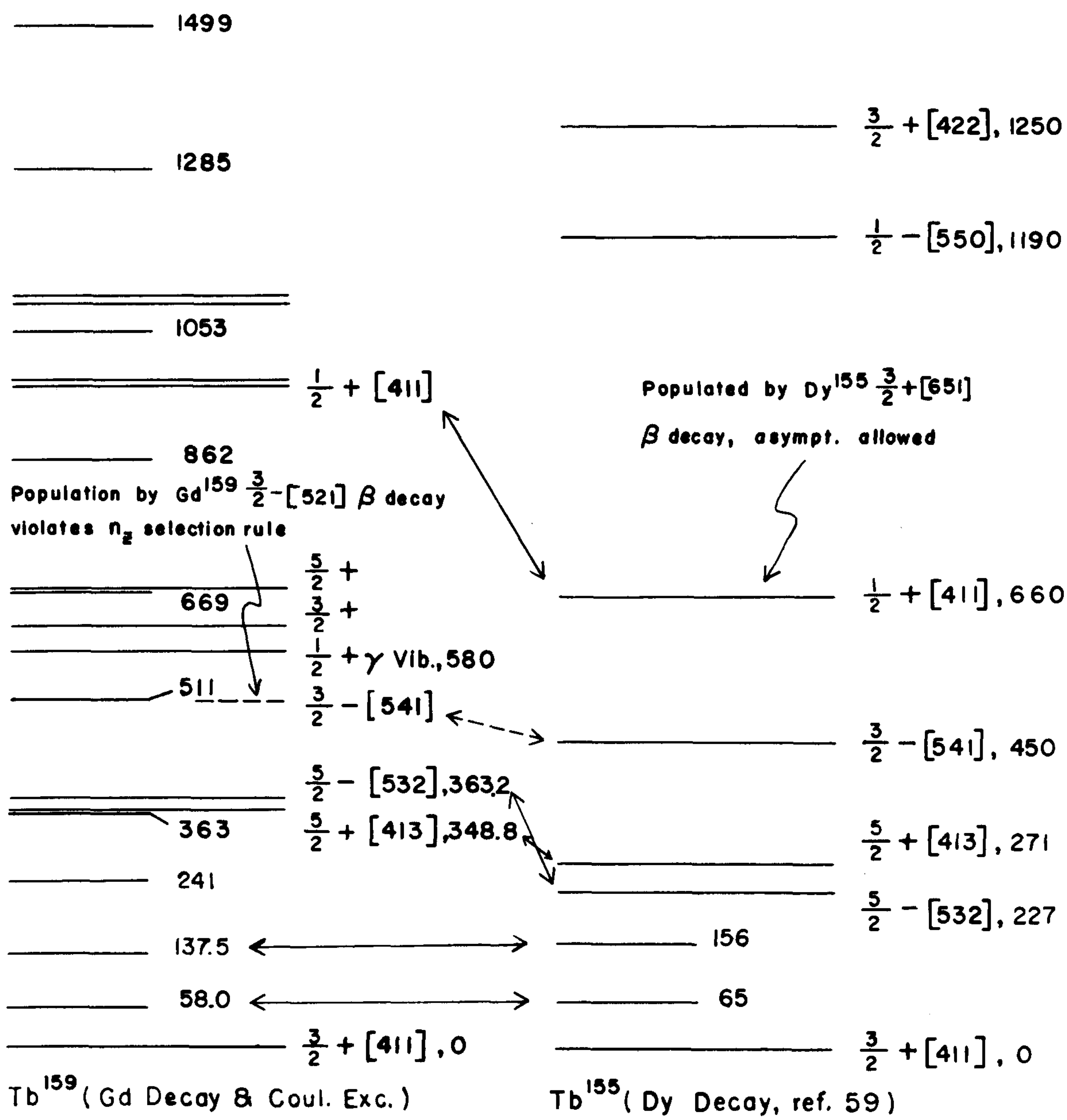

FIG VII - 6

furthermore, in Tb^{155} the states listed exhaust the possibilities for Nilsson-type single-particle states, as is evident from comparison to the Nilsson diagram, Fig. VI-17. Dy^{155} is assigned as a 3/2-[651] state. The beta decay to the Tb^{155} 3/2-[541] state is then allowed according to the beta-decay asymptotic selection rules[24], since $\Delta N = -1$. $\Delta n_z = 1$, $\Delta \Lambda = 0$. The corresponding state is not seen in the decay of Gd^{159} 3/2-[521], $\Delta N = 0$, $\Delta n_z = 0$, $\Delta \Lambda = 2$, because it is hindered by these rules, and would be only very weakly discernible even if unhindered, as in Tb^{155}. It is not seen in the decay of Dy^{159} by reason of energetics. Also E1 excitation or decay transitions are forbidden in the limit of infinite deformation[24], so that they are hindered in the rotational region relative to the "single-particle" estimates, by factors of $\sim 10^4$ to 10^6. The state probably would not be seen dy Diamond et al.[35] because of this and also the small conversion coefficient associated with the relatively high energy and low multipolartiy. If, as may be the case in Tb^{155}, the band based on this state has the same inertia constant as the ground-state band, a level of about 588 keV decaying to the ground-state band with 588-, 530- and 450.5-keV radiation would be expected, as well as 472-keV radiation from the 530-keV level. The first two of these would be obscured by other strong lines, but there is some indication that one or both of the other two may be present, especially the 432-keV radiation in the gamma-particle coincident spectra. Further indication of the E1 character of the supposed excitation is the suppression of this state in the coincidence spectra. This situation would be expected on the basis of the angular distribution of the inelastic ions accompanying the excitations, shown in Fig. II.7 of ref. 1, which for $\xi \approx 0$, unlike the E2 case, is strongly peaked at forward angles, causing suppression from coincidence with backscattered ions.

However, a difficulty with this interpretation is the unretarded B(E1) value it requires. Also, the enhancement at 2.28 MeV/amu is too great. The state probably is not an octupole-vibrational state (which would be expected at lowest energies here in the middle of the rotational region), because these states are excited primarily through enhanced E3 transitions, not E1, and also because the state (along with the 363-keV state) is not discernable in the early 1-MeV/amu spectrum in Fig. VII-5.

The obvious interpretation, which fits the behavior well, is annihilation radiation due to nuclear reactions from O^{16} on primarily H^1, C^{12} and O^{16} in the vacuum-system pump oil, which even cryogenic trapping could not totally eliminate. This is corroborated by an enhancement of this radiation brought about by not gating the counting apparatus off during the 95 msec. intervals between beam bursts. Evidence for the presence of low-Z contaminants resulting from observation of a high-energy singles Tb gamma-ray spectrum, is contained in Table VII-3, which indicates that there are meny lines accountable as transitions in products of $O^{16}(O^{16},x)$ and $C^{12}(O^{16},x)$ reactions, where x p, pn, n, nn, pnn, etc. The singles gamma-ray spectrum, from 1 MeV up, is essentially identical to a

Table VII-3

Obs. ray, approx. energy MeV	Possible transitions: P^{29}	P^{30}	P^{31}	Si^{29}	Si^{30}	Al^{26}	Al^{27}
0.835						0.824	0.834
1.02			0.96			1.01	1.013
1.27		1.26	1.27				
1.36	1.38					1.34	
1.62				1.59		1.64	
1.75	1.72						1.72
2.00	1.96	1.97	1.99	2.03		2.08	1.98
2.22			2.23		2.24		2.22
2.50		2.54					
2.72		2.72				2.73	2.74
2.98		2.94					2.98

Some contributing reactions:

$O^{16}(O^{16}, ppn)P^{29} \xrightarrow[4.45\,sec\,\beta^+]{} Si^{29}$

$O^{16}(O^{16}, pn)P^{30} \xrightarrow[2.55\,sec\,\beta^+]{} Si^{30}$

$O^{16}(O^{16}, p)P^{31}$ stable

$O^{16}(O^{16}, pnn)Si^{29}$ stable

$O^{16}(O^{16}, pn)Si^{30}$ stable

$O^{16}(O^{16}, n)S^{31} \xrightarrow[3\,sec\,\beta^+]{} P^{31}$

$O^{16}(O^{16}, nn)S^{30}$ }
$O^{16}(O^{16}, nnn)S^{29}$ } No available level data.

$C^{12}(O^{16}, pn)Al^{26} \xrightarrow[6.6\,sec\,\beta^+]{} Mg^{26}$ stable

$C^{12}(O^{16}, p)Al^{27}$ stable

$C^{12}(O^{16}, n)Si^{27} \xrightarrow[4.9\,sec.\,\beta^+]{} Al^{27}$

$C^{12}(O^{16}, nn)Si^{26} \xrightarrow[2.1\,sec\,\beta^+]{} Al^{26} \xrightarrow[6.6\,sec\,\beta^+]{} Mg^{26}$

high-energy spectrum obtained from an even-A rare-earth target at another laboratory[227], which indicates conclusively the common-contaminant origin of its features.

The enhancement of the 348-keV radiation in the singles relative to the coincidence spectra is not due to the fact of that level, rather than the 363-keV level, being the 5/2- [523] level populated by an E1 process (which would place these levels in the same order as the corresponding levels in Tb^{155} as given by Takahashi), but rather to the relative emphasis of multiple processes in the ground-state band for the backward projectile scattering angles. Also, Coulomb excitation yields of Diamond et al.[35] indicate E2 excitation of the 348-keV level. The 363-keV conversion data of Nielsen et al.[47] and Metzger and Todd[51] indicate E1 decay, with the direct lifetime measurement giving the expected order-of-magnitude hindrance. (However the conversion coefficient and K/LM... due to Malik et al.[49] for their 361-keV transition indicated M1+70%E2 decay, and also on the basis of a Gd^{159} ground state with $I\pi$=3/2- and the observed log ft value the 361-keV state spin was assigned 1/2+ . So there has not been absolutely unanimous agreement about the nature of these levels.)

Comparison of the overall shape of the 580-keV band deexcitation with calculated (gamma-ion coincident) photopeak intensities in Fig. VI-24 suggests that only $\mathcal{R} = \pm 1$ with M1 deexcitation and $|\mathcal{R}| = \infty$ with E2 or M1 deexcitation, among the cases calculated, are consistent with the spectra. The latter is appropriate for a vibrational band.

Predicted laboratory spectral profiles were obtained from the calculated photopeak heights for the assumed 580-keV band, $|\mathcal{R}| = \infty$, and the cases of pure M1 and pure E2 deexcitation, on the assumption of an intrinsic matrix element equal to $B_{sp}(E2)$. The overall profile shapes indicate that to distinguish M1 from E2 or mixed decay would be virtually impossible from the NaI intensity observations.

The intrinsic matrix element connecting the 580-keV band to the ground-state band was found by comparing the population of the 580-keV level as estimated from its deexcitation intensity with the population of certain ground-state band members as estimated from gamma-ray population and depopulation transition intensities and comparing with theoretical populations. Since the ground-state band theoretical populations were calculated on the assumption of $Q_o = 8.1$, and the upper-band populations on the assumption of the intrinsic interband matrix element equalling $B_{sp}(E2)$, this procedure relates this matrix element to the ground-state Q_o. The total population probability $\mathcal{P}_i$ of the i^{th} ground-state band member is related to its excitation probability P_i and the decay transition probabilities $I_{ij} = \mathcal{P}_i t_{ij}$, $\sum_{j \neq i} t_{ij} = 1$, to levels $j \neq i$ via the relations

$$\begin{aligned} I_{i,i-\mu} &= \mathcal{P}_i t_{i,i-\mu} \qquad (\mu = 1,2;\ i \geq \mu) \\ \mathcal{P}_i &= P_i + I_{i+1,i} + I_{i+2,i} \qquad (i \geq 0) \end{aligned} \tag{VII-21}$$

from which

$$P_i = I_{i,i-1} + I_{i,i-2} - I_{i+1,i} - I_{i+2,i} \quad . \tag{VII-22}$$

Here $I_{ij} = I_{ij}^{(\gamma)} (1 + \alpha_{ij}^{tot})$ is a transition intensity, and $I_{ij}^{(\gamma)}$ is the corresponding gamma-ray intensity. For populations of the 241-keV level one has

$$P(MCE) = I(183) + I(103.5) - I(122) - I(270) \qquad \text{(VII-23)}$$

and for the 343-keV level,

$$P(MCE) = I(122) + I(225.5) - I(148) - I(306) \qquad \text{(VII-24)}$$

where the numbers in parantheses are the transition energies in keV. This method bypasses the need to know the ground-state band E2/M1 mixing ratios. Using calculated spectrum profiles as a guide, photopeak heights for the relevant transitions were estimated from the experimental data, and reduced to transition intensities by correcting for resolution, peak/total, absorption, efficiency and internal-conversion effects. This gave unnormalized excitation populations, which were compared to the calculated populations to give normalization factors permitting the comparison of the unnormalized observed yields of higher-band deexcitations with the calculated single-particle yields. Estimating from the data and using calculated profiles as a guide, the result of the comparison is

$$B_{intr} \equiv |\langle -\tfrac{1}{2} | \mathcal{M}(E2) | \tfrac{3}{2} \rangle|^2 = (3.3 \pm 1) B_{sp}(E2) \qquad \text{(VII-25)}$$

if the deexcitation is assumed to be pure E2, or

$$B_{intr} = (2.9 \pm 0.8) B_{sp}(E2) \qquad \text{(VII-26)}$$

if the deexcitation is assumed to be pure M1. The difference reflects the greater percentage of the total band decay represented by the 580-keV decay in the latter case. 580-keV band population and depopulation intensity ratios for the case of symmetry corrections characterized by $|\mathcal{R}_{if}| = \infty$, appropriate to vibrational states, were employed here.

The combined spectrum profile of the ground-state band and the 580-keV band with this value of the intrinsic matrix element reproduces satisfactorily the observed profile.

Diamond et al.[35] found a somewhat smaller value, $\sum \epsilon_\gamma B(E2) = 1.5\ B_{sp}(E2)$, with an uncertainty of $\sim$19%, for the total excitation to the 580-keV band. Because of the addition property of the Clebsch-Gordon coefficients this es equal to the intrinsic matrix element. They concluded on the basis of their conversion-electron line intensities and average theoretical 580-keV band deexcitation conversion coefficient that the decay is predominantly M1. An intrinsic matrix element twice as large would imply on this basis predominantly E2 decays.

As mentioned above, E2 deexcitation is required for pure vibrational transitions even in the present symmetry-modified case. Their Doppler-broadening argument, however, still would imply the presence of a significant M1 component.

No observations of transitions as high as $\sim$900-keV were possible, as they were too weak to show above the background.

Gamma-gamma coincident spectra were obtained with the apparatus set up as explained in Section V. Two runs, in the second of which a Victoreen 200 x 100-channel two-dimensional analyser was used, yielded essentially identical results. The expected cascade relationships among the gamma rays depopulating the first six excited states in the ground-state band were confirmed, constituting an important verification of the nature of these transitions as depopulating a rotational band. There seems to be evidence for the presence of gamma rays expected in the depopulation of the assumed 580-keV band, but the poor quality of counting statistics that could be acquired in a reasonable running time, and the presence of a background of gamma rays of high multiplicity which are efficiently detected in the gamma-gamma coincidence mode, precludes a detailed assessment of the coincidence relationships other than the foregoing. The resemblance of the 511-keV gated spectrum and the two-dimensional M.C.A. spectra in coincidence with higher-energy regions of the y-coordinate singles spectrum to a background spectrum (run on a different occasion), and the paucity of good detail in a total gamma-gamma coincidence spectrum, are indicative of the magnitude of the coincident-background problem. The background again is probably due to nuclear reactions with low-Z target contaminants, especially the C^{12} and O^{16} in the vacuum pump oil. Possible remedies include utalizing triple gamma-gamma-particle coincidences with NaI(Tl) detectors, and the use of Ge semiconductor detectors with their inherently good energy resolution in gamma-ion or gamma-gamma coincidence modes. These would be feasible with the higher currents available from tandem van de Graaf accelerators, but experience has shown that they could not be done in reasonalbe times using the HILAC. Also, extremely "clean" vacuum systems, especially in the target area, seem indispensable. Substantial data-improvement is unlikely, however, without substantially higher

B. Holmium

Single and backscattered-ion coincident spectra of 4.08 MeV/amu O^{16} on Ho^{165} appear in Fig. VII-7. As mentioned above it was not expected that there would be any appreciable population of single-particle states on Ho, and this has been confirmed except for one feature. The coincidence spectrum shows the ground-state band deexcitation transitions, and interband deexcitations that turn out to be from $K = K_0 \pm 2$ gamma-vibrational states. The singles spectrum shows the expected smaller relative populations of higher ground-state band members, and perhaps some 511-keV on top of the 514-keV band. Switching off the machine gate which blanks the apparatus between the beam bursts enhances the 511-keV line. There is also a gamma-ray line at 360 keV which can be associated with the ground-state transition of a 361-keV state, observed by Persson et al.[125] and others in Dy^{165} decay, which deexcites via M2 with a 1.5 msec. half life. This state has been assigned the Nilsson 3/2+[411] classification. The only alternative Nilsson states this low in energy would be 1/2+[411] and 5/2+[413], neither of which decay primarily by M2. Diamond et al.[35] have found that conversion-electron yield data following Coulomb excitation by O^{16} ions with 44- and 60-MeV bombarding energies indicate population either by E3 direct, or by E2 to the 580-keV band members followed by deexcitation to this level, or both. As mentioned previously, E1 transitions are K-forbidden but M2 and E3 transitions are allowed by the K- and the asymptotic selection rules between the 3/2+[411] and 7/2-[523] intrinsic

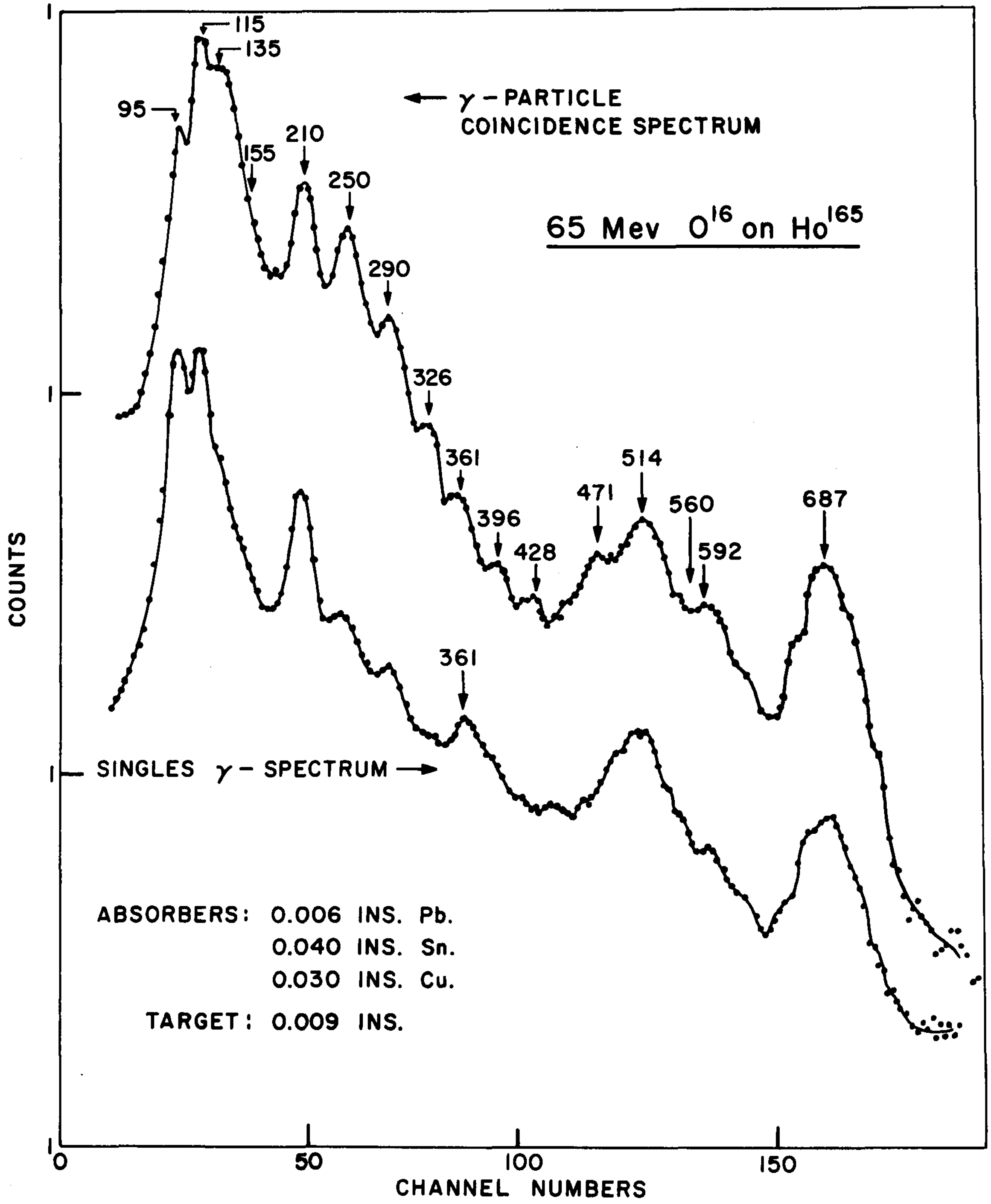

115
135
95
γ - PARTICLE COINCIDENCE SPECTRUM
210
155
250
65 Mev O^{16} on Ho^{165}
290
326
361
514
471
560
687
396
428
592
361
SINGLES γ - SPECTRUM
COUNTS
ABSORBERS: 0.006 INS. Pb.
0.040 INS. Sn.
0.030 INS. Cu.
TARGET: 0.009 INS.
1
1
1
1
0
50
100
150
CHANNEL NUMBERS

FIG VII - 7

states, which may account for the population of this state.

An analysis of the ground-state band energies is presented in Table VII-4 and Fig. VII-8. The energies are found to obey the relation

$$E_I = E_0 + AI(I+1) + BI^2(I+1)^2$$
$$A = 10.676 \pm 0.011 \text{ keV} \qquad \text{(VII-27)}$$
$$B = -3.792 \pm 0.076 \text{ eV}$$

These values agree within experimental error with the results of Diamond et al.[35]: $A = 10.65 \pm 0.04$ keV, $B = -3.2 \pm 0.7$ eV. A "C"-term if present would be of the form $C(-1)^{I+1/2}(I-5/2) \times (I-3/2)(I-1/2)(I+1/2)(I+3/2)(I+5/2)(I+7/2)$, and would occur in the seventh order of perturbation theory, not the first, as in $K = 1/2$ decoupling, or third, as in Tb^{159}. As such it would be expected to be small, if there is any reasonable convergence of the perturbation series. The observed spectra indicate that $|C| \lesssim 10^{-7}$. Band-mixing with the 1/2+[411] state is of course parity-forbidden in this case.

Data obtained with a cooled germanium semiconductor detector are shown in Fig. VII-9. In addition to ground-state transitions they show transitions from 514-keV and 566-keV members of the 514-keV band and from the 687-keV state. There is also deexcitation from the 361-keV state, since the expected intensity of the 361-keV transition in the ground-state band is at least five times less than the observed 361-keV intensity. On this spectrum appeared non-repeating features at 342.5 keV and ~548 keV, and an extremely faint indication of a line at

Table VII-4

Ho^{165} Ground-State Band Parameters

I	$2(I+1) \equiv x$	Assumed $E_I - E_{I_0}$, keV	$E_{I+1} - E_I$	$\frac{E_{I+1}-E_I}{2(I+1)} \equiv y$	Weight w *
$K=7/2=I_0$	81	0	94.697	10.5219	25000
9/2	121	94.697±0.004	115±1	10.5454	110
11/2	169	210±1	135±1	10.3846	130
13/2	225	345±1	154±1	10.2667	149
15/2	289	500±1	172±2	10.1176	85
17/2	361	671±2	190±2	10.0000	95
19/2	441	861±3	206±5	9.8095	42
21/2	529	1067±4	222±6	9.6522	38
23/2	625	1289±5	-----	-------	------

$$* \quad \frac{E_{I+1} - E_I \pm \delta(E_{I+1} - E_I)}{2(I+1)} \equiv y \pm \delta y \; ; \quad w = \frac{10}{|\delta y|}$$

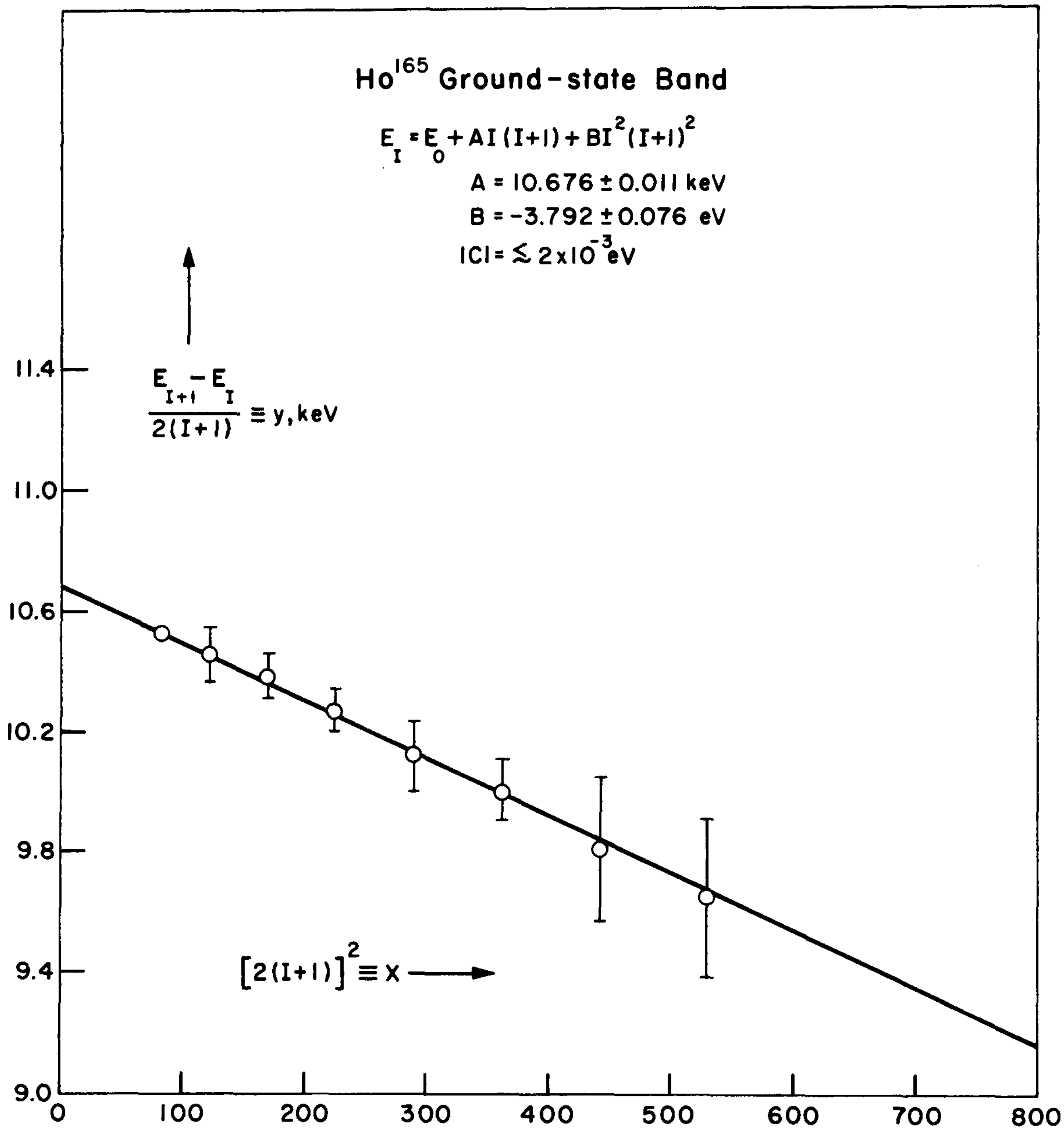

Ho^{165} Ground-state Band
$E_I = E_0 + AI(I+1) + BI^2(I+1)^2$
A = 10.676 ± 0.011 keV
B = −3.792 ± 0.076 eV
|C| = ≲ 2x10^{-3} eV
$\frac{E_{I+1} - E_I}{2(I+1)} \equiv y$, keV
$[2(I+1)]^2 \equiv x$
11.4
11.0
10.6
10.2
9.8
9.4
9.0
0
100
200
300
400
500
600
700
800

FIG VII - 8

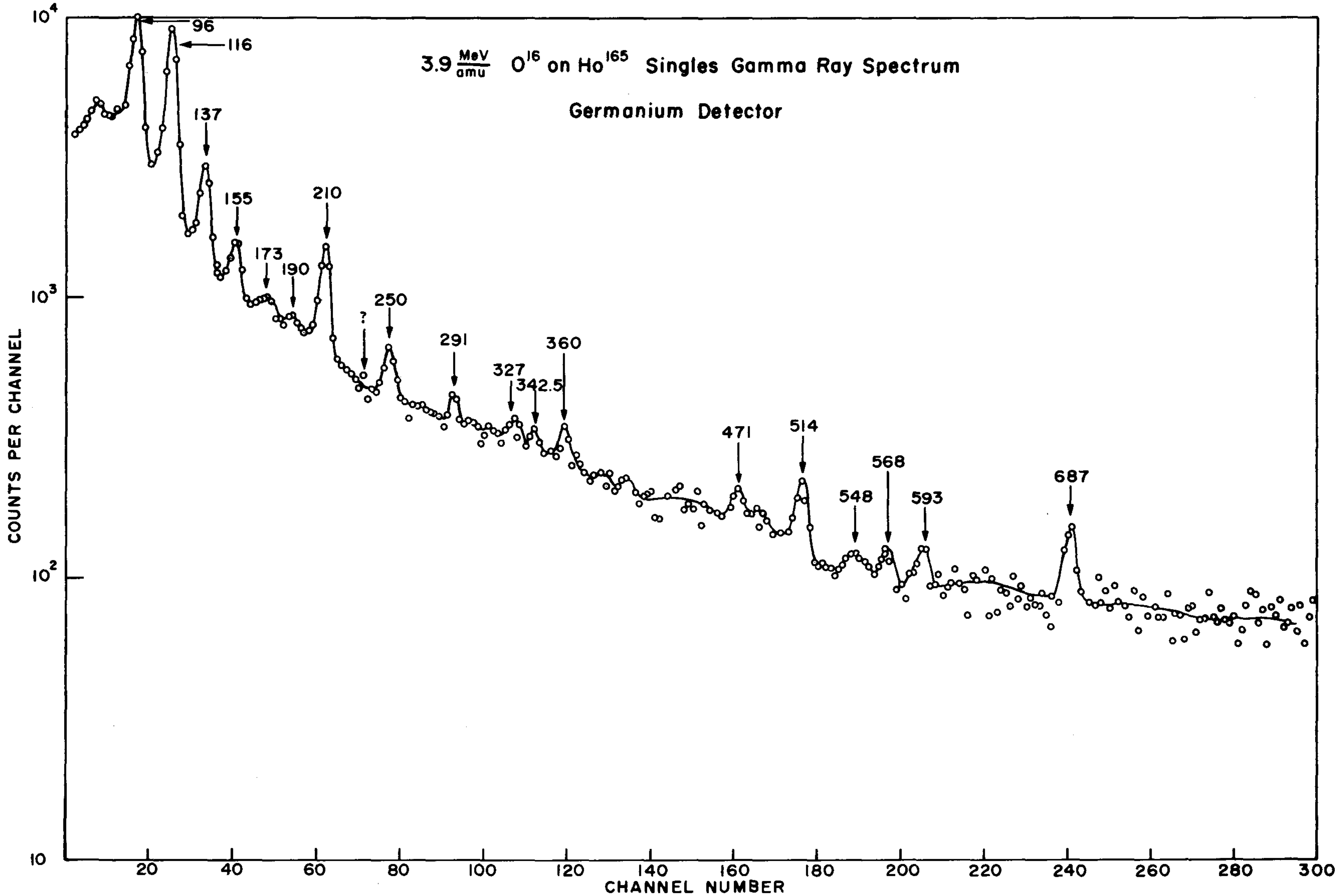
3.9 MeV/amu O16 on Ho165 Singles Gamma Ray Spectrum
Germanium Detector
96
116
137
155
173
190
210
?
250
291
327
342.5
360
471
514
548
568
593
687
COUNTS PER CHANNEL
CHANNEL NUMBER
10
10²
10³
10⁴
20
40
60
80
100
120
140
160
180
200
220
240
260
280
300

FIG VII - 9

245 keV corresponding to one of two unassigned lines seen by Diamond et al.

Predicted ground-state band spectrum profiles generated from gamma-ray response shapes and calculated photopeak heights were used as interpretative guides. Again the overall observed features could be reproduced with the 514-keV and 687-keV band profiles added in, but no sharp conclusions from the higher ground-state band transitions about the precise Q_0 value could be made. From comparison of the spectrum in Fig. VII-7 with the calculated photopeak heights, it appears that the assumed conversion coefficient $\delta^2(95) = 0.04$ is approximately correct. This conclusion is subject to the accuracy of the various applied instrumental corrections.

Calculated deexcitation spectrum profiles for the assumed 514-keV and 687-keV bands were obtained for respective spin assignments $K = K_0 - 2$ and $K = K_0 + 2$. These are for the cases of single E2 excitation followed by pure E2 deexcitation, in accord with the anticipated vibrational character of the states and with the average conversion coefficient measurements by Diamond et al. There are no symmetry modifications in this case. Comparison of a superposition of these and the calculated ground-state band profile with the observed spectra indicates fairly conclusively the assignments of 3/2- and 11/2-.

The intraband matrix element was determined from the data in the same way as in the case of Tb. The excitation of the 210-keV state is given by

$$P(MCE) = I(115) + I(210) - I(135) - I(290) \quad \text{(VII-28)}$$

and for the 345-keV state, by

$$P(MCE) = I(135) + I(250.3) - I(155) - I(326). \quad \text{(VII-29)}$$

Populations were calculated from observed gamma-ray intensities and compared to the theoretical populations calculated for Q_o 7.5 and 8.0, to give the normalization factor allowing comparison of the experimental higher-band unnormalozed yields with the intensities calculated on the premise that B_{intr} $B_{sp}(E2)$. The results were, for the 514-keV band,

$$B_{intr}(514) = (2.5 \pm 0.5) B_{sp}(E2) \quad \text{(VII-30)}$$

for the choice $Q_o = 7.5$, or

$$B_{intr}(514) = (2.2 \pm 0.5) B_{sp}(E2) \quad \text{(VII-31)}$$

for the choice $Q_o = 8.0$; and for the 687-keV band,

$$B_{intr}(687) = (3.0 \pm 0.5) B_{sp}(E2) \quad \text{(VII-32)}$$

for $Q_o = 7.5$, or

$$B_{intr}(687) = (2.6 \pm 0.5) B_{sp}(E2)$$

for $Q_o = 8.0$. Again these values are higher than those found by Diamond et al., $1.9 B_{sp}$ and $1.7 B_{sp}$ respectively, but not by a very great percentage. Upon combining calculated ground-state and higher-band profiles the general aspect of the observed spectrum was reproduced, but the higher ground-state band gamma rays were found to be somewhat too intense. This could indicate that the true Q_o value is a bit larger. A value of ~ 8.8 or so would bring the B_{intr} values into good agreement with those in ref. 35, and would increase the relative excitation of the highest observed ground-state-band gamma rays by factors of from ~ 2 to ~ 4.

C. Lutetium

NaI(Tl) gamma-ion coincident and gamma singles spectra from 4.08 MeV/amu O^{16} on Lu^{175} are displayed in Fig. VII-10. Unlike Ho, which has as its ground state a relatively isolated negative-parity Nilsson state generated from the $h_{11/2}$ shell, Lu has a positive-parity ground state which is connected by E2 transition moments to other low-lying positive-parity Nilsson states: a 5/2+[402], and at somewhat higher energy, 1/2+[411]. There should be a low-lying 9/2-[514] state, and lying rather high, 11/2-[505], 3/2+[402] and 1/2+[400] states. None of the last three have been identified; of the first three, beta decays to Lu^{175} populate the 5/2+ and 9/2- states, and possibly the 1/2+[411] state as well. The 9/2- state is seen in various Lu and Ta isotopes lying rather low in energy, and happens to be the ground state in Lu^{173}, according to Harmatz et al.[65] There would be high-lying states for the next higher major shell with $N=6$, positive parity and $N=5$, negative parity.

Because of the possibility of Coriolis mixing with the 1/2+[411] band, now not parity-forbidden, as well as higher order stretching effects, contributing to an alternating C-term in the ground-state band energies, it would have been of interest to try to detect such a term. Unfortunately a number of circumstances prevented a really definitive check, but indications are that the C-term is negligible in this case also. Firstly, there appears to be a strong transition at 486 ± 3 keV, appearing in the coincidence spectrum, attributed to a vibrational state. Somewhat lower in energy than Tb and Ho gamma-vibrational states,

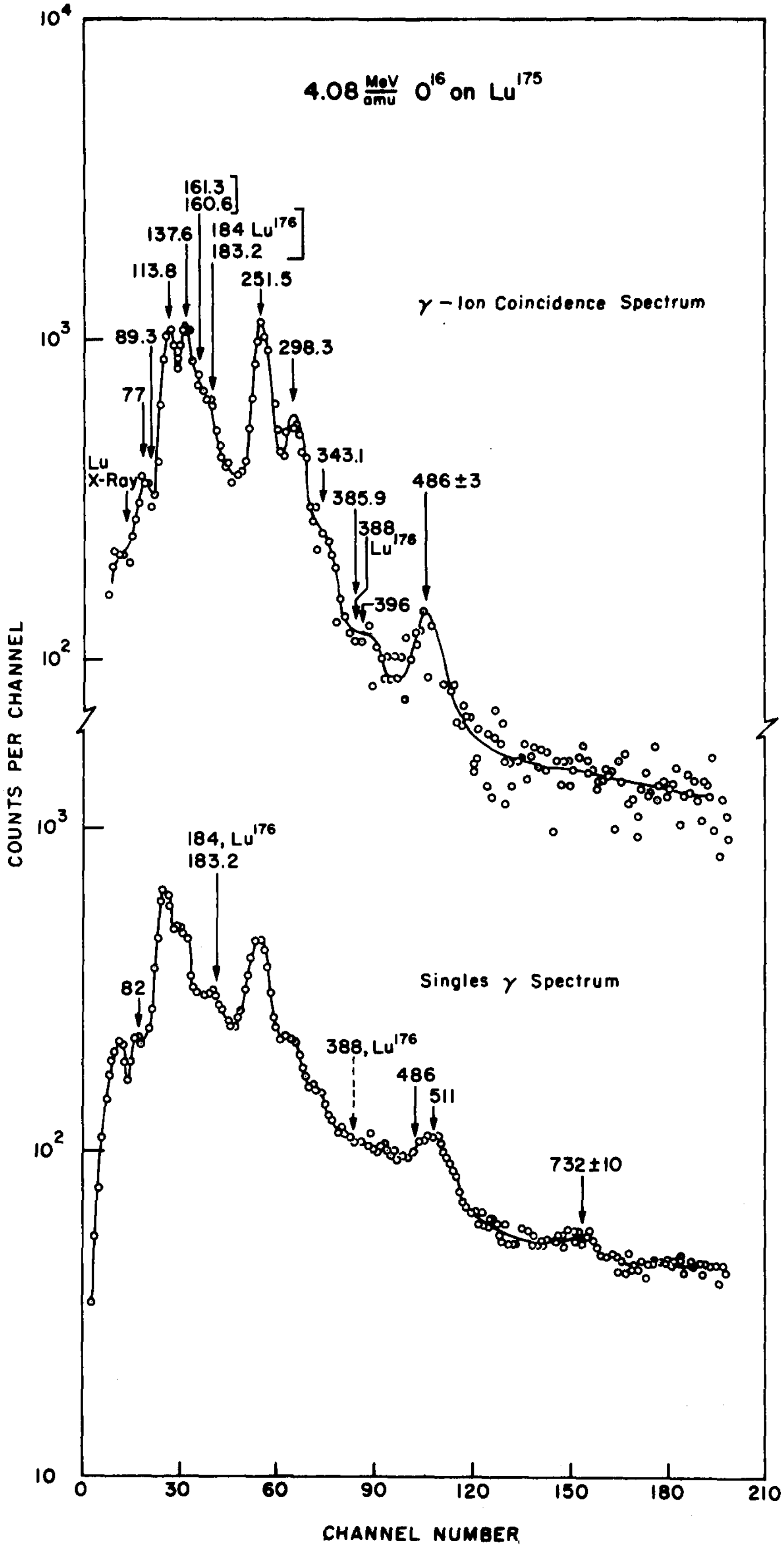

$4.08 \frac{MeV}{amu}$ O^{16} on Lu^{175}
γ – Ion Coincidence Spectrum
Singles γ Spectrum
161.3
160.6
137.6
184 Lu^{176}
183.2
113.8
251.5
89.3
298.3
77
Lu
X-Ray
343.1
385.9
486±3
388
Lu^{176}
396
184, Lu^{176}
183.2
82
388, Lu^{176}
486
511
732±10
COUNTS PER CHANNEL
CHANNEL NUMBER

FIG VII - 10

if obscures the higher Lu ground-state band deexcitation transitions, which have somewhat higher energies than corresponding Ho and Tb ground-state band transitions. It was decided to predict higher ground-state band transition energies from "A" and "B" terms only, as found from the first two excited levels, and compare with the observed spectra. This also led to some difficulties.

The definitive determination of energies of Lu transitions is the bent-crystal gamma-spectrometer work of Hatch et al.[178], who found for the lowest ground-state band transition energies,

$$\begin{aligned} E_{9/2} - E_{7/2} &\equiv E_1 = 113.81 \pm 0.02 \text{ keV} \\ E_{11/2} - E_{9/2} &\equiv E_2 = 137.65 \pm 0.05 \text{ keV.} \end{aligned} \qquad \text{(VII-34)}$$

With energies given by $E_I = E_0 + AI(I+1) + BI^2(I+1)^2$, one finds

$$\begin{aligned} E_1 &= 9A + (9^3/2)B \\ E_2 &= 11A + (11^3/2)B \end{aligned} \qquad \text{(VII-35)}$$

Values of A and B, of the level energies and of the transition energies were calculated for $E_1 = 113.81$ keV, $E_2 = 137.65$ keV and for various combinations of $E_1 = 113.79$, 113.83 keV and $E_2 = 137.60$ keV, 137.70 keV. The deviations in the energies were about the same for E_1 low, E_2 high as for E_1 high, E_2 low, etc. The largest deviations were adopted as the given uncertsinties, Table VII-5. The locations of transitions of these energies are shown on the NaI spectra, and are found to correspond to the experimental results. The calculated values of A and B are:

Table VII-5

keV	CC	LL	LH	HL	HH
E_1*	113.81±0.02	113.79	113.79	113.83	113.83
E_2*	137.65±0.05	137.60	137.70	137.60	113.70
A	12.9126	12.9152	12.8967	12.9286	12.9102
-10^3 B	6.596	6.712	6.258	6.934	6.480

I	E, keV		
	Levels	Transitions	
7/2	0	-----	-----
9/2	113.81±0.02	113.81±0.02	-----
11/2	251.46±0.07	137.65±0.05	251.46±0.07
13/2	412.08±0.19	160.62±0.16	298.27±0.21
15/2	594.63±0.53	183.21±0.34	343.17±0.50
17/2	797.95±1.1	202.66±0.56	385.87±0.89
19/2	1020.7 ± 2.0	222.8 ± 0.9	426.1 ± 1.5
21/2	1261.3 ± 3.2	240.6 ± 1.3	463.4 ± 2.1
23/2	1518.2 ± 7	256.9 ± 1.7	497.5 ± 2.9

* $E_1 \equiv E_{9/2} - E_{7/2}$ $\quad$ A = 12.913 ± 0.016 keV

$E_2 \equiv E_{11/2} - E_{9/2}$ $\quad$ B = -6.60 ± 0.34 eV

$$A = 12.913 \pm 0.016 \text{ keV}$$
$$B = -6.60 \pm 0.34 \text{ eV} \qquad \text{(VII-36)}$$

A singles gamma-ray spectrum obtained with a cooled Ge detector, from 3.90 MeV/amu O^{16} on Lu^{175}, is shown in Fig. VII-11. Among the identifiable features shown thereon, the most prominant are the ground-state-band deexcitations.

The transition at 89 keV is probably the 89.3-keV E2 transition from the 7/2+ rotational to the 5/2+[402] state. The 113.81-keV and 137.65-keV transitions appear at the correct positions. The shape of the 161-keV transition peak is peculiar, obviously a composit. Ge spectra were run at 4.52, 3.00 and 2.60 MeV/amu incident energies as well; this feature appeared, also as a composit, on the 4.52 and 3.00 MeV/amu spectra, but was too weak to observe at 2.60 MeV/amu. It is probably composed of the anticipated 160.62 ± 0.16-keV ground-state-band transition, the 161.3 ± 0.2-keV $1/2+ \rightarrow 5/2+$ transition[178] which is seen because the transition to the ground state would be M3-E4 and much slower, and possibly the 165.2-keV transition in Ta^{181}. If the 1/2+ state is 1/2+[411], then the E2 transition is asymptotically allowed although delayed by a factor of $\sim 10^5$, but the M3 transition to the ground state is asymptotically forbidden. The lower-energy part of this feature (161 keV as apposed to 164 keV) seemed relatively a bit more prominant in the 4.5 MeV/amu spectrum. In general, weak features that should have been the most prominant in the spectrum taken at this energy were harder to identiry because the background was

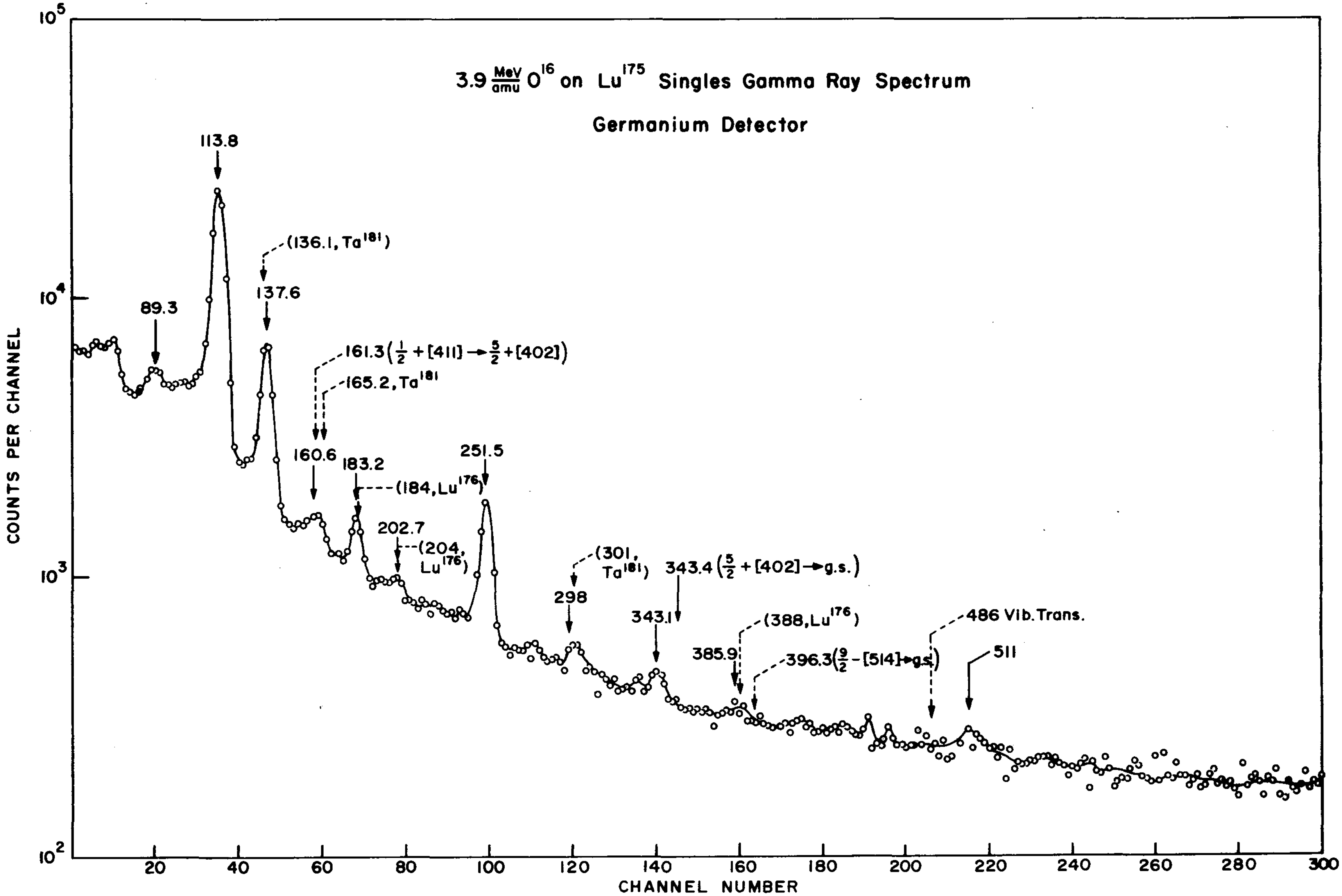

3.9 MeV/amu O16 on Lu175 Singles Gamma Ray Spectrum
Germanium Detector
113.8
(136.1, Ta181)
137.6
89.3
161.3 (1/2 + [411] → 5/2 + [402])
165.2, Ta181
160.6
183.2
(184, Lu176)
251.5
202.7
(204, Lu176)
(301, Ta181)
298
343.4 (5/2 + [402] → g.s.)
343.1
(388, Lu176)
385.9
396.3 (9/2 − [514] → g.s.)
486 Vib. Trans.
511
COUNTS PER CHANNEL
CHANNEL NUMBER

FIG VII - 11

markedly higher than for the three lower energies. The anticipated 183.21 ± 0.34-keV transition was present but too intense, because of the presence of the overlying 184-keV transition in Lu^{176}, which cnstitutes 2.6% natural isotopic abundance in the Lu target. This transition complex was prominant at 3 and 2.6 MeV/amu, and present but somewhat obscured by the excessive background at 4.5 MeV/amu. A ~183-keV transition too intense for Lu^{175} ground-state band deexcitation is present in the NaI singles spectrum also. The very weak feature observed at 195 ± 1 keV in this spectrum was successively stronger at the lower bombarding energies, attaining a peak height within a factor of 2 of that for the 183-keV peak at 2.6 MeV/amu. This feature is not visible in the NaI spectra. It is not anticipated among the low-Z background transitions and is not found in Lu^{176} or Ta^{181} spectra. None of the states generated from the next higher major shell, 1/2-[541] , 3/2-[532] , 1/2+[660] , 3/2+[651] , 1/2-[530] in rough order of excitation energy, can be excited via E1, so the transition is probably due to background but from an unknown source.

The anticipated 202.66 ± 0.56-keV ground-state band transition is noticeable here, but with some uncertainty, again because of an overlying transition: 204-keV, in Lu^{176}. The feature at this energy is no longer noticeable at 3 and 2.6 MeV/amu but is more prominant than the 183-keV line at 4.5 MeV/amu, suggesting a strong enhancement of second-excited state populations at this energy in Lu^{176}, together with a prominant M1 deexcitation to the first excited state, competing favorably with the 301-keV decay to the ground-state.

The next recognizable feature is the strong line in the correct position for the anticipated 251.46 ± 0.07-keV transition in the Lu^{175} ground-state band. The weak line at 279 ± 1 keV did not appear in any of the other spectra and is either spurious or else real but too weak to observe at lower bombarding energies or against the higher background at the higher bombarding energy. Again it is not anticipated among Lu^{176}, Ta^{181} or low-Z reaction background transitions. The feature at ch. 120, which appears about the same in the 2.6 and 3 MeV/amu spectra but not at all above background in the 4.5 MeV/amu spectrum, is slightly too high for the anticipated 298.27 ± 0.21-keV ground-state band transition, but is right at the energy, 301 keV, of the 11/2+ → 7/2+ ground-state band transition in Ta^{181}. The next recognizable feature, weak or indiscernable at lower bombarding energies and, against the background, at the higher energy, is at the correct position for the anticipated 343.17 ± 0.50-keV ground-state band transition, but is composed partly of an overlying 343.40 ± 0.08-keV ^{178} 5/2+[502] → ground state single-particle transition. No significant detail at higher energies was present in any of the other spectra. The very weak feature around channel 160 is in the correct position for the 388-keV transition in Lu^{176}, which is seen in the NaI gamma-ion coincident spectrum as well. It obscures the anticipated 385.9 ± 0.9-keV Lu^{175} ground-state band transition. No further significant detail is present, except a suggestion of the 511-keV radiation (and perhaps a very slight suggestion of some 486-keV radiation).

The conclusions that can be drawn here are that the data are compatable, in so far as can be discerned, with the extrapolations of the lowest ground-state band transitions with just the "A" and "B" terms in energy, with the "C" term less than $\sim 10^{-7}$ keV again. The first two levels of Lu^{176}, and of contaminating Ta^{181} which was used as target backing, were populated, as well as possibly the 343.4-keV 5/2+ single-particle level.

Further features of the NaI spectra are the 511-keV annihilation radiation together with a slight suggestion of a slightly lower-energy transition, and a weak 732 ± 10-keV line in the singles spectrum, and in the gamma-ion coincidence spectrum a strong line at 486 ± 3 keV. The 732-keV line could be deexcitation from the 750 ± 100-keV parent level deduced by Bernstein and Graetzer[144] from yield observations of a 258-keV K internal conversion line following Coulomb excitation by protons at two different bombarding energies. However this line did not appear in the coincidence spectrum, so that it is probably a background line, although such a line does not occur among anticipated lines from low-Z contaminants or Lu^{176} ot Ta^{181}. The possibility of E1 excitation of a 7/2-[532] state seems unlikely since the E1 transition is forbidden by the Λ and n_z asymptotic selection rules, and would be as highly retarded as the E1 transition to the 396.3-keV 9/2-[514] level, which is also forbidden by the Λ and n_z rules. The 396-keV transition is not seen in the singles spectrum, but this could be due in part to obscuration by higher-energy lines.

Comparison of calculated ground-state band photopeak heights with the NaI gamma-ion coincidence spectrum indicates that the estimate $\delta^2(114) = 0.20$ is too small by a factor of ~ 2; this conclusion is subject to the accuracy of the ratio of e.g. the 114-keV and 251-keV absorption factors. With $\delta^2 \sim 0.4$, the fall-off rate for the higher $I \rightarrow I-2$ transitions in the experimental spectrum is correct, so that $Q_0 \sim 8$ is approximately correct.

The 486-keV feature has the correct width, after background subtraction, for a single prominant line, a characteristic of deexcitation of a $K = K_0 + 2 = 11/2$ gamma-vibrational band, and not the aspect corresponding to deexcitation of a $K = 3/2$ band.

If the state is a $K = 11/2$ gamma-vibrational state, there should be a fairly prominant 372-keV deexcitation to the 114-keV level. Unfortunately this is obscured by the Lu^{176} 388-keV line as well as by possible 386-keV ground-state band and 396-keV particle transitions. Also, if the state is $K = 11/2$, a tendency is suggested for $K = K_0 - 1/2$ states to occur at low energies for lower values of Z, and $K = K_0 + 1/2$ for higher values of Z, with both present in Ho^{165}. It would be interesting to see whether or not any theoretical basis for this behavior exists.

The intrinsic matrix element was estimated just as before, referred to the estimate $Q_0 = 8.0$ for the ground-state band. Here only the 251-keV level could be used:

$$P(MCE) = I(137.6) + I(251.5) - I(160.6) - I(343.2). \quad \text{(VII-37)}$$

The result, on using the derived yield normalization factor to allow comparison to the observed 486-keV gamma-ray intensity and that calculated for a single-particle strength intrinsic matrix element, is

$$B_{intr} = (3.4 \pm 0.3)B_{sp}.$$

VIII. Conclusion

The odd-Z, even-N nuclei in the rotational region spanning the area between 50 and 82 protons and 82 and 126 neutrons were Coulomb excited with oxygen ions of energies up to 4 MeV/amu.

Deexcitation gamma radiation subsequent to excitation of states up to spin 23/2 was observed in the Tb^{159} and Ho^{165}, and to 13/2 in the Lu^{175} ground-state bands (possibly to 17/2 in Lu but for certain overlying transitions obscuring the transitions depopulating the 15/2+ and 17/2+ members). Energy analysis of these bands indicated the presence of terms proportional to $I(I+1)$ and to $I^2(I+1)^2$. It was seen that for an odd-A core-plus-nucleon model with quadrupole surface deformations these are the main anticipated terms in the energies and characterize respectively the rotational component to the motion, and the modification thereto due to the rotation-vibration coupling term in the Hamiltonian, dependent on both the orientation and shape coordinates. In Tb there was found to be a third term in the rotational energies proportional to $(-1)^{I+\frac{1}{2}}(I-\frac{1}{2})(I+\frac{1}{2})(I+\frac{3}{2})$, with a coefficient about the same size as that of the vibration-rotation term, ~6 eV. It was shown how two alternative mechanisms could account for such a term. One of these is band mixing between the Nilsson state 3/2+[411], which corresponds to the Tb ground state, and the relatively low-lying 1/2+[411] state. The rotational band based on the latter state exhibits the well-known decoupling term in the energies, $a(-1)^{I+\frac{1}{2}}(I+\frac{1}{2})$. The coefficient a is related to an intrinsic matrix element with respect to the Nilsson-type state wave functions; calculated values agree with the observed values for bands built on nuclear levels corresponding to this state, e.g., the Tm^{169} ground state, ~ 0.8. With the energy modifications in this band reflected in the perturbation energy denominators, the C-term in a $K=3/2$ band results. The term in the Hamiltonian responsible for this mixing is the so-called Coriolis term, essentially the $\vec{I} \cdot \vec{j}$ cross term in $R^2=(\vec{I}-\vec{j})^2$, which is not diagonal in the usual pure-band representation.

The decoupling in $K=1/2$ bands is due to diagonal terms in the matrix elements of this term with respect to $K=1/2$-band wave functions which are suitably symmetrized for the situation of invariance with respect to reflections in the core equatorial plane. For $K>1/2$ there are no such diagonal terms and hence no decoupling in a pure band, since all off-diagonal terms vanish by reason of their differing spins I.

The second mechanism involves the equatorial symmetry of the wave function in conjunction with an $(\vec{I} \cdot \vec{j})^3$ energy term which has diagonal matrix elements with respect to state functions in a $K=3/2$ band. It was seen how such a term arises from higher powers of $R^2=(\vec{I}-\vec{j})^2$ in a phenomenological expansion of the core inertial moments in powers of the core angular momentum. This expansion also results in many small energy corrections, including $I^2(I+1)^2$ contributions, minor modifications or "renormalizations" of the inertia moments and the constant terms in the energy expressions, an $I(I+1)$ -dependent correction to a in $K=1/2$ bands, and the like, all related in a complex fashion to the model expansion parameters. While a unique determination of many of these is neither possible nor meaningful, the assignment of all the $I^2(I+1)^2$ terms to this mechanism results in a value of $B^{(1)}$ (Equation VII-10), the coefficient of R^2 in the expansion of $1/\mathfrak{T}^{\circ}$, of 0.047, a reasonable value corresponding to a usual centrifugal flattening out of the nuclear shape. Of course, the major part of the $I^2(I+1)^2$ term is actually due to the shape-orientation coupling term neglected in the model under discussion, so that $B^{(1)}$ is probably smaller than this. Also, if most of the C-term in Tb is ascribed to this mechanism, then C is related to the diagonal matrix element $\langle \chi_{\frac{3}{2}} | j_{+'} | \chi_{-\frac{3}{2}} \rangle$ and $B^{(2)}$, and provides an addition to the mixing mechanism for which the size of $\langle \chi_{\frac{3}{2}} | j_{+'} | \overline{\chi}_{-\frac{1}{2}} \rangle$ as calculated from Nilsson functions is too small by a factor of ~ 4.

No low-lying suitably decoupled $K=1/2$ bands of negative parity are anticipated for Ho^{165} from the Nilsson model, and higher decoupling occurs in the seventh order of perturbation theory, so that no alternating energy term is anticipated, and none found. Lu^{175} can have decoupling again only in the seventh order, so with reasonable convergence of the perturbation expansion, no observable alternating correction should arise from this cause. The 1/2+[411] state is not forbidden from admixing with the 7/2+[404] ground state by parity but will not be admixed by the Coriolis term in second order because $|\Delta\Omega| = 3$, so again no alternating energy perturbations should arise. The data indicate that very probably none exist for this nucleus, although a series of remarkable coincidences precluded an absolutely definitive check on this.

Calculations of excitation and subsequent deexcitation intensities indicate no significant deviations from the majority of the values of Q_0 and E2/M1 mixing associated with the ground-state band radiations reported from radioactive source work and previous Coulomb excitation studies.

Among other features in the spectra, the most prominent were found to be associated with a 580-keV band in Tb^{159}, 514 and 687-keV bands in Ho^{165}, and a 486-keV band in Lu^{175}. Referred to assumed values of Q_0 of ~ 8 for the ground-state bands, the intrinsic matrix elements connecting the base states of these bands with the nuclear ground states were found to be from ~ 2 to ~ 3 single-particle units (as defined by Alder et al.[1], including the statistical factor $(2\lambda + 1)$). These values are higher than can be accounted for by intrinsic E2 matrix elements between Nilsson single-particle states even in the presence of Coriolis mixing, suggesting collective enhancement. For odd-A nuclei, there are three possible quadrupole vibrational bands, two gamma-vibrational with $K = K_0 \pm 2$, and the beta band with $K = K_0$. Beta bands tend to be high-lying in this region of the periodic table.

Conversion electron data obtained by Diamond et al.[35] on Tb and Ho and Ge gamma spectra for Ho obtained in this work gave energy parameters suggesting that the 580 and 514-keV bands were K_0-2 gamma bands, and 687-keV band, a K_0+2 gamma band. Analysis to determine deexcitation gamma-ray profiles and comparison with the spectra obtained in this work indicate that these are correct assignments, and that the 486-keV state in Lu^{175} is due to a $K=K_0+2$ gamma band, with the K_0+2 bands decaying predominantly via E2. The spectrum profiles did not permit a determination of the K_0-2 band decays in Tb and Ho as being predominantly E2 and M1. In either case, for pure vibrational states, M1 decay is forbidden, even though in Tb symmetry modifications destroy the M1 K-forbiddenness. If the 580-keV band were a single-particle state the Alaga rules for a pure band would become symmetry-modified, with possible gross alterations in the deexcitation profile. The data indicate that the symmetry modification characterized by $|\mathcal{R}| = \infty$, required for a pure vibrational state, provides the best fit to the data.

In Tb and 348-keV state observed in radioactive decay work and assigned as 5/2+ [413] was fairly strongly excited, giving a deexcitation profile that suggest $\delta^2(348) \sim 0.4$, and an intrinsic E2 matrix element of about one single-particle unit. A possibility of E1 excitation of an anticipated low-lying 3/2- [541] state was ruled out, as discussed above.

In Ho a 361-keV line from a level assigned from previous source work as 3/2+ [411] was observed. The lowest electromagnetic transition multipolarities for the Ho ground state, 7/2- [523] to this state were M2 and E3. It is possible that this state is populated from the 5/2- gamma-vibrational state via M2 or E1 decay.

In Lu some evidence for excitation of a 343.4-keV level assigned from previous source work as 5/2+[502] was present in the singles gamma spectra, but no observable radiation from any further single-particle levels.

The general predictions of the rotational model in its odd-A context appear to be confirmed by this work, and the occurrence of the expected main higher-order effects was noted. However the limitations inherent in the available amount of beam and the resolution or efficiency of the detectors placed acute limitations on the quality of the data and on the amount of detailed information that could be extracted from it. Substantial advance in data quality will have to await the availability of higher beam currents to permit better coincidence suppression of background, expecially for Ge gamma-ray detectors. This is prerequisite to a more detailed probe of the many perturbations and mixing effects that can arise from the simple core-plus-nucleon type phenomenology.

IX. Appendicies

Appendix 1. Least Squares Formulae for the Straight Line

$y = a_o + a_1 x$

Data: (x_i, y_i); weights w_i; $i = 1, \ldots, n$.

x_i known exactly.

Residuals: $\delta_i = y_i - (a_{oLS} + a_{1LS} x_i)$

$$a_{oLS} = \frac{[wx][wxy] - [wy][wx^2]}{D}$$

$$a_{1LS} = \frac{[wx][wy] - [w][wxy]}{D}$$

$$D \equiv [wx]^2 - [w][wx^2]$$

$$[ab] \equiv \sum_{i=1}^{n} a_i b_i$$

$$\sigma_{a_o} = \sqrt{\frac{[w\delta^2][wx^2]}{(n-2)|D|}}$$

$$\sigma_{a_1} = \sqrt{\frac{[w\delta^2][w]}{(n-2)|D|}}$$

Appendix 2. Rayleigh-Schrodinger Scheme

Exact problem: $H|\Psi_n\rangle = E_n|\Psi_n\rangle$

Corresponding zero-order problem: $H^{(0)}|n\rangle = E_n^{(0)}|n\rangle$

Expansions:
$$H = \sum_{\nu=0}^{\infty} \lambda^{\nu} H^{(\nu)}$$
$$E_n = \sum_{\nu=0}^{\infty} \lambda^{\nu} E_n^{(\nu)}$$
$$|\Psi_n\rangle = \sum_{\nu=0}^{\infty} \lambda^{\nu} |\Psi_n^{(\nu)}\rangle$$

Substitution in the exact problem, equating of terms with like powers of λ, and use of the relations:

$$|\Psi_n^{(\nu)}\rangle = \sum_{\rho} |\rho\rangle\langle\rho|\Psi_n^{(\nu)}\rangle \equiv |n\rangle\langle n|\Psi_n^{(\nu)}\rangle + \sum_{\rho\neq n} |\rho\rangle\langle\rho|\Psi_n^{(\nu)}\rangle\,;$$
$$\langle m|n\rangle = \delta_{mn}\,; \quad \langle\Psi_m|\Psi_n\rangle = \delta_{mn}$$

results in the following first, second and third-order corrections to the energies and wave functions:

$$E_n^{(1)} = \langle n|H^{(1)}|n\rangle$$
$$E_n^{(2)} = \langle n|H^{(2)}|n\rangle + \sum_{\rho\neq n} \frac{\langle n|H^{(1)}|\rho\rangle\langle\rho|H^{(1)}|n\rangle}{E_n^{(0)} - E_\rho^{(0)}}$$
$$E_n^{(3)} = \langle n|H^{(3)}|n\rangle + \sum_{\rho\neq n} \frac{\langle n|H^{(2)}|\rho\rangle\langle\rho|H^{(1)}|n\rangle + \langle n|H^{(1)}|\rho\rangle\langle\rho|H^{(2)}|n\rangle}{E_n^{(0)} - E_\rho^{(0)}}$$
$$+ \sum_{\rho\neq n}\sum_{\sigma\neq n} \frac{\langle n|H^{(1)}|\rho\rangle\langle\rho|H^{(1)}|\sigma\rangle\langle\sigma|H^{(1)}|n\rangle}{(E_n^{(0)} - E_\rho^{(0)})(E_n^{(0)} - E_\sigma^{(0)})}$$
$$- \langle n|H^{(1)}|n\rangle \sum_{\rho\neq n} \frac{\langle n|H^{(1)}|\rho\rangle\langle\rho|H^{(1)}|n\rangle}{(E_n^{(0)} - E_\rho^{(0)})^2}$$

$$|\psi_n\rangle = |n\rangle\left\{1+\langle n|\psi_n^{(1)}\rangle+\langle n|\psi_n^{(2)}\rangle+\langle n|\psi_n^{(3)}\rangle+\dots\right\}$$

$$+\sum_{\rho\neq n}\frac{|\rho\rangle\langle\rho|H^{(1)}|n\rangle}{E_n^{(0)}-E_\rho^{(0)}}\left\{1+\langle n|\psi_n^{(1)}\rangle+\langle n|\psi_n^{(2)}\rangle+\dots\right\}$$

$$+\left(-\langle n|H^{(1)}|n\rangle\sum_{\rho\neq n}\frac{|\rho\rangle\langle\rho|H^{(1)}|n\rangle}{(E_n^{(0)}-E_\rho^{(0)})^2}+\sum_{\rho\neq n}\frac{|\rho\rangle\langle\rho|H^{(2)}|n\rangle}{E_n^{(0)}-E_\rho^{(0)}}+\sum_{\rho\neq n}\sum_{\sigma\neq n}\frac{|\rho\rangle\langle\rho|H^{(1)}|\sigma\rangle\langle\sigma|H^{(1)}|n\rangle}{(E_n^{(0)}-E_\rho^{(0)})(E_n^{(0)}-E_\sigma^{(0)})}\right)$$

$$\times\left\{1+\langle n|\psi_n^{(1)}\rangle+\dots\right\}+\left[\sum_{\rho\neq n}\frac{|\rho\rangle\langle\rho|H^{(3)}|n\rangle}{E_n^{(0)}-E_\rho^{(0)}}\right.$$

$$+\sum_{\rho\neq n}\sum_{\sigma\neq n}\frac{|\rho\rangle\langle\rho|H^{(2)}|\sigma\rangle\langle\sigma|H^{(1)}|n\rangle+|\rho\rangle\langle\rho|H^{(1)}|\sigma\rangle\langle\sigma|H^{(2)}|n\rangle}{(E_n^{(0)}-E_\rho^{(0)})(E_n^{(0)}-E_\sigma^{(0)})}$$

$$+\sum_{\rho\neq n}\sum_{\sigma\neq n}\sum_{\tau\neq n}\frac{|\rho\rangle\langle\rho|H^{(1)}|\sigma\rangle\langle\sigma|H^{(1)}|\tau\rangle\langle\tau|H^{(1)}|n\rangle}{(E_n^{(0)}-E_\rho^{(0)})(E_n^{(0)}-E_\sigma^{(0)})(E_n^{(0)}-E_\tau^{(0)})}$$

$$-\langle n|H^{(1)}|n\rangle\sum_{\rho\neq n}\sum_{\sigma\neq n}\left(\frac{1}{E_n^{(0)}-E_\rho^{(0)}}+\frac{1}{E_n^{(0)}-E_\sigma^{(0)}}\right)\frac{|\rho\rangle\langle\rho|H^{(1)}|\sigma\rangle\langle\sigma|H^{(1)}|n\rangle}{(E_n^{(0)}-E_\rho^{(0)})(E_n^{(0)}-E_\sigma^{(0)})}$$

$$+\left(\langle n|H^{(1)}|n\rangle\right)^2\sum_{\rho\neq n}\frac{|\rho\rangle\langle\rho|H^{(1)}|n\rangle}{(E_n^{(0)}-E_\rho^{(0)})^3}-\langle n|H^{(2)}|n\rangle\sum_{\rho\neq n}\frac{|\rho\rangle\langle\rho|H^{(1)}|n\rangle}{(E_n^{(0)}-E_\rho^{(0)})^2}$$

$$\left.-\sum_{\rho\neq n}\frac{|\rho\rangle\langle\rho|H^{(1)}|n\rangle}{(E_n^{(0)}-E_\rho^{(0)})^2}\sum_{\sigma\neq n}\frac{\langle n|H^{(1)}|\sigma\rangle\langle\sigma|H^{(1)}|n\rangle}{E_n^{(0)}-E_\sigma^{(0)}}-\langle n|H^{(1)}|n\rangle\sum_{\rho\neq n}\frac{|\rho\rangle\langle\rho|H^{(2)}|n\rangle}{(E_n^{(0)}-E_\rho^{(0)})^2}\right]$$

$$\times\left\{1+\dots\right\}+\dots$$

$\langle n|\psi_n^{(\nu)}\rangle$ are related to normalization of $|\psi_n\rangle$; $\langle\psi_n|\psi_n\rangle=1$ implies $\langle n|\psi_n^{(\nu)}\rangle=\frac{(i\chi_n)^\nu}{\nu!}$, χ_n real but otherwise arbitrary. Hence $\left\{1+\sum_{\nu=1}^{\infty}\langle n|\psi_n^{(\nu)}\rangle\right\}=e^{i\chi_n}$, a phase factor. One may set $\chi_n\equiv 0$.

Appendix 3. Tables of Ground-State Band Calculations

Table A-1

$$P_{I_f I_0}(\theta, q, \xi = 0) \approx (2I_f + 1) \sum_I{}' \begin{pmatrix} I_f & I_0 & I \\ -K & K & 0 \end{pmatrix}^2 P_I[q(\theta)]$$

$P_{I_f K}$, $K = I_0 = 3/2,\ 7/2$:

$K = 3/2$

$P_{\frac{5}{2},\frac{3}{2}}$	$\frac{18}{35}P_2$	$\frac{1}{21}P_4$
$P_{\frac{7}{2},\frac{3}{2}}$	$\frac{2}{7}P_2$	$\frac{2}{7}P_4$
$P_{\frac{9}{2},\frac{3}{2}}$	$\frac{5}{11}P_4$	$\frac{10}{143}P_6$
$P_{\frac{11}{2},\frac{3}{2}}$	$\frac{7}{33}P_4$	$\frac{45}{143}P_6$
$P_{\frac{13}{2},\frac{3}{2}}$	$\frac{28}{65}P_6$	$\frac{7}{85}P_8$
$P_{\frac{15}{2},\frac{3}{2}}$	$\frac{12}{65}P_6$	$\frac{28}{85}P_8$
$P_{\frac{17}{2},\frac{3}{2}}$	$\frac{135}{323}P_8$	$\frac{12}{133}P_{10}$
$P_{\frac{19}{2},\frac{3}{2}}$	$\frac{55}{323}P_8$	$\frac{45}{133}P_{10}$
$P_{\frac{21}{2},\frac{3}{2}}$	$\frac{66}{161}P_{10}$	$\frac{11}{115}P_{12}$
$P_{\frac{23}{2},\frac{3}{2}}$	$\frac{26}{161}P_{10}$	$\frac{198}{575}P_{12}$

$K = 7/2$

$P_{\frac{9}{2},\frac{7}{2}}$	$\frac{15}{33}P_2$	$\frac{350}{1287}P_4$	$\frac{14}{429}P_6$	$\frac{1}{2431}P_8$
$P_{\frac{11}{2},\frac{7}{2}}$	$\frac{6}{55}P_2$	$\frac{54}{143}P_4$	$\frac{21}{143}P_6$	$\frac{21}{2431}P_8$
$P_{\frac{13}{2},\frac{7}{2}}$	$\frac{98}{429}P_4$	$\frac{735}{2431}P_6$	$\frac{245}{4199}P_8$	$\frac{1}{969}P_{10}$
$P_{\frac{15}{2},\frac{7}{2}}$	$\frac{2}{39}P_4$	$\frac{70}{221}P_6$	$\frac{770}{4199}P_8$	$\frac{14}{969}P_{10}$
$P_{\frac{17}{2},\frac{7}{2}}$	$\frac{693}{4199}P_6$	$\frac{99}{323}P_8$	$\frac{557}{7429}P_{10}$	$\frac{18}{10925}P_{12}$
$P_{\frac{19}{2},\frac{7}{2}}$	$\frac{11}{323}P_6$	$\frac{91}{323}P_8$	$\frac{4550}{22287}P_{10}$	$\frac{210}{10925}P_{12}$
$P_{\frac{21}{2},\frac{7}{2}}$	$\frac{1001}{7429}P_8$	$\frac{2002}{6555}P_{10}$	$\frac{154}{1725}P_{12}$	$\frac{22}{10025}P_{14}$
$P_{\frac{23}{2},\frac{7}{2}}$	$\frac{195}{7429}P_8$	$\frac{567}{2185}P_{10}$	$\frac{5}{23}P_{12}$	$\frac{77}{3335}P_{14}$

$P_{I_f}(K=5/2)$

q	$P_{5/2}$	$P_{7/2}$	$P_{9/2}$	$P_{11/2}$	$P_{13/2}$	$P_{15/2}$	$P_{17/2}$	$P_{19/2}$	$P_{21/2}$	$P_{23/2}$
0.0	0	0	0	0	0	0	0	0	0	0
0.5	.0434	.0245	.0006	0	0	0	0	0	0	0
1.0	.1475	.0871	.0091	.0044	.0003	.0001	0	0	0	0
1.5	.2514	.1612	.0380	.0194	.0025	.0011	.0001	.0000	0	0
2.0	.2972	.2162	.0911	.0500	.0113	.0054	.0008	.0003	.0000	.0000
2.5	.2647	.2325	.1544	.0935	.0330	.0167	.0036	.0017	.0002	.0001
3.0	.1792	.2080	.2012	.1382	.0700	.0382	.0120	.0057	.0012	.0005
3.5	.0895	.1570	.2061	.1685	.1160	.0699	.0269	.0152	.0044	.0020
4.0	.0414	.1048	.1668	.1724	.1555	.1058	.0583	.0324	.0121	.0060

$P_{I_f}(K=7/2)$

q	$P_{9/2}$	$P_{11/2}$	$P_{13/2}$	$P_{15/2}$	$P_{17/2}$	$P_{19/2}$	$P_{21/2}$	$P_{23/2}$
0.0	0	0	0	0	0	0	0	0
0.5	.0395	.0097	.0003	.0001	0	0	0	0
1.0	.1264	.0387	.0047	.0012	.0001	.0000	0	0
1.5	.2269	.0846	.0202	.0061	.0010	.0003	.0000	.0000
2.0	.2920	.1394	.0530	.0187	.0048	.0014	.0003	.0001
2.5	.2975	.1884	.0985	.0422	.0151	.0051	.0013	.0004
3.0	.2504	.2151	.1447	.0764	.0347	.0138	.0047	.0015
3.5	.1786	.2147	.1761	.1151	.0641	.0302	.0125	.0047
4.0	.1185	.1750	.1812	.1472	.0984	.0549	.0270	.0118

Table A-2

Z_2, Element	M_2 [219] (At.wt.,amu)	Z_2/M_2	$\frac{Z_2/M_2}{(Z_2/M_2)_{Ag}}$
4 Be	9.012	.4438	1.0190
13 Al	26.98	.4818	1.1062
28 Ni	58.71	.4769	1.0949
29 Cu	63.54	.4564	1.0454
47 Ag	107.9	.4356	1.0000
79 Au	197.0	.4010	0.9206
82 Pb	207.2	.3957	0.9085
65 Tb	158.9	.4091	0.9391
67 Ho	165.0	.4061	0.9322
71 Lu	175.0	.4057	0.9314

$R(E, Z_2)$, after E. L. Hubbard[224]

E, MeV/amu	13 Al	28 Ni	29 Cu	47 Ag	79 Au	82 Pb
1	3.1	4.5	4.2	5.5	7.5	8.0
2	5.6	7.9	7.8	10.0	14.0	14.0
3	8.7	11.8	11.8	15.1	21.0	20.5
4	12.3	16.2	16.4	20.6	28.6	27.7
5	16.7	21.6	21.8	27.1	37.5	36.3
$6\frac{1}{4}$	23.0	29.1	29.4	36.3	50.1	48.0
$7\frac{1}{2}$	30.3	37.4	38.1	46.7	64.0	62.0

	$[R(Z,Z_2{}'\ 47(Ag))/R(E,Z_2)][(Z_2/M_2)/(Z_2/M_2)_{Ag}]$					
1	.6235	.8958	.8001	1	1.2554	1.3219
2	.6195	.8650	.8173	1	1.2889	1.2719
3	.6373	.8556	.8188	1	1.2803	1.2334
4	.6605	.8610	.8341	1	1.2781	1.2217
5	.6817	.8727	.8429	1	1.2739	1.2170
$6\frac{1}{4}$	.7009	.8777	.8486	1	1.2706	1.2014
$7\frac{1}{2}$	.7177	.8862	.8548	1	1.2616	1.2062

Table A-3

Interpolated Range-Energy Data

Z_2, Element	E, MeV/amu 1	2	3	4	5	$6\frac{1}{4}$	$7\frac{1}{2}$
	$\mathcal{R}(E;\ Z_2,\ Z_{2Ag})$						
47 Ag	1	1	1	1	1	1	1
65 Tb	1.1431	1.1625	1.1577	1.1564	1.1541	1.1522	1.1472
67 Ho	1.1590	1.1806	1.1752	1.1738	1.1712	1.1691	1.1635
71 Lu	1.1908	1.2167	1.2102	1.2086	1.2054	1.2030	1.1962
79 Au	1.2544	1.2889	1.2803	1.2781	1.2739	1.2706	1.2616
	$R(E,\ Z_2)$, mg./cm.^{2}						
65 Tb	6.695	12.38	18.61	25.37	33.31	44.54	57.05
67 Ho	6.832	12.66	19.04	25.94	34.05	45.52	58.29
71 Lu	7.032	13.06	19.62	26.73	35.07	46.89	59.98

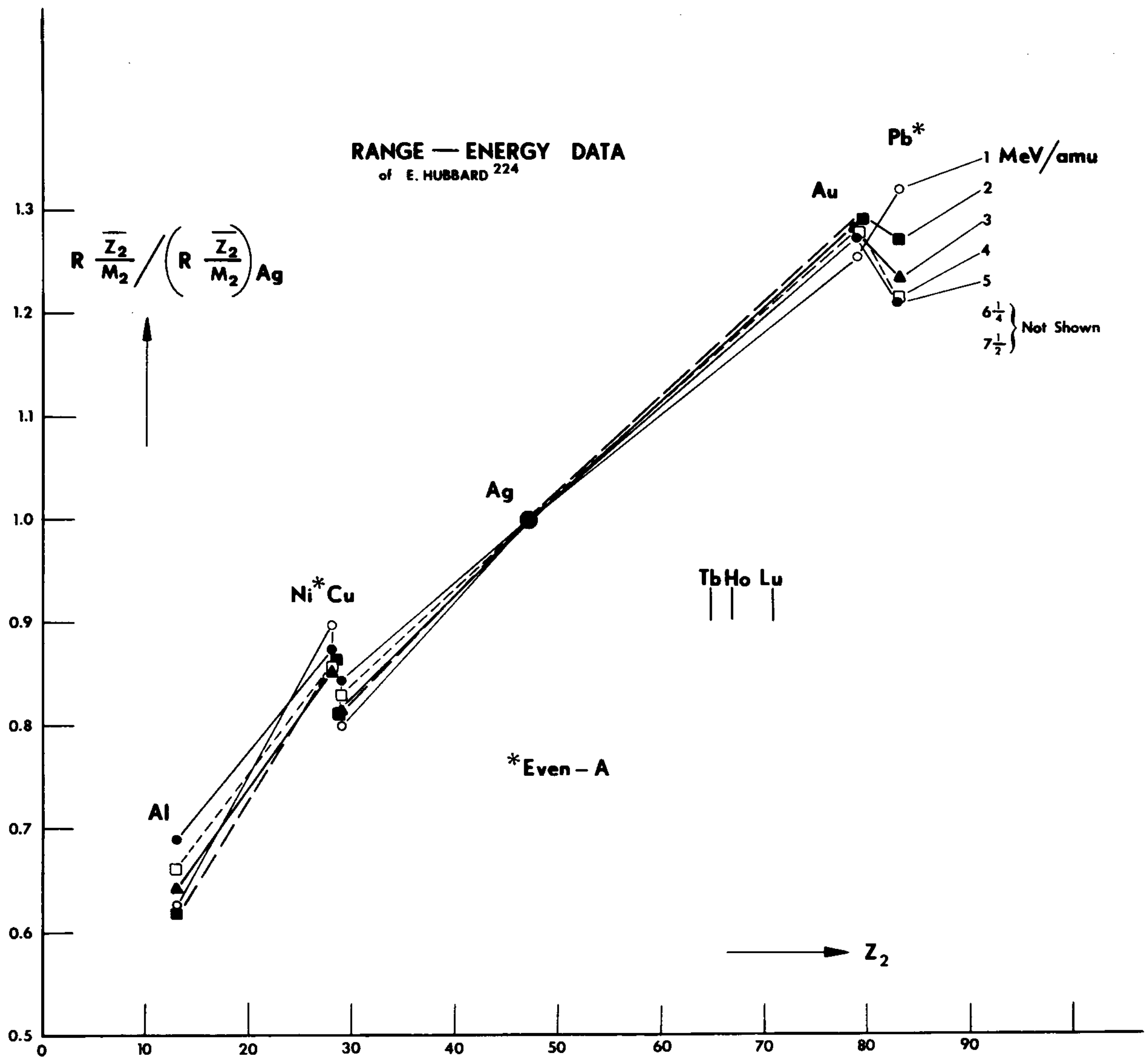

RANGE — ENERGY DATA
of E. HUBBARD 224
$R \frac{\overline{Z_2}}{M_2} \Big/ \left(R \frac{\overline{Z_2}}{M_2}\right)_{Ag}$
1.3
1.2
1.1
1.0
0.9
0.8
0.7
0.6
0.5
0
10
20
30
40
50
60
70
80
90
Al
Ni* Cu
Ag
Au
Pb*
Tb Ho Lu
*Even – A
1 MeV/amu
2
3
4
5
$6\frac{1}{4}$
$7\frac{1}{2}$
Not Shown
Z_2

FIG A-1

Table A-4

E_2 MeV/amu	$\sum_j d\sigma_R(\theta_{jCM}, E_2)$, cm.^{2}/nucl. Tb	Ho	Lu	
4.08	1.345×10^{-25}	1.430×10^{-25}	1.609×10^{-25}	
4.060	1.358	1.443	1.625	
3.922	1.455	1.546	1.741	
3.781	1.566	1.664	1.874	
3.637	1.692	1.798	2.025	
3.484	1.844	1.960	2.206	
3.442	1.889			At disc. cutoff depths.
3.433		2.018		
3.421			2.288	

E_2	$\bar{q}$ Tb, Q_o=8.1	Ho, Q_o=7.5	8.0	Lu, Q_o=8.0	
4.08	2.901	2.543	2.712	2.438	
4.060	2.879	2.524	2.693	2.420	
3.922	2.734	2.397	2.556	2.297	
3.781	2.588	2.269	2.420	2.175	
3.637	2.441	2.140	2.283	2.052	
3.484	2.297	2.013	2.148	1.930	
3.442	2.248				At disc. cutoff depths.
3.433		1.963	2.094		
3.421				1.872	

Intratarget Kinematics

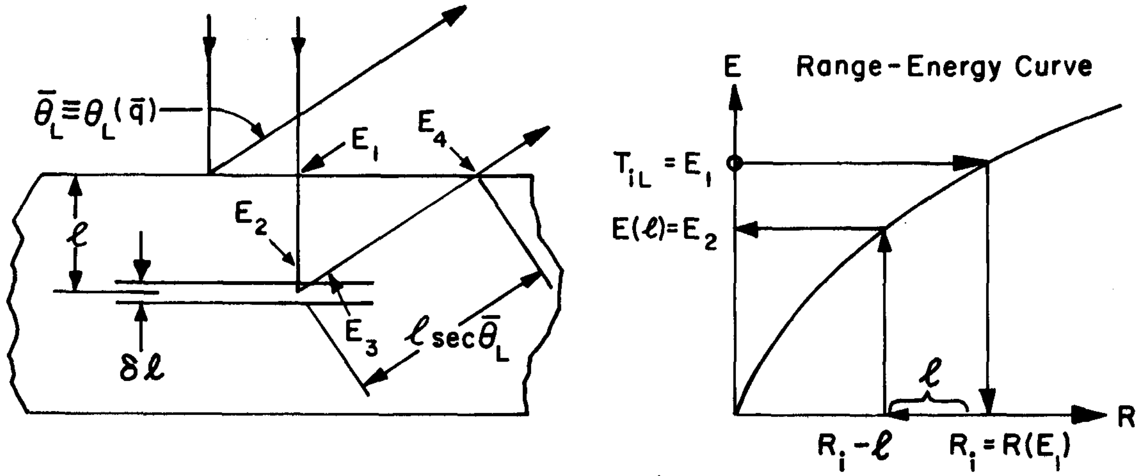

$$E_1 \xrightarrow[\text{Curve}]{\text{Range-Energy}} E_2(\ell, E_1) \xrightarrow[\text{Equation}]{\text{Q}} E_3(\ell, \bar{\theta}_L, E_1) \xrightarrow[\text{Curve}]{\text{Range-Energy}} E_4(\ell, \bar{\theta}_L, E_1)$$

Range-energy curve : $R = f(E)$ or $E = \mathfrak{f}(R)$

$E_1 = T_{iL} =$ "machine energy"

$E_2(\ell, T_{iL}) =$ effective incident energy at depth ℓ in target

$E_2(\ell, T_{iL}) = \mathfrak{f}\left[f(T_{iL}) - \ell\right]$

$E_3(\ell, \bar{\theta}_L, T_{iL}) =$ projectile energy subsequent to "quasi-elastic" Coulomb exciting event $(Q \approx 0)$

$$E_3(\ell, \bar{\theta}_L, T_{iL}) = \frac{E_3(\ell, \bar{\theta}_L, T_{iL})}{E_2(\ell, T_{iL})} E_2(\ell, T_{iL}) \equiv \epsilon(\bar{\theta}_L, E_2)\, E_2(\ell, T_{iL})$$

$E_4(\ell, \bar{\theta}_L, T_{iL}) =$ emergent scattered ion energy

$$E_4(\ell, \bar{\theta}_L, T_{iL}) = \mathfrak{f}\left\{f\left[E_3(\ell, \bar{\theta}_L, T_{iL})\right] - \ell \sec\bar{\theta}_L\right\}$$

Cutoff depth ℓ_{cut} : $E_4(\ell_{cut}, \bar{\theta}_L, T_{iL}) = E_{4cut}(T_{iL}) =$ energy corresp. to particle discriminator setting.

FIG A-2

Table A-5

Ground-State Band Energies for Depopulation Computations

i	I	E_i	$E_{i,i-1}$ *	$E_{i,i-2}$ *	$E_{i,i-1}$ **	$E_{i,i-2}$ **	k_i $\frac{\Delta E}{511}$ $\frac{keV}{keV}$ **	k'_i $\frac{\Delta E}{511}$ $\frac{keV}{keV}$ **
0	I_o= 3/2	0						
1	5/2	58.00±.01	58.00±.01#		58.0		.1135	.2691
2	7/2	137.50±.02	79.50±.02#	(137.5±.02)#	79.5	137.5	.1556	.2691
3	9/2	241 ±1	103.5	183 ±2	103.5	183.0	.2025	.3581
4	11/2	363 ±1	122	225 ±2	122	225.5	.2388	.4413
5	13/2	511 ±3		270 ±3	148	270	.2846	.5284
6	15/2	669 ±4		306 ±3	158	306	.3092	.5988
7	17/2	862 ±5		351 ±4	193	351	.3777	.6859
8	19/2	1053 ±6		384 ±4	191	384	.3738	.7515
9	21/2	1285 ±6		423 ±5	232	423	.4540	.8278
10	23/2	1499 ±7		446 ±5	214	446	.4188	.8728
0	I_o= 7/2	0						
1	9/2	94.697±.004#	94.697±.004#		94.7		.1815	
2	11/2	210 ±1	115 ±1	210±1	115.3	210	.2256	.4110
3	13/2	345 ±1	135 ±1	250±2	135	250.3	.2642	.4898
4	15/2	500 ±1	155 ±1	290±2	154	290	.3041	.5675
5	17/2	671 ±2	173 ±2(Ge)	326±3	172	326	.3366	.6380
6	19/2	861 ±3	180 ±2(Ge)	361±3	190	361	.3718	.7065
7	21/2	1067 ±4		396±4	206	396	.4031	.7750
8	23/2	1289 ±5		428±4	222	428	.4344	.8376
0	I_o= 7/2	0 ##			##	##		
1	9/2	113.81±.02	113.81±.02#		113.81±.02		.2227	
2	11/2	251.46±.07	137.65±.05#	251.3±.5#	137.65±.05	251.46±.07	.2694	.4921
3	13/2	412.08±.19			160.62±.16	298.27±.21	.3143	.5837
4	15/2	594.64±.53			182.56±.34	343.18±.50	.3573	.6716
5	17/2	797.95±1.1			203.31±.56	385.87±.89	.3979	.7551
6	19/2	1020.67±2.0			222.72±.9	426.03±1.5	.4358	.8337
7	21/2	1261.30±3.2			240.63±1.3	240.63±2.1	.4709	.9068
8	23/2	1518.08±7.			256.78±1.7	497,41±2.9	.5025	.9734

* Observed. ** From adopted level energies. # Previous source work.

\## Extrapolation from source work using $E_I = E_o + AI(I+1) + BI^2(I+1)^2$.

Table A-6

$\Delta E_{i,i-1}$ Transitions, Theoretical I.C. Coefficients

i	k_i	$\alpha_2(K)$	$\alpha_2(L)$	$\alpha_2(M)$	$\alpha_2(N)$	$\sum\alpha_2$	$\beta_1(K)$	$\beta_1(L)$	$\beta_1(M)$	$\beta_1(N)$	$\sum\beta_1$
Terbium											
1	.1135										
2	.1556	1.90	3.18	1.49	.44	7.01	3.62	.476	.210	.120	4.43
3	.2025	1.04	.980	.448	.15	2.62	1.74	.226	.100	.0600	2.13
4	.2388	.654	.492	.203	.078	1.43	1.06	.138	.0640	.0385	1.30
5	.2896	.381	.207	.0918	.039	.719	.630	.0804	.0371	.0220	.770
6	.3092	.314	.154	.0685	.030	.567	.525	.0671	.0310	.0180	.641
7	.3777	.173	.0646	.0281	.0138	.280	.303	.0382	.0171	.0104	.369
8	.3738	.179	.0678	.0295	.0150	.291	.312	.0395	.0177	.0106	.380
9	.4540	.0890	.0266	.0144	.00520	.132	.158	.0204	.00879	.0048	.192
10	.4188	.128	.0425	.0185	.00980	.199	.222	.0287	.0127	.0074	.271
Holmium											
1	.1853	1.23	1.64	.790	.195	3.86	2.53	.365	.158	.0950	3.15
2	.2256	.795	.740	.335	.0940	1.96	1.52	.215	.0944	.0570	1.89
3	.2642	.525	.378	.167	.0550	1.12	.979	.133	.0622	.0385	1.21
4	.3014	.347	.204	.0905	.0355	.677	.676	.0903	.0422	.0258	.834
5	.3366	.252	.126	.0563	.0245	.456	.494	.0648	.0294	.0180	.606
6	.3718	.186	.0810	.0252	.0153	.318	.369	.0491	.0220	.0130	.453
7	.4031	.146	.0566	.0251	.0112	.239	.296	.0393	.0174	.0099	.363
8	.4344	.117	.0421	.0186	.0081	.186	.239	.0317	.0142	.0079	.239
Lutetium											
1	.2227	.695	.940	.495	.143	2.27	2.23	.293	.140	.075	2.74
2	.2594	.441	.419	.201	.0660	1.13	1.31	.180	.0825	.0450	1.62
3	.3143	.299	.214	.0958	.0350	.644	.888	.118	.0538	.0300	1.09
4	.3573	.214	.122	.0540	.0210	.411	.612	.0827	.0373	.0215	.754
5	.3979	.159	.0792	.0350	.0150	.288	.431	.0599	.0268	.0160	.534
6	.4358	.121	.0550	.0237	.0104	.210	.339	.0459	.0208	.0120	.418
7	.4709	.100	.0408	.0172	.00755	.166	.274	.0372	.0166	.0093	.337
8	.5025	.0835	.0318	.0132	.00535	.134	.228	.0312	.0137	.0077	.281

i	k_i'	$\alpha_2'(K)$	$\alpha_2'(L)$	$\alpha_2'(M)$	$\alpha_2'(N)$	$\sum\alpha_2'$
Terbium						
1						
2	.2691	.473	.290	.126	.0510	.940
3	.3581	.203	.0808	.0353	.0168	.339
4	.4413	.0963	.0295	.0128	.0060	.145
5	.5284	.0630	.0179	.00742	.00180	.0901
6	.5988	.0452	.0109	.00455	.00130	.0620
7	.6869	.0310	.00673	.00284	.00084	.0414
8	.7515	.0240	.00496	.00204	.00062	.0316
9	.8278	.0187	.00365	.00147	.00045	.0243
10	.8728	.0163	.00310	.00121	.000375	.0210
Holmium						
1						
2	.4110	.138	.0525	.0233	.0102	.224
3	.4898	.0810	.0263	.0113	.0053	.124
4	.5675	.0545	.0151	.00530	.00305	.0790
5	.6380	.0397	.00990	.00415	.00202	.0558
6	.7065	.0298	.00690	.00285	.00137	.0409
7	.7750	.0234	.00508	.00206	.00099	.0315
8	.8376	.0189	.00398	.00159	.00074	.0252
Lutetium						
1						
2	.4921	.0886	.0345	.0143	.00610	.144
3	.5837	.0553	.0180	.00747	.00335	.0841
4	.6716	.0370	.0109	.00445	.00213	.0545
5	.7551	.0275	.00728	.00295	.00140	.0391
6	.8337	.0214	.00526	.00210	.00104	.0298
7	.9068	.0175	.00405	.00158	.0080	.0239
8	.9734	.0148	.00324	.00127	.00065	.0200

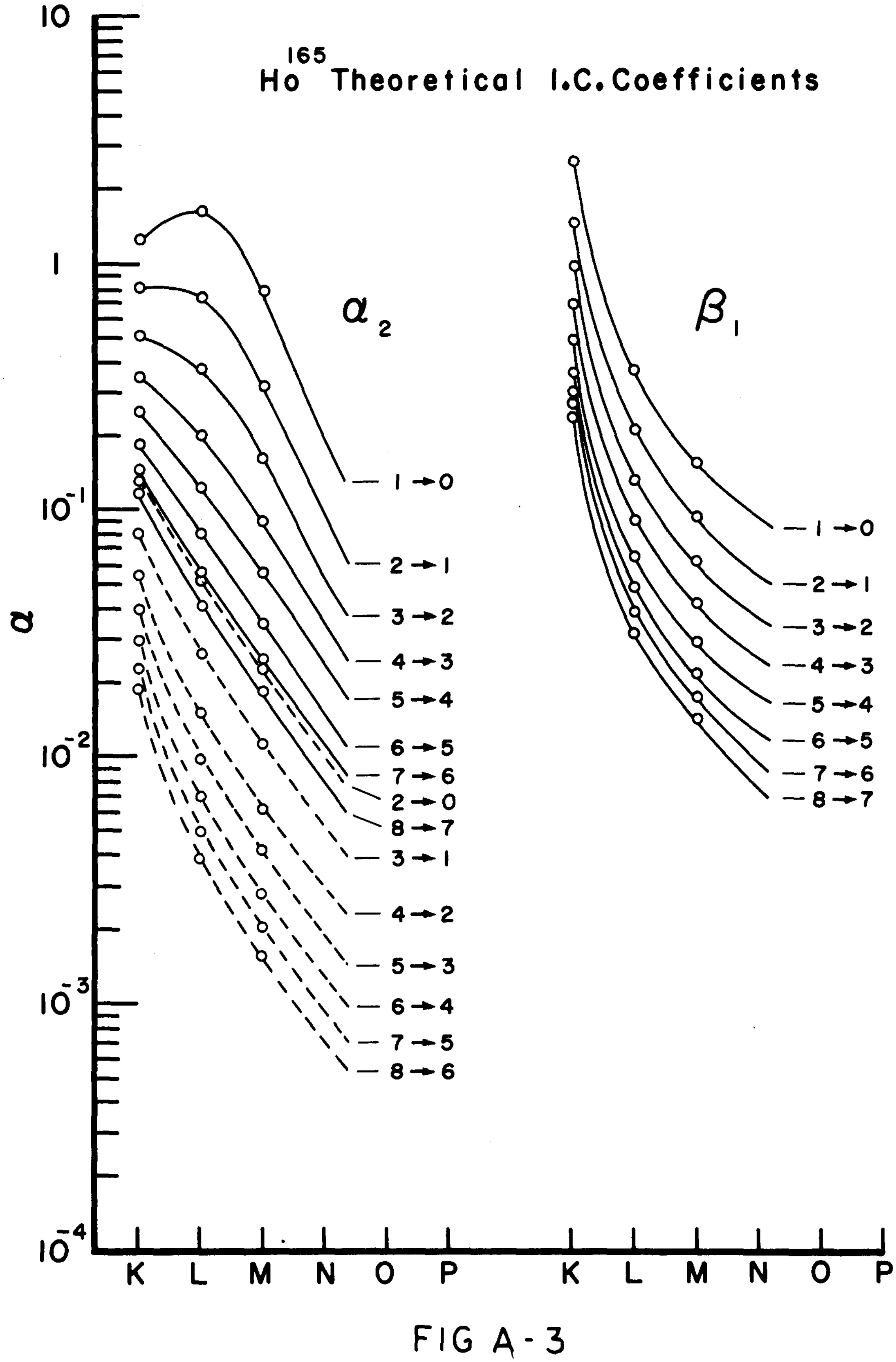

Ho^{165} Theoretical I.C. Coefficients
α_2
β_1
α
10
1
10^{-1}
10^{-2}
10^{-3}
10^{-4}
K L M N O P
K L M N O P
1 → 0
2 → 1
3 → 2
4 → 3
5 → 4
6 → 5
7 → 6
2 → 0
8 → 7
3 → 1
4 → 2
5 → 3
6 → 4
7 → 5
8 → 6
1 → 0
2 → 1
3 → 2
4 → 3
5 → 4
6 → 5
7 → 6
8 → 7

FIG A-3

Table A-7

Matrices for the Ground-State Band Depopulation Problem---

Pure M1 and Pure E2 Decay Cases

$$= \begin{pmatrix} 1 & 0 & 0 & 0 & 0 & \cdots \\ -t_{10} & 1 & 0 & 0 & 0 & \cdots \\ -t_{20} & -t_{21} & 1 & 0 & 0 & \cdots \\ 0 & -t_{31} & -t_{32} & 1 & 0 & \cdots \\ 0 & 0 & -t_{42} & -t_{43} & 1 & \cdots \\ \vdots & \vdots & \vdots & \vdots & \vdots & \ddots \end{pmatrix}; \quad \|t_{M1}\| = \begin{pmatrix} 1 & 0 & 0 & 0 & 0 & \cdots \\ -1 & 1 & 0 & 0 & 0 & \cdots \\ 0 & -1 & 1 & 0 & 0 & \cdots \\ 0 & 0 & -1 & 1 & 0 & \cdots \\ 0 & 0 & 0 & -1 & 1 & \cdots \\ \vdots & \vdots & \vdots & \vdots & \vdots & \ddots \end{pmatrix};$$

$$\left. \begin{array}{ccccccccccc} & 0 & 0 & 0 & 0 & 0 & 0 & 0 & 0 & 0 & 0 \\ & 1 & 0 & 0 & 0 & 0 & 0 & 0 & 0 & 0 & 0 \\ .419 & -.28581 & 1 & 0 & 0 & 0 & 0 & 0 & 0 & 0 & 0 \\ & -.90692 & -.09308 & 1 & 0 & 0 & 0 & 0 & 0 & 0 & 0 \\ & 0 & -.96354 & -.03646 & 1 & 0 & 0 & 0 & 0 & 0 & 0 \\ & 0 & 0 & -.98033 & -.01967 & 1 & 0 & 0 & 0 & 0 & 0 \\ & 0 & 0 & 0 & -.99010 & -.00990 & 1 & 0 & 0 & 0 & 0 \\ & 0 & 0 & 0 & 0 & -.99140 & -.00860 & 1 & 0 & 0 & 0 \\ & 0 & 0 & 0 & 0 & 0 & -.99582 & -.00418 & 1 & 0 & 0 \\ & 0 & 0 & 0 & 0 & 0 & 0 & -.99515 & -.00485 & 1 & 0 \\ & 0 & 0 & 0 & 0 & 0 & 0 & 0 & -.99781 & -.00218 & 1 \end{array} \right) = \|t^{Tb}_{E2}|$$

$$\begin{pmatrix} 1 & 0 & 0 & 0 & 0 & 0 & 0 & 0 & 0 \\ -1 & 1 & 0 & 0 & 0 & 0 & 0 & 0 & 0 \\ -.63755 & -.36245 & 1 & 0 & 0 & 0 & 0 & 0 & 0 \\ 0 & -.84213 & -.15787 & 1 & 0 & 0 & 0 & 0 & 0 \\ 0 & 0 & -.91888 & -.08112 & 1 & 0 & 0 & 0 & 0 \\ 0 & 0 & 0 & -.94969 & -.05031 & 1 & 0 & 0 & 0 \\ 0 & 0 & 0 & 0 & -.96544 & -.03456 & 1 & 0 & 0 \\ 0 & 0 & 0 & 0 & 0 & -.97561 & -.02439 & 1 & 0 \\ 0 & 0 & 0 & 0 & 0 & 0 & -.98125 & -.01875 & 1 \end{pmatrix} = \|t^{Ho}_{E2}\|;$$

$$\begin{pmatrix} 1 & 0 & 0 & 0 & 0 & 0 & 0 & 0 & 0 \\ -1 & 1 & 0 & 0 & 0 & 0 & 0 & 0 & 0 \\ -.69874 & -.30126 & 1 & 0 & 0 & 0 & 0 & 0 & 0 \\ 0 & -.87474 & -.12526 & 1 & 0 & 0 & 0 & 0 & 0 \\ 0 & 0 & -.92879 & -.07121 & 1 & 0 & 0 & 0 & 0 \\ 0 & 0 & 0 & -.95492 & -.04508 & 1 & 0 & 0 & 0 \\ 0 & 0 & 0 & 0 & -.96888 & -.03112 & 1 & 0 & 0 \\ 0 & 0 & 0 & 0 & 0 & -.97704 & -.02296 & 1 & 0 \\ 0 & 0 & 0 & 0 & 0 & 0 & -.98238 & -.01762 & 1 \end{pmatrix} = \|t^{Lu}_{E2}\|.$$

Table A-8

$1/\delta_i^2$: i	Tb $\delta_i^2=.01$	Tb .015	Tb .02	Ho .04	Lu .20
1	100.00	66.67	50.00	25.00	5.000
2	114.04	76.02	57.02	25.62	5.194
3	115.15	76.76	57.57	26.36	5.379
4	125.92	83.95	62.96	27.13	5.577
5	120.67	80.45	70.91	28.05	5.799
6	141.81	94.54	70.91	28.80	6.053
7	122.56	81.71	61.28	29.98	6.348
8	156.76	104.51	78.38	31.02	6.697
9	130.57	86.71	65.03		
10	183.64	122.43	91.82		

Terbium

i	$\frac{1+\alpha_2^{i,i-2}}{1+\alpha_2^{i,i-1}}$	$\mathcal{R}_i^{E2}$	$\frac{1}{1+\mathcal{R}_i^{E2}} = t_{i,i-1}^{E2}$	$1-t_{i,i-1}^{E2} = t_{i,i-2}^{E2}$
0				
1			1.	0.
2	1.940/8.01	2.4988	.28581	.71419
3	1.336/3.62	9.7433	.09308	.90692
4	1.145/2.43	26.431	.03646	.96354
5	1.0901/1.719	49.833	.01967	.98033
6	1.0620/1.567	99.651	.00994	.99006
7	1.0414/1.280	115.33	.00860	.99140
8	1.0316/1.291	238.17	.00418	.99582
9	1.0243/1.132	205.01	.00485	.99515
10	1.0210/1.199	456.57	.00219	.99781

i	$\frac{1+\beta_1^{i,i-1}}{1+\alpha_2^{i,i-1}}$	$m_i \equiv 1 + \frac{1}{\delta_i^2}\frac{1+\beta_1^{i,i-1}}{1+\alpha_2^{i,i-1}}$ $\delta_i^2=.01$	.015	.02
0				
1				
2	5.43/8.01	78.305	52.538	39.652
3	3.13/3.62	100.560	67.373	50.782
4	2.30/2.43	120120	80.457	60.594
5	1.770/1.719	125.25	83.832	63.121
6	1.641/1.567	149.51	95.986	72.241
7	1.369/1.280	132.09	88.390	66.542
8	1.380/1.291	168.57	112.71	84.786
9	1.192/1.132	137.95	92.302	69.476
10	1.271/1.199	195.67	130.72	98.334

Table A-8 (Cont.)

i	Terbium $\frac{1}{\mathcal{R}_i} = \frac{m_i}{\mathcal{R}_i^{E2}}$ $\delta_i^2 = .01$	.015	.02	$1 - t_{i,i-2} = t_{i,i-1}$ .01	.015	.02
0						
1				1.	1.	1.
2	31.337	21.025	15.868	.96908	.95459	.94072
3	10.321	6.9149	5.2120	.91167	.87366	.83902
4	4.5476	3.0440	2.2925	.81974	.75272	.69628
5	2.5134	1.6823	1.2667	.71538	.62179	.55883
6	1.5003	0.96322	0.72494	.60005	.49063	.42027
7	1.1453	0.76640	0.57696	.53386	.43388	.36587
8	0.70778	0.47324	0.35599	.41444	.32122	.26253
9	0.67291	0.45024	0.33890	.40224	.31046	.25312
10	0.42856	0.28631	0.21537	.29999	.22258	.17720

i	$\frac{1}{1+1/\mathcal{R}_i} = t_{i,i-2}$ $\delta_i^2 = .01$	.015	.02
0			
1			
2	.03092	.04541	.05928
3	.08833	.12634	.16098
4	.18026	.24728	.30372
5	.28462	.37281	.44117
6	.39995	.50937	.57973
7	.46614	.56612	.63413
8	.58556	.67878	.73747
9	.59776	.68954	.74688
10	.70001	.77742	.82280

Holmium

i	$\frac{1+\alpha_2^{i,i-2}}{1+\alpha_2^{i,i-1}}$	R_i^{E2}	$\frac{1}{1+R_i^{E2}} = t_{i,i-1}^{E2}$	$1-t_{i,i-1}^{E2} = t_{i,i-2}^{E2}$
1			1.	
2	1.224/2.96	1.7590	.36245	.63755
3	1.124/2.12	5.3342	.15787	.84213
4	1.0790/1.677	11.328	.08112	.91888
5	1.0558/1.459	18.875	.05031	.94969
6	1.0409/1.318	27.938	.03456	.96544
7	1.0315/1.239	40.008	.02439	.97561
8	1.0252/1.186	52.328	.01875	.98125

($\delta_1^2 = .04$)

i	$\frac{1+\beta_1^{i,i-1}}{1+\alpha_2^{i,i-1}}$	$m_i \equiv 1+\frac{1}{\delta_i^2}\frac{1+\beta_1^{i,i-1}}{1+\alpha_2^{i,i-1}}$	$\frac{1}{R_i} = \frac{m_i}{R_i^{E2}}$	$1-t_{i,i-2} = t_{i,i-1}$	$\frac{1}{1+1/R_i} = t_{i,i-2}$
1				1.	
2	2.89/2.96	26.020	14.792	.93668	.06332
3	2.21/2.12	28.480	5.3392	.84225	.15775
4	1.834/1.677	30.674	2.7079	.73031	.26969
5	1.606/1.459	31.876	1.6888	.62809	.37191
6	1.453/1.318	32.744	1.1720	.53960	.46040
7	1.363/1.239	33.986	0.84948	.45931	.54069
8	1.293/1.186	34.816	0.66535	.39953	.60047

Lutetium

i	$\frac{1+\alpha_2^{i,i-2}}{1+\alpha_2^{i,i-1}}$	R_i^{E2}	$\frac{1}{1+R_i^{E2}} = t_{i,i-1}^{E2}$	$1-t_{i,i-1}^{E2} = t_{i,i-2}^{E2}$
1			1.	
2	1.144/2.13	2.3194	.30126	.69874
3	1.0841/1.644	6.6876	.13008	.86992
4	1.0545/1.411	13.043	.07121	.92879
5	1.0391/1.288	21.185	.04508	.95492
6	1.0298/1.210	31.136	.03112	.96888
7	1.0239/1.166	42.554	.02296	.97704
8	1.0200/1.134	55.757	.01762	.98238

($\delta_1^2 = .20$)

i	$\frac{1+\beta_1^{i,i-1}}{1+\alpha_2^{i,i-1}}$	$m_i = \frac{1}{\delta_1^2}\frac{1+\beta_1^{i,i-1}}{1+\alpha_2^{i,i-1}}$	$\frac{1}{R_i} = \frac{m_i}{R_i^{E2}}$	$1-t_{i,i-2} = t_{i,i-1}$	$\frac{1}{1+1/R_i} = t_{i,i-2}$
1				1.	
2	2.62/2.13	7.3883	3.1855	.76108	.23892
3	2.09/1.644	7.8386	1.1721	.53962	.46038
4	1.754/1.411	7.9330	0.60823	.37820	.62180
5	1.534/1.288	7.9067	0.37322	.27178	.72822
6	1.418/1.210	8.0939	0.25995	.20632	.79368
7	1.337/1.166	8.2787	0.19455	.16286	.83714
8	1.281/1.134	8.5652	0.15360	.13315	.86685

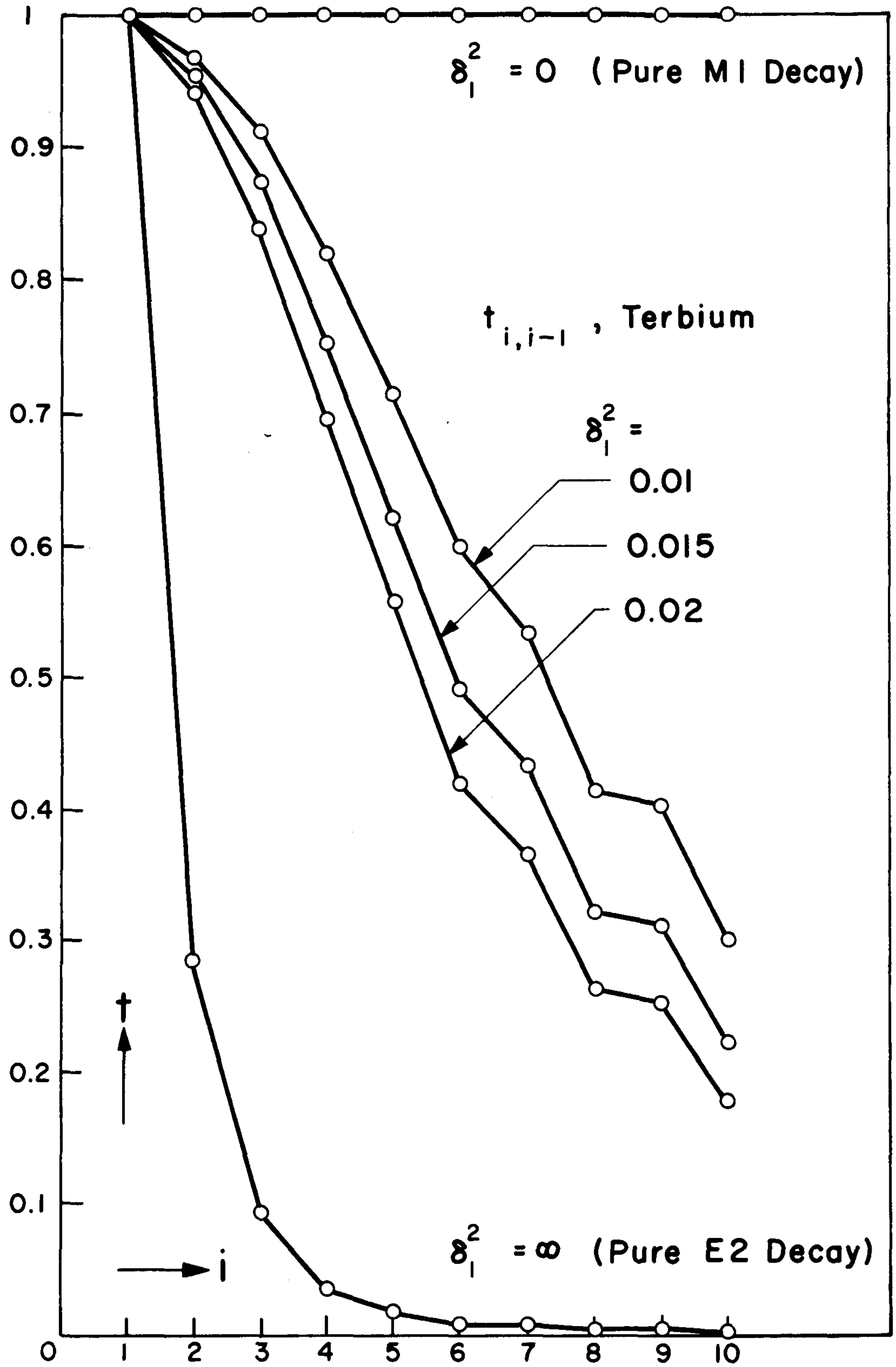

1
0.9
0.8
0.7
0.6
0.5
0.4
0.3
0.2
0.1
0
1
2
3
4
5
6
7
8
9
10
$\delta_1^2 = 0$ (Pure M1 Decay)
$t_{i,i-1}$, Terbium
$\delta_1^2 =$
0.01
0.015
0.02
t
i
$\delta_1^2 = \infty$ (Pure E2 Decay)

FIG A - 4a

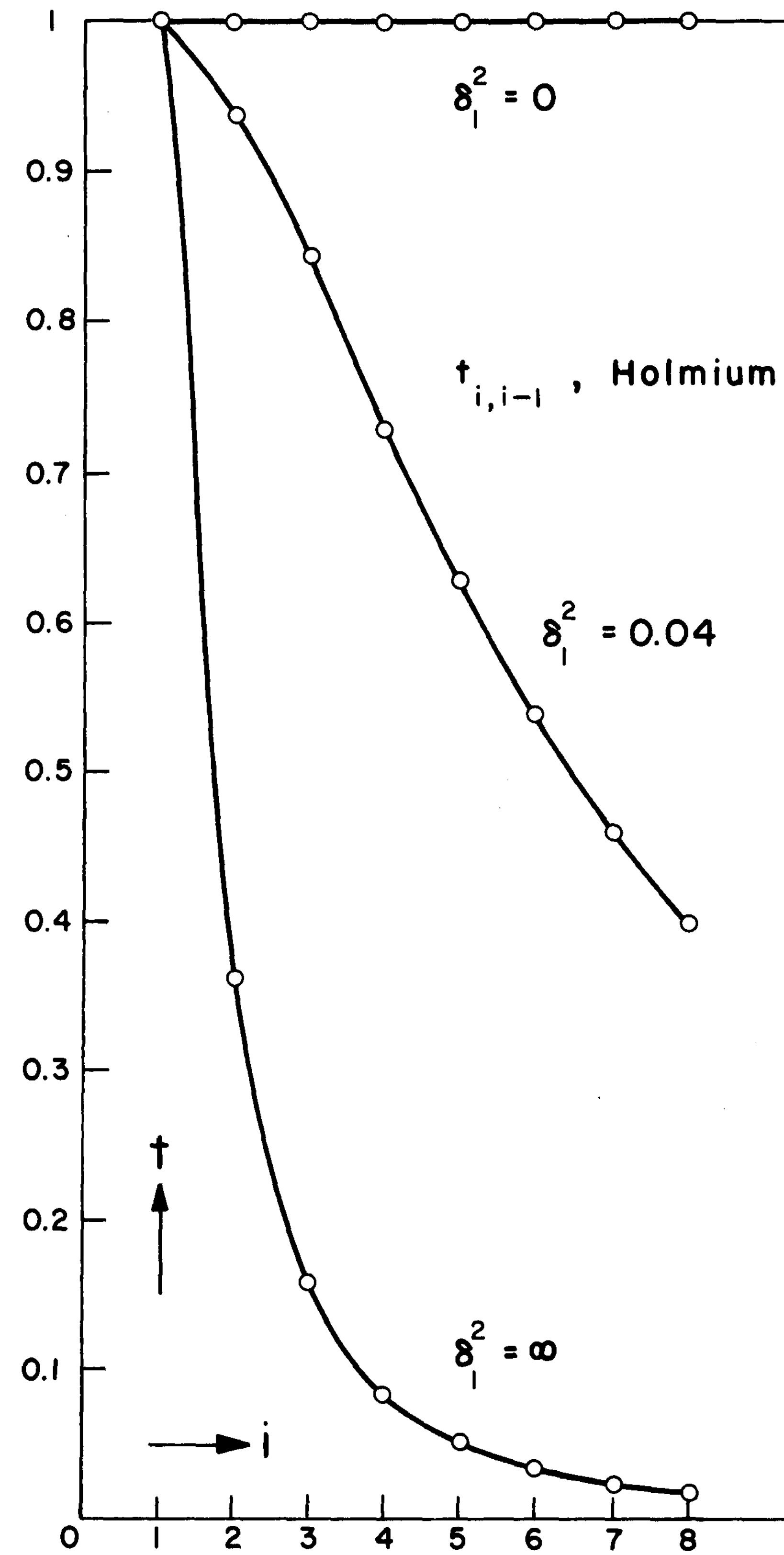

1
0.9
0.8
0.7
0.6
0.5
0.4
0.3
0.2
0.1
0
1
2
3
4
5
6
7
8
$\delta_1^2 = 0$
$t_{i,i-1}$, Holmium
$\delta_1^2 = 0.04$
$\delta_1^2 = \infty$
t
i

FIG A-4b

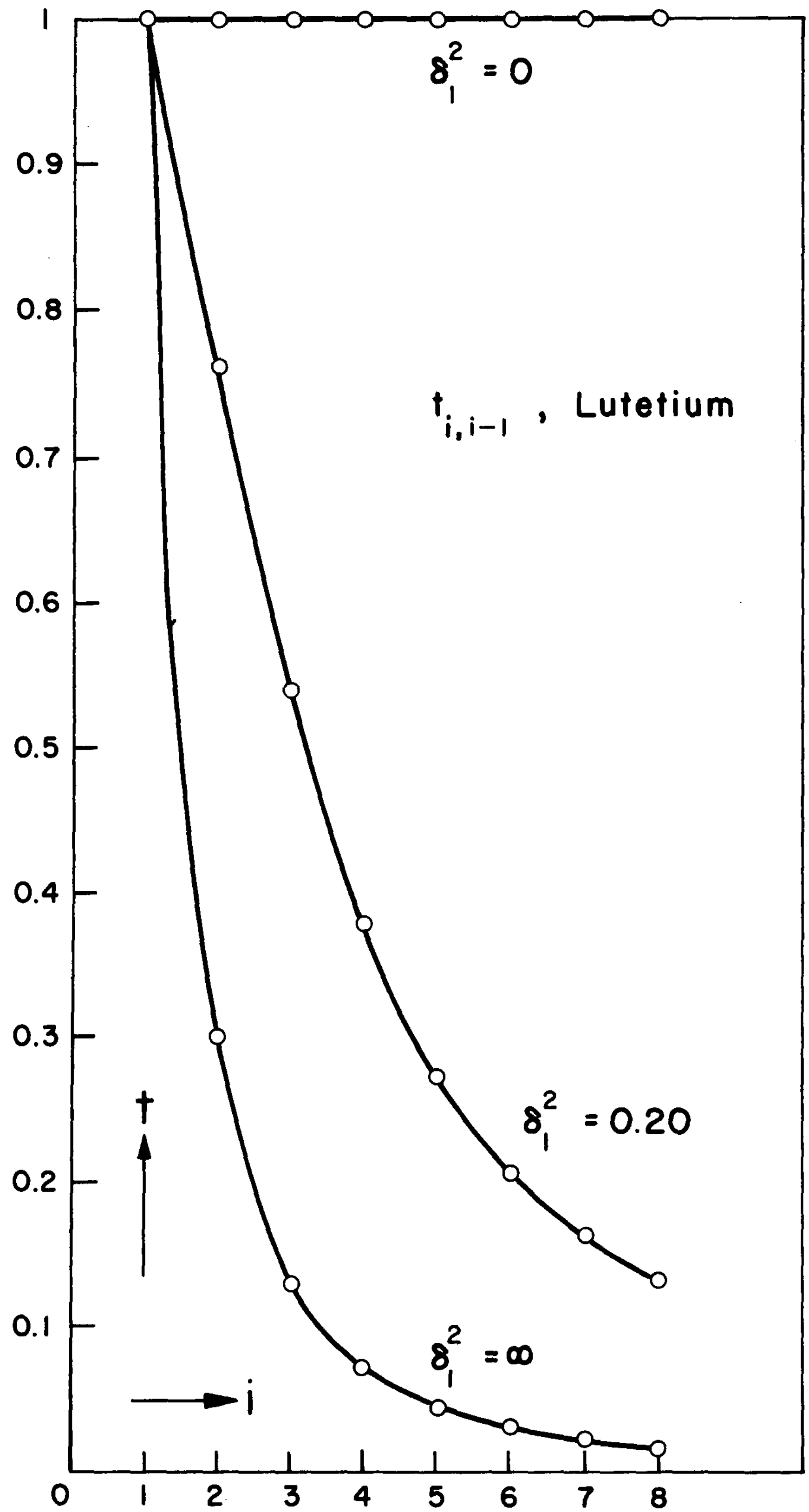

1
0.9
0.8
0.7
0.6
0.5
0.4
0.3
0.2
0.1
0
1
2
3
4
5
6
7
8
$\delta_1^2 = 0$
$t_{i,i-1}$, Lutetium
$\delta_1^2 = 0.20$
$\delta_1^2 = \infty$
t
i

FIG A-4c

Table A-9

Inverted Depopulation Matrices

Terbium, $\delta_1^2 = \infty$:

0	0	0	0	0	0	0	0	0	0
1	0	0	0	0	0	0	0	0	0
.28581	1	0	0	0	0	0	0	0	0
.93352	.09308	1	0	0	0	0	0	0	0
.30942	.96694	.03646	1	0	0	0	0	0	0
.92124	.11027	.98105	.01967	1	0	0	0	0	0
.31550	.95844	.04584	.99026	.00994	1	0	0	0	0
.91603	.11757	.97301	.02802	.99149	.00860	1	0	0	0
.31801	.95492	.04972	.98624	.01404	.99586	.00418	1	0	0
.91314	.12164	.96853	.03267	.98674	.01339	.99517	.00485	1	0
.31931	.95310	.05172	.98414	.01617	.99370	.00635	.99783	.00219	1

Terbium, $\delta_1^2 = 0.01$:

0	0	0	0	0	0	0	0	0	0
1	0	0	0	0	0	0	0	0	0
.96908	1	0	0	0	0	0	0	0	0
.97179	.91167	1	0	0	0	0	0	0	0
.97131	.92759	.81974	1	0	0	0	0	0	0
.97145	.92305	.87105	.71538	1	0	0	0	0	0
.97139	.92486	.85053	.82921	.60005	1	0	0	0	0
.97142	.92402	.86010	.77668	.78648	.53387	1	0	0	0
.97140	.92450	.85449	.80744	.67731	.80682	.41444	1	0	0
.97142	.92421	.85785	.78905	.74257	.64365	.76446	.40224	1	0
.97141	.92442	.85550	.80199	.69688	.75788	.51945	.82068	.29999	1

Terbium, $\delta_1^2 = 0.015$:

0	0	0	0	0	0	0	0	0	0
1	0	0	0	0	0	0	0	0	0
.95459	1	0	0	0	0	0	0	0	0
.96031	.87366	1	0	0	0	0	0	0	0
.95890	.90489	.75272	1	0	0	0	0	0	0
.95426	.88836	.84083	.62179	1	0	0	0	0	0
.95661	.89678	.79596	.81444	.49063	1	0	0	0	0
.95528	.89202	.82136	.70537	.77899	.43388	1	0	0	0
.95618	.89526	.80412	.77940	.58328	.81815	.32122	1	0	0
.95557	.89302	.81601	.72836	.71822	.55318	.78927	.31046	1	0
.95604	.89475	.80676	.76804	.61333	.75916	.42540	.84652	.22258	1

Terbium, $\delta_1^2 = 0.02$:

0	0	0	0	0	0	0	0	0	0
1	0	0	0	0	0	0	0	0	0
.94072	1	0	0	0	0	0	0	0	0
.95026	.83902	1	0	0	0	0	0	0	0
.94735	.88791	.69628	1	0	0	0	0	0	0
.94864	.86635	.83028	.55883	1	0	0	0	0	0
.94788	.87884	.75259	.81459	.42027	1	0	0	0	0
.94836	.87042	.80185	.65241	.78789	.36587	1	0	0	0
.94800	.87676	.76552	.77200	.51678	.83352	.26253	1	0	0
.94826	.87239	.79266	.68267	.71927	.48424	.81333	.25312	1	0
.94805	.87597	.76456	.75627	.55267	.77162	.36014	.86765	.17721	1

Table **A-9** (Cont.)

Holmium, $\delta_1{}^2 = \infty$:

$$\begin{pmatrix} 1 & 0 & 0 & 0 & 0 & 0 & 0 & 0 & 0 \\ 1 & 1 & 0 & 0 & 0 & 0 & 0 & 0 & 0 \\ 1 & .36245 & 1 & 0 & 0 & 0 & 0 & 0 & 0 \\ 1 & .89935 & .15787 & 1 & 0 & 0 & 0 & 0 & 0 \\ 1 & .40601 & .93169 & .08112 & 1 & 0 & 0 & 0 & 0 \\ 1 & .87452 & .19681 & .95377 & .05031 & 1 & 0 & 0 & 0 \\ 1 & .42220 & .90630 & .11115 & .96718 & .03456 & 1 & 0 & 0 \\ 1 & .86349 & .21411 & .93331 & .07267 & .97646 & .02439 & 1 & 0 \\ 1 & .43048 & .89332 & .12656 & .95041 & .05222 & .98171 & .01875 & 1 \end{pmatrix} = \|u\|$$

Holmium, $\delta_1{}^2 = 0.04$:

$$\begin{pmatrix} 1 & 0 & 0 & 0 & 0 & 0 & 0 & 0 & 0 \\ 1 & 1 & 0 & 0 & 0 & 0 & 0 & 0 & 0 \\ 1 & .93668 & 1 & 0 & 0 & 0 & 0 & 0 & 0 \\ 1 & .94667 & .84225 & 1 & 0 & 0 & 0 & 0 & 0 \\ 1 & .94398 & .88479 & .73031 & 1 & 0 & 0 & 0 & 0 \\ 1 & .94498 & .86898 & .83061 & .62809 & 1 & 0 & 0 & 0 \\ 1 & .94452 & .87627 & .78443 & .79932 & .53960 & 1 & 0 & 0 \\ 1 & .94478 & .87232 & .80941 & .70654 & .78853 & .45931 & 1 & 0 \\ 1 & .94462 & .87469 & .79441 & .76225 & .63906 & .78398 & .39953 & 1 \end{pmatrix} = \|u\|$$

Lutetium, $\delta_1{}^2 = \infty$:

$$\begin{pmatrix} 1 & 0 & 0 & 0 & 0 & 0 & 0 & 0 & 0 \\ 1 & 1 & 0 & 0 & 0 & 0 & 0 & 0 & 0 \\ 1 & .30126 & 1 & 0 & 0 & 0 & 0 & 0 & 0 \\ 1 & .90911 & .13008 & 1 & 0 & 0 & 0 & 0 & 0 \\ 1 & .34454 & .93895 & .07121 & 1 & 0 & 0 & 0 & 0 \\ 1 & .88366 & .16650 & .95813 & .04508 & 1 & 0 & 0 & 0 \\ 1 & .36132 & .91403 & .09881 & .97029 & .03112 & 1 & 0 & 0 \\ 1 & .87167 & .18367 & .93840 & .06632 & .97775 & .02296 & 1 & 0 \\ 1 & .37031 & .90116 & .11360 & .95437 & .04780 & .98279 & .01762 & 1 \end{pmatrix} = \|u\|$$

Lutetium, $\delta_1{}^2 = 0.20$:

$$\begin{pmatrix} 1 & 0 & 0 & 0 & 0 & 0 & 0 & 0 & 0 \\ 1 & 1 & 0 & 0 & 0 & 0 & 0 & 0 & 0 \\ 1 & .76108 & 1 & 0 & 0 & 0 & 0 & 0 & 0 \\ 1 & .87107 & .53962 & 1 & 0 & 0 & 0 & 0 & 0 \\ 1 & .80268 & .82588 & .37820 & 1 & 0 & 0 & 0 & 0 \\ 1 & .85249 & .61742 & .83101 & .27178 & 1 & 0 & 0 & 0 \\ 1 & .81295 & .78289 & .47162 & .84976 & .20632 & 1 & 0 & 0 \\ 1 & .84304 & .64438 & .77248 & .36591 & .87074 & .16287 & 1 & 0 \\ 1 & .80092 & .76446 & .51167 & .78534 & .29478 & .88854 & .13315 & 1 \end{pmatrix} = \|u\|$$

Table A-10

Level # i	$10^2 P_i$	$10^2\mathcal{P}_i = 10^2\sum_{k=1}^{10} P_k u_{kI}$, Terbium, Uncorrected: $\delta_I^2 = 0$	0.01	0.015	0.02	∞
1	17.76	56.67	55.59	55.00	54.55	41.02
2	16.09	38.91	37.06	36.34	35.72	25.69
3	11.303	22.82	20.94	20.30	19.81	14.59
4	6.975	11.52	10.418	10.119	9.932	8.550
5	2.666	4.545	3.871	3.703	3.599	3.030
6	1.366	1.879	1.686	1.647	1.631	1.530
7	0.3292	0.5128	0.4140	0.3994	0.3904	0.3519
8	0.1524	0.1836	0.1687	0.1668	0.1659	0.1616
9	0.02208	0.0312	0.0248	0.0241	0.0237	0.0021
10	0.00909	0.0091	0.0091	0.0091	0.0091	0.0091

i	$10^2\mathcal{P}_i = 10^2\sum_{k=1}^{10} P_k u_{ki}$, Terbium, Corrected: $\delta_I^2 = 0$	0.01	0.015	0.02	∞
1	56.67	55.59	55.00	54.55	41.02
2	38.91	37.06	36.34	35.72	25.69
3	22.82	20.94	20.30	19.81	14.59
4	11.52	10.419	10.119	9.933	8.550
5	4.546	3.872	3.704	3.600	3.031
6	1.880	1.687	1.648	1.632	1.530
7	0.5141	0.4150	0.4003	0.3913	0.3529
8	0.1849	0.1694	0.1674	0.1666	0.1619
9	0.0325	0.0257	0.0250	0.0247	0.0231
10	0.0104	0.0096	0.0095	0.0095	0.0094

i	$10^2 P_i$	$10^2\mathcal{P}_i = 10^2\sum_{k=1}^{8} P_k u_{ki}$, Holmium, $Q_0 = 7.5$, Uncorr.: $\delta_I^2 = 0$	0.04	∞
1	23.17	44.90	43.60	34.64
2	12.70	21.73	20.43	16.08
3	5.765	9.029	8.236	6.702
4	2.259	3.264	2.935	2.532
5	0.7094	1.0047	0.8837	0.7703
6	0.2252	0.2593	0.2628	0.2428
7	0.0535	0.0701	0.0601	0.0538
8	0.0166	0.0166	0.0166	0.0166

i	$10^2\mathcal{P}_i = 10^2\sum_{k=1}^{8} P_k u_{ki}$, Holmium, $Q_0 = 7.5$, Corr.: $\delta_I^2 = 0$	0.04	∞
1	44.90	43.60	34.64
2	21.73	20.43	16.08
3	9.033	8.239	6.705
4	3.268	2.938	2.533
5	1.0085	0.8867	0.7741
6	0.2991	0.2648	0.2436
7	0.0739	0.0629	0.0568
8	0.0204	0.0178	0.0173

Level # i	$10^2 P_i$	$10^2 \mathcal{P}_i = 10^2 \sum_{k=1}^{8} P_k u_{ki}$, Holmium, Q_0 8.0, Uncorr. $\delta_1^2 = 0$	0.04	∞
1	25.694	50.58	48.93	39.01
2	13.781	24.89	23.30	18.04
3	6.852	11.110	10.086	8.064
4	2.844	4.258	3.798	3.239
5	0.9792	1.414	1.237	1.0875
6	0.3258	0.4347	0.3841	0.3530
7	0.0833	0.1089	0.0935	0.0838
8	0.0256	0.0256	0.0256	0.0256
i		$10^2 \mathcal{P}_i = 10^2 \sum_{k=1}^{8} P_k u_{ki}$, Holmium, Q_0 8.0, Corr. $\delta_1^2 = 0$	0.04	∞
1		50.59	48.94	39.02
2		24.90	23.31	18.05
3		11.116	10.091	8.069
4		4.264	3.803	3.241
5		1.420	1.242	1.0926
6		0.4411	0.3875	0.3544
7		0.1153	0.0982	0.0889
8		0.0320	0.0278	0.0268
i	$10^2 P_i$	$10^2 \mathcal{P}_i = 10^2 \sum_{k=1}^{8} P_k u_{ki}$, Lutetium, Uncorrected $\delta_1^2 = 0$	0.20	∞
1	27.212	50.54	45.80	38.41
2	14.128	23.33	19.86	17.36
3	5.989	9.203	7.550	6.864
4	2.271	3.214	2.659	2.519
5	0.6748	0.9432	0.7628	0.7281
6	0.2064	0.2684	0.2272	0.2220
7	0.0472	0.0620	0.0492	0.0475
8	0.0148	0.0148	0.0148	0.0148
i		$10^2 \mathcal{P}_i = 10^2 \sum_{k=1}^{8} P_k u_{ki}$, Lutetiom, Corrected $\delta_1^2 = 0$	0.20	∞
1		50.54	45.80	38.41
2		23.33	19.86	17.36
3		9.207	7.552	6.867
4		3.218	2.660	2.520
5		0.9467	0.7653	0.7306
6		0.2719	0.2284	0.2227
7		0.0655	0.0517	0.0482
8		0.0183	0.0152	0.0155

Appendix 4. Gamma-Ray Instrumental Effects

<u>Absorption</u>: In the runs in which the data to be compared with the calculated spectra were acquired the graded X-ray sheilds were for Tb, 0.030 in. Cu; for Ho, 0.030 in. Cu and 0.030 in. Cu, 0.040 in. Sn, 0.009 in. Pb; and for Lu, 0.030 in. Cu, 0.040 in. Sn, 0.009 in. Pb. The targets in these runs were thin discs machined down from slices cut from ingots, and were of thicknesses 0.010 in. for Ho and Lu, 0.018 in. for Tb. The entire thicknesses were active in attenuating the radiation, since the entire path during exciting events penetrated only to a minute distance into the target. This can be seen from the discriminator cutoff depths:

Experiment:	Target dens., gm./cm.^{3}	Cutoff depth mg./cm.^{2}	in.
4.08 $\frac{\text{MeV}}{\text{amu}}$ O^{16} on Tb^{159}	8.253	4.43	2.113×10^{-4}
Ho^{165}	8.799	4.58	2.049×10^{-4}
Lu^{175}	9.849	4.80	1.919×10^{-4}

The chamber contributes 0.040 in. Al and $\sim$1/64 in. $\approx$0.016 in. Teflon (polytetrafluoroethylene), and the crystal cans, 0.032 in. Al and 1/16 in. Al_2O_3 in the overall obsorption. The total absorption is given by

$$I/I_0 = e^{-\sum_i \lambda_i d_i} \qquad \text{(A4-1)}$$

where d_i is the thickness and λ_i the absorption coefficient of the i^{th} absorber. This is a consequence of the exponential absorption in a single absorbing material characterized by the constant λ,

$$I(d)/I_o = e^{-\lambda d} = e^{-\lambda_o \sigma_b d}, \tag{A4-2}$$

$$\lambda = 10^{-24} \mathcal{N} \sigma_b \rho / A, \tag{A4-3}$$

in which σ_b is the atomic cross section (cross section per atom) for photon interactions removing photons from the incident beam, in barns, $\mathcal{N} = 6.0226 \times 10^{23}$ is Avogadro's number, ρ is the absorber density in gm./cm.^{3}, A the atomic weight in amu and d the depth in the absorber in cm. at which the beam intensity is I(d) when the intensity at zero depth is I_o. Since the cross sections depend on incident energy, so do the absorption coefficients. Densities, atomic weights and photon cross sections employed are listed in Table A-11.

The aluminum thickness includes the equivalent Al thickness d'_{Al} from the Al_2O_3 in the crystal cans, as follows: 1/16 in. Al_2O_3, m.w.(2Al)/m.w.(Al_2O_3) $= 53.96/101.96 = 0.52923$; d'_{Al} $(\rho_{eff}(Al)/\rho(Al))(1/16\ in.) = 0.52923\,\rho(Al_2O_3)/\rho(Al) \times (1/16\ in.) = 0.52923 \times 3.5/(2.699 \times 16) = 0.04289$ in. The oxygen thickness includes the oxygen part of the Al_2O_3, which has the effective density $\rho_{eff}(O) = \rho(Al_2O_3)[1-(m.w.(2Al)/m.w.(Al_2O_3))]$ $= 3.5 \times (1-0.52923) = 1.6477$ gm./cm.^{3}, which is used in calculating λ_o for oxygen. The path length through the oxygen of this effective density is increased by 1/3 to allow for the approximate effect of the carbon and the fluorene in the Teflon. Teflon, $(C_2F_4)_n$, has a specific gravity[219] ranging from 2.1 to 2.3; here, I used 2.2. 1/64 in. of Teflon with $\rho = 2.2$ gm./cm.^{3} has the same areal density as 0.0209 in. $= 0.33 \times (1/16)$ in. of material of density equal to the effective

Table A-11

σ_b(Tb, Ho, Lu), barns

E_γ	50 Sn	53 I	65 Tb	67 Ho	71 Lu	74 W	82 Pb	92 U
			Interpolated					
40	3800	4610	8300	9100	10300	2460	3620	5650
50	2070	2560	4800	5280	6280	1340	1970	3080
60	1280	1570	3070	3380	4060	819	1220	1870
80	588	731	1500	1660	2020	2350	571	879
100	326	404	850	948	1160	1330	1880	497
150	118	145	295	327	401	462	660	994
200	6319	76	145	160	197.5	228	324	484
300	32.1	37.0	63.5	69.2	83.0	94.6	130	188
400	22.6	25.3	39.8	43.0	50.0	56.3	75.8	108
500	18.2	20.1	30.0	32.1	36.5	40.1	52.4	73.3
600	15.7	17.3	24.7	26.3	29.6	32.2	41.1	56.3
800	13.0	14.1	19.3	20.3	22.5	24.1	29.8	39.0
000	11.3	12.2	16.2	17.0	18.7	20.0	24.2	30.8
500	9.11	9.76	12.4	12.9	14.2	15.2	18.0	22.1
000	8.07	8.66				13.4	15.9	19.4

edge	E_K=29.2keV	33.2keV	51.99keV*	55.60keV*	63.31keV*	69.5keV	88.0keV	115.6keV
σ_b	1200	1080	---	---	---	559	447	343
	8730	7660	---	---	---	3350	2620	1890

* K edges are below the lowest-energy ground-state band transitions of 58.00 keV, 94.70 keV and 113.81 keV respectively.

Absorber Materials

	Z	At. Wt.	ρ(gm./cm.^{3})
Cu	29	63.54	8.92
Sn	50	118.69	7.28
Pb	82	207.19	11.3
Al	13	26.98	2.70
Tb	65	158.93	8.25
Ho	67	164.94	8.80
Lu	71	174.99	9.85
O	8	16.00	----
Al_2O_3	--	M.W. 101.96	~3.5

oxygen density in Al_2O_3, $\rho = 1.65$ gm./cm.^{3}. Approximating the $_6C$ and $_9F$ photon cross sections by the $_8O$ cross section is then equivalent to adding 33% to the path length in the "equivalent-density" oxygen. The absorption fractions for each absorber component were calculated and combined to yield total absorption factors for the relevant conditions. The total absorption fractions as a function of energy are given in Table A-12.

Efficiency: Total photon detection efficiencies were taken from tables of E. Wolicki[220] The height h refers to the beam-spot-to-crystal-face distance. The efficiencies for a $1\frac{1}{2}$ in. x 2 in. NaI(Tl) crystal as a function of h and, as interpolated from the tables, for the present experimental situations, are shown in Table A-13 and Fig. A-5.

Photopeak fraction and resolution: A series of spectra were obtained with thin gamma-ray sources in the identical geometry to the experiments in order to duplicate the scattering and attenuation effects. The sources were prepared by evaporating drops of solutions of salts containing the radioactive elements on $\frac{1}{4}$-mil Mylar and covering with cellophane tape. This procedure produced sources, each of the order of from one tenth to ten microcuries, about the size of the beam spot and with negligible absorption or backscatter or filling of the valley between the Compton edge and photopeak due to small-angle scattering, of which particularly the latter two are quite noticeable with standard sealed-source casings. These sources were placed in the

Table A-12

Total Absorption Factors

$I(d)/I_o$

E	Case: A	B	C	D
50 keV	.006916*	.01891*	.000001854*#	.00000120*#
60	.04101	.07796	.0002588#	.0003866*#
80	.1960	.2676	.01913#	.01644#
100	.3639	.4330	.03117	.02853
150	.6138	.6524	.2559	.2481
200	.7136	.7355	.4573	.4502
300	.7881	.7988	.6447	.6410
400	.8196	.8266	.7179	.7157
600	.8523	.8570	.7839	.7826
800	.8707	.8745	.8142	.8133
1000	.8838	.8871	.8354	.8346
1500	.9048	.9074	.8643	.8637

A Tb, 0.030 in. Cu abs.

B Ho, 0.030 in. Cu abs.

C Ho, 0.030 in. Cu, 0.040 in. Pb, 0.009 in. Pb abs.

D Lu, 0.030 in. Cu, 0.040 in. Sn, 0.009 in. Pb abs.

* Fictitious extrapolation of rare-earth absorptions from above the rare-earth K-edge.

\# Below the Pb K-edge.

Table A-13

Calculated Efficiencies for $1\frac{1}{2}$ in. by 2 in. NaI(Tl) Crystals[220]

E, keV	h = 0	0.4	0.5	0.75	1.0	1.25	1.5	2.0	3.0	4.0
60	.500	.395	.370	.313	.264	.222	.187	.135	.0763	.0478
80	.500	.392	.367	.309	.259	.217	.183	.132	.0747	.0469
100	.500	.386	.361	.302	.252	.211	.177	.128	.0723	.0456
150	.495	.357	.330	.271	.224	.186	.156	.112	.0645	.0412
200	.464	.314	.228	.234	.192	.159	.133	.0968	.0565	.0367
300	.377	.241	.220	.178	.146	.122	.103	.0753	.0450	.0298
400	.322	.202	.184	.149	.122	.102	.0862	.0637	.0384	.0257
500	.286	.178	.162	.131	.108	.0900	.0762	.0564	.0343	.0231
600	.264	.163	.149	.120	.0990	.0826	.0702	.0520	.0317	.0216
800	.234	.143	.131	.106	.0872	.0730	.0620	.0461	.0282	.0191
1000	.214	.130	.119	.0963	.0794	.0665	.0565	.0421	.0259	.0175
1500	.183	.111	.101	.0817	.0674	.0565	.0481	.0359	.0222	.0151
2000	.167	.100	.0916	.0742	.0613	.0514	.0437	.0327	.0202	.0138
3000	.153	.0913	.0834	.0676	.0558	.0469	.0399	.0299	.0185	.0126

E, keV	h=1.867cm. (A,B)	h=1.986cm. (C,D)
60	.149	.136
80	.146	.133
100	.140	.129
150	.122	.113
200	.106	.0975
300	.0820	.0762
400	.0688	.0642
500	.0608	.0570
600	.0564	.0525
800	.0500	.0468
1000	.0451	.0426
1500	.0387	.0361
2000	.0352	.0330

A,B: Cu absorber

C,D: Cu-Sn-Pb absorber

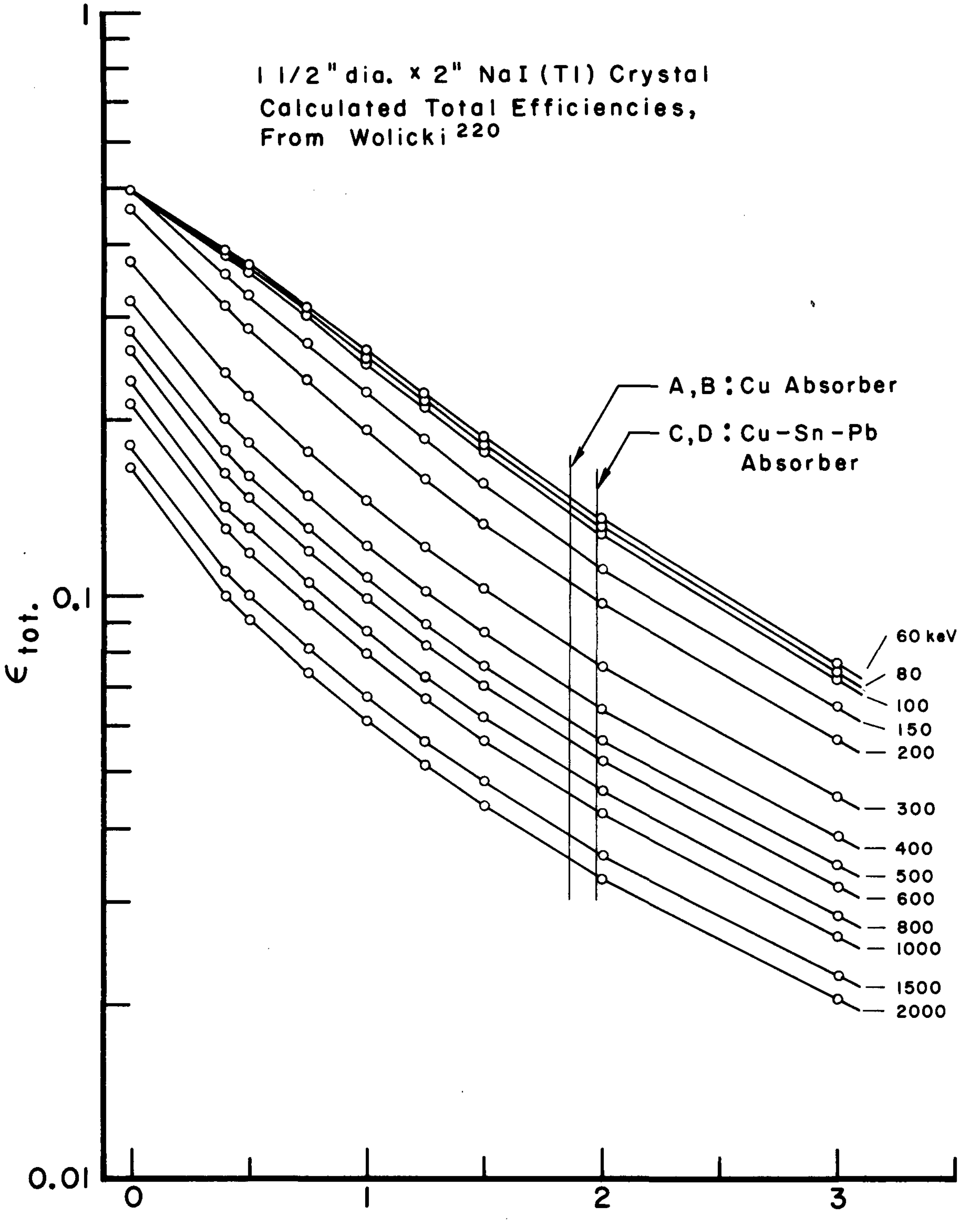
1 1/2" dia. × 2" NaI (Tl) Crystal
Calculated Total Efficiencies,
From Wolicki[220]
A,B : Cu Absorber
C,D : Cu-Sn-Pb Absorber
60 keV
80
100
150
200
300
400
500
600
800
1000
1500
2000
1
0.1
0.01
$\epsilon_{tot.}$
0
1
2
3
h, cm

FIG A-5

target chamber, taped in position right adjascent to the target surface, with the apparatus set up as for a data run. Because of the predetermined geometries, the counting rates and consequent averall system gain shifts were somewhat randomly variable from source to source, making each spectrum generally slightly shifted in gain from the corresponding calibration spectrum. Calibration spectra were run at various counter distances and a fixed counting rate set to approximate the average counting rate during data runs.

The sources employed, and the gamma-ray energies and resolutions obtained from the source spectra are listed in Table A-14. The resolutions are shown in Fig. A-6, on a log-log plot, together with a line corresponding to a $1/\sqrt{E}$ law. That the observed resolution decreases more slowly than expected on the basis of statistical causes is due to the greater variability of depth in the NaI crystal at which the detection events occur for the more penetrating higher-energy gamma rays, with a concomitant greater spread in extinction by the crystal of its own light output, an effect that can be somewhat only by yse of a light pipe between the crystal and the photomultiplier, at some cost in light intensity and consequent deterioration in fast-timing circuit performance.

Values of escape peak-to-photopeak intensity ratios from Wabstra et al.[126] for the iodine X-ray escape peaks which occur at energies $E_{esc} = E_{\gamma} - 28.5$ keV, and of 180^{o} backscatter peak and Compton edge energies[126, 222] given by

Activity[221]	E_γ, keV[221]	Daughter X-ray[126] $\overline{E}_K$, keV	Gamma-Ray Photopeak Pos., Ch. No. n_p	F.w.h.m., Channels Δn	Resolution $\mathcal{R} = \frac{\Delta n}{n_o + 6}$
${}_{25}Mn^{54} \xrightarrow[290d.\epsilon]{} {}_{24}Cr^{54}$	837.7±0.8 (522±20, weak)	Low	198.9	16.5	8.05%
${}_{55}Cs^{137} \xrightarrow[30y.\beta^-]{} {}_{56}Ba^{137}$	661.6±0.1	32.88	159.6	14.55	8.79%
${}_{38}Sr^{85} \xrightarrow[65d.\epsilon]{} {}_{37}Rb^{85}$	513±2	Low	128.0	13.05	9.74%
${}_{11}Na^{22} \xrightarrow[2.6y.\beta^+]{} {}_{10}Ne^{22}$	511.0 annihil. (1274±2)	V. low	120.5	12.25	9.68%
${}_{4}Be^{7} \xrightarrow[53d.\epsilon]{} {}_{3}Li^{7}$	477.3±0.4	V. low	117.9	12.2	9.84%
${}_{50}Sn^{113} \xrightarrow[\epsilon]{} {}_{49}In^{113}$	392.4±0.6 (255.1±0.4)	24.70	94.0	10.65	10.65%
${}_{80}Hg^{203} \xrightarrow[46.5d.\beta^-]{} {}_{81}Tl^{203}$	279.14±0.03	74.62	66.6	8.65	11.91%
${}_{58}Ce^{139} \xrightarrow[140d.\epsilon]{} {}_{57}La^{139}$	166.0±0.5	34.18	36.8	6.0	14.02%
${}_{48}Ce^{144} \xrightarrow[285d.\beta^-]{} {}_{59}Pr^{144} \xrightarrow[17m.\beta^-]{} {}_{60}Nd^{144}$	133.9; (many others)	36.82(Pr) 38.18(Nd)	25.8	5.5	15.94%
${}_{48}Cd^{109} \xrightarrow[470d.\epsilon]{} {}_{47}Ag^{109}$	87.8±0.2 87.8, I-escape	22.60 Esc. = 9.0	16.5 9.0	3.88 4.02	17.23% 27.08%

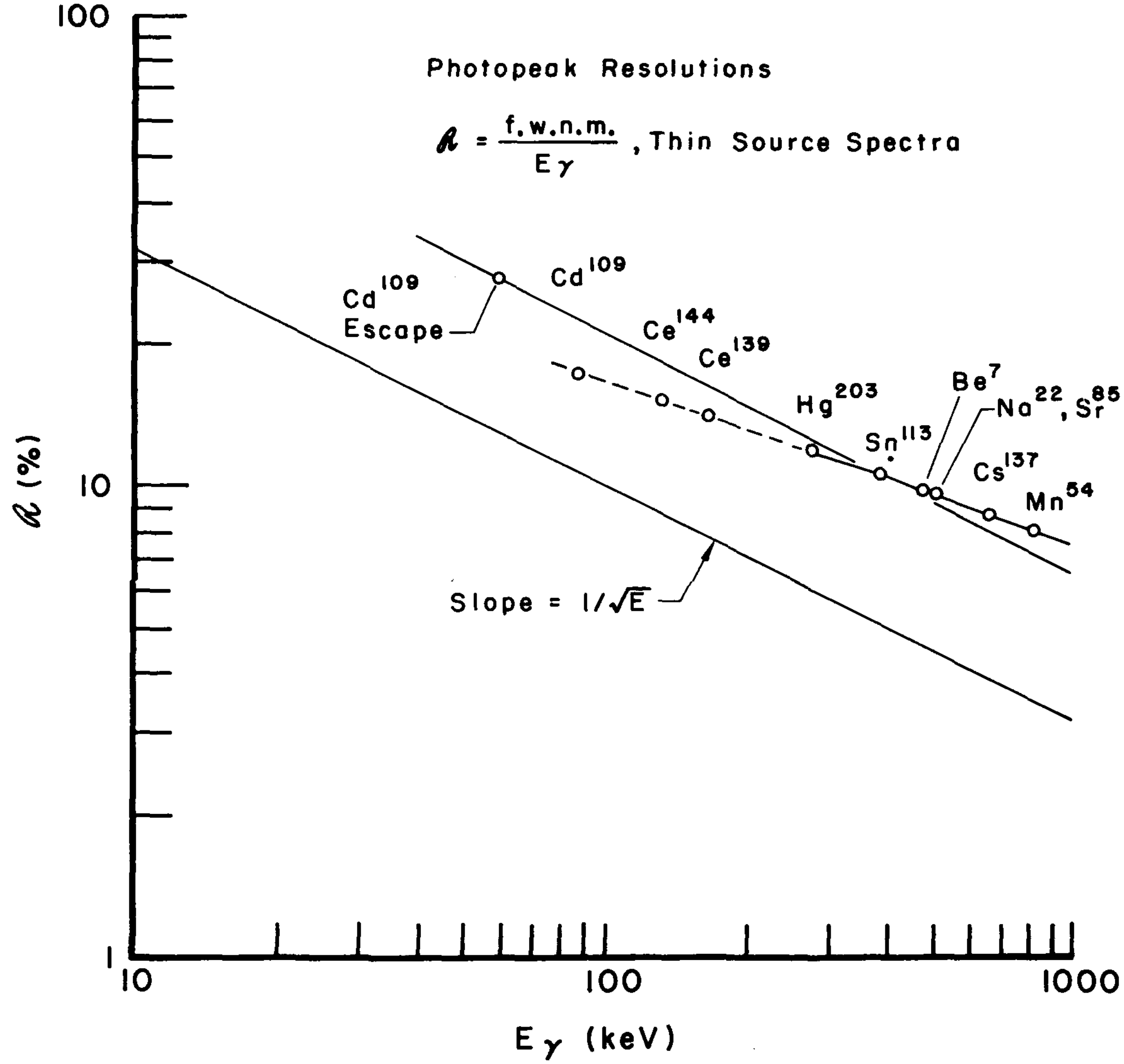
Photopeak Resolutions
$\mathcal{R} = \frac{f.w.n.m.}{E\gamma}$, Thin Source Spectra
100
10
1
$\mathcal{R}$ (%)
Cd^{109} Escape
Cd^{109}
Ce^{144}
Ce^{139}
Hg^{203}
Sn^{113}
Be^{7}
Na^{22}, Sr^{85}
Cs^{137}
Mn^{54}
Slope = $1/\sqrt{E}$
10
100
1000
$E\gamma$ (keV)

FIG A-6

$$\frac{E_\pi}{m_e c^2} = \frac{1}{2+1/\varepsilon}, \quad \frac{E_c}{m_e c^2} = \frac{1}{\varepsilon + 1/2}, \quad E_\pi + E_c = E_\gamma ; \qquad \text{(A4-4)}$$

$$\left(\frac{h\nu'}{h\nu}\right)_{180^\circ} = \frac{1}{1+2\varepsilon}, \quad \left(\frac{T_e}{h\nu}\right)_{180^\circ} = \frac{1}{1+1/2\varepsilon}, \quad h\nu' + T_e = h\nu, \qquad \text{(A4-5)}$$

were employed as guides in interpreting response shapes between the available source energies. Here $\varepsilon = h\nu/m_e c^2$ $E_\gamma/511.0$ keV, and $h\nu'$ and T_e are the scattered-photon and struck-electron energies after a Compton collision in which the photon is scattered through 180°.

The most reliable way to obtain peak-to-total ratios is to observe them experimentally. Contributing to the total response are the photopeak, the Compton distribution, the X-ray escape peak, backscatter radiation from the apparatus (particularly portions of the phototubes and their metal housings and tin-lead shields adjascent to the crystals), and radiation that has been scattered through small angles with slight downward energy shifts when passing through the target, chamber wall, X-ray shields and crystal cans. The significant portion of the total response is that portion caused by "primary" gamma rays directly from the target, which includes all contributions except the backscatter features. The backscatter contributions were graphically subtracted from the standard observed gamma-ray line shapes, and the ratios of photopeak areas to the residual total areas were obtained directly from these plots. Ce^{144} presented extra difficulties due to the presence of the high-energy β^--bremsstrahlung present, and to the presence of other gamma rays, particularly an 80.6-keV gamma ray in the Pr^{144} daughter[221] which has 80- and 134-keV levels populated in the Ce^{144} β^--decay, and some more levels populated in the subsequent gamma deexcitations.

The peak-to-total results are shown in Fig. A-7. The product of the attenuation, efficiency and peak-to-total factors were multiplied by the calculated gamma-ray intensities $I_{ij}^{(\gamma)}$ to yield the theoretical photopeak intensities $I_{pij}^{(\gamma)}$. To construct "photopeak heights" or relative positions of the tops of the calculated photopeaks from their calculated intensities or areas, it was assumed that they were Gaussian, with height h and f.w.h.m. Δ. They are given analytically by

$$\mathcal{f}(E) = he^{-\frac{4\ln 2}{[\mathcal{R}(E_\gamma)]^2}\left(\frac{E-E_\gamma}{E_\gamma}\right)^2} \equiv he^{-\lambda(E-E_\gamma)^2} \qquad \text{(A4-6)}$$

Here $\mathcal{R} = \Delta/E_\gamma$ is the resolution. A curve of this form encloses an area enclosed by the x-axis given by

$$A = h\sqrt{\frac{\pi}{\lambda}} \ . \qquad \text{(A4-7)}$$

Hence,

$$h = \sqrt{\frac{4\ln 2}{\pi\Delta^2}}\, A = \frac{0.93937}{\Delta} A \ . \qquad \text{(A4-8)}$$

A is to be identified with $I_{pij}^{(\gamma)}$. A plot of $f \equiv h/I_{pij}^{(\gamma)} = 0.93937/\Delta$ appears in Fig. A-8. The predicted spectrum profiles were constructed by drawing on a semilog plot the photopeak parabolas of appropriate resolutions and relative heights and affixing thereto the remainders of the standard response shapes, including backscatter peaks. The instrumental correstions were also applied in the photopeak height gamma-ray intensity, as required.

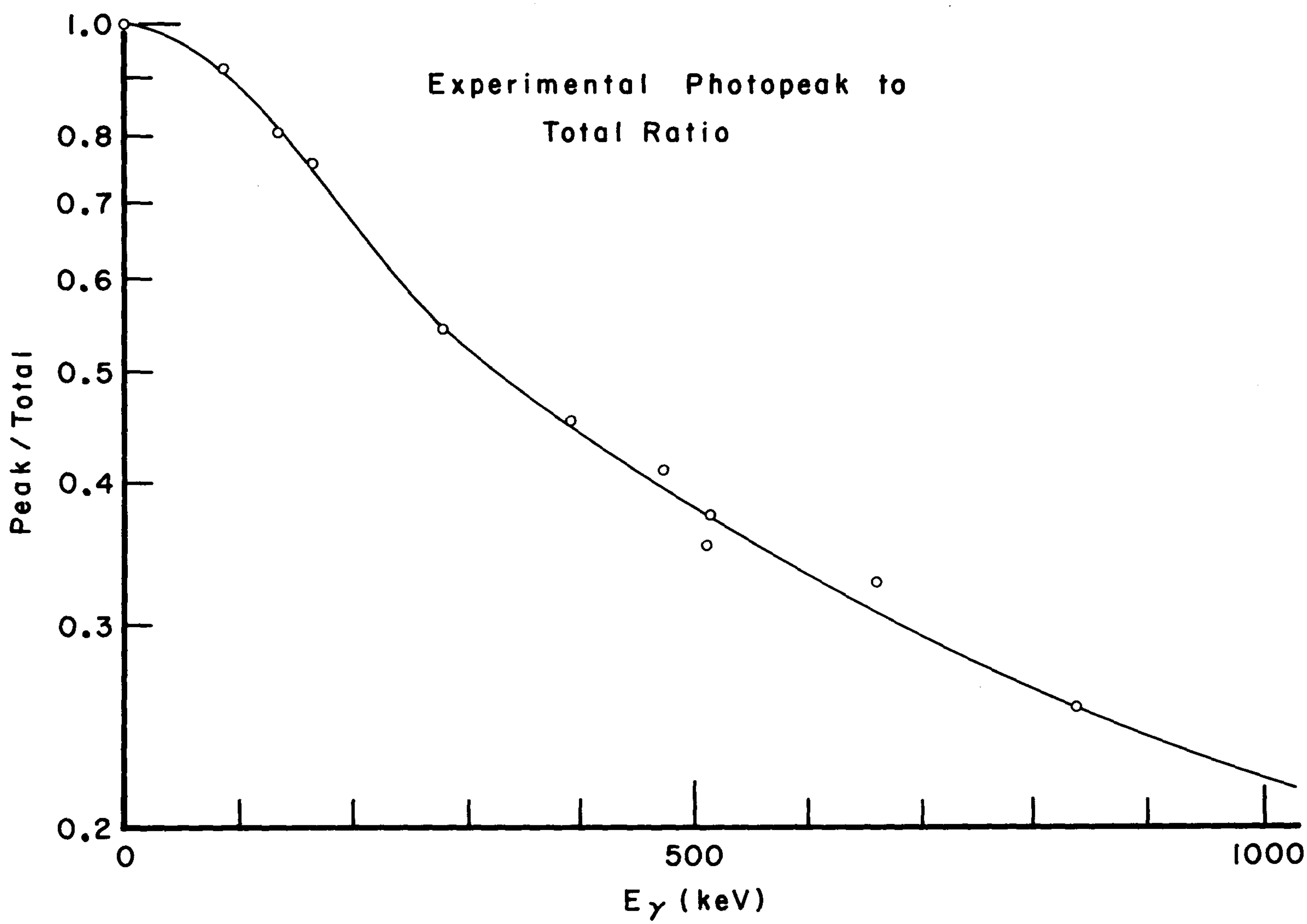

Experimental Photopeak to Total Ratio
1.0
0.8
0.7
0.6
0.5
0.4
0.3
0.2
Peak / Total
0
500
1000
Eγ (keV)

FIG A-7

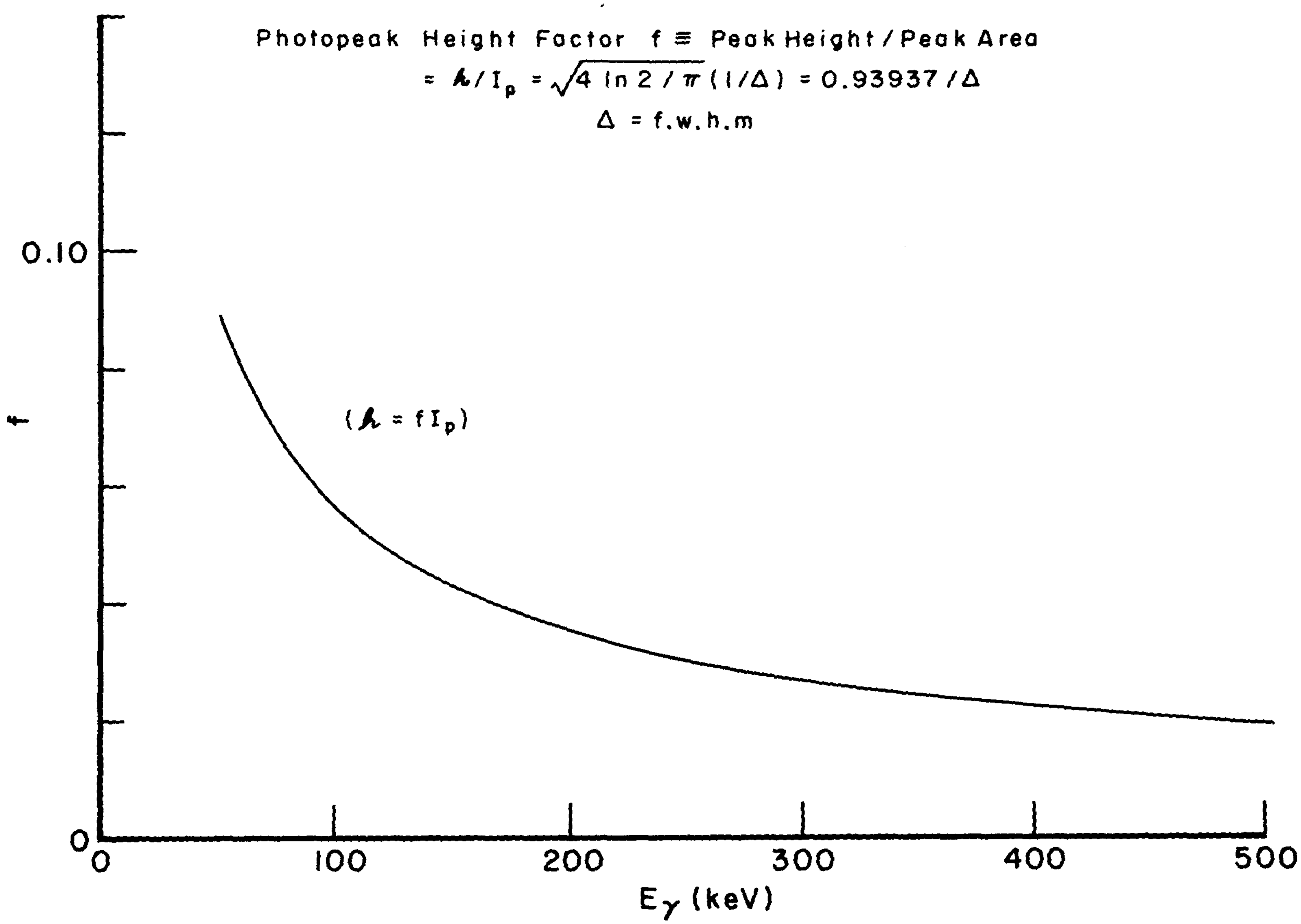
Photopeak Height Factor f ≡ Peak Height / Peak Area
$= h/I_p = \sqrt{4 \ln 2/\pi}\,(1/\Delta) = 0.93937/\Delta$
Δ = f.w.h.m
0.10
f
$(h = fI_p)$
0
0
100
200
300
400
500
E_γ (keV)

FIG A-8

Table A-15

Terbium

ξ	$\sum \frac{d\sigma_{E2}}{d\Omega} \delta\Omega$	$E_{i\,eff}$, $\frac{MeV}{amu}$	$(E_{ieff}-E'_{iev})eB_{sp}$	$\sum \frac{d\sigma_{E2}}{d\Omega}\delta\Omega$ $\frac{barn}{nucl.}$	$E_{i\,eff}$	$(E_{ieff}-E'_{iev})eB_{sp}$	$\sum \frac{d\sigma_{E2}}{d\Omega}\delta\Omega$
		348.1 keV			429 keV		
0	.06280						
.1	.05639	4.594	.02819	.001588	5.282	.03239	.001826
.2	.04489	2.899	.01773	.000796	3.318	.02037	.000914
.3	.03333	2.215	.01352	.000451	2.547	.01552	.000517
.4	.02361	1.831	.01114	.0002633	2.105	.01280	.0003024
.5	.01616	1.579	.009591	.0001549	1.816	.01102	.0001780
.6	.01080	1.399	.008485	.0000917	1.610	.009746	.0001053
.7	.007022	1.264	.007329	.0000515	1.454	.009796	.0000617
.8	.004495	1.158	.006993	.0000314	1.332	.008030	.0000361
		580 keV			617 keV		
0							
.1		6.459	.03959	.002233	6.732	.04126	.002325
.2		4.076	.02490	.001117	4.248	.02594	.001163
.3		3.116	.01897	.000632	3.247	.01976	.000698
.4		2.575	.01564	.0003695	2.684	.01630	.0003848
.5		2.222	.01346	.0002155	2.316	.01402	.0002265
.6		1.970	.01190	.0001287	2.053	.01240	.0001339
.7		1.779	.010736	.0000754	1.855	.01118	.0000785
.8		1.631	.009811	.0000441	1.699	.010216	.0000459
		675 keV			763 keV		
0							
.1		7.148	.04380	.002468	7.758	.04753	.002679
.2		4.511	.02754	.001236	4.896	.02988	.001341
.3		3.448	.02098	.000699	3.736	.02276	.000758
.4		2.851	.01730	.000409	3.094	.01876	.000443
.5		2.461	.01489	.0002405	2.670	.01614	.0002610
.6		2.181	.01317	.0001422	2.368	.01428	.0001542
.7		1.970	.01187	.0000833	2.151	.01287	.0000902
.8		1.804	.010844	.0000487	1.986	.01176	.0000528
		971 keV			979 keV		
0							
.1		9.112	.05581	.003144	9.162	.05610	.00316
.2		5.752	.03507	.001574	5.784	.03526	.001583
.3		4.398	.02672	.000891	4.422	.02686	.000895
.4		3.636	.02202	.000520	3.656	.02214	.000523
.5		3.138	.01894	.0003060	3.156	.01905	.000308
.6		2.783	.01676	.0001819	2.799	.01685	.0001820
.7		2.514	.01510	.0001060	2.529	.01518	.0001066
.8		2.302	.01379	.0000620	2.316	.01387	.0000624

Table A-15 (Cont.)

Terbium (Cont.)

ξ		$E_{ieff}\ \frac{MeV}{amu}$	$(E_{ieff}-E'_{lev})eB_{sp}$	$\sum\frac{d\sigma_{E2}}{d\Omega}\delta\Omega\ \frac{barn}{nucl.}$	E_{ieff}	$(E_{ieff}-E'_{lev})eB_{sp}$	$\sum\frac{d\sigma_{E2}}{d\Omega}\delta\Omega$
		1087 keV			1103 keV		
0							
.1		9.823	.06013	.00339	9.921	.06072	.003424
.2		6.204	.03780	.001697	6.265	.03817	.001712
.3		4.743	.02879	.000959	4.790	.02908	.000969
.4		3.922	.02373	.000560	3.961	.02396	.000556
.5		3.385	.02042	.0003300	3.418	.02061	.0003332
.6		3.002	.01805	.0001950	3.032	.01823	.0001970
.7		2.712	.01627	.0001142	2.739	.01643	.0001153
.8		2.491	.01490	.0000670	2.509	.01501	.0000674

Holmium

	$\sum\frac{df_{E2}}{d\Omega}\delta\Omega$	514.2 keV			566 keV		
0	.06320						
.1	.05673	6.067	.03704	.00339	6.469	.03948	.002240
.2	.04561	3.828	.02326	.001697	4.082	.02483	.001122
.3	.03365	2.926	.01775	.000959	3.119	.01892	.000637
.4	.02378	2.401	.01463	.000560	2.579	.01560	.000371
.5	.01626	2.086	.01260	.0003300	2.225	.01342	.0002184
.6	.01083	1.849	.01114	.0001950	1.972	.01189	.0001289
.7	.007073	1.671	.010043	.0001142	1.782	.010703	.0000757
.8	.004536	1.530	.009180	.0000670	1.632	.009782	.0000443

		638 keV			687 keV		
0							
.1		7.006	.04265	.00242	7.361	.04491	.002547
.2		4.422	.02689	.001215	4.647	.02824	.001276
.3		3.380	.02049	.000689	3.552	.02125	.000724
.4		2.794	.01689	.000402	2.936	.01773	.000422
.5		2.411	.01453	.0002363	2.534	.01527	.000248
.6		2.138	.01286	.0001392	2.246	.01350	.0001463
.7		1.931	.01170	.0000828	2.029	.01217	.0000861
.8		1.768	.010723	.0000485	1.858	.01112	.0000504

		820 keV		
0				
.1		8.285	.05053	.002867
.2		5.230	.03177	.001434
.3		3.998	.02420	.000815
.4		3.305	.01995	.0004745
.5		2.852	.01717	.0002792
.6		2.529	.01518	.0001644
.7		2.285	.01368	.0000967
.8		2.092	.01250	.0000567

Table A-15 (Cont.)

Lutetium

	$\sum \frac{d\sigma_{E2}}{d\Omega}\delta\Omega$	$E_{ieff,amu}\frac{MeV}{}$	$(E_{ieff}-E'_{1ev})cB_{sp}$	$\sum \frac{d\sigma_{E2}}{d\Omega}\delta\Omega \frac{barn}{nucl.}$	E_{ieff}	$(E_{ieff}-E'_{1ev})cB_{sp}$	$\sum \frac{d\sigma_{E2}}{d\Omega}\delta\Omega$
		343.40 keV			432.7 keV		
0	.06374						
1	.05729	4.800	.02854	.001634	5.601	.03328	.001906
2	.04562	3.028	.01795	.000819	3.534	.02093	.000955
3	.03388	2.314	.01368	.000464	2.701	.01596	.000541
4	.02405	1.912	.01128	.0002713	2.232	.01316	.0003165
5	.01643	1.649	.009712	.0001596	1.926	.01132	.0001862
6	.01091	1.462	.008592	.0000937	1.707	.010018	.0001093
7	.007150	1.329	.007797	.0000557	1.541	.009029	.0000645
8	.004589	1.209	.007083	.0000325	1.411	.008252	.0000379
		495 keV			514.4 keV		
0							
1		6.126	.03640	.002085	6.286	.03734	.002140
.2		3.866	.02289	.001045	3.966	.02349	.001072
.3		2.954	.01745	.000592	3.031	.01790	.000607
.4		2.441	.01438	.000346	2.505	.01476	.0003550
.5		2.106	.01238	.0002034	2.161	.01270	.0002088
.6		1.867	.010952	.0001195	1.916	.01124	.0001227
.7		1.687	.009876	.0000706	1.731	.010130	.0000724
.8		1.544	.009025	.0000414	1.584	.009257	.0000424
		646 keV			665 keV		
0							
.1		7.318	.04346	.002488	7.461	.04430	.002538
.2		4.618	.02733	.001246	4.709	.02786	.001272
.3		3.529	.02082	.000707	3.599	.02123	.000720
.4		2.918	.01717	.000413	2.975	.01750	.0004215
.5		2.518	.01478	.0002430	2.566	.01506	.0002467
.6		2.232	.01307	.0001426	2.276	.01333	.0001454
.7		2.016	.01178	.0000841	2.055	.01220	.0000872
.8		1.846	.010773	.0000494	1.882	.010978	.0000504

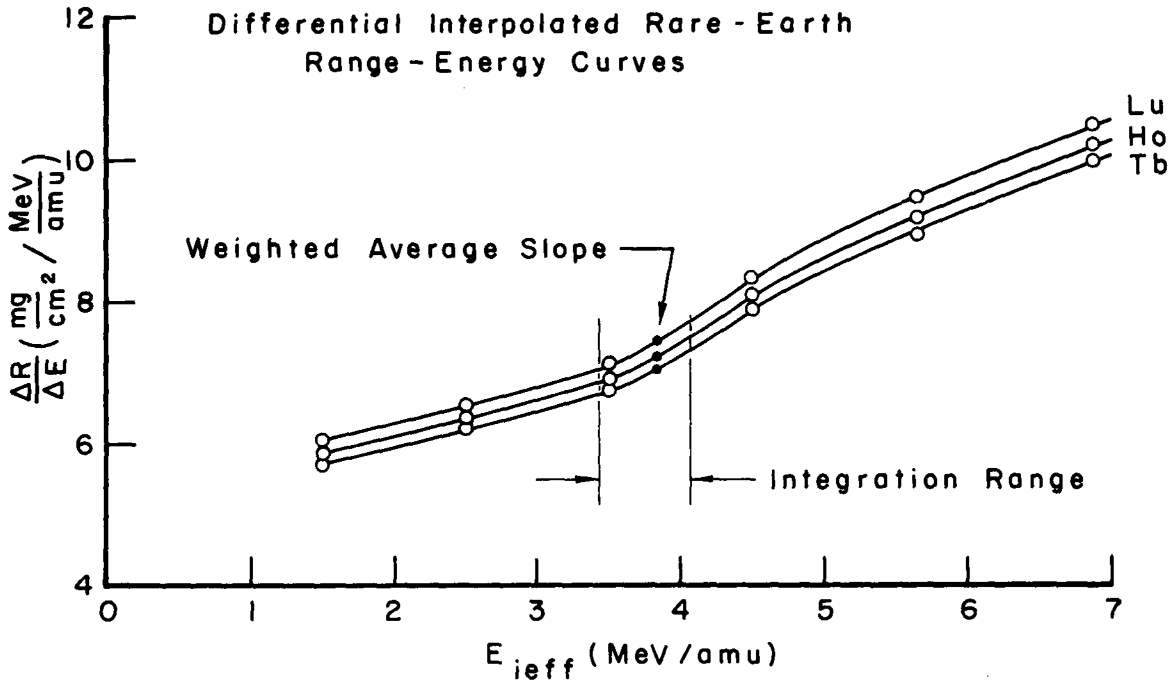

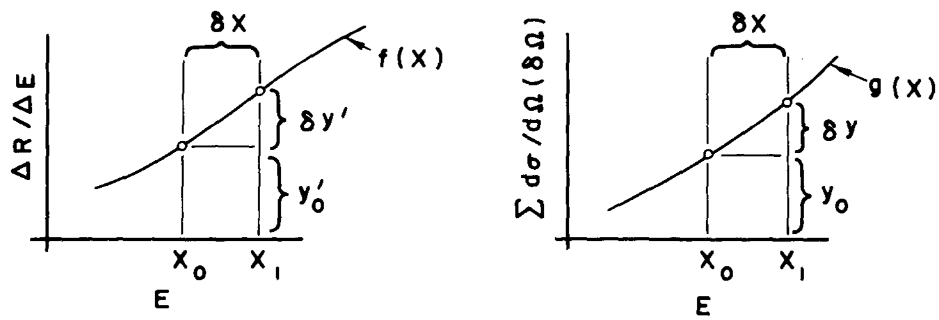

$$\overline{f} \equiv \frac{\int_{X_0}^{X_1} f(X)\,g(X)\,dX}{\int_{X_0}^{X_1} g(X)\,dX} \approx \frac{y_0' y_0 + \frac{1}{2}(y_0 \delta y' + y_0' \delta y) + \frac{1}{3}\delta y' \delta y}{y_0 + \frac{1}{2}\delta y} = -\overline{\frac{d\ell}{dE}}$$

FIG A-9

Table A-16

Computation of Weighted Average Range-Energy Slopes

E_{lev}, keV	y_0 $\frac{barn}{nucl.}$	y_0' $\frac{mg./cm.^2}{MeV/amu}$	y $\frac{barn}{nucl.}$	y' $\frac{mg./cm.^2}{MeV/amu}$	$\mathcal{F}=-\frac{d\bar{\ell}}{dE}$ $\frac{mg./cm.^2}{MeV/amu}$
Tb 348.1	.01068	6.72	.00297	.63	7.048
429	.00975	6.72	.00312	.63	7.049
580	.00792	6.72	.00326	.63	7.053
617	.00752	6.72	.00329	.63	7.054
674	.00693	6.72	.00330	.63	7.057
763	.00610	6.72	.00329	.63	7.057
971	.00432	6.72	.00301	.63	7.062
979	.00424	6.72	.00299	.63	7.062
1087	.00351	6.72	.00282	.63	7.065
1103	.00342	6.72	.00279	.63	7.065
Ho 514.2	.00846	6.86	.00324	.66	7.208
566	.00793	6.86	.00327	.66	7.209
638	.00716	6.86	.00330	.66	7.209
687	.00665	6.86	.00330	.66	7.212
820	.00535	6.86	.00320	.66	7.215
Lu 343.4	.01004	7.07	.00307	.70	7.435
432.7	.00892	7.07	.00319	.70	7.438
514.2	.00792	7.07	.00327	.70	7.440
646	.00660	7.07	.00330	.70	7.443
665	.00633	7.07	.00330	.70	7.444

Table A-17

Gamma-Ray Decay Fractions, 348-keV Band

I_i	I_f	ΔE_{if}, keV	$\chi_{if}^{(\gamma)}$ $\frac{C_E}{C_M} = \infty$	10^4	10^3	10^2	1	0
5/2	3/2	348.1	5.636×10^{-1}	6.150×10^{-1}	6.987×10^{-1}	7.250×10^{-1}	7.285×10^{-1}	7.285×10^{-1}
5/2	5/2	290.1	3.399×10^{-1}	2.902×10^{-1}	2.095×10^{-1}	1.842×10^{-1}	1.808×10^{-1}	1.807×10^{-1}
5/2	7/2	210.6	3.807×10^{-2}	2.979×10^{-2}	1.632×10^{-2}	1.210×10^{-2}	1.153×10^{-2}	1.152×10^{-2}
5/2	9/2	107.1	2.590×10^{-4}	1.782×10^{-4}	4.682×10^{-5}	5.592×10^{-6}	5.714×10^{-8}	0
7/2	3/2	429	8.108×10^{-1}	6.404×10^{-1}	2.384×10^{-1}	3.242×10^{-2}	3.376×10^{-4}	0
7/2	5/2	371	1.634×10^{-2}	1.432×10^{-1}	4.826×10^{-1}	6.504×10^{-1}	6.767×10^{-1}	6.768×10^{-1}
7/2	7/2	291.5	1.253×10^{-1}	1.452×10^{-1}	2.016×10^{-1}	2.291×10^{-1}	2.334×10^{-1}	2.335×10^{-1}
7/2	9/2	188	1.435×10^{-2}	1.413×10^{-2}	1.389×10^{-2}	1.373×10^{-2}	1.370×10^{-2}	1.370×10^{-2}
7/2	11/2	66	2.075×10^{-5}	2.662×10^{-5}	6.102×10^{-6}	8.297×10^{-7}	8.639×10^{-9}	0

Table A-1[illegible]

Predicted Gamma-Ray Intensities, 348.1-keV Band

I_i	I_f	ΔE_{if}, keV	$\frac{C_E}{C_M} = \infty$	10^4	10^3	10^2	1	0
			$I_{if}^{(M)} = P_i \chi_{if}^{(M)}$, barn/nucl-mg./cm.^{2}					
5/2	3/2	348.1	1.325×10^{-3}	1.446×10^{-3}	1.643×10^{-3}	1.704×10^{-3}	1.713×10^{-3}	1.713×10^{-3}
5/2	5/2	290.1	7.990×10^{-4}	6.823×10^{-4}	4.925×10^{-4}	4.330×10^{-4}	4.250×10^{-4}	4.249×10^{-4}
5/2	7/2	210.6	8.950×10^{-5}	7.004×10^{-5}	3.838×10^{-5}	2.844×10^{-5}	2.711×10^{-5}	2.709×10^{-5}
5/2	9/2	107.1	6.089×10^{-7}	4.190×10^{-7}	1.101×10^{-7}	1.315×10^{-8}	1.343×10^{-10}	0
7/2	3/2	429	2.363×10^{-3}	1.893×10^{-3}	6.948×10^{-4}	9.449×10^{-5}	9.838×10^{-7}	0
7/2	5/2	371	4.762×10^{-5}	4.175×10^{-4}	1.407×10^{-3}	1.896×10^{-3}	1.972×10^{-3}	1.973×10^{-3}
7/2	7/2	291.5	3.651×10^{-4}	4.233×10^{-4}	5.877×10^{-4}	6.678×10^{-4}	6.803×10^{-4}	6.805×10^{-4}
7/2	9/2	188	4.181×10^{-5}	4.117×10^{-5}	4.048×10^{-5}	4.001×10^{-5}	3.993×10^{-5}	3.993×10^{-5}
7/1	11/2	66	6.047×10^{-8}	4.844×10^{-8}	1.778×10^{-8}	2.418×10^{-9}	2.518×10^{-11}	0

$P_{348.1\ keV} = 2.351 \times 10^{-3}$ barn/nucl-mg./cm.^{2}

$P_{429\ keV} = 2.914 \times 10^{-3}$ barn/nucl-mg./cm.^{2}

Table A-19

Gamma-Ray Decay Fractions, 580-keV Band

$\chi_{if}^{(\gamma)}$, Pure E2$\downarrow$

I_i	I_f	ΔE_{if}, keV	$\mathcal{R} = 0$	$\mathcal{R} = 1$	$\mathcal{R} = -1$	$\mathcal{R} = \pm i$	$\lvert\mathcal{R}\rvert = \infty$	Pure M1$\downarrow$
1/2	3/2	580	.2937	.9295	.1563	.6215	.8620	.9806
1/2	5/2	522	.6937	.0609	.8307	.3670	.1273	---
3/2	3/2	617	.6780	0	.8649	.5796	.5060	.4616
3/2	5/2	559	.0362	.5863	.1039	.2631	.4324	.5149
3/2	7/2	479.5	.2746	.4001	.0219	.1467	.0512	.9765
5/2	3/2	674	.5671	.4916	.0630	.3896	.2282	.0998
5/2	5/2	616	.2411	.4703	.0602	.3736	.4911	.5222
5/2	7/2	536.5	.0671	.0209	.6037	.1596	.2431	.3594
5/2	9/2	433	.1149	.0090	.2584	.0683	.0260	.3594
7/2	3/2	763	.1752	.0590	.1232	.1111	.0451	---
7/2	5/2	705	.5950	.0596	.5547	.4614	.3239	.1725
7/2	7/2	625.5	.1081	.1456	.3041	.2743	.4452	.5355
7/2	9/2	522	.0622	.5657	.0070	.1123	.1638	.2723
7/2	11/2	400	.0515	.1560	.0040	.0327	.0133	.2723

Predicted Gamma-Ray Intensities, 580-keV Band

I_i	I_f	ΔE_{if}, keV	$I_{if}^{(\gamma)}$, Pure E2↑, Pure E2↓. $\mathcal{R}_{\uparrow,\downarrow} = 0$	$\mathcal{R} = 1$	$\mathcal{R} = -1$	$\mathcal{R} = \pm i$	$\lvert\mathcal{R}\rvert = \infty$
1/2	3/2	580	1.266×10^{-4}	3.607×10^{-3}	6.739×10^{-5}	1.486×10^{-3}	1.487×10^{-3}
1/2	5/2	522	2.991×10^{-4}	2.364×10^{-4}	3.582×10^{-4}	7.911×10^{-4}	2.195×10^{-4}
3/2	3/2	617	1.121×10^{-3}	0	5.461×10^{-3}	1.916×10^{-3}	8.366×10^{-4}
3/2	5/2	559	5.987×10^{-5}	0	6.562×10^{-4}	8.700×10^{-4}	7.150×10^{-4}
3/2	7/2	479.5	4.539×10^{-4}	0	1.382×10^{-4}	4.850×10^{-4}	8.470×10^{-5}
5/2	3/2	674	8.477×10^{-4}	4.593×10^{-3}	1.046×10^{-5}	8.412×10^{-4}	1.516×10^{-4}
5/2	5/2	616	3.604×10^{-4}	4.388×10^{-3}	1.000×10^{-5}	6.065×10^{-4}	3.262×10^{-4}
5/2	7/2	536.5	1.003×10^{-4}	1.957×10^{-4}	1.003×10^{-4}	3.446×10^{-4}	1.615×10^{-4}
5/2	9/2	433	1.718×10^{-4}	8.377×10^{-5}	4.292×10^{-5}	1.475×10^{-4}	1.728×10^{-5}
7/2	3/2	763	6.955×10^{-5}	5.851×10^{-6}	1.100×10^{-4}	5.501×10^{-5}	4.474×10^{-6}
7/2	5/2	705	2.362×10^{-4}	5.911×10^{-6}	4.954×10^{-4}	2.285×10^{-4}	3.214×10^{-5}
7/2	7/2	625.5	4.292×10^{-5}	1.444×10^{-5}	2.716×10^{-4}	1.358×10^{-4}	4.418×10^{-5}
7/2	9/2	522	2.468×10^{-5}	5.614×10^{-5}	6.246×10^{-6}	5.559×10^{-5}	1.626×10^{-5}
7/2	11/2	400	2.045×10^{-5}	1.548×10^{-5}	3.594×10^{-6}	1.617×10^{-5}	1.315×10^{-6}

Predicted Gamma-Ray Intensities, 580-keV Band

$I_{if}^{(\gamma)}$, Pure E2 ↑, Pure M1 ↓.

I_i	I_f	ΔE_{if}, keV	$\mathcal{R}\uparrow = 0$	$\mathcal{R} = 1$	$\mathcal{R} = -1$	$\mathcal{R} = \pm i$	$\lvert\mathcal{R}\rvert = \infty$
1/2	3/2	580	4.227×10^{-4}	3.805×10^{-3}	4.228×10^{-4}	2.114×10^{-3}	1.691×10^{-3}
1/2	5/2	522	0	0	0	0	0
3/2	3/2	617	7.631×10^{-4}	0	2.914×10^{-3}	1.526×10^{-3}	7.631×10^{-4}
3/2	5/2	559	8.512×10^{-4}	0	3.250×10^{-3}	1.702×10^{-3}	8.512×10^{-4}
3/2	7/2	479.5	0	0	0	0	0
5/2	3/2	674	1.491×10^{-4}	9.319×10^{-4}	1.657×10^{-5}	2.154×10^{-4}	6.627×10^{-5}
5/2	5/2	616	7.805×10^{-4}	4.878x10-3	8.673×10^{-5}	1.127×10^{-3}	3.469×10^{-4}
5/2	7/2	536.5	5.371×10^{-4}	3.357×10^{-3}	5.968×10^{-5}	7.759×10^{-4}	2.387×10^{-4}
5/2	9/2	433	0	0	0	0	0
7/2	3/2	763	0	0	0	0	0
7/2	5/2	705	6.847×10^{-5}	1.712×10^{-5}	1.541×10^{-4}	8.542×10^{-5}	1.712×10^{-5}
7/2	7/2	625.5	2.126×10^{-4}	5.314×10^{-5}	4.782×10^{-4}	2.652×10^{-4}	5.314×10^{-5}
7/2	9/2	522	1.081×10^{-4}	2.702×10^{-5}	2.432×10^{-4}	1.348×10^{-4}	2.702×10^{-5}
7/2	11/2	400	0	0	0	0	0

Table A-21

Tb Gamma-Ray Decay Fractions and Intensities, 971-keV Band

ΔE_{if} keV	$t_{if}^{(M)}$ Pure M1↓	$I_{if}^{(\gamma)}$, Pure E2↑, Pure M1↓ $R = 0$	$R = 1$	$R = -1$	$R = \pm i$	$\lvert R\rvert = \infty$
971	.9945	2.603×10^{-4}	2.343×10^{-3}	2.603×10^{-4}	1.302×10^{-3}	1.041×10^{-3}
913	0	0	0	0	0	0
979	.4421	4.561×10^{-4}	0	1.824×10^{-3}	9.121×10^{-4}	4.560×10^{-4}
921.0	.5521	5.696×10^{-4}	0	2.278×10^{-3}	1.139×10^{-3}	5.696×10^{-4}
841.5	0	0	0	0	0	0
1087	.08593	7.305×10^{-5}	2.029×10^{-4}	8.117×10^{-6}	1.055×10^{-4}	3.247×10^{-5}
1029.0	.4998	4.249×10^{-4}	1.180×10^{-3}	4.721×10^{-5}	6.138×10^{-4}	1.889×10^{-4}
949.5	.4091	3.478×10^{-4}	9.660×10^{-4}	3.864×10^{-5}	5.023×10^{-4}	1.546×10^{-4}
846	0	0	0	0	0	0
1103	0	0	0	0	0	0
1045.0	.1488	3.671×10^{-5}	9.178×10^{-6}	8.261×10^{-5}	4.589×10^{-5}	9.178×10^{-6}
965.5	.5216	1.287×10^{-4}	3.217×10^{-5}	2.896×10^{-4}	1.609×10^{-4}	3.217×10^{-5}
862	.3248	8.014×10^{-5}	2.003×10^{-5}	1.803×10^{-4}	1.002×10^{-4}	2.003×10^{-5}
740	0	0	0	0	0	0

Table A-22

Ho Gamma-Ray Decay Fractions and Intensities, 514-keV Band

I_i	I_f	ΔE_{if} keV	$\langle I_i \tfrac{3}{2} 2 2 \| I_f \tfrac{7}{2}\rangle^2 \left(\frac{\Delta E_{if}}{\Delta E_{i_0 f_0}}\right)^5$	$t^{(\gamma)}_{ifE2}$	$I^{(\gamma)}_{if} = P_i t^{(\gamma)}_{ifE2}$
3/2	7/2	514.2	1.000	.9887	2.610×10^{-3}
5/2	7/2	566	4.444×10^{-1}	.5253	7.839×10^{-4}
5/2	9/2	471.3	3.895×10^{-1}	.4604	6.869×10^{-4}
7/2	7/2	638	1.333×10^{-1}	.3274	1.795×10^{-4}
7/2	9/2	543.3	2.171×10^{-1}	.5331	2.922×10^{-4}
7/2	11/2	428	5.188×10^{-2}	.1274	6.982×10^{-5}
9/2	7/2	Est.729.7	2.424×10^{-2}	.1050	1.168×10^{-5}
9/2	9/2	635.0	1.059×10^{-1}	.4587	5.100×10^{-5}
9/2	11/2	519.7	8.612×10^{-2}	.3731	4.189×10^{-5}
9/2	13/2	384.7	1.196×10^{-2}	.7146	5.763×10^{-6}
11/2	7/2	Est.845.1	2.020×10^{-3}	.0158	1.488×10^{-7}
11/2	9/2	750.4	2.745×10^{-2}	.2144	2.022×10^{-6}
11/2	11/2	635.1	6.207×10^{-2}	.4847	4.572×10^{-6}
11/2	13/2	500.1	3.248×10^{-2}	.2536	2.393×10^{-6}
11/2	15/2	345.1	2.745×10^{-3}	.02144	2.022×10^{-7}

Table A-23

Ho Gamma-Ray Decay Fractions and Intensities, 687-keV Band

I_i	I_f	ΔE_{if} keV	$t^{(\gamma)}_{ifE2}$	$I^{(\gamma)}_{if} = P_i t^{(\gamma)}_{ifE2}$
11/2	7/2	687	.8275	3.206×10^{-3}
11/2	9/2	592.3	.1516	5.873×10^{-4}
11/2	11/2	477	.01321	5.116×10^{-5}
11/2	13/2	342	.0003892	1.508×10^{-6}
11/2	15/2	187	.000001359	5.264×10^{-9}
13/2	7/2	(820)	0	0
13/2	9/2	725.3	.7443	7.443×10^{-1}
13/2	11/2	610	.2227	2.227×10^{-1}
13/2	13/2	475	.02301	2.301×10^{-2}
13/2	15/2	320	.0006246	6.246×10^{-4}
13/2	17/2	149	.000001157	1.157×10^{-6}

Table A-24

Predicted Decay Fractions and Gamma-Ray Intensities, 343-keV Band

			$x_{if}^{(\gamma)}$				$I_{if}^{(\gamma)}=P_i x_{if}^{(\gamma)}$			
I_i	I_f	ΔE_{if}	$\delta^2(343.4)=\infty$	0.25	0.1	0	$\delta^2(343.4)=\infty$	0.25	0.1	0
5/2	7/2	343.4	.8537	.9187	.9231	.9285	2.016×10^{-2}	2.170×10^{-2}	2.180×10^{-2}	2.193×10^{-2}
5/2	9/2	229.6	.09123	.01197	.005199	0	2.155×10^{-3}	2.828×10^{-4}	1.228×10^{-4}	0
7/2	7/2	432.8	.9113	.5109	.4456	.3888	1.880×10^{-2}	1.054×10^{-2}	9.194×10^{-3}	8.022×10^{-3}
7/2	9/2	319.0	.04504	.4280	.4905	.5448	9.292×10^{-4}	8.831×10^{-3}	1.012×10^{-2}	1.124×10^{-2}
7/1	11/2	181.3	.01497	.003498	.001627	0	3.088×10^{-4}	7.216×10^{-5}	3.357×10^{-5}	0
9/2	7/2	546.7	.5179	.2233	.1483	.07286	3.712×10^{-3}	1.600×10^{-3}	1.063×10^{-3}	5.222×10^{-4}
9/2	9/2	432.9	.4606	.5040	.5150	.5262	3.301×10^{-3}	3.612×10^{-3}	3.691×10^{-3}	3.771×10^{-3}
9/2	11/2	295.2	.001046	.2241	.2809	.3380	7.494×10^{-6}	1.606×10^{-3}	2.013×10^{-3}	2.423×10^{-3}
9/2	13/2	134.6	.001855	.0006270	.0003146	0	1.329×10^{-5}	4.494×10^{-6}	2.255×10^{-6}	0
11/2	7/2	684.5	.1250	.05772	.03179	0	1.146×10^{-5}	5.290×10^{-6}	2.913×10^{-6}	0
11/2	9/2	570.7	.6405	.3905	.2946	.1756	5.870×10^{-5}	3.578×10^{-5}	2.700×10^{-5}	1.613×10^{-5}
11/2	11/2	433.1	.2207	.3825	.4445	.5213	2.022×10^{-5}	3.513×10^{-5}	4.074×10^{-5}	4.777×10^{-5}
11/2	13/2	272.4	.0002701	.1309	.1810	.2429	2.475×10^{-8}	1.197×10^{-5}	1.658×10^{-5}	2.226×10^{-5}
11/2	15/2	89.9	.0001459	.00006737	.00003727	0	1.337×10^{-8}	6.173×10^{-9}	2.301×10^{-9}	0

Table A-25

Lu Gamma-Ray Decay Fractions and Intensities, 486-keV Band

I_i	I_f	ΔE_{if}, keV	$\chi_{if}^{(\gamma)}$	$I_{if}^{(\gamma)} = P_i \chi_{if}^{(\gamma)}$
11/2	7/2	486 2	8.893×10^{-1}	4.300×10^{-3}
11/2	9/2	372.2	9.011×10^{-2}	4.357×10^{-4}
11/2	11/2	234.5	2.300×10^{-3}	1.112×10^{-5}
11/2	13/2	73.9	1.112×10^{-6}	5.377×10^{-4}
11/2	15/2	Neg.	0	0

X. References

1. K. Alder et al., Rev. Mod. Phys. 28, 432 (1956).
2. J. M. Blatt and V. F. Weisskopf, Theoretical Nuclear Physics (John Wiley & Sons, Inc., New York, 1952).
3. K. Alder and A. Winther, Kgl. Danske Videnskab. Selskab Mat. Fys. Medd. 32, No. 8 (1960).
4. M.E. Rose, Elementary Theory of Angular Momentum (John Wiley & Sons, Inc., New York, 1957).
5. A. R. Edmonds, Angular Momentum in Quantum Mechanics (Princeton University Press, New Jersey, 1957).
6. A Bohr, Kgl. Danske Videnskab. Selskab Mat. Fys. Medd. 26, No. 14 (1952).
7. R. K. Osborn and E. D. Klema, Phys. Rev. 100, 822 (1955).
8. A. Bohr and B. Mottelson, Kgl. Danske Videnskab. Selskab Mat. Fys. Medd. 27, No. 18 (1955).
9. S. G. Nilsson, Kgl. Danske Videnskab. Selskab Mat. Fys. Medd. 29, No. 16 (1955).
10. K. Gottfried, Phys. Rev. 103, 1017 (1956).
11. T. D. Newton, Can. J. Phys. 38, 700 (1960).
12. R. H. Lemmer, Phys. Rev. 117, 1551 (1960).
13. J. P. Davidson and J. Chi, Electromagnetic Lifetimes and Properties of Nuclear States, N.A.S. - N.R.C. 974 (L962).
14. A. Kerman, Kgl. Danske Videnskab. Selskab Mat. Fys. Medd. . 30, No. 15 (1956).
15. D. Inglis, Phys. Rev. 97, 701 (1955).
16. A. Bohr and B. Mottelson, Kgl. Videnskab. Selskab Mat. Fys. Medd. 30, No.1 (1955).
17. D. Inglis, Phys. Rev. 96, 1059 (1954).
18. S. Belyaev, Kgl. Danske Videnskab. Selskab Mat. Fys. Medd. 31, No. 11 (1959).
19. M. Baranger, Phys. Rev. 120, 957 (1960).

20. A. Kerman, Ann. Phys. 12, 300 (1961).

21. J. P. Elliott, Proc. Roy. Soc. (London), A245, 128 (1958).

22. G. Alaga, K. Alder, A. Bohr, and B. Mottelson, Kgl. Danske Videnskab. Selskab Mat. Fys. Medd. 29, No. 9 (1955).

23. A. Bohr and B. Mottelson, "On the Theory of Rotational Spectra"

24. B. Mottelson and S. G. Nilsson, Kgl. Danske Videnskab. Selskab Mat. Fys. Skr. 1, No. 8 (1959).

25. U. Hauser, Electromagnetic Lifetimes and Properties of Nuclear States, N.A.S. - N.R.C. 974 (1962).

26. F. Villers, Ann. Rev. Nucl. Science 7, 185 (1957).

27. D. Hill and J. A. Wheeler, Phys. Rev. 89, 1102 (1955).

28. J. A. Wheeler and J. J. Griffin, Phys. Rev. 108, 311 (1957).

29. J. Yoccoz, Proc. Phys. Soc. (London) A70, 308 (1957).

30. R. F. Peierls and J. Yoccoz, Proc. Phys. Soc. (London) A70, 381 (1957).

31. F. Villers, Nucl. Phys. 3, 240 (1957).

32. M. A. Preston, Physics of the Nucleus (Addison-Wesley Publ. Co., Inc., Mass., 1962) ch. 10.

33. D. Brink, progr. in Nucl. Phys. 8, 97 (1961).

34. A. Bohr and B. Mottelson, Beta and Gamma Ray Spectroscopy, K. Siegbahn, ed., (North Holland Publ. Co., Amsterdam, 1955).

35. R. Diamond, B. Elbek, and F. Stephens, Nucl. Phys. 43, 560 (1963).

36. M. Pool and L. Quill, Phys. Rev. 53, 437 (1938).

37. Krisberg, Pool, and Hibdon, Phys. Rev. 74, 44 (1948).

38. B. H. Ketelle, Brookhaven Natl. Lab. Rept. No. BNL C-9, 109 (1949).

39. F. D. S. Butement, Phys. Rev. 75, 1276 (1949).

40. F. D. S. Butement, Proc. Phys. Soc. (London) A63, 532 (1950).

41. W. C. Jordan, J. M. Cork, and S. B. Burson, Phys. Rev. 92, 315 (1953).

42. W. H. Sullivan, Trilinear Chart of Nuclides, (U.S. Atomic Energy Commission, Washington, D.C., 1956).

43. N. Marty, Comp. Rend. 241, 385 (1955).

44. R. Barloutaud and R. Ballini, Comp. Rend. 241, 389 (1955).

45. R. Ballini and R. Barloutaud, J. Phys. Rad. 17, 534 (1956).

46. J. Quidort, quoted by R. Ballini and Barloutaud, J.Phys. Rad. 17, 534 (1956).

47. K. O. Nielsen, O. B. Nielsen, and O. Skilbreid, Nucl. Phys. 7, 561 (1958).

48. L.A. Sliv and I.M. Band, Tables of Internal Conversion Coefficients of Gamma Rays, I and II (Akad. Nauk SSSR, Leningrad, 1956 and 1958; translation by U. of Ill. Phys. Dept., 57 ICC-K1, 58 ICC-1, (unpubl.).

49. S. S. Malik, N. Nath, and C. E. Mandeville, Phys. Rev. 112, 262 (1958).

50. M. E. Rose, Internal Conversion Coefficients (North Holland Publ. Co., Amsterdam, 1958).

51. F. R. Metzger and W. B. Todd, Nucl. Phys. 13, 177 (1959).

52. S. Gorodetzky, R. Manquenouille, R. Richert, and A. Knipper, J. Phys. Rad. 22, 699 (1961).

53. S. Gorodetzky, R. Manquenouille, R. Richert, and A. Knipper, Electromagnetic Lifetimesand Properties of Nuclear States, N.A.S. - N.R.C. 974 (1962).

54. R. Manquenouille, Ann. de Phys. 6, 1122 (1961).

55. G. A. Vartapetyan, Z. A. Petrosyan, and A. G. Khudaverdyan, Sov. Phys. J.E.T.P. 14, 1213 (1962).

56. B. N. Subba-Rao, Nucl. Phys. 36, 342 (1962).

57. R. W. Sharp and W.W. Beuchner, Phys. Rev. 109, 1698 (1958).

58. A. Y. Cabezas et al., Phys. Rev. 122, 1796 (1961).

59. K. Takahashi, J. Phys. Soc. (Japan)17, 1229 (1962).

60. I.M. Govil and C.S. Khurana, Nucl. Phys. 49, 29 (1963).

61. B. H. Ketelle, Phys. Rev. 76, 1256 (1949).

62. F.D.S. Butement, Proc. Phys. Soc. (London) A64, 395 (1951).

63. F.D.S. Butement, Proc. Phys. Soc. (London) A64, 428 (1951).

64. J. W. Mihelich, B. Harmatz, and T. Handley, Phys. Rev. 108, 989 (1957).

65. B. Harmatz, T. H. Handley, and J. W. Mihelich, Phys. Rev. 114, 1082 (1959).

66. B. H. Ketelle and A. R. Brossi, Phys. Rev. 116, 98 (1959).

67. R. C. Greenwood and E. Brannen, Phys. Rev. 120, 1411 (1960).

68. G. Alaga, Phys. Rev. 100, 432 (1955).

69. E. E. Berlovich, M. P. Bonitz, and M. K. Nikitin, Sov. Phys. J.E.T.P. 13, 525 (1961).

70. E. E. Berlovich, Electromagnetic Lifetimes and Properties of Nuclear States, N.A.S. - N.R.C. 974 (1962).

71. J. M. Baker and B. Bleaney, Proc. Phys. Soc. (London) A68, 257 (1955).

72. T. Huus, J. Bjerregaard, and B. Elbek, Kgl. Danske Videnskab. Selsakb Mat. Fys. Medd. 30, No. 17 (1956).

73. M. Martin, P. Marmier, and J. de Boer, Helv. Phys. Acta 31, 435 (1958).

74. I. Lindgren, Nucl. Phys. 32, 151 (1962).

75. J. M. Baker and B. Bleaney, Proc. Roy. Soc. (London) A254, 156 (1958).

76. H. Ryde, L. Persson, and K. Oelsner-Ryde, Arkiv Fys. 23, 195 (1963).

77. L. Persson, to be publ.

78. F. W. Aston, Proc. Roy. Soc. (London) A146, 46 ( ).

79. T. L. Collins, F. M. Rourke, and F. A. White, Phys. Rev. 105, 196 (1957).

80. H. Mark and G.T. Paulissen, Phys. Rev. 100, 813 (1955).

81. N. P. Heydenburg and G. M. Temmer, Phys. Rev. 100, 150 (1955).

82. N. P. Heydenburg and G. M. Temmer, Phys. Rev. 104, 981 (1956).

83. E. L. Chupp, J. W. M. DuMond, F. J. Gordon, R. C. Jopson, and H. Mark, Phys. Rev. 112, 518 (1958).

84. O. Nathan and V. I. Popov, Nucl. Phys. 21, 631 (1960).

85. M. C. Olesen and B. Elbek, Nucl. Phys. 15, 134 (1960).

86. H. Schüler and T. Schmidt, Naturwiss. 22, 730 (1934).

87. C. A. Hutchison, Jr. and E. Wong, J. Chem. Phys. 29, 754 (1958).

88. E. G. Fuller and M. S. Weiss, Phys. Rev. 112, 560 (1958).

89. R. T. Birge, Rev. Mod. Phys. Suppl. 1, 1 (1929).

90. R. A. Lyttleton, The Stability of Rotating Liquid Masses, (Cambridge Univ. Press, London, 1953).

91. E. M. Bernstein, Electromagnetic Lifetimes and Properties of Nuclear States, N.A.S. - N.R.C. 974 (1962).

92. J. de Boer, G. Goldring, and H. Winkler, Proc. Third Conf. on Reactions between Complex Nuclei, Asilomar, Calif., Apr., 1963, A. Ghiorso et al., ed. (Univ. of Calif. Press, 1963).

93. R. H. Lemmer and A.E.S. Green, Phys. Rev. 119, 1043 (1960).

94. J. Marsh and S. Sugden, Nature 136, 102 (1935).

95. G. Hevesy and H. Levi, Nature 136, 103 (1935); Kgl. Danske Videnskab. Selskab Mat. Fys. Medd. 14, No. 5 (1936); Nature 137, 185 (1936).

96. H. Slätis, Arkiv Mat. Astron. Fys. A33, No. 17 (1947).

97. W. Bothe, Z. Naturforsch. 1, 179 (1946).

98. R. Sher, H. Kouts, and K. Downes, Phys. Rev. 87, 523 (1952).

99. B. Dzelepov and A. Konstantini, Compt. Rend. U.S.S.R. 30, 701 (1941).

100. S. Eklund, Arkiv Mat. Astron. Fys. A28, No. 3 (1941).

101. A. F. Clark, Phys. Rev. 61, 203, 242 (1942).

102. A. Flammersfeld, Naturwiss. 32, 68 (1944); Z. Naturforsch. 1, 190 (1946).

103. M. Inghram, R. Hayden, and D. Hess, Phys. Rev. 71, 270 (1947).

104. M. Inghram, A. Shaw, D. Hess, and R. Hayden, Phys. Rev. 72, 515 (1947).

105. N. Hole, Arkiv Mat. Astron. Fys. A36, No. 2 (1948).

106. R. Caldwell, Phys. Rev. 78, 407 (1950).

107. W. Wright and M. Deutsch, Phys. Rev. 82, 277 (1951).

108. J. Kahn, ORNL - 1089, 1951 (unpubl.)

109. J. Mihelich and E. Church, Phys. Rev. 85, 690 (1952).

110. W. C. Jordan, J. M. Cork, and S. B. Burson, Phys. Rev. 92, 1218 (1953).

111. G. Weber, Z. Naturforsch. 9A, 115 (1954).

112. E. Rodriguez-Mayquez, Anales Real Soc. Espan. Fis y Quim., Ser. A 50, 95 (1954).

113. L. Grenags and A.Meessen, J. Phys. Rad. 20, 61 (1959).

114. J. Kane, R. Sher, and E. Weinstock, Bull. Am. Phys. Socl, Ser. II 3, 209A (1958).

115. F. Bonhoeffer, H. Hennies, and A. Flammersfeld, Z. Physik 155, 488 (1959).

116. C. Hammer and M. Stewart, Phys. Rev. 106, 1001 (1957).

117. R. Tornau, Z. Physik 159, 101 (1960).

118. A. Hashizume, T. Takahashi, Y. Tendo, and Y. Enomoto, J. Phys. Soc. (Japan) 15, 2175 (1960).

119. T. von Egidy, Ann. der Physik 7, 221 (1962).

120. E. L. Church and J. Weneser, Phys. Rev. 104, 1382 (1956).

121. T. A. Green and M. E. Rose, Phys. Rev. 110, 105 (1958).

122. T. Novakov and R. Stepic, Phys. Let. 3, 82 (1962).

123. A. S. Reiner, Nucl. Phys. 5, 544 (1958).

124. E. 1. Church and J. Weneser, Bull. Am. Phys. Soc., Ser. II 7, 490 (1962).

125. L. Persson, R. Hardell, and S. Nilsson, Arkiv Fys. 23, 1 (1963).

126. A. Wapstra et al., Nuclear Spectroscopy Tables (North Holland Publ. Co., Amsterdam, 1959).

127. G. White-Grodstein, X Ray attenuation Coefficients from 10 keV to 100 MeV, NBS Circular No. 583 (1957).

128. S. Hultberg. Arkiv Fys. 15, 307 (1959).

129. F. Cranston, J. Starner, and M. Bunker, Bull. Am. Phys. Soc., Ser. II 4, 292 (1959).

130. A. G. W. Cameron, At. Energy Canada Rept. CRP-690 (1957); Can. J. Phys. 35, 1021 (1957).

131. F. Everling, L. A. König, J. H. E. Mattauch, and A. H. Wapstra, Nucl. Phys. 18, 529 (1960).

131a. P. Seeger, Nucl. Phys. 25, 1 (1961).

132. S. Hultberg and R. Stockendal, Arkiv Fys. 14, 565 (1959).

133. C. De Vries, E. J. Bleeker, and N. Solomons-Grobben, Nucl. Phys. 18, 454 (1960).

134. G. A. Graves, L. M. Langer, and R. D. Moffat, Phys. Rev. 88, 344 (1952).

135. R. E. Maerker and R. D. Birkhoff, Phys. Rev. 89, 1159 (1953).

136. F. P. Cramston, M. E. Bunker, and J. W. Starner, Bull. Am. Phys. Soc. 5, 255 (1960).

137. B. Harmatz et al., Phys. Rev. 119, 1345 (1960).

138. R. M. Diamond, B. Elbek, G. Igo, and F. S. Stephens, UCRL-9302, 1960 (unpubl.)

139. E. Bernstein and H. Lewis, Phys. Rev. 105, 1524 (1957).

140. G. Goldring and T. Paulisson, Phys. Rev. 103, 1314 (1956).

141. J. Baker and B. Bleaney, Proc. Phys. Soc. (London) A68, 1090 (1955).

142. E. Bernstein and H. Lewis, Bull. Am. Phys. Soc., Ser. II 1, 47 (1956).

143. H. Kopfermann, Kernmomente (Akad. Verlagsges., Frankfurt, 1956).

144. E. Bernstein and R. Graetzer, Phys. Rev. 119, 1321 (1960).

145. Lutgen and Winther, private communication to Diamond et al.

146. O. Prior, Arkiv Fys. 14, 451 (1959).

147. F. D. S. Butement, Proc Phys. Soc. (London) A63, 775 (1950).

148. G. Wilkinson and H. Hicks, UCRL-744, 1950 (unpubl.)

149. J. Zylicz, Z. Sujkowski, J. Jastrzebski, O. Wotczek, S. Chojnacki, and I. Yutlandov, Polish Acad. Sciences Rept. PAN-358/I-A, Inst. Nucl. Reasearch, Warsaw, 1962 (unpubl.)

150. H. Ryde, L. Persson, and K. Oelsner-Ryde, Arkiv Fys. 23, 171 (1963).

151. O. I. Grigoriev, B. S. Kusnetsev, N. S. Shimanskaya, and I. Y. Yutlandov, Izvest. Akad. Nauk S.S.S.R., Ser. Fiz. 22, 850 (1958).

152. V. G. Soloviev, Kgl. Danske Vidensakb. Selskab Mat. Fys. Skr. 1, No.11, (1961).

153. H. Schüler and T. Schmidt, Naturwiss. 23, 69 (1935).

154. W. T. Leland, Phys. Rev. 77, 634 (1950).

155. F. K. McGowan, Phys. Rev. 85, 142, 151 (1952).

156. T. Stribel, Z. Naturforsch. 10a, 894 (1955).

157. R. Watson and A. Freeman, J. Appl. Phys., 33 Suppl., 1086 (1962).

158. B. Bleaney, Proc. Phys. Soc. (London) A68, 937 (1955).

159. B. Judd and I. Lindgren, Phys. Rev. 122, 1802 (1961).

160. B. Wybourne, J. Chem. Phys. 37, 1807 (1962).

161. L.S. Goodman, H. Kopfermann, and K. Schlüpmann, Naturwiss. 49, 101 (1962).

162. D. A. Tipler, P. Axel, N. Stein, and D.C. Sutton, Phys. Rev. 129, 2096 (1963).

163. G. Wilkinson and H. Hicks, UCRL-233, 1948 (unpubl.); Phys. Rev. 75, 696 (1949).

164. J. M. Cork, A. E. Stoddard, W. C. R. Rutledge, C. Branyan, and J. Le Blanc, Phys. Rev. 78, 299 (1950).

165. J. M. Cork, H. B. Keller, W. C. R. Rutledge, and A. E. Stoddard, Phys. Rev. 78, 95 (1950).

166. J. M. Cork et al., Phys. Rev. 75, 1133, 1778 (1949).

167. J. M. Cork, Nucleonics 7, No. 5, 24 (1950).

168. A Hedgran and S. Thulin, Phys. Rev. 81 1072 (1951).

169. S. Burson, K. W. Blair, H. B. Keller, and S. Wexler, Phys. Rev. 83 62 (1951).

170. S. Burson and W. Rutledge, ANL-4746, 1951 (unpubl.); Phys. Rev. 86, 633 (1952).

171. Bashilev, Antoneva, Dzhelepov, and Dolgentseva, Izvest. Akad. Nauk S.S.S.R., Ser. Fiz. 17, 437 (1953).

172. A. Burford, J. Perkins, and S. Haynes, Phys. Rev. 95, 303 (1954); 99, 3 (1955).

173. N. Marty, Compt. Rend. 240, 963 (1955).

174. H. de Waard, Phil. Mag. 46, 445 (1955).

175. L. Akerlind, B. Hartmaan, and T. Wiedling, Phil. Mag. 46, 448 (1955).

176. J. Mize, M. Bunker, and J. Starner, Phys. Rev. 100, 1390 (1955).

177. J. M. Cork, M. K. Brice, L. C. Schmid, and R. G. Helmer, Phys. Rev. 101, 1042 (1956).

178. E. Hatch, F. Boehm, P. Marmier, and J. DuMond, Phys. Rev. 104, 745 (1956).

179. T. Weidling, Directional Correlation Measurements and Some Other Related Investigations of Excited Nuclei (Uppsala, Almquist, & Wilksells, Boktryckeri, AB (1956), Thesis, Univ. of Stockholm, 1956).

180. H. Vartapetian, Compt. Rend. 244, 65 (1957).

181. M. Grace, C. Johnson, R. Scurlock, and R. Taylor, Phil. Mag. (8) 2, 1079 (1957).

182. E. Klema, Phys. Rev. 109, 1652 (1958).

183. F. McGowan, ORNL - 1705 (unpubl.) p. 18.

184. D. M. Chase and L. Wilets, Phys. Rev. 101, 1038 (1956).

185. E. Bernstein and H. Lewis, Phys. Rev. 105, 1524 (1957).

186. E. Berlovich, Sov. Phys. J.E.T.P. 6, 1176 (1958).

187. J. Daniels, J. Lamarche, and M. Le Blanc, Can. J. Phys. 36, 997 (1958).

188. H. Vartapetian, Ann. de Phys. 3, 569 (1958).

189. G. Manning and J. Rogers, Nucl. Phys. 15, 166 (1960).

190. A. Gnedich, L. Kryukova, and V. Muravena, Sov. Phys. J.E.T.P. 11, 524 (1960).

191. V. Bozhko, I. Zalyubovskil, and A. Tutubalin, Izvest. Akad. Nauk S.S.S.R., Ser. Fiz. 24, 847 (1960).

192. K. Hoffman, I. Krause, W. Schmidt-Ott, and A. Flammersfeld, Z. Physik 160, 201 (1960).

193. U. Hauser, K. Runge, and G. Knissel, Nucl. Phys. 27, 632 (1961).

194. A. Blaugrund, Y. Dar, and G. Goldring, Phys. Rev. 120, 1328 (1960).

195. J. Thun, Z. Grabowski, M. El-Nesr, and G. Bruce, Nucl. Phys. 29, 1 (1962).

196. E. Bashandy, and M. El-Nesr, Arkiv Fys. 21, 65 (1962).

197. B. Deutsch, Nucl. Phys. 30, 191 (1962).

198. J. Lindskog, T. Sundström, and P. Sparrman, Arkiv Fys. 23, 341 (1963).

199. B. Elbek, M. Olesen, and O. Skilbreid, Nucl. Phys. 10, 294 (1959).

200. A. H. Reddoch, to be publ.

201. E.E. Berlovich, Y. K. Gusev, V. V. Il'in, and M. K. Nikitin, Sov. Phys. J.E.T.P. 16, 1144 (1963).

202. S. G. Nilsson and O. Prior, Kgl. Danske Videnskab. Selskab Mat. Fys. Medd. 32, No. 16 (1961).

203. N. P. Heydenburg and G. M. Temmer, Phys. Rev. 93, 906 (1954).

204. A. Stendel, Naturwiss. 44, 371 (1957).

205. G. Goldring, Phys. Rev. 127, 2151 (1962).

206. H. Gollnow, Z. Physik 103, 443 (1936).

207. P. Klinkenberg, Re. Mod. Phys. 24, 63 (1952).

208. I. Kamei, Phys. Rev. 99, 789 (1955).

209. K. Murakawa and I. Kamei, Phys. Rev. 105, 671 (1957).

210. L. Goodman, "Symp. on Quadrupole Moments," Univ. of Kyoto, Japan, 1956 (unpubl.).

211. A. Stendel, Z. Physik 152, 599 (1958).

212. J. Blaise, J. Bauche, S. Gerstenkorn, and F. Tompkins, J. Phys. Rad. 22, 417 (1961).

213. G. Ritter, Phys. Rev. 126, 240 (1960).

214. A. Reddoch and G. Ritter, Phys. Rev. 126, 1493 (1962).

215. H. Yoshida and C. L. Lin, Phys. Let. 3, 107 (1962).

216. K. T. Hecht, Selected Topics in Nuclear Structure, B. J. Verhaar, ed., (North Holland Publ. Co., Amsterdam, 1964).

217. J. P. Davidson, Rev. Mod. Phys. 37, 105 (1965).

218. J. M. DuMond et al., Rev. Mod. Phys. 27, 363 (1955).

219. C. Hodgman et al., ed., Handbook of Chemistry and Physics, 45th Ed. (Chemical Rubber Publ. Co., Ohio, 1962).

220. E. A. Wolicki, R. Jastrow, and F. Brooks, U. S. Naval Research Lab. Rept. NRL-4833, 1956(unpubl.).

221. 1960 Nuclear Data Tables, Part 4, N.A.S. - N.R.C., Washington, D.C. (1961).

222. R.D. Evans, The Atomic Nucleus (McGraw-Hill Book Co., Inc., N.Y., 1955).

223. L. C. Northcliff, Ann. Rev. Nucl. Phys. 5, 13 (1965).

224. E. L. Hubbard, UCRL-9053, Jan., 1960 (unpubl.).

225. R. Graetzer et al., Nucl. Phys. 39, 124 (1962).

226. H. Lütgen and A. Winther, Kgl. Danske Videnskab. Selskab Mat. Fys. Skr. 2, No. 6, (1964).

205. G. Goldring, Phys. Rev. 127, 2151 (1962).

206. H. Gollnow, Z. Physik 103, 443 (1936).

207. P. Klinkenberg, Re. Mod. Phys. 24, 63 (1952).

208. I. Kamei, Phys. Rev. 99, 789 (1955).

209. K. Murakawa and I. Kamei, Phys. Rev. 105, 671 (1957).

210. L. Goodman, "Symp. on Quadrupole Moments," Univ. of Kyoto, Japan, 1956 (unpubl.).

211. A. Stendel, Z. Physik 152, 599 (1958).

212. J. Blaise, J. Bauche, S. Gerstenkorn, and F. Tompkins, J. Phys. Rad. 22, 417 (1961).

213. G. Ritter, Phys. Rev. 126, 240 (1960).

214. A. Reddoch and G. Ritter, Phys. Rev. 126, 1493 (1962).

215. H. Yoshida and C. L. Lin, Phys. Let. 3, 107 (1962).

216. K. T. Hecht, Selected Topics in Nuclear Structure, B. J. Verhaar, ed., (North Holland Publ. Co., Amsterdam, 1964).

217. J. P. Davidson, Rev. Mod. Phys. 37, 105 (1965).

218. J. M. DuMond et al., Rev. Mod. Phys. 27, 363 (1955).

219. C. Hodgman et al., ed., Handbook of Chemistry and Physics, 45th Ed. (Chemical Rubber Publ. Co., Ohio, 1962).

220. E. A. Wolicki, R. Jastrow, and F. Brooks, U. S. Naval Research Lab. Rept. NRL-4833, 1956(unpubl.).

221. 1960 Nuclear Data Tables, Part 4, N.A.S. - N.R.C., Washington, D.C. (1961).

222. R.D. Evans, The Atomic Nucleus (McGraw-Hill Book Co., Inc., N.Y., 1955).

223. L. C. Northcliff, Ann. Rev. Nucl. Phys. 5, 13 (1965).

224. E. L. Hubbard, UCRL-9053, Jan., 1960 (unpubl.).

225. R. Graetzer et al., Nucl. Phys. 39, 124 (1962).

226. H. Lütgen and A. Winther, Kgl. Danske Videnskab. Selskab Mat. Fys. Skr. 2, No. 6, (1964).

227. G. Seaman, Multiple Coulomb Excitation Studies in Even-Even Samaruim Nuclei (Thesis, Yale Univ., 1965).

228. Nuclear Data Sheets, N.A.S.-N.R.C., Washington, D.C.